NEOTECTONICS OF SOUTH-CENTRAL COASTAL CALIFORNIA

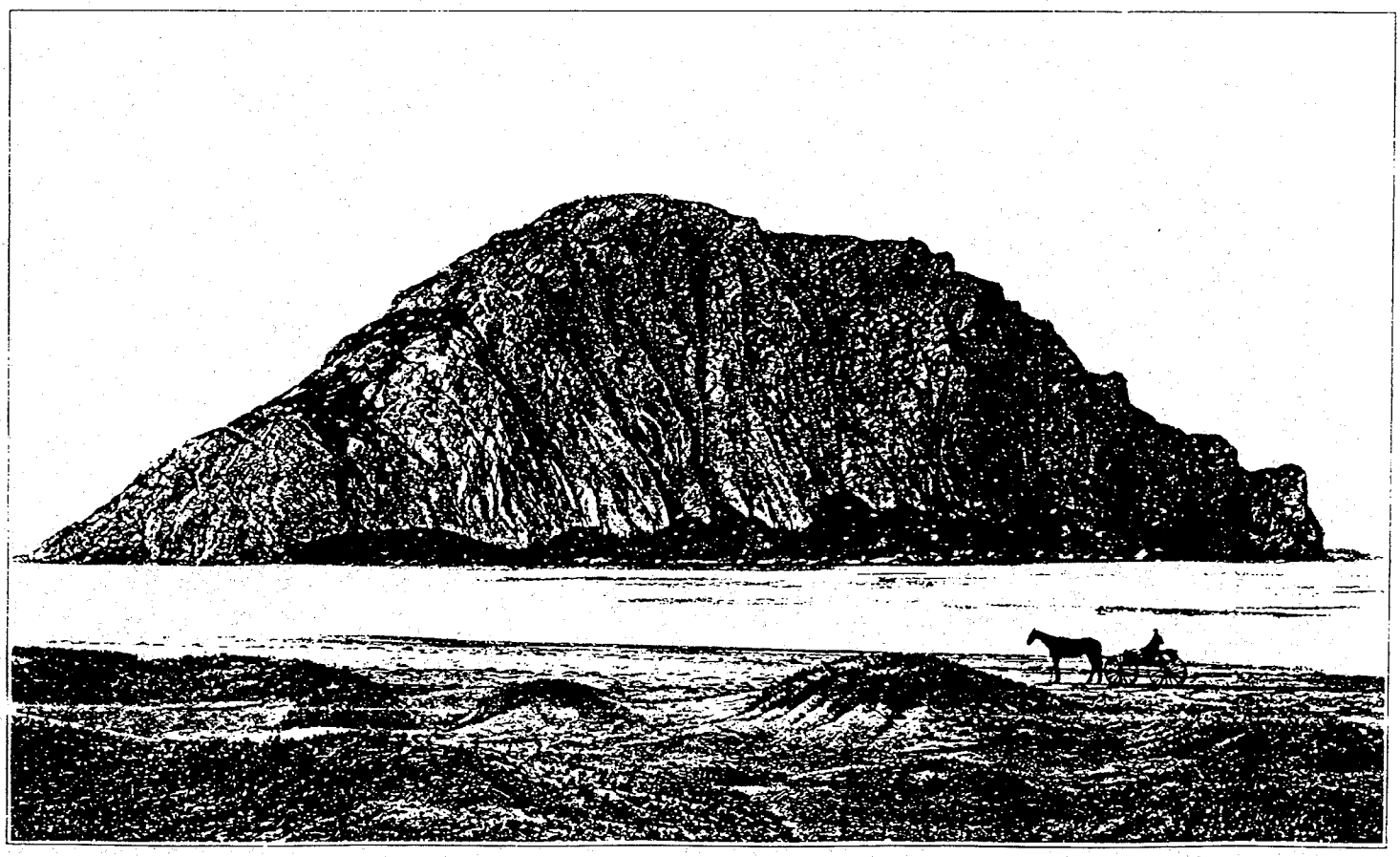

FRIENDS OF THE PLEISTOCENE

Pacific Cell

1990 Fall Field Trip

September 21 - 23, 1990

FIELD TRIP GUIDEBOOK

FRIENDS OF THE PLEISTOCENE
PACIFIC CELL

1990 FALL FIELD TRIP

SEPTEMBER 21-23, 1990

FIELD TRIP GUIDEBOOK

NEOTECTONICS OF SOUTH-CENTRAL COASTAL CALIFORNIA

Organized and Edited by

William R. Lettis
Kathryn L. Hanson
Keith I. Kelson
John R. Wesling

Trip Leaders

Michael Angell
Doug Clark
N. Timothy Hall
Kathryn Hanson
Keith Kelson
William Lettis
Anthony Orme
Tom Rockwell
John Wesling

TABLE OF CONTENTS

TABLE OF CONTENTS
(continued)

TABLE OF CONTENTS
(continued)

LIST OF FIGURES (continued)

TABLE OF CONTENTS
(continued)

LIST OF FIGURES (continued)

TABLE OF CONTENTS
(continued)

LIST OF FIGURES (continued)

TABLE OF CONTENTS
(continued)

CONTRIBUTED ARTICLES[1]

[1]The contents of these articles are the sole responsibility of their respective authors and have not been edited by the field trip organizers. It is suggested that you contact the individual authors regarding permission to cite specific articles. In addition, we have not appended the plates for these figures. If you would like a copy of the plates for one or more of the articles, please send a written request to Kathryn Hanson at Geomatrix Consultants, Spear Street Tower, Suite 717, San Francisco, California 94105.

NEOTECTONICS OF SOUTH-CENTRAL COASTAL CALIFORNIA

INTRODUCTION

Welcome to south-central coastal California - a region characterized and formed by active coastal erosion and tectonic deformation. Primarily motivated by hydrocarbon exploration in the onshore and offshore Santa Maria basin and by seismic hazard assessment for the Diablo Canyon Power Plant near Point Buchon, the tectonics of this coastal region has been the focus of numerous onshore and offshore geological, geophysical, and seismological studies during the past several years. This field trip will summarize the key findings of many of these studies and will discuss the implications and integration of this extensive suite of recently acquired data for assessing the regional tectonic setting.

Although these data allow new or updated interpretations of the geology in this region, there are still several unresolved or controversial issues regarding the history, style, and kinematics of late Cenozoic deformation in south-central coastal California. The more significant of these issues include:

- What is the history of deformation and contemporary style and rate of deformation along the various components of the San Gregorio/Hosgri fault system?

- Are "blind" thrust faults beneath active folds important tectonic elements in this region? If so, how should they be identified and characterized for seismic hazards evaluation?

- Is crustal shortening in the Los Osos/Santa Maria domain (east of the Hosgri fault zone) accommodated by rigid block uplift along discrete reverse faults, by folding and displacement along "blind" thrust faults at depth, or both?

- Is transpressional strain along the Pacific/North American plate margin partitioned into nearly pure tangential and normal strain components along south-central coastal California? If so, where and at what scale does strain partitioning occur and how should this phenomenon be addressed in the evaluation of seismic hazards?

During the course of this field trip we will observe many of the geologic relationships that are critical for addressing these unresolved or controversial issues and will discuss alternative interpretations that satisfy the existing data and observations. In addition, many of these issues are addressed in the series of articles and "in-progress" manuscripts that are appended to this guidebook.

In light of the importance of coastal processes in shaping the geology of this region, we will spend much of this field trip on the scenic beaches of south-central coastal California. We will convene on Friday morning at Montaña de Oro State Park campground near the beach of Spooner's Cove (Fig. 1). From the campground, we will drive north to the historic harbor of San Simeon Cove where we will examine field relationships along

the San Simeon fault zone. We will discuss the structural association of this strike-slip fault with the Hosgri fault zone, which lies entirely offshore south of San Simeon Point. On Saturday, we will focus on the nature and rate of deformation within and along the margins of the Irish Hills, which form the western part of the San Luis Range, one of several northwest-trending structural blocks within the onshore Santa Maria Valley region. On Sunday, we will examine structural and geomorphic relationships along the southwestern margin of the San Luis Range and then assess late Cenozoic deformation within the Santa Maria Valley and along the northwestern margin of, and within, the uplifting Casmalia Hills. We will have the opportunity to evaluate the style of deformation within and along the margins of the Casmalia Hills and compare this style of deformation to that associated with the San Luis Range to the north.

ACKNOWLEDGEMENTS

Many people contributed their time and support to make this FOP trip a reality. We wish to thank the contributors and co-leaders of this trip for their willing and cooperative efforts in assembling this production.

Part of the expense of planning this trip and preparing the guidebook was provided by the Professional Development Funds of Geomatrix Consultants, Inc., and of William Lettis and Associates. The Pacific Gas and Electric Company also provided technical support and funding for time and expenses for several contributors.

Special thanks goes to Deborah Ahrens of Geomatrix Consultants for her marathon typing efforts and for her assistance in handling field trip correspondence. We also are appreciative of the graphics group at Geomatrix, in particular Carolyn Mosher, for their efforts over the past four years, represented in part by the graphics for much of this guidebook.

Much of the research to be presented on this trip was generated in response to addressing conditions to the operating license of the Diablo Canyon Power Plant. Under the direction of Lloyd S. Cluff, Pacific Gas and Electric Company designed and implemented the Long-Term Seismic Program (LTSP) to reevaluate the seismic design basis for the plant as required by this license condition. As part of this program, a four-year comprehensive study of the neotectonics of south-central coastal California was conducted by PG&E and its consultants. Many papers included in this volume are a direct result of research supported by this program.

In conjunction with the review of the Diablo Canyon LTSP, the Nuclear Regulatory Commission provided support for additional independent research in south-central coastal California. Under the direction of Drs. Bert Slemmons and Richard Schweikert of the Center for Neotectonic Studies, University of Nevada, studies were conducted by Doug Clark, Steve Nichman, Katie Killeen, and Barbara Matz that contributed greatly to the understanding of Quaternary stratigraphy and structure in the region.

We will be spending much of the first day of the field trip on the Hearst Ranch near San Simeon. We are grateful to the Hearst Corporation and, in particular, Ranch Manager Harlan Brown, for support during our field studies in 1986 and for land access during this field trip.

TECTONIC OVERVIEW OF SOUTH-CENTRAL COASTAL CALIFORNIA

The 1990 Pacific Cell Friends of the Pleistocene field trip will review the geomorphic and tectonic evolution of the onshore Santa Maria basin region in south-central coastal California. We will visit many outcrops and discuss several lines of direct and indirect reasoning that bear on the tectonic setting of the onshore Santa Maria basin (Fig. 1). The onshore physiography of the Santa Maria basin region is expressed as a series of west-northwest-trending ranges and valleys between the more west-trending western Transverse Ranges to the south and the more north-trending Santa Lucia and San Rafael ranges to the northeast and east. Detailed and reconnaissance geologic studies conducted at various localities within the onshore Santa Maria basin region indicate that ranges and valleys generally reflect areas of Quaternary uplift and subsidence (or low rate of uplift), respectively. Most ranges are bordered by or associated with Quaternary active reverse or thrust faults (Fig. 2).

The west-northwest-trending structural grain and style of deformation in the onshore Santa Maria basin and adjacent areas is unique in the south-central coastal California region (Fig. 2). The structural grain is transitional between the east-west-trending structural grain of the western Transverse ranges and the north-northwest-trending grain of the Santa Lucia and San Rafael ranges. To the west, the west-northwest-trending reverse faults within the onshore Santa Maria Basin terminate against the north-northwest-trending San Simeon and Hosgri fault zones. West of these fault zones, the offshore Santa Maria basin is characterized by gradual block subsidence, scattered faults, and in some regions, by broad, late Cenozoic folds that are subparallel to the Hosgri and San Simeon fault zones.

We call the transitional region between the Western Transverse Ranges and southern California Coast Ranges the Los Osos/Santa Maria domain (Fig. 2) (Lettis and others, 1989). The domain is bordered by the Santa Ynez River fault trend on the south, the Oceanic-West Huasna-Little Pine-Foxen Canyon fault system on the northeast and east, and the San Simeon and Hosgri fault zones to the west and southwest (Fig. 2). We further divide the domain into a series of west-northwest-trending, elongated structural blocks that are bordered by known or postulated west-northwest-trending reverse faults. These blocks are the Cambria, San Luis/Pismo, Santa Maria Valley, Solomon Hills, Casmalia, Purisima Hills, and Vandenburg/Santa Ynez Valley blocks.

Two models have been proposed to explain the pattern of uplift and subsidence observed in the domain. Based on structural modeling, Namson and Davis (1990) conclude that the region is as a fold and thrust belt underlain by a regional decollement. According to this model, Franciscan Complex basement behaves as a brittle, horizontally layered medium and uplift of the ranges results from fault-bend or fault-propagation folding above ramps that branch upward from a regional decollement. Alternatively, detailed geological and geophysical studies conducted in the northern part of the domain indicate that Quaternary deformation is characterized by range-front reverse faulting and block uplift, tilting or subsidence of individual structural blocks, and that little or no active folding or

faulting is present within the blocks. This model is similar to the model proposed by Luyendyk and others (1980) wherey clockwise rotation of the western Transverse Ranges is accommodated by crustal shortening and lateral movement of rigid blocks in the Los Osos/Santa Maria domain.

Regardless of the model, the pattern and nature of deformation within the Los Osos/Santa Maria domain requires that the region is undergoing north-northeast-directed crustal shortening. The rates of convergence for these models range between 0.3 and 6.7 mm/yr. Based on geodetic data, Fiegl and others (1990) model an integrated rate of deformation across the southern part of the domain of 7 ± 1 mm/yr, which can be resolved into 6 ± 2 mm/yr of N30°E-directed crustal shortening and 3 ± 1 mm/yr of right-lateral shear across this axis. Lettis and others (this volume [a]) interpret that the shortening is related to transpression along the Pacific North American plate margin modified by clockwise rotation of the western Transverse Ranges. Clockwise rotation of the western Transverse Ranges (e.g., Luyendyk and others, 1980, 1985; Luyendyk and Hornafius, 1987), which is underlain by thickened continental crust, compresses the Los Osos/Santa Maria domain, which is underlain primarily by the Franciscan Complex, against the relatively stable Salinian crust that underlies large parts of the Santa Lucia and San Rafael ranges to the northeast.

FIELD TRIP GUIDE: DAY 1

Friday, 21 September 1990

Compiled by:	K. Hanson, W. Lettis, and N.T. Hall.
Assembly Point:	Parking area at Spooner's Cove - Montaña de Oro State Park. We will drive to our first field stop overlooking San Simeon Bay. Please minimize the number of cars by car pooling (essential for access to Hearst Ranch!)
Assembly Time:	7:45 am
Departure Time:	8:00 am
Route:	Montaña de Oro State Park to San Simeon area (Figs. 3 and 4).

QUATERNARY BEHAVIOR OF THE SAN SIMEON AND HOSGRI FAULT ZONES

INTRODUCTION

The San Simeon and Hosgri fault zones are prominent structural features along the coast of south-central California (Fig. 2). The San Simeon fault zone trends northwest subparallel to the central California coast for 87 km from near Lopez Point on the north to Point Estero on the south. The fault zone intersects the coast and is exposed onshore from San Simeon Bay to north of Ragged Point, a distance of about 20 km. Detailed geologic mapping conducted along the onshore reach of the fault zone near San Simeon Point document its geologic character as a major Quaternary

right-slip fault (Hall, 1975; Weber, 1983). More recent paleoseismic investigations provide new data for characterizing the late Quaternary behavior of the fault zone (Hanson and others, 1987; Hall and others, 1987; PG&E, 1988; Hanson and Lettis, this volume; Hall and others, this volume).

The Hosgri fault zone, however, lies entirely offshore where comparable geologic mapping and paleoseismic investigations cannot be performed. Evidence for the style and timing of deformation along this fault is primarily derived from remote techniques such as seismic reflection profiles, side-scan sonar data, and potential field data, supplemented by analyses of bathymetry and seismicity data. Using a variety of these data sets, the fault has been variously interpreted as an active listric thrust fault (Crouch and others, 1984), an inactive, former basin-margin normal fault (Davis and McIntosh, 1987), and an active right-slip fault (McCulloch, 1987; Hamilton, 1987; PG&E, 1988; Lettis and others, this volume [a]). Based on regional and detailed geophysical, geologic, stratigraphic, and tectonic analyses, most authors interpret that the strike-slip character of the San Simeon fault zone extends southward onto the Hosgri fault zone, and that these two faults comprise the southern two components of the larger San Gregorio/Hosgri fault system (Silver, 1974, 1978; Graham and Dickinson, 1976, 1978a, 1978b; Hall, 1975, 1978; Greene, 1977; Leslie, 1980, 1981; Clark and others, 1984; PG&E, 1988). Understanding the structural relationship between the well-documented San Simeon fault zone and the Hosgri fault zone is essential for describing the contemporary tectonic behavior and seismic potential of the Hosgri fault zone, as well as for assessing the tectonic setting and nature of Quaternary deformation along the south-central margin of California. A variety of geophysical and geological data have been used to evaluate the nature of the interaction between the San Simeon and Hosgri fault zones in the offshore region between San Simeon and Estero bays. These studies indicate that the faults form an en echelon right stepover and that they are structurally related via an intervening, actively subsiding pull-apart basin (Lettis and others, this volume [a]).

We will spend much of the first day of this field trip reviewing geologic, geomorphic, pedologic, and geophysical data that address the Quaternary behavior of the San Simeon and Hosgri fault zones. Today, our route includes six localities:

- **Field Stop 1-1:** We will visit an overview of San Simeon Bay to discuss offshore geophysical data between San Simeon Bay and Estero Bay.

- **Field Stop 1-2:** We will walk along the beach at San Simeon Cove to the San Simeon fault zone, where we will discuss evidence of Quaternary faulting.

- **Field Stop 1-3:** We will walk from Field Stop 1-2 to an exposure of the fault zone in a small Borrow Pit. We will discuss results from extensive trenching at this site.

- **Field Stop 1-4:** We will view a prominent flight of emergent marine terraces and discuss age-estimates based on comparison to Pleistocene sea-level curves, relative soil development, uranium-series dating, and thermoluminescence dating.

- **Field Stop 1-5**: We will walk from Field Stop 1-4 to a second trenching site that provided data on the sense, rate, timing, and amount of late Quaternary slip on the San Simeon fault zone.

- **Field Stop 1-6**: We will continue our walk to a third trenching site that provided evidence of the sense of slip and net slip of a Holocene faulting event. We will return to Montaña de Oro State Park after Field Stop 1-6.

GENERAL DIRECTIONS TO STOP 1-1

From Spooner's Cove, drive north along Pecho Valley Road (Montaña de Oro State Park access road) into the town of Los Osos. At 3.2 miles, Pecho Valley Road will make a sharp right turn and become Los Osos Valley Road. Proceed 1.5 miles through the town of Los Osos and turn left (north) on South Bay Boulevard. Drive 3.9 miles to Highway 1 north. Proceed north on Highway 1 for 28.2 miles to the vista view turnout along the west side of the Highway. Use extreme care in making the left turn into the turnout. The following road log details the route and describes several geologic features between Montaña de Oro and San Simeon Bay.

ROAD LOG TO STOP 1-1

Odometer Cum.	Odometer Int.	
0.0	0.0	Pecho Valley Road generally follows the back edge of the first emergent (Q_1) marine terrace in Montaña de Oro, which we correlate to marine oxygen isotope substage 5a (~80 ka). Remnants of at least 12 marine terraces are present in the region between Montaña de Oro State Park and the town of Los Osos. These terraces extend up to elevations of approximately 250 m and represent one of the most complete flight of Pleistocene marine terraces in the region. We will have the opportunity to discuss the distribution and significance of these terraces tomorrow.
2.8	2.8	Crossing projected trend of Los Osos fault zone. Emergent marine terraces are not present in the Morro Bay area northeast of the Los Osos fault zone. Morro Bay occupies part of a late Cenozoic structural basin informally named the Morro Bay basin. We will discuss the structural setting of this basin tomorrow. Note the well-developed eolian sand spit across the entrance to Morro Bay and the ramp of dune sand along the southern margin of the bay. North of the bay is Morro Rock, the westernmost outcrop of a linear west-northwest trending alignment of Oligocene dacite intrusions called the Morro Rock-Islay Peak Complex. Potassium-argon age analysis of dacite from Morro Rock yielded an age of 22.1 ± 0.9 Ma (Turner, 1968; Turner and

others, 1970). The intrusions form a series of resistant peaks along the northern margin of the Los Osos Valley, including Bishop Peak and Islay Peak overlooking the town of San Luis Obispo. Hall (1981b) suggests that emplacement of the dacite was structurally controlled by the San Luis Obispo transform fault, which he infers was the initial transform fault between the Pacific and North American plates.

3.6 0.8 *Pecho Valley Road bends sharply to right and becomes Los Osos Valley Road.*

5.1 1.5 *South Bay Boulevard. Turn left (north) toward Morro Bay.*

6.9 1.8 *Cross Los Osos Creek.* Note the tidal marsh of Morro Bay State Park on left.

8.4 1.5 South Bay Boulevard crosses the pass between Black Hill (on left) and Cerro Cabrillo (on right). These hills are part of the Morro Rock-Islay Peak dacite intrusive complex.

9.0 0.6 *Intersection with Highway 1; go under overpass, turn left (north) onto Highway 1.*

15.4 6.4 The town of Cayucos is built primarily on a broad emergent marine terrace informally named the Cayucos terrace. Marine deposits on this terrace are fossiliferous and are approximately 120 ka based on uranium-series dating of coral (Veeh and Valentine, 1967; Ku and Kern, 1974; Muhs and others, 1988; Stein and others, 1989; and D. Muhs, personal communication) and paleoclimatic analysis of invertebrate faunal assemblages (Kennedy and others, 1988). The shoreline angle elevation (elevation of the inner edge of the terrace at the intersection of the wave-cut abrasion platform and the paleo-sea cliff) of this terrace is close to the estimated paleo-sea level (~ +6 m) for the 120 ka highstand. Because of this and the absence of higher marine terraces along this stretch of coastline, we conclude that there has been little or no late Quaternary uplift of this part of the coastal region. The Cayucos terrace increases in elevation to the north and is absent in the Morro Bay region to the south indicating that there has been south-directed Quaternary tilting in this region.

19.6 4.2 We are now crossing the Cambria fault. This fault is a high-angle fault that juxtaposes Cretaceous sandstone and Franciscan Complex rocks (Hall and others, 1979). The fault intersects

the coastline between Cayucos Point and the mouth of Ellsly Creek. A down-to-the-south step in the 120 ka Cayucos terrace is coincident with the fault trace and indicates possible late Quaternary fault activity (Hall and others, 1979; Weber, 1983). Alternatively, the step may have originated by lithologically controlled differential erosion of the wave-cut platform. Recently acquired uranium-series ages (Muhs, personal communication, 1990) from coral collected on both sides of the fault indicate that the terrace is the same age across the fault and that the step does not represent two different aged terraces.

25.4 5.8 *Highway 1 passes the wonderful town of Harmony (pop. 18); there is an excellent pasta restaurant on Main Street.*

27.3 1.9 *Continue north on Highway 1 past the intersection with Highway 46, which leads to Paso Robles.*

32.8 5.5 We are driving along the Tripod terrace, the first emergent terrace along this stretch of coastline. Weber (1983) correlated this terrace to the 120 ka Cayucos terrace to the south. Springs within the dune sand to the east (right) side of the highway likely represent the approximate elevation of a higher wave-cut platform that is largely buried by a sheet of eolian sand.

34.3 1.5 *Crossing San Simeon Creek.* A flight of marine terraces forms a sequence of broad platforms extending east to the Santa Lucia Range. The Oceanic-West Huasna fault, a northeast-dipping reverse fault, lies at the base of this range.

35.3 1.0 At 12:00 on the skyline, the Oceanic-West Huasna fault system merges with the San Simeon fault zone. The San Simeon fault zone lies directly offshore and is responsible, in part, for development of the linear coastline from this location south to Point Estero.

36.1 0.8 *Crossing Pico Creek.* North of Pico Creek, the Tripod terrace becomes the second emergent terrace. We interpret the first emergent terrace, the San Simeon terrace of Weber (1983), is interpreted to be approximately 80 ka (correlative to marine oxygen isotope substage 5a). Several large remnant sea stacks, visible east of Highway 1, are preserved near the back edge of the Tripod terrace.

37.2 1.1 *Turn left (west) from Highway 1 into Vista View parking lot (STOP 1-1).*

Field Stop 1-1 - San Simeon Bay Overview

The San Simeon fault zone intersects the coastline at San Simeon Cove in the northwestern corner of San Simeon Bay. The fault forms the prominent northeast-facing escarpment visible of San Simeon Point. To the northwest, the fault merges with the Oceanic-West Huasna fault system along the base of the prominent Santa Lucia range front. We will visit five localities along the southern part of the onshore reach of the San Simeon fault zone, beginning at San Simeon Cove (Fig. 5). Geologic mapping, drilling and trenching studies at these localities provide evidence that the San Simeon fault zone is a right-lateral, strike slip fault with a late Quaternary slip rate of 1 to 3 mm/yr.

Offshore to the southeast, the San Simeon fault zone approaches and structurally interacts with the Hosgri fault zone between San Simeon Bay and Estero Bay. To investigate the nature of this interaction, we acquired and analyzed a variety of offshore geophysical and geological data, which we will discuss at this stop. Our interpretation of these data indicates that (1) the San Simeon and Hosgri fault zones are prominent basement-involved structures that laterally terminate in the near-offshore between San Simeon Bay and Point Estero (Fig. 6); (2) the faults overlap one another for a distance of about 10 to 12 kilometers and form a 5-kilometer wide en echelon right stepover; and (3) a subsiding basin bordered by normal faults and containing late Pliocene and younger deposits exists within the stepover region. A subsiding basin within a right stepover between two right-slip faults is a widely recognized structural feature variously referred to as a pull-apart basin (Burchfield and Stewart, 1966; Mann and others, 1983), a releasing step or bend (Crowell, 1974), or a dilational jog (Sibson, 1985, 1986a, 1986b). Based on the right en echelon fault stepover, the intervening pull-apart basin structure, and the documented right-slip character of the onshore San Simeon fault zone, we conclude that lateral slip is transferred between the San Simeon fault zone and the northern Hosgri fault zone via the pull-apart basin (Lettis and others, this volume [a]).

Empirical and theoretical kinematic studies of strike-slip fault systems indicate that an en echelon step between offset strands of a strike-slip fault produces a characteristic style and pattern of deformation dependent on both the orientation of the stepover (right-stepping or left-stepping) and the sense of slip on the fault system (e.g., Hempton and Dunn, 1984; Hempton and Neher, 1986). Furthermore, the dimensions and age of the basins are related to rates of slip along the master bounding faults (Rodgers, 1908; Woodcock and Fischer, 1986). From these studies we infer that a time-averaged late Pliocene-Quaternary lateral slip rate of 1 to 4 mm/yr is transferred across the basin between the southern San Simeon and northern Hosgri fault zones.

Analysis of an extensive suite of geophysical, seismological, and geological data along the entire Hosgri fault zone provides additional evidence supporting an interpretation of predominantly strike-slip behavior of the Hosgri fault zone in the contemporary tectonic setting. An important criterion for evaluating the style of faulting along the Hosgri fault zone is the ratio of horizontal slip rate to vertical slip rate. Using a lateral rate of 1 to 3 mm/yr (based on paleoseismic and

Quaternary mapping studies conducted along the San Simeon fault zone, the rate of slip necessary to produce the San Simeon/Hosgri pull-apart basin, consideration of regional tectonics, and geodetic rates of crustal shortening in south-central California) and a vertical slip rate of 0.1 to 0.4 mm/yr (based on conservative estimates of the rate of vertical separation of a mid-Pliocene unconformity (2.8 Ma) across the fault zone), the ratio of horizontal to vertical slip ranges from 2:1 to 30:1. These ratios indicate that the Hosgri fault zone is predominantly a strike slip fault with a subordinate component of dip slip.

The Hosgri fault zone also exhibits many characteristics comparable to other strike slip faults in the world such as:

- Reversals in the sense of vertical separation both down dip and along strike of the fault.
- The presence of local intra-fault zone pull-apart basins at right-releasing stepovers.
- Compressional and extensional flower structures having associated intra-fault zone anticlinal and synclinal folding.
- The fault zone and individual fault strands within the zone are linear at regional scale (greater than 20 km) and curvilinear to linear at local scale (less than 20 km). Fault trace sinuosity is less than 1:1, similar to other known strike slip faults.

Tectonic, kinematic and regional stress data indicate that the Hosgri fault zone decouples regional crustal shortening of differing orientations within the Los Osos/Santa Maria domain and the offshore Santa Maria basin, requiring lateral slip on the Hosgri fault zone.

ROAD LOG TO **STOP 1-2**

Odometer Cum.	Odometer Int.	
0.0	0.0	*Return to vehicles and continue north on Highway 1. Reset odometer.*
0.4	0.4	*Crossing Little Pico Creek.* The shoreline angle for the San Simeon terrace is exposed in the seacliff directly north of the mouth of Little Pico Creek at an elevation of 7 m. Natural exposures of the soil developed in the San Simeon terrace deposits were described and collected along the sea cliff south of the creek mouth. We are driving again on the Tripod (~120 ka) terrace. Note the continued presence of numerous relict sea stacks near the back edge of this terrace. The Tripod terrace, like the modern wave-cut platform in this area, is highly irregular where developed on chert and metavolcanic knockers within the Franciscan Complex.
1.8	1.4	*Turn left (west) onto San Simeon Road - the entrance to W.R. Hearst State Beach. To the east is the entrance road to the Hearst Castle State Historical Monument parking area. Drive 0.2 mile*

and park along San Simeon road rather than entering the park. The older buildings along the beach are part of the old San Simeon Bay port. The materials used to construct Hearst Castle were shipped to this port and carried up the hill to the Castle. Assemble on the beach near the lagoon at the mouth of Arroyo del Puerto - north of San Simeon Pier. We will walk north toward San Simeon Point to San Simeon Cove (Stop 1-2) at the northwest end of the bay. As we walk, note the older gravel deposits from Arroyo del Puerto Creek exposed in the low sea cliff. These gravels rest on Franciscan Complex basement locally exposed at the base of the cliff. The wave-cut platform of the San Simeon terrace, which is well exposed south of San Simeon pier, is absent along this reach of the coast either due to fluvial erosion by Arroyo del Puerto or because it is tectonically tilted down-to-the-west into the San Simeon fault zone.

Field Stop 1-2 - San Simeon Cove

The San Simeon fault zone intersects the coastline at San Simeon Cove in the northwestern corner of San Simeon Bay (Fig. 5). At this location, the fault zone is about 120 m wide and consists of two or possibly three major fault strands (Fig. 7). A fossiliferous, shallow marine, pebbly sandstone has been tectonically emplaced along the fault zone between the highly resistant diatomite and chert beds of the Monterey Formation that underlie San Simeon Point to the southwest and less resistant rocks of the Franciscan Complex to the northeast. Hall (1976) tentatively correlated the fossiliferous sandstone with the Pliocene and Pleistocene Careaga Formation in the Santa Maria basin to the south. Restoration of the offset Careaga suggests up to 85 km of cumulative right-lateral displacement. Alternatively, the sandstone may have accumulated in a nearby offshore basin, such as the San Simeon/Hosgri pull-apart basin described at our previous stop, in which case, the cumulative displacement is less than 2 km.

The lowest emergent wave-cut platform, called the San Simeon Point (Q1) terrace, is beveled onto the Careaga (?) and the Monterey formations. Based on a uranium-series age of bone, soil-profile development, and correlation of the terrace sequence to the marine oxygen isotope record, this terrace is estimated to be 60 or 80 ka (see Hanson and others, this volume, for a discussion of the ages and correlation of marine terraces in the San Simeon region). The wave-cut platform is separated vertically about 2.5 m across the western-most strand of the fault zone, indicating late Quaternary activity. The Q1 terrace is assumed to step down to the northeast across the inferred easternmost major strand of the fault zone, but relationships in this region are obscured by thick colluvium from overlying dune deposits.

The Careaga Formation forms a small fault-bounded prominence at San Simeon Cove (Fig. 7). On the southwestern side of this prominence, branching and anastamosing cemented shears cut the Careaga (?)

Formation but do not displace the overlying marine terrace platform. The most prominent of these shears strikes N28°W and dips 53° NE. On the northeast side of the prominence, Careaga (?) beds are overlain by tilted estuarine deposits with a thermoluminescence age of 193,000 ± 47,000 years (Glenn Berger, personal communication, 1987). Here, the Careaga (?) Formation, the estuarine beds, and the overlying San Simeon Point (Q1) terrace wave-cut platform and its basal marine terrace deposits are cut by a small fault. A distinctive oxidized layer within the basal marine terrace deposits is vertically separated about 8 cm across this fault indicating late Pleistocene activity. This location is cited by Weber (1983) as demonstrating late Pleistocene and probable Holocene activity based on fractures and displaced soil lamellae observed within the overlying dune sand. .Manson (1985) cited the study by Weber in concluding that the San Simeon fault zone is "... sufficiently active and, well-defined ..." to be designated an Alquist-Priolo special studies zone.

The San Simeon fault zone extends offshore to the southeast from the seacliff exposure into San Simeon Bay (Fig. 5). Rock samples collected from the floor of San Simeon Bay by a diver-geologist show that a strip of sandy bottom separates the Monterey Formation from the Franciscan Complex. The sandy bottom may represent a less resistant fault slice of the Careaga (?) Formation as is exposed onshore or perhaps a buried fluvial channel. The distribution of lithologies offshore indicates that the approximate N35°E trend of the San Simeon fault zone observed onshore extends offshore for at least 2 km southeast of San Simeon Point.

DIRECTIONS TO **FIELD STOP 1-3**

*From San Simeon Cove we will walk to **Stop 1-3** at the Borrow Pit. Follow the beach back toward the pier to the end of the eucalyptus grove. At this point follow the dirt trail up the sea cliff, cross the fence (use care) onto the Hearst Ranch and follow the general trend of the fault zone to the Borrow Pit site (Fig. 5). In order to minimize our impact on the Hearst Ranch property, please* ***do not smoke*** *and cross fences only at designated crossings.*

Field Stop 1-3 - Borrow Pit Site

During our initial phases of mapping at San Simeon, a major strand of the San Simeon fault zone was observed in a small sand quarry, informally named the Borrow Pit, located about 600 m northwest of the San Simeon Cove (Fig. 8). The pit is excavated in an older dune complex that locally veneers the late Pleistocene marine terraces in this area. The exposed trace of the San Simeon fault zone is a clay-rich zone of fault gouge that is up to 1.5 m wide and locally contains exotic boulders and cobbles derived from Franciscan Complex rocks and from deeply weathered basal marine terrace deposits. We excavated five trenches, five exploratory pits and drilled numerous boreholes at this site (Fig. 8). The fault exposed in trenches (Fig. 9), the eastern Borrow Pit trace, is marked by a prominent vertical to subvertical sheet of gouge that separates dune sand on the west from the San Simeon-Q2 (80 or 105 ka) or Tripod-Q3 (120 ka) marine terrace deposits. The presence of shears and clay gouge within unconsolidated to moderately-consolidated late Pleistocene or younger dune sand and

apparent disruption of soil horizons formed in the dune sand suggests that multiple-slip events occurred during the late Pleistocene and/or Holocene.

In addition to the eastern trace, stratigraphic and structural relationships inferred from trench exposures and borehole data suggest that there is at least one additional prominent late Pleistocene fault trace. These relationships are discussed in Hall and others (this volume). Structural and stratigraphic relationships across the entire fault zone at the Borrow Pit Site are illustrated on cross sections AA' and BB' (Fig. 10). These sections, which synthesize mapping, trenching, drilling, and shallow seismic refraction data, show a complex fault zone approximately 180 m wide that consists of at least six strands. The apparent vertical separation across these strands is variably down-to-the-east and down-to-the-west. Fossiliferous marine deposits encountered below the dune sand in several drill holes contain fauna interpreted by G. Kennedy (written communication, 1986) to be early Quaternary (pre-500 ka) and possibly Pliocene in age. We believe these deposits are correlative with the Careaga (?) Formation exposed at San Simeon Bay and occupy a similar structural position as a fault slice between the Monterey Formation and Franciscan Complex bedrock.

In summary, trenching and drilling investigations at the Borrow Pit site confirm that: (1) the San Simeon fault zone consists of multiple splays that manifest both down-to-the-east and down-to-the-west apparent vertical separations, (2) the most recent activity on one major strand, the eastern Borrow Pit fault, was essentially pure right-lateral strike slip, (3) this faulting clearly cuts dune sand of late Pleistocene age, and (4) this faulting also disrupts the topsoil developed on the dune sand, strongly suggesting Holocene activity.

LUNCH

Return to our cars along San Simeon Road. We will eat lunch at San Simeon State Park. Picnic tables and restroom facilities are available in the state park. The historic (1852) Sebastian's General Store is an excellent place to obtain miscellaneous supplies (at tourist prices).

DIRECTIONS TO **FIELD STOP 1-4**

Reassemble at the cars at 1:00 pm. We will drive and repark the cars at the area designated PARK 2 on Figure 5. Follow the frontage road past the San Simeon store to the intersection with Highway 1. Cross Highway 1 and enter the main gate into the Hearst Ranch headquarters. Follow ranch roads as indicated on Figure 5 around the Hearst airstrip to the PARK 2 site. We will walk a short distance to "Bull Knoll" overlook (Stop 1-4).

Field Stop 1-4 - "Bull Knoll" Overlook

From the vantage point of "Bull Knoll" (or close to it depending on the number and size of bulls presently in residence), we can get a good view of the coastal region along the onshore San Simeon fault zone. This area is characterized by a prominent flight of emergent marine terraces disrupted by late Quaternary faulting along the San Simeon fault zone. In order to constrain the Pleistocene slip rate for the San Simeon

fault zone, we performed a detailed mapping of marine terraces across the southern onshore reach of the fault zone. To assess the elevation of wave-cut platforms in areas covered by eolian and alluvial deposits, we drilled 94 boreholes and excavated 31 soil and exploratory pits. Uranium-series dating of one bone sample from the lowest emergent marine terrace and thermoluminescence dating of silt from estuarine deposits underlying the second emergent terrace provide some age control. However, due to the limited amount of datable material recovered from marine terrace deposits in the San Simeon area, other less direct dating and correlation techniques, including comparison of geomorphic expression, relative altitudinal spacing of marine terraces, and comparison of relative soil profile development, also were employed to correlate and estimate the ages of terraces across the fault zone. A discussion of the distribution, correlation, age, and uplift of marine terraces (including a summary of soil geomorphological studies that will be discussed by T. Rockwell at this Stop) is provided in Hanson and others (this volume).

We have mapped flights of four and five marine terraces to the northeast and southwest, respectively, of the southern onshore reach of the San Simeon fault zone (Fig. 11). From youngest to oldest, they are the San Simeon Point (Q1), San Simeon (Q2), Tripod (Q3), Oso (Q4), and La Cruz (Q5) terraces. They are interpreted to correlate with marine oxygen-isotope stages 3 or 5a (60 to 80 ka), 5a or 5c (80 to 105 ka), 5e (120 ka), 7 (210 ka), and 9 (330 ka).

The terraces are clearly displaced vertically and laterally across the San Simeon fault zone. The fault zone is characterized locally by a prominent northeast-facing escarpment as we observed at Stop 1-1. A longitudinal profile showing the elevations of shoreline angles of terraces on both sides of the fault zone illustrates that terraces southwest of the main active traces of the fault are warped up adjacent to the fault zone (Fig. 12). The highest rate of Pleistocene uplift (0.24 m/ka) occurs within and directly southwest of the fault zone. The apparent fold deformation in this area suggests that a concealed low-angle, southwest-vergent fault may splay from the high-angle San Simeon fault zone. Comparable low-angle fault components along a high-angle strike-slip fault zone are observed on seismic records across both the San Gregorio fault to the north near Seal Cove and the Hosgri fault zone to the south between Point Buchon and Point Sal. Northeast of the San Simeon fault zone there is no apparent folding or deformation of marine terraces and the significantly low uplift rate in this region (0.16 $\pm$ 0.01 m/ka) is only slightly less than the uplift rate (0.17 $\pm$ 0.02 m/ka) for areas southwest of the fault zone outside of the region of warping.

Mapping of the marine terrace strandlines indicates that right lateral displacement is the main component of slip on the San Simeon fault zone and that late Pleistocene deformation has been concentrated along two or possibly three primary fault traces within a zone of shearing and warping up to 500 meters wide. Estimated lateral slip rates based on the present locations of strandlines for the San Simeon (~ 80 or 105 ka), Tripod (120 ka), and Oso (210 ka) terraces, and paleogeographic reconstructions of the shoreline configurations during their development, range from about 0.4 to 11 mm/yr with the best constrained values ranging from 1 to 3 mm/yr (see Hanson and Lettis, this

volume). Slip rates based on deflections and apparent offset of drainages across the primary active traces of the San Simeon fault zone are in agreement with the values estimated from the marine terrace study.

Bull Knoll is situated on a largely stripped remnant of the Oso (Q4) terrace in the region of highest uplift. This terrace remnant is bounded by two active traces of the San Simeon fault zone. The main active trace is expressed by a series of tonal contrasts, vegetation lineaments, and side hill benches and scarps that flank the northeastern slope of Bull Knoll. Exposures in exploration and soil test pits indicate that secondary fault traces are present along the southwest flank.

Looking to the southwest, we get a good view of the extensive dune complex that mantles most of the area along the southern onshore San Simeon fault zone. Using scattered bedrock outcrops and subsurface data from a number of boreholes on San Simeon Point, we have documented that during the development of the Oso (~210 ka) and Tripod (~120 ka) paleoshorelines, islands occupied the present location of San Simeon Point. The present configuration of the shoreline, which consists of a large headland southwest of the fault zone, and an embayment beach to the northeast is fairly recent, having first developed during San Simeon time (~105 or 80 ka). The presence or absence of such headland/bay configurations is an important factor that we considered in estimating lateral offset based on the present configurations of marine terrace strandlines (see Hanson and Lettis, this volume).

DIRECTIONS TO FIELD STOP 1-5

From "Bull Knoll" we will walk downhill to the southeast to the Airport Creek site (Stop 1-5).

Field Stop 1-5 - Airport Creek Site

The Airport Creek site is located within the San Simeon fault zone about 900 m northwest of the Borrow Pit site (Fig. 5). Paleoseismic investigations conducted at this locality provide data to evaluate several key fault parameters such as sense and rate of slip, timing of the most recent slip, and slip per event for a prominent Holocene fault strand within the San Simeon fault zone. We briefly summarize below some of the key observations and results from these investigations. Hall and others (this volume) provide a more detailed discussion.

Two geomorphic features indicate Holocene faulting at the site: a local 1.8-m right-deflection of the channel margin along Airport Creek and a subtle topographic trough bounded by low scarps in unconsolidated materials on the southeastern side of the creek (Fig. 13). Based on this surface evidence, we excavated seven trenches and two exploratory pits at the site to evaluate faulting that occurred during the late Pleistocene and Holocene.

The faulting exposed in trenches at the Airport Creek site consists of from one to three distinct strands that occur within a 9- to 12-m wide zone of highly sheared materials (Fig. 14). At least one fault strand cuts the base of the soil A horizon and clearly demonstrates late Holocene activity on the San Simeon fault zone. The structural expression of the youngest faulting is quite variable from trench to trench and ranges from a nearly horizontal

single trace in trench T-4, to a nearly vertical single trace in trench T-1, to multiple west-dipping traces in trenches T-2 and T-5. The strike of the individual fault planes is also variable and ranges from N25°W to N41°W. Four of the trenches crossed a major strand of the fault with apparent down-to-the-east vertical separation. Grooves and striae on the main fault plane, however, plunge 2° to 11° southeast, indicating that movement on the fault has been predominantly strike slip.

Geomorphic features and stratigraphic evidence exposed in the trenches demonstrate that during the early Holocene Airport Creek was partially ponded against the northeast side of the fault. In the late Holocene, Airport Creek incised its channel between 3 and 4.5 m into these alluvial deposits. The steep walls of this channel are right-laterally deflected 1.8 m where they cross the active fault (Fig. 13). Although the creek changes direction near the fault, both channel walls display 1.8 m of right-lateral displacement, which we believe probably occurred during the late Holocene. It is likely that the channel deflection occurred during one, or at most two, slip events on the active fault trace.

The rate of slip on the main fault trace exposed in the Airport Creek trenches can be estimated from the dislocated southern margin of the early Holocene terrace deposit (Fig. 13) and from a geometric analysis of vertically separated soil horizons exposed in trench T-1 (Fig. 15). The fluvial terrace margin is a poorly constrained piercing point that intersects the main fault trace at Airport Creek from the east at a low angle in the vicinity of trench T-2. The piercing point west of the fault is less well constrained but must lie between trenches T-1 and T-5, giving a right separation of ranging from 10 to 20 m. The age of this terrace margin is also uncertain but may be on the order of 6,500 to 7,725 years based on radiocarbon ages of sediment within the terrace deposits and estimated sedimentation rates. From this age span, we estimate a slip rate that falls within the range of 1.3 to 3.1 mm/yr.

For additional estimates of slip rate at the Airport Creek site, we focused on trench T-1. By making several assumptions (see Hall and others, this volume), we used the vertical separation of soil stratigraphic units correlated across the fault in this trench to estimate an average Holocene horizontal slip rate of 1.0 to 1.4 mm/yr. The progressive decrease of vertical separations upsection in trench T-1 also provides good evidence for multiple slip-events on this fault. Although this fault appears to be the primary active trace within the fault zone, it is but a part of a broader fault zone. Hence, the slip rate calculated for this trace probably represents a minimum value for the San Simeon fault zone.

Using the range of slip rates estimated from both the vertical separations observed in trench T-1 (1.0 to 1.4 mm/yr) and from the displaced Airport Creek terrace margin (1.3 to 3.1 mm/yr) plus our estimate of net slip per event of 0.9 to 1.8 m, we estimate the average time between slip events to range from 643 to 1385 years. However, because the active fault observed at Airport Creek is a single trace, its estimated slip rate probably represents a minimum value for the San Simeon fault zone. Likewise, the calculated recurrence interval may underestimate the occurrence of ground rupturing events within the broader fault zone.

DIRECTIONS TO **FIELD STOP 1-6**

From the Airport Creek site, we will walk to the northwest (past the parked cars) along the active trace of the fault to the Oak Knoll Creek site (Stop 1-6). Geomorphic expression of the fault zone, including springs, vegetation, lineaments, tonal contrasts, and side hill benches are present on the east side of Bull Knoll and the elevated region northwest of Bull Knoll. The broad flat surface extending to the northeast is the La Cruz marine terrace, which we interpret to be 330 ka (correlative to marine oxygen isotope stage 9).

Field Stop 1-6 - Oak Knoll Creek Site

Oak Knoll Creek crosses the San Simeon fault zone orthogonally and is marked by a prominent right deflection of the valley margins and by deformed fluvial terrace deposits. We excavated six trenches in the Oak Knoll Creek area to identify the locations of the primary traces of the San Simeon fault zone and to assess their late Quaternary fault behavior (Fig. 16). Trenches T-1, T-2, T-2A, and T-3 were excavated to depths of 4.5 m or more in the semiconsolidated Holocene deposits of fluvial terrace Qt5 (5.5 to 7.9 ka) on the south margin of the Oak Knoll Creek. Trenches T-1, T-2, and T-2A intersected an active strand of the San Simeon fault zone. Initially, we intended to extend trench T-3 an additional one hundred meters or more to the northeast to detect other active, more easterly strands within the fault zone. However, unstable trench walls and homogeneous, poorly stratified overbank deposits required an alternative approach. We subsequently excavated trenches T-4 and T-5 south of the creek in a hillside area of shallow bedrock overlain by a thin veneer of alluvial and colluvial materials. Trench T-5 revealed a sheared contact between Franciscan greenstone and Holocene (?) colluvium.

Figure 17a is a diagrammatic oblique view of the Oak Knoll Creek site showing the approximate relative positions of trenches T-1, T-2, T-2A, and T-3, the active strand observed in trenches T-1 and T-2, and the approximate projected position of the more easterly strand encountered in trench T-5. Detailed logging along the north wall of trench T-2 revealed a vertical fault in alluvium having a strike of N26°W at the bottom of the trench 4.5 m below the surface. At a depth of 1.5 m, the strike of the fault plane is rotated clockwise to N14°W suggesting right-lateral strike slip. A sand bed whose thickness changes abruptly across the fault is located at a depth of 1.5 to 2.1 m in the trench T-2. A second trench (T-2A), hand-excavated parallel to the fault, provided a three-dimensional view of the sand bed and was used to measure variations in its thickness for construction of an isopach map. The equal-thickness contours yielded excellent piercing points on the fault from which we were able to evaluate vertical and lateral components of fault displacement (Fig. 17b). Detrital charcoal collected from above and below the sand bed indicate it was deposited in the interval between 6250 ± 120 and 5540 ± 120 radiocarbon years B.P. We concluded from detailed analysis of the fault exposed in trenches T-2 and T-2A that the most recent slip event on the fault has the following characteristics:

1. Horizontal right slip component = 1.2 ± 0.03 m

2. Vertical slip component (east-side-up) = 0.2 m

3. Net slip: 1.23 ± 0.04 m

4. Poorly defined slickensides and grooves on the fault plane indicate that the slip vector plunges 10° to 15° to the north (an 11°N plunge best fits the observed horizontal and vertical slip components)

5. Slip occurred within the last 5540 ± 120 radiocarbon years B.P.

Whether this slip occurred during one or more than one event cannot be conclusively resolved with the present data. However, the amount of vertical separation between correlated terrace deposits measured across the fault remains constant to the bottom of the trench and indicates that the upper 4.5 m of the Oak Knoll terrace section have undergone similar amounts of displacement, which supports a single event hypothesis. The fault dislocates the base of the A horizon of the surface soil suggesting that the latest slip event might be considerably younger than 5540 ± 120 radiocarbon years B.P. The absence of clear evidence for multiple events and the down-to-the-west sense of vertical separation contrasts with the paleoseismic record observed at Airport Creek and indicates that although a late Holocene displacement occurred, this strand is a different subparallel fault to the one described earlier at Airport Creek (**Stop 1-5**).

The trenches excavated at Oak Knoll Creek apparently did not cross the major Holocene strands of the San Simeon fault zone. The trenches may have been unfavorably located within an en echelon step in the fault trace and thus missed the active portion of the fault. Recently active strands may also occur beneath the isolated knob that lies in the gap between trenches T-3 and T-4.

Return to the cars and retrace the route to our campsite at Montaña de Oro State Park.

END OF DAY 1

FIELD TRIP GUIDE: DAY 2
Saturday, 22 September 1990

Compiled by: W. Lettis, J. Wesling, and M. Angell

Assembly Point: Drive to parking area at Spooner's Cove - Montaña de Oro State Park. Please minimize number of vehicles by car pooling. From this location, we will walk to our first field stop on a marine terrace north of Islay Creek.

Assembly Time: 7:45 am

Departure Time: 8:00 am

Route: Montaña de Oro State Park to Avila Beach, via the Los Osos Valley and See Creek Canyon (Fig. 18).

QUATERNARY DEFORMATION OF THE SAN LUIS RANGE (PART I)

INTRODUCTION

On Saturday we will examine the geomorphic, stratigraphic and tectonic history of the Irish Hills (Fig. 18) that form the northwestern part of the northwest-trending San Luis Range in San Luis Obispo County. Our campground, Montaña de Oro State Park, is situated on the northwestern coastal margin of the hills. As part of the San Luis Range, the Irish Hills are one of a series of northwest-trending ranges in the onshore Santa Maria basin of south-central California (Fig. 2). As described earlier in this guidebook, the

onshore Santa Maria basin is undergoing north-northeast-directed crustal shortening with uplift of the ranges and subsidence or low rates of uplift of the intervening valleys. The San Luis Range is bounded by the Los Osos fault zone on the northeast and a series of small reverse faults, the Olson, San Luis Bay, Wilmar Avenue, Pecho, and Oceano faults, on the southwest (Fig. 19). Within the Irish Hills, a thick sequence of Miocene and Pliocene volcanic and marine deposits overlies Franciscan basement and is deformed into the Pismo Syncline (Hall and others, 1979), a large, northwest-trending synclinorium.

Two alternative explanations or models have been proposed to describe the style, pattern and rate of crustal shortening in the onshore Santa Maria basin. Namson and Davis (1990) propose that the region is underlain by one or more blind thrust faults with uplift of the ranges produced by fault-propagation or fault-bend folding. Lettis and others (1989, this volume [a]) propose that crustal shortening is accommodated, at least in part, by rigid block uplift along bordering range-front reverse faults with little or no folding within the ranges. These two models have important implications for identifying and characterizing active faults for seismic hazard evaluation. Today and tommorrow morning, we will explore these alternative models by evaluating the style and rate of deformation of the Irish Hills. Tomorrow afternoon, we will continue this discussion by visiting the Casmalia Range - a similar northwest-trending structural range south of the San Luis Range within the onshore Santa Maria basin.

A variety of stratigraphic units and geomorphic surfaces are present in the Irish Hills region from which to evaluate the style and rate of late Tertiary and Quaternary deformation within and bordering the hills. We have conducted extensive field mapping, drilling and trenching investigations of these deposits and surfaces to assess the presence of active folding and to identify and characterize active faulting. Today we will visit five localities within and along the northeastern margin of the Irish Hills (Fig. 18):

- **Field Stop 2-1**: We will inspect marine terraces preserved along the coastal perimeter of the Irish Hills and across the axial trace of the Pismo Syncline.

- **Field Stop 2-2**: We will discuss the Los Osos fault zone at an overview of Morro Bay.

- **Field Stop 2-3**: We will review the paleoseismic history of the Los Osos fault zone based on detailed mapping and trenching investigations.

- **Field Stop 2-4**: In the synclinal core of the Irish Hills we will discuss alternative tectonic models for development of the Pismo syncline, uplift of the Irish Hills, and implications for seismic hazard evaluation.

- **Field Stop 2-5**: We will discuss implications of the marine terrace sequence along the southwestern flank of the Irish Hills for evaluating deformation within and along the southwestern margin of the hills.

Assemble at Spooner's Cove parking lot. We will walk to

Stop 2-1 on the lowest emergent terrace.

Field Stop 2-1 - Montaña de Oro, Spooner's Cove Overview (Fig. 18)

Remnants of at least 12 marine terraces are present along the coastal perimeter of the Irish Hills from Morro Bay to San Luis Obispo Bay (Fig. 20) (Hanson and others, this volume, Plate 2). **Stop 2-1** is located on the lowest marine terrace above Spooner's Cove, within walking distance of our campsite. At Spooner's Cove, these terraces have shoreline angle elevations ranging from 12 ± 2 m to 235 ± 3 m (Figs. 20 and 21). The lower three terraces are well-preserved, laterally continuous surfaces that are correlated to oxygen isotope stages 5a (80 ka), 5e (120 ka), and 7 (210 ka) on the basis of uranium-series ages of coral and vertebrate bone samples, amino-acid racemization analyses on molluscs, cool versus warm water invertebrate faunal assemblages, and correlation to paleo-sea-level high stands. The higher, older terraces are correlated to oxygen isotope stages 9 (330 ka) and older, indicating that the terrace record extends well beyond 500 ka (Hanson and others, this volume). At this location, at least five terraces are visible. We are standing on the lowest emergent terrace, which is approximately 80 ka.

To the north, this terrace sequence extends beneath a complex sequence of late Pleistocene and Holocene eolian deposits (Orme, 1990). This complex is exposed along 14 km of ocean front from Islay Creek northward to beyond Morro Rock, and extends up to 8 km inland. The sequence is particularly well exposed in 30- to 50-m-high bluffs for 2 km northward from Islay Creek to Hazard Canyon, where a succession of beach, colluvial, alluvial, and eolian deposits overlie the Q1 raised shore platform. North from Hazard Canyon, the Q1 platform and non-eolian deposits are not present perhaps because of downwarping and faulting associated with the Los Osos fault zone, or because they either never accumulated or were flushed out by west-flowing terrestrial drainages. However, the eolian sequence continues northward onto and beneath the 6.5 km-long, 300 to 650 m-wide Morro Bay sand barrier (Fig. 22). The following eolian sequence, which overlies the Q1 marine deposits and platform, may be observed looking northward from the large midden (SLO 1) immediately north of Islay Creek:

Active Dunes: unvegetated tongues of sand, 6 to 8 m thick, formed or reactivated over the past 200 years by a combination of vegetation destruction (fire, grazing, military activity, off-road vehicles), engineering modifications to the Morro Bay entrance channel, and possible relative sea-level rise.

Younger Parabolic and Lobate Dunes: variably vegetated, these dunes form 10-m-high bluffs south of the Morro barrier. They postdate an extensive fire around 1730 ± 90 yr BP that may have been caused by lightning or pre-Chumash hunting peoples.

Older Parabolic Dunes: capped by a pronounced charcoal horizon dated at 1730 ± 90 yr BP, these dunes overlie a strong paleosol on which midden materials and artifacts occur that have yielded ^{14}C ages between 3080 ± 90 yr BP 1 km north of Islay Creek and 4160 ± 70 yr BP beneath SLO 1. Only the noses of

the parabolas now survive but it is likely that these dunes accumulated from reworked transverse or barchanoid dunes on a coastal ramp following the main Flandrian transgression.

Paleodunes: a 15- to 45-m-thick sequence of variably indurated dunes, reddish yellow to strong brown in color, rises from below present sea level beneath the Morro barrier to feather out around 300 m against the Irish Hills. Although they include weak paleosols and are capped by a strong paleosol older than 4160 ± 70 yr BP, the age of these dunes is uncertain. However, by analogy with a dated sequence of paleodunes near Point Sal, it is likely that the Morro Bay paleodunes were emplaced between 30 ka and 20 ka BP, on a falling sea level during the transition from marine oxygen isotope stage 3 to 2 (Orme, this volume).

The above sequence reveals a hiatus between the suggested age of the shore platform and associated deposits of around 80 ka (Hanson and others, this volume), and the inferred age of the paleodunes between 20 and 30 ka (Orme, this volume). This gap could be attributed to erosion. Alternatively, the gap could be narrowed if: (1) the lower part of the paleodunes and the underlying alluvial/colluvial deposits are older than 30 ka, or (2) the marine deposits are less than 80 ka. These alternatives are discussed by Orme (this volume).

The flight of marine terraces, which occupies the western and southwestern margins of the Irish Hills, provides an excellent late Quaternary strain gauge from which to evaluate the locations, patterns, and rates of folding and faulting within the Irish Hills. Presence of the elevated flight of marine terraces indicates continued Quaternary uplift of the hills. Based on the terrace ages, elevations of shoreline angles, and elevation of sea level at the time of terrace formation, the northern Irish Hills have been elevated at the rate of 0.24 ± 0.02 m/ka (Hanson and others, this volume).

A longitudinal profile showing terrace shoreline angle elevations and terrace correlations for this part of the coast is presented on Figure 21. This stretch of coastline crosses the axial trace of the Pismo syncline, related folds, and the projected traces of the Edna and San Miguelito faults within the hills. At **Stop 2-1**, we are approximately on the axial trace of the Pismo syncline (Fig. 19). Our model of terrace correlation (Fig. 21) indicates that the marine terraces have not been folded, tilted, or faulted; they record uniform uplift of the hills along this part of the coast. To the north, the marine terrace sequence is abruptly truncated by the projected trace of the Los Osos fault zone. As we will see at **Stop 2-2**, there is no evidence that suggests the terrace sequence is warped down adjacent to the Los Osos fault zone.

Although the Quaternary marine terraces are not deformed by the Pismo syncline and the San Miguelito and Edna faults, Tertiary strata as young as middle to late Pliocene in age are folded. These relations suggest that a change in style of deformation occurred within the hills about 1 to 3.5 Ma. Synclinal folding with continued subsidence and marine deposition occurred until at least 3.5 Ma and perhaps 2 Ma as indicated by syndepositional folding of the middle to late

Pliocene Squire Member of the Pismo Formation. The marine terrace record, however, indicates a structural inversion such that the former synclinal depocenter now occupies the core of an uplifting range.

The argument for a change in style of deformation is predicated on the assumption that the marine terraces accurately reflect and record the style of late Quaternary deformation. We argue that this assumption is valid and that the shoreline angles of these terraces can be mapped with sufficient accuracy to resolve the rate, pattern, and style of deformation. As we will discuss at **Stop 2-4**, arguments have been put forward that folding within the Irish Hills is continuing today and that the marine terraces either do not record the folding or that folding is concentrated in narrow zones along the margins of the range and cannot be recognized in the terrace record.

GENERAL DIRECTIONS TO **STOP 2-2**

> *Return to our vehicles at Spooner's Cove assembly point, Montaña de Oro campground. Drive north 3.2 miles on Pecho Valley Road (leaving Montaña de Oro State Park) to Rodman Drive. Turn right (east) into Cabrillo Estates and stay on Rodman Drive for 0.8 miles to Alamo Drive. Turn right on Alamo Drive, proceed 0.2 miles to the end of road, and park (Fig. 18).*

ROAD LOG TO **STOP 2-2**

Odometer Cum.	Odometer Int.	
0.0	0.0	As we drive north from Spooner's Cove toward Morro Bay, note the dune sand deposits of several different ages on our left and the flight of eolian veneered marine terraces on our right. The stand of eucalyptus trees was planted, in part, to stabilize the dune field.
3.2	3.2	*Turn right (east) onto Rodman Drive.*
3.8	0.6	Note the exposure of diatomaceous siltstone of the Miguelito Member of the Pismo Formation in the roadcut on the right (south). This bedrock is the last exposure of bedrock on the northern flank of the Irish Hills in this area; the top of bedrock drops off to over 150 m below sea level in the Morro Bay basin to the north.
4.0	0.2	*Turn right (south) onto Alamo Drive. Drive 0.2 miles to end of road and park. We will walk to an overview of the Morro Bay region.*

Field Stop 2-2 - Los Osos Fault Zone, Overview

Stop 2-2 provides an overview of the Los Osos fault zone, which separates the elevated Irish Hills to the south from the subsiding Morro Bay to the north (Fig. 23). The fault zone in this area is buried beneath the Morro Bay dune complex, and its presence at this location is based largely on indirect geomorphic and stratigraphic evidence. The marine terrace sequence, which

is continuous between here and **Stop 1-1**, terminates abruptly across the projection of the Los Osos fault zone. The longitudinal profiule of marine terrace shoreline angles (Fig. 21) shows that the terraces are not tilted, folded or warped down to the northeast as they approach the Los Osos fault zone. The abrupt truncation of the terraces suggests that the range front is not the steep limb of an anticline. The foundation excavation for the home at 2787 Rodman Drive near this field stop exposed marine terrace deposits at an elevation 125 m.

There are no marine terraces in the Morro Bay area. Subsurface data from wells drilled by the California Department of Water Resources and the U.S. Geological Survey, and geophysical data in the adjacent offshore region, indicate that a deep, but locally restricted, subsiding basin is present in the southern Morro Bay area directly northeast of the Los Osos fault zone (Figs. 23 and 24). The basin is informally referred to as the Morro Bay basin. Onshore, the basin is approximately 6 km long and 3 to 4 km wide at the coast. Gravity data suggest that the basin extends offshore an additional 2 to 3 km to the northwest. Basement in the center of the basin is at a depth of more than 189 m below sea level. In general, bedrock around the perimeter of the basin consists of Franciscan Complex rocks, whereas Pliocene and Quaternary deposits occupy the center of the basin. The presence of Pliocene rocks in the basin indicates that subsidence was occurring during the late Tertiary and may have begun even earlier. Continued subsidence during Quaternary time is indicated by the presence of Quaternary sediments at depths exceeding 160 m below sea level. These depths exceed maximum levels of sea level lowering during Pleistocene low stands and, therefore, cannot be attributed to fluvial incision. The nature, rate and possible causes of subsidence of the Morro Bay basin are discussed by Lettis and Hall (this volume).

Truncation of the marine terrace sequence by the Los Osos fault zone and subsidence of the Morro Bay basin provide indirect constraints on the rate of slip for the Los Osos fault zone (Fig. 24). Based on the elevations of marine terraces, the Irish Hills are uplifting at a rate of 0.24 $\pm$ 0.02 m/ka. Based on the depth to bedrock in Morro Bay, the Morro Bay basin is subsiding at some rate of less than 0 and probably less than -0.2 m/ka (Lettis and Hall, this volume). Furthermore, borehole data indicate that subsidence is generally restricted to the Morro Bay region and does not extend southeast into the Los Osos Valley. Thus, the total rate of vertical separation across the Los Osos fault zone is about 0.24 m/ka and locally as high as 0.44 m/ka. Assuming that the fault dips 30° to 60° southwest, the net slip rate for the Los Osos fault zone is 0.2 to 0.8 mm/yr.

GENERAL DIRECTIONS TO **STOP 2-3**

Return to Pecho Valley Road via Rodman Drive, turn right (north). Pecho Valley Road will make a sharp right bend after 0.5 miles and will become Los Osos Valley Road. Drive through the town of Los Osos and proceed 9.0 miles from the intersection with Rodman Drive to Valle Vista Road. Turn right on Valle Vista Road and park. We will walk to ***Stop 2-3*** *(Fig. 18).*

ROAD LOG TO **STOP 2-3**

Odometer (reset odometer)

Cum.	Int.	
0.0	0.0	*Return to vehicles and retrace route along Alamo Drive.*
0.2	0.2	*Turn left (west) onto Rodman Drive.*
1.0	0.8	*Turn right (north) onto Pecho Valley Road.*
1.5	0.5	*Pecho Valley Road makes sharp right turn and becomes Los Osos Valley Road.*
4.2	2.7	Note the exposure of Pleistocene dune sand in the roadcut on the north side of Los Osos Valley Road. The dune sand forms an extensive sand ramp along the southern margin of the Morro Bay area. The older dune sand has been extensively dissected and forms progressively less continuous remnants to the east within Los Osos Valley. As we drive east on Los Osos Valley Road, the Los Osos fault zone is at the base of the Irish Hills on the right (south). Los Osos Valley Road extends down the heart of the Los Osos Valley. After leaving the locally subsiding Morro Bay basin near the coast, most of the Los Osos Valley is floored by thin alluvial deposits (typically less than 100 feet) underlain by bedrock of the Franciscan Complex. Shallow bedrock implies either no subsidence or a low rate of uplift of the valley relative to the Irish Hills.
7.0	2.8	Note the well preserved scarps, spring lines and deflected drainages along the Los Osos fault zone for the next 3.0 miles to **Stop 2-3**.
10.0	3.0	*Turn right onto Valle Vista Road and park. We will walk from here to Stop 2-3.*

Field Stop 2-3 - Los Osos Fault Zone, Cuesta Property

Detailed mapping and paleoseismic investigations were conducted at several localities along the Los Osos fault zone. These include the Ellsworth, Ingley, Cuesta, Brughelli, and Guidetti sites (Fig. 25) (Lettis and Hall, this volume). **Stop 2-3** is at the Cuesta site on the outskirts of the town of San Luis Obispo. At this stop, we will discuss the results of our paleoseismic investigations on the Cuesta property as well as on the nearby Ellsworth and Ingley properties (Fig. 26). These three sites are located along the geomorphically well-expressed central reach of the Irish Hills segment of the Los Osos fault zone. Discontinuous scarps, closed depressions, spring lines, tonal lineaments, and deflected drainages define a fault zone from ½ to 1 km wide (Lettis and Hall, this volume, Plate 1). Based on the prominent geomorphic expression of the fault zone, results of our paleoseismic studies, and independent mapping conducted by the California Division of Mines and Geology (CDMG), this reach of the fault zone has been zoned an Alquist-Priolo special studies zone by CDMG (Treiman, 1988).

A series of discontinuous lobate scarps, spring lines and stream knickpoints preserved within Quaternary deposits at the Cuesta site (Fig. 27) suggest that the fault has had Quaternary displacement. We excavated three trenches at the Cuesta site. These trenches revealed a series of high- and low- angle reverse faults that displace upper Pleistocene and Holocene deposits (Fig. 28). Structural and stratigraphic relations indicate that this faulting is probably secondary deformation in the hanging wall of a southwest-dipping reverse fault that either does not reach the surface at this locality or reaches the surface northeast of Los Osos Valley Road. The primary reverse fault was exposed in Trench 2 at the Ingley site (Fig. 29). Stratigraphic and structural relationships in this trench indicate late Holocene activity on at least three southwest-dipping fault planes. Based on the amount of displacement and estimated age of the displaced strata in this trench, we estimate a slip rate of 0.07 to 0.33 mm/yr. From these relationships, we conclude that the Los Osos fault zone is an active seismogenic reverse or thrust fault. The fault dips southwest beneath the Irish Hills and is responsible, in part, for uplift of the hills. The down-dip geometry of the fault is uncertain. Based on observed stratigraphic and structural relationships exposed at the Cuesta and Ingley sites, we interpret that the fault may dip 30° to 60° to the southwest (Fig. 30).

GENERAL DIRECTIONS TO **STOP 2-4**

Return to Los Osos Valley Road, turn right (east). Drive 0.9 miles to Perfumo Canyon Road. Turn right (southwest) onto Perfumo Canyon Road and proceed 6.1 miles to ridge crest of Irish Hills, ***Stop 2-4.***

ROAD LOG TO **STOP 2-4**

Odometer Cum.	Int.	
0.0	0.0	*Return to Los Osos Valley Road and reset odometer. Turn right (east) toward San Luis Obispo.*
0.3	0.3	Note the encroaching suburban development of San Luis Obispo. Due to extensive grading, it is not clear where the Los Osos fault zone is located in this area. Predevelopment aerial photography shows several tonal lineaments and break-in-slopes in the area, suggesting that the Los Osos fault zone extends through the town at or near the southern margin of the valley.
0.9	0.6	*Turn right (southwest) onto Perfumo Canyon Road.* Before the turn, note that Laguna Lake is visible in the distance between the houses on our left (north). The lake is an internally drained natural basin possibly formed, in part, by tectonic impoundment along one or more traces of the Los Osos fault zone. In addition, overbank levee deposits along San Luis Obispo Creek and alluvial fan deposits from the Irish Hills have contributed to impoundment of the lake.

1.9 1.0 Note the large outcrops of serpentinite, metavolcanics, and greywacke sandstone along Perfumo Canyon. We are driving through an area underlain by Franciscan Complex along the northeastern limb of the Pismo syncline.

7.0 5.1 Ridge crest of Irish Hills. **Stop 2-4.**

Field Stop 2-4 - Pismo Syncline, Central Irish Hills

This stop is located within the Franciscan Complex along the NE limb of the Pismo syncline. The syncline is a large, northwest-trending synclinorium within the San Luis Range that deforms the Miocene Obispo and Monterey formations and the Miocene to Pliocene Pismo Formation (Fig. 31). To the northeast and southwest, the syncline is flanked by subparallel anticlines cored, in part, by basement rocks of the Franciscan Complex and an unnamed Cretaceous sandstone and shale sequence comparable to the Great Valley sequence. Rocks of the Franciscan Complex in roadcuts along Perfumo Canyon between here and the Los Osos Valley form the core of one of these anticlines.

At **Stop 2-4**, we can observe in the distance to the northeast, the "Seven Sisters" of the Morro Rick-Islay Peak dacite complex. These dacite plugs are 33 ma and represent the core of a linear volcanic chain. The linear trend of the dacite plugs are probably structurally controlled. Hall (1981) interprets the plugs to lie along the San Luis Obispo transform fault - the original transform between the North American and Pacific plates in the late Oligocene. The Pismo syncline lies to the southwest of us and as we drive to our next stop you will observe beds of the Monterey and Pismo formations deformed by the syncline. The involvement of Pismo Formation in the continued development of the syncline and possibly bordering anticlines indicates that crustal shortening via folding occurred through much of the Pliocene. Folding is not limited to the well bedded Tertiary strata but also incorporates the underlying heterogeneous Franciscan Complex as well. Crustal shortening via folding implies the presence of a detachment fault at depth beneath the fold. Geometric modeling techniques (Suppe, 1983) indicate that the location, geometry, and dimensions of a fold are governed by the location and dimensions of ramps in the underlying detachment fault. Namson and Davis (1990) and PG&E (1990) constructed retrodeformable balanced cross sections to evaluate the presence, location, and activity of potential blind thrust faults beneath the Irish Hills (Figs. 31 and 32; Lettis and others, this volume [b]). Inherent to these modeling techniques are the assumptions that Franciscan basement behaves as a brittle, bedded medium and that deformation proceeds by plane-strain (e.g., no out-of-the-plane loss of mass via faulting, ductile flow, tilting, etc.).

These retrodeformable cross sections suggest that the Irish Hills are underlain by one or more blind thrust faults. Movement on these thrust faults produced anticlinal deformation within the Irish Hills. The Pismo syncline developed as a result of growth of two adjacent anticlines. The model by Namson and Davis (1990) predicts an uplift rate for the Irish Hills of up to 17 m/ka and a pattern of uplift that would produce continued anticlinal folding within the hills (Fig. 33). This rate and

pattern is incongruent with the uniform uplift rate of about 0.2 m/ka determined from the marine terrace data. The retrodeformable models developed by PG&E (1990) (Figs. 34 and 35) are consistent within an uplift rate of about 0.2 m/ka and apparent uniform uplift across the crest of the Irish Hills (Fig. 36). In these models folding is concentrated in narrow zones along the northeastern and southwestern flanks of the range.

Among the assumptions made to construct these sections are that strike-slip deformation in this region is negligible, and that the primary structure of the Pismo syncline is the result of slip on faults within Franciscan Complex basement. These assumptions are required by the tehcniques used to predict fault geometries at depth, however, local and regional geologic evidence indicates they may not be completely valid. Lateral slip and decoupling of deformation at shallow depths within the Franciscan Complex basement is not addressed by these methods, and therefore may have a negative effect on the applicability of these models.

An important issue for seismic hazard evaluation is whether blind thrust faults that underlie the Irish Hills are active today. Based on the marine terrace sequence that is not deformed across the axial trace of these folds, we interpret that thrust faulting and folding of the Irish Hills is no longer an active process. This style of deformation ceased in the late Pliocene or early Quaternary and has been replaced by rigid block uplift along bordering reverse faults such as the Los Osos fault zone.

Alternative cross sections that portray the Los Osos fault zone as a major seismogenic structural feature extending through the entire crust or joining with the Hosgri fault zone at depth as a flower structure are difficult to restore and present significant kinematic problems. Although such models may be appropriate to approximate local tectonic conditions, they provide no information on the distribution of slip and fault geometries at depth.

If thrust faulting and folding is an ongoing active process, several interesting and perplexing problems must be resolved. Why are the marine terraces uplifted uniformly across the axial traces of the folds? How can the Los Osos fault zone, a major seismogenic feature, extend through the underlying thrust fault to reach crustal depths at which large magnitude earthquakes occur (7 to 12 km)?

GENERAL DIRECTIONS TO **STOP 2-5**

> *Return to our vehicles and continue 0.2 mile on Perfumo Canyon Road to the summit, where the road becomes See Canyon Road. Drive down See Canyon Road for 7.1 miles to San Luis Bay Drive. Turn right (west) onto San Luis Bay Drive and proceed about 1.2 miles to Avila Beach Drive. Turn right (west) onto Avila Beach Drive and proceed 0.7 miles to Cave Landing Road. Turn left (south) onto Cave Landing Road and proceed 0.6 miles to the dirt parking lot above Mallagh Landing.*

ROAD LOG TO **STOP 2-5**

Odometer	
Cum.	Int.

0.0	0.0	*Return to vehicles and reset odometer. Continue on Perfumo Canyon Road.*
0.2	0.2	Road enters Tertiary bedrock as mapped by Hall and others (1979).
7.3	7.1	*Turn right (west) onto San Luis Bay Drive.*
8.5	1.2	*Turn right (west) onto Avila Beach Drive.*
8.9	0.4	Note northeast-dipping beds of the Monterey Formation on the southwest limb of the Pismo syncline.
9.2	0.3	*Turn left (south) onto Cave Landing Road.* The road crosses the headwall of a large landslide complex. The San Miguelito fault trends northwest through this landslide complex.
9.8	0.6	*Proceed over the hill and park in the dirt parking lot on Mallagh Point. We will walk down the dirt road to* ***Stop 2-5*** *on the stage 5e marine terrace overlooking Pirates Cove.*

Field Stop 2-5 - Mallagh Landing, San Miguelito Fault

Mallagh Landing is an old sea port in San Luis Obispo Bay rumored to have been used by pirates prior to settlement of the harbor area. Large iron rings for securing ships and stone steps are carved in the cliff at Mallagh Point. The small cove east of Mallagh Point is knwon locally as Pirate's Cove, and is a popular sunbathing spot. Mallagh Landing lies along the southwestern margin of the San Luis Range, along which is preserved a sequence of mappable emergent marine terraces. This sequence has been delineated along the coast line from the Montaña de Oro area (**Stop 2-1**), around Point Buchon and Point San Luis, and along the southwestern margin of the San Luis Range to the Nipomo Mesa (Fig. 19). As shown by Hanson and others (this volume) and Lettis and others (this volume [b]), the marine terrace sequence provides an excellent strain gauge from which to measure Quaternary deformation of the San Luis Range. Figure 37 shows elevation of terrace shoreline angles along the coast between Avila Beach and Arroyo Grande.

At Mallagh Landing, there is particularly good preservation of this marine terrace sequence, although many of the wave-cut platforms are buried, stripped, and/or very discontinuous. The terrace sequence includes discontinuous remnants of the 80 or 100 ka platform on the western side of Mallagh Point, a continuous remnant of the 120 ka wave-cut platform in Pirate's Cove and around Mallagh Point, and several remnants of higher terraces identified via borehole and geophysical data. The oil tanks northwest of Mallagh Point are situated on Q4 marine terrace (greater than 330 ka). Elevations and ages of the lower terraces indicate a late Pleistocene uplift rate of 0.12 $\pm$ .02 m/ka, which is substantially lower than the uplift rate of 0.20 $\pm$ 0.02 m/ka determined in the Montaña de Oro area (Hanson and others, this volume). The lower uplift rate here at Mallagh Landing reflects deformation along the southwestern margin of the San Luis Range.

Based on the elevations and distributions of marine terraces between Point Buchon and Santa Maria River, we have identified three west-northwest-trending faults that exhibit late Pleistocene displacement of the emergent marine terrace sequence (Lettis and others, this volume [b]). These faults, the Wilmar Avenue, San Luis Bay, and Olson faults, will be discussed tomorrow morning at **Stop 3-1**. The marine terrace sequence also crosses two faults, the San Miguelito and Pismo faults, previously identified by Hall and others (1979) and Hall (1973). Neither of these faults displaces Quaternary marine terraces identified along the margin of the San Luis Ranges (Lettis and others, this volume [b]).

The marine terrace sequence preserved at Mallagh Landing provides data on the late Quaternary history of the San Miguelito fault. This sequence crosses the San Miguelito fault in the topographic saddle east of the parking lot. This fault displaces the Tertiary Pismo Formation and is considered to be an important structural element within the Irish Hills by Hall and others (1979). Trench excavations and detailed mapping conducted by PG&E (1988) revealed a complex kinematic history within the fault zone. Stratigraphic evidence suggests the fault originated as a northeast-dipping, basin-bounding normal fault at the southwest margin of the Pismo basin. Trench investigations and stratigraphic displacements across this fault indicate that a significant amount of strike-slip deformation post-dates the normal deformation. In addition, map-scale stratigraphic relationships and near-vertical slickensides observed in trench exposures across the central portion indicate post-Miocene to late Pliocene reverse separation. However, both the 120 ka and 80 ka shoreline angles show no displacement across the San Miguelito fault, indicating that it has not been active in the late Pleistocene (Fig. 37). Elevations of older, higher shoreline angles on boths sides of the fault suggest no post-500 ka displacement along the fault (Hanson and others, this volume; Lettis and others, this volume [b]).

From this location, you are free to stay and enjoy the sunset, visit the wonderful town of Avila Beach, or head back to Montaña de Oro State Park campground. Tomorrow we will address the southwestern structural boundary of the San Luis Range (Irish Hills) and compare the tectonic history of this range with the style and rate of deformation in the Casmalia Range, which, on a clear day, is visible to the south across San Luis Obispo Bay.

END OF DAY 2

FIELD TRIP GUIDE: DAY 3

Sunday, 23 September 1990

Compiled by:	K. Kelson, W. Lettis, J. Wesling, D. Clark
Assembly Point:	Parking area at Montana de Oro State Park. From this location, we will drive to our first stop on the beach in the city of Pismo Beach.
Assembly Time:	7:45 am
Departure Time:	8:00 am
Route:	Montana de Oro State Park to Casmalia Hills, via Pismo Beach and the Santa Maria Valley (Figs. 38a and 38b).

QUATERNARY DEFORMATION OF THE SAN LUIS RANGE (PART II), THE SANTA MARIA VALLEY, AND THE CASMALIA RANGE

INTRODUCTION

On Sunday morning we will continue our discussion of the Quaternary deformation of the San Luis Range, focusing on its southwestern margin. This margin is bordered by a broad zone of discontinuous reverse faults, including the Wilmar Avenue, San Luis Bay, Olson, Oceano, and Pecho faults (Lettis and others, this volume [b]). Because most of these faults either are buried by extensive eolian and alluvial deposits, lie offshore, or are difficult to access with a large group, we will concentrate on discussing the geometry and late Quaternary history of the Wilmar Avenue, San Luis Bay, and Olson faults. We will also continue our discussion of models proposed to describe the style, pattern, and rate of crustal shortening in the region.

During the latter half of the day we will address the Quaternary deformation of the Casmalia Range, a west-northwest-trending structural block that lies south of the San Luis Range. Several Quaternary stratigraphic units and geomorphic surfaces on the margins of the Casmalia Range allow assessments of the style and rate of range uplift, the presence or absence of active folding, and the style and recency of deformation on the bordering Orcutt Frontal (Casmalia) and Lions Head faults. Therefore, studies of this range provide another data set to compare models of crustal shortening within the Los Osos/Santa Maria domain. Detailed investigations of Quaternary deposits and landforms within and adjacent to the range are summarized by Clark (this volume).

As shown on Figures 38a and 38b, today we will visit four localities (the fourth is optional):

- **Field Stop 3-1:** We will visit the sea-cliff exposure of the Wilmar Avenue fault in the city of Pismo Beach, and discuss its implications for deformation along the southwestern margin of the San Luis Range. At this stop, we will also review the results of detailed studies to assess the late Quaternary behavior of the San Luis Bay and Olson faults.

- **Field Stop 3-2:** We will visit an overview of the southwestern boundary of the San Luis Range near the town of Nipomo, and discuss models of regional crustal shortening.

- **Field Stop 3-3:** We will view deformed upper Pliocene to upper Pleistocene deposits along the northeastern margin of the Casmalia

Range, and discuss their implications for uplift and deformation of the range block.

- **Field Stop 3-4 (optional):** We will visit an overview in the central part of the Casmalia Range of the well-preserved flight of marine terraces near Point Sal. We will discuss evidence of deformation within the range and along its southwestern margin.

Please note that parking will be limited at Field Stop 3-4. We ask that participants carpool as much as possible. We will make a brief stop at the base of the range to allow people to park their cars and ride with others.

GENERAL DIRECTIONS TO **STOP 3-1**

From the Spooner's Cove parking area at Montaña de Oro State Park, drive north 3.7 miles along Pecho Valley Road. At the sharp right bend, Pecho Valley Road becomes Los Osos Valley Road. Continue along Los Osos Valley Road for 11.0 miles to Highway 101. Turn right (south) onto Highway 101 and proceed 8.7 miles to the Pismo Beach exit. After exiting Highway 101, turn right onto Price Street, and then immediately turn left onto the access road to the Kon Tiki Inn. Park in the Bank of America parking lot and walk down to the beach via the stairs behind the Kon Tiki Inn. Once on the beach, turn right (northwest) and walk about 150 m to Stop 3-1.

ROAD LOG TO **STOP 3-1** (Fig. 38a)

Odometer Cum.	Odometer Int.	
0.0	0.0	*From Spooner's Cove parkign area at Montaña de Oro State Park, drive north along Pecho Valley Road.*
3.7	3.7	*Pecho Valley Road makes a sharp right bend and becomes Los Osos Valley Road. Continue to the east along Los Osos Valley Road.*
12.2	8.5	*Intersection with Valle Vista Road; location of yesterday's Stop 2-3.*
12.5	0.3	Note the encroaching suburban development of San Luis Obispo. Due to extensive grading, it is not clear where the Los Osos fault zone is located in this area. Predevelopment aerial photography shows several tonal lineaments and break-in-slopes in the area, suggesting that the Los Osos fault zone extends through the town at or near the southern margin of the valley.
13.3	0.8	Laguna Lake is visible in the distance between the houses on our left (north). The lake is an internally drained natural basin possibly formed, in part, by tectonic impoundment along one or more traces of the Los Osos fault zone. In addition, overbank levee deposits along San Luis Obispo Creek and

alluvial fan deposits from the Irish Hills have contributed to impoundment of the lake.

14.4 1.1 Several high, flat surfaces along the Irish Hills range front to the south are preserved remnants of fluvial terraces formed along San Luis Obispo Creek that formed as the creek incised through the rising Irish Hills. San Luis Obispo Creek flows south through the hills generally subparallel to Highway 101 to San Luis Obispo Bay near Avila Beach. To the north, these fluvial terraces must have been graded to the floor of Los Osos Valley, but they now project well above the floor of the valley. We interpret these fluvial terraces to be uplifted and truncated by the Los Osos fault zone.

14.7 0.3 *Intersection with Highway 101. Turn right (south) and proceed south on Highway 101.*

15.2 0.5 Highway 101 crosses the Los Osos fault zone near the base of the escarpment. High fluvial terrace remnants are preseved along San Luis Obispo Creek on both sides of Highway 101.

15.9 0.7 Note the exposures of serpentinite, graywacke, and mélange of the Franciscan Complex on both sides of Highway 101.

18.0 2.1 Southwest-dipping Tertiary strata on the east side of San Luis Obispo Creek Valley form the northeastern limb of the Pismo syncline.

18.4 3.7 *San Luis Bay Drive/Avila Beach exit. Continue south on Highway 101.*

19.8 0.4 Strata of the Tertiary Pismo Formation are exposed in the roadcut and dip northeast into the axis of the Pismo suncline. Over the next 3 to 4 miles, Highway 101 lies on terrace deposits overlying the substage 5e 120 ka wave-cut platform. Several fossil localities along this stretch of the coastline have been dated via uranium/thorium, amino acid racemization, and faunal assemblage methods (Hanson and others, this volume). Discontinuous remnants of the substage 5a 80 ka marine terrace occur in the sea cliff in the Shell Beach vicinity. To the left (east), discontinuous remnants of the 200 ka wave-cut platform are preserved. This terrace sequence provides a long-term uplift rate for the San Luis Range, in the Avila Beach to Pismo Beach area, of about 0.13 m/ka (Hanson and others, this volume).

23.3 3.5 The large paleo-sea stack between northbound and southbound lanes of Highway 101 is composed of resistant, silicified tuff of the Miocene Obispo Formation. This stack

is one of several that form an east-west-trending alignment extending into the near-offshore region, to the northwest.

23.4 0.1 *Exit Highway 101 at the Pismo Beach exit. Turn right (south) onto Price Street, and then immediately turn left onto the access road to the Kon Tiki Inn.*

23.6 0.2 *Park in the Bank of America parking lot on the left. We will walk down to the beach through the Kon Tiki Inn. Stop 3-1 is located on the beach at the sea cliff about 150 m northwest of the stairs from the Kon Tiki Inn.*

Field Stop 3-1: Wilmar Avenue Sea-cliff Exposure, Pismo Beach

The town of Pismo Beach lies on deposits overlying the 120 ka marine platform, which is exposed in the sea cliff here at **Stop 3-1**. This terrace is present along most of the coastline along the southwestern margin of the San Luis Range between here and Montaña de Oro (**Stop 2-1**). As shown by Hanson and others (this volume) and Lettis and others (this volume [b]), the marine terrace seqeunce provides an excellent strain gauge to measure Quaternary deformation of the San Luis Range. Figure 37 shows the elevations of terrace shoreline angles along the coast between Avila Beach and Arroyo Grande. the 120 ka platform exposed at **Stop 2-5** is continuous and not displaced from Mallagh Landing to Pismo Beach, where it lies at approximately the same elevation. The sequence of terraces along this reach of the coastline suggest an uplift rate of 0.12 ± 0.02 m/ka for this part of the San Luis Range (Hanson and others, this volume).

The southwestern margin of the San Luis Range is bordered by a complex zone of late Quaternary reverse faults that strike west-northwest and dip moderately to the northeast (Fig. 19; Lettis and others, this volume [b]). Major structures within this zone include the Wilmar Avenue, San Luis Bay, Olson, Pecho, and Oceano faults, all of which have poor geomorphic expression. Only the San Luis Bay and Wilmar Avenue faults are well exposed in outcrop. Late Quaternary slip rates for the onshore parts of the Olson, San Luis Bay, and Wilmar Avenue faults are based primarily on disruptions of late Quaternary marine terraces (Hanson and others, this volume; Lettis and others, this volume [b]).

Our field stop is at the only presently known exposure of the Wilmar Avenue fault, located along the present sea cliff near Wilmar Avenue in Pismo Beach. The fault zone exposed in the sea cliff is approximately 4 ± 2 m wide and contains shears that range in strike from N40W to east-west and dip from 45 to 70 degrees to the northeast (Fig. 39). The fault juxtaposes Oligocene to lower Miocene Rincon and Obispo Formations over the Pliocene Squire Member of the Pismo Formation. Slickensides and mullions on the southeasternmost fault plane are subparallel to fault dip. These striae and the presence of older bedrock overlying younger bedrock indicate predominantly reverse displacement.

The marine wave-cut platform exposed in the sea cliff near Wilmar Avenue is displaced by the fault with a net vertical separation of 6.4 m (Fig. 40). This platform is interpreted to be 120 ka

(Hanson and others, this volume). However, the platform on the downthrown side of the main fault may have been partially reoccupied by a later sea-level stand; if so, the cumulative net vertical separation of the 120 ka platform across the fault zone is only about 4.3 m. Assuming a range in fault dip of 45 to 70 degrees and a range in vertical separation of 4.3 to 6.4 m, these separations suggest an average late Pleistocene net slip rate of 0.04 to 0.08 mm/yr.

To the southwest of the main fault trace, a southwest-dipping subsidiary fault displaces distinct beds within the terrace deposits overlying the 120 ka marine platform (Fig. 40). These beds have progressively lower amounts of vertical separation up section, which most likely are a result of multiple syndepositional faulting events. The bedrock-parallel attitude of the subsidiary fault strand and its southwesterly dip suggest that it is probably a flexural slip fault related to formation of a footwall syncline (Fig. 40). Because the syncline appears to be related to slip on the primary fault strand, growth of the syncline probably is related to slip on the subsidiary fault. Therefore, episodic slip on the subsidiary fault probably reflects episodic slip on the primary fault strand.

Two other generally east-west-trending reverse fault are present along the onshore part of the southwestern margin of the San Luis Range. Both of these faults, the San Luis Bay and Olson faults, have been identified based on disruptions of the late Quaternary marine terrace sequence. The San Luis Bay fault has poor geomorphic expression and is observed in only one location, a roadcut and sea-cliff exposure about 0.3 km west of the town of Avila Beach (Fig. 41). In this exposure, the fault displaces the 120 ka marine terrace and younger overlying colluvial deposits. Based on elevations of the 120 ka strandline on both sides of the fault, there is 5 to 8.5 m of cumulative post-120 ka vertical separation across the fault (Hanson and others, this volume). A strand of the San Luis Bay fault exposed in the sea-cliff near Avila Beach displaces late Quaternary fluvial deposits (Lettis and others, this volume [b]). Charcoal from these deposits yielded a radiocarbon age of 21,040 ± 850 yr B.P., indicating latest Quaternary movement. The fault strand that displaces these deposits dips about 40° to the northeast; slickensides on the fault plane indicate essentially dip slip movement.

The San Luis Bay fault is interpreted to continue west from the Avila Beach exposure to the coastline near Rattlesnake Canyon (Fig. 41). In the Rattlesnake Canyon area, there is about 7.0 to 7.4 m of vertical separation of the 120 ka strandline as a result of faulting and down-to-the south warping. Based on these data and separations at the Avila Beach exposure, the estimated post-120 ka rate of vertical separation ranges from 0.04 to 0.07 mm/yr. Based on a range in fault dip from 40 to 70 degrees, these data yield a range in average slip rate of 0.4 to 0.11 mm/yr, which is comparable to that estimated for the Wilmar Avenue fault.

The Olson fault is a west-trending fault that intersects the coastline about 6.4 km northwest of Point San Luis (Fig. 41), and is interpreted to be the northeasternmost element of the zone of faults along the southwestern margin of the San Luis Range. The 120 ka marine platform has 4.1 to 6.4 m of vertical separation across the Olson fault, and the 80 ka platform has 1.5 to 4.6 m of vertical separation. These data

suggest a rate of vertical separation ranging from 0.03 to 0.05 mm/yr.

Investigations of marine terrace ages and elevations indicate that the San Luis Range has undergone late Quaternary uplift as a relatively rigid crustal block with little to no internal deformation (Hanson and others, this volume; Lettis and others, this volume [b]). Most of the uplift probably occurred along the northeastern margin of the range via displacement along the Los Osos fault zone (Lettis and Hall, this volume), and along the southwestern margin of the range via distributed displacement on the Wilmar Avenue, San Luis Bay, Olson, Oceano, and Pecho faults (Lettis and others, this volume [b]). The lack of emergent marine terraces and substantial sedimentation within the Santa Maria Valley suggest that the zone of faulting along the southwestern margin of the range represents a zone of transition between uplift and subsidence. The complex and laterally discontinous nature of this zone suggests that this margin is a complex, diffuse zone. This contrasts with the northwestern margin of the range, which is bordered by the comparatively simple, discrete Los Osos fault zone.

GENERAL DIRECTIONS TO **STOP 3-2**

*Return to vehicles via the Kon Tiki Inn stairs. Proceed southeast on Price Street for 0.7 miles through the city of Pismo Beach. Merge onto Highway 101 southbound, and proceed 8.8 miles to the Los Berros/Thompson Avenue exit. Turn left (east) onto Thompson Avenue and proceed 2.3 miles to Mehlschau Road. Turn left onto Mehlschau Road and proceed 0.2 miles to **Stop 3-2**. Park off the road (Fig. 38).*

ROAD LOG TO **STOP 3-2**

Odometer Cum.	Odometer Int.	
0.0	0.0	*Return to vehicles via stairs at Kon Tiki Inn. Return to Price Street via parking lot access road. Reset odometer. At Price Street, turn right (southeast) and drive through the city of Pismo Beach.*
0.7	0.7	*Merge onto Highway 101 (south).* In this area, the highway follows the trend of both the late Pleistocene (~120 ka) shoreline and the Wilmar Avenue fault. The inland trend of the paleo-shoreline indicates that most of the Nipomo Mesa and the Santa Maria Valley were submerged during Pleistocene sea level highstands. Namson and Davis (1990) postulate that this stretch of the highway approximately coincides with the axial trace of the San Luis anticline. Several remnants of wave-cut platforms (as indicated by pholad borings and/or marine deposits) suggest that the long-term uplift of this part of the San Luis Range is about 0.13 mm/yr.
1.3	0.6	Sand quarry within small drainage to the left (north) of the highway. Based on detailed geologic mapping, trenching, and drilling in this quarry, informally termed the Farmboy Quarry to honor a fine nearby restaurant, the amount of late Quaternary separation on the

Wilmar Avenue fault is comparable to that determined from the sea-cliff exposure (**Stop 3-1**). These investigations also show that the hanging wall block of the fault is characterized by a broad, steep-limbed anticline and substantial distributed brittle deformation in the Pliocene Squire Member of the Pismo Formation. On the right (south) side of the highway, artificial exposures indicate that the Squire Member is subhorizontal and also characterized by distributed brittle deformation. Remnants of the 120 ka wave-cut platform on both sides of the highway have approximately 4.3 to 6.4 m of vertical separation (Lettis and others, this volume [b]). Assuming a 35- to 70-degree fault dip, these data suggest a post-120 ka slip rate for the Wilmar Avenue fault of 0.04 to 0.08 mm/yr. These relations also indicate that the surface fault trace coincides with Highway 101 in this area.

5.3 4.0 The large cone-shaped hill to the left (east) side of the highway is Picacho Hill. Pholad-bored wave-cut platforms and marine deposits are well exposed in the numerous gullies along the southwestern flank of Picacho Hill. Southwest of U.S. Highway 101, the flight of marine terraces appear to be disrupted along the projected trend of the Wilmar Avenue fault. Vertical separation of two terraces estimated to be approximately 560 and 430 ka across the fault in the Picacho area indicate a net slip rate of 0.04 to 0.10 mm/yr, which is comparable to the net slip rate across the Wilmar Avenue fault zone in Pismo Beach.

7.4 2.1 Maison Beutz winery accessible via this exit. (Last time we checked, the tasting room hours were 2 to 5 pm.)

8.8 1.4 *Exit Highway 101 at the Los Berros/Thompson Avenue exit.*

9.1 0.3 *Turn left (east) onto Thompson Avenue.* Over the next 2 or so miles, road cuts expose unconsolidated gravels that contain pholad-bored cobbles. Based on correlation of marine terraces with those near Arroyo Grande and Pismo Beach, the wave-cut platform associated with those deposits is probably about 560 ka.

11.4 2.3 *Turn left (northeast) onto Mehlschau Road.*

11.6 0.2 ***Stop 3-2.*** *Park off the road.*

Field Stop 3-2: The Southwestern Margin of the San Luis Range, near Nipomo

Stop 3-2 is located within a flight of marine terraces that extend from Highway 101 to the southwestern flank of the San Luis Range to the east. The two most prominent marine terraces in this area at elevations of approximately 88 m and 110 m are

relatively flat and moderately dissected (Fig. 42). Remnants of a third terrace of an elevation of about 155 m are observed in the vicinity of Los Berros Creek. Road cuts and natural outcrops near Nipomo expose marine terrace deposits on wave-cut platforms that are beveled across the Obispo and Monterey Formations. Based on correlation of these terraces with the dated flight of marine terraces at Pismo Beach, these terraces are older than 500 ka. The terrace shoreline angles in the Nipomo region indicate uniform uplift at a rate of 0.15 m/ka with no apparent folding and a possible slight northwestward tilt toward Pismo Beach where uplift rates are about 0.13 m/ka. Southwest of Highway 101, the location and elevation of younger middle and late Pleistocene terraces are obscured by thick dune deposits underlying Nipomo Mesa.

The marine terrace sequence steps down to the southwest into the subsiding Santa Maria Valley across a series of northwest-dipping reverse faults. These faults include the Wilmar Avenue fault along Highway 101 and the Oceano fault and inferred unnamed structures southwest of Highway 101. Because of extensive eolian deposits, fluvial erosion, parallelism of the fault trend and marine strandlines, and limited land access, assessment of the characteristics of the Wilmar Avenue fault is difficult southeast of the Picacho Hill area. The location of the surface trace is inferred by an alignment of several subtle geomorphic and geologic features, including a straight segment of Nipomo Creek ("Nipomo lineament") and a postulated Tertiary basin margin south of the town of Nipomo. This basin margin is inferred on the basis of field mapping and water well data that indicate a substantial change in the elevation of the top of Franciscan Complex rocks across the projected trend of the Wilmar Avenue fault (Lettis and others, this volume [b]). Outcrops northeast of U.S. Highway 101 near Nipomo expose Franciscan rocks overlain by Quaternary marine deposits at an elevation of 88 $\pm$ 2 m. Water well data southwest of the highway show that probable Tertiary sandstone and shale are present between an elevation of 51 m and the bottom of the well at -74 m. The lack of Franciscan Complex rocks in this well suggests the presence of a steep Tertiary basin margin approximately coincident with southeastward projection of the Wilmar Avenue fault. Based on water well data, the elevation of the base of the Quaternary deposits across the projection of the Wilmar Avenue fault changes by approximately 37 m. The Oceano fault and unnamed structures west of Highway 101 are recognized on geophysical records and from interpretation of water and oil well data.

Stop 3-2 is also located along the axial trace of the Point San Luis antiform proposed by Namson and Davis (1990). According to the retrodeformable model of Namson and Davis (1990), this anticline is deforming (uplifting) at a rate of about 0.5 m/ka or greater. Because of the uniform uplift and lack of folding recorded by the marine terrace sequence, we interpret that the Point San Luis anticline, if it exists, is not a late Quaternary structure. This would imply that the underlying thrust fault proposed by Namson and Davis (1990) also is not active as currently modeled.

The range front of Tematate Ridge to the northeast is, in part, a resistant lithologic contact within the Obispo Tuff and, in part, the back edge or former sea cliff of the middle to late Quaternary marine terrace sequence. To the southwest across the

Santa Maria Valley, the Casmalia Hills form the skyline on a clear day. Our next two stops will address the structural and stratigraphic setting of these hills.

GENERAL DIRECTIONS TO **STOP 3-3**

Retrace the route along Mehlschau Road back to Thompson Avenue. Turn left (to the southeast) and drive 5.0 miles to the intersection with Highways 101 and 166. Turn right, go under the overpass, and then turn left to get onto southbound Highway 101. Continue on southbound Highway 101 across the Santa Maria Valley for 9.6 miles to the Clark Avenue (Orcutt) exit. Turn right (west) and continue 3.4 miles through the town of Orcutt to Highway 1 (Cabrillo Highway). Turn right (northwest) and drive 2.6 miles to Black Road. Turn left (southwest) and continue for 0.5 miles until Airox Road branches off to the left. Park along Airox Road; we will walk west along Black Road to the bridge over the railroad track (Figs. 38a and 38b).

ROAD LOG TO **STOP 3-3**

Odometer Cum.	Int.	
0.0	0.0	*Return to vehicles, reset odometers, and drive southwest on Mehlschau Road.*
0.2	0.2	*Turn left on Thompson Avenue.*
1.2	1.0	Driving through scenic Nipomo. The Wilmar Avenue fault and the linear segment of Nipomo Creek that composes the Nipomo Creek lineament lie to the right. Highway 101 lies on the Nipomo Mesa, which is mantled by Quaternary eolian deposits.
5.2	4.0	*Turn right on Highway 166, go under overpass, then turn left onto southbound Highway 101.*
5.6	0.4	Crossing the broad, sandy bed of the Santa Maria River. The Wilmar Avenue fault may extend to the southern end of the Nipomo Mesa, and if so, its location is constrained by exposures of late Quaternary deposits in the bluffs along the northern margin of the Santa Maria River. Fluvial deposits exposed in these bluffs consist of primarily silt and clay, and are overlain by a thick sequence of eolian deposits. The contact between the fluvial and eolian deposits is exposed continuously along the bluffs for a distance of about 2 km west of Nipomo Creek. If the Wilmar Avenue fault has had late Pleistocene activity in this area, it is approximately coincident with Highway 101 near the confluence of Nipomo Creek and the Santa Maria River. For the next six or seven miles we will be crossing the Santa Maria Valley and the Santa Maria oil field.
14.8	9.2	*Exit Highway 101 at Clark Avenue. Turn right (west) toward the town of Orcutt.*
17.1	2.3	*Highway 135 overpass.*

18.2 1.1 *Intersection with Highway 1 (Cabrillo Highway). Turn right (northwest).* To the left (southwest) lies the northeastern margin of the Casmalia Range. Note the topographic scarps along the base of the range. Clark (this volume) notes that these features are steeply-dipping to vertical "dip slopes" of resistant beds within the upper Pliocene to lower Pleistocene Paso Robles Formation, commonly mantled by a veneer of upper Pleistocene Orcutt Sand.

20.8 2.6 *Intersection with Black Road. Turn left (southwest).*

21.3 0.5 *Airox Road branches off to the left. Turn left and park along Airox Road. We will walk west along Black Road to the bridge over the railroad track.*

Field Stop 3-3: The Northeastern Margin of the Casmalia Block, Airox Road

Stop 3-3 provides an opportunity to view deformation along the northeastern margin of the Casmalia Range, which is bordered by the southwest-dipping Orcutt Frontal fault. Surface deformation along this fault is recorded by steeply northeast-dipping to overturned upper Pliocene to lower Pleistocene alluvial sediments of the Paso Robles Formation, northeast-dipping (up to 22 degrees) and locally faulted middle and upper Pleistocene Orcutt sand, and overlying tilted(?) alluvium. Matz and Slemmons (1987) identified prominent west-northwest-trending, potentially fault-related lineaments at the base of the range front, along the inferred trace of the Orcutt Frontal fault. These features are steeply-dipping to vertical "dip slopes" of resistant beds within the Paso Robles Formation, commonly mantled by a veneer of Orcutt Sand (Clark, this volume). Deformation along the Orcutt Frontal fault is expressed mainly by folding or tilting of Neogene strata, with discontinuous, secondary surface faulting in the hanging-wall block.

At **Stop 3-3**, we will look at deformation of the Paso Robles Formation, the Orcutt Sand, and a Quaternary fluvial deposit. Based on paleocurrent indicators and the presence of exotic clasts, the Quaternary fluvial deposit is associated with a southwesterly-flowing paleo-drainage that originated in the San Rafael Mountains. About 0.7 km south of the inferred trace of the Orcutt Frontal fault, the deposit dips 7 to 9 degrees to the northeast, indicating at least that much middle or late Quaternary tectonic tilting and/or folding. These and other similar deposits that have northeast dips occur only within about 1 km of the inferred trace of the Orcutt Frontal fault, suggesting that fold deformation is localized along the fault. The Orcutt Frontal fault has an estimated minimum late Quaternary dip-slip rate of 0.16 to 0.34 mm/yr (Clark, this volume).

As we will note at **Stop 3-4**, a well-preserved flight of marine terraces along the northwestern and southwestern margins of the Casmalia Range suggest that the range is being uplifted at a rate of 0.14 to 0.17 mm/yr (Clark, this volume). The terrace shoreline angles indicate that the predominant style of late Quaternary surface deformation in the Casmalia Range is uniform, block-style uplift. However, there is significant localized folding along the Orcutt Frontal fault and minor reverse

movements on the Lions Head fault. This pattern of range emergence indicated by marine and fluvial terraces can be interpreted in at least two ways: (1) uplift of a rigid structural block along high-angle reverse faults with localized drag folding at the surface on the Orcutt Frontal fault; or (2) continued anticlinal folding of the Casmalia Range above a listric blind thrust or reverse fault. The second model is favored based on the implied continuity in style with earlier Pleistocene fault-propagation style folding (Nitchman, 1988; Namson and Davis, 1990).

GENERAL DIRECTIONS TO **STOP 3-4**

Return to vehicles, and retrace route along Black Road to Highway 1. Turn left (northwest) on Highway 1 and drive 5.4 miles to Brown Road. Turn left (west). Drive 3.9 miles up Corralitos Canyon, to where Brown Road veers to the right away from Corralitos Ranch. Because parking is limited at ***Stop 3-4****, please park your car here and ride with others, if possible. Continue into the range along Brown Road for approximately 2.6 miles, to the crest of the Casmalia Range. Park where possible for* ***Stop 3-4*** *(Fig. 38b).*

ROAD LOG TO **STOP 3-4**

Odometer *(reset odometer)*

Cum.	Int.	
0.0	0.0	*Return to vehicles and retrace route along Black Road to Highway 1.*
0.5	0.5	*Turn left (northwest) on Highway 1.*
5.9	5.4	*Turn left (west) on Brown Road.* As we drive into the Casmalia Range along Corralitos Canyon, notice the oversteepened range front coincident with the Orcutt Frontal fault. Further into the range, a variety of stratigraphic units are exposed. Pliocene and Quaternary anticlinal uplift and reverse faulting have brought to the surface Mesozoic basement (Point Sal ophiolite and Knoxville Formation). Overlying Neogene, predominantly marine strata of the Santa Maria basin are also deformed. If it is possible to see through the dust of the car ahead, notice the bright red cobble conglomerate at the side of the road. This is the upper Oligocene-lower Miocene Lospe Formation, a coarse alluvial unit deposited unconformably on the Point Sal ophiolite. Hall (1981) believes that the Lospe at Point Sal is equivalent to alluvial deposits at San Simeon, and cited this as one of several piercing points indicative of about 80 km of right-lateral displacement along the San Gregorio-Hosgri fault.
9.8	3.9	*Brown Road veers to the right away from Corralitos Ranch. Because parking is limited at Field Stop 3-4, please park your car here and ride with others, if possible.*
9.9	0.1	*Crossing Corralitos Creek.*

10.4 0.5 *Intersection with dirt road branching to the right. Stay on Brown Road (straight ahead) to the crest of the Casmalia Range.*

12.4 2.0 *Crest of the Casmalia Range. Park where possible.*

Field Stop 3-4 (optional): The Casmalia Range, Point Sal Ridge

Stop 3-4 is an overview of the marine terraces near Point Sal. A well preserved flight of at least nine marine terraces with shoreline angle elevations of 9 to 265 m is present on the southwest flank of the Casmalia Range (on Vandenberg Air Force Base), and continues to the north, where all but the lowest one or two marine terraces are buried by thick dune sand. Comparison of the marine terrace altitudinal spacing with global sea level curves suggests that the ages of the two lowest marine terraces are 83 ka and 120 ka (oxygen isotope substages 5a and 5e, respectively). These data suggest a 0.14 to 0.17 mm/yr uplift rate for the Casmalia Range (Clark, this volume). Bulk fossil and coral samples from several of the terraces currently are being analyzed for faunal assemblage and U/Th relative and absolute age dates.
Surveyed shoreline angle elevations of the inferred 83 ka and 120 ka marine terraces between the Lions Head fault and Point Sal indicate uniform late Quaternary range uplift, with no significant internal faulting, tilting, or folding. The wave-cut platform geometries of two higher marine terraces (shoreline angle elevations of 163 and 265 m) also indicate uniform block-style uplift. A single shoreline angle measurement at Mussel Rock suggests localized late Quaternary tilting or folding north of Point Sal. To the south, the Lions Head fault at its seacliff exposure is a steep, NE-dipping reverse fault. The 120 ka marine terrace has 1.4 m of vertical separation across a normal fault in the hanging wall of the Lions Head fault. This fault is interpreted as a secondary "bending-moment" fault associated with reverse displacement at depth. The cumulative rate of vertical separation of middle and late Quaternary marine terraces across the Lions Head fault is no more than 0.01 to 0.02 mm/yr (Clark, this volume).

END OF DAY 3

REFERENCES

Berger, G., 1987, personal communication.

Burchfield, B.C., and J.H. Stewart, 1966, "Pull-apart" origin of the central segment of Death Valley, California: Geological Society of America Bulletin, v. 77, p. 439-442.

Clark, D.G., this volume, Late Quaternary tectonic deformation in the Casmalia Range, coastal south-central California.

Clark, J. C., Brabb, E. E., Greene, H. G., and Ross, D. C., 1984, Geology of Point Reyes Peninsula and implications for San Gregorio fault history: in Crouch, J. K., and Bachman, S. B. (eds.), Tectonics and Sedimentation Along the California Margin; Pacific Section S.E.P.M., v. 38, p. 67-86.

Crouch, J., and Bachman, S.B., and Shay, J.T., 1984, Post-Miocene compressional tectonics along the central California margin: in Crouch, J., and Bachman, S.B., eds., Tectonics and Sedimentation Along the California Margin; Pacific Section, S.E.P.M., v. 38, p. 37-54.

Crowell, J. C., 1974, Sedimentation along the San Andreas fault, in Doff, R. H., Modern and Ancient Geosynclinal Sedimentation: Special Publication, Society of Economic Paleontologists and Mineralogists, v. 19, p. 292-303.

Fairbanks, H.W., 1904, Description of the San Luis quadrangle: Geologic atlas of the United States, San Luis folio, California: No. 101, U.S. Geological Survey.

Davis, T., and McIntosh, K.D., 1987, A retrodeformable structural solution across the southern Coast Ranges and implications for seismically active structures (abs.): Geological Society of America, Cordilleran Section Meeting Abstracts with Program, v. 19, no. 6, p. 447.

Feigl, K.L., King, R.W., and Jordan, T.H., 1990, Geodetic measurement of tectonic deformation in the Santa Maria fold and thrust belt, California: Journal of Geophysical Research, v. 95, no. B3, p. 2679-2699.

Graham, S. A. and Dickinson, W. R., 1976, The San Gregorio Fault as a major right-slip fault of the San Andreas fault system (abs.): Geological Society of America Abstracts with Programs, v. 8, p. 890.

Graham, S. A., and Dickinson, W. R., 1978a, Evidence for 115 kilometers of right slip on the Gregorio-Hosgri fault trend: Science, v. 199, p. 179-81.

Graham, S. A., and Dickinson, W. R., 1978b, Apparent offsets of on-land geologic features across the San Gregorio-Hosgri fault trend: in Silver, E. A. and Normack, W. R., (eds), San Gregorio-Hosgri Fault Zone, California: California Division of Mines and Geology, Special Report 137, p. 13-23.

Green, H.G., 1977, Geology of the Monterey Bay region: U.S. Geological Survey Open-File Report 77-718, 347 p.

Hall, C.A., Jr., 1975, San Simeon-Hosgri fault system, coastal California: economic and environmental implications: Science, v. 190, No. 1221, p. 1291-1294.

Hall, C.A., Jr., 1976, San Simeon-Hosgri Fault System, Coastal Central California: Economic and Environmental Implications: Geological Society of America Abstracts with Programs, v. 8, p. 378.

Hall, C.A., Jr., 1978, Origin and development of the Lompoc-Santa Maria pull- apart basin and its relation to the San Simeon-Hosgri strike-slip fault, western California: in Silver, E.A., and Normack, W.R. (eds.), San Gregorio-Hosgri fault zone, California, California Division of Mines and Geology Special Report 137, p. 25-31.

Hall, C.A., Jr., 1981a, Chapter 17 - Evolution of the western Transverse Ranges microplate: Late Cenozoic faulting and basinal development: in Ernst, W.G. (ed.), The Geotectonic Development of California, Rubey Volumn, no. 1, Prentice-Hall, Inc., Englewood Cliffs, New Jersey, p. 559-582.

Hall, C.A., Jr., 1981b, San Luis Obispo transform fault and middle Miocene rotation of the western Transverse Ranges, California: Journal of Geophysical Research, v. 86, no. B2, p. 1015-1013.

Hall, C.A., Jr., Ernest, W.G., Prior, S.W., and Wiese, J.W., 1979, Geologic map of the San Luis Obispo-San Simeon Region, California: U.S. Geological Survey Miscellaneous Investigations Series, Map I-1097, Scale 1:48,000.

Hall, N. T., Hunt, T. D., Vaughan, P. A., Bickner, F., and Lettis, W. R., 1987, Trenching and mapping investigations of the late Quaternary behavior of the San Simeon fault, San Luis Obispo County, California (abs.): Geological Society of America Abstracts with Programs, Cordilleran Section, v. 19, no. 6, p. 385.

Hall, N.T., Hunt, T.D., and Vaughn, P., this volume, Holocene Behavior of the San Simeon Fault Zone, South Central Coastal California.

Hamilton, D. H., 1987, Characterization of the San Gregorio-Hosgri fault system, coastal central California (abs.): Geological Society of America Abstracts with Programs, Cordilleran Section, v. 19, no. 6, p. 385.

Hanson, K. L., Lettis, W. R., and Mezger, L., 1987, Late Pleistocene deformation along the San Simeon fault zone near San Simeon, California (abs.): Geological Society of America Abstracts with Programs, Cordilleran Section, v. 19, no. 6, p. 386.

Hanson, K.L., Wesling,J.R., Lettis, W.R., Kelson, K.I., and Mezger, L., this volume, Correlation, ages, and uplift rates of Quaternary marine terraces, south-central coastal California.

Hanson, K.L. and Lettis, W.R., this volume, Pleistocene slip rate for the San Simeon fault zone based on offset marine terraces and displaced drainages.

Hempton, M.R., and Dunne, L.A., 1984, Sedimentation in pull-apart basins: active examples in eastern Turkey: Journal of Geology, v. 92, p. 513-530.

Hempton, M.R., and Neher, K., 1986, Experimental fracture, strain and subsidence patterns over en echelon strike-slip faults: implications for the structural evolution of pull-apart basins: Journal of Structural Geology, v. 8, p. 597-605.

Kennedy, G., (Los Angeles County Museum of Natural History, written communication, 1986)

Kennedy, G.L., Wehmiller, J.F., and Muhs, D.R., 1988, Late Pleistocene climatic change: evidence from coastal San Luis Obispo County, central California: American Quaternary Association Program and Abstracts, p. 126.

Ku, T.-L., and Kern, J.P., 1974, Uranium-series age of the upper Pleistocene Nestor terrace, San Diego, California: Geological Society of America Bulletin, v. 85, p. 1713-1716.

Leslie, R.B., 1980, Continuity and tectonic implications of the San Simeon-Hosgri fault zone, Central California: unpublished Master Thesis, University of California at Santa Cruz, California.

Leslie, R.B.,1981, Continuity and tectonic implications of the San Simeon-Hosgri fault zone, central California: U.S. Geological Survey Open-File Report 81-430.

Lettis, W.R., and Hall, N.T., this volume, The Los Osos fault zone, San Luis Obispo County, California.

Lettis, W. R., Hall, N. T., and Hamilton, D. H., 1989, Quaternary tectonics of south-central coastal California (abs.): 28th International Geological Congress, Abstracts, v. 2, p. 2-285.

Lettis, W.R., DiSilvestro, K., Hanson, K.L., and Shiller, J.I., this volume [a], The San Simeon/Hosgri pull-apart basin: analysis of offshore data.

Lettis, W.R., N.T. Hall, K.L. Hanson, K.I. Kelson, and J.R. Wesling, this volume [b], Quaternary Deformation of the San Luis Range, San Luis Obispo County, California.

Luyendyk, B.P., Kamerling, M.J., and Terres, R.R., 1980, Geometric model for Neogene crustal rotations in southern California: Geological Society of America Bulletin, Part I, v. 91, p. 211-217.

Luyendyk, B.P., Kamerling, M.J., Terres, R.R., and Hornafius, J.S., 1985, Simple shear of southern California during the Neogene: Journal of Geophysical Research, v. 90, p. 12,454-12,466. (1075)

Luyendyk, B.P., and Hornafius, J.S., 1987, Chapter 11 - Neogene crustal rotations, fault slip, and basin development in southern California: in Ingersoll, R.V., and Ernst, W.G., eds., Cenozoic Development of Coastal California: Rubey Volume, v. 6, Prentice-Hall, Inc., Englewood Cliffs, New Jersey, p. 259-283.

Mann, P., Hempton, M. R., Bradley, D. C., and Burke, K., 1983, Development of pull-apart basins: Journal of Geology, v. 91, p. 529-554.

Manson, M., 1985, San Simeon fault zone and Cambria fault, San Luis Obispo County, California: California Division of Mines and Geology Fault Evaluation Report FER-170, p. 12.

Matz, B., and Slemmons, D.B., 1987, Remote sensing study of the Pismo syncline and the Santa Maria Basin, central coastal California: Geological Society of America Abstracts with Programs, v. 19, p. 429.

McCulloch, D. S., 1987, Regional geology and hydrocarbon potential of offshore central California; in Scholl, D. W., Grantz, A., and Vedder, J., eds., Geology and Resource Potential of the Continental Margin of Western North America and Adjacent Ocean Basins, Beaufort Sea to Baja California: American Association of Petroleum Geologists, Circum Pacific Earth Science, v. 6, p. 353-401.

Muhs, D.R., Kennedy, G.L., and Rockwell, T., 1988, Uranium-series ages of corals from marine terraces, Pacific Coast of North America: implications for the timing and magnitude of late Pleistocene sea-level changes: American Quaternary Association, Program and Abstracts, p. 140.

Muhs, D.R., 1990, personal communication.

Namson, J.S., and Davis, T.L. 1990, in review, Subsurface study of the late Cenozoic structural geology of the Santa Maria basin, western Transverse Ranges and southern Coast Ranges, California.

Nitchman, S.P. 1988, Tectonic geomorphology and neotectonics of the San Luis Range, San Luis Obispo County, California: M.S. Thesis, University of Nevada, Reno, 120 p.

Orme, A.R., 1990, The instability of Holocene coastal dunes: the case of the Morro dunes, California; in Nordtrom, K.F., Psuty, N.P., and Carter, R.W.G., eds., Coastal Dunes: Form and Process: New York and Chichester, John Wiley and Sons, p. 317-338.

Orme, A.R., this volume, Late Quaternary coastal dunes of the Santa Maria area: a synopsis.

Pacific Gas and Electric Company (PG&E), 1988, Diablo Canyon power plant long term seismic program report: Pacific Gas and Electric Company, San Francisco, California.

Rodgers, D.A., 1980, Analysis of pull-apart basin development produced by en echelon strike-slip faults: in Ballance, P.F., and Reading, H.G., eds., Sedimentation in Oblique-Slip Mobile Zones, International Association of Sedimentologists Special Publication 4, p. 27-41.

Sibson, R.H., 1985, Stopping of earthquake ruptures at dilational fault jogs: Nature, v. 316, p. 248-251.

Sibson, R. H., 1986a, Brecciation processes in fault zones: inferences from earthquake rupturing: Pageoph, v. 124, nos. 1/2, p. 159-175.

Sibson, R. H., 1986b, Rupture interaction with fault jogs: in Earthquake Source Mechanics, Das, S., Boatwright, J., and Sholz, C.H., (eds.), Maurice Ewing Series 6, American Geophysical Union Monography 37, p. 157-168.

Silver, E. A., 1974, Structural interpretation from free-air gravity on the California continental margin, 35° to 40°N (abs.): Geological Society of America Abstracts with Programs, v. 6, no. 3, p. 253.

Silver, E.A., 1978, The San Gregorio-Hosgri fault zone: An Overview: in Silver, E.A., and Normark, W.R., eds., San Gregorio-Hosgri Fault Zone, California: California Division of Mines and Geology Special Report 137, p. 1-2.

Stein, R.S., and Ekstrom, G., 1989, Rupture sequence and fault geometry beneath the 100-km-long New Idria-Colinga-Kettleman Hills segmented fold chain: EOS, Transactions of the American Geophysical Union, v. 70, p. 1368.

Suppe, J., 1983, Geometry and kinematics of fault-bend folding: American Journal of Science, v. 283, p. 684-721.

Treiman, 1989, Los Osos fault zone: California Division of Mines and Geology Fault Evaluation Report FER-200.

Turner, D.L., Surdam, R.C., and Hall, C.A., 1970, The Obispo formation and associated volcanic rocks in the central California Coast Ranges - K-Ar ages and biochronologic significance: Geological Society of America Abstracts with Programs, v. 2, no. 2, p. 155.

Veeh, H.H., and Valentine, J .W., 1967, Radiometric ages of Pleistocene fossils from Cayucos, California: Geological Society of America Bulletin, v. 78, p. 547-550.

Weber, G.E., 1983, Geologic investigation of the marine terraces of the San Simeon Region and Pleistocene Activity of the San Simeon fault zone, San Luis Obispo County, California: U.S. Geological Survey Technical Report 66.

Woodcock, N.H., and Fischer, M., 1986, Strike-slip Duplexes: Journal of Structural Geology, v. 8, no. 7, p. 725-735.

1075F(FOP)

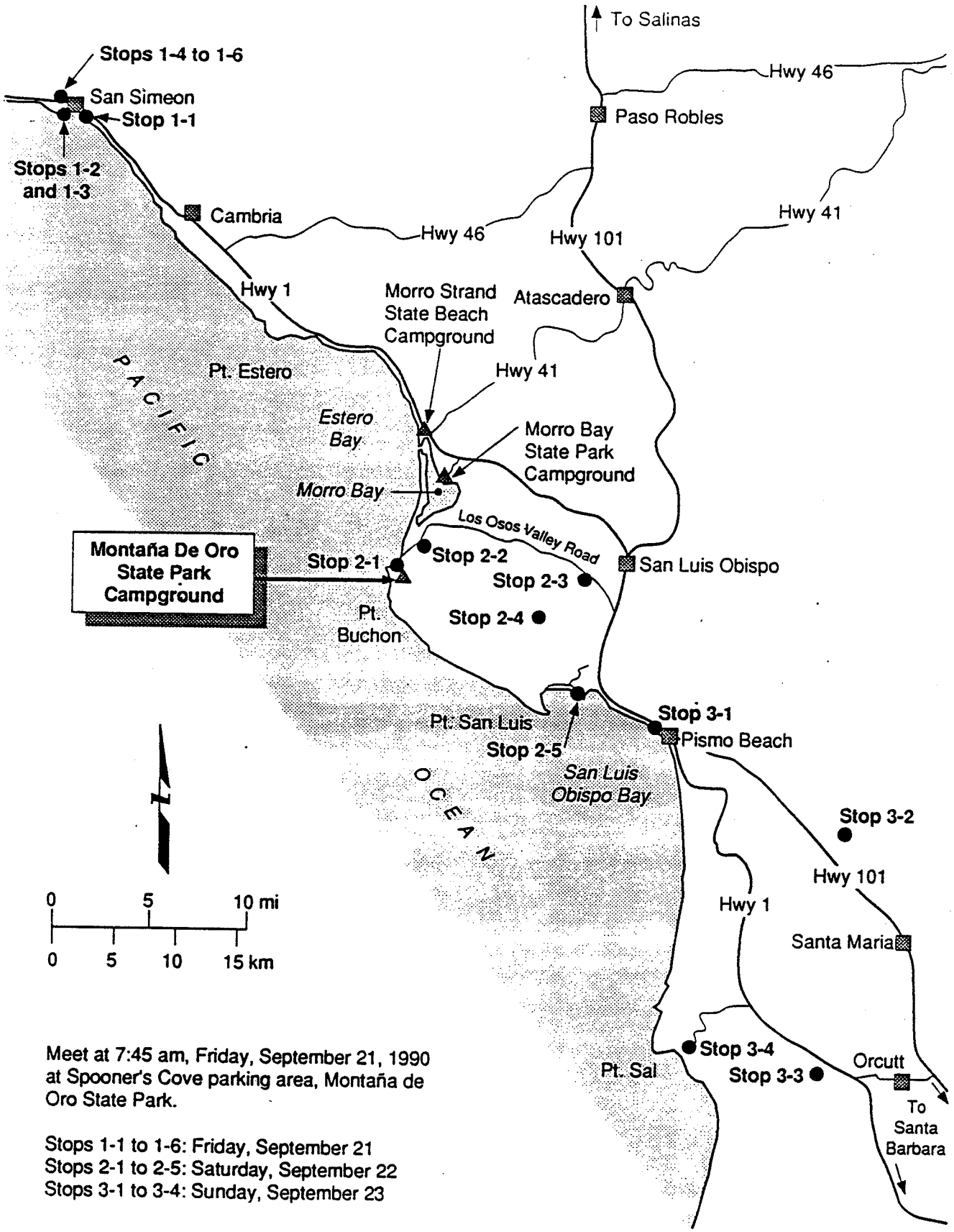

Meet at 7:45 am, Friday, September 21, 1990 at Spooner's Cove parking area, Montaña de Oro State Park.

Stops 1-1 to 1-6: Friday, September 21
Stops 2-1 to 2-5: Saturday, September 22
Stops 3-1 to 3-4: Sunday, September 23

Figure 1. Regional map showing locations of field stops and Montaña de Oro State Park campground.

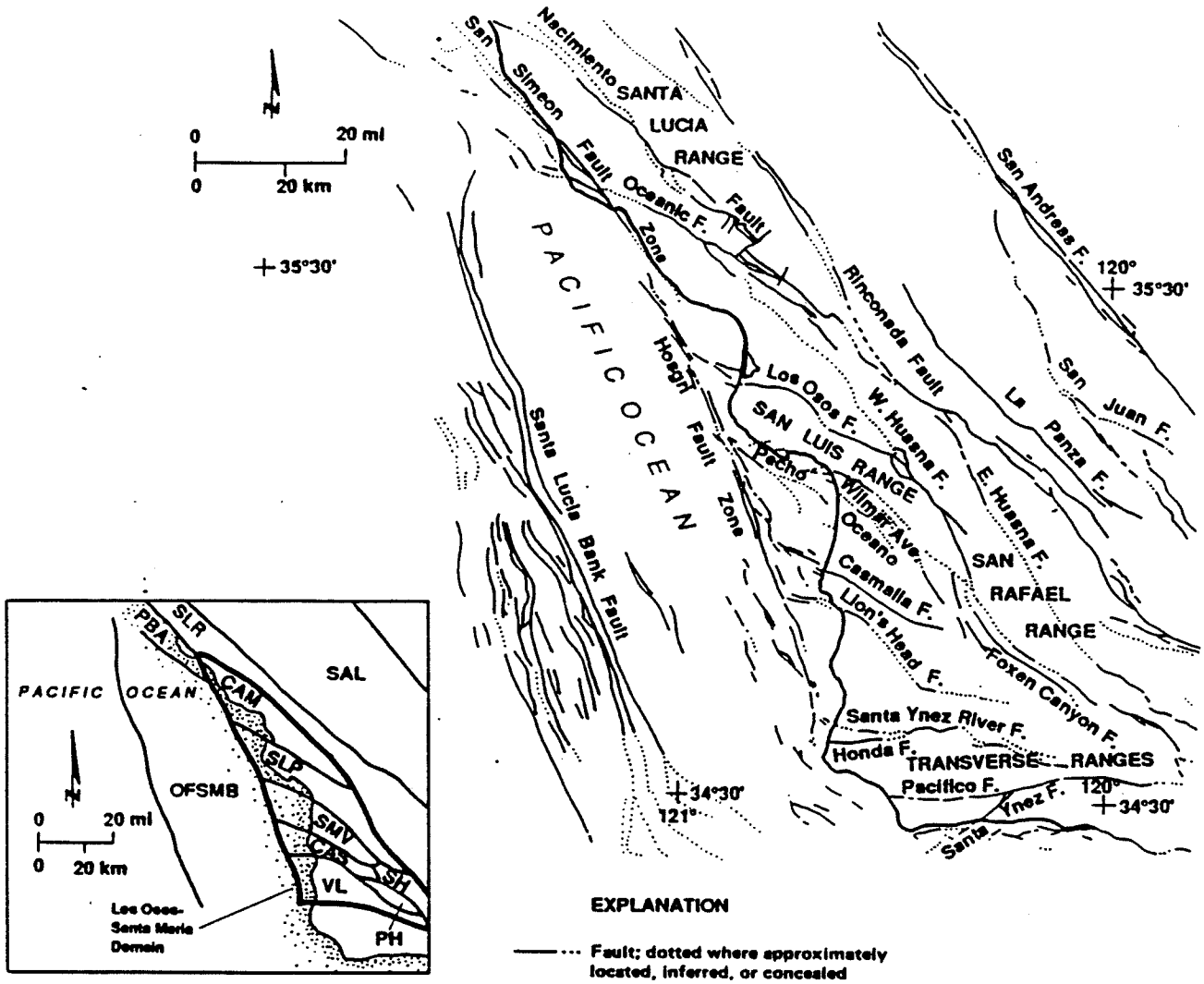

Figure 2. Map of structural blocks and faults in the south-central California coastal region. SAL = Salinian block, SLR = Santa Lucia Range block, PBA = Piedras Blancas anticlinorium, CAM = Cambria block, SLP = San Luis/Pismo block, OFSMB = Offshore Santa Maria basin block, SMV = Santa Maria Valley block, CAS = Casmalia block, VL = Vandenberg/Lompoc block, PH = Purisima Hills block, SH = Solomon Hills block. (After Lettis and others, this volume).

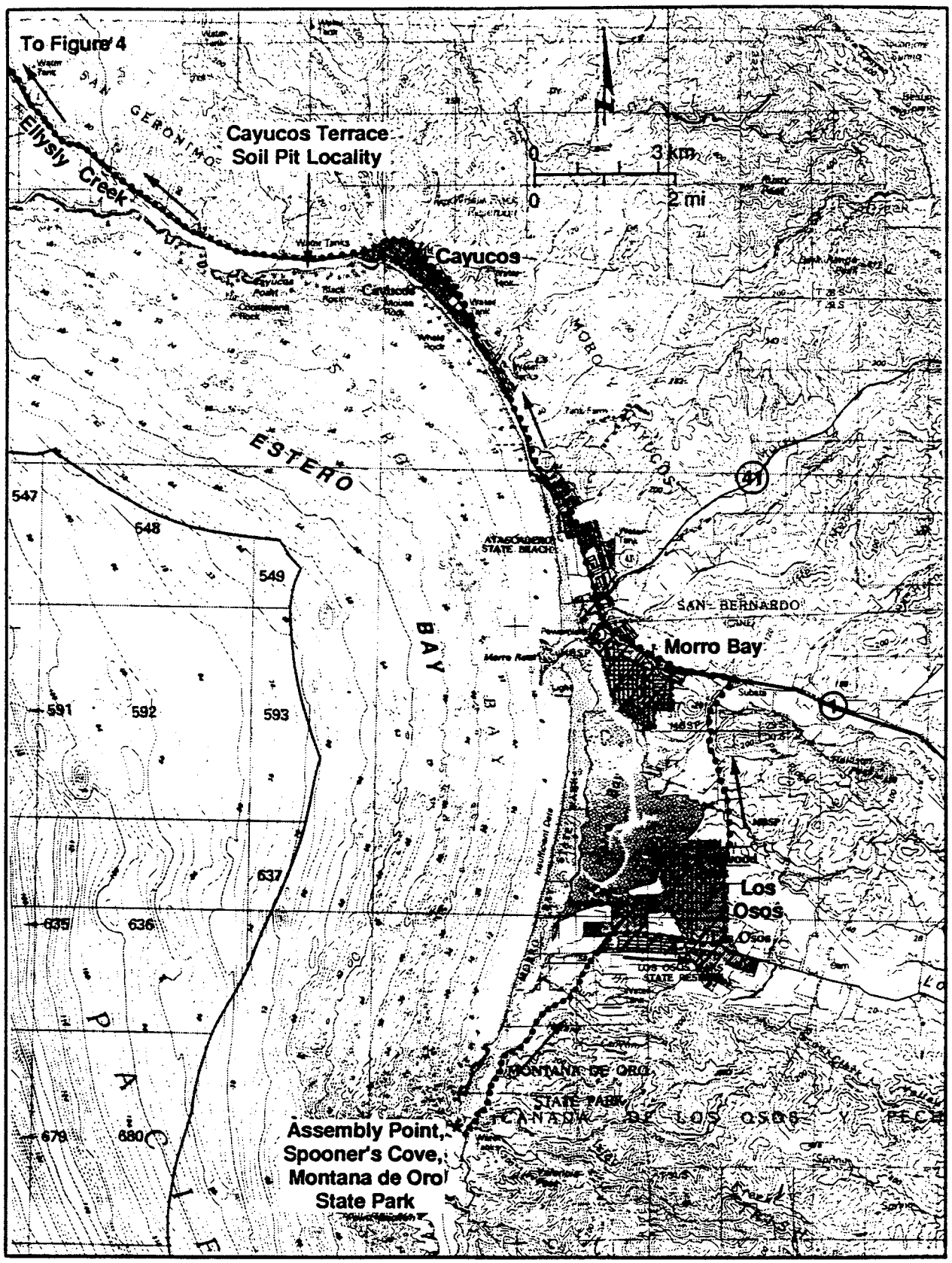

Figure 3. Location map showing field trip route (Day 1) - Morro Bay to Cayucos area.

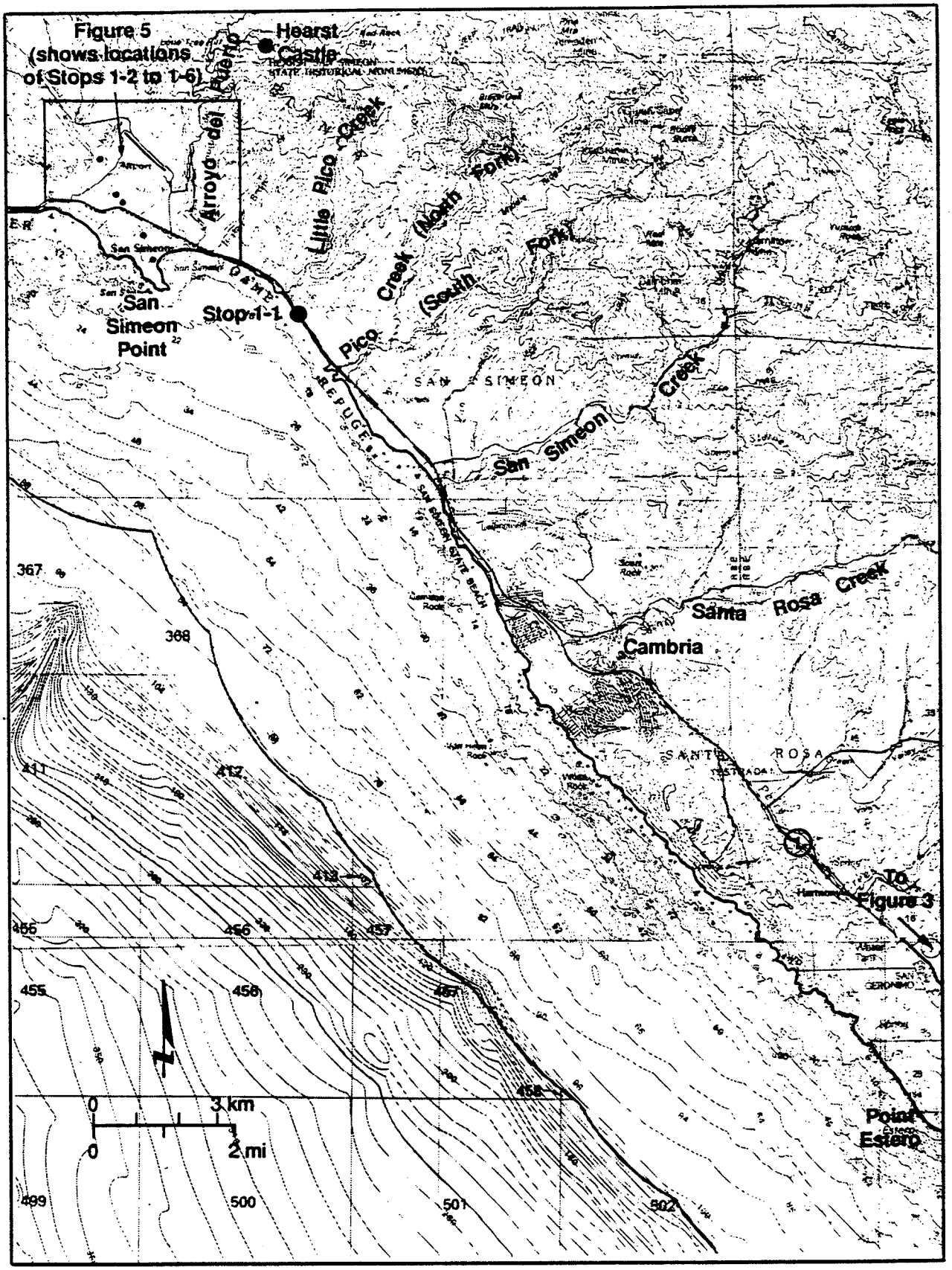

Figure 4. Location map showing field trip route (Day 1) - Point Estero to San Simeon Point.

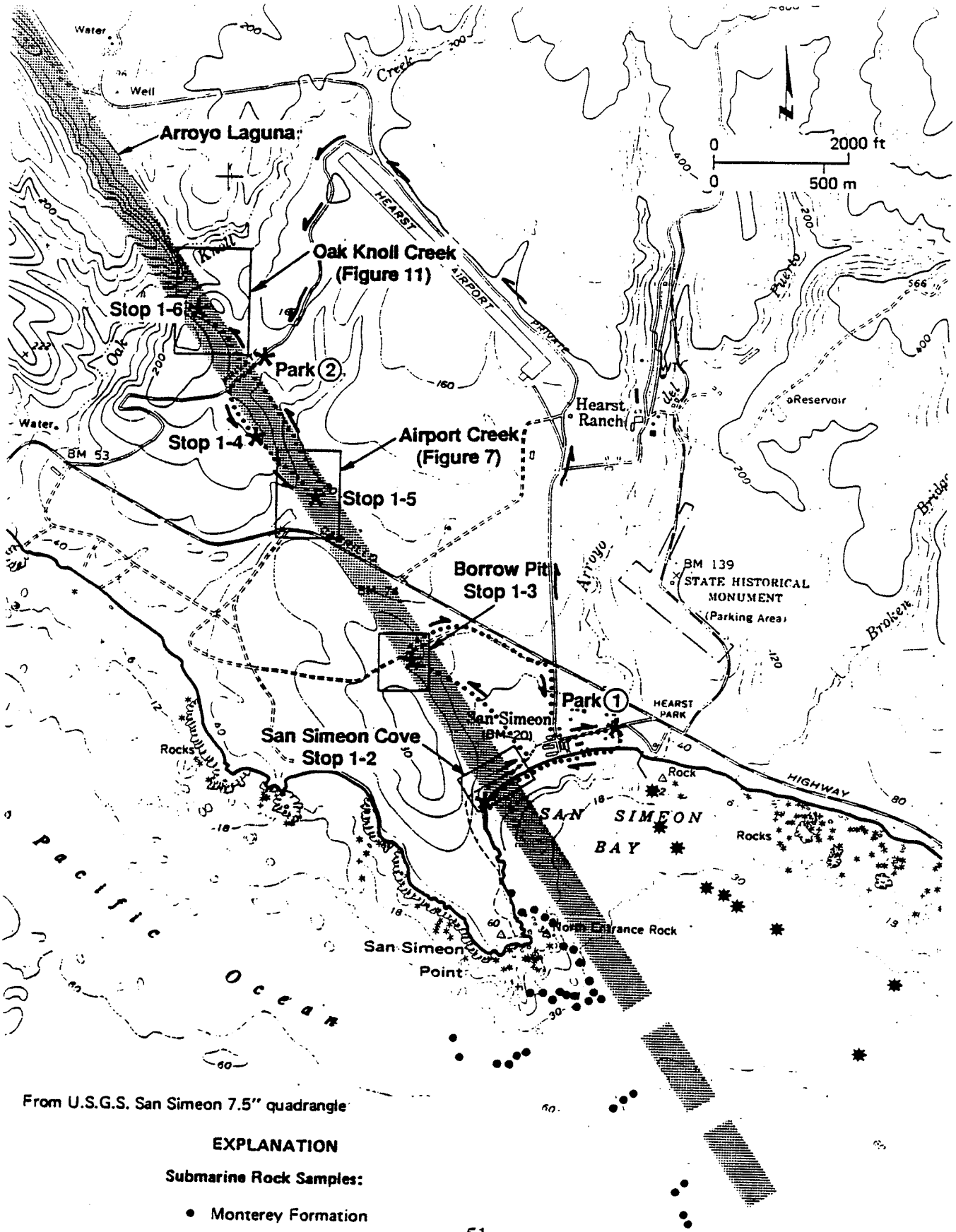

From U.S.G.S. San Simeon 7.5" quadrangle

EXPLANATION

Submarine Rock Samples:

- Monterey Formation
- Franciscan Complex

Approximate trend of the San Simeon fault zone

Figure 5. Map showing detailed study areas, locations of field stops 1-2 to 1-6, and location of submarine rock samples along the San Simeon fault zone

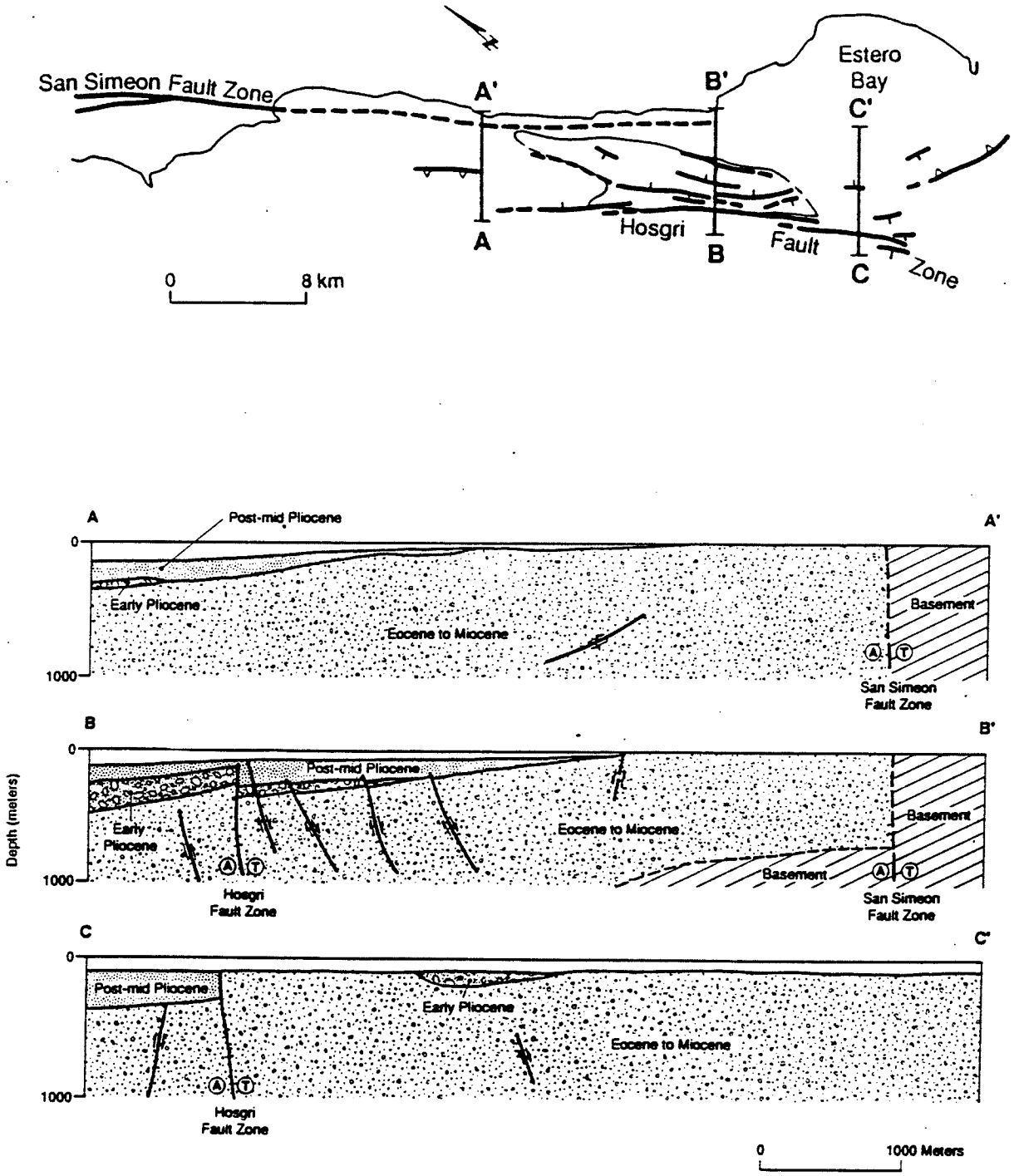

Figure 6. Geologic sections illustrating stratigraphic and structural relationships north of the San Simeon/Hosgri pull-apart (A-A'), through the pull-apart (B-B'), and south of the pull-apart (C-C').

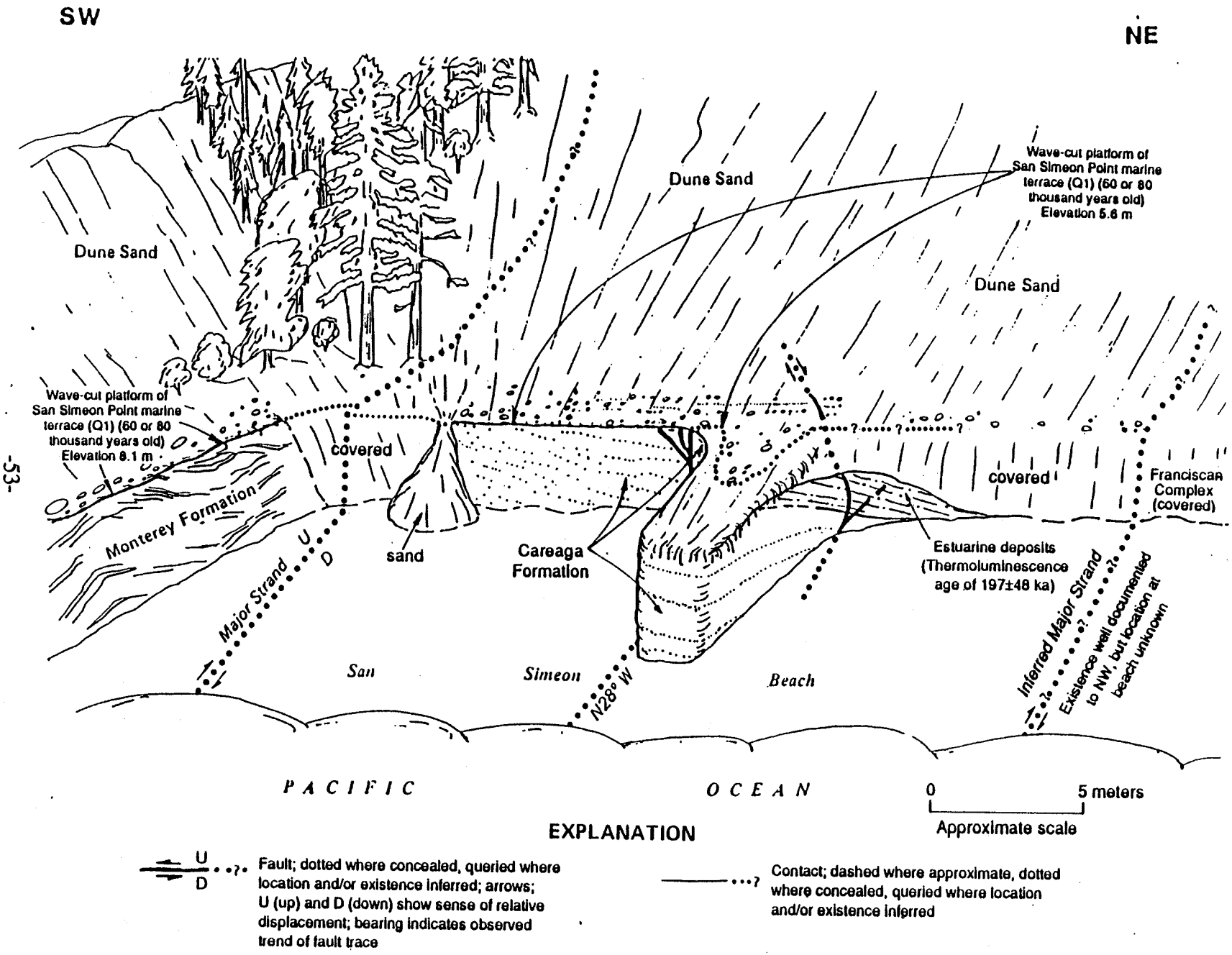

Figure 7. Gull's eye view of S[illegible] Simeon fault zone at San Simeon Cove.

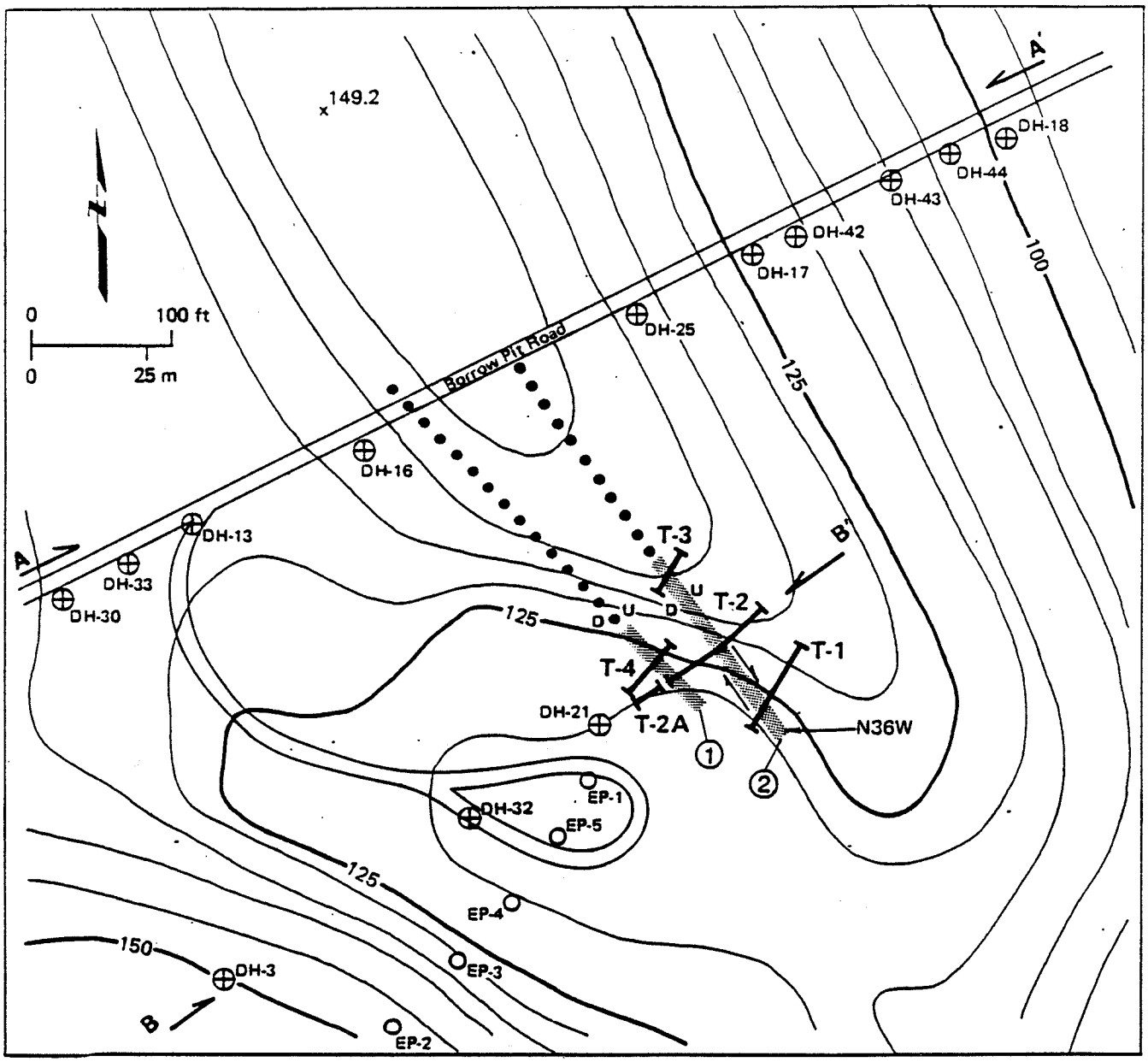

EXPLANATION

30"-wide backhoe trench

DH-16 — 5"-diameter flight-auger hole

EP-1 — 30"-wide backhoe exploratory pit

A — A' — Line of cross section (Figure 10)

125 — Topographic contour showing elevation in feet; contour interval 5'

N48W — Trace of fault exposed in trenches; dotted where concealed and extended by auger-hole data; arrows show sense of slip; bearing indicates observed trend of fault trace

① — Western Borrow Pit trace (inferred)

② — Eastern Borrow Pit trace

Figure 8. Map of Borrow Pit site showing locations of trenches, auger holes, and exploratory pits.

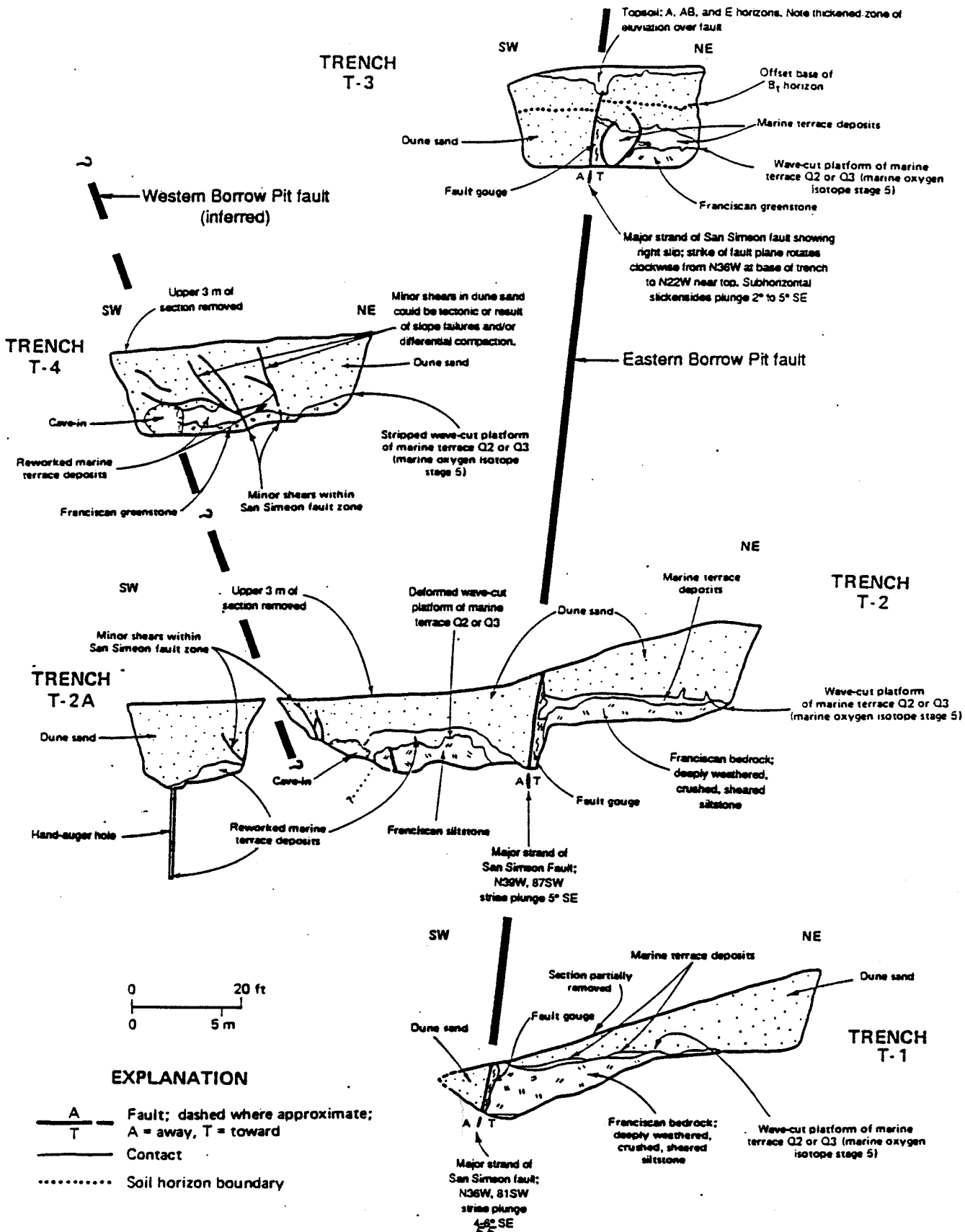

Figure 9. Simplified logs of Borrow Pit trenches showing major strand of San Simeon fault (view to NW).

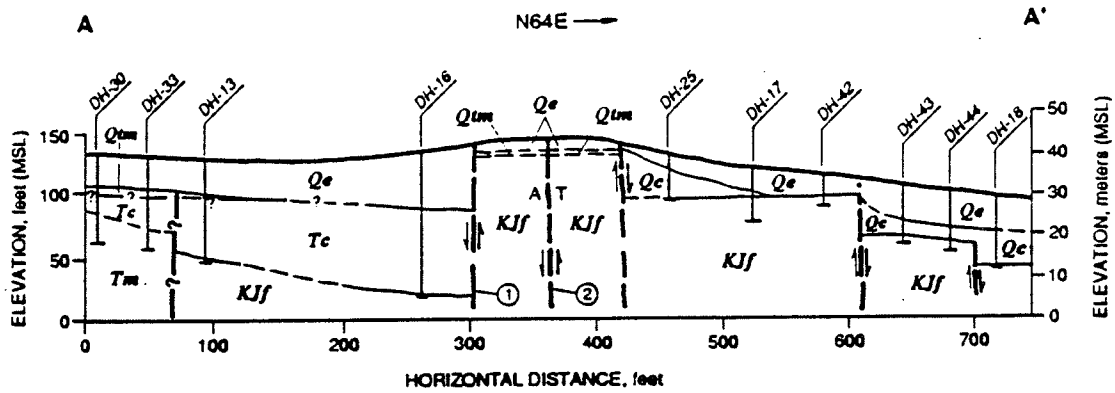

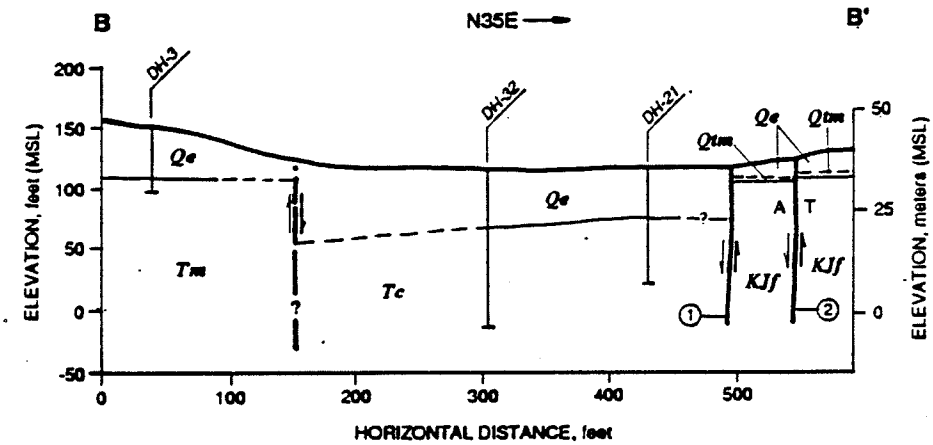

EXPLANATION

Qtm	Quaternary marine terrace deposits
Qe	Quaternary eolian deposits
Qc	Quaternary colluvium
Tc	Careaga Formation
Tm	Monterey Formation
KJf	Franciscan Complex

Fault; dashed where approximately located, dotted where concealed, queried where uncertain; A/T (away/toward) and arrows indicate apparent relative direction of displacement

DH-30 — 5"-diameter flight-auger hole

① — Western Borrow Pit fault

② — Eastern Borrow Pit fault

For locations of cross sections, see Figure 8

Figure 10. Cross sections through the Borrow Pit site showing multiple strands within the San Simeon fault zone. Section A - A' is drawn along the Borrow Pit Road; section B - B' is drawn across the trenching site.

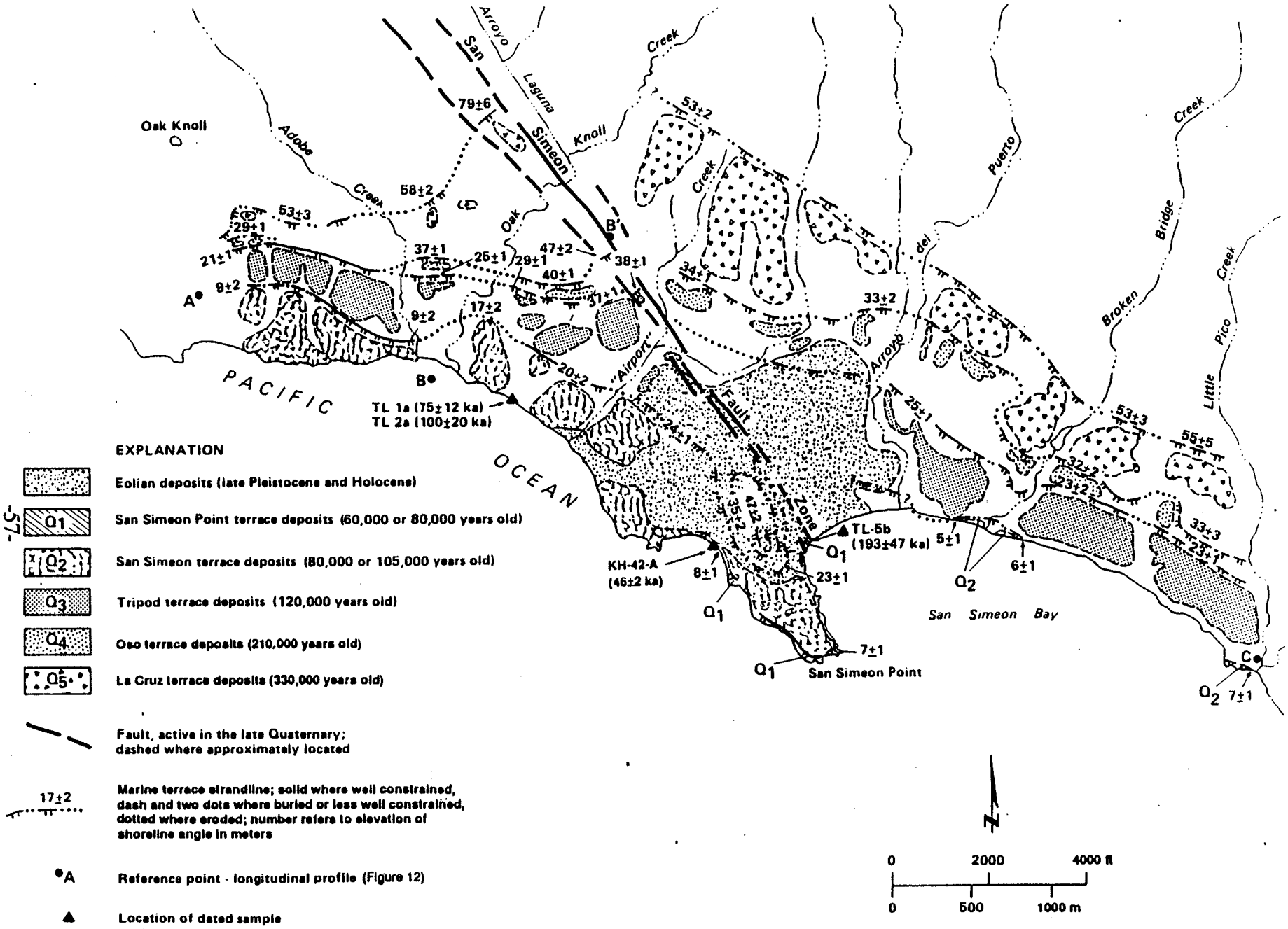

Figure 11. Geologic map of marine terraces along the Southern onshore reach of the San Simeon fault zone.

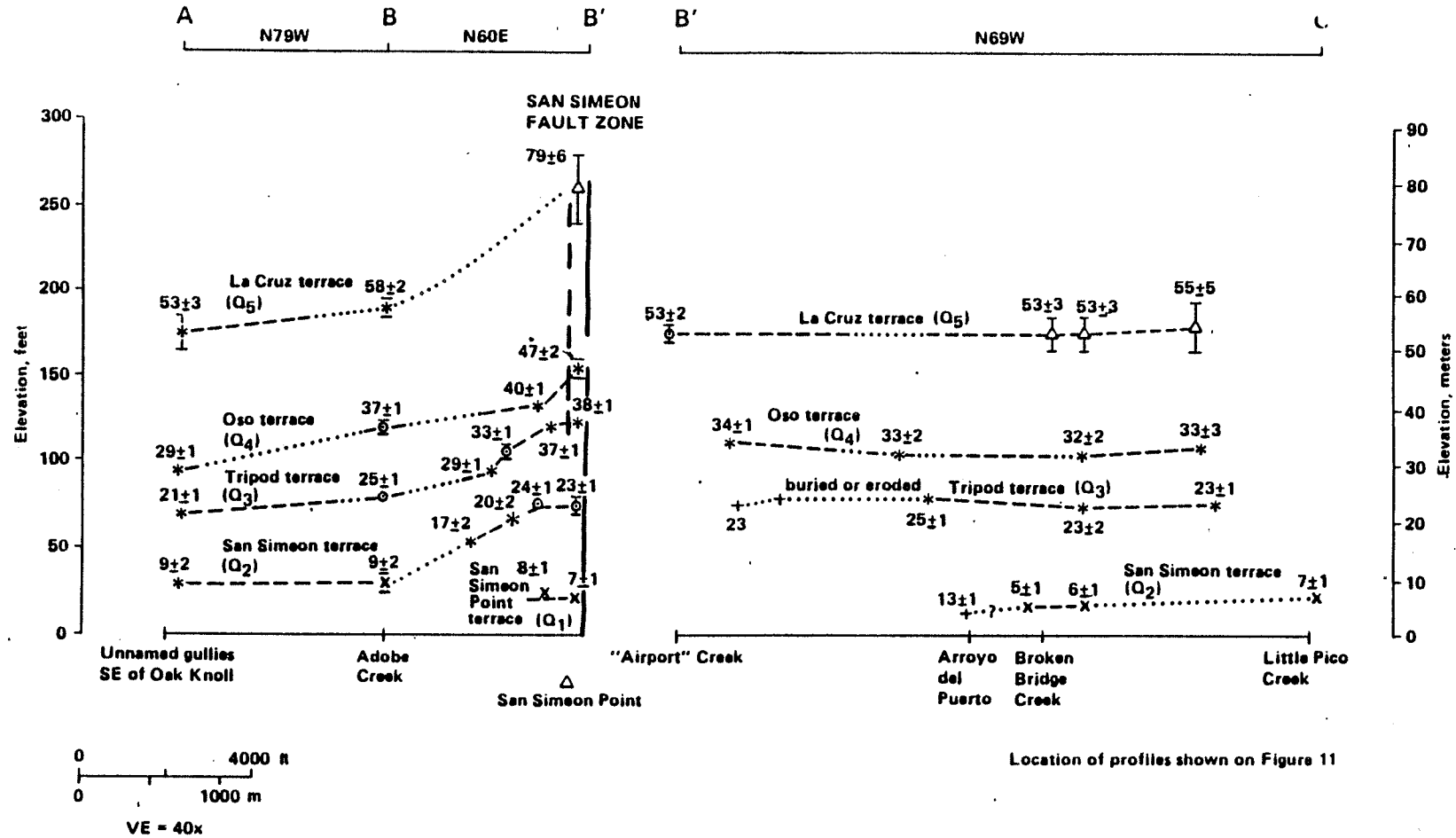

EXPLANATION

Lines

- ——— ⦣ with well exposed wave cut platform (WCP)
- - - - - ⦣ without well expressed wave cut platform
- ····· Eroded ⦣

General note: Error bars are shown except where symbol is larger than error.

Symbols

- ⦣ Shoreline angle
- x ⦣, elevation based on surveying of exposed ⦣ (meters)
- ⊙ ⦣; elevation based on drill hole projections (meters)
- * ⦣; elevation based on projection of surveyed wcp exposed in seacliff, stream cut or soil pit (meters)
- △ ⦣; elevation estimated from bedrock outcrops plotted on USGS 7.5' topographic quadrangle map (meters). Contour interval 40 feet
- + Elevation of bedrock surfaces (meters)

Figure 12. Longitudinal profile of marine terraces along the southern onshore San Simeon fault zone.

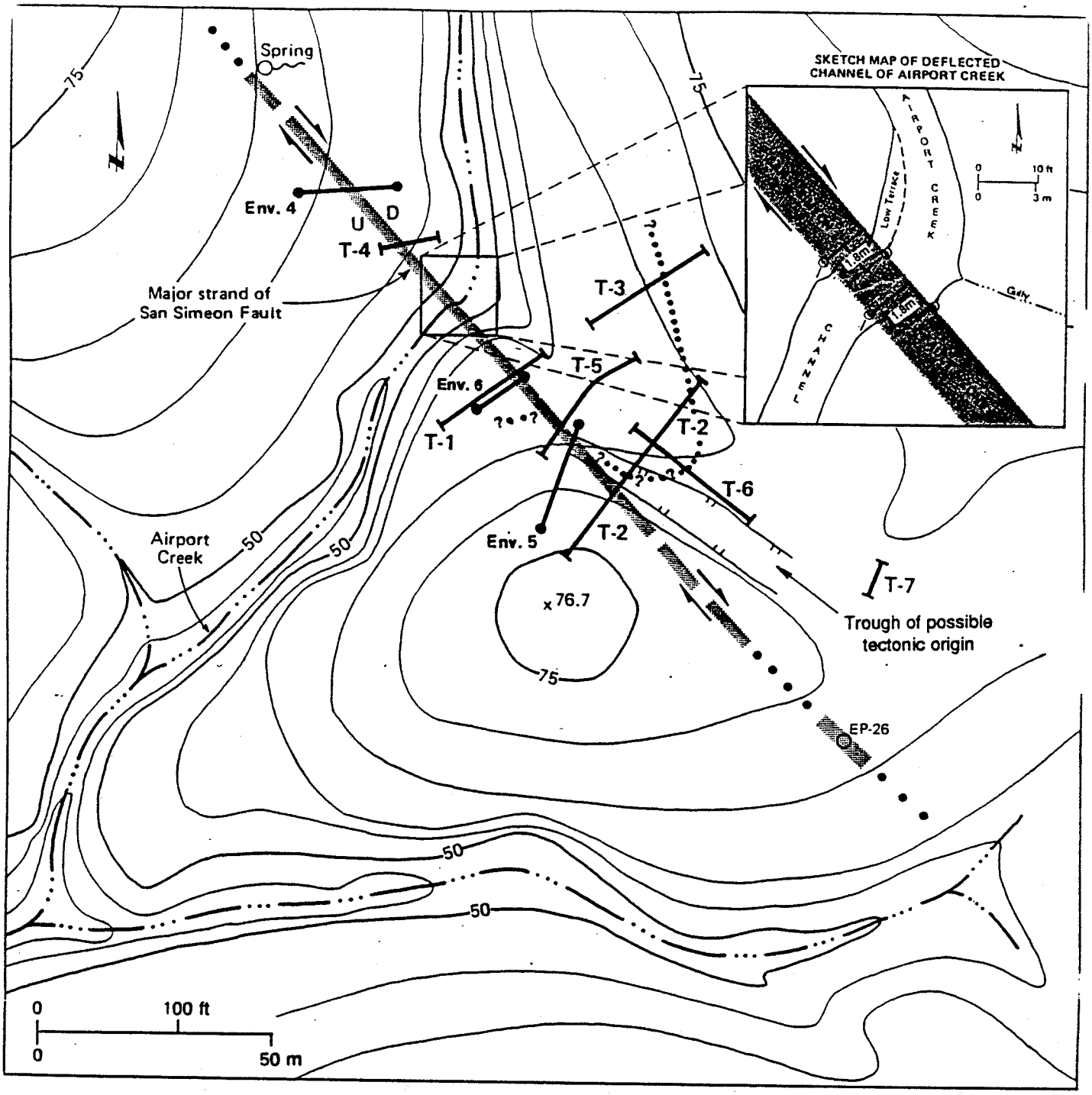

EXPLANATION

T-4 — 30"-wide backhoe trench

Env. 4 — Backhoe trench excavated by Envicom in 1977

EP-26 — 30"-wide backhoe exploratory pit

50 — Topographic contour showing elevation in feet; contour interval 5'

U D — Trace of fault exposed in trenches; dashed where approximate, dotted where concealed; U=up, D=down; arrows indicate relative sense of horizontal displacement

? — Approximate limit of Holocene fluvial terrace surface; queried where poorly constrained

Figure 13. Map of Airport Creek site showing locations of trenches, exploratory pits, and deflected channel.

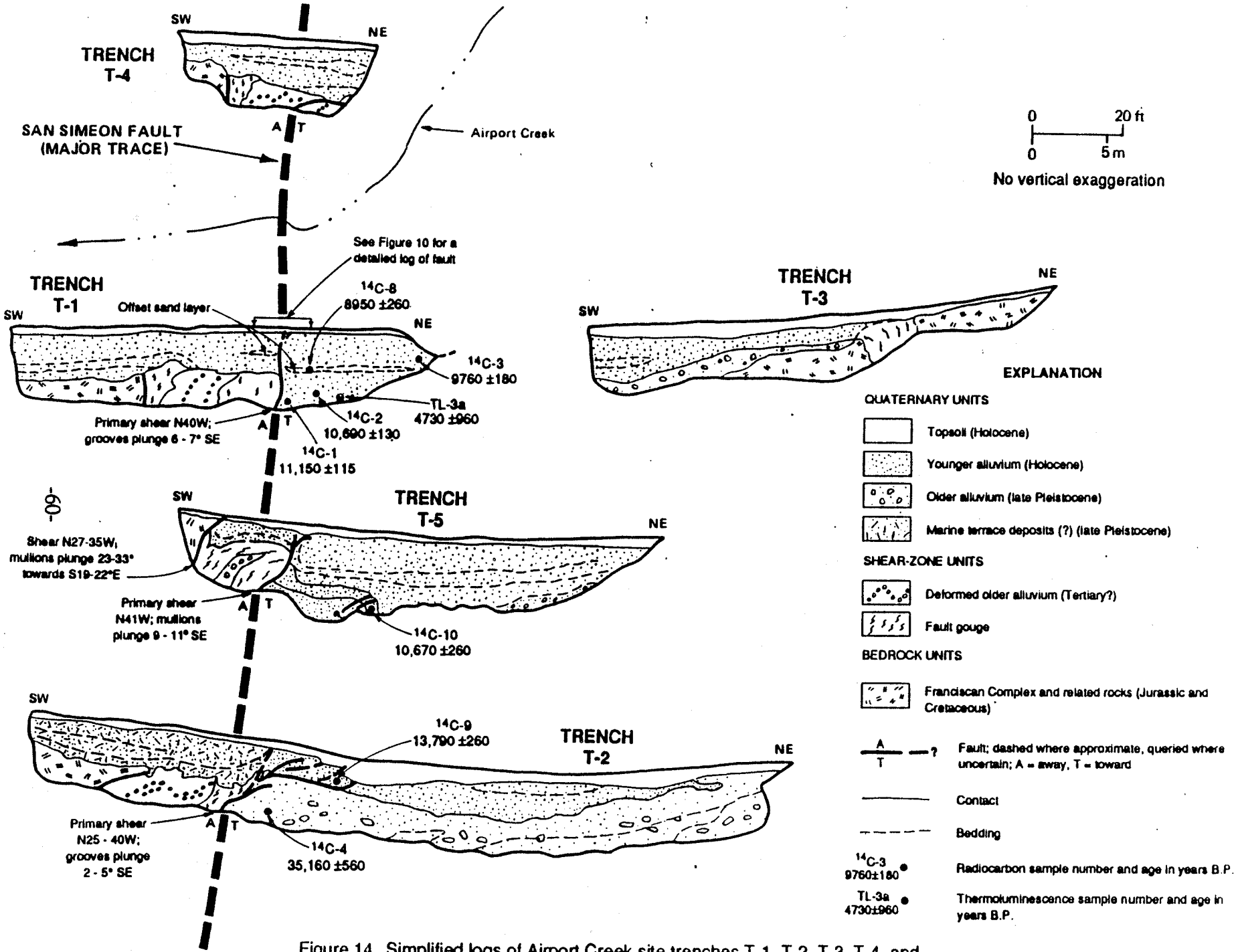

Figure 14. Simplified logs of Airport Creek site trenches T-1, T-2, T-3, T-4, and T-5 showing a major strand of the San Simeon fault (view to NW).

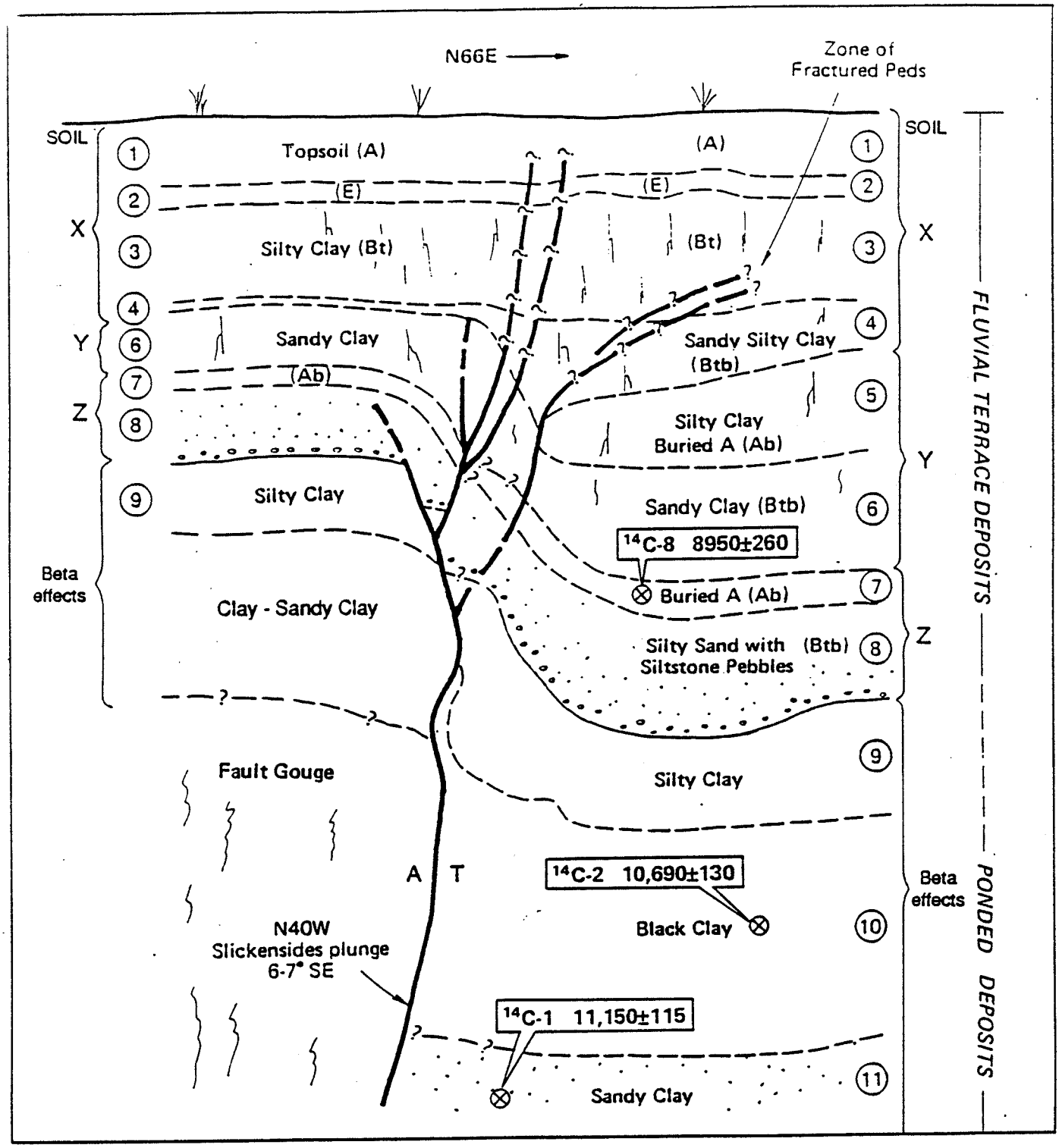

EXPLANATION

X — Modern soil

Y, Z — Buried paleosols

A T — Fault; dashed where approximately located, queried where uncertain, A/T (away, toward) indicate apparent relative sense of displacement

Contact; dashed where approximately located, queried where uncertain

⊗ — Radiocarbon sample; age in years B.P.

0 — 2 ft
0 — 1 m
No vertical exaggeration

Figure 15. Detailed log of San Simeon fault strand exposed in NW wall of Airport Creek trench T-1.

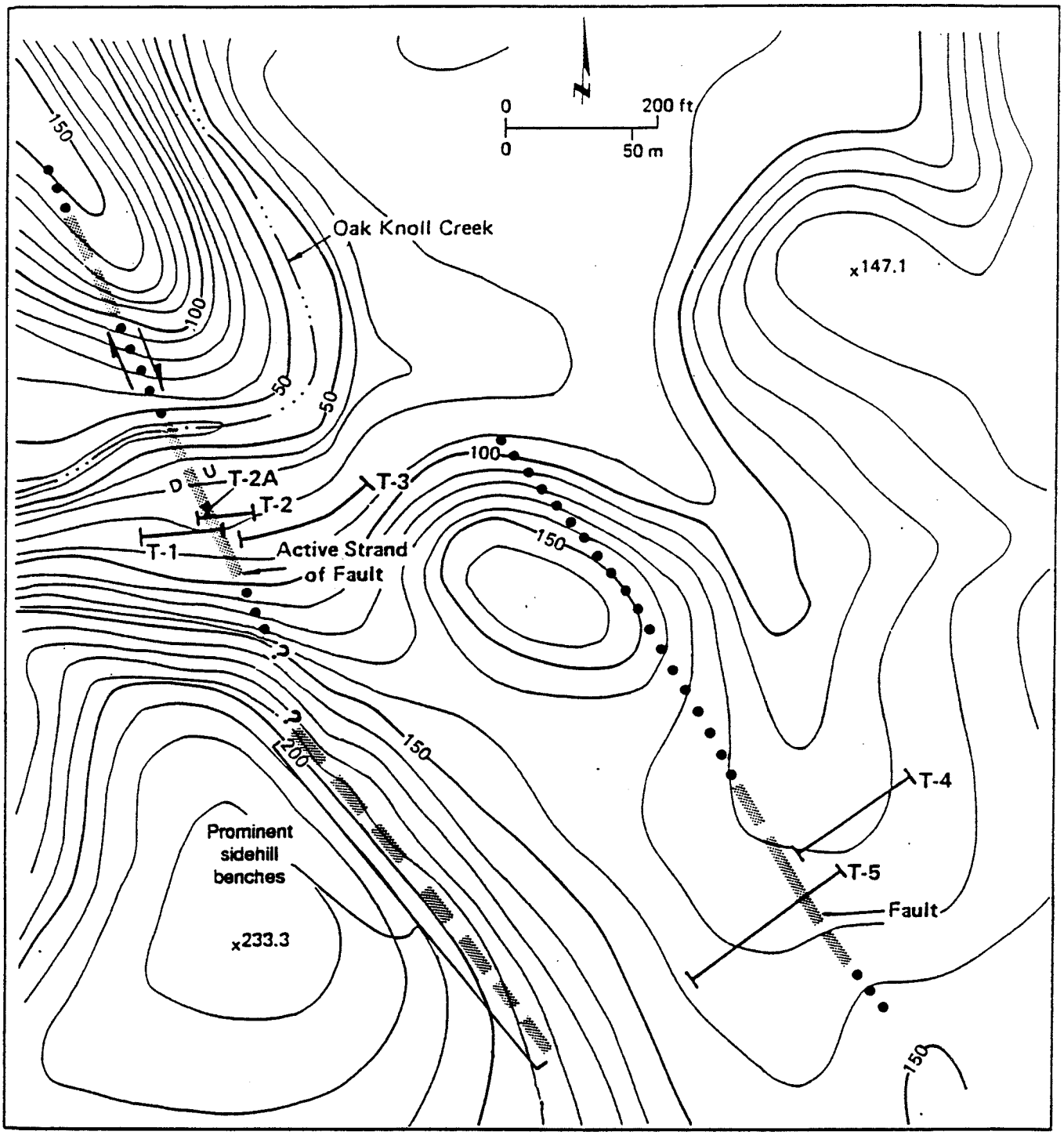

EXPLANATION

30"-wide backhoe trench

150 Topographic contour showing elevation in feet; contour interval 10'

U D ?

Trace of fault exposed in trenches; dashed where approximate, dotted where concealed or inferred, queried where connection uncertain; U = up, D = down; arrows indicate sense of horizontal displacement

Figure 16. Map of Oak Knoll Creek site showing location of trenches.

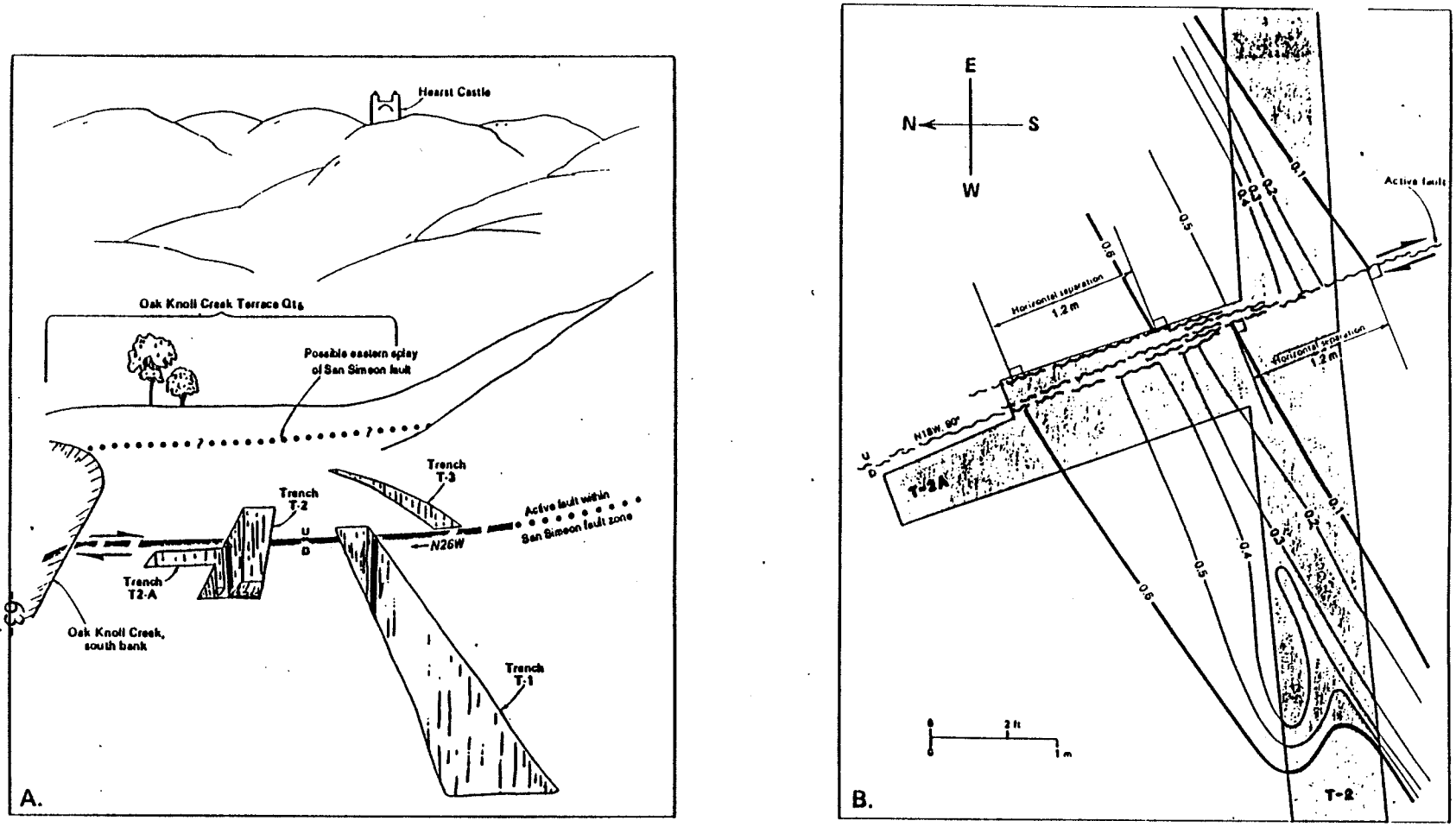

EXPLANATION

Trace of fault exposed in trenches; dashed where approximate, dotted where concealed; U=up, D=down; arrows indicate relative direction of displacement

N26W — Trend of fault

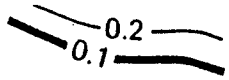

Isopachs (lines of equal thickness) on clayey sand marker horizon; contour interval 0.1 ft. Heavy contours used as piercing points

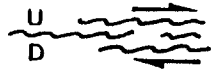

Fault; U=up, D=down; paired arrows indicate relative sense of displacement

N18W, 90° — Orientation of fault at elevation of clayey sand marker horizon

Figure 17. A. Sketch showing an active fault within the San Simeon fault zone exposed in trenches on Oak Knoll Creek fluvial terrace Qt_5.
B. Isopach of clayey sand marker horizon showing right-lateral separation across active San Simeon fault trace.

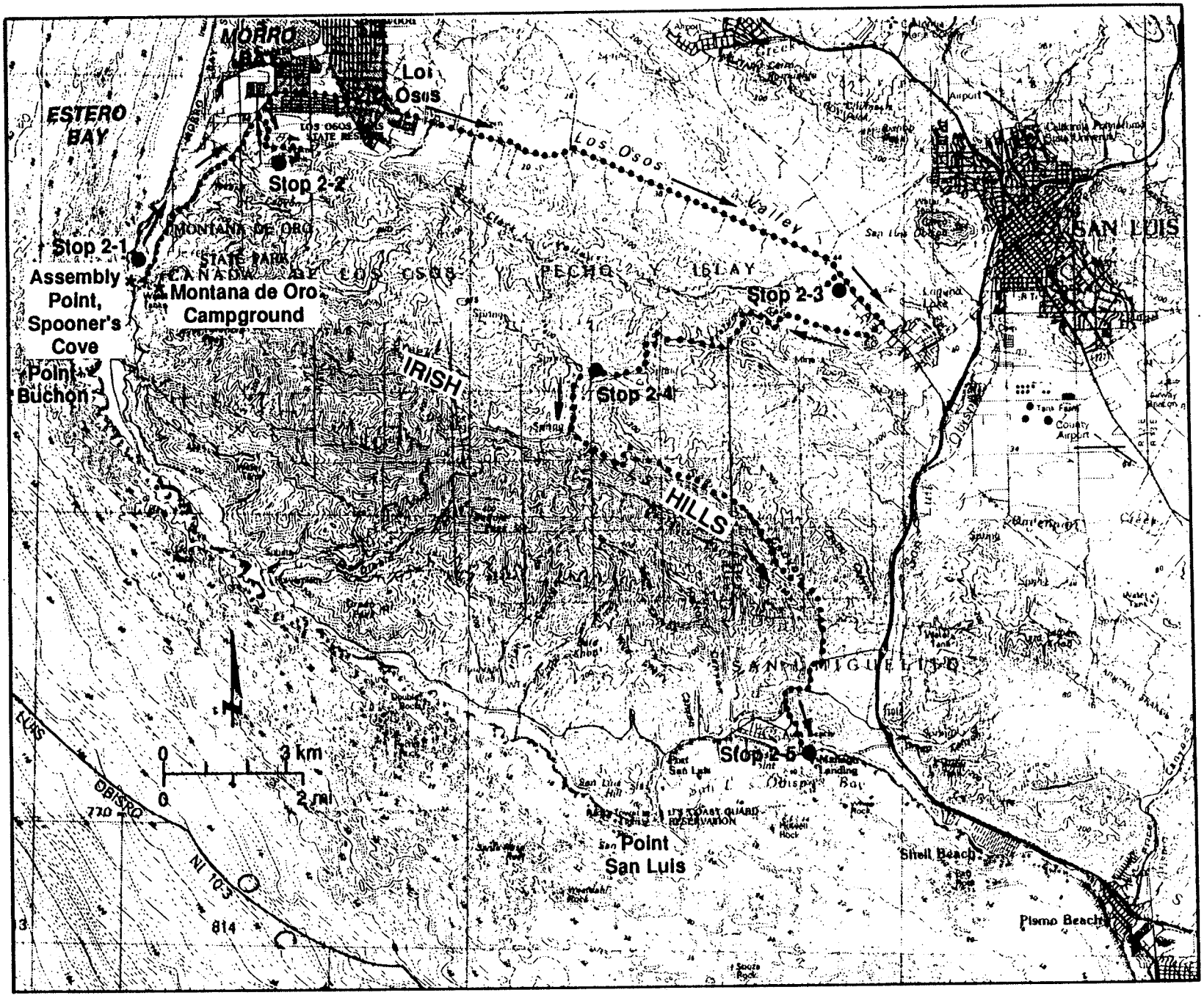

Figure 18. Location map showing field trip route (Day 2).

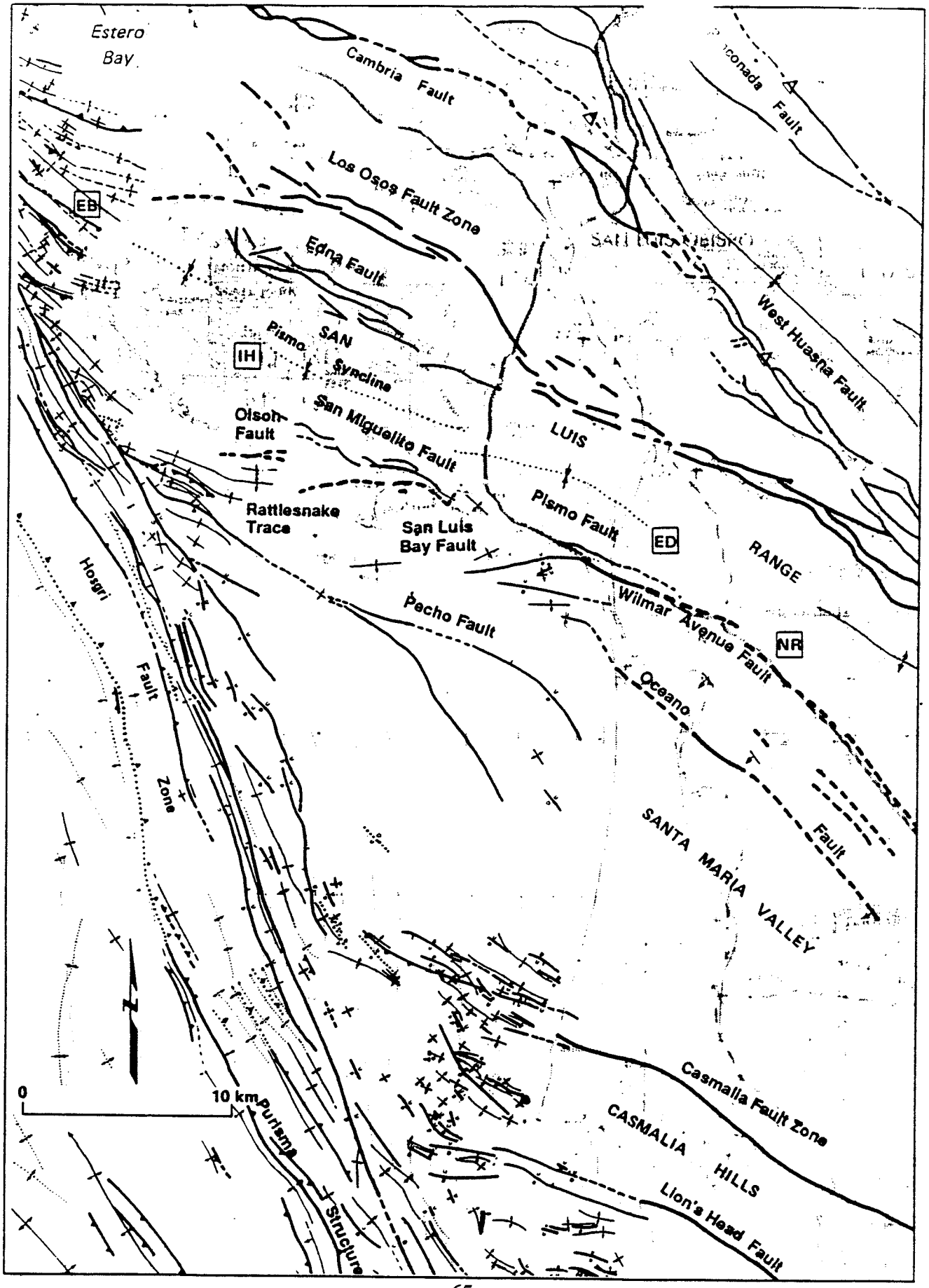

Figure 19. Map of faults and folds in the onshore and offshore regions of south-central California. Subblocks of the San Luis Range are: EB, Estero Bay; IH, Irish Hills; ED, Edna; and NR, Newsom Ridge.

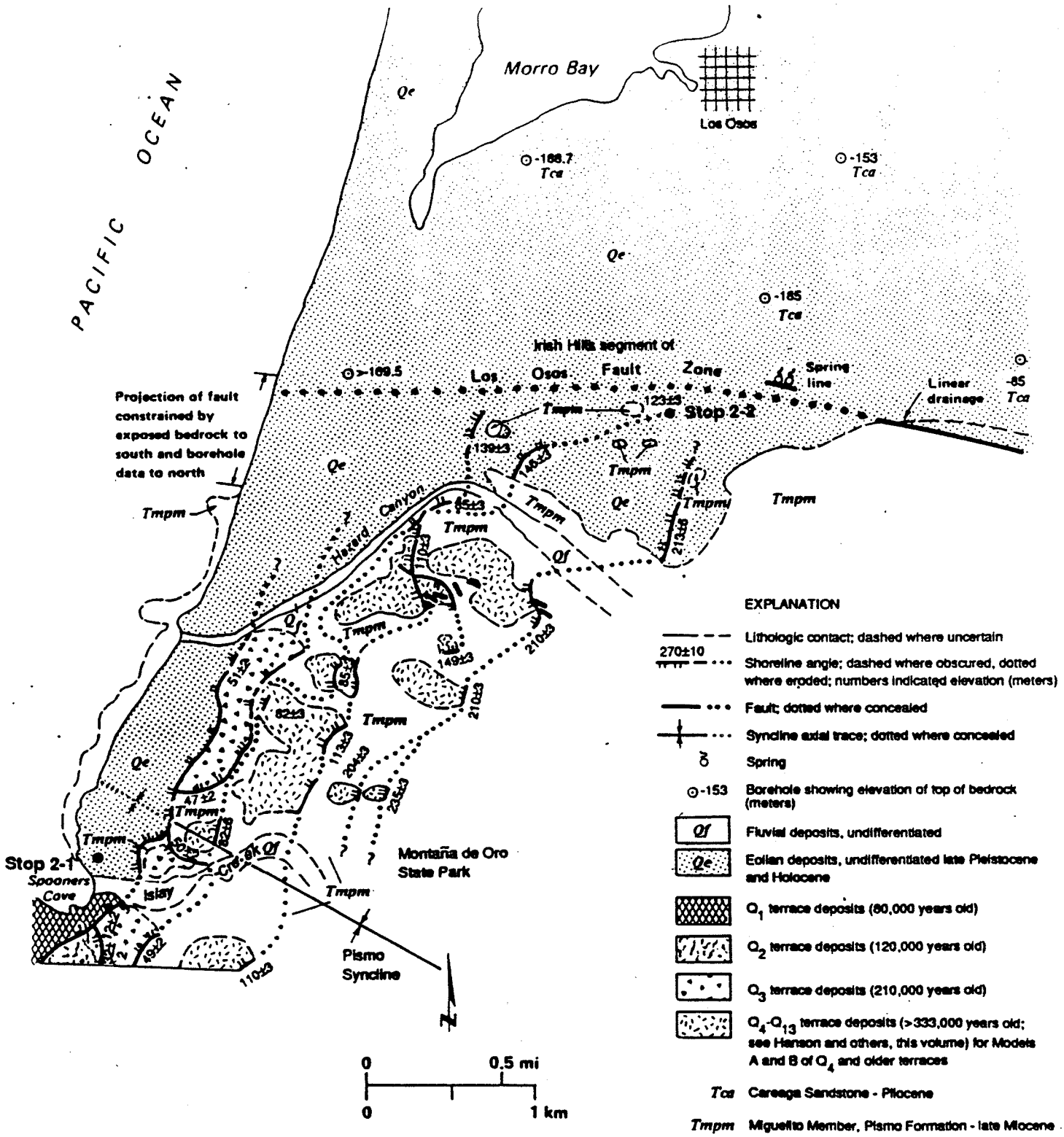

Figure 20. Generalized geologic map of Quaternary deposits in the Montaña de Oro and Morro Bay areas illustrating distribution of marine terraces and interpreted location of the Los Osos fault zone. (After Hanson and others, this volume).

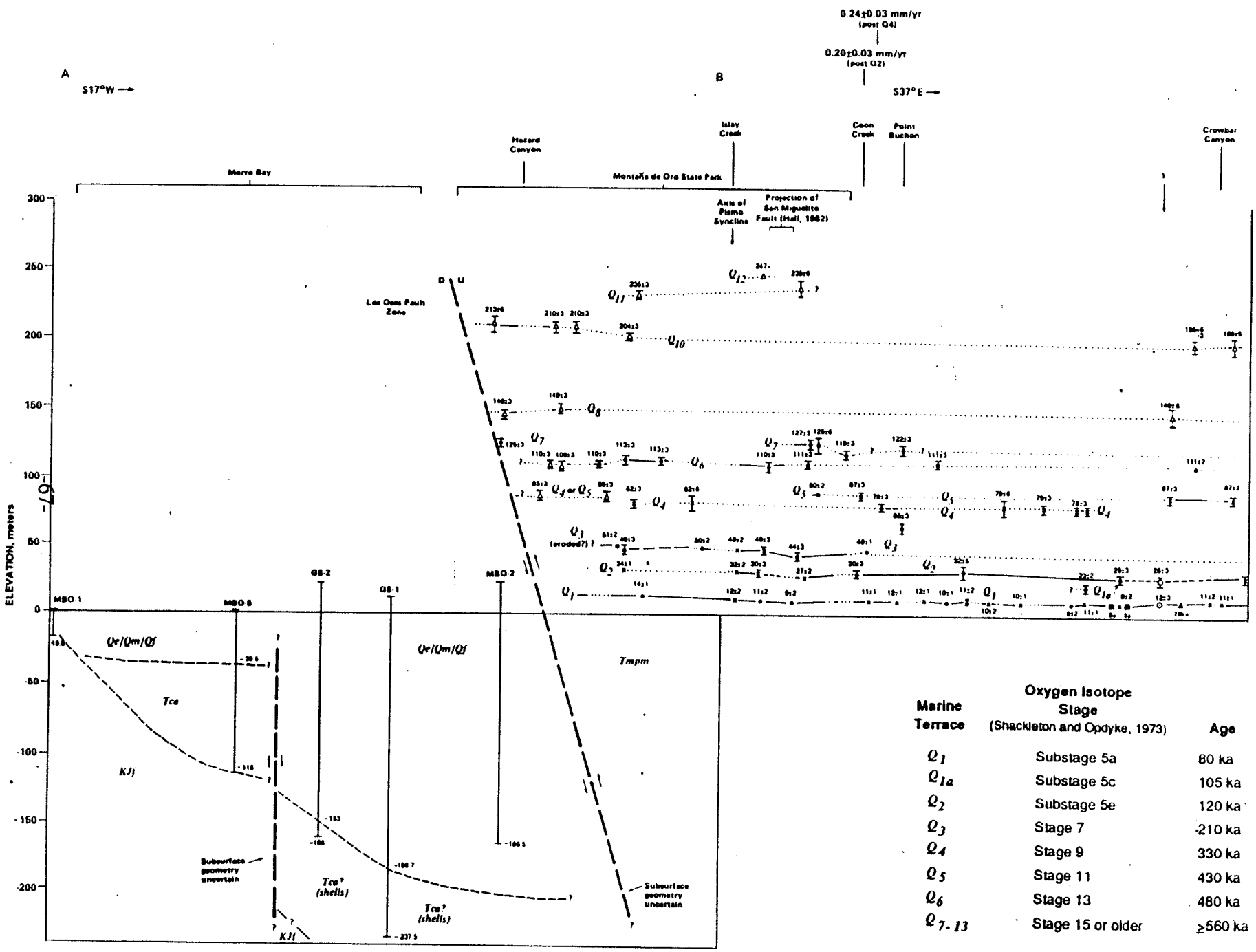

Marine Terrace	Oxygen Isotope Stage (Shackleton and Opdyke, 1973)	Age
Q_1	Substage 5a	80 ka
Q_{1a}	Substage 5c	105 ka
Q_2	Substage 5e	120 ka
Q_3	Stage 7	210 ka
Q_4	Stage 9	330 ka
Q_5	Stage 11	430 ka
Q_6	Stage 13	480 ka
Q_{7-13}	Stage 15 or older	≥560 ka

Figure 21. Lor nal profiles of marine terraces betwe rro Bay and Crowbar Canyon cross the Pismo Syncline and n of the San ault. No ver eration. For location of Hanson and others (th volume)

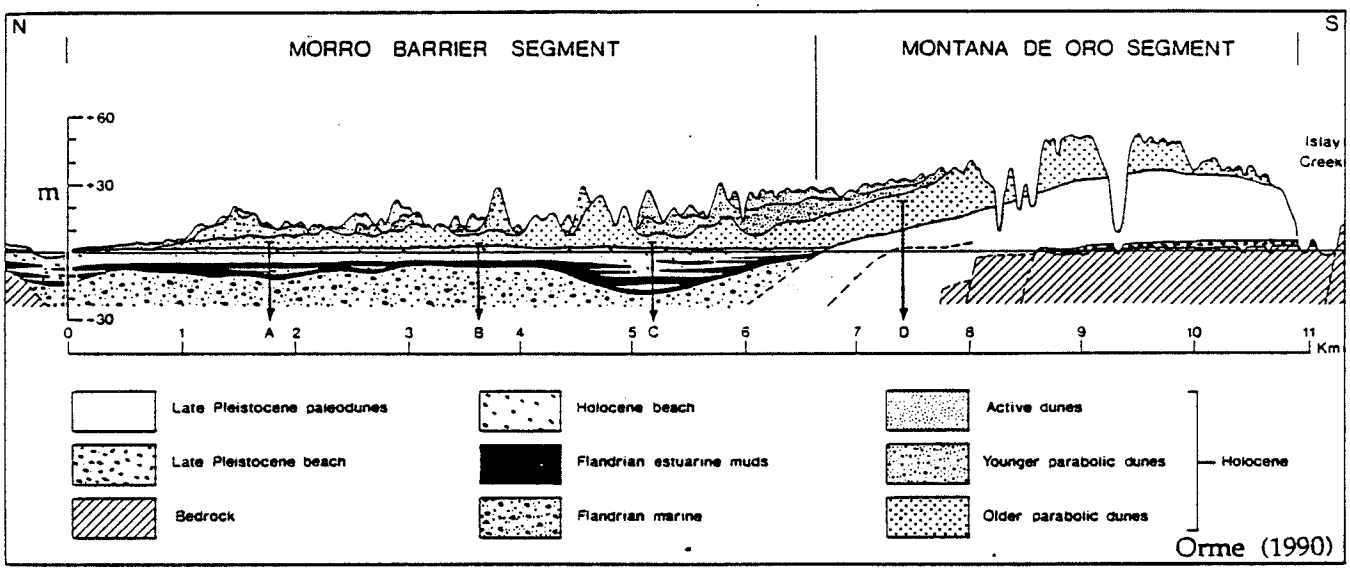

Figure 22. Cross section of late Quaternary dunes and other deposits, Morro Bay, California.

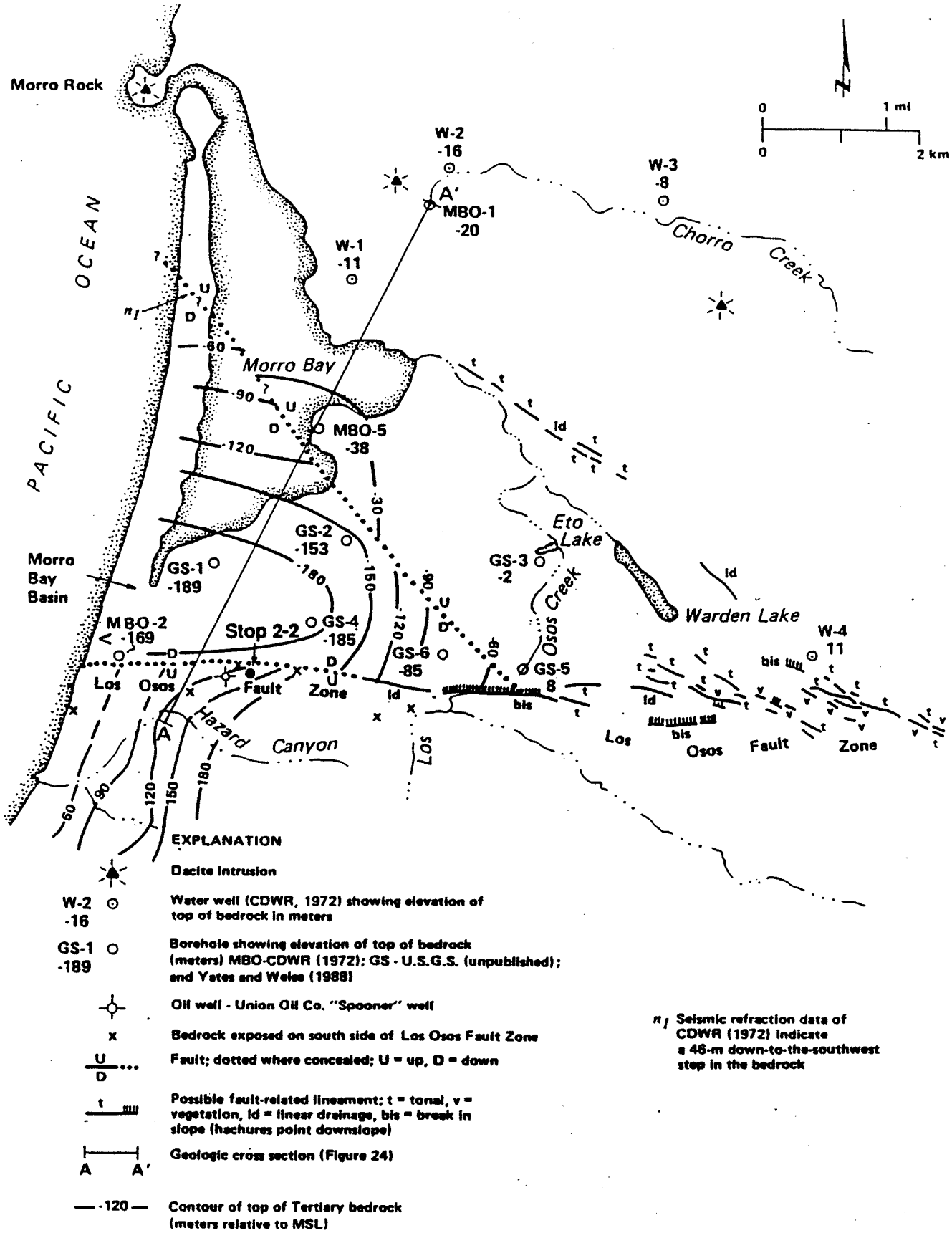

Figure 23. Map of Morro Bay showing locations of wells and interpreted location of the Los Osos fault zone and the Morro Bay basin.

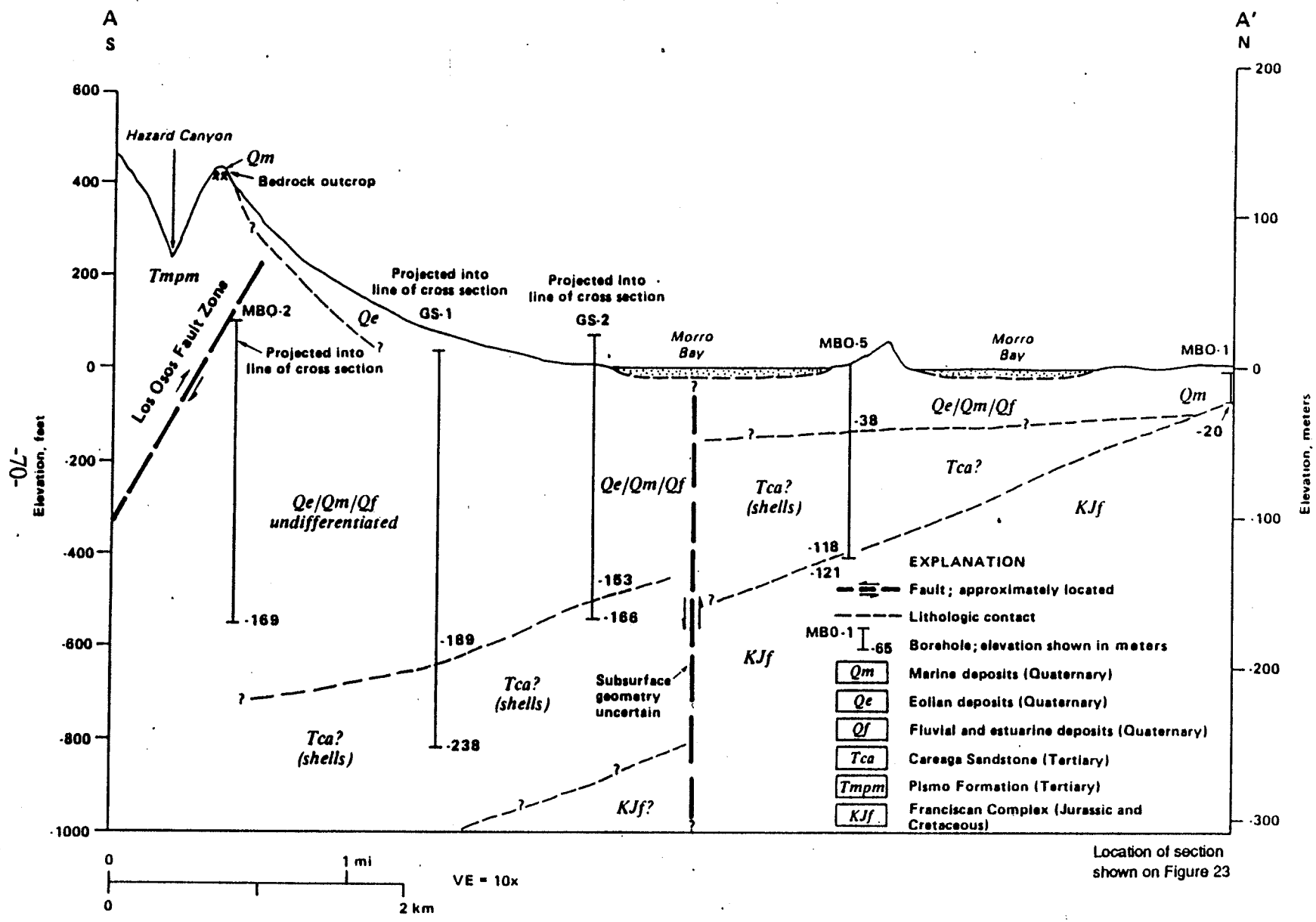

Figure 24. Geologic cross section across Morro Bay area illustrating str[illegible]raphic and structural relationships associated with the Morro Bay basin.

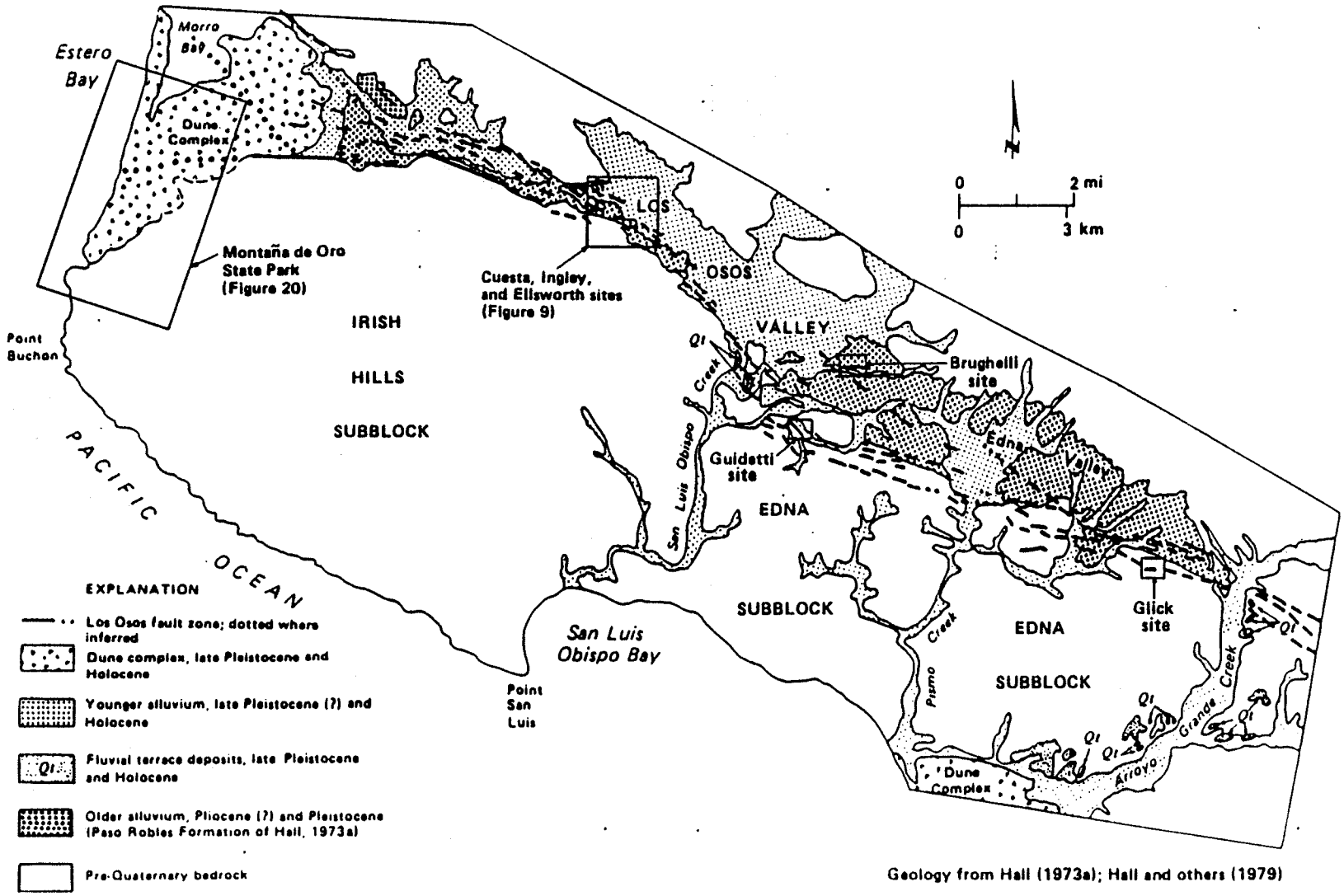

Figure 25. Map showing distribution of Pliocene (?) and Quaternary alluvial deposits along the Los Osos fault zone and the location of areas of detailed geologic investigation.

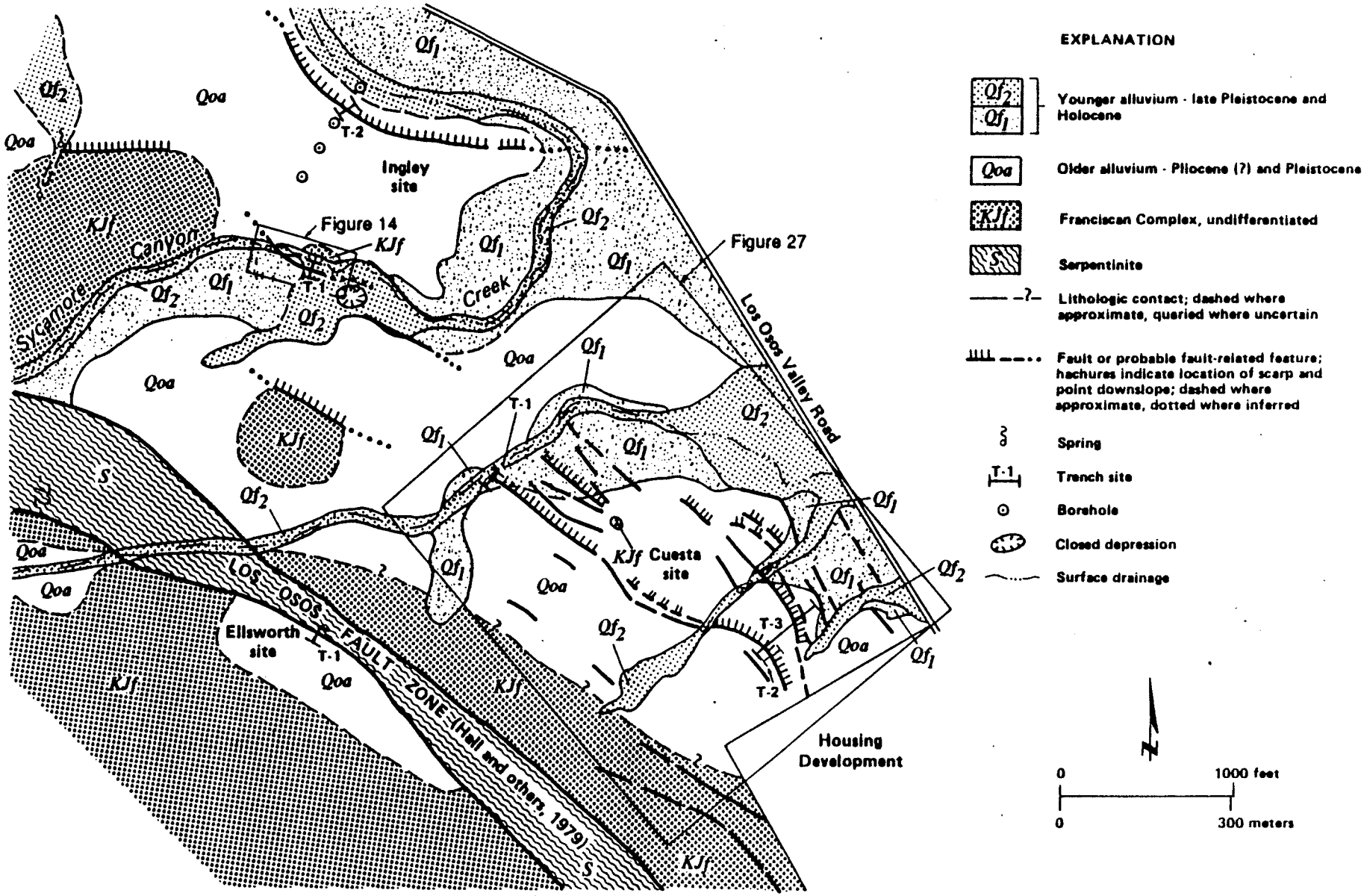

Figure 26. Geologic map of the Cuesta, Ingley, and Ellsworth sites showing location of the Los Osos fault identified by Hall and others (1979) and additional faults and fault-related features identified during this geologic investigation.

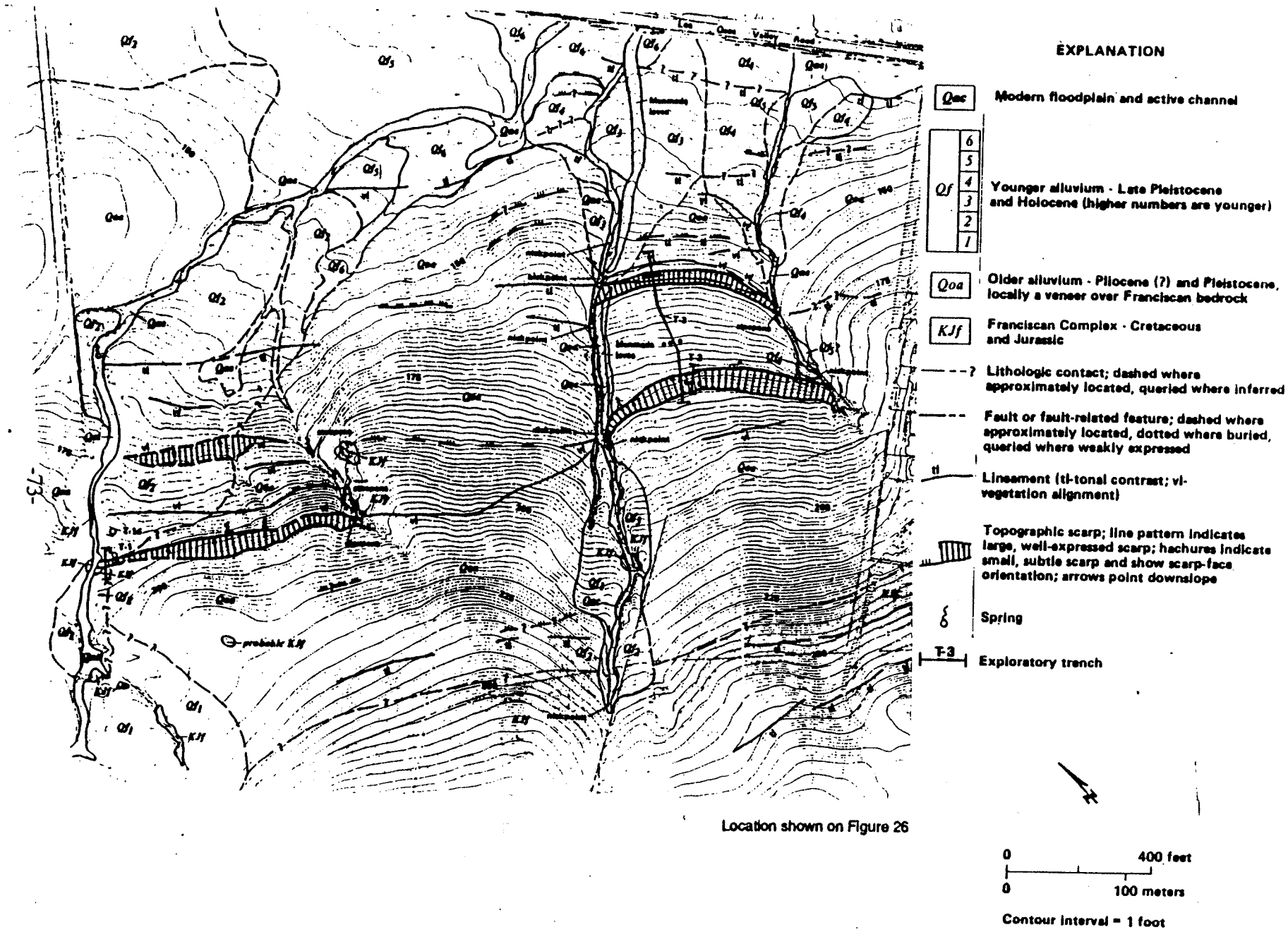

Figure 27. Detailed geologic map of the northeastern part of the Cuesta site, Los Osos fault zone.

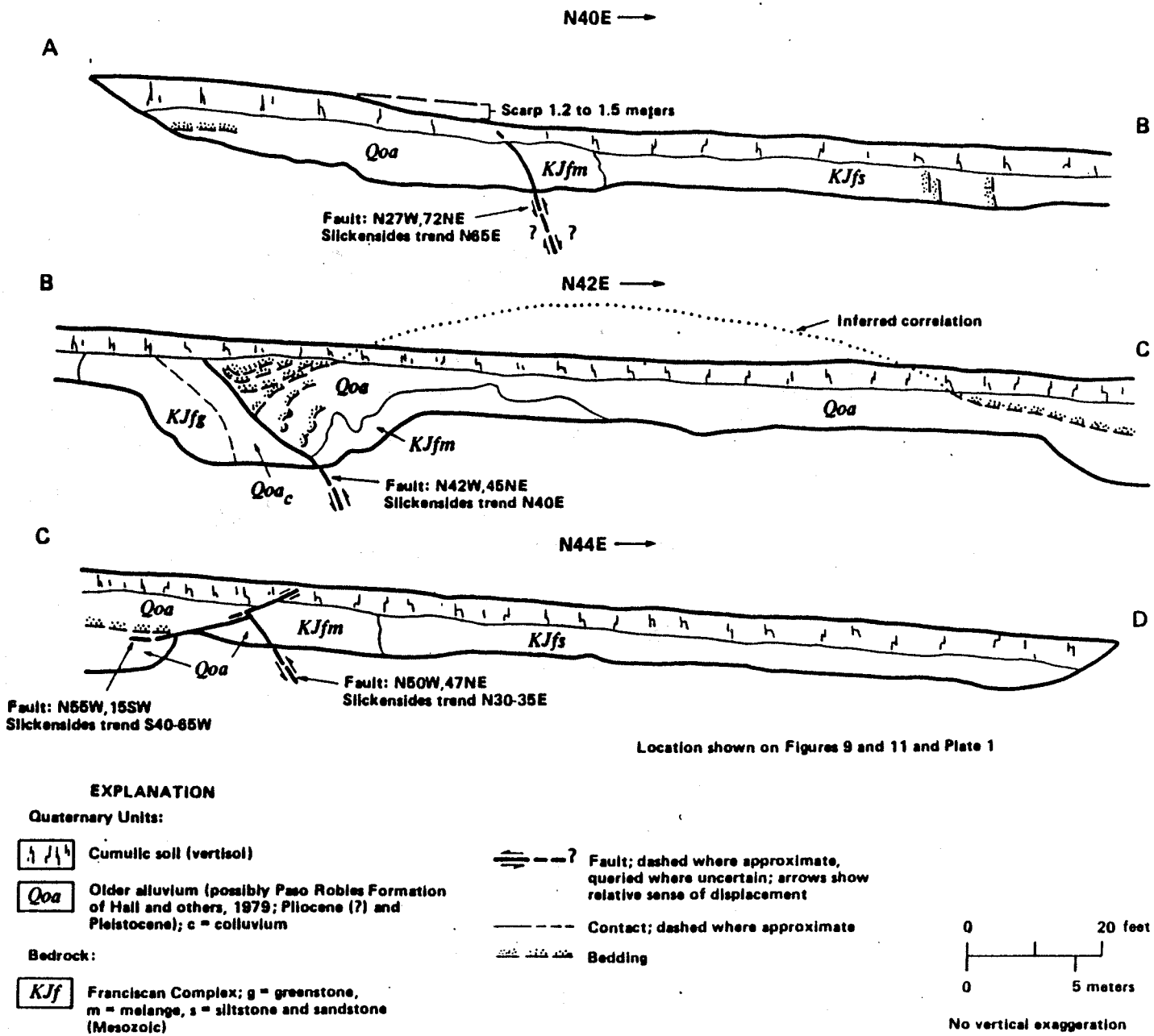

Figure 28. Diagrammatic log of Cuesta Trench T-3 showing dip-slip faults in the inferred hanging wall block of the Los Osos fault.

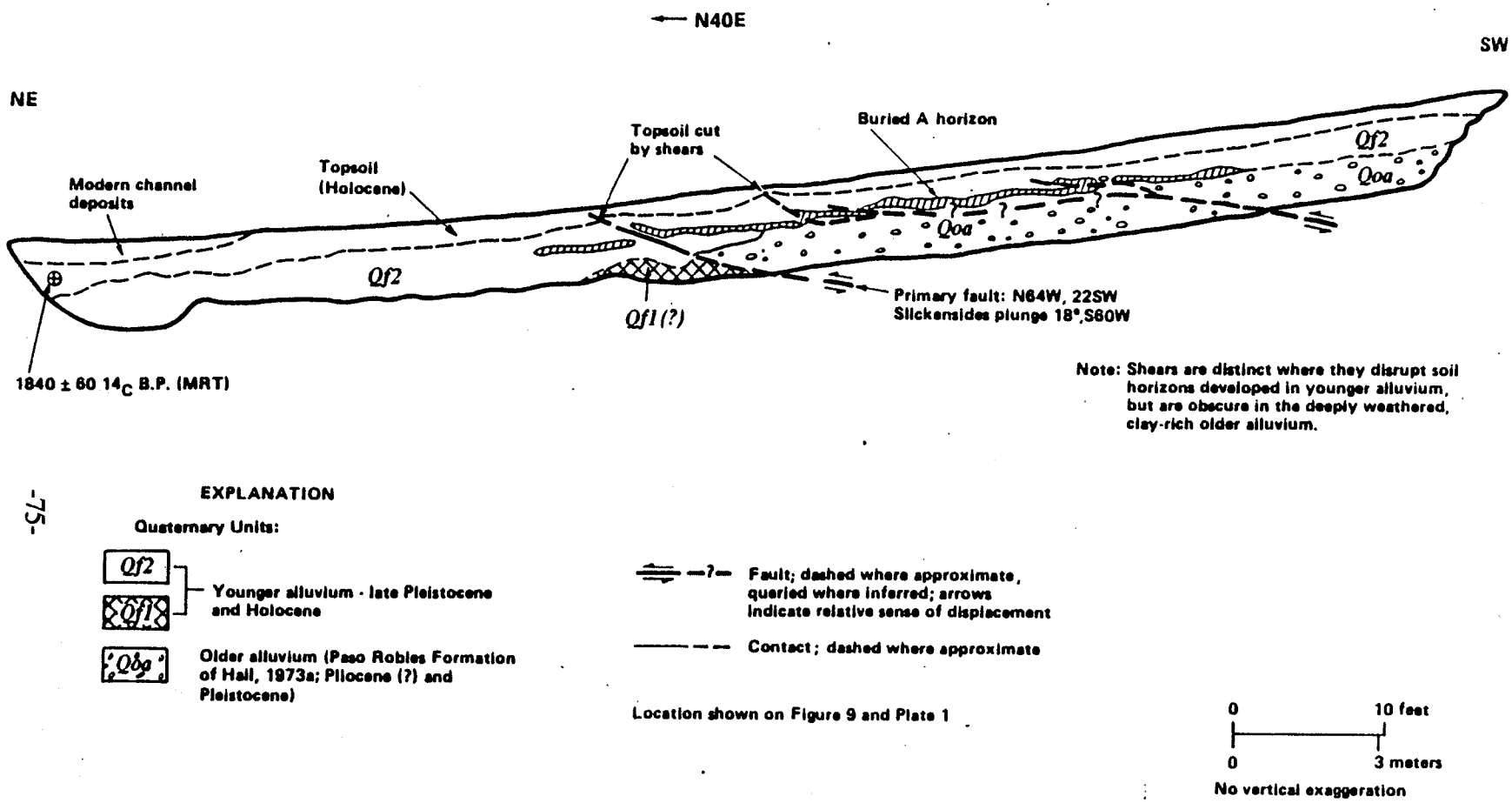

Figure 29. Diagrammatic log of Ingley trench T-2 showing primary zone of thrusting within the Los Osos fault zone.

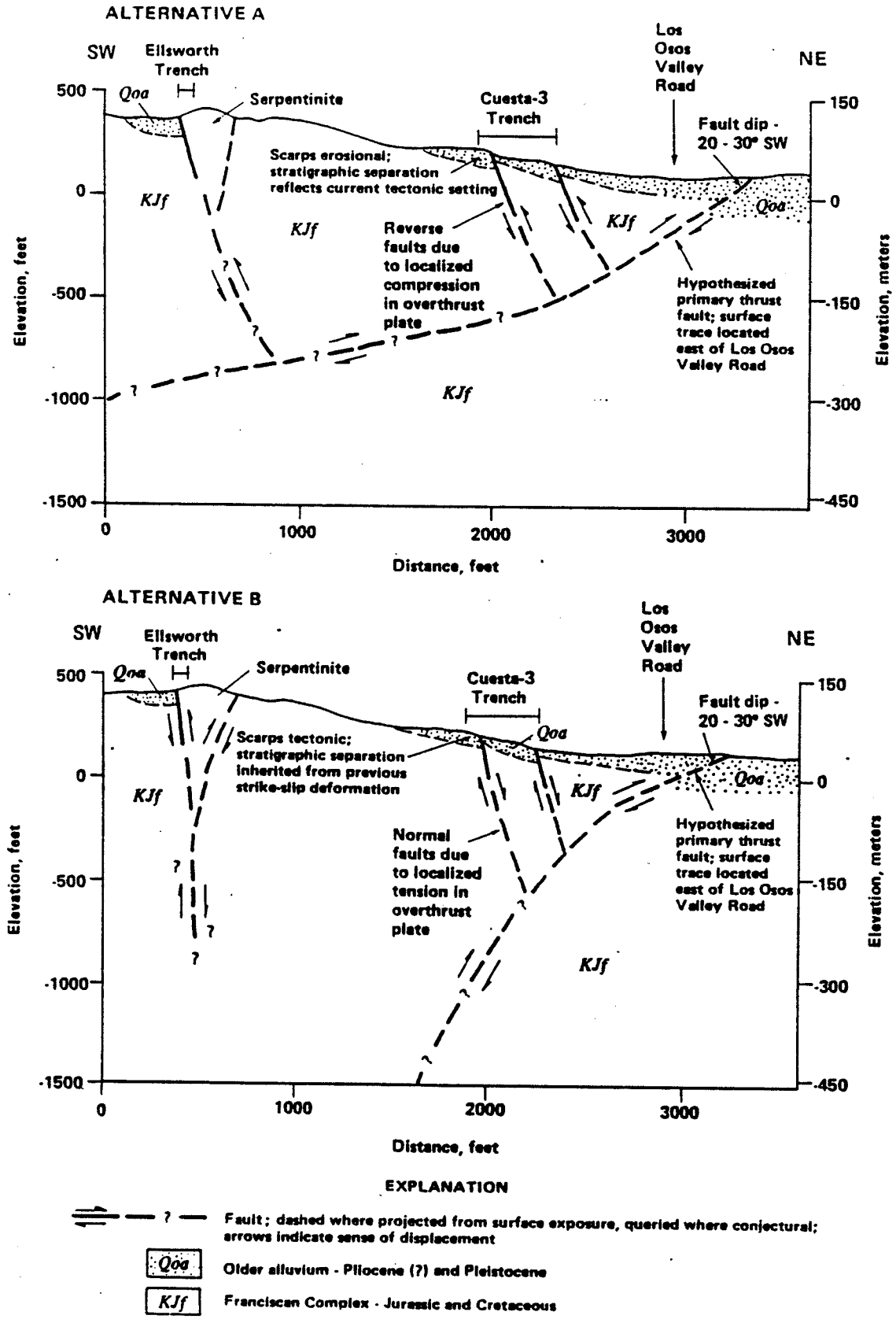

Figure 30. Schematic geologic cross sections between the Ellsworth and Cuesta properties illustrating alternative interpretations of fault geometry based on near-surface stratigraphic, geomorphic and structural relationships. A - primary fault flattens with depth; B - primary fault steepens with depth.

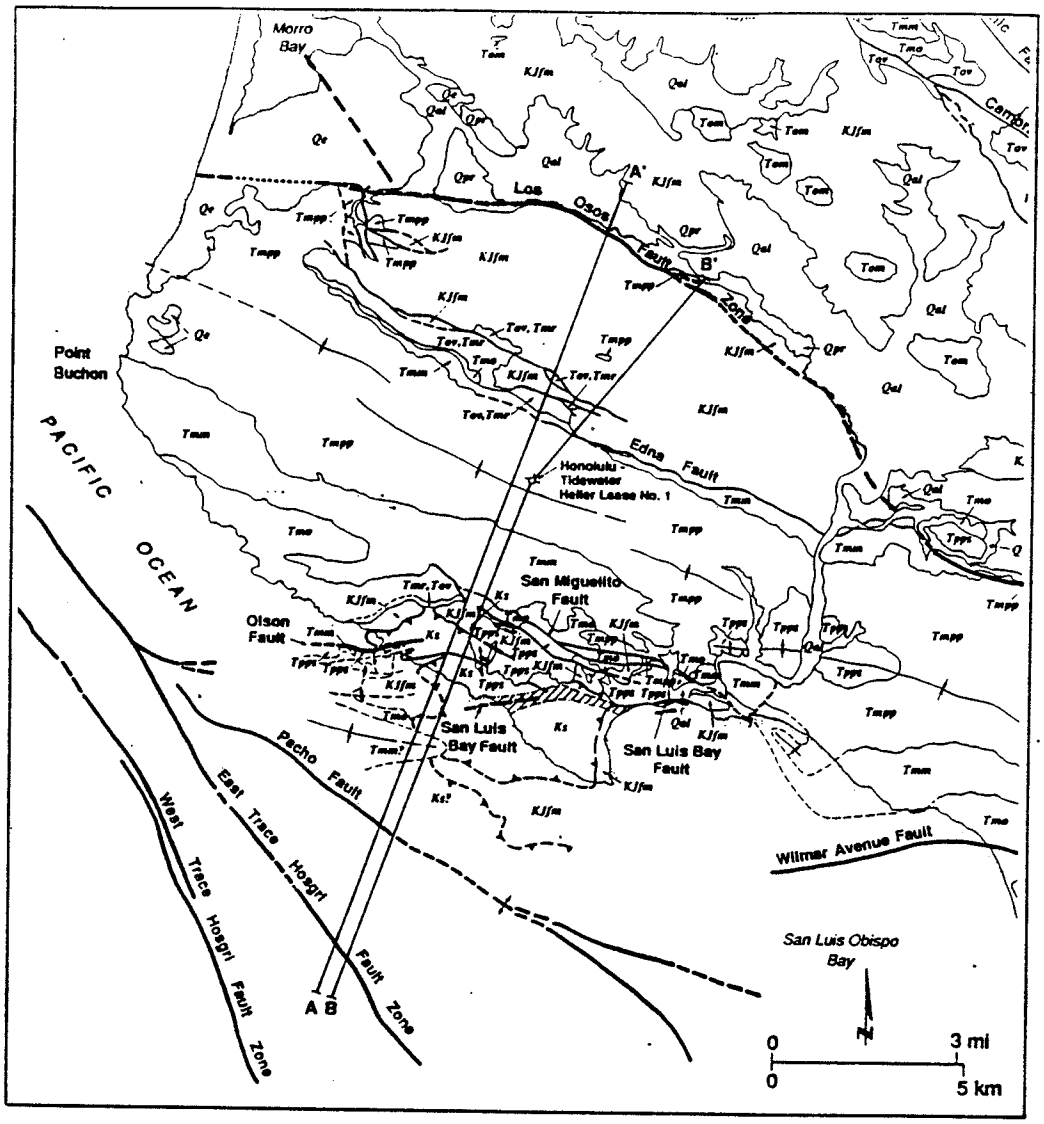

EXPLANATION

Geologic Symbols

- Fault; dashed where approximately located, dotted where concealed; teeth on inferred upper plate of thrust fault; heavy line where fault offsetting Squire Member and younger geologic units
- Contact, dashed where approximately located
- Onshore trace of San Luis Bay fault
- Anticline, dashed where approximately located
- Syncline, dashed where approximately located

Stratigraphic Units

Quaternary	*Qal*	Alluvium
	Qe	Eolian deposits
Pliocene	*Tpps*	Squire Member of the Pismo Formation
Pliocene-Miocene	*Tmpp*	Undifferentiated Pismo Formation
Miocene	*Tmm*	Monterey Formation
	Tmo	Obispo Formation
Oligocene	*Tmr*	Rincon Formation
	Tov	Vaqueros Sandstone
	Tom	Morro Rock-Islay Hill Complex
Jurassic-Cretaceous	*Ks*	Undifferentiated sandstone, siltstone, and conglomerate
	KJfm	Franciscan Complex rocks

Figure 31. Geologic map of the Irish Hills showing locations of prominent folds and faults in the region and location of cross sections A A' and B B'.

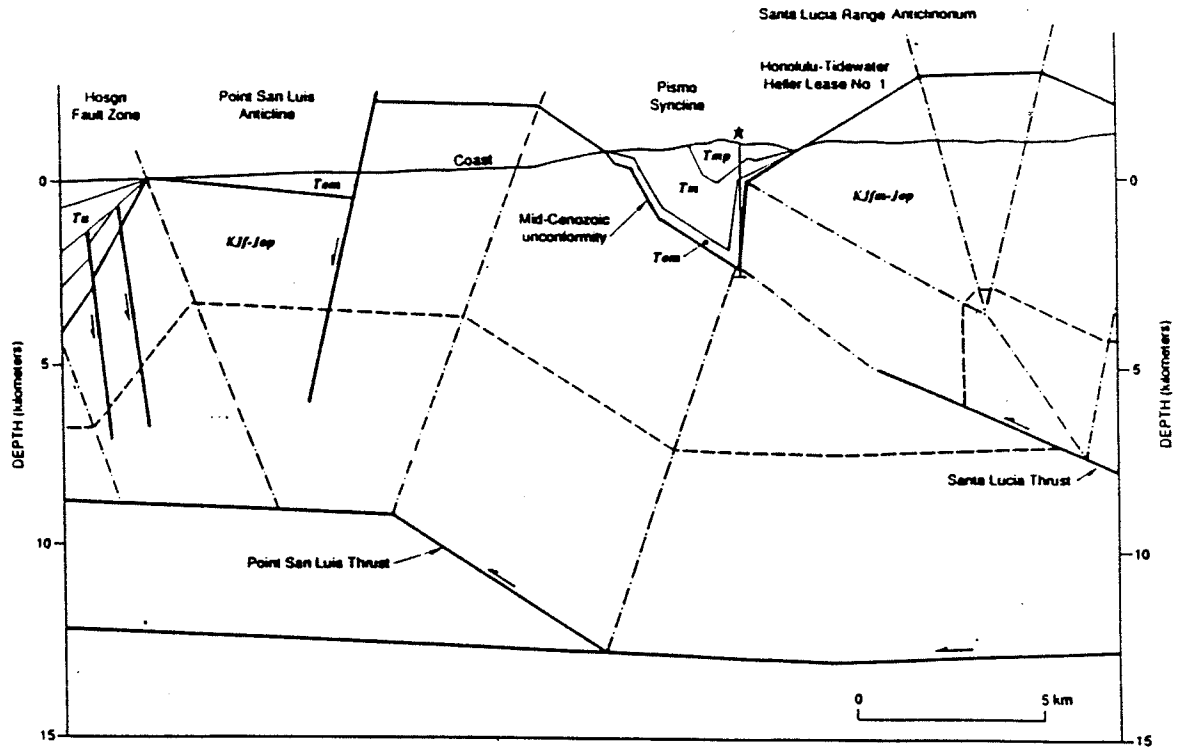

DEFORMED

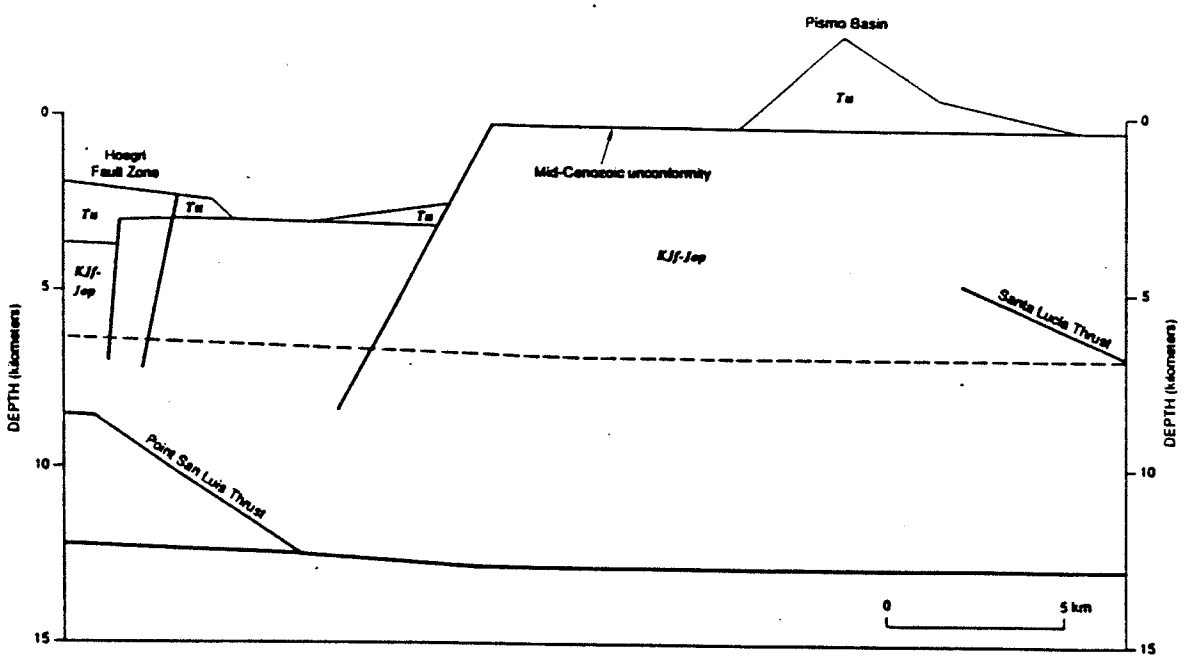

RESTORED

Figure 32. Balanced cross section across the Irish Hills by Namson and Davis (1990).

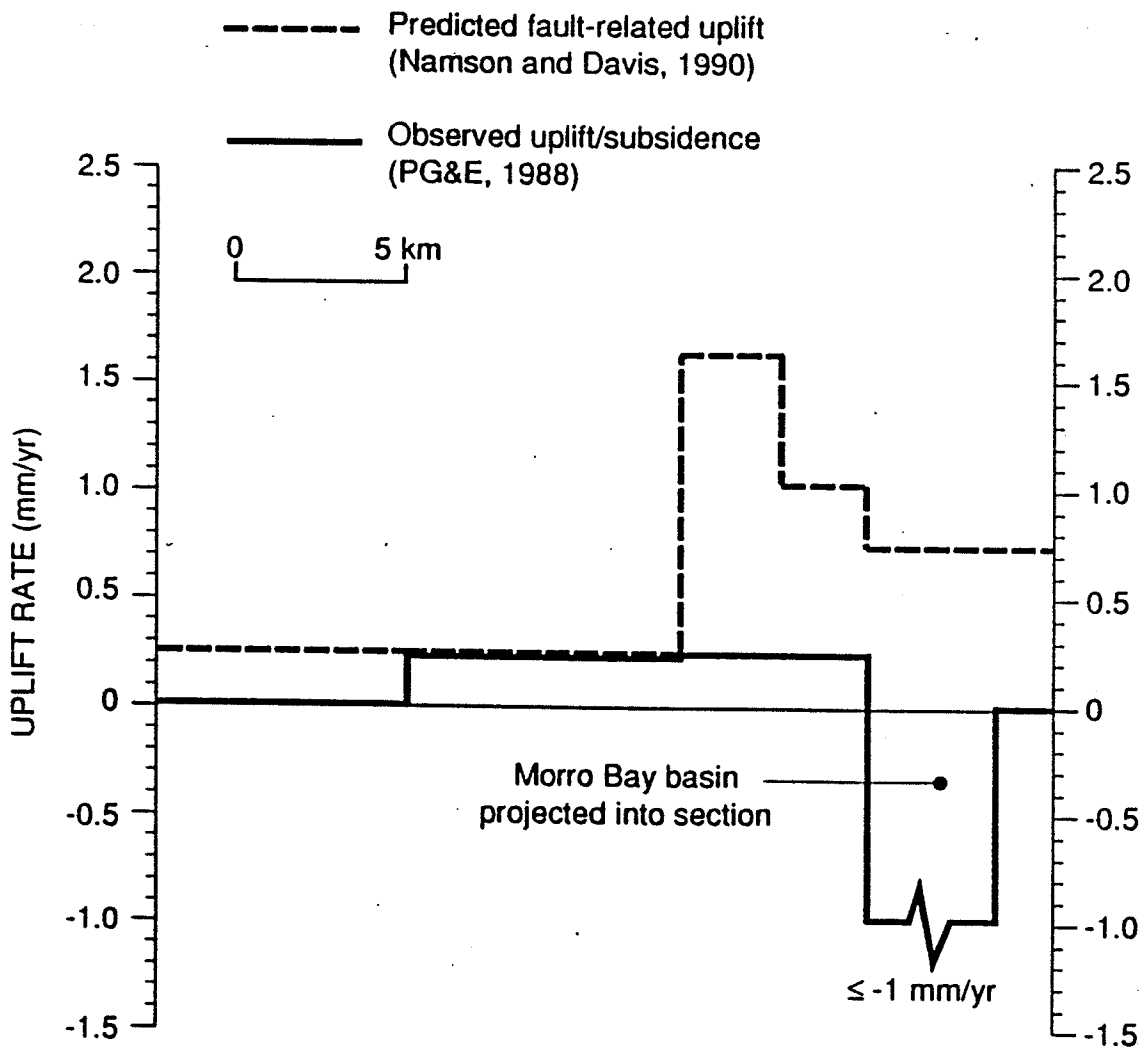

Figure 33. Predicted uplift (Namson and Davis, (1990).

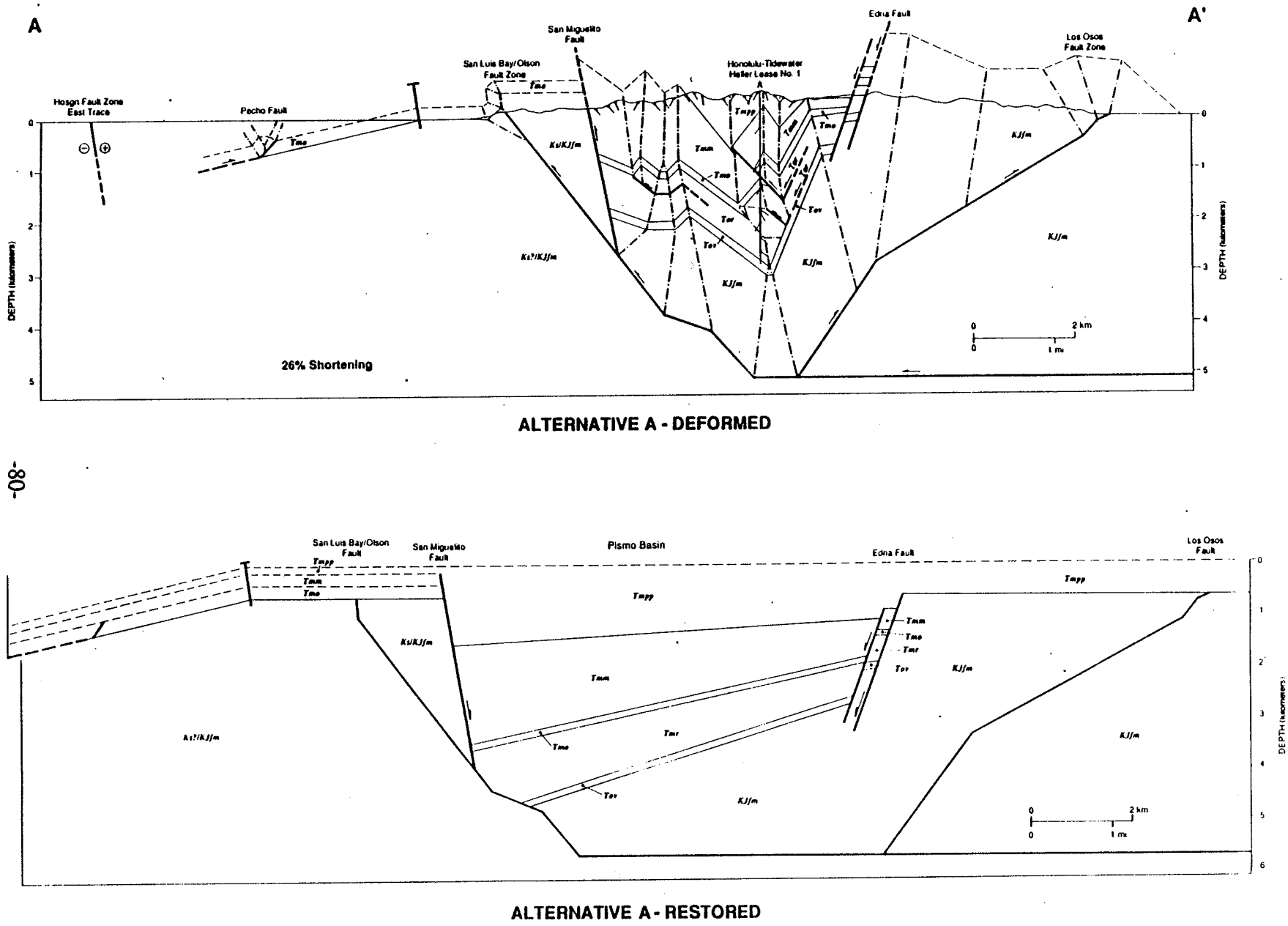

Figure 34. Alternative balanced cross sections (A A') across the Irish Hills by PG&E (1990).

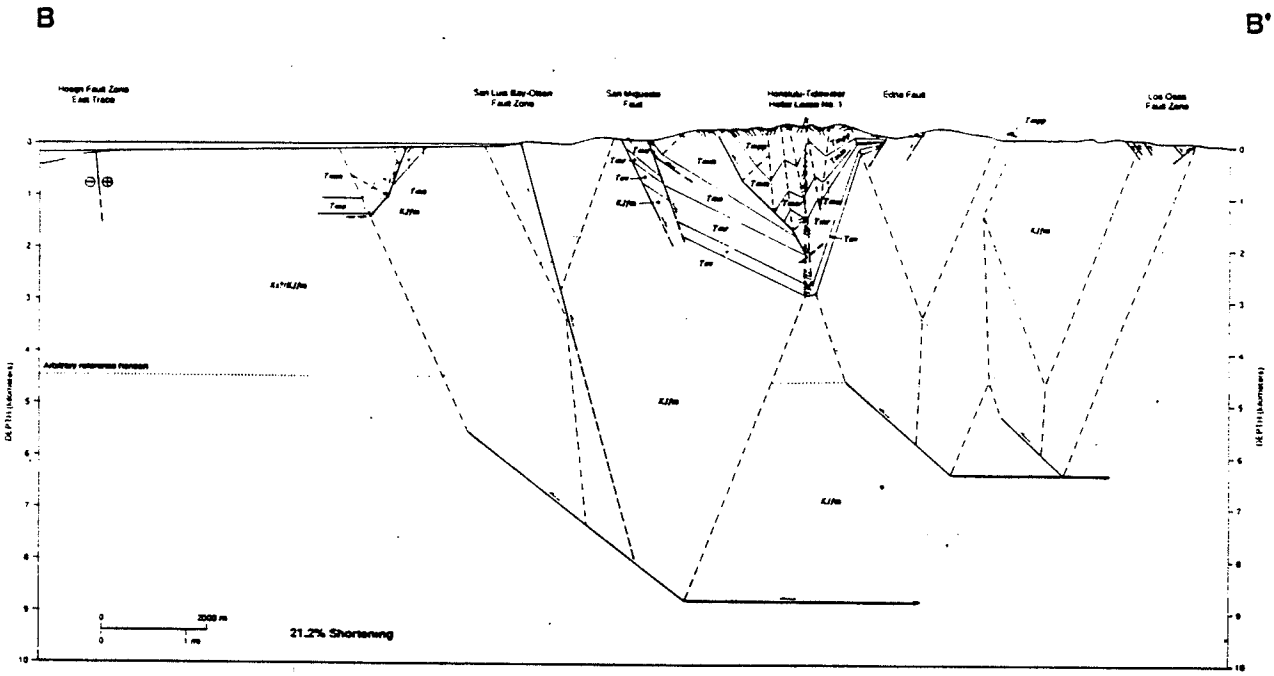

ALTERNATIVE B - DEFORMED

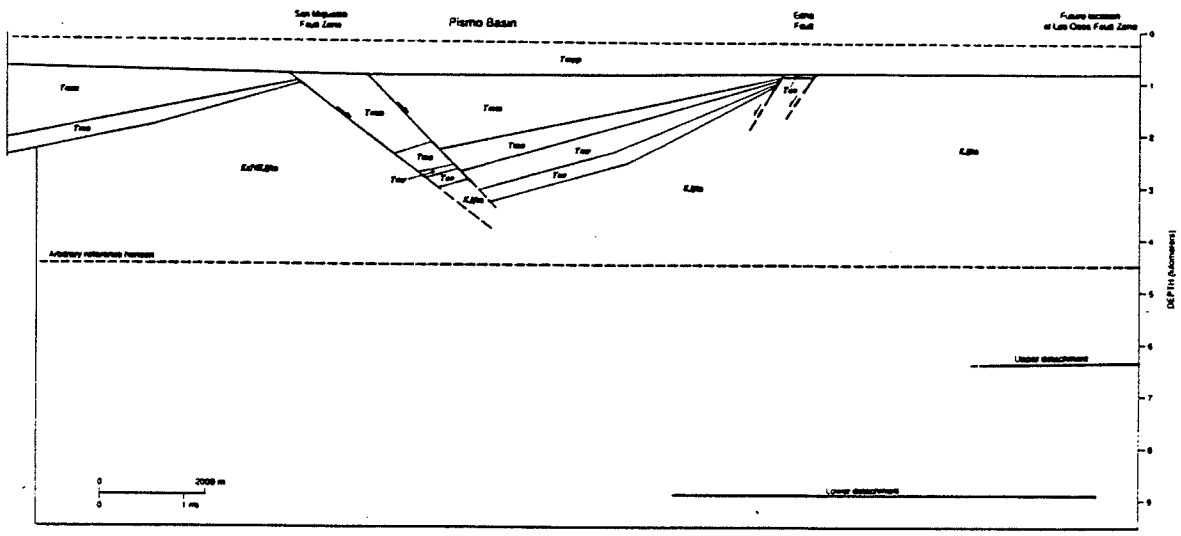

ALTERNATIVE B - RESTORED

Figure 35. Alternative balanced cross sections (B-B') across the Irish Hills by PG&E (1990).

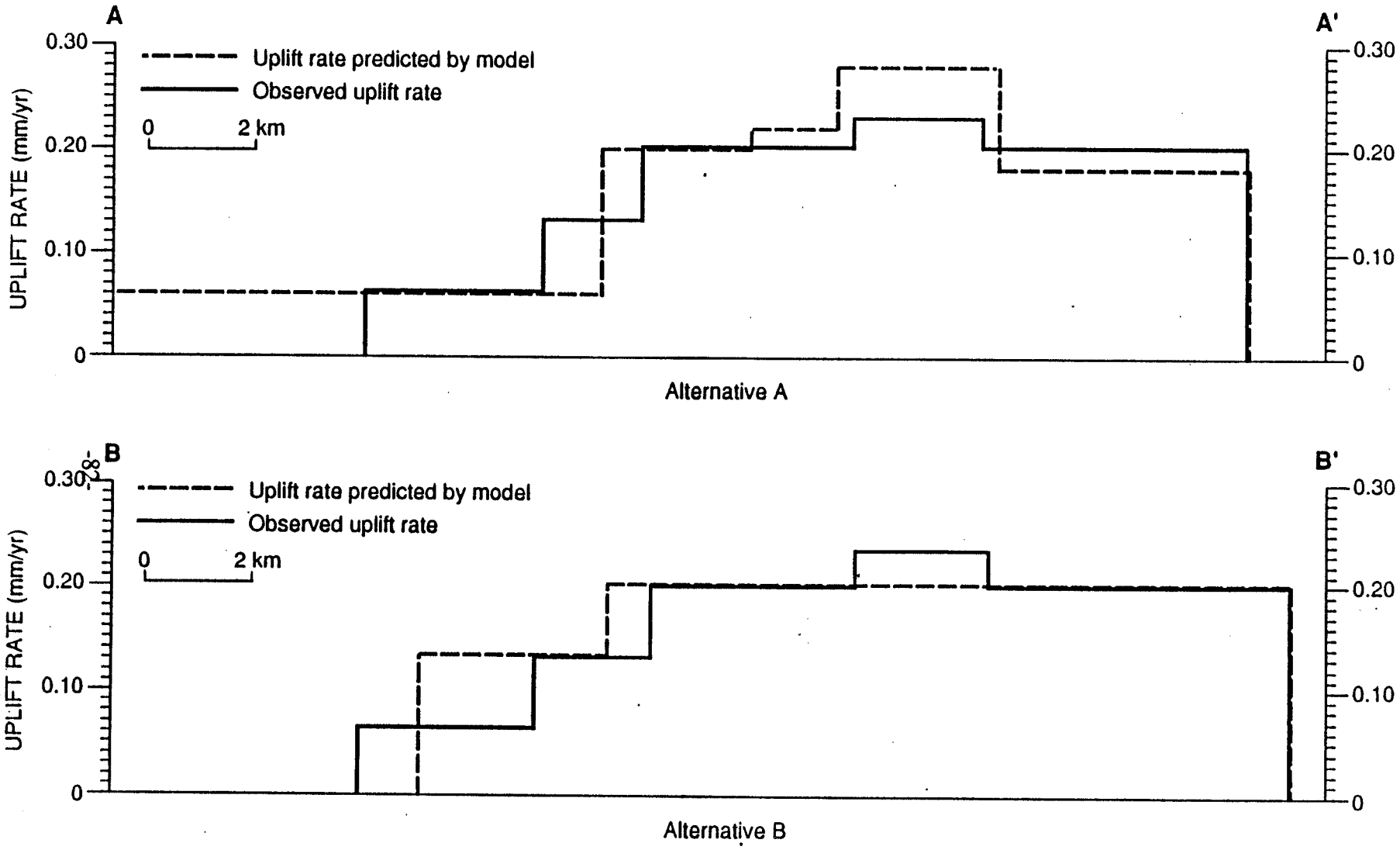

Figure 36. Predicted uplift (PG&E, 1990).

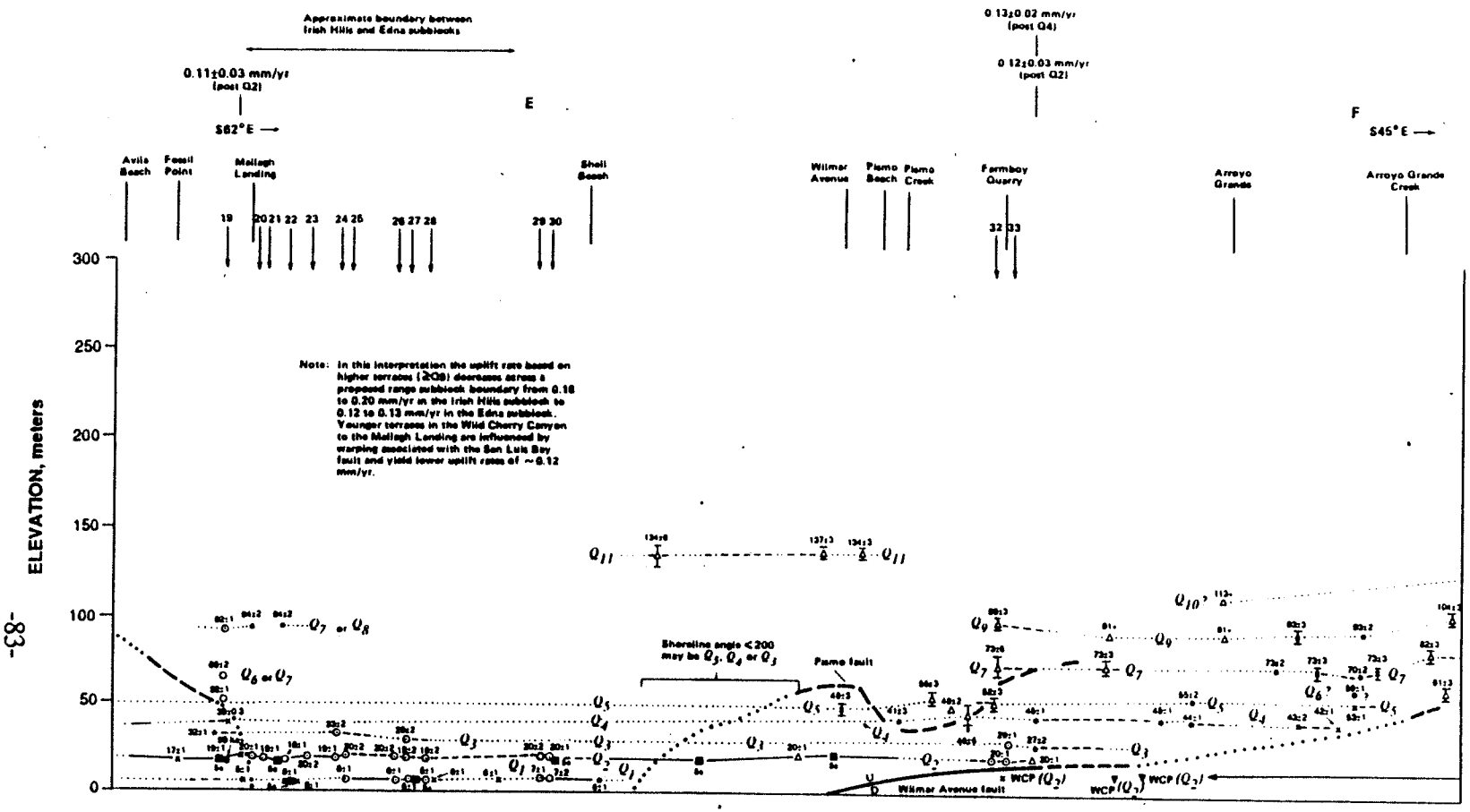

Marine Terrace	Oxygen Isotope Stage (Shackleton and Opdyke, 1973)	Age
Q_1	Substage 5a	80 ka
Q_{1a}	Substage 5c	105 ka
Q_2	Substage 5e	120 ka
Q_3	Stage 7	210 ka
Q_4	Stage 9	330 ka
Q_5	Stage 11	430 ka
Q_6	Stage 13	480 ka
$Q_{7\text{-}13}$	Stage 15 or older	>560 ka

Figure 37. Longitudinal profiles of marine terraces between Avila Beach and Arroyo Grande, crossing the San Miguelito, Pismo, and Wilmar Avenue faults. No vertical exaggeration. For location of profile , see Hanson and others (this volume).

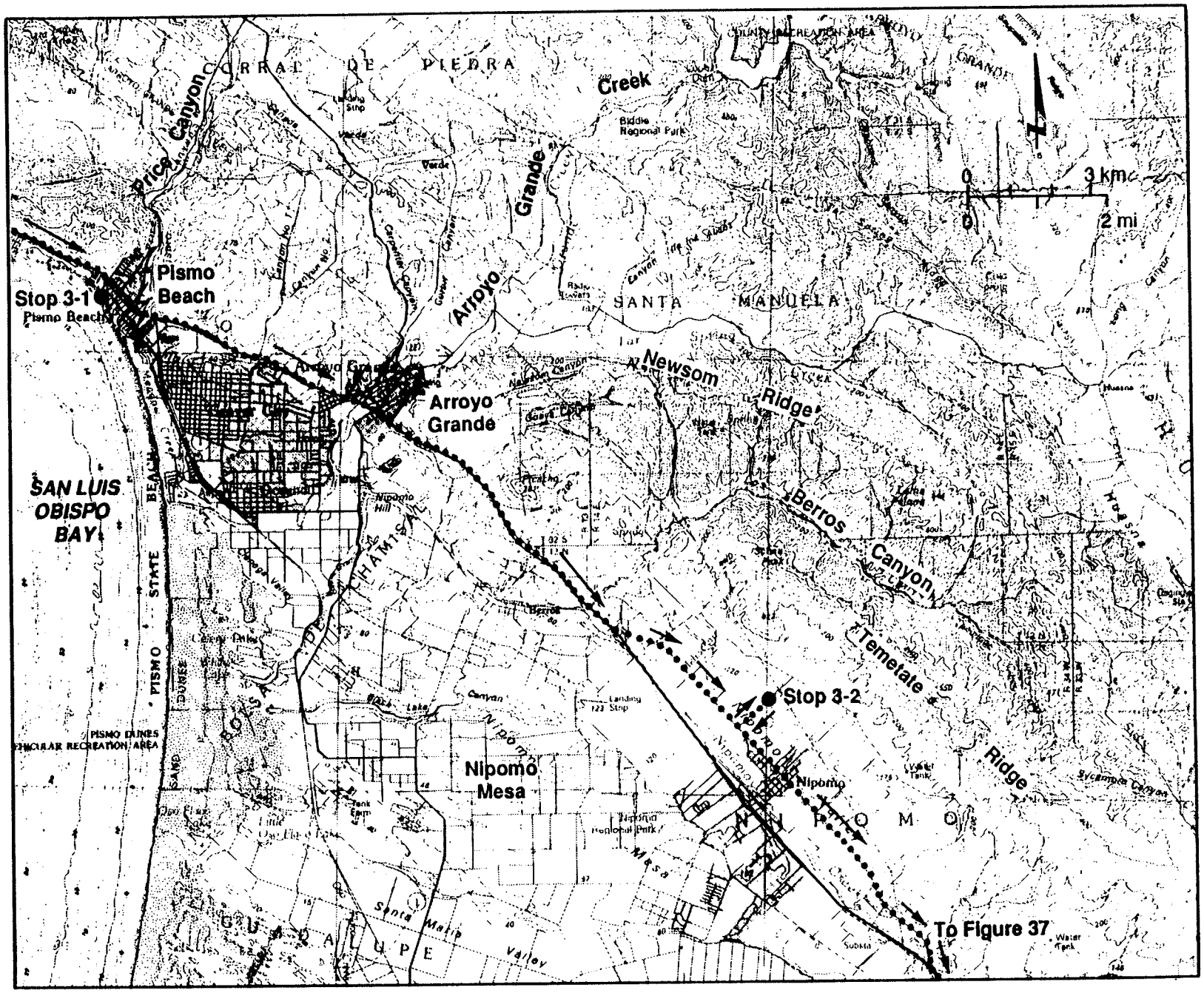

Figure 38a. Location map showing field trip route (Day 3) - Pismo Beach to Nipomo.

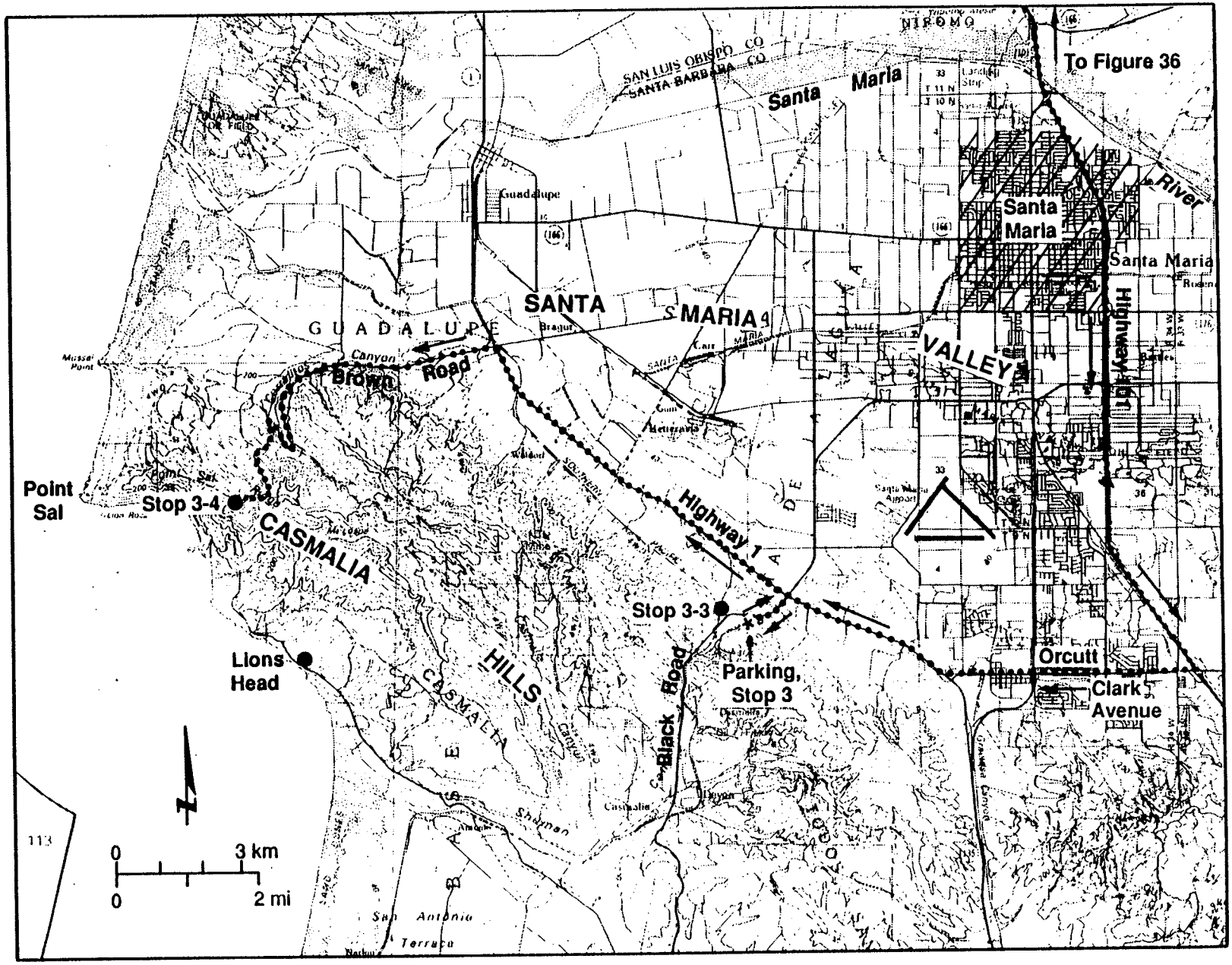

Figure 38b. Location map showing field trip route (Day 3) - Santa Maria to Point Sal.

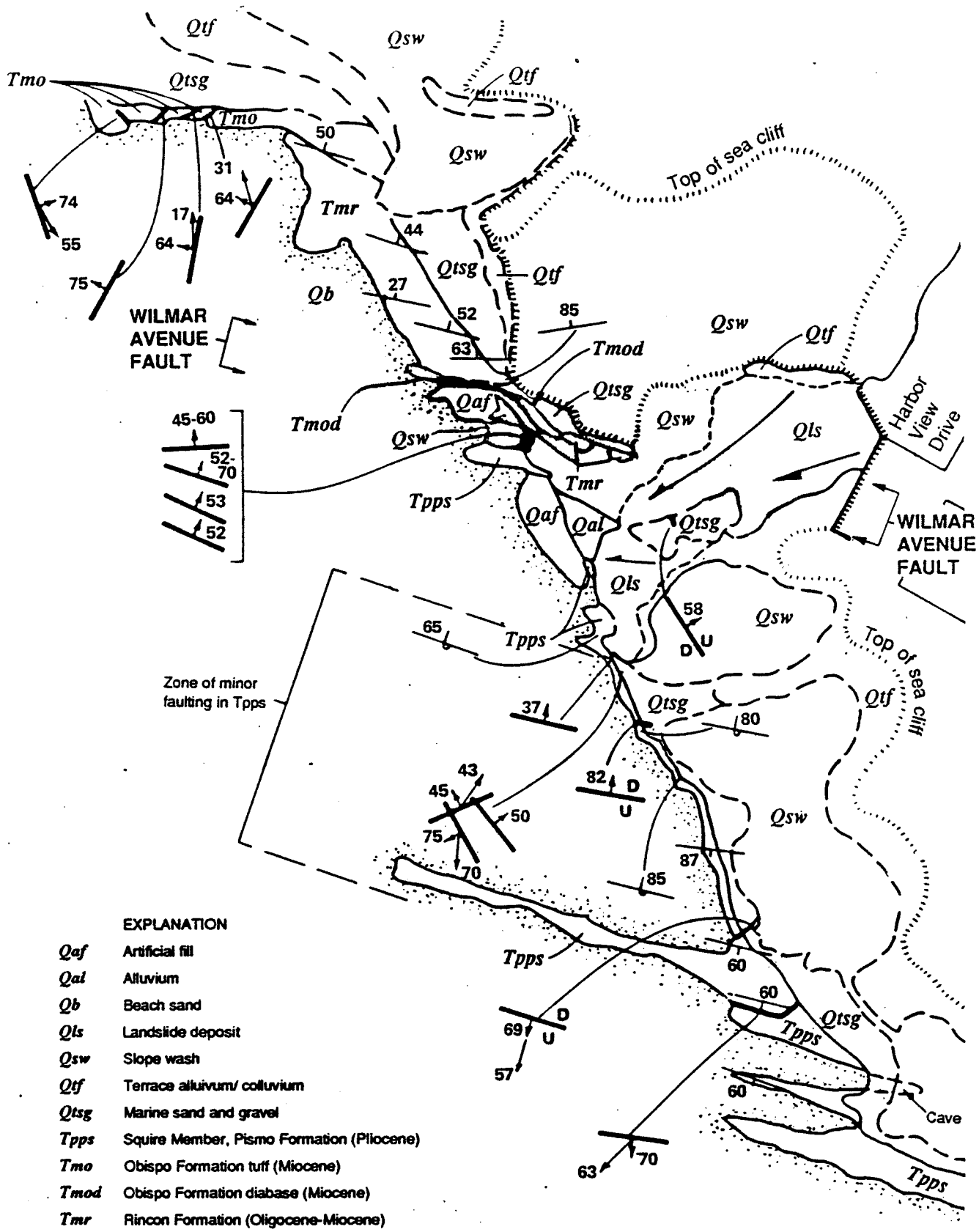

Figure 39. Geologic map of the sea-cliff exposure of the Wilmar Avenue fault, Pismo Beach.

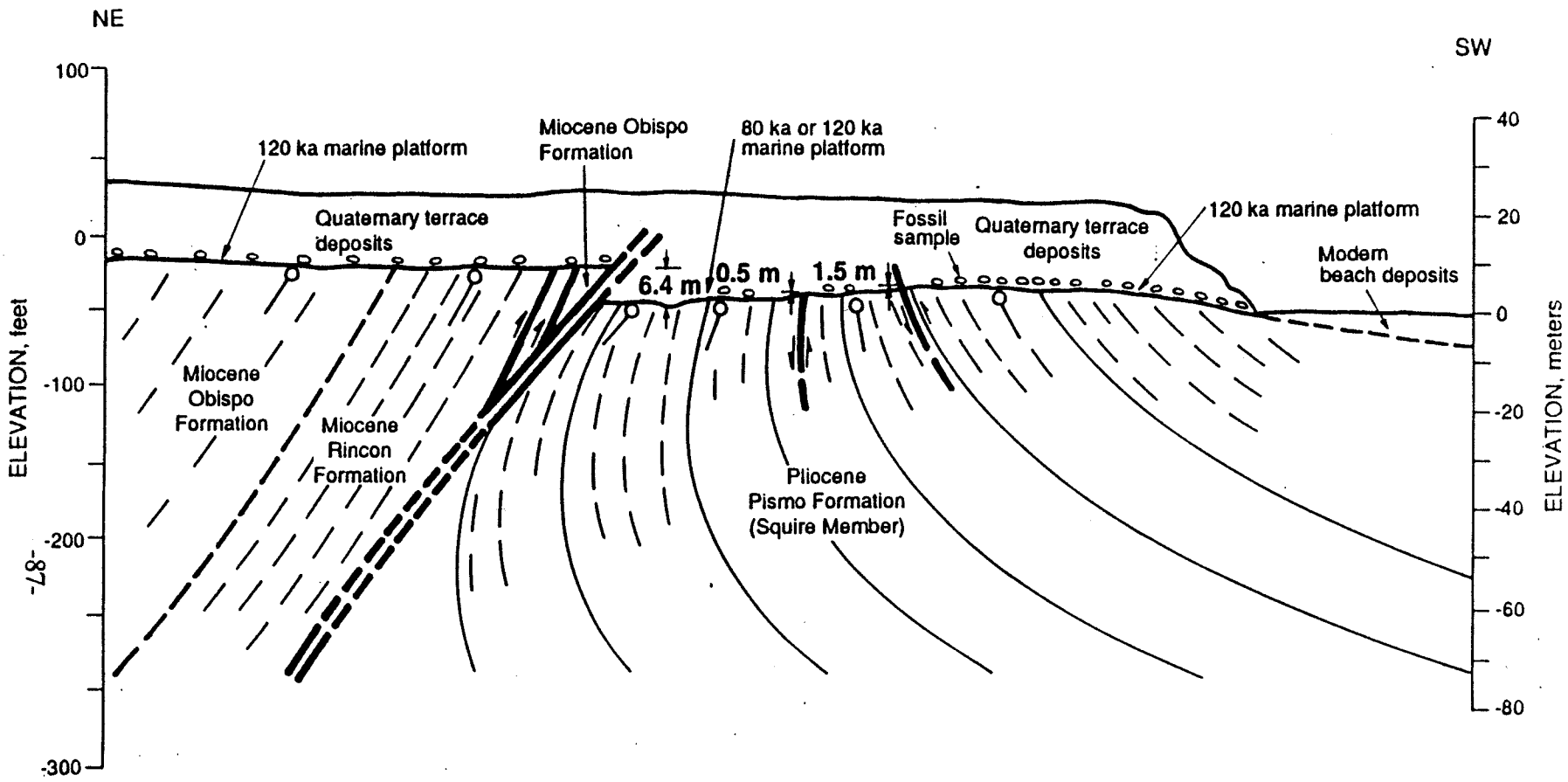

Figure 40. Schematic geologic section across the Wilmar Avenue fault exposed in the sea cliff, Pismo Beach .

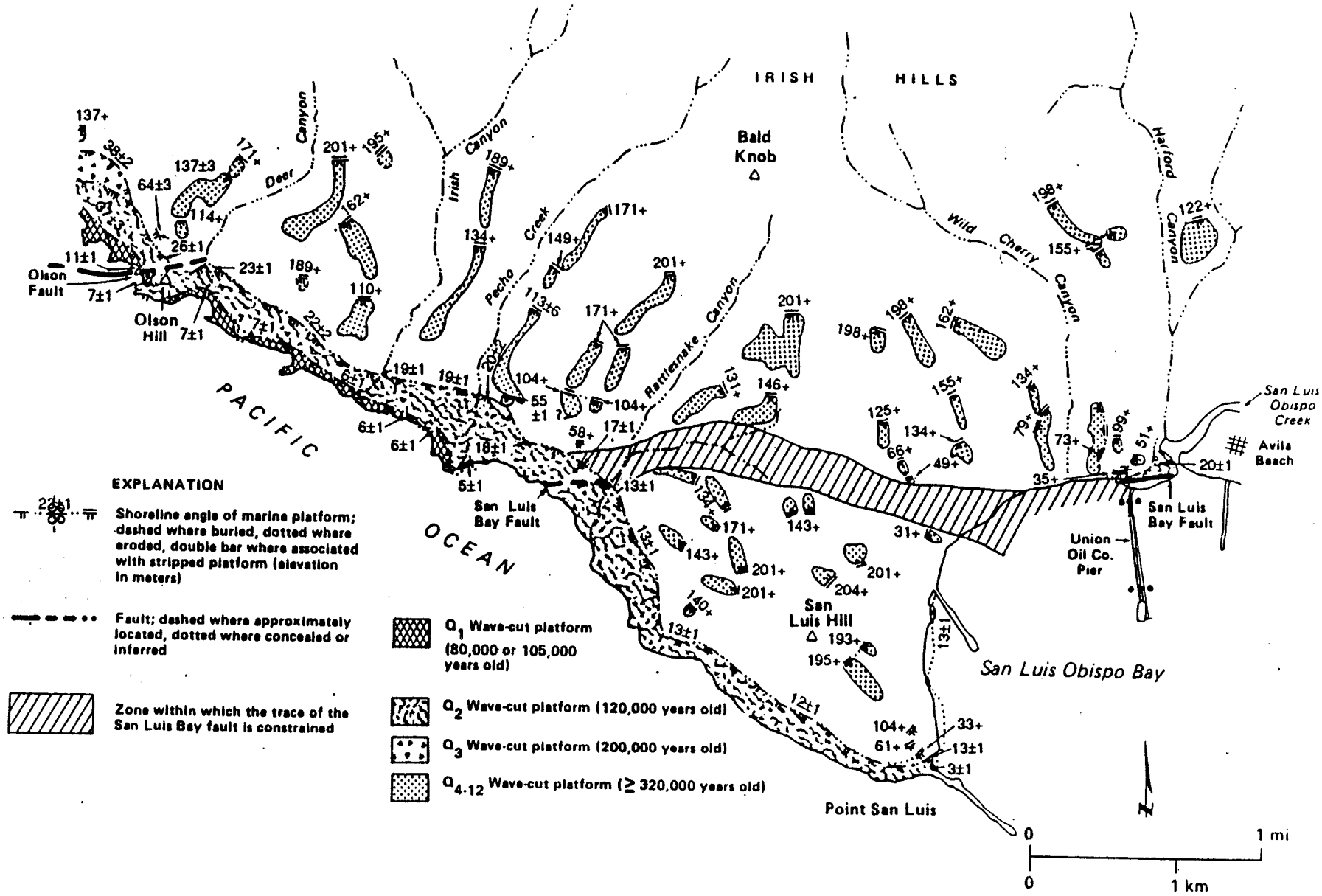

Figure 41. Map of marine wave-cut platforms in the vicinity of the San Luis Bay and Olson faults.

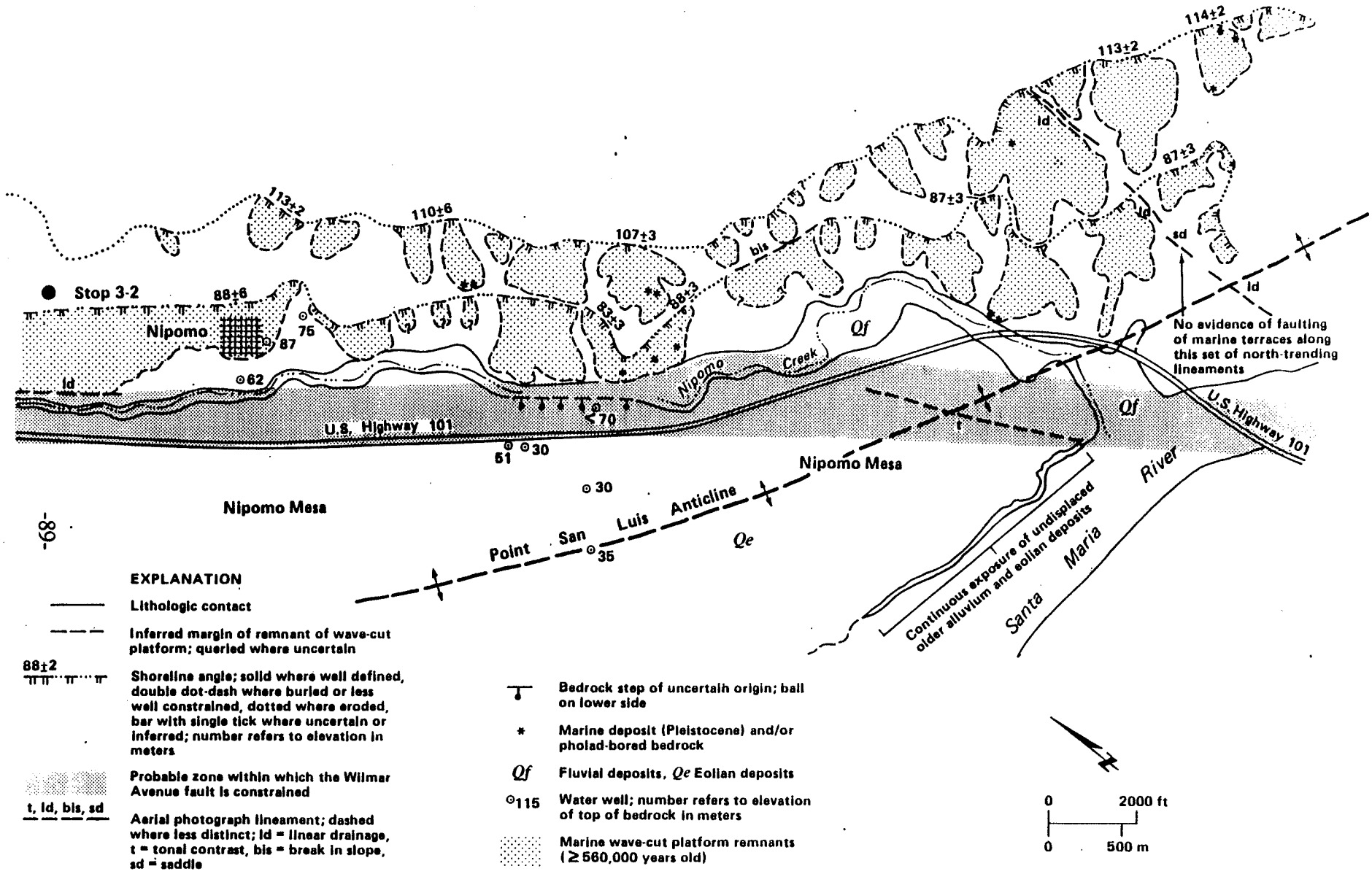

Figure 42. Map of marine wave-cut platforms near the town of Nipomo showing the inferred axial trace of the San Luis anticline proposed by Namson and Davis (1990).

THE SAN SIMEON/HOSGRI PULL-APART BASIN SOUTH-CENTRAL COASTAL CALIFORNIA

W.R. Lettis
William Lettis and Associates, Lafayette, California

L. DiSilvestro, K.L. Hanson
Geomatrix Consultants, Inc., San Francisco, California

and **J.I. Shiller**
Vapor Extraction Technology, San Diego, California

ABSTRACT

The San Simeon and Hosgri fault zones are prominent structural features along the coast of south-central California. The San Simeon fault zone comes onshore for about 20 kilometers between Ragged Point and San Simeon Point where detailed mapping and paleoseismic investigations indicate that it is a large, dextral fault with an estimated slip rate ranging from 1 to 3 millimeters per year. The Hosgri fault zone, however, lies entirely offshore where conventional geologic investigations cannot be performed to determine its style and rate of activity.

Understanding the structural relationship between the well-documented San Simeon fault zone and less well-documented Hosgri fault zone is essential for describing the contemporary tectonic behavior and seismic potential of the Hosgri fault zone, as well as for assessing the tectonic setting and nature of Quaternary deformation along the south-central margin of California. In this study, we examine a suite of geophysical and geological data acquired in the San Simeon Bay to Estero Bay region where the Hosgri and San Simeon fault zones interact. Our interpretation of these data indicate that: (1) the Hosgri and San Simeon fault zones are prominent basement-involved structures that terminate in the near-offshore between San Simeon Bay and Point Estero; (2) the faults overlap one another for a distance of about 10 to 12 kilometers and form a 5-kilometer wide en echelon right stepover; and (3) a subsiding basin bordered by normal faults and containing late Pliocene and younger deposits exists within the stepover region.

Theoretical modeling and empirical studies of pull-apart basins worldwide show that the dimensions of the pull-apart basin are related to cumulative lateral slip on the bordering master faults. Based on the geometry, dimensions and age of the San Simeon/Hosgri pull-apart structure, we infer that a time-averaged lateral slip rate of at least 1 to 4 millimeters per year is transferred across the basin between the southern San Simeon and northern Hosgri fault zones and, thus, that the Hosgri fault zone is a prominent dextral fault along the coast of south-central California.

INTRODUCTION

The San Simeon and Hosgri fault zones are prominent structural features along the coast of south-central California (Figure 1). Detailed geologic mapping and paleoseismic investigations conducted along the onshore

reach of the San Simeon fault zone near San Simeon Point document its geologic character as a major Quaternary right-slip fault (Hall, 1975; Weber, 1983; Hall et al., 1987; Hanson et al., 1987; PG&E, 1988; Hanson and Lettis, in review; Hall and Hunt, in review). The Hosgri fault zone, however, lies entirely offshore, where comparable geologic mapping and paleo-seismic investigations cannot be performed. Evidence for the style and timing of deformation along this fault is primarily derived from remote techniques such as seismic reflection profiles, side-scan sonar data, and potential field data, supplemented by analyses of bathymetry and seismicity data. Using a variety of these data sets, the fault has been variously interpreted as an active listric thrust fault (Crouch et al., 1984), an inactive, former basin-margin normal fault (Davis and McIntosh, 1987), and an active right-slip fault (McCulloch, 1987; Hamilton, 1987; PG&E, 1988). Based on regional and detailed geophysical, geologic, stratigraphic, and tectonic analyses, most authors interpret that the strike-slip character of the San Simeon fault zone extends southward onto the Hosgri fault zone, and that these two faults comprise the southern two components of the larger San Gregorio/Hosgri fault system (Silver, 1974, 1978; Graham and Dickinson, 1976, 1978a, 1978b; Hall, 1975, 1978; Greene, 1977; Leslie, 1980, 1981; Clark et al., 1984; PG&E, 1988).

Understanding the structural relationship between the San Simeon fault zone and the Hosgri fault zone is essential for describing the contemporary tectonic behavior and seismic potential of the Hosgri fault zone, as well as for assessing the tectonic setting and nature of Quaternary deformation along the south-central margin of California. These two faults approach one another in the near-offshore region between San Simeon Bay and Estero Bay (Figure 1). The nature of this fault interaction can theoretically take one of several forms: the two faults may merge as one through-going laterally continuous fault as proposed by Leslie (1980, 1981); the faults may extend to the north and south, respectively, as two distinct, separate, subparallel structures having little or nor kinematic or structural interaction, as proposed by Hoskins and Griffiths (1971), PG&E (1988), and Hamilton and Willingham (1977); the two faults may progressively or abruptly die out as they approach one another, in which case, strain along the faults would be consumed by secondary deformation at or along the fault terminations; or the two faults may be en echelon components of the same fault system, in which case, slip is transferred wholly or in part between the two faults across an en echelon stepover as proposed by PG&E (1988).

In an effort to define and document the structural interaction between the San Simeon and Hosgri fault zones, we acquired and interpreted a variety of geophysical and geological data in the San Simeon Bay to Estero Bay region. Our studies show that the San Simeon and Hosgri fault zones are distinct basement-involved faults that terminate in the near-offshore region. Where these faults overlap, they form a 5-kilometer-wide, en echelon right stepover that contains a subsiding late Tertiary and Quaternary basin. The presence of a sub-siding basin within a right stepover between two right-slip faults is a widely recognized structural feature referred to as a pull-apart basin (Burchfield and Stewart, 1966; Mann et al., 1983), a releasing step or bend (Crowell, 1974), or a dilatational jog (Sibson, 1985, 1986a, 1986b). Empirical and theoretical kinematic studies of strike-

slip fault systems indicate that en echelon steps between offset strands of strike-slip faults produce a characteristic style and pattern of deformation dependent on both the orientation of the stepover (right-stepping or left-stepping) and the sense of slip on the fault system.

Based on the right en echelon fault stepover, the intervening pull-apart structure, and the documented right-slip character of the onshore San Simeon fault zone, we conclude that lateral slip is transferred between the San Simeon fault zone and the northern Hosgri fault zone via the pull-apart basin. If the Hosgri fault zone is interpreted to be a thrust fault, strike-slip on the San Simeon fault zone must progressively or abruptly die out southward, and the lateral strain must be absorbed on splay faults or folds. However, based on our studies of the geology and geophysics in the San Simeon Bay-Estero Bay region, no candidate structures of this type are present to accommodate the lateral strain from the San Simeon fault zone.

In this paper, we describe the evidence for the San Simeon/Hosgri pull-apart basin, the dimensions and structural history of the basin, and implications drawn from this structure in assessing the sense and rate of slip along the Hosgri fault zone. Based on empirical and theoretical studies of pull-apart basins worldwide that relate dimensions and age of the basins to rates of slip along the master bounding faults, we also estimate the rate of lateral slip on the Hosgri and San Simeon fault zones. We compare these rates with independently derived rates from the San Simeon fault zone onshore and discuss the implications of the pull-apart basin for seismic rupture segmentation along the Hosgri and San Simeon fault zone.

REGIONAL SETTING

The San Gregorio/Hosgri fault system is a complex system of faulting that is subparallel to and lies primarily offshore from the central California coast (Figure 1). This system of faults branches from the San Andreas fault near Bolinas Lagoon on the north (Jennings, 1975) and dies out to the southeast near Point Arguello (Cummings et al., 1987; PG&E, 1988). From the time the Hosgri fault zone was first identified in 1970 (Wolf and Wagner, 1970; Hoskins and Griffiths, 1971; Wagner, 1974), the major focus of research on the San Gregorio/Hosgri fault system was the estimation of the amount and timing of large-scale, right-slip displacement that had occurred along it. Based on interpreted offset stratigraphic units, cumulative Cenozoic lateral offsets of 80 to 150 kilometers have been proposed for all or parts of the fault system (Silver, 1974; Hall, 1975; Graham, 1976; Graham and Dickinson, 1976, 1978a, 1978b; Greene, 1977; Silver and Normark, 1978; Seiders, 1979; Blake et al., 1978; Clark et al., 1984). In contrast to these estimates, several authors have argued for lesser amounts of Neogene lateral offset along the southern part of the fault system, ranging from near zero on the Hosgri fault zone (Crouch et al., 1984) to estimates of less than 30 kilometers on the Hosgri and San Simeon fault zones (Hamilton and Willingham, 1977, 1978, 1979; Seiders, 1979; Hamilton, 1984).

The cumulative lateral displacement occurred over time intervals that span several different tectonic settings. The fault system may have evolved in the Oligocene to early Miocene as transform faulting replaced subduction along the North American plate margin (Atwater, 1970; Atwater and Molnar, 1973;

Graham, 1978; McCulloch, 1987; Hall, 1981). The presence of large Miocene basins along the continental shelf of California suggests that early faulting along the fault system was extensional or transtensional (McCulloch, 1987; McCulloch and Lewis, 1988). In the early Pliocene, a change in relative plate motion between the Pacific and North American plates placed the plate margin under a component of compression (Page and Engebretson, 1984; Engebretson et al., 1985; Cox and Engebretson, 1985; Harbert and Cox, 1989). Estimates of subsequent deformation on all or part of the fault system range from purely thrust (Crouch et al., 1984) to convergent strike slip (for example, Hall, 1975; PG&E, 1988).

Interpretation of contemporary deformation along the Hosgri fault zone is hindered by two important factors: first, the entire fault system is offshore, where established techniques for assessing Quaternary activity (for example, mapping, trenching, drilling) cannot be performed; and second, the fault system has an imprint of preexisting deformation that spans significant changes in tectonic setting. For example, investigation of the fault zone by geophysical techniques provides images of the upper crust from the sea floor to several kilometers that reflect the composite structural and stratigraphic history of the fault. The assessment of Quaternary activity on the Hosgri fault zone, therefore, must come from an integrated interpretation of offshore geophysical data combined with geologic, seismologic, and tectonic analyses of the fault's structural association with the San Gregorio, Sur, and San Simeon fault zones to the north.

The San Gregorio, Sur, and San Simeon fault zones, although primarily offshore, come onshore at four locations, and investigations of their Quaternary activity have been performed there. Geologic studies of the San Gregorio fault zone at Seal Cove and Año Nuevo near Santa Cruz (Weber and Lajoie, 1977, 1979a, 1979b), the Sur fault zone in the Point Sur area (Hall, 1989), and the San Simeon fault zone in the Point Piedras Blancas area (PG&E, 1988; Hall, 1975; Envicom, 1977; Weber et al., 1981; Weber, 1983; Manson, 1985; Hanson and Lettis, in review; and Hall and Hunt, in review) indicate that these faults are prominent right-slip fault zones.

The San Simeon fault zone is a prominent structural feature where it is locally exposed onshore from the San Simeon Point to north of Ragged Point, a distance of 20 kilometers (Figure 1). At the northern end of San Simeon Bay, the fault zone consists of major boundary faults that define a zone about 120 meters wide. The zone splays to the northwest and has several traces that trend more westerly than the N35°W strike of the main eastern trace of the fault zone. Although the dominant sense of displacement along major strands within the zone is right-slip, the more westerly trending fault splays have a component of dip-slip displacement (Hall,1975; PG&E, 1988; Weber, 1983; Hanson and Lettis, in review).

Several studies have been performed to quantify the rate of lateral slip across the San Simeon fault zone. Based on reconnaissance mapping of marine terraces between Cayucos and Cape San Martin and correlation of marine terraces across the San Simeon fault zone, Weber (1983) interpreted a Pleistocene right-lateral slip rate of between 5 and 19 millimeters per year, with a preferred estimate of 8 to 10 millimeters per year for the past 350 to 400 thousand years. Based on a subsequent detailed analysis of deflected stream drainages and

more detailed marine terrace mapping, supplemented by drilling and soil-profile development studies in the San Simeon Point region directly north of San Simeon Bay, PG&E (1988) and Hanson and Lettis (in review) estimate right-lateral slip rates of 1 to 3 millimeters per year during the past 200 thousand years. Similarly, PG&E (1988) and Hall and Hunt (in review) estimate a minimum Holocene right-lateral slip rate of 1 to 2 millimeters per year, on the basis of offset fluvial deposits exposed in trench excavations along Oak Knoll Creek and Airport Creek. In each of these studies, a minor amount of upthrow on the western block vertical separation is also recognized, with the ratio of lateral to vertical separation ranging from 5:1 to 20:1.

Quaternary activity on the Hosgri fault zone is less well-constrained than on the San Simeon fault zone, primarily because it lies entirely offshore where comparable Quaternary mapping and paleoseismic investigations cannot be performed. Crouch et al. (1984) cite down-on-the-west basement separation across the Hosgri fault zone, the presence of subparallel folds in the offshore Santa Maria Basin, thrust focal mechanisms of microseismicity in south-central coastal California, and shallow-dipping reflectors on seismic reflection data to infer that the Hosgri fault zone is one of a region-wide system of west-verging, shallow-dipping listric thrust faults. Retrodeformable cross sections prepared by Davis and McIntosh (1987) and Namson and Davis (1990) that are based on limited offshore geophysical data and selected onshore geologic data suggest that the Hosgri fault zone is a steeply northeast dipping, rotated former basin-margin normal fault that is not active in the contemporary tectonic regime. These interpretations, however, do not provide an estimated slip rate for the Hosgri fault zone, nor do they address the structural association of the fault system with the known (PG&E, 1988) strike-slip San Simeon fault zone to the north.

Detailed analysis of seismic reflection data, geologic and geomorphic data, seismicity data directly related to the Hosgri, and consideration of regional tectonic kinematics have led PG&E (1988) and Lettis et al. (1989) to interpret that right slip is the dominant contemporary sense of displacement along the Hosgri fault zone. These authors cite reversals in apparent sense of vertical separation both down-dip and along strike, linearity of the trace, a steeply dipping fault plane, negative and positive flower structures with associated folding and thrusting, strike-slip earthquake focal mechanisms, and local pull-apart basins as indicative of a right-slip fault system.

DATA

To evaluate the lateral continuity of the Hosgri and San Simeon fault zones and the nature of their interaction, we conducted a program of geophysical exploration, seafloor sampling, and geomorphic analyses in the near-shore coastal region between San Simeon Bay and Estero Bay. Geophysical data consist of both common depth point (CDP) and shallow high-resolution seismic reflection data, with a line spacing of approximately 2 km and 1 km, respectively (Figure 2). These data are part of an extensive suite of approximately 16,000 km of offshore seismic data obtained by PG&E (1988) for their evaluation of offshore geologic structure. The data used in this study are shown in Table 1 and include both CDP and high resolution data shot between 1976 and 1986 using sparker, watergun, and airgun sources. With the exception of the

Comap Alaska, Aquatronics, and CGI seismic lines, the CDP data are deep-penetration (2 sec or more two-way travel time (TWTT)) and 24-fold or greater. High resolution seismic reflection data were acquired with sparker, boomer, airgun, or sleeve exploder sources, with stratigraphic penetration down to 1 to 2 sec. These data are acquired with systems operating at higher frequencies (up to 35 Hz) than the conventional CDP surveys and, therefore, provide information about the upper 50 to 100 msec of record that are lost on CDP records. These data were processed using the data processing sequence shown in Table 2. State-of-the-art processing techniques were used to improve imaging of the vertical extent and dip of the elements forming the fault zone, as well as the stratigraphic definition of units critical to age determination of structural events.

Data quality of both the CDP and high-resolution seismic data is variable depending upon the source and geologic complexity. Both stacked and migrated data sets were used in the interpretation process. Geologic interpretations beneath about 1 sec TWTT were based primarily on the CDP data. Seafloor geomorphic features and shallow-crustal deformation above about one second TWTT were identified primarily from the high-resolution data set. The interpreted time sections were converted to depth-corrected sections using a velocity model developed from an integrated analysis of the CDP seismic data and well information from the offshore Santa Maria Basin, and extrapolated into the Estero Bay/San Simeon Bay region. The velocity model was applied to the seismic sections to create depth sections approaching spatially correct geometric orientations for interpretation of stratigraphic thickness and structural deformation. Regional aeromagnetic data published by McCulloch and Chapman (1977) and Beyer and McCulloch (1988) were used to assist in the interpretation of depth to basement.

In addition to the interpretation of geophysical data, we collected samples of bedrock exposed in seafloor outcrops in shallow coastal areas, primarily to evaluate the offshore continuity of the San Simeon fault zone and to assess the age of Tertiary units interpreted on the seismic data. Lithologic samples and bedding attitudes were acquired from the seafloor by diver geologists in San Simeon Bay and along the coast between Cambria and Point Estero (Figure 2). Onshore, the San Simeon fault zone juxtaposes rocks of the Franciscan Complex on the east against rocks of the Miocene Monterey Formation on the west, with an intervening tectonic slice of Pliocene to Pleistocene conglomerate sandstone mapped as the Careaga Formation by Hall (1975). We used the distribution of these lithologies to constrain the location of the San Simeon fault zone in San Simeon Bay. Farther offshore to the south, near-shore lithologic samples and geomorphic features such as scarps, lineaments, and the morphology of the coastline were used to constrain the location of the San Simeon fault zone (PG&E, 1988).

RESULTS

Analysis of data from the offshore region between San Simeon Bay and Estero Bay indicate that (1) the Hosgri and San Simeon fault zones are prominent basement-involved structures that terminate in the near-offshore between San Simeon Bay and Point Estero; (2) the faults overlap one another for a distance of about 10 to 12 kilometers and form a 5-kilometer-wide, right en echelon stepover; and (3) a subsiding basin bordered

by normal faults and containing late Pliocene and younger deposits exists within the stepover region.

The locations of near-surface geologic structures and morphologic features in the San Simeon Bay/Estero Bay region are shown on Figure 2. The vertical distribution of these structures and late Cenozoic deposits in the area are shown on seismic reflection profiles S-1 through S-6 (Figures 3 through 8). These profiles were selected from the extensive suite of data examined to provide uniform spatial coverage of the area and to illustrate the shallow stratigraphy and structure of subsiding basin between the northern Hosgri fault zone and the southern San Simeon fault zone. Profiles S-1 through S-5 are roughly normal to the regional structural grain (Figure 2) and illustrate the down-dip geometry and sense of vertical separation of faults identified in the area. Profile S-6 is parallel to the regional structural grain and illustrates the lateral continuity and along-strike terminations of the subsiding basin. Below, we describe the locations and nature of terminations of the San Simeon and Hosgri fault zones; this is followed by a description of stratigraphic units identified from the seismic data in the intervening subsiding basin, and discussion of the geometry and dimensions of the intervening subsiding basin.

Location and Terminations of the San Simeon and Hosgri Fault Zones

The location of the San Simeon and Hosgri fault zones in the near offshore region between Estero Bay and San Simeon Bay is shown on Figure 2. The San Simeon fault zone extends S38°E from its well-constrained location onshore at San Simeon Bay for a distance of 38 to 40 kilometers to a southern termination offshore from Point Estero (Figure 2). Along this reach, the fault zone is inferred to have one or more prominent traces within a zone up to 1 kilometer wide, similar to the character of the fault zone onshore directly north of San Simeon Bay (PG&E, 1988; Hanson and Lettis, in review). For 5 kilometers southeast of the onshore San Simeon Bay exposure, the location of the fault zone is constrained by (1) the distribution of offshore lithologies (determined from sea-bottom hand-collected samples) that shows the Tertiary Monterey Formation juxtaposed against Franciscan Complex rocks across a narrow linear zone of sandy sea bottom, inferred to represent a slice of the less competent Pliocene and Pleistocene Careaga Formation (Figure 2); (2) a series of low, east-facing seafloor steps comparable to the east-facing scarps mapped by Weber (1983) and Hanson and Lettis (in review) onshore to the north (Figure 2); and (3) disrupted sea floor imaged on high-resolution seismic data shot by Scammon within San Simeon Bay (PG&E, 1988). South of San Simeon Bay, the fault zone is inferred to lie shoreward of our geophysical data coverage. Because the Cambria coastline is not cut by a fault comparable in size to the fault zone observed onshore at San Simeon Bay (Hall et al., 1979), we interpret the San Simeon fault zone to lie in a narrow linear corridor between the coastline and the shoreward limit of the geophysical data. A shore-parallel syncline observed on the near-shore geophysical data for a distance of 15 kilometers in this area (Figure 2) and the straight, possibly structurally controlled, rocky coastline supports the inference that a major shore-parallel structural feature is present near the coast.

We project the fault zone southeast from this straight section of coastline an additional 17 kilometers to a point near Point Estero, based on the presence of southwest-facing

seafloor scarps. No geomorphic expression of a fault is observed south of a point near the latitude of Point Estero. Geophysical data in northern Estero Bay show an unbroken, northeast-dipping stratigraphic section along the projection of the fault zone (Figures 6 and 9), indicating that the San Simeon fault zone does not extend into Estero Bay along the southeastern trend established by the high-resolution geophysical data in San Simeon Bay and the linear Cambria coastline.

The northern Hosgri fault zone extends across the eastern part of Estero Bay and terminates approximately 10 kilometers north of the latitude of Point Estero (Figure 2). From south to north, the fault trend bends from N25°W to N45°W. Throughout this reach, the location of the fault is well constrained from the grid of seismic data and is marked locally by disruptions in seafloor bathymetry. The fault zone is imaged primarily as abrupt lateral changes in reflection character or as near-vertical to steeply dipping reflection-free zones of incoherent energy. Comparable features are observed in seismic sections across the San Andreas fault zone in Cholame Valley (Shedlock et al., 1990) and across active and inactive strike-slip faults in both interplate and intraplate settings (Lemiszki and Brown, 1988). The primary fault traces are high-angle to a depth of 1 to 2 sec (TWTT), below which reduced data quality precludes interpretation. The fault typically separates a thick section of coherent reflectors interpreted to be Tertiary strata on the west from a zone of incoherent energy typical of Franciscan basement on the east (Figures 3 through 8).

The northern termination of the Hosgri fault zone is defined on the seismic data by a change in structural style and the character and recency of near-surface faulting. In contrast to the zone of incoherent energy representing elevated basement observed on the east side of the Hosgri fault zone to the south (Figures 3 through 8), a zone of coherent reflectors interpreted to be Tertiary strata that are deformed into a series of asymmetric folds extend across the projection of the Hosgri fault zone north of its termination (Figure 12). In addition, the near-surface, post- mid-Pliocene fault deformation prevalent along the northern Hosgri fault zone dies out at the northern termination of the fault zone and is not evident along the projected trend of the fault to the north (Figure 9).

The geologic and geophysical data, therefore, indicate the Hosgri and San Simeon fault zones are basement-involved structures that terminate in the near-offshore region between San Simeon Bay and Estero Bay, and clearly are not a laterally continuous fault zone as suggested by Leslie (1981). The map pattern of faulting (Figure 2) defines an en echelon right step about 5 kilometers wide. The two faults overlap one another by 10 to 12 kilometers, or potentially less, depending on the inferred southern extent of the San Simeon fault zone along the Cambria coastline. The regional strike of the Hosgri and San Simeon fault zone (N25°W and N38°W, respectively) defines an overall, regional left bend in the fault system across the en echelon right step between the two fault traces.

Stratigraphy

The pattern and style of structural deformation in the region between the Hosgri and San Simeon fault zones were assessed primarily from the distribution and disruption of Cenozoic deposits and stratigraphic unconformities observed on the seismic data. Unconformities identified

from well data and seismic character in the region include the top of basement, top of Miocene, mid-Pliocene (or early/late Pliocene), and late Wisconsinan unconformities. The older three unconformities produce moderate to strong, coherent reflectors having a distinct seismic signature, and are mappable horizons on the CDP seismic reflection data (Figures 3 through 8). The late Wisconsinan unconformity is observed locally in the near-offshore region on high-resolution boomer and sparker data, and provides important information for identifying areas of late Pleistocene and Holocene deformation.

Clark et al., (in press) provide a description of the chronostratigraphy of the central offshore Santa Maria Basin. A generalized stratigraphic column for the offshore Santa Maria Basin based on their work is shown on Table 3. Although offshore well data are not available in the San Simeon Bay/Estero Bay area to provide detailed stratigraphic information, the unconformities identified in this region are correlated to the unconformities identified by Clark et al. (in press) in the Santa Maria Basin and well data offshore of Point Sal and Point Arguello on the basis of loop-tied geophysical data. Basement in the study area is inferred to consist of Mesozoic Franciscan Complex rocks and undifferentiated Cretaceous and Paleogene sandstones and shales that crop out locally in the onshore Cambria region (Hall et al., 1979). The top of basement unconformity is an extensive, regional surface throughout the offshore Santa Maria Basin; it probably represents an erosional episode during the global late Oligocene (22 to 25 million years ago) low sea-level stand (McCulloch, 1987; McCulloch and Lewis, 1988).

Miocene deposits in the offshore Santa Maria Basin consist of the Obispo, Point Sal, and Monterey formations and the lower part of the Sisquoc Formation (Clark et al., in press). The top of Miocene unconformity separates the lower part of the Sisquoc from the Pliocene upper part of the Sisquoc Formation, and can be traced over most of the offshore basin on seismic data (Clark et al., in press). Based on diatom zonations from the onshore Santa Maria Basin, Dumont (1989) places the age of the Miocene/Pliocene boundary at 5.3 million years ago. This date is in close agreement with the chronology of the AAPG Correlation of the Stratigraphic Units of North America for the Santa Maria Basin (Bishop and Davis, 1984), with Berggren et al. (1985), and with Barron (1986).

Pliocene deposits in the offshore Santa Maria Basin consist of the upper part of the Sisquoc Formation and the informally named "Foxen" formation (Clark et al., in press). These two units are separated by a mid-Pliocene unconformity. The unconformity can be mapped on seismic data over most of the basin, although not as consistently as the top of Miocene unconformity. Clark et al. (in press) assign an age of 3.4 million years to the uppermost Sisquoc beds beneath the unconformity, and an age of 2.8 to 1.7 million years to the top of the "Foxen" formation overlying the unconformity. Thus, the age of the mid-Pliocene unconformity is bracketed to be younger than 3.4 and older than 2.8 million years. Near Point Buchon directly south of Estero Bay, the mid-Pliocene unconformity is overlain by the Squire Member of the Pismo Formation. The Squire Member is stratigraphically equivalent to the "Foxen" formation and contains a late Pliocene pecten fauna (Hall, 1973). The presence of late-Pliocene strata above the mid-Pliocene unconformity onshore indicates that the mid-Pliocene

unconformity in the offshore Estero Bay area is probably at least 2 to 3 million years old.

The late Wisconsinan unconformity is preserved locally in the near-shore environment. We interpret the unconformity to be an erosional surface carved during the late Wisconsinan low sea-level stand, which culminated approximately 18,000 years ago. Deposits overlying the unconformity reflect post-18,000 years near-shore marine sedimentation.

The top of Miocene unconformity is identified throughout the San Simeon Bay/Estero Bay region and provides an excellent marker horizon for assessing post-Miocene (5.3 million years ago) deformation. Figure 10 is an isopach map of sediment thickness overlying the post-Miocene unconformity, illustrating the loci and pattern of depocenters in the area.

The distribution of post-Miocene sediments and location of deformation in the San Simeon Bay/Estero Bay region indicates that the Hosgri and San Simeon fault zones overlap in a right-stepping, en echelon manner. The intervening 5-kilometer-wide region is occupied by a subsiding basin. The mid-Pliocene unconformity structure map (Figure 9) and seismic lines S1, S2 and S3 (Figures 3, 4, and 5) indicate this subsiding basin is a west-southwest-tilted asymmetric half-graben.

Sediments at the base of the half-graben are estimated to be "Foxen" equivalent or older. Two unconformities are identified in the basin. We interpret the lower unconformity to be the top Miocene unconformity, and the higher unconformity to be the mid-Pliocene unconformity. Alternatively, we cannot preclude that the lower unconformity is the mid-Pliocene unconformity and the higher unconformity is some younger, local unconformity such as the Pliocene/Pleistocene unconformity that is recognized discontinuously in parts of the onshore Santa Maria basin. In this latter case, the subsiding basin between the Hosgri and San Simeon fault zones would be a much younger, more rapidly developing structural feature than we have interpreted.

The higher unconformity is a strong reflector in the southern part of the basin (Figures 5, 6, and 7), but is absent in the northern part of the basin (Figure 3). Figure 9 is a time-structure map of the higher (mid-Pliocene) unconformity. Absence of the unconformity in the northern part of the basin indicates that either the unconformity was uplifted and eroded or a preexisting structural high in this area prevented development of the unconformity and subsequent deposition of overlying late Pliocene and younger sediment.

The distribution and thickness of post-late Wisconsinan sediment in the region is shown on Figure 11. The distribution of these deposits reflects the most recent depositional patterns in the near-offshore region between San Simeon Bay and Estero Bay. As shown on Figure 11, these deposits are not spatially associated with nearby large streams along the Cambria coastline. These deposits, therefore, probably reflect depositional patterns primarily from longshore drift. The post-late Wisconsinan deposits form a relatively flat carapace over the older basin deposits within the central and southwestern part of the basin between the Hosgri and San Simeon fault zones. The deposits thicken locally in several isolated depocenters, often attaining thicknesses of up to 12 meters, indicating that subsidence of the intervening basin is continuing in late Quaternary time.

Dimensions and Geometry of the San Simeon/Hosgri Pull-Apart Basin

The distribution and thickness of late Cenozoic deposits described above clearly define a subsiding late Cenozoic basin locally restricted to the overlapping region of the right-stepping, en echelon stepover between the Hosgri and San Simeon fault zones. As shown by the mid-Pliocene unconformity structure contour map (Figure 9), the basin forms an elongate or "lazy Z" shape, 15 to 18.5 kilometers long and 3 to 5 kilometers wide at its widest point near the basin center. The isopach map of Pliocene and younger sediment (Figure 10), indicates that the subsiding basin is deepest along its western and southwestern margin proximal to the Hosgri fault zone. In this area, the basin contains Pliocene and younger deposits up to 260 meters thick.

The geometry and size of the basin is structurally controlled by the Hosgri fault zone to the southwest, the San Simeon fault zone to the northeast, and a series of more northerly trending faults with apparent normal separation within the basin (Figures 9 and 12). At least four east-dipping apparent normal faults are evident within the basin (Figures 5, 6, and 12(B)). In map view, these faults strike north-south and intersect the Hosgri fault zone at 10- to 20-degree angles (Figures 2 and 9). The apparent normal separation indicates that these faults are extensional or transtensional structures. Greater displacement and closer spacing of the faults in the western and southwestern part of the stepover region produced a southwest-tilted half-graben leading to the thicker accumulation of Pliocene and younger deposits observed in this area. The southwestern-most normal fault and the Hosgri fault zone converge southward (Figure 5) and form the south-western structural margin of the basin.

North of latitude 35°23′, the Hosgri fault zone ceases to define the western structural margin of the basin. In this area, the north-south-trending normal faults diverge from the N25°W to N45°W-trending Hosgri fault zone and define a more irregular basin edge that trends obliquely across the stepover to the San Simeon fault zone on the east (Figures 9 and 10). The northeastern and eastern edge of the basin is partly controlled by the eastern-most normal fault observed on the seismic records and by the inferred southeastern extension of the San Simeon fault zone (Figure 9). The poorly-defined southern edge of the basin, where Pliocene deposits thin and pinch to the south, does not appear to be fault controlled (Figures 8 and 10).

DISCUSSION

A structural basin bordered by and containing extensional faults exists in the en echelon right stepover between the Hosgri and San Simeon fault zones. Active Quaternary extension and subsidence of the basin is indicated by (1) normal fault displacement of the mid-Pliocene unconformity and late-Wisconsinan unconformity, especially in the northern part of the basin; (2) the distribution and thickening of post-mid-Pliocene and post-late-Wisconsinan sediment within the basin against the apparent normal faults and the Hosgri fault zone along the western and southwestern margins of the basin (Figures 5, 6 and 12); and (3) Pliocene and younger deposits are gently warped down along the margins of the subsiding basin (Figures 3 through 8).

The occurrence of active, localized subsidence between two en echelon fault strands can be used to infer the style of faulting on the basin-margin faults. For examples, King (1985) and Barka and

Kadinsky-Cade (1989) describe the kinematics and occurrence of subsiding basins between en echelon strike-slip faults. Based on the right-stepping en echelon geometry of the southern San Simeon fault zone and northern Hosgri fault zone and the well-documented right-slip behavior of the San Simeon fault zone onshore to the north, we interpret the locally subsiding basin between these two faults to be a tectonic pull-apart basin. Kinematic considerations require that right slip is transferred across the pull-apart between the San Simeon and Hosgri fault zones and, thus, that the Hosgri fault zone is a prominent right-slip fault in the near-coastal region of south-central California.

A similar origin has been proposed for a large number of Quaternary basins along strike-slip fault zones throughout the world including: the Dead Sea Basin and Gulf of Aqaba basins along the Dead Sea Rift (Quennell, 1958; Ben-Avraham, 1985; Ten-Brink and Ben-Avraham, 1989); the Niksar and Erzincan basins along the North Anatolian fault (Barka and Kadinsky-Cade, 1988); the Cholame Valley along the San Andreas fault zone (Shedlock et al., 1990); the Hamner Basin along the Hope fault in New Zealand (Freund, 1971); the Carioco Basin in the southern Caribbean Sea (Schubert, 1982); the La Gonzalez Basin along the Bocono fault zone in Venezuela (Schubert, 1980); and several basins along the Haiyuan, Xianshuihe, and Fuyun fault zones in China (Deng et al., 1986). Recent publications (for example, Aydin and Nur, 1982; Mann et al., 1983; and Bahat, 1983) provide reviews of these previously recognized stepovers and suggest structural models for pull-apart basin development.

The San Simeon/Hosgri pull-apart basin exhibits several features in common with other pull-apart basins or dilatational jogs recognized along strike-slip faults throughout the world. The geometry of the San Simeon/Hosgri basin defines an elongated "lazy Z" pattern characteristic of young active pull-apart basins bounded by right-slip or "master" faults (Mann et al., 1983) (Figures 13, 14, and 16). The San Simeon/ Hosgri pull-apart basin is similar to other "lazy Z"-shaped basins in that there are no large transverse faults connecting the master boundary faults. The margins of the San Simeon/Hosgri pull-apart basin are characterized by a gentle downwarping of sediments into the stepover region (for example, Figure 8) and resemble similar margins along the Cholame Valley pull-apart basin (Shedlock et al., 1990) (Figure 15) and the Dead Sea Rift (Kashai and Croker, 1987; Reches, 1987) (Figure 15). All these pull-apart structures are similar in that each is characterized by localized, asymmetric subsidence, which has resulted in the formation of a tilted half grabens (for example, Figure 16).

The San Simeon/Hosgri pull-apart basin also contains numerous, relatively short, apparent normal faults that are subparallel to, rather than strongly oblique to, the bordering strike-slip master faults. These normal faults form an en echelon "relay" pattern across the basin. Subparallel normal faults within pull-apart basins are observed in many areas, such as the Niksar basin (Hempton and Dunne, 1983), Gulf of Aqaba (Ben-Avraham, 1985), and the Cholame Valley basin (Shedlock et al., 1990) (Figures 13, 14, and 15). Localized uplift of basement and either removal of or non-development of the top of Miocene and mid-Pliocene unconformities (Figure 10) along the northern margin of the San Simeon/ Hosgri pull-apart basin is also comparable to "compressional bulges" around the perimeter

of other pull-apart basins where the master bordering strike-slip faults are non-parallel and form an overall, regional left-restraining bend across the basin. Excellent examples of these compressional bulges occur along the margins of the Hanmer basin (Freund, 1971) and the Erzincan basin (Barka and Kadinsky-Cade, 1988).

Estimated Rate of Slip Transferred Across the Stepover

The region within an en echelon stepover between two strike-slip faults deforms in response to the relative motion of the strike-slip faults (Mann et al., 1983). The degree of deformation and the extent of basin development in the stepover region are dependent on four parameters: the slip rate, cumulative displacement on the fault system, dimensions of the stepover, and the effective transfer of slip across the stepover. By evaluating these parameters for the San Simeon/Hosgri stepover, we can estimate the amount and rate of strike slip transferred across the stepover.

Empirical, theoretical, and experimental studies strongly indicate that basin dimensions are related to cumulative displacement along the master faults over a given period of time. For example, using a mathematical model based on elastic dislocation theory, Rodgers (1980) modeled the structural development of pull-apart basins between lengthening parallel master faults and first proposed a relationship between basin depth and master-fault displacement. The principal variables in this development are the amount of overlap of the two en echelon master faults, the spacing between these faults, the amount of displacement along the faults, and whether or not the faults intersect the earth's surface. Depending on the amount of overlap and spacing between the master faults, the depth of the basin formed between two en echelon strike-slip faults typically ranges from 10 to 15 percent of the fault displacement (Rodgers, 1980).

Hempton and Dunne (1984) compared modern and ancient pull-apart basins and suggested that the thickness of sediment in kilometers (y) is related to the length in kilometers of a pull-apart basin parallel to master fault overlap (x) by the equation $y = 0.8x + 0.26$. They hypothesized that subsidence of the pull-apart basin depends on the amount of crustal stretching, which, in turn, is a function of strike-slip displacement on the master faults. Subsequent claybox experiments by Hempton and Neher (1986) showed that subsidence is accommodated in the stepover area by oblique-slip on many Riedel and conjugate Riedel shears distributed throughout the stepover area. Subsidence (y, centimeters) exhibits a linear relationship with the master fault displacement (x, in centimeters) described by the equation $y = 0.36x - 1.4$.

Woodcock and Fischer (1986) also note that a simple volume balance at an en echelon fault offset suggests that the instantaneous uplift or subsidence rate in the stepover region could be of the same order as the slip rate on the bounding fault. Their numerical estimate of the rate of subsidence at an offset is represented by the equation

$$\text{subsidence rate} = (h \div l) \times (\text{slip rate})$$

where (h) is depth of the basin in kilometers and (l) is the length of the basin in kilometers along strike. This calculation gives a maximum rate, since in natural systems some of the excess volume is accommodated by lateral bending of the fault walls and distributed uplift or subsidence around the bend.

Based on the empirical relationships of Rodgers (1980) and Woodcock and Fischer (1986), we have used the geometry and dimensions of the San Simeon/Hosgri pull-apart basin (Figure 17) to estimate the long-term rate of lateral slip that must be transferred across the stepover region in order to develop the pull-apart (Table 4). In these calculations, we assume that the sediments infilling the basin range in age from Holocene to mid-Pliocene (2.8 million years) or early Pliocene (less than 5.3 million years) (Table 3). As discussed previously, there are no well data with which to evaluate directly either the lithology or age of the sedimentary strata within the pull-apart basin. Two prominent unconformities are observed in the pull-apart basin on the seismic data (Figures 3 through 7). We correlate the stratigraphically lower unconformity to the top of Miocene unconformity (5.3 million years) mapped elsewhere in the offshore Santa Maria Basin on the basis of seismic character and loop-tied geophysical data. Alternatively, this unconformity may be equivalent to the younger mid-Pliocene unconformity interpreted to be 2.8 to 3.4 million years old. Because of the uncertainties of ages of sediments within the basin, therefore, we have calculated slip rates based on sediment thicknesses and ages implied by both interpretations (Table 4).

In addition, we have estimated slip rate using both the thickness of post-late-Wisconsinan (18,000 years old) sediment and approximate values of master fault overlap in the stepover region (Table 4). The maximum thickness of post-late-Wisconsinan sediment is 12 meters in several small, localized areas along the Hosgri fault zone and along one of the normal faults that transect the basin (Figure 11). We also subjectively use a value of 6 meters for the thickness of post-late-Wisconsinan sediment to better approximate the thickness of sediment throughout the basin minus the background thickness of post-late-Wisconsinan sediment on the shelf outside the basin. In this manner, we better approximate the thickness of sediment due to tectonic subsidence and impoundment of sediment within the basin. Because of the uncertainty in measuring the thickness of post-late-Wisconsinan sediment in the basin due to subsidence (and thus equating this value to basin depth to structural relief) and the relatively young age of the deposits, the estimated slip rates calculated from these values is also uncertain. The values do, however, indicate that lateral slip on the order of millimeters per year is occurring on the bordering master faults in order to develop the basin.

We estimate master fault overlap to be 10 $\pm$ 5 kilometers. The range of 5 to 15 kilometers is used to account for the probable minimum and probable maximum length of fault overlap. The minimum of 5 kilometers assumes that the San Simeon fault zone extends to the southeast through San Simeon Bay, where it separates the Franciscan Complex from Monterey Formation (based on diver geology and is detected on Scammon seismic data), to the Cambria coastline, where it is inferred to trend subparallel to a prominent syncline in Tertiary strata and thus separates Tertiary strata offshore from the Cambria slab basement complex onshore. The maximum value of 15 kilometers assumes that the San Simeon fault zone extends southeast to beyond Point Estero and accounts for the length of the observed pull-apart basin, which is about 15 to 18 kilometers long and is an indirect measure of fault overlap.

The equations developed by Hempton and Neher (1986) and Hempton and Dunne (1984) were not used to estimate slip rates in this study. The equation developed by Hempton and Dunne (1984) relates sediment thickness to basin length and does not provide a direct measure of fault displacement over a period of time. The equation developed by Hempton and Neher (1986) relates basin subsidence to master-fault displacement based on claybox experiments. Their studies show that basin subsidence does not begin until a threshold of cumulative fault displacement is achieved, after which there is a linear relationship between basin subsidence and fault displacement. The threshold of cumulative fault displacement at a crustal scale is likely to be different, because of the rheological properties of the crust, and thus the equation developed by Hempton and Neher (1986) is not valid for this analysis.

The estimated slip rates presented in Table 2 range from about 1 to 4 millimeters per year. We consider these rates to be minimum estimates for the lateral slip rates on the bordering strike slip faults for the following reasons:

- Thickness of basin sediment is used as an indirect measure of structural relief and is predicated on the assumption that the basin is closed and has little or no loss of sediment. Because the Hosgri/San Simeon basin lies offshore, however, the thickness of strata contained within the basin above the lowest mapped unconformity (our interpreted top of Miocene, Figures 3 through 7, or alternatively, the mid-Pliocene) has been reduced by subsequent erosional events. At least two unconformities (for example, the interpreted mid-Pliocene unconformity (Figures 3 through 7) and the late Wisconsinan unconformity), occur stratigraphically above the top of Miocene unconformity. These unconformities represent periods of erosion and/or intervals of non-deposition during periods of climatically-controlled low sea level.

- At least some lateral slip on the bordering master faults is likely accommodated by local compressional structures north and south of the pull-apart and by inefficient (or non-ideal) transfer of slip and structural evolution of the pull-apart basin.

- The late Pliocene and Pleistocene Careaga Formation occurs as a fault sliver within the San Simeon fault zone at San Simeon Bay about 5 to 10 kilometers north of the pull-apart basin. The Careaga Formation at this location is a fossiliferous marine conglomeratic deposit containing abundant angular clasts of locally reworked Monterey Formation shale and black chert. The fossil assemblage and local reworking of Monterey clasts, many of which are pholad-bored, indicates near-shore deposition, perhaps in the late Pliocene San Simeon/Hosgri pull-apart basin. The outcrop of Careaga at San Simeon Bay, therefore, may represent a faulted slice of the San Simeon/Hosgri pull-apart basin transported roughly 5 to 10 kilometers northward in the past 2 million years, or a slip rate of 2.5 to 5 millimeters per year on the San Simeon fault zone.

- The age of sediment in the basin is not well constrained and may be considerably younger than the 5.3- and 2.8-million-year estimates used in the slip rate calculations.

Despite these limitations, the minimum estimated slip rates compare favorably with those derived independently from paleoseismic investigations conducted along the onshore reach of the San Simeon fault zone. These investigations yielded slip rate estimates of 1 to 3 millimeters per year over the past 200,000 years (PG&E, 1988; Hanson and Lettis, in review) and 1 to 2 millimeters per year during the Holocene (PG&E, 1988; Hall and Hunt, in review). We conclude, therefore, that the lateral slip rate along the northern Hosgri fault zone is a minimum of 1 to 4 millimeters per year, and is likely to be comparable to slip rates reported along the onshore San Simeon fault zone.

Implications of the San Simeon/Hosgri Pull-Apart Basin for Seismic Hazard Assessment

Various researchers postulate that releasing stepovers or dilatational jogs are potential segmentation points to the propagation of seismic rupture along a fault zone (for example, Sibson, 1985, 1986; King, 1986; Kneupfer et al., 1989). Abrupt changes in the amount of slip accompanying individual earthquakes, for example, are commonly associated with releasing or dilatational stepovers (Clark, 1972; Tchalenko and Berberian, 1975; Sieh, 1978; Sibson, 1986). Pull-apart basins are coincident with the ends of several historical ruptures along the North Anatolian fault zone in Turkey (Barka and Kadinsky-Cade, 1988) and the Cholame Valley along the San Andreas fault zone in central California also appears to have hindered or terminated surface rupture associated with historical earthquakes (Brown and Vedder, 1967; Aki, 1979; Allen, 1968; and Shedlock et al., 1990). Similarly, studies of seismicity associated with the 1979 M_L 5.9 Coyote Lake earthquake on the Calaveras fault indicate that coseismic rupture associated with the earthquake terminated at a dilatational jog or right-releasing step (Bouchon, 1982; Lin and Helmberger, 1983) and that subsequent, post-seismic slip transferred to an en echelon fault segment about 2 kilometers to the southwest (Reasenberg and Ellsworth, 1982; Sibson, 1986b). In a systematic evaluation of a large number of historical fault ruptures, Knuepfer (1989) and Knuepfer et al. (1989) documented very few cases in which coseismic rupture propagated across releasing stepovers 5 kilometers or more wide.

These observations and the growing body of theoretical and empirical evidence strongly indicate that large releasing stepovers along strike-slip fault systems are effective, long-lived segmentation points to coseismic rupture. The San Simeon/Hosgri pull-apart basin is up to 5 kilometers wide and up to 18 kilometers long. It is the largest known extensional stepover along the entire San Gregorio/San Simeon/Hosgri fault system. The stepover clearly separates the northern Hosgri fault zone from the southern San Simeon fault zone, and likely separates ruptures occurring on these two fault zones.

CONCLUSIONS

Analysis of geophysical and geological data from the near-offshore region between San Simeon Bay and Estero Bay shows that the northern Hosgri fault zone and southern San Simeon fault zone are related to one another via a right, en echelon stepover. An extensional, subsiding basin bordered by and containing normal faults occurs locally

within the stepover region. Based on kinematic arguments and comparisons with subsiding basins along strike-slip faults worldwide, we interpret the subsiding basin between the Hosgri and San Simeon fault zones to be a tectonic pull-apart basin.

The San Simeon/Hosgri pull-apart basin accommodates the lateral slip on the two bordering strike-slip faults. Based on empirical, theoretical, and experimental modeling techniques that relate pull-apart dimensions to cumulative lateral slip on the bordering master faults, we estimate minimum slip rates of 1 to 4 millimeters per year for the southern San Simeon and northern Hosgri fault zones. These slip rates are consistent with time-averaged late Quaternary and Holocene slip rates estimated from paleoseismic investigations and geologic mapping along the southern onshore reach of the San Simeon fault zone.

Seismic hazard analyses require that estimates be made of likely rupture lengths along fault zones. A growing body of theoretical and empirical data indicates that extensional releasing stepovers or dilatational jogs often are effective segmentation points to coseismic rupture along strike-slip fault systems. The San Simeon/Hosgri pull-apart basin is the largest known extensional releasing stepover along the entire San Gregorio/San Simeon/Hosgri fault system. Based on its geometry and stratigraphic relationships, the basin appears to be a major, long-lived segmentation point separating the southern San Simeon and northern Hosgri fault zones.

REFERENCES

Aki, K., Characterization of barriers on an earthquake fault: Journal of Geophysical Research, 84, 6140-6148, 1c^F9.

Allen, C.R., The tectonic environments of seismically active and inactive areas along the San Andreas fault system; in Kovach, R., A. and Nur, eds., Proceedings of the Conference on Geologic Problems of the San Andreas Fault System, Stanford University Publications in Geological Sciences, 11, 70-92, 1968.

Atwater, T., Implications of plate tectonics for the Cenozoic tectonic evolution of western North America: Geological Society of America Bulletin, 81, 3513-3536, 1970.

Atwater, T., and P. Molnar, Relative motion of the Pacific and North American plates deduced from sea-floor spreading in the Atlantic, Indian, and South Pacific oceans: in Kovach, R. L., and Nur, A., (eds.), Proceedings of the Conference on Tectonic Problems of the San Andreas Fault System, Stanford University Publications in Geological Sciences, 13, 136-148, 1973.

Aydin, A., and A. Nur, Evolution of pull-apart basins and their scale independence: Tectonics, 1, 91-105, 1982.

Bahat, D., New aspects of rhomb structures: Journal of Structural Geology, 5, 591-601, 1983.

Barka, A.A., and K. Kadinsky-Cade, Effects of restraining stepovers on earthquake rupture; in Schwartz, D.P., and Sibson, R.H., (eds.), Fault Segmentation and Controls of Rupture Initiation and Termination: U.S. Geological Survey Open File Report 89-315, 67-79, 1989.

Barka, A.A., and K. Kadinsky-Cade, Strike-slip fault geometry in Turkey and its influence on earthquake activity: Tectonics, 7, 663-684, 1988.

Barron, J. A., Updated diatom biostratigraphy for the Monterey Formation of California; in Siliceous Microfossils and Microplankton Studies of the Monterey Formation and Modern Analogs, R.E. Casey and J.A. Barron, eds., Pacific Section, Society of Econ. Paleontologists and Mineralogists, Book 45, 1986.

Ben-Avraham, Z., Structural framework of the Gulf of Elat (Aqaka), Northern Red Sea: Journal of Geophysical Research, 90, 703-726, 1985.

Berggren, W.A., D.V. Kent, J.J. Flynn, and J.A. Van Couvering, Cenozoic geochronology: Geological Society of America Bulletin, 96, 1407-1418, 1985.

Beyer, L.A., and D.S. McCulloch, Free-air gravity anomaly map of the offshore Santa Maria Basin: U.S. Geological Survey Open-File Report, 1 map, scale 1:125,000, 1988, in preparation.

Bishop, C.C., and J.F. Davis, Correlation of Stratigraphic Units of North America (COSUNA) project, Southern California region: The American Association of Petroleum Geologists, 1984.

Blake, M.C., R.H. Campbell, T.H. Dibblee, D.G. Howell, T.H. Nilsen, W.R. Normark, J.G. Vedder, and E.A. Silver, Neogene basin formation and hydrocarbon accumulation in relation to the plate tectonic evolution of the San Andreas fault system, California: American Association of Petroleum Geologists Bulletin, 62, 344-372, 1978.

Bouchon, M., The rupture mechanism of the Coyote Lake earthquake of 6 August 1979 inferred from near-field data: Bulletin of the Seismological Society of America, v. 72, p. 745-757, 1982.

Brown, R.D., Jr., and J.G. Vedder, Surface tectonic fractures along the San Andreas fault: U.S. Geological Survey Professional Paper 579, 2-23, 1967.

Burchfield, B.C., and J.H. Stewart, 1966, "Pull-apart" origin of the central segment of Death Valley, California: Geological Society of America Bulletin, 77, 439-442, 1966.

Clark, D.H., N.T. Hall, D.H. Hamilton, and R.G. Heck, Structural analysis of late Neogene deformation in the central offshore Santa Maria Basin, California: Journal of Geophysical Research, in press.

Clark, J.C., E.E. Brabb, H.G. Greene, and D.C. Ross, Geology of Point Reyes Peninsula and implications for San Gregorio fault history; in J.K. Crouch and S.B. Bachman (eds.), Tectonics and Sedimentation Along the California Margin: Pacific Section S.E.P.M., 38, 67-86, 1984.

Clark, M.M., Surface rupture along the Coyote Creek fault: U.S. Geological Survey Professional Paper 787, 55-86, 1972.

Cox, A., and D. Engebretson, Change in motion of Pacific plate at 5 Myr BP.: Nature, 313, 472-272, 1985.

Crain, W.E., W.E. Mero, and D. Patterson, Geology of the Point Arguello field; in R.V. Ingersoll and W.E. Ernst (eds.): Cenozoic Basin Development of Coastal California, Rubey Vol. VI, Englewood Cliffs, New Jersey, Prentice Hall, p. 405-426, 1987.

Crouch, J., S.B. Bachman, and J.T. Shay, Post-Miocene compressional tectonics along the central California margin; in J. Crouch, and S.B Bachman (eds.), Tectonics and Sedimentation Along the California Margin: Pacific Section, S.E.P.M., 38, 37-54, 1984.

Crowell, J.C., Sedimentation along the San Andreas fault; in R.H. Doff, Modern and Ancient Geosynclinal Sedimentation: Special Publication, Society of Economic Paleontologists and Mineralogists, 19, 292-303, 1974.

Cummings, D., T.A. Johnson, and R.A. Gaal, Shallow structural geology, offshore Santa Maria to Point Arguello, central California (abs.): Geological Society of America Abstracts with Programs, Cordilleran Section, 19, 369, 1987.

Davis, T.L., and K.D. McIntosh, A retrodeformable structural solution across the southern Coast Ranges and implications for seismically active structures (abs.): Geological Society of America Abstracts with Programs, Cordilleran Section Meeting, 19, 370, 1987.

Deng, Q., S. Chen, F. Song, S. Zhu, Y. Wang, W. Zhang, D. Jiao, B.C. Burchfield, P. Molnar, L. Royden, and P. Zhang, Variations in the geometry and amount of slip on the Haiyuan (Nanxi haushan) fault zone, China and the surface rupture of the 1920 Haiyuan earthquake: American Geophysical Union, Maurice Ewing Series, 6, 169-182, 1986.

Dumont, M.P., 1989, The Monterey Formation and biostratigraphy: an overview; in T.C. Mackinnon (ed.), Oil in the California Monterey Formation: American Geophysical Union Field Trip Guidebook T311, 28th International Geological Congress, 28-32, 1989.

Engebretson, D.C., A. Cox, and R.G. Gordon, Relative motions between oceanic and continental plates in the Pacific basin: Geological Society of America Special Paper 206, 59 p., 1985

Envicom, Fault investigation, Hearst Ranch environmental data base: unpublished report for the Hearst Corporation, 1977.

Freund, R., The Hope fault: A strike slip fault in New Zealand: New Zealand Geological Survey Bulletin, 86, 49, 1971.

Graham, S.A., Tertiary sedimentary tectonics of the central Salinan block of California: unpublished Ph.D. thesis, Stanford University, California, 510 p., 1976.

Graham, S.A., 1978, Role of the Salinian Block in the evolution of the San Andreas fault system, California: American Association of Petroleum Geologists Bulletin, 62, 2214-2231, 1978.

Graham, S.A. and W.R. Dickinson, The San Gregorio Fault as a major right-slip fault of the San Andreas fault system (abs.): Geological Society of America Abstracts with Programs, 8, 890, 1976.

Graham, S.A., and W.R. Dickinson, Evidence for 115 kilometers of right slip on the Gregorio-Hosgri fault trend: Science, 199, 179-81, 1978a.

Graham, S.A., and W.R. Dickinson, Apparent offsets of on-land geologic features across the San Gregorio-Hosgri fault trend; in E.A. Silver and W.R. Normack (eds), San Gregorio-Hosgri Fault Zone, California: California Division of Mines and Geology, Special Report 137, 13-23, 1978b.

Greene, H.G., Geology of the Monterey Bay region: U.S. Geological Survey Open-File Report 77-718, 347 p., 1977

Hall, C.A., Jr., San Simeon-Hosgri fault system, coastal California: economic and environmental implications: Science, 190, 1291-1294, 1975.

Hall, C.A., Jr., Origin and development of the Lompoc-Santa Maria pull-apart basin and its relation to the San Simeon-Hosgri strike-slip fault, western California; in E.A. Silver and W.R. Normark (eds.), San Gregorio-Hosgri fault zone, California: California Division of Mines and Geology Special Report 137, 25-31, 1978.

Hall, C.A., Jr., San Luis Obispo transform fault and middle Miocene rotation of the western Transverse Ranges, California: Journal of Geophysical Research, 86, 1015-1013, 1981.

Hall, C.A., Jr., San Gregorio-San Simeon-Hosgri fault, Point Sur, California (abs.): Program, 64th Annual Meeting, Pacific Section AAPG-SEPM, 1989.

Hall, C.A., Jr., W.G. Ernst, S.W. Prior, and J.W. Wiese, Geologic map of the San Luis Obispo-San Simeon region, California: U.S. Geological Survey, Miscellaneous Investigations Map I-1097, 1979.

Hall, N.T., and T.D. Hunt, Holocene behavior of the San Simeon fualt zone, south-central coastal California; in I.B. Alterman (ed.), Seismotectonics of Central and Coastal California: Geological Society of America Special Paper, in review.

Hall, N.T., T.D. Hunt, P.A. Vaughan, F. Bickner, and W.R. Lettis, Trenching and mapping investigations of the late Quaternary behavior of the San Simeon fault, San Luis Obispo County, California (abs.): Geological Society of America Abstracts with Programs, Cordilleran Section, 19, 385, 1987.

Hamilton, D.H., The tectonic boundary of coastal Central California: Ph.D. dissertation, Stanford University, 290 p, 1984.

Hamilton, D.H., 1987, Characterization of the San Gregorio-Hosgri fault system, coastal central California (abs.): Geological Society of America Abstracts with Programs, Cordilleran Section, 19, 385, 1987.

Hamilton, D.H., and C.R. Willingham, Hosgri fault zone: structure, amount of displacement, and relationship to structures of the western Transverse Ranges (abs.): Geological Society of America Abstracts with Program, 9, 429, 1977.

Hamilton, D.H., and C.R. Willingham, Evidence for a maximum of 20 km of Neogene right slip along the San Gregorio fault zone of central California (abs.): EOS (Transactions, American Geophysical Union), 59, 1210, 1978.

Hamilton, D.H., and C.R. Willingham, The coastal boundary zone of central California (abs.): Geological Society of America, Abstracts with Programs, Cordilleran Section Meeting, 11, 81, 1979.

Hanson, K.L., and W.R. Lettis, in review, Estimated Pleistocene slip rate for the San Simeon fault zone, south-central coastal California; in I.B. Alterman (ed.), Seismotectonics of Central and Coastal California: Geological Society of America Special Paper, in review.

Hanson, K.L., W.R. Lettis, and L. Mezger, Late Pleistocene deformation along the San Simeon fault zone near San Simeon, California (abs.): Geological Society of America Abstracts with Programs, Cordilleran Section, 19, 386, 1987.

Harbert, W., and A. Cox, Late Neogene motion of the Pacific plate: Journal of Geophysical Research, 94, 3052-3064, 1989.

Hempton, M.R., and L.A. Dunne, Sedimentation in pull-apart basins: active examples in eastern Turkey: Journal of Geology, 92, 513-530, 1984.

Hempton, M.R., and Neher, K., Experimental fracture, strain and subsidence patterns over en echelon strike-slip faults: implications for the structural evolution of pull-apart basins: Journal of Structural Geology, 8, 597-605, 1986.

Hoskins, E.G. and J.R. Griffiths, 1971, Hydrocarbon potential of northern and central California offshore; in I.H. Cram (ed.), Future petroleum provinces of the United States — their geology and potential: American Association of Petroleum Geologists Memoir 15, 212-228, 1971.

Isaacs, C.M., M.A. Keller, V.A. Gennai, K.C. Stewart, and J.E. Taggart, Jr., Preliminary evaluation of Miocene lithostratigraphy in the Point Conception COST well, OCS-CAL 780164 No. 1, off southern California; in C.M. Isaacs, R.E. Garrison, S.A. Graham, and W.A. Jensky, II (eds.), Petroleum Generation and Occurrence in the Miocene Monterey Formation, California: Pacific Section, Society of Economic Paleontologists and Mineralogists, 1983.

Jennings, C.W., Fault map of California with locations of volcanoes, thermal springs and thermal wells: California Division of Mines and Geology Geologic Data Map No. 1, scale 1:750,000, 1985.

Kashai, E.L., and P.F. Croker, Structural geometry and evolution of the Dead Sea - Jordan rift system as deduced from new subsurface data: Tectonophysics, 141, 33-60, 1987.

King, G.C.P., 1986, Speculations on the geometry of the initiation and termination processes of earthquake rupture and its relation to morphology and geological structure: PAGEOPH, 124, 567-585, 1986.

Knuepfer, P.L., Implications of the characteristics of endpoints of historical surface fault ruptures for the nature of fault segmentation; in D.P. Schwartz, and R.H. Sibson, (eds.), Fault Segmentation and Controls of Rupture Initiation and Termination: U.S. Geological Survey Open-File Report 89-315, 193-228, 1989.

Knuepfer, P.L.K., E.M. Baltzer, and J.M. Turko, Repeatibility of fault rupture segments and earthquake potential: U.S. Geological Survey, National Earthquake Hazards Reduction Program, Final Technical Report, Contract No. 14-08-0001-G1527, 1989.

Lemiszki, P.J., and L.D. Brown, Variable crustal structure of strike-slip fault zones as observed on deep seismic reflection profiles: Geological Society of America Bulletin, 100, 665-676, 1988.

Leslie, R.B., Continuity and tectonic implications of the San Simeon-Hosgri fault zone, Central California: unpublished Master Thesis, University of California at Santa Cruz, California, 1980.

Leslie, R.B., Continuity and tectonic implications of the San Simeon-Hosgri fault zone, central California: U.S. Geological Survey Open-File Report 81-430, 1981.

Lettis, W.R., N.T. Hall, and D.H. Hamilton, Quaternary tectonics of south-central coastal California (abs.): 28th International Geological Congress, Abstracts, 2, 2-285, 1989.

Liu, J.-L., and D.V. Helmberger, The near-source ground motion of the 6 August 1979 Coyote Lake, California, earthquake: Bulletin of the Seismological Society of America, 73, 201-218, 1983.

Mann, P., M.R. Hempton, D.C. Bradley, and K. Burke, Development of pull-apart basins: Journal of Geology, 91, 529-554, 1983.

Manson, M., San Simeon fault zone and Cambria fault, San Luis Obispo County, California: California Division of Mines and Geology Fault Evaluation Report FER-170, 12 p., 1985.

McCulloch, D.S., Regional geology and hydrocarbon potential of offshore Central California: U.S. Geological Survey Professional Paper (in press), 127 p., 1987.

McCulloch, D.S., and R.H. Chapman, Maps showing residual magnetic intensity along the California coast, lat. 37°30'N to 34°30'N: U.S. Geological Survey Open File Report 77-79, 14 aeromagnetic maps, scale 1:250,000, 1977.

McCulloch, D.S., and S.D. Lewis, Offshore resource geology of central California: in U.S. Geological Survey Research on Energy Resources - 1988 Program and Abstracts, U.S. Geological Survey Circular 1025, 34, 1988.

McCulloch, D.S., J.G. Vedder, H.C. Wagner, and R.G. Bruns, Geological setting; in H.E. Cook (ed.), Geologist Studies of the Point Conception Deep Stratigraphic Test Well, OCS-CAL 78-164 No. 1, Outer Continental Shelf, Southern California: U.S. Geological Survey Open-File Report 79-1218, 1979.

Namson, J.S., and T.L. Davis, Subsurface study of the late Cenozoic structural geology of the Santa Maria basin, western Transverse Ranges and southern Coast Ranges, California (in review), 1990.

Pacific Gas and Electric Company, Appendix 2.5E, Final Safety Analysis Report for Diablo Canyon Nuclear Power Plant: U.S. Atomic Energy Commission Docket Nos. 50-275 and 50-323, 1975.

Pacific Gas and Electric Company, Final Report of the Diablo Canyon Long Term Seismic Program: U.S. Nuclear Regulatory Commission Docket Nos. 50-275 and 50-323, 1988.

Page, B.M., and D.C. Engebretson, Correlations between the geologic record and computed plate motions for central California: Tectonics, 3, 133-155, 1984.

Quennell, A.M., The structural and geomorphic evolution of the Dead Sea Rift: Journal of the Geological Society of London, 114, 1-24, 1958.

Reasenberg, P., and W.L. Ellsworth, Aftershocks of the Coyote Lake, California earthquake of August 6, 1979; a detailed study: Journal of Geophysical Research, 87, 10,637-10,665, 1982.

Reches, Z., Mechanical aspects of pull-apart basins and push-up swells with applications to the Dead Sea transform: Tectonophysics, 141, 75-88, 1987.

Rodgers, D.A., Analysis of pull-apart basin development produced by en echelon strike-slip faults; in P.F. Balance and H.G. Reading (eds.), Sedimentation in Oblique-slip Mobile Zones: Int. Assoc. Sediment. Special Publication 4, 27-41, 1980.

Schubert, C., Late-Cenozoic pull-apart basins, Bocono fault zone, Venezuelan Andes: Journal of Structural Geology, 2, 463-468, 1980.

Schubert, C., Origin of Cariaco basin, southern Caribbean Sea: Marine Geology, 47, 345-360, 1982.

Seiders, V.M., 1979, San Gregorio-Hosgri fault zone south of Monterey Bay, California: A reduced estimate of maximum displacement: U.S. Geological Survey Open File Report 79-385, 10 p., 1979

Shedlock, K.M., T.M. Brocher, and S.T. Harding, Shallow structure and deformation along the San Andreas fault in Cholame Valley, California, based on high-resolution reflection profiling: Journal of Geophysical Research, in press.

Sibson, R.H., 1985, Stopping of earthquake ruptures and dilational jogs: Nature, 316, 248-251, 1985.

Sibson, R.H., Brecciation processes in fault zones: inferences from earthquake rupturing: Pageoph, 124, 159-175, 1986a.

Sibson, R.H., Rupture interaction with fault jogs; in S. Das, J. Boatwright, and C.H. Sholz (eds.), Earthquake Source Mechanics, Maurice Ewing Series 6, American Geophysical Union Monography, 37, 157-168, 1986b.

Sieh, K.E., Slip along the San Andreas fault associated with the great 1857 earthquake: Bulletin of the Seismological Society of America, 68, 1421-1448, 1978.

Silver, E.A., 1974, Structural interpretation from free-air gravity on the California continental margin, 35° to 40°N (abs.): Geological Society of America Abstracts with Programs, 6, 253, 1974.

Silver, E.A., 1978, The San Gregorio-Hosgri fault zone: an overview; in E.A. Silver, and W.R. Normark (eds.), San Gregorio-Hosgri Fault Zone, California: California Division of Mines and Geology Special Report 137, 1-2, 1978.

Silver, E.A., and W.R. Normark, San Gregorio-Hosgri fault zone, California: California Division of Mines and Geology Special Report 137, 567 p., 1978.

Tchalenko, J.S., and M. Berberian, Dasht-e-Bayaz fault, Iran: earthquake and earlier related structures in bedrock: Geological Society of America Bulletin, 86, 703-709, 1^D5.

ten-Brink and Ben-Avraham, The anatomy of a pull-apart basin; seismic reflection observations of the Dead Sea Basin: Tectonics, 8, 1989.

Wagner, H.C., Marine geology between Cape San Martin and Point Sal, south-central California offshore: U.S. Geological Survey Open-File Report 74-252, 17 p., 1974.

Weber, G.E., Geologic investigation of the marine terraces of the San Simeon region and Pleistocene activity of the San Simeon fault zone, San Luis Obispo County, California: U.S. Geological Survey Technical Report 66, 1983.

Weber, G.E., and K.R. Lajoie, Late Pleistocene and Holocene tectonics of the San Gregorio fault zone between Moss Beach and Point Año Nuevo, San Mateo County, California (abs.): Geological Society of America Abstracts with Programs, 19, 524, 1977.

Weber, G.E., and K.R. Lajoie, Late Pleistocene rates of movement along the San Gregorio fault zone, determined from offset of marine terrace shoreline angles; in G.E. Weber, K.R. Lajoie, and G.B. Griggs (eds.), Coastal Tectonics and Coastal Geologic Hazards in Santa Cruz and San Mateo Counties, California, Field Trip Guide for Cordilleran Section of the Geological Society of America, 75th Annual Meeting, 101-111, 1979a.

Weber, G.E., and K.R. Lajoie, Evidence for Holocene movement on the Frijoles fault near Point Año Nuevo, San Mateo County, California; in G.E. Weber, K.R. Lajoie, and G.B. Griggs (eds.), Coastal Tectonics and Coastal Geologic Hazards in Santa Cruz and San Mateo Counties, California, Field Trip Guide for Cordilleran Section of the Geological Society of America, 75th Annual Meeting, 92-100, 1979b.

Weber, G.E., L.K. Oshiro, D.F. Brown, P.A. McCrory, Evidence for Late Pleistocene or Holocene faulting Along the San Simeon Fault Zone at San Simeon Bay, San Luis Obispo County, California (abs.): Geological Society of America Abstracts with Program, 12, 113, 1981.

Wolf, S.C., and H.C. Wagner, Preliminary reconnaissance marine geology of area between Santa Lucia escarpment and Point Buchon, California: unpublished U.S. Geological Survey administrative report, 5 p, 1970.

Woodcock, N.H., and M. Fischer, M., 1986, Strike-slip duplexes: Journal of Structural Geology, 8, 725-735, 1986.

Table 1

COMMON-DEPTH-POINT GEOPHYSICAL DATA BASE

Acquisition Contractor	Date Shot	Owner/ Client	Primary System Energy Source	CDP (Fold)	Record Length (km)	Survey Length (km)	General Survey Area
Aquatronics	1974	PG&E	Sparker	6	1.3	479	Point Arguello to San Simeon within 10 km of coast line
Consolidated Geotechnical (CGI)	1976	CGI/PG&E	Sparker (30 kj)	12	2	1,340	Santa Maria Basin, Point Conception to Cape San Martin
Comap Alaska	1986	PG&E	Water guns (160 cu in)	24	2	500	San Luis Bay to Cape San Martin, within 6 km of coast line
Fairfield Industries	1979	Minerals Management Services	Sleeve exploder	12	1	4,720	Santa Maria Basin, Point Conception to Point Estero
JEBCO Seismic Inc	1988	JEBCO/PG&E	Air guns (3,380 cu in)	60	4	58	Northeastern Santa Maria Basin, Point San Luis to Point Piedras Blancas
Western Geophysical, Inc.	1974	Western Geophysical/ PG&E	Air guns	46	6	220	Eastern Santa Maria Basin, Point Arguello to Estero Bay
Western Geophysical, Inc.	1975 & 1982	Western Geophysical/ PG&E	Air guns	46 & 60	6	250	Northeastern Santa Maria Basin, Point Buchon to Cape San Martin
	Total kilometers of common-depth-point line					11,929	

Table 2

TYPICAL DATA PROCESSING SEQUENCE USED FOR CDP SEISMIC REFLECTION DATA ACQUIRED BETWEEN POINT ESTERO AND SAN SIMEON POINT

1. Demultiplex.
2. Gain recovery.
3. Deconvolution - spiking or predictive with time variant gates.
4. Bandwidth filter.
5. Sort - common depth point gathers and add water depth statics.
6. Vector multi-prestack - water bottom and long period multiple attenuator (proprietary to Seisdata Services, Inc.).
7. Velocity analysis every 1/2-mile or less along the line as structural complexity demands.
8. Normal moveout application.
9. Trace muting.
10. Common depth point stack.
11. Time variant filter.
12. Automatic gain control 250 to 500 ms gate depending on data type.
13. Noise rejection filter (NRF) - enhances primary energy and attenuates severe steeply dipping diffracted energy with near water velocity. NRF is similar to 2-D FK filter.
14. Remove water depth statics applied in Step 5.
15. Wave equation migration - frequency domain operator using smoothed RMS stacking velocity field converted to average velocity via Dix's equation for depth conversion.
16. Film display of Steps 12, 13, and 15.

TABLE 3. RELATIONSHIP OF STRATIGRAPHIC UNITS IN CENTRAL AND SOUTHERN OFFSHORE SANTA MARIA BASIN (Modified from Clark et al., 1989)

Central Area	Age	Southern Area*	Years B.P.
	Early Pleistocene		1.7 to 2.8 Ma
"Foxen" & younger	Late Pliocene	Upper Pico & younger	
	Late Pliocene		3.4 Ma
"upper" Sisquoc	Early Pliocene	Lower Pico (upper Sisquoc)	
	Base Pliocene		5.3 Ma
"lower" Sisquoc	Top Miocene	Santa Margarita (lower Sisquoc)	
			6.0 to 8.0 Ma
Monterey		Monterey	
			15.0 to 15.7 Ma
Point Sal		Point Sal	16.0 to 17.0 Ma
Obispo		Tranquillon	15.3 to 17.0 Ma
	Base Miocene		22 to 25 Ma
Paleogene(?) Undiff.		Unknown	
			67.0 Ma
Cretaceous(?) Undiff.		Jalama Espada	100 Ma
			140.0 Ma
Franciscan Complex	Jurassic	Franciscan Complex	

NOTES:

----- unconformity
——— conformable contact

*After McCulloch et al., 1979; Isaacs et al., 1983; and Crain et al., 1987

TABLE 4. ESTIMATED SLIP RATES ON SAN SIMEON AND HOSGRI FAULT ZONES BASED ON GEOMETRY OF SAN SIMEON/HOSGRI PULL-APART BASIN

Model	Observed Basin Depth (assume basin depth is ≥ observed sediment thickness)	Calculated Offset or Basin Stretching	Estimated Subsidence Rate (calculated from sediment thickness and sediment age)	Observed Master-Fault Overlap (assume overlap = offset or basin stretching)	SLIP RATE: Estimated Age of Sediment		
					5.3 Ma	2.8 Ma	18 Ka
Rodgers (1980)							
y = 0.10 x (where o = 2s) y = basin depth x = offset s = separation (spacing between master faults) o = overlap	y = 0.28 km (maximum post top of Miocene or post-mid-Pliocene sediment thickness)	x ≥ 2.8 km	(not applicable)	----	≥ 0.53 mm/yr	≥ 1.0 mm/yr	---
	y ≥ 0.012 km (maximum post-late-Wisconsinan sediment thickness)	x ≥ 0.12 km		----	----	----	≥ 6.7 mm/yr
	y ≥ 0.006 km (average post-late-Wisconsinan sediment thickness)	x ≥ 0.08 km		----	----	----	≥ 3.3 mm/yr
	---	---		x = 10 ± 5 km	1.9 ± 0.9 mm/yr	3.6 ± 1.8 mm/yr	----
Woodcock and Fischer (1986)							
subsidence rate = $\frac{y}{x}$ slip rate y = depth x = length of basin	y = 0. 28 km	(not applicable)	0.28 km/5.3 Ma = 0.05 mm/yr	x = 10 ± 5 km	1.8 ± 0.9 mm/yr	----	---
	y = 0.28 km		0.28 km/2.8 Ma = 0.10 mm/yr	x = 10 ± 5 km	----	3.6 ± 1.8 mm/yr	---

FIGURE CAPTIONS

Figure Number	Title
1	Regional map showing the location of the Hosgri and San Simeon fault zones in south-central coastal California.
2	Map of geologic structures in the San Simeon Bay to Estero Bay region showing locations of seismic lines.
3	Migrated seismic line S-1 (a) and interpretation (b). MPU is the mid-Pliocene unconformity and TMU is the top of Miocene unconformity.
4	Migrated seismic line S-2 (a) and interpretation (b). MPU is the mid-Pliocene unconformity and TMU is the top of Miocene unconformity.
5	Migrated seismic line S-3 (a) and interpretation (b). MPU is the mid-Pliocene unconformity and TMU is the top of Miocene unconformity.
6	Migrated seismic line S-4 (a) and interpretation (b). MPU is the mid-Pliocene unconformity and TMU is the top of Miocene unconformity.
7	Migrated seismic line S-5 (a) and interpretation (b). MPU is the mid-Pliocene unconformity and TMU is the top of Miocene unconformity.
8	Interpreted line drawing of seismic line S-6. MPU is the mid-Pliocene unconformity and TMU is the top of Miocene unconformity.
9	Time-structure map on mid-Pliocene unconformity.
10	Isopach map of post Miocene sediments.
11	Isopach map of post-late-Wisconsinan deposits.
12	Geologic sections illustrating stratigraphic and structural relationships north of the San Simeon/Hosgri pull-apart (A-A´), through the pull-apart (B-B´) and south of the pull-apart (C-C´). See Figure 11 for location of sections.
13	Comparison of the San Simeon/Hosgri pull-apart with the Dead Sea and Gulf of Aqaba pull-apart basins.

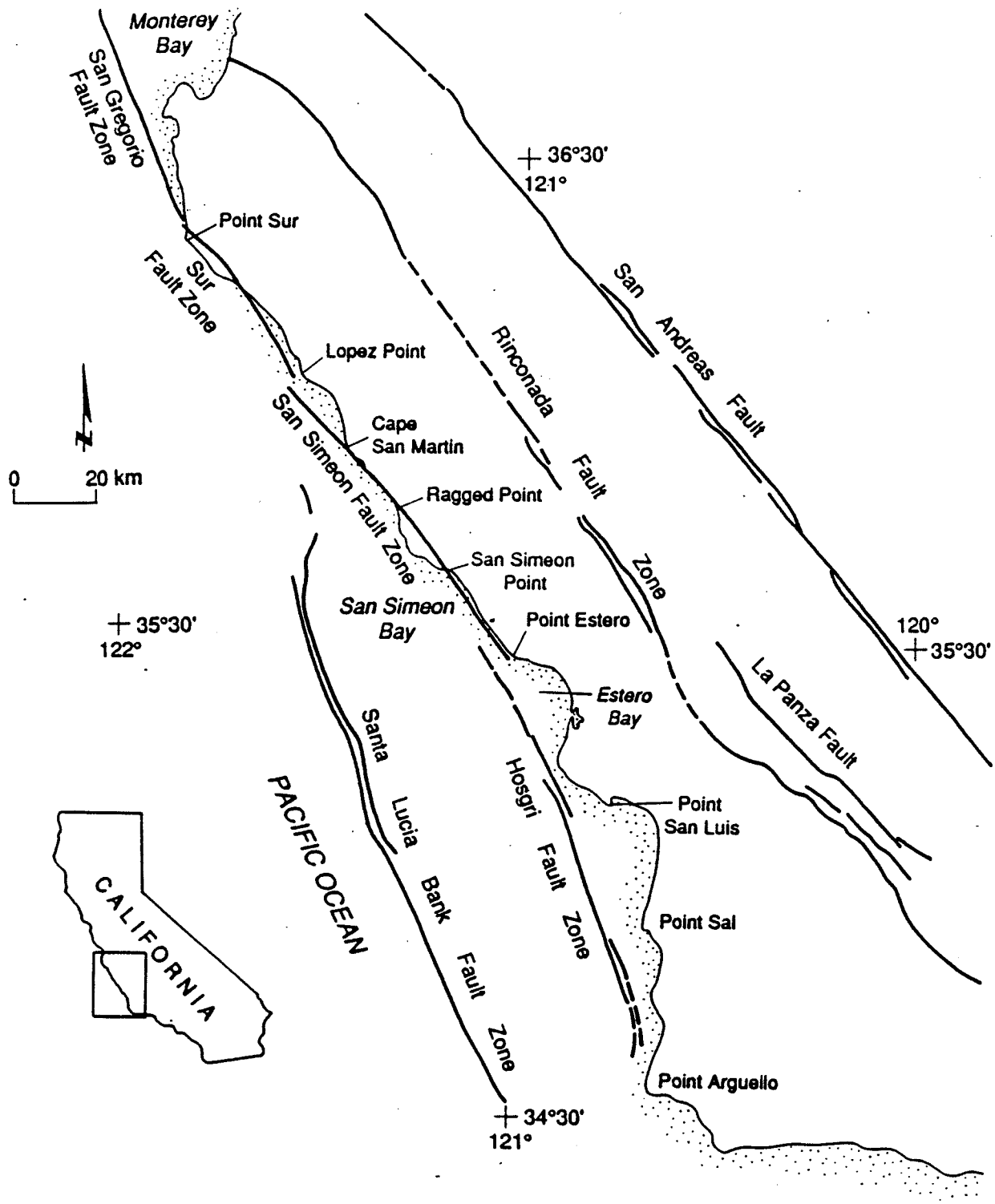
Monterey Bay
San Gregorio Fault Zone
Point Sur
Sur Fault Zone
Lopez Point
Cape San Martin
San Simeon Fault Zone
Ragged Point
San Simeon Point
San Simeon Bay
Point Estero
Estero Bay
Point San Luis
Point Sal
Point Arguello
Rinconada Fault Zone
San Andreas Fault
La Panza Fault
Santa Lucia Bank Fault Zone
Hosgri Fault Zone
PACIFIC OCEAN
CALIFORNIA
0 20 km
36°30'
121°
35°30'
122°
120°
35°30'
34°30'
121°

Figure 1.

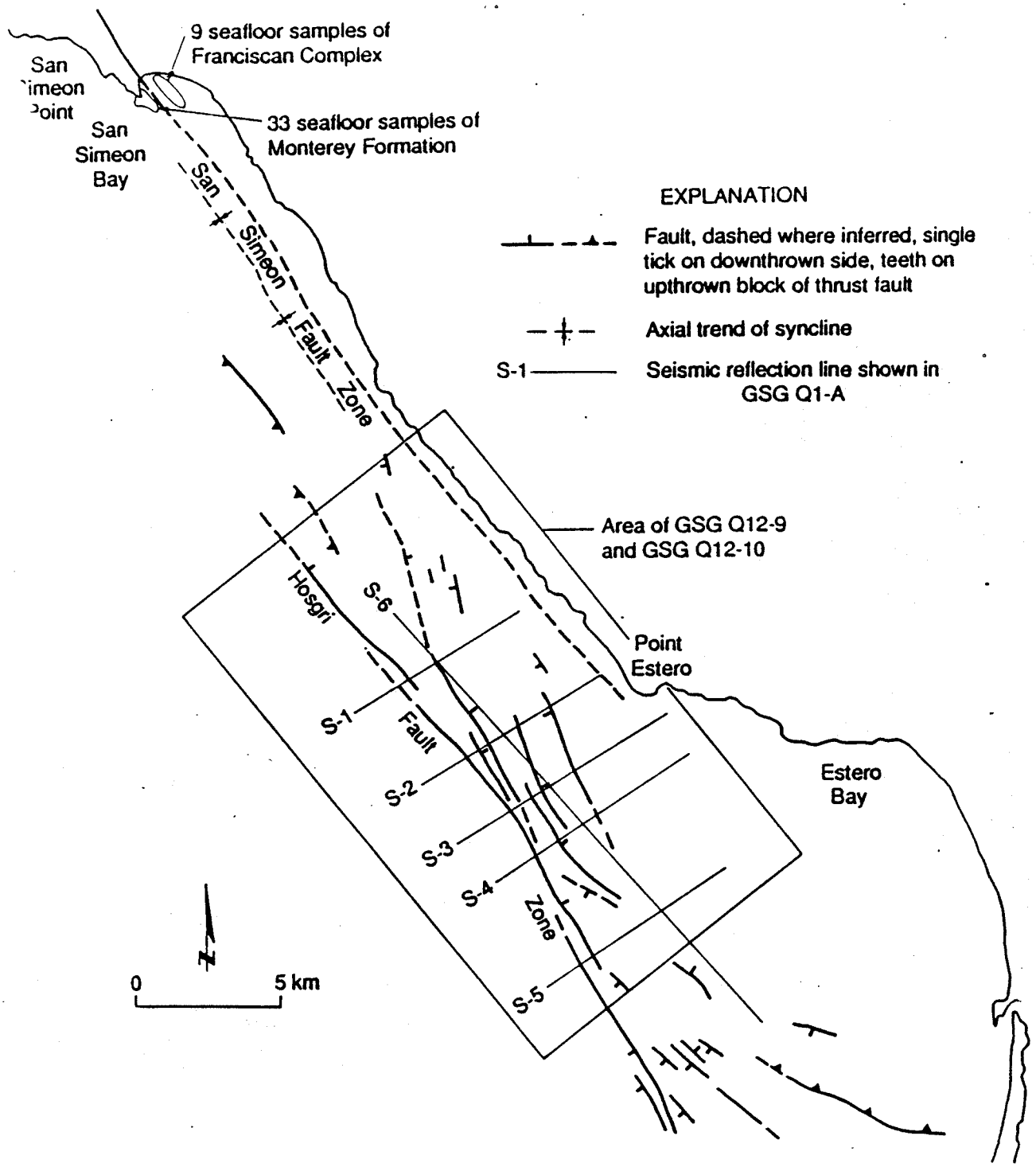
9 seafloor samples of Franciscan Complex
San Simeon Point
San Simeon Bay
33 seafloor samples of Monterey Formation
San Simeon Fault Zone
EXPLANATION
Fault, dashed where inferred, single tick on downthrown side, teeth on upthrown block of thrust fault
Axial trend of syncline
S-1
Seismic reflection line shown in GSG Q1-A
Area of GSG Q12-9 and GSG Q12-10
Hosgri
S-6
S-1
Fault
S-2
S-3
S-4
Zone
S-5
Point Estero
Estero Bay
N
0
5 km

Figure 2.

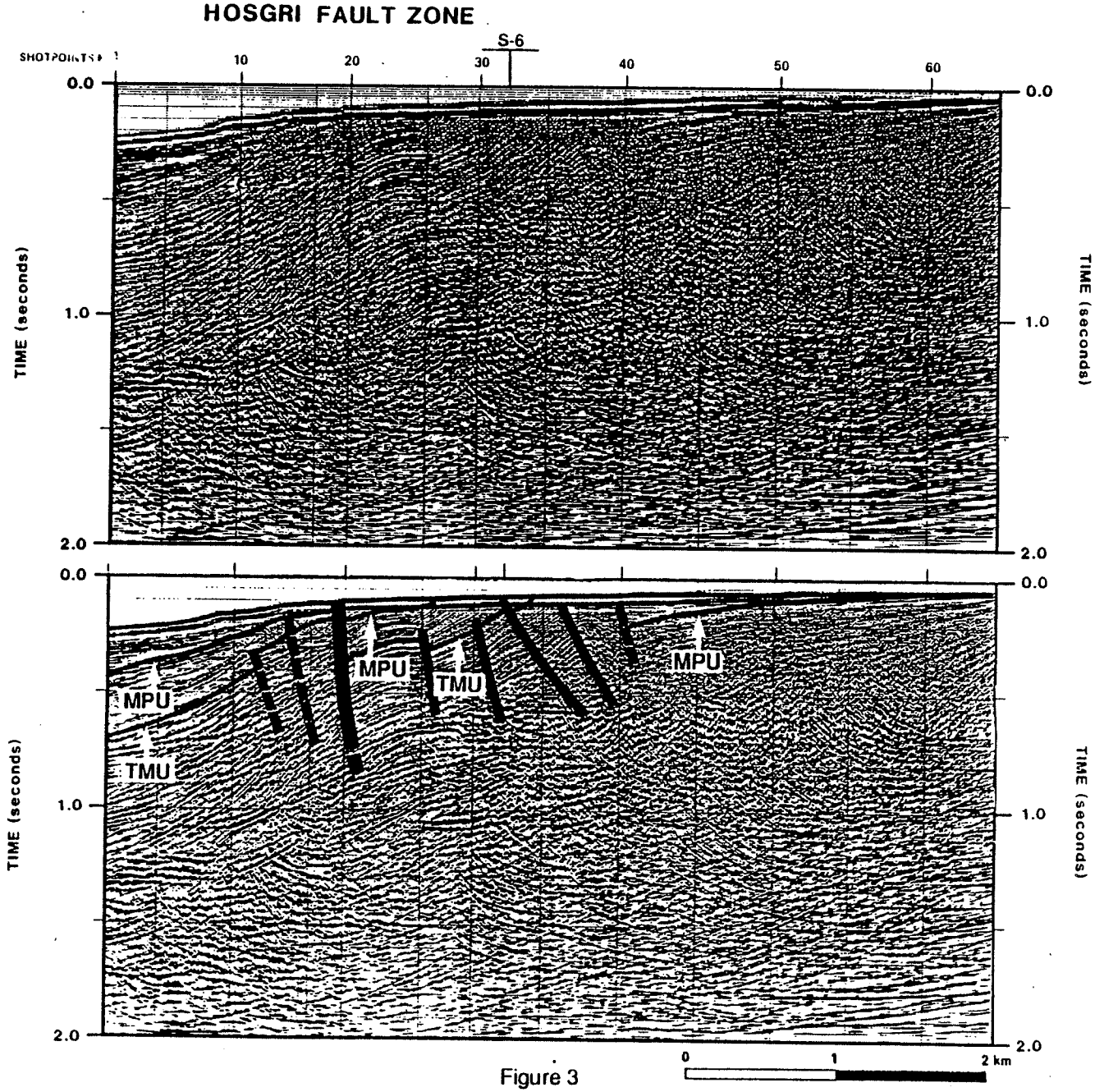

Figure 3

Migrated seismic line S-1 (a) and interpretation (b). MPU is the mid-Pliocene unconformity and TMU is the top of Miocene unconformity .

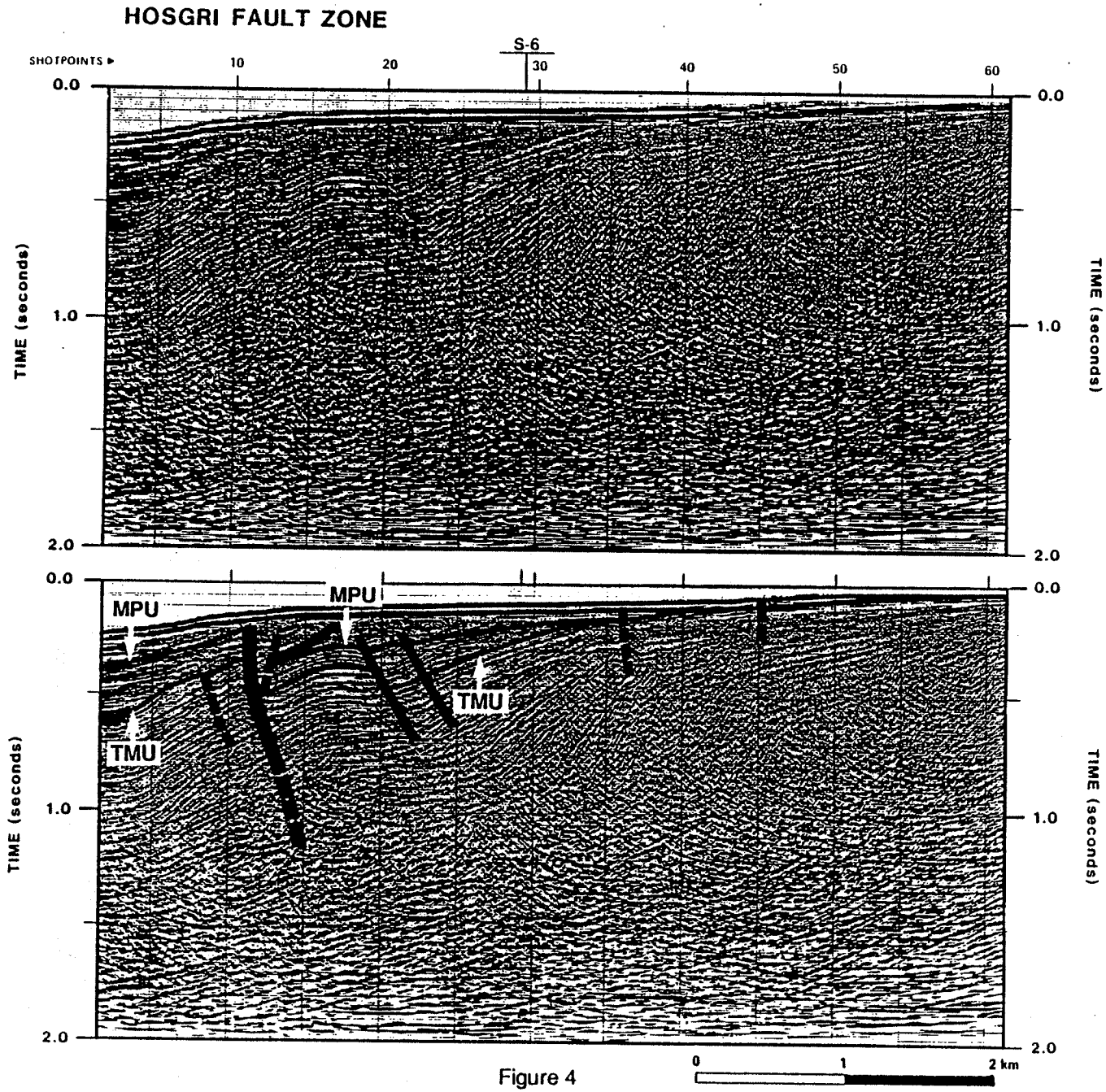

Figure 4

Migrated seismic line S-2 (a) and interpretation (b). MPU is the mid-Pliocene unconformity and TMU is the top of Miocene unconformity

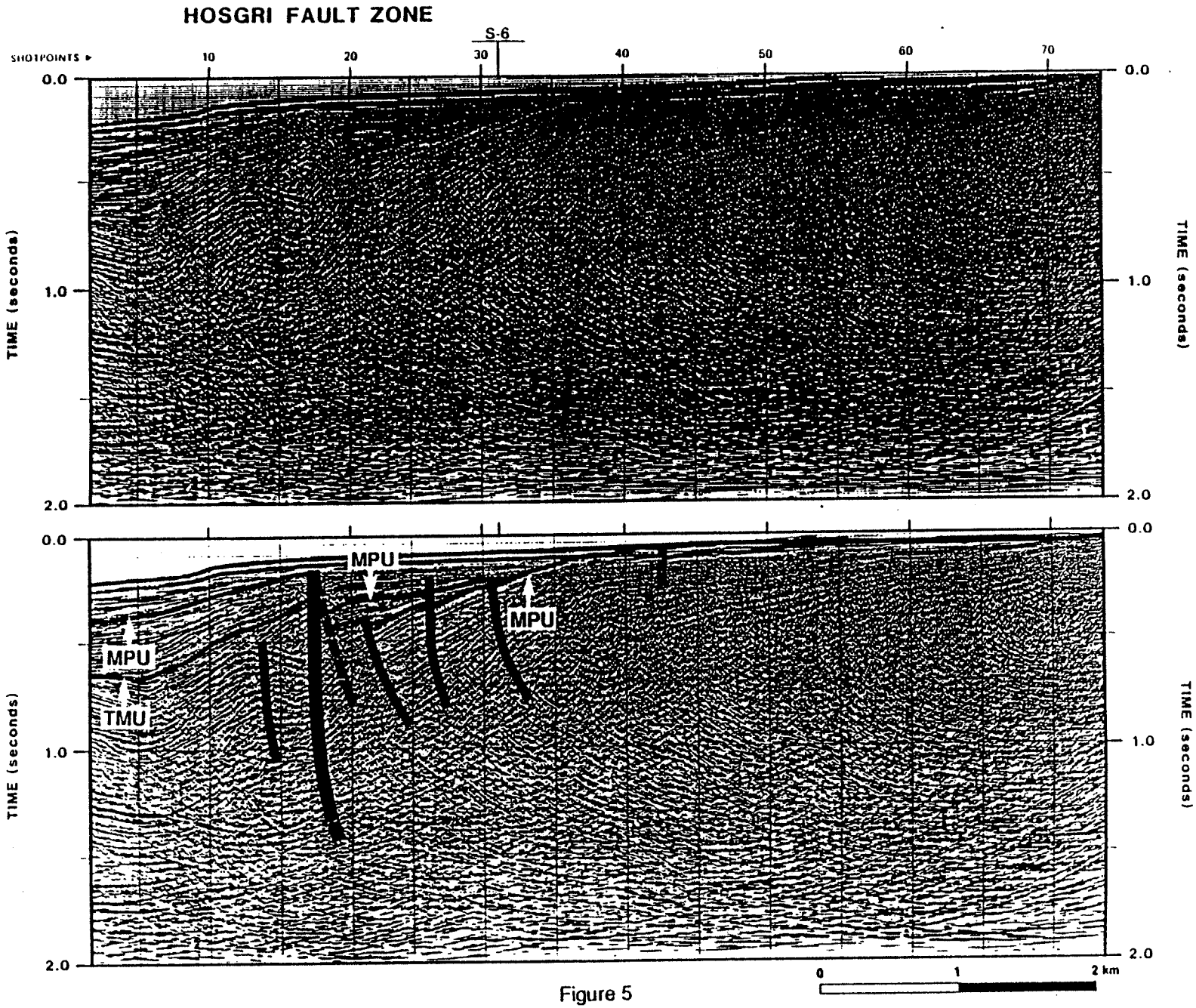

Figure 5

Migrated seismic line S-3 (a) and interpretation (b). MPU is the mid-Pliocene unconformity and TMU is the top of Miocene unconformity

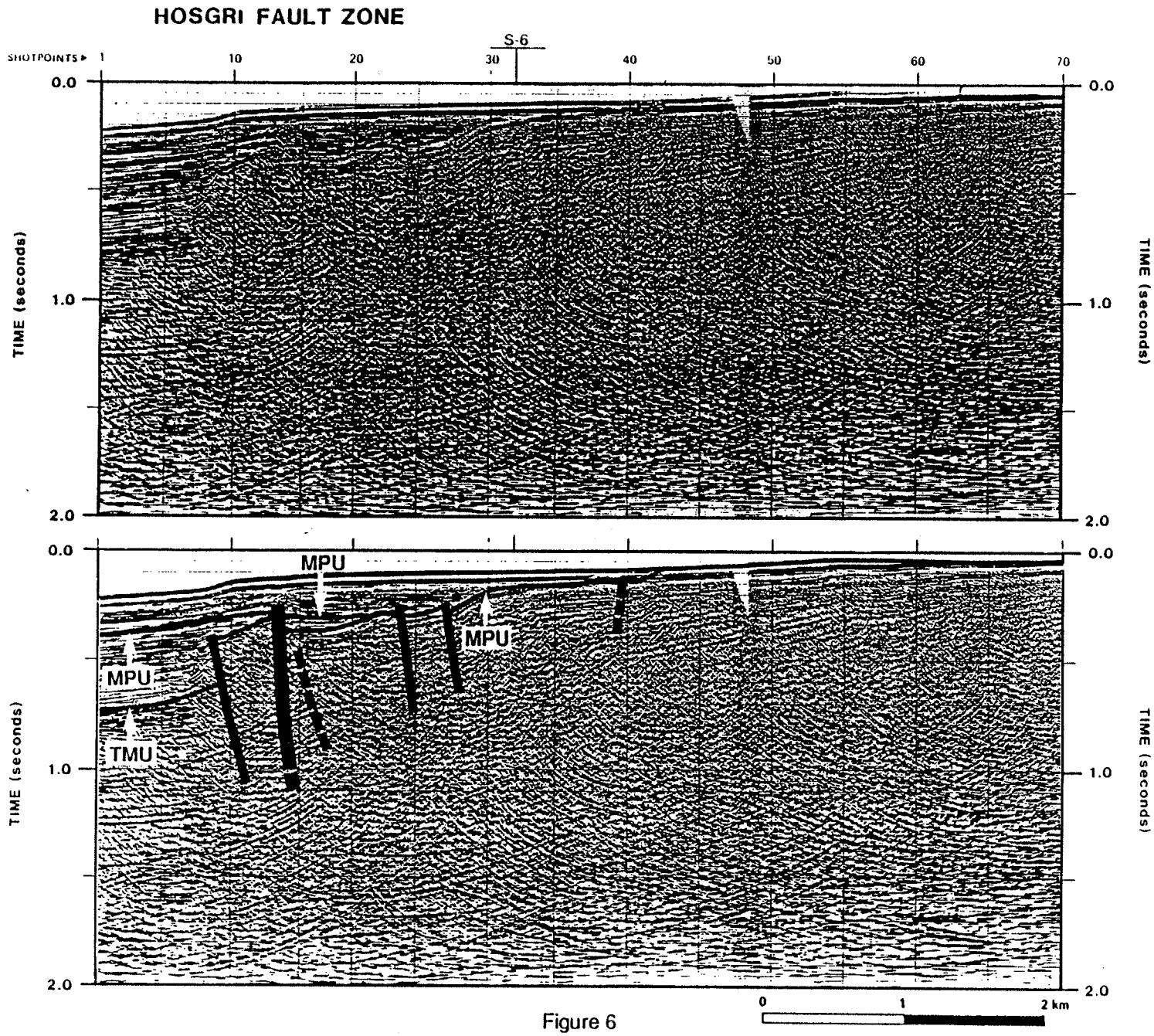

Figure 6

Migrated seismic line S-6 (a) and interpretation (b). MPU is the mid-Pliocene unconformity and TMU is the top of Miocene unconformity

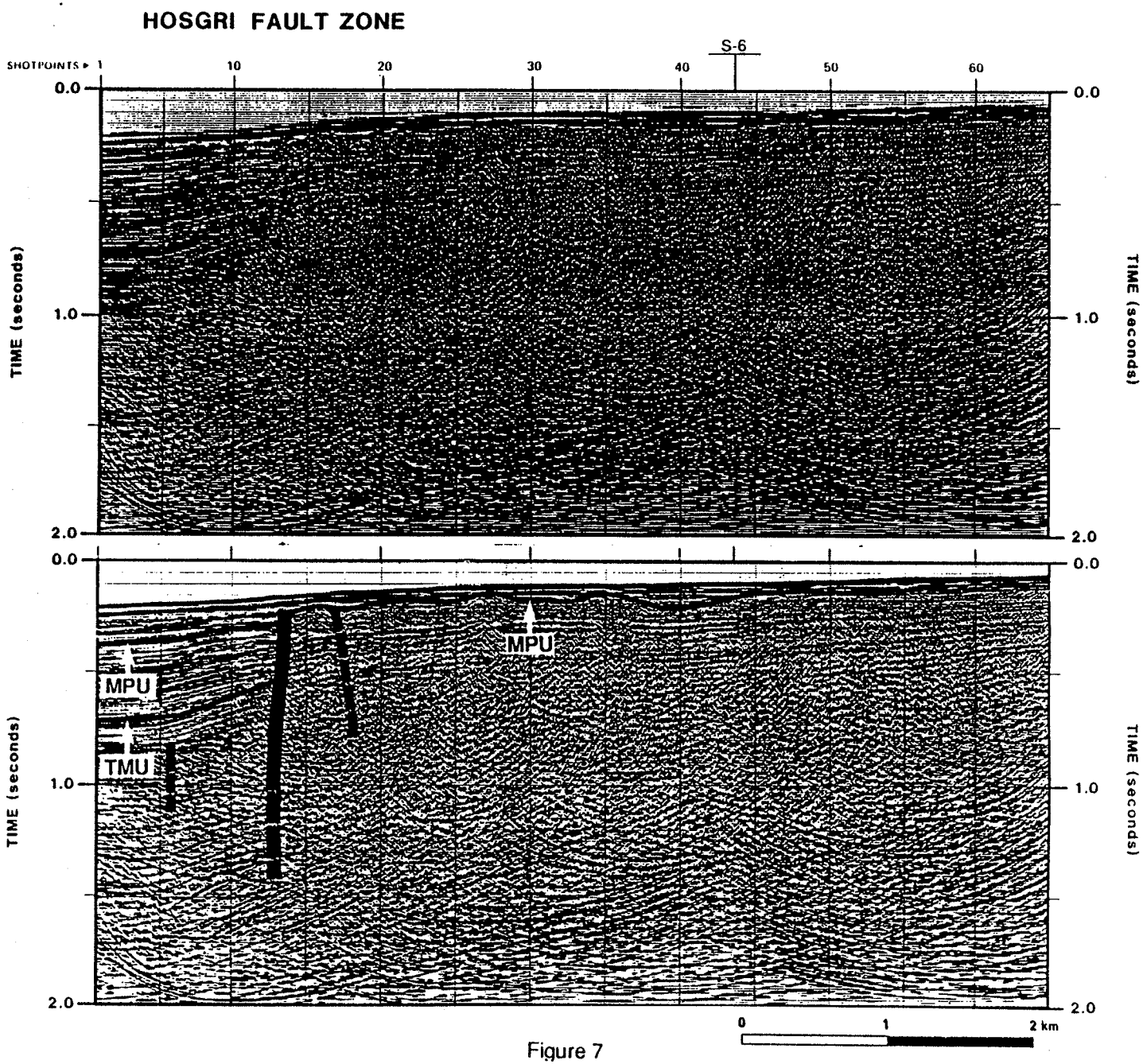

Figure 7

Migrated seismic line S-5 (a) and interpretation (b). MPU is the mid-Pliocene unconformity and TMU is the top of M[illegible] unconformity

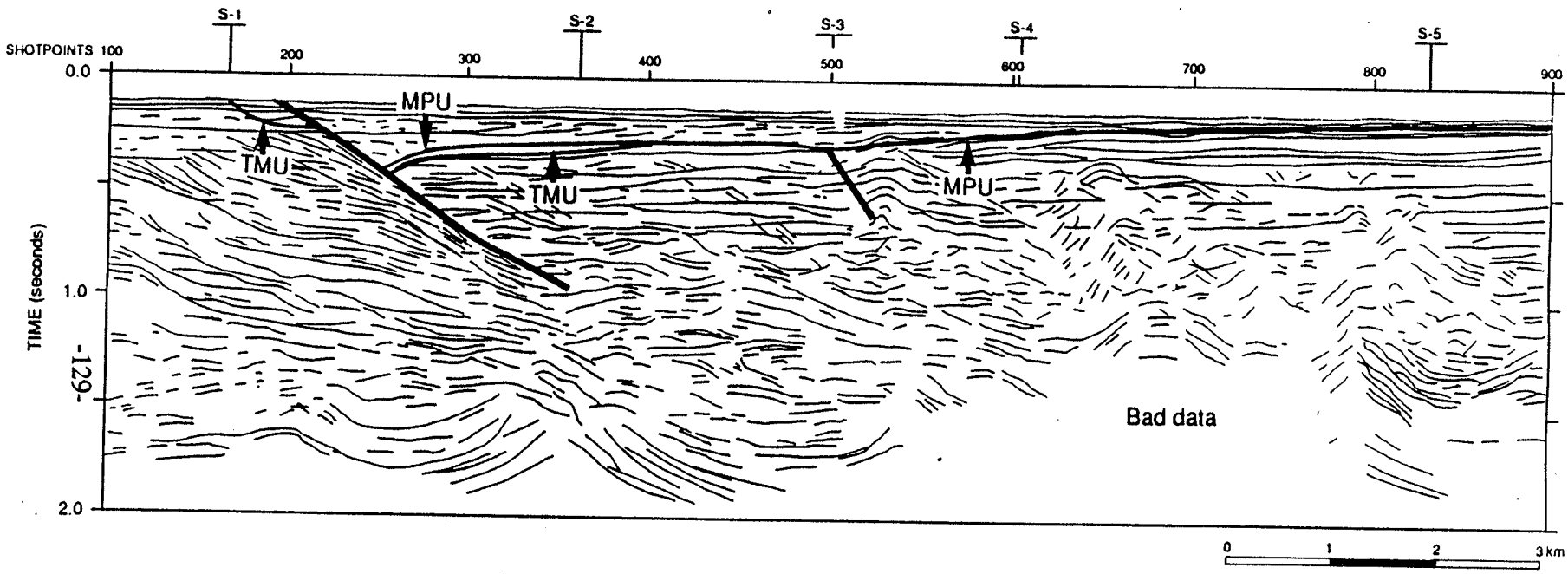

Figure 8. Interpreted line drawing of seismic line S-6. MPU is the mid-Pliocene unconformity and TMU is the top unconformity.

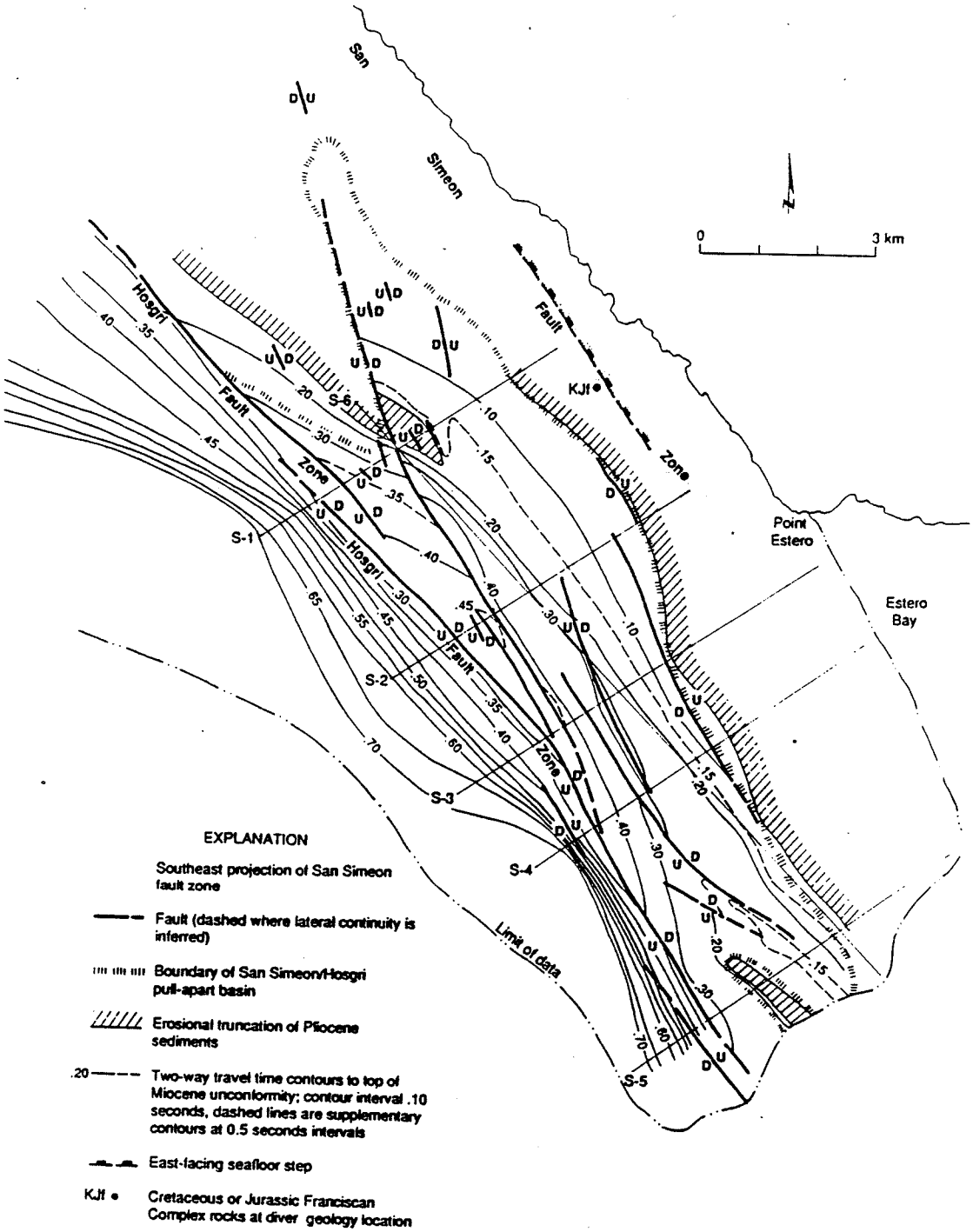
San
Simeon
Fault
Zone
Hosgri
Fault
Zone
Hosgri
Fault
Zone
Point
Estero
Estero
Bay
KJf
S-1
S-2
S-3
S-4
S-5
S-6
0
3 km
Limit of data
EXPLANATION
Southeast projection of San Simeon fault zone
Fault (dashed where lateral continuity is inferred)
Boundary of San Simeon/Hosgri pull-apart basin
Erosional truncation of Pliocene sediments
.20 Two-way travel time contours to top of Miocene unconformity; contour interval .10 seconds, dashed lines are supplementary contours at 0.5 seconds intervals
East-facing seafloor step
KJf Cretaceous or Jurassic Franciscan Complex rocks at diver geology location

Figure 9.

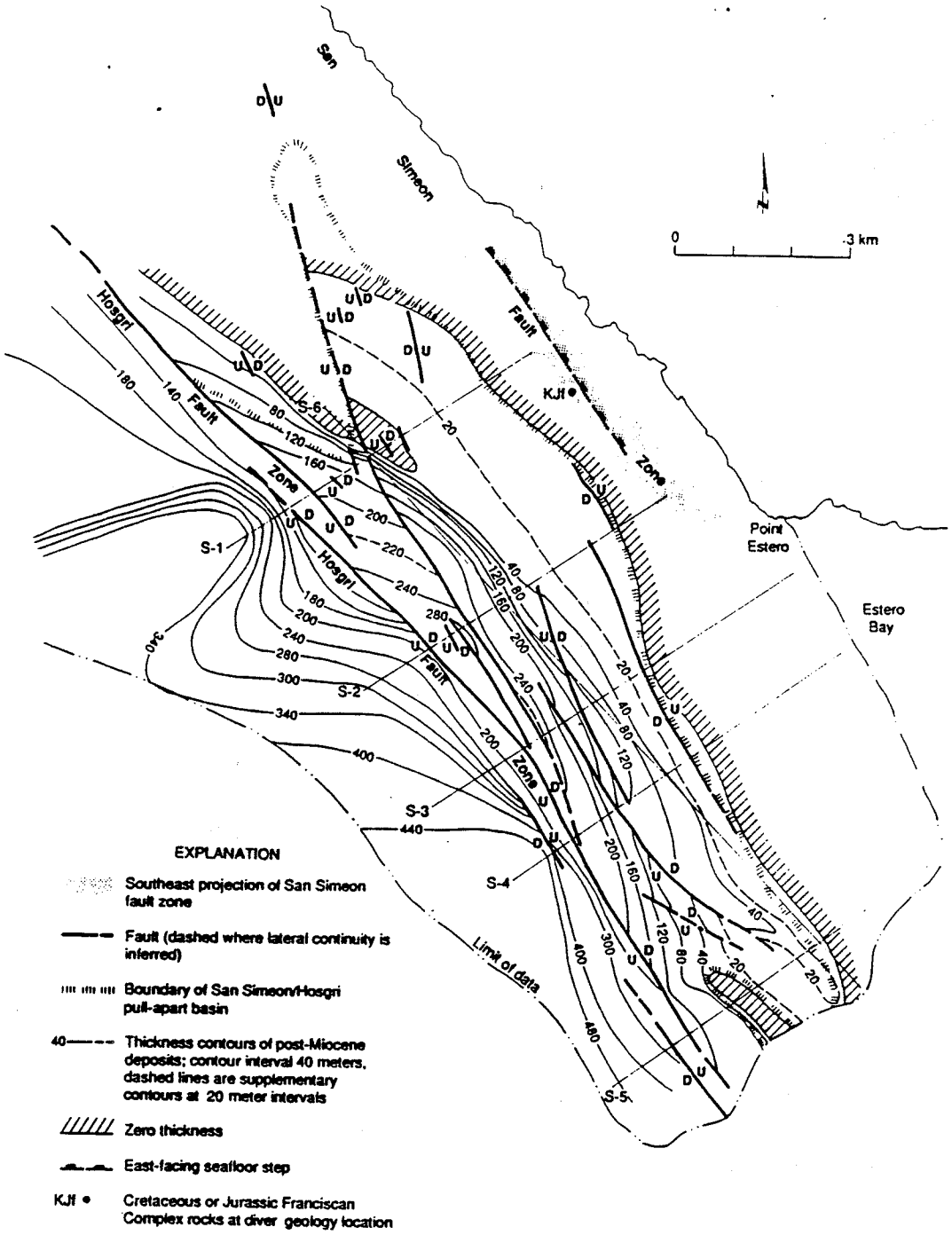
San
Simeon
Fault
Zone
Hosgri
Fault
Zone
Hosgri
Fault
Zone
Point
Estero
Estero
Bay
0
3 km
KJf
S-1
S-2
S-3
S-4
S-5
S-6
Limit of data
EXPLANATION
Southeast projection of San Simeon fault zone
Fault (dashed where lateral continuity is inferred)
Boundary of San Simeon/Hosgri pull-apart basin
Thickness contours of post-Miocene deposits; contour interval 40 meters, dashed lines are supplementary contours at 20 meter intervals
Zero thickness
East-facing seafloor step
KJf
Cretaceous or Jurassic Franciscan Complex rocks at diver geology location

Figure 10.

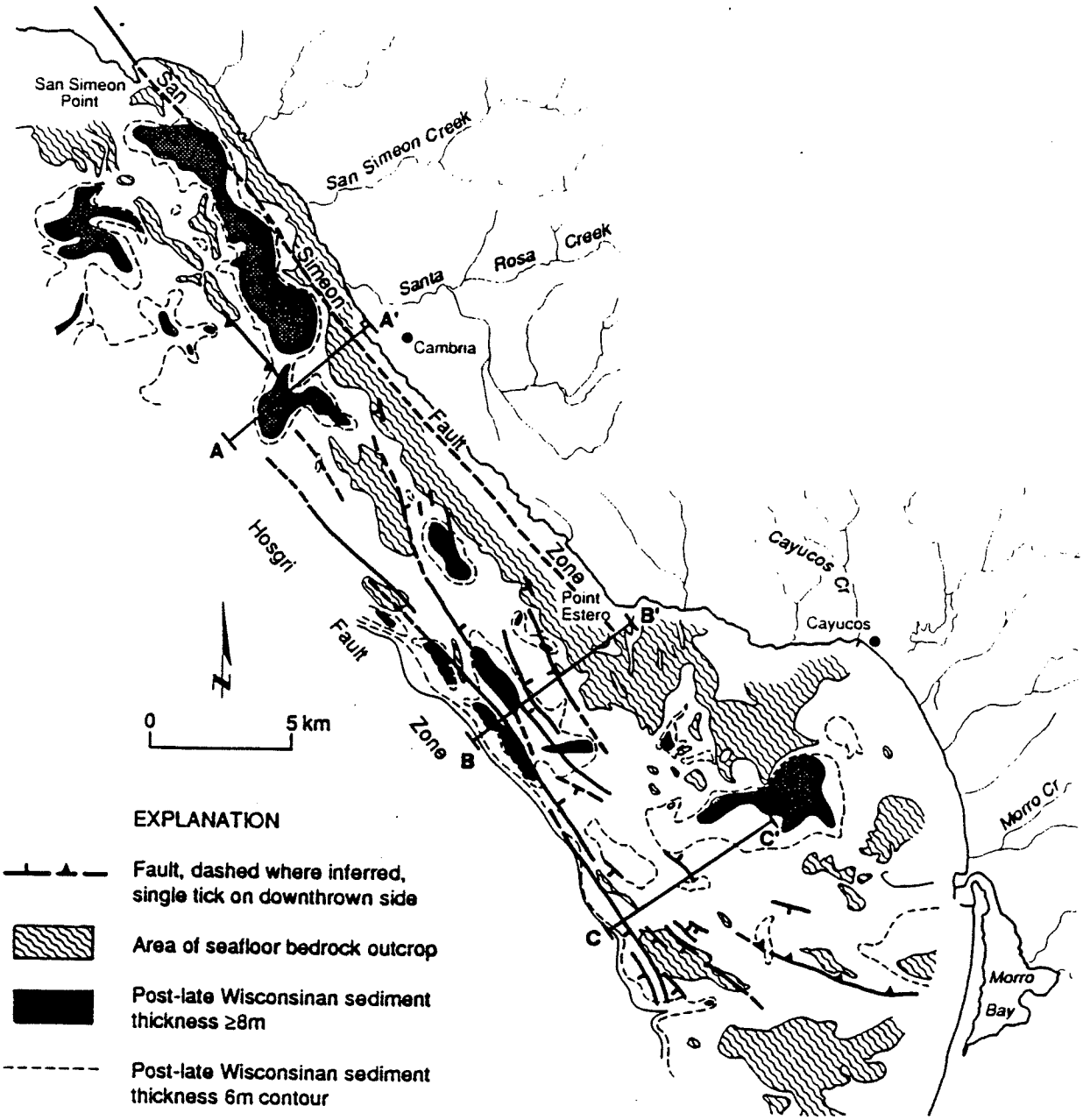
San Simeon Point
San Simeon Creek
Santa Rosa Creek
San Simeon Fault Zone
Cambria
A
A'
Hosgri Fault Zone
Point Estero
B
B'
Cayucos Cr
Cayucos
C
C'
Morro Cr
Morro Bay
N
0
5 km
EXPLANATION
Fault, dashed where inferred, single tick on downthrown side
Area of seafloor bedrock outcrop
Post-late Wisconsinan sediment thickness ≥8m
Post-late Wisconsinan sediment thickness 6m contour

Figure 11.

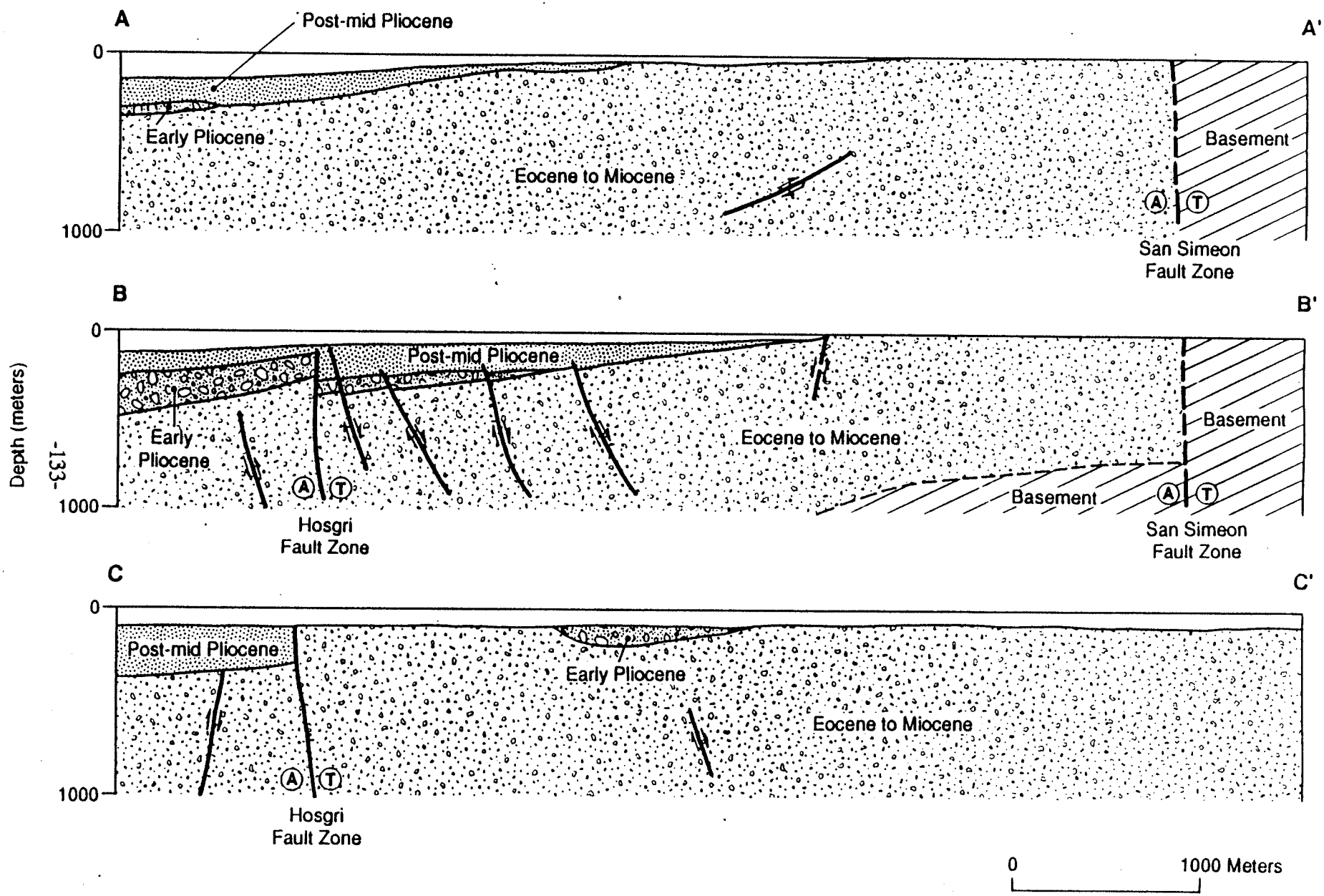
A
A'
Post-mid Pliocene
Early Pliocene
Eocene to Miocene
Basement
San Simeon
Fault Zone
B
B'
Post-mid Pliocene
Early
Pliocene
Eocene to Miocene
Basement
Basement
Hosgri
Fault Zone
San Simeon
Fault Zone
C
C'
Post-mid Pliocene
Early Pliocene
Eocene to Miocene
Hosgri
Fault Zone
0
1000
Depth (meters)
0
1000 Meters

Figure 12.

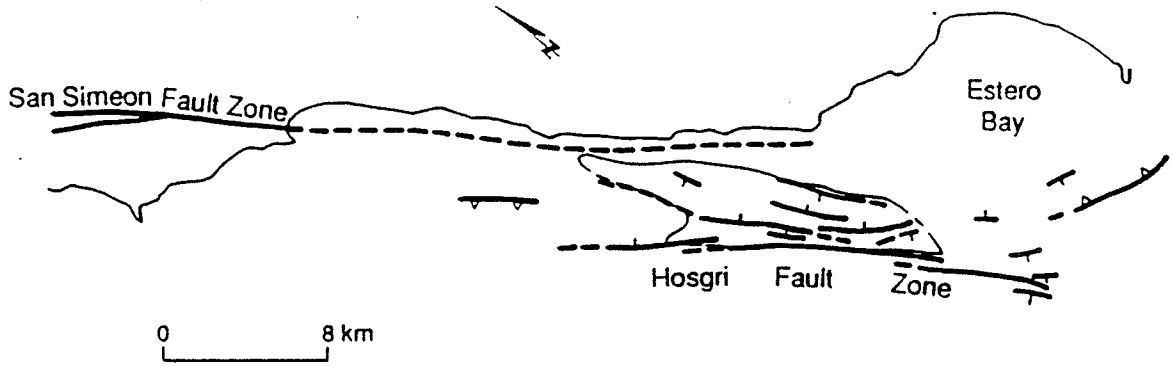

A. Hosgri/San Simeon Stepover

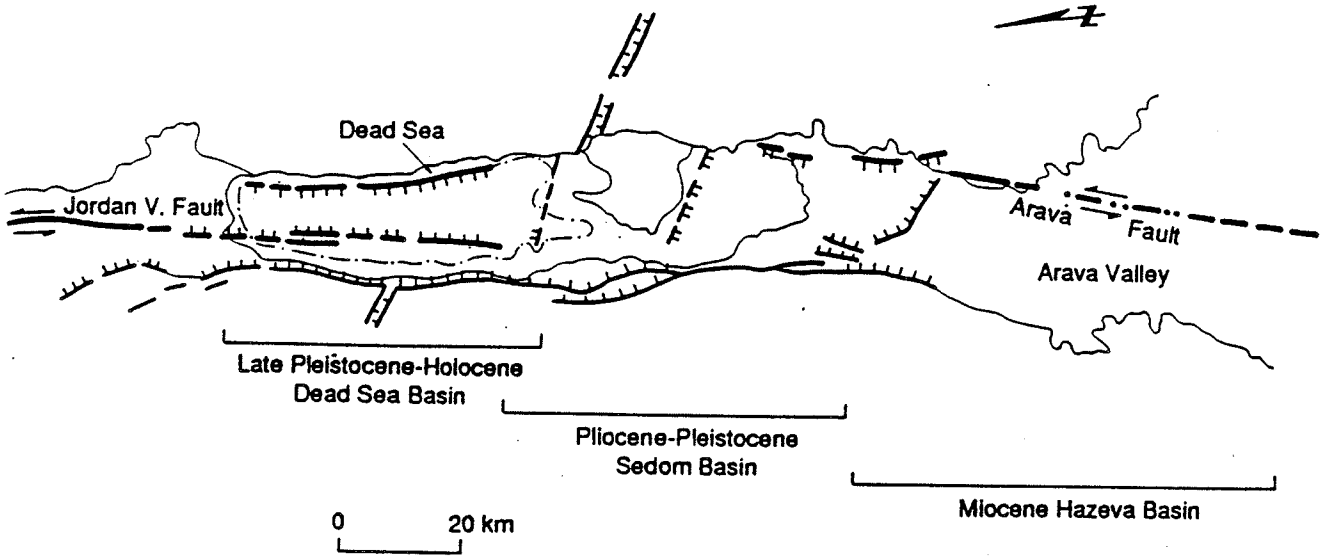

B. Dead Sea Fault Zone (Manspeizer, 1985)

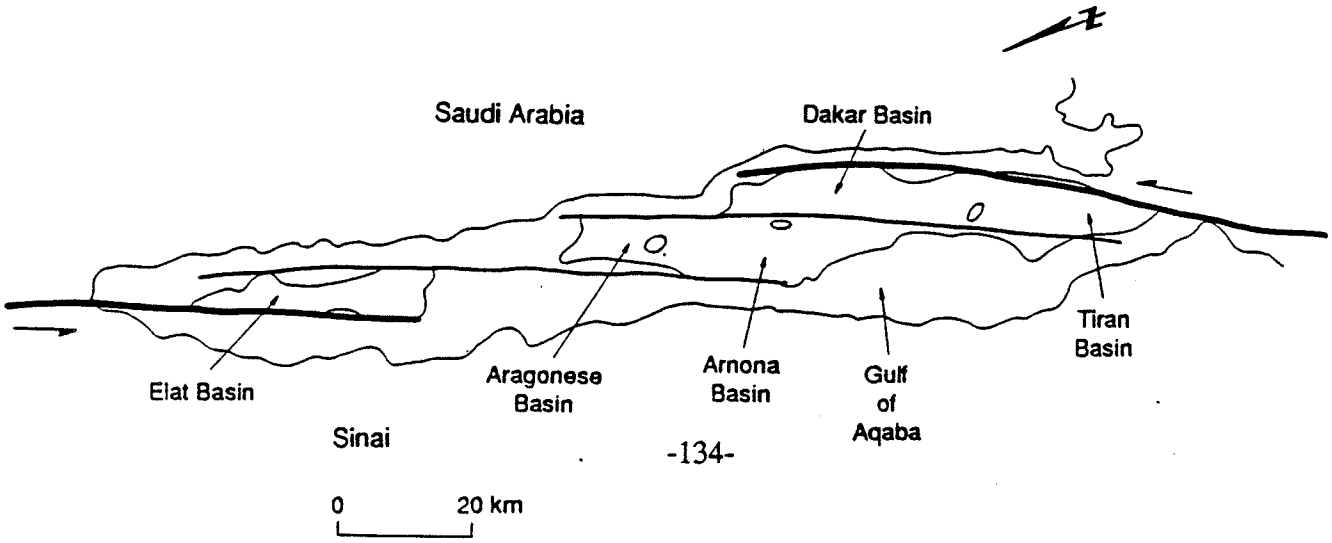

Figure 13.

C. Dead Sea Valley - Gulf of Aqaba (Ben-Avraham, 1985)

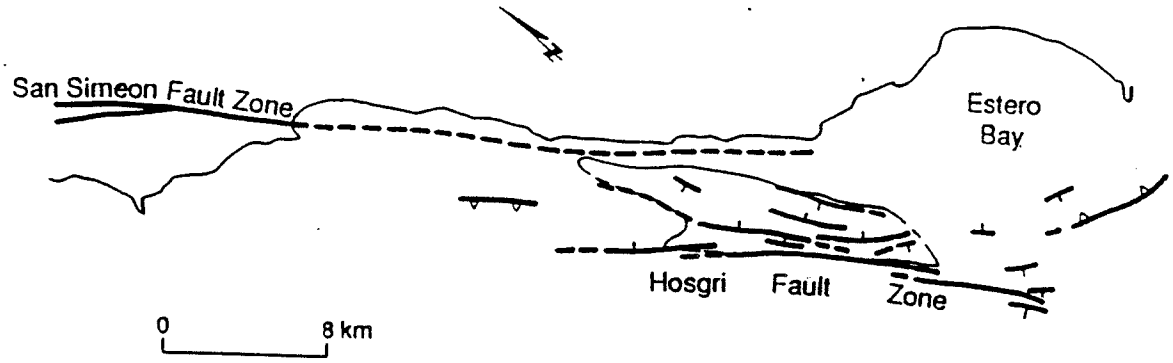

A. Hosgri/San Simeon Stepover

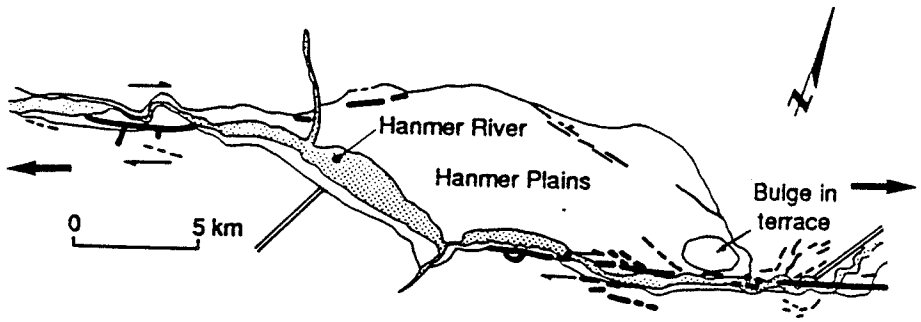

B. Hanmer Plains, Hope Fault Zone, New Zealand (Freund, 1971)

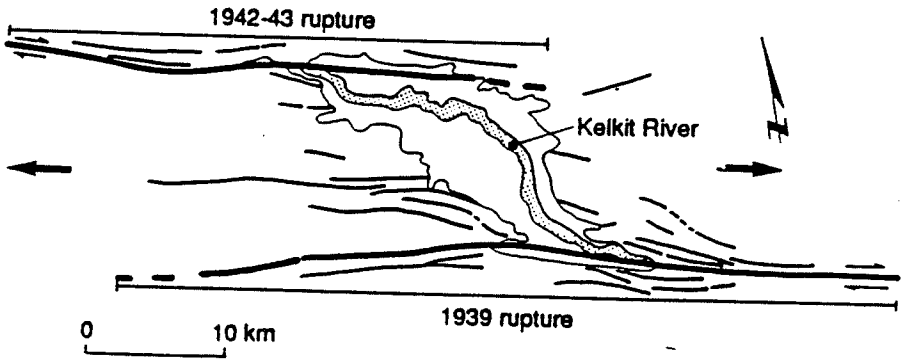

C. Niksar Pull-apart Basin, North Anatolian Fault Zone, Turkey (modified from Hempton and Dunne, 1983)

Figure 14.

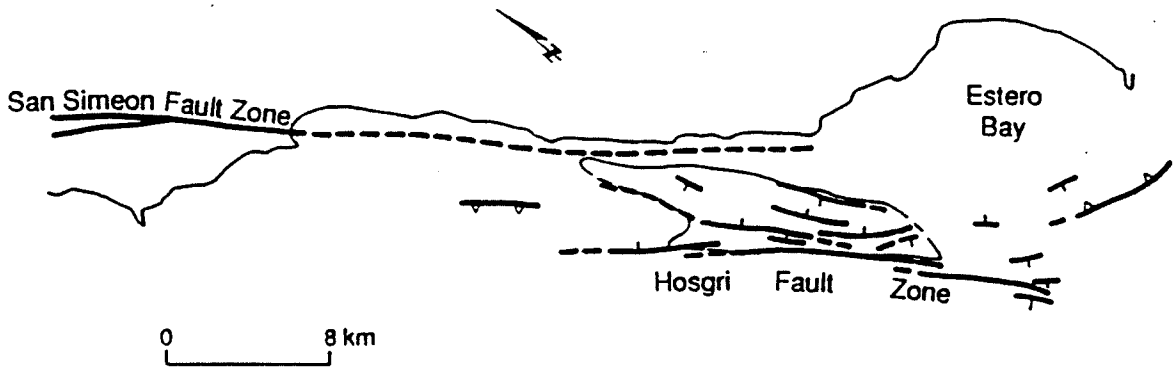

A. Hosgri/San Simeon Stepover

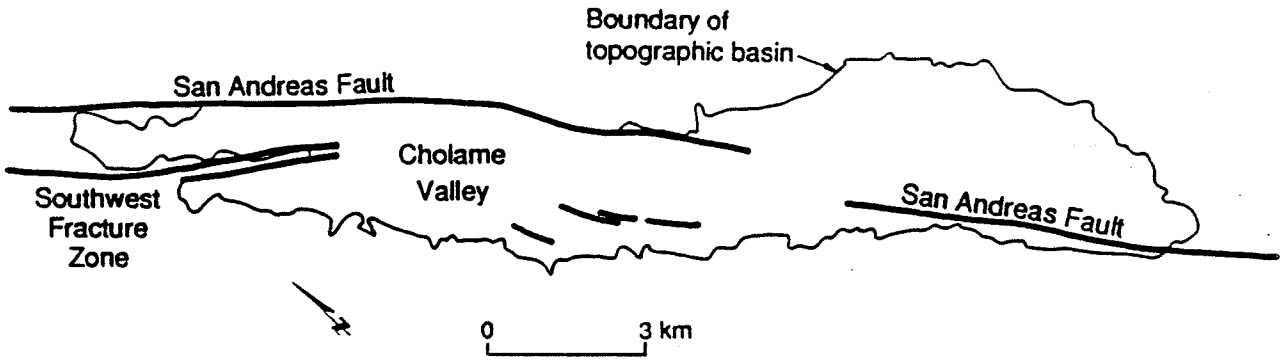

B. Cholame Valley Pull-Apart Basin

Figure 15.

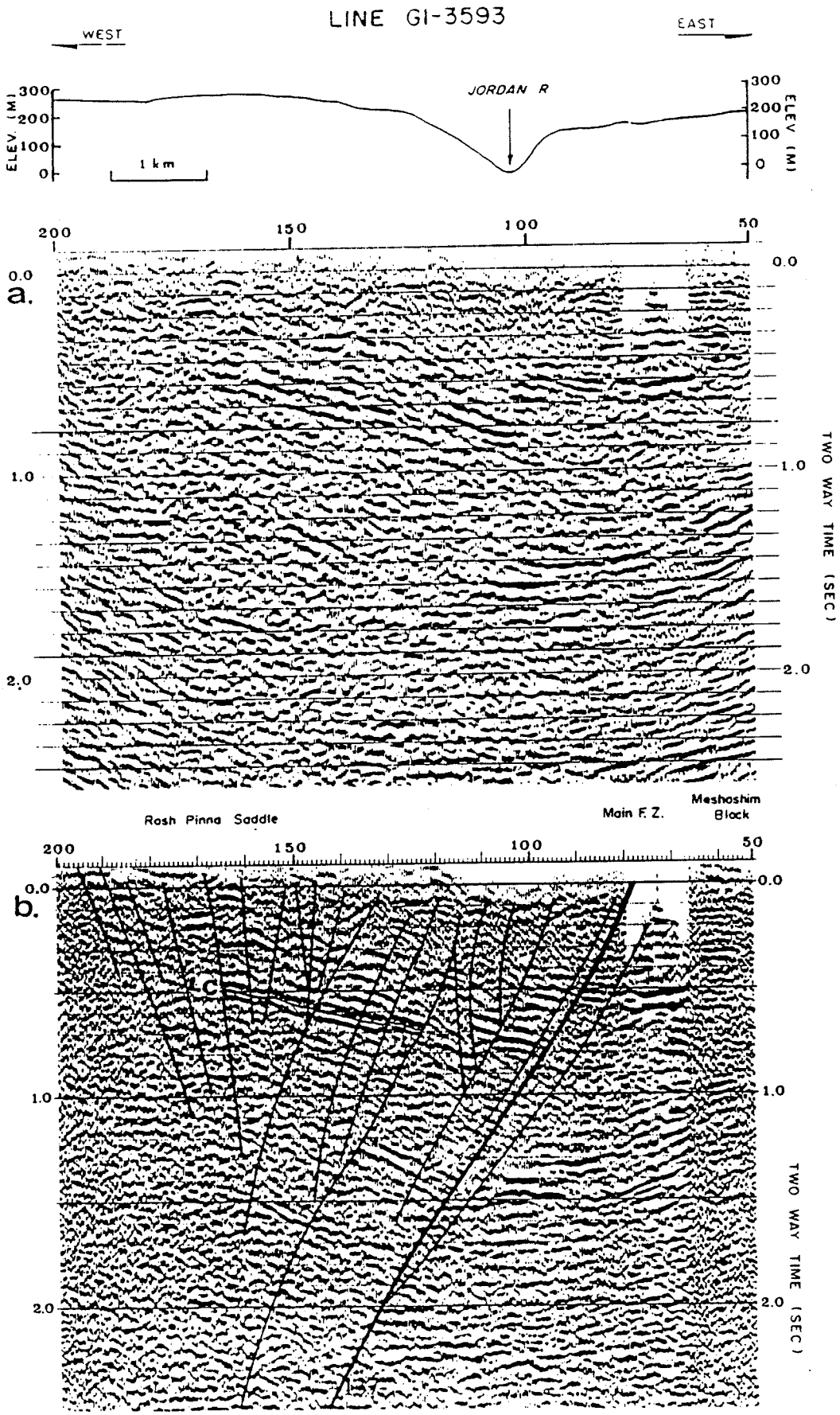

From Rothstein and Bartov, 1989

Figure 16.

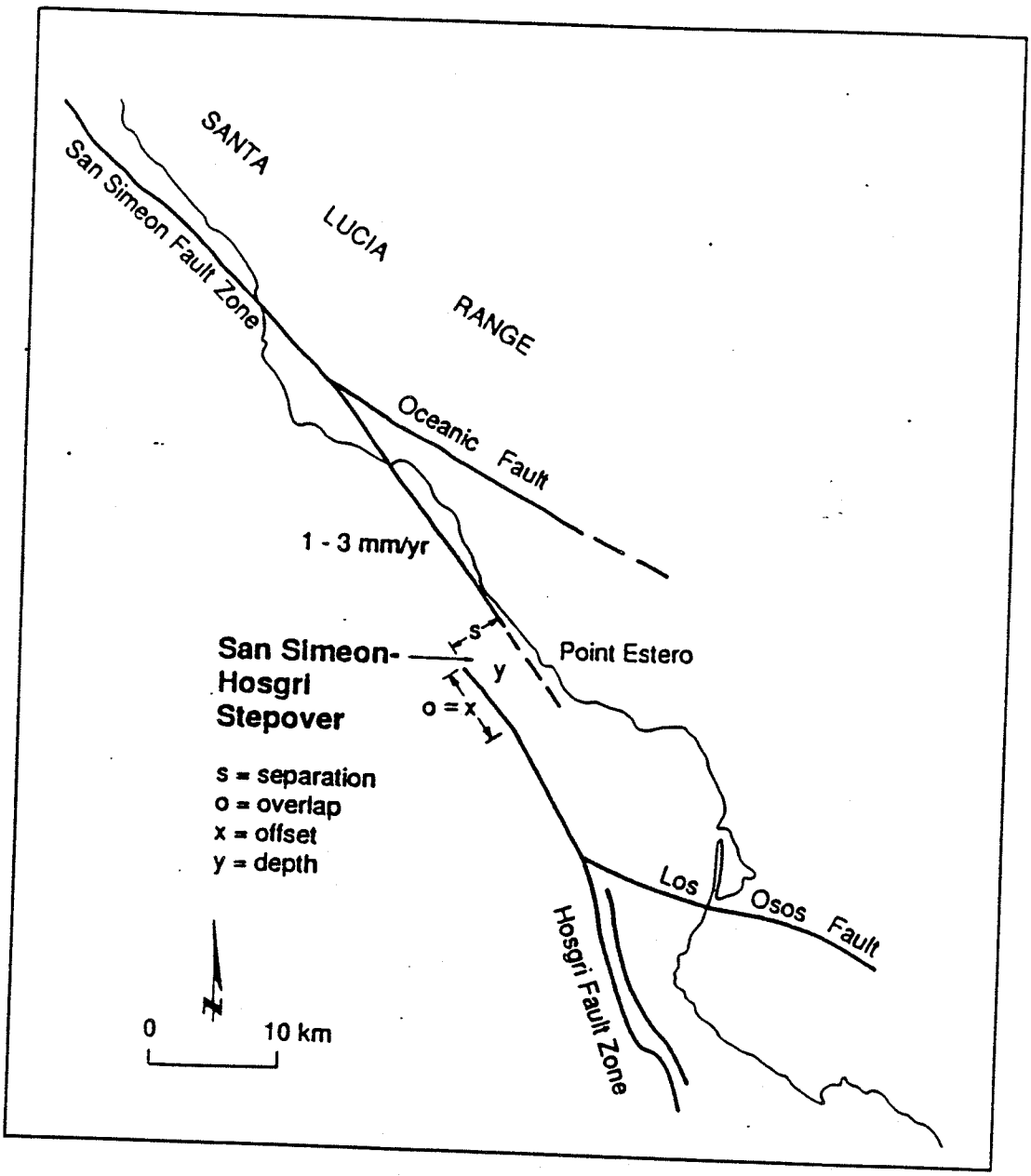
SANTA
LUCIA
RANGE
San Simeon Fault Zone
Oceanic Fault
1 - 3 mm/yr
San Simeon-
Hosgri
Stepover
s
y
o = x
Point Estero
s = separation
o = overlap
x = offset
y = depth
Los Osos Fault
Hosgri Fault Zone
0
10 km

Figure 17

CORRELATION, AGES, AND UPLIFT RATES OF QUATERNARY MARINE TERRACES: SOUTH-CENTRAL COASTAL CALIFORNIA

Kathryn L. Hanson, John R. Wesling
Geomatrix Consultants, Inc., San Francisco, California

William R. Lettis, Keith Kelson
William Lettis and Associates, Lafayette, California

and **Lili Mezger**
University of Oregon, Eugene, Oregon

ABSTRACT

Emergent Quaternary marine terraces are present along most of the south-central California coastline from San Simeon on the north to the Santa Maria Valley on the south. Detailed mapping of these terraces provides new data for assessing the locations, style, and rates of Quaternary deformation in the region. This paper describes the distribution, correlation, and ages of these terraces near San Simeon and between Morro Bay and the Santa Maria Valley.

In the San Simeon study area, sequences of four and five marine terraces have been mapped to the northeast and southwest, respectively, of the southern onshore reach of the San Simeon fault zone. From youngest to oldest, they are the San Simeon Point (Q1), San Simeon (Q2), Tripod (Q3), Oso (Q4), and La Cruz (Q5) terraces. They are interpreted to correlate with marine oxygen-isotope stages 3 or 5a (60 or 80 ka), 5a or 5c (80 or 105 ka), 5e (120 ka), 7 (210 ka), and 9 (330 ka). A uranium-series age of 46 $\pm$ 2 ka, and a weighted mean thermoluminescence age of 83 $\pm$ 10 ka have been obtained for samples collected from the lowest two emergent terraces, respectively, on the southwestern side of the fault zone. Estimated ages and correlation of terraces across the San Simeon fault zone are based on lateral correlation of the Tripod terrace to the well-dated ~120 ka Cayucos terrace, comparison of relative soil profile development, and comparison of geomorphic expression and terrace altitudinal spacing. Comparison of the relative altitudinal spacing of terraces to paleo-sea-level curves developed from worldwide data indicates uplift rates of approximately 0.17 $\pm$ 0.02 m/ka southwest, and 0.16 $\pm$ 0.01 m/ka northeast of the fault and approximately 0.24 m/ka for the uplifted and warped areas within the fault. Terrace altitudinal spacing for the lowest three terraces on San Simeon Point, however, indicates that uplift during the past 120 ka in this area has not been uniform adjacent to the active traces of the San Simeon fault zone.

In the San Luis Obispo study area, a flight of at least twelve elevated marine terraces is present between Morro Bay

and the northwestern margin of the Santa Maria Valley. The lower two terraces (Q1 and Q2) in this sequence are interpreted to correlate to marine oxygen-isotope substages 5a (80 ka), and 5e (120 ka), respectively. These correlations are well constrained by 10 uranium-series ages of coral and vertebrate bone samples, 12 amino acid racemization analyses, and 14 paleoclimatic analyses of invertebrate faunal assemblages. The ages of the lower two terraces provide local calibration of the terrace sequence for correlation with paleo–sea-level curves developed from worldwide data. For terraces equal to or younger than about 330 ka, we have estimated terrace ages and uplift rates by correlating shoreline angle elevation and terrace altitudinal spacing to these curves. Uplift rates based on the present elevation of the 120 ka terrace in this region range from approximately 0.06 to 0.24 m/ka.

Late Pleistocene uplift rates throughout the entire coastal region between San Simeon to the Santa Maria Valley are comparable to rates observed elsewhere in California that are on the order of 0.1 to 0.3 m/ka in tectonic regimes characterized by predominantly strike-slip faulting. The rates are considerably less than maximum rates of 3 to 5 m/ka for the region directly south of the Mendicino Triple Junction and 5 to 7 m/ka for areas characterized by significant crustal shortening such as the Ventura anticline in the Transverse Ranges, and 0.8 m/ka for the Santa Cruz Mountains region adjacent to the restraining bend in the San Andreas fault.

Estimates of the position of sea level (with respect to the present) during the ~80-ka-high sea stand range from about -19 m to near the present level. Estimated paleo-sea level during the ~80 ka high sea stand in the San Luis Obispo study area, assuming a + 6 m paleo-sea-level estimate for the ~120 ka terrace and uniform uplift since formation of the ~120 ka terrace, is - 4 ± 1 m (relative to present sea level). This value is in general agreement with other recent estimates from coastal California, Mexico, and Japan, but is significantly higher than previous estimates from New Guinea and Barbados.

INTRODUCTION

Emergent marine terraces have long been recognized as useful indicators of long-term crustal deformation in tectonically active coastal regions (Bradley and Griggs, 1976; Weber, 1983; Lajoie and others, 1979, 1982; Lajoie, 1986). On both local and regional scales, they constitute the longest, most detailed, and a really extensive records of late Quaternary crustal deformation (Lajoie, 1986).

Emergent marine terraces are remnants of abandoned wave-cut platforms preserved in steplike sequences along uplifted coastlines. They commonly occur within a few hundred meters above present sea level. A wave-cut platform and associated beach and near-shore deposits are observed along the present coastline and thus provide a modern analog (Fig. 1). The shoreline angle (also known as the platform back edge) is the intersection between the gently seaward-dipping relict platform and the

steeper relict sea cliff. It lies within 1 m of the location and elevation of the abandoned marine shoreline referred to as a strandline. The wave-cut platform is commonly covered by a veneer of shallow-water sand and gravel, which locally contains marine vertebrate and invertebrate fossils. On uplifted platforms, marine deposits are generally buried by a wedge of subaerially derived alluvium and/or colluvium, which may reach a thickness of 10 to 20 m or more that thins toward the sea. Because of this, shoreline angles of older, higher marine terraces are typically subdued and seldom exposed.

The present elevations of emergent Pleistocene marine terraces reflect vertical tectonic movements and/or global sea-level fluctuations. In general, flights of marine terraces higher than present sea level are the geologic record of periodic glacio-eustatic sea-level highstands superimposed on a rising coastline (Fig. 2) (Broecker and others, 1968; Mesolella and others, 1969; Matthews, 1973). Although strandlines also form during sea-level lowstands, geomorphic evidence for these strandlines is generally destroyed by wave erosion or submerged during subsequent sea level transgressions.

Emergent marine terraces are present along most of the south-central California coast from San Simeon on the north to the Santa Maria Valley on the south. We have mapped these terraces to provide new data for assessing the locations, style, and rates of Quaternary deformation in the region. Areas of detailed mapping are shown on Figure 3 and include the San Simeon and San Luis Obispo areas. In this report we first present a summary of age and paleo–sea-level data for marine terrace sequences worldwide based on recently published and in-progress studies. These data provide a framework for evaluating the ages of marine terraces in our study area, and estimating long-term rates of uplift based on these terraces. Secondly, descriptions of the terrace sequences in the San Simeon and San Luis Obispo areas are provided, followed by discussions of ages, correlation, and uplift rates for each study area. Detailed mapping and dating of marine terraces in these areas allows for better estimates of slip rates of faults that displace the terraces and provides constraints on patterns and rates of uplift and folding that can be used to evaluate various tectonic models that have been proposed for the region. Such studies are reported in detail in companion papers by Hanson and Lettis (this volume), Lettis and others (this volume), and Lettis and Hall (this volume).

QUATERNARY SEA-LEVEL HISTORY

Ages for sea-level high stands during the past 700,000 years have been estimated by various workers based on uranium-series dating of coral associated with former shorelines in New Guinea (Veeh and Chappell, 1970; Bloom and others, 1974), Barbados (Mesolella and others, 1969; Bender and others, 1979) and coastal California (Muhs and others, 1987, 1988), and on correlations to interglacial periods inferred from the oxygen-isotope records of deep sea cores

(Shackleton and Opdyke, 1973; and Chappell and Shackleton, 1986). Table 1 presents a compilation of these age estimates.

Detailed studies of these terrace sequences also has provided information on the paleo-sea level at which individual terraces formed. Paleo–sea-level data have been obtained by subtracting well-documented constant-rate tectonic uplift from the relative sea-level record of emergent coral reefs on the Huon Peninsula of Papua, New Guinea (Veeh and Chappell, 1970; Bloom and others, 1974; Chappell, 1983; Bloom and Yonekura, 1985; and Chappell and Shackleton, 1986). Uranium-series ages of fossil corals from New Guinea provide a paleo–sea-level curve back to approximately 200 ka (Fig. 2 and Table 1). Longer paleo–sea-level records on Barbados in the West Indies provide less detailed sea-level curves extending back approximately 640,000 to 700,000 years (Table 1) (Broecker and others, 1968; Mesolella and others, 1969; Matthews, 1973; Bloom and others, 1974; and Bender and others, 1979). The record of sea-level fluctuations provided by these data are in general agreement with paleoclimate data interpreted from oxygen-isotope ratios in deep-sea cores (Shackleton and Opdyke, 1973; Bender and others, 1979; and Shackleton, 1987).

Paleo-sea level during the last major interglacial highstand, approximately 120,000-125,000 years B.P., has been well documented in several locations throughout the world. Estimates of the elevation of this paleo-sea level range from 2 to 10 meters above the present sea level (Thurber and others, 1965; Veeh, 1966; Thomson and Walton, 1972; Ku and others, 1974; Neumann and Moore, 1975; Marshall and Thom, 1976; Harmon and others, 1978, 1981; Schubert and Szabo, 1978; Szabo and others, 1978; Szabo, 1979; Cronin and others, 1981) with a value of 6 m commonly used. Because the 120,000 year-old strandline is a well-preserved and well-dated terrace along many coastlines, it is generally used for estimating and comparing uplift rates within and between various coastal regions.

Paleo–sea-level estimates for other interglacial highstands and selected lowstands are presented in Table 1. It should be noted that there are conflicting estimates of paleo-sea level at ~80 ka and 105 ka. Studies in Barbados (Bender and others, 1979), New Guinea (Chappell and Shackleton, 1986), and Haiti (Dodge and others, 1983) suggest that sea level was at -16 to -18 m at 105 ka and -15 to -16 m at 80 ka, relative to present (Muhs, in press). Bloom and Yonekura (1985), using a different method, estimate that paleo-sea level at ~80 ka and ~105 ka were -7 and 0 m, respectively, based on new regressions of the New Guinea data. These estimates are in agreement with recent studies by Muhs and others (1987, 1988), who propose that paleo-sea level at ~80 ka and ~105 ka along the coast of southern California and northern Baja California, Mexico, were -5 ± 2 m and -2 ± 2 m, respectively. Other studies in Japan (Machida, 1975), Bermuda (Vacher and Hearty, 1989), the Mediterranean area

(Hearty and others, 1986), and the Atlantic Coastal Plan (Szabo, 1985), also indicate that sea level during the 80 ka highstand was significantly higher, in some cases close to the present level.

DATING OF MARINE TERRACES AND ESTIMATION OF UPLIFT RATES

A variety of numerical-, calibration-, and correlation-dating techniques were used during this study to estimate the ages of the marine terrace sequences, and document the lateral correlation of sequences of marine terraces. These techniques include:

Numerical

- Uranium-series dating of invertebrate coral and vertebrate bone and teeth samples (Table 2)

Calibration

- Relative degree of soil profile development
- Amino acid racemization of marine mollusk shells (Table 2)
- Thermoluminescence analysis (Table 3)

Correlation

- Correlation of marine terraces to paleo-sea levels based on terrace altitudinal spacing
- Paleoclimatic analysis of marine invertebrate faunal assemblages and correlation to the dated marine terraces (Table 2).

The most reliable numerical ages obtained during this study are from the lowest two marine terraces. Direct dating of older marine terraces is difficult because of the lack of material suitable for dating. One approach to estimate ages of higher terraces is to calculate an uplift rate based on the known age and elevation of the lower dated terraces and assume that this uplift rate is uniform over time (Chappell and Veeh, 1978; Muhs and Szabo, 1982; Hanks and others, 1984; and Ward, 1985). This technique, however, is not applicable in areas where the uplift rate has not been uniform throughout the period of time represented by the terrace sequence. Often it is not known whether an assumption of uniform uplift rate over time is valid.

Graphical comparison of the relative spacing of terraces within the sequence to paleo–sea-level curves based on worldwide data is another approach to estimate ages of marine terraces and evaluate temporal and spatial changes in uplift rates (Pillans, 1983; Weber, 1983; Bull, 1985). Spacings of shoreline angles within a flight of terraces depends on: 1) position of sea level at the time of terrace formation (paleo-sea level), 2) intervals of time between consecutive sea-level highstands, 3) rates of uplift, and 4) erosion of pre-existing terraces. We have used two different graphical methods to compare the relative spacing

of terraces to the paleo–sea-level record in order to estimate the ages of undated terraces and evaluate long-term uplift rates and possible changes in uplift rates over time. These methods include the inferred uplift rate plots and predicted uplift rate plots as described below.

Inferred Uplift Rate Graphs

Inferred uplift-rate graphs locate by graphical comparison the most likely position of local terraces in the sequence of global marine terraces (Bull, 1985). In this method, inferred uplift is calculated by subtracting the elevation at which the terrace formed relative to modern sea level (paleo-sea level) from the present elevation of the shoreline angle of that terrace based on an assumed correlation to one of the global high-stands (Table 1). Inferred uplift is then plotted against terrace age and the slope of the resultant line is the inferred uplift rate. Diagrams that show uplift values plotted against inferred ages for a flight of terraces can be used to indicate how accurately the age-estimates predict the inferred uplift of other terraces in the flight. These diagrams provide a basis for evaluating the most probable ages of undated terraces in a sequence where one or more terraces have been dated, as well as the ages of a sequence of undated terraces.

Predicted-Uplift Graphs

An alternative graphical approach for evaluating long-term uplift and terrace ages by terrace spacing is illustrated in Figure 4. Based on estimates of the ages and paleo-sea levels of global highstands (Table 1, last column) lines are drawn predicting the present elevation of marine terraces given differing rates of long-term constant uplift. In this graphical approach, which we refer to as a predicted-uplift graph, uncertainties in the estimated values of paleo-sea level are indicated by the envelope drawn around each line. If the age of a terrace in the sequence is known, this graph can be used to predict the elevations of other terraces in the sequence assuming uplift has been constant. One advantage to this graphical approach is that it is possible to visually differentiate uncertainties in paleo-sea level estimates from uncertainties or errors in measurement of the present shoreline angle elevations. Also, this technique allows for an estimation of the range in values of long-term constant uplift permitted by the data. This graph is similar in appearance to the relation diagram presented by Pillans (1983). However, in contrast to our approach, which assumes age and paleo sea level to evaluate uplift rate, Pillans' technique makes assumptions about uplift rates to estimate likely ages of terraces.

In general, both techniques used in this study provide the same value for an average long-term uplift rate. Representative inferred uplift-rate graphs for selected areas in the San Simeon and San Luis Obispo study areas are provided in subsequent text figures and on Plate 4. Predicted-uplift graphs showing results of long-term average uplift rates based on several terraces are not presented graphically in this paper. The estimates for the post-Q2 (120 ka) terrace uplift rate given at the top of Plate 4 are based on the predicted-uplift technique.

Factors that must be considered in using both graphic techniques are that some emergent Pleistocene terraces may be missing or laterally discontinuous as a result of sea-cliff retreat during subsequent highstands, and that disruption of the terrace sequence by faulting or folding may alter the apparent number and spacing of terraces in the sequence. For these reasons we have used primarily uplift rates based on the elevation of the 120 ka terrace for comparing uplift between various coastal regions.

In addition, we have considered the variability between paleo-sea level and the actual elevation at which the paleo-shoreline angle formed. The modern shoreline angle at some locations along the coast between Point Buchon and Point San Luis appears to be forming at elevations of approximately 1 to 3 m above mean sea level. Detailed measurement of the variability along the coastline at Punta Bunda, northern Baja California, Mexico, indicate a comparable range of 2.5 ± 1.0 m for the elevation of the modern shoreline angle (Rockwell, 1987). In our plots we have assumed that this variation is probably accounted for given the range in uncertainties for paleo-sea level and measurement of shoreline elevations.

TECHNIQUES USED TO ESTIMATE SHORELINE ANGLE ELEVATIONS

Accurate measurement of terrace shoreline angle elevations is critical to estimates of uplift rate. The accuracy with which shoreline angle elevations are measured is often a function of the scale and contour interval of available base maps. Base maps used in this study varied in scale from 1:1200 to 1:24,000 and in contour interval from 2 to 40 ft (0.6 to 12 m). Along the coastline from Montaña de Oro State Park to Point San Luis and at Mallagh Landing a professional survey crew established a series of control points (accurate to 0.3 m) to provide additional elevation control. Using these control points and bench marks shown on topographic maps, the elevations of wave-cut platforms, shoreline angles, and shallow boreholes were surveyed using a stadia rod and an Abney level or Brunton compass level. The accuracy of these surveys ranged from 0.3 to 1.0 m. Similar elevation control was available in areas northeast of U.S. 101 between Arroyo Grande and Pismo Beach, where detailed surveys and topographic maps have been made for urban development.

The measured shoreline angle elevations of higher marine terraces veneered by marine deposits are generally accurate from ± 2 to 6 m, depending on the available topographic control. Where a terrace is stripped of marine and terrestrial deposits (and thus may have been lowered by fluvial or hillslope erosion), the estimated elevation of the stripped bedrock surface is considered to be a minimum value for the wave-cut platform. Estimates of the shoreline angle for these stripped wave-cut platforms are generally considered only to be accurate to within 6 m. The elevations of wave-cut platforms and shoreline angles exposed in the modern sea cliff were measured with a Brunton compass level or Abney level and stadia rod

relative to sea level at a known time and were then corrected to mean sea level using published tide charts.

Drilling and shallow seismic refraction surveys provided additional information on the elevations of shoreline angles in areas where natural exposures of shoreline angles and wave-cut platforms are limited or not available. Elevations of shoreline angles are estimated by projecting the wave-cut platform where exposed in a sea cliff, stream or gully cut, or determined from drilling to its intersection with the projected paleo-sea cliff slope (Fig. 1). The old sea cliff is frequently mappable in the field or on aerial photographs on the basis of an inflection point in topography across the erosionally modified sea cliff. It is assumed that the natural seaward slopes of wave-cut platforms generally vary from 20 to 40 m/km (1° to 2.3°) along the inner portion of the wave-cut platform (from the shoreline angle to about 300 to 600 m offshore) and from 7 to 17 m/km (½° to 1°) along the outer edge (greater than 300 to 600 m from the sea cliff) (Bradley and Griggs, 1976). This technique results in a range of estimated elevations of a shoreline angle, particularly over wider terraces. Also, the technique is not applicable if tectonic tilting has occurred. However, it does enable both the recognition of multiple wave-cut platforms that are obscured by thick alluvial and colluvial aprons and the assessment of tilting or deformation of the original slope of the platform. Another factor that must be considered in using this technique is the irregularities that commonly occur on some platforms. These irregularities are generally a function of the variable resistance and bedding attitudes of different geologic units. Topographic steps of 3 m, for example, are common between sandstone and shale units on wave-cut platforms formed on bedrock of the Franciscan Complex, and irregularities (sea-stacks) of 12 to 15 m can be caused by large chert and metavolcanic knockers in the mélange of the Franciscan Complex. Ridges approximately 1.5 to 3.3 m high occur along the strike of bedding in platforms developed across the more resistant zeolitized tuff in the Obispo Formation. Relatively smooth terraces are formed in more uniform and less resistant bedrock, such as sandstone of the Squire Member of the Pismo Formation. Irregularities from 0.3 to 1.0 m are commonly observed for wave-cut platforms developed in this bedrock.

SAN SIMEON STUDY AREA

A well developed flight of emergent marine terraces is present in the San Simeon coastal area. Previous workers in the area (Pacific Gas and Electric Company, 1974, 1975; Hall, 1975; Envicom, 1977; Weber, 1983; and Hamilton, 1984) noted deformation of in the marine terraces, particularly the lowest terraces across traces of the San Simeon fault zone, and concluded that the San Simeon fault had experienced late Pleistocene activity. The most detailed study of marine terraces in the San Simeon coastal area was provided by Weber (1983), who mapped the coastal region from Ragged Point south to Cayucos.

In order to constrain better the slip rate for the San Simeon fault zone (Hanson

and Lettis, this volume), we undertook a detailed study of marine terraces across the southern onshore reach of the San Simeon fault zone, where the fault zone is the narrowest and where the most complete sequences of marine terraces are present on both sides of the fault zone. In addition to mapping existing exposures at a scale of 1:2,400, a series of 94 boreholes were drilled, and 31 soil and exploration pits were excavated to determine the elevation of buried wave-cut platforms in areas covered by extensive eolian and alluvial deposits. Uranium-series dating of one bone sample from the lowest emergent marine terrace and thermoluminescence dating of silt from estuarine deposits underlying the second emergent terrace provide some age control. However, due to the limited amount of datable material observed in marine terrace deposits in the San Simeon area, other less direct dating and correlation techniques, including comparison of geomorphic expression and relative altitudinal spacing of marine terraces, and comparison of relative soil profile development, were also employed to correlate and date terraces across the fault zone.

Description of Marine Terraces

Sequences of four and five marine terraces have been mapped to the northeast and southwest, respectively, of the southern onshore reach of the San Simeon fault zone (Fig. 5). Detailed mapping and subsurface data are presented on Plate 1, and a longitudinal profile illustrating the elevations of shoreline angles on both sides of the fault zone is presented on Figure 6. With some modification of the terminology developed by Weber (1983), names have been designated for the five marine terraces mapped in detail along the southern portion of the onshore reach of the San Simeon fault zone. From youngest to oldest, they are the San Simeon Point (Q1), San Simeon (Q2), Tripod (Q3), Oso (Q4), and La Cruz (Q5) terraces. Higher (older) terraces were noted in reconnaissance studies, but were not mapped in detail due to the lack of lateral continuity and difficulty in estimating ages.

San Simeon Point Terrace (Q1). This is the youngest and lowest emergent marine terrace present in the San Simeon coastal area. The San Simeon Point Terrace had not been previously delineated as a separate terrace by Weber (1983). The terrace is present only within and to the southwest of the San Simeon fault zone and occurs as a narrow (typically less than 46 m wide) discontinuous bench around San Simeon Point (Fig. 5). A remnant of this terrace is present above the exposure of faulted Careaga sandstone at San Simeon State Beach and is displaced by the San Simeon fault zone. The shoreline angle of the San Simeon Point terrace lies at an elevation of 6.4 to 8.5 m and is well exposed in at least three locations around San Simeon Point. Along the southwest margin of San Simeon Point the terrace appears to merge with the outer part of the San Simeon terrace (Q2). The exact nature of this contact is obscured by a thick cover of eolian deposits.

San Simeon Terrace (Q2). The San Simeon terrace (Fig. 5) correlates to the San Simeon wave-cut platform as

mapped by Weber (1983). Weber included this wave-cut platform and the next higher one (the Tripod wave-cut platform) in a single composite terrace he called the Piedras Blancas terrace. The San Simeon terrace is the lowest emergent terrace that is present on both sides of the San Simeon fault zone.

On the northeastern side of the fault zone, the terrace occurs as a series of discontinuous, narrow (less than 67 m wide) strips along the coast from immediately south of Arroyo del Puerto, where the shoreline angle is about 5 $\pm$ 1 m, to Little Pico Creek, where the shoreline angle is higher, about 7 $\pm$ 1 m. The terrace, which gradually decreases in elevation south of Little Pico Creek, cannot be traced south of Cambria (Weber, 1983). The shoreline angle is well exposed in the sea cliff near the mouth of Broken Bridge Creek and directly north of Little Pico Creek (Fig. 5). The terrace is present farther to the northwest than had been mapped by Weber (1983), and although there appears to be some tilt in a general north to northwest direction, there does not appear to be extensive downwarping of the wave-cut platform toward the fault zone as postulated by Weber (1983). Fluvial erosion and subsequent burial by extensive eolian sand has modified and obscured the platform near its intersection with the San Simeon fault zone on the northeastern side of the fault. The San Simeon terrace may be preserved for a distance of at least 460 m north of Arroyo del Puerto based on a fairly continuous drop in bedrock between Arroyo del Puerto and the San Simeon fault zone (Fig. 5; Plate 1). This step in bedrock is inferred from the following observations: (1) bedrock in a 3 to 4 m terrace exposed along the north bank of Arroyo del Puerto rises abruptly in the vicinity of the access road to San Simeon village to an elevation of 6 m (Plate 1); (2) the step in bedrock appears to be coincident with a southwest-facing break in slope that extends north to the vicinity of geophysical lines 5 and 16 (Plate 1); and (3) a down-to-the-southwest step in the surface of bedrock along this trend is suggested by geophysical data from line 19 and by drilling and geophysical data along line 5 (Plate 1). This step in bedrock may be coincident with the strandline of the San Simeon terrace, or alternatively, and equally likely, it may represent a fluvial channel margin. The possible northward extent of the San Simeon terrace, however, is constrained by borehole data to lie south of the access road to the Borrow Pit locality (Plate 1).

The elevation of the shoreline angle for the San Simeon terrace is considerably higher within and directly southwest of the fault zone. Around San Simeon Point the elevation of the shoreline angle is as high as 24 $\pm$ 1 m, but with increasing distance from the active traces of the fault zone the elevation decreases to 9 $\pm$ 2 m. North of the Arroyo del Oso fault the elevation of the shoreline angle is 6.1 to 7.6 m, comparable to the elevation of the shoreline angle northeast of the fault zone. In contrast to the northeast side of the fault zone, the terrace is considerably wider, ranging in width from 122 to 730 m along the stretch of coastline between Oak Knoll and San Simeon Point. However,

northwest of the Oak Knoll area the terrace, as mapped by Weber (1983), narrows and is generally less than 84 m wide.

Tripod Terrace (Q3). The Tripod terrace was defined by Weber (1983) as the upper platform in the Piedras Blancas composite terrace. The Tripod terrace is generally the broadest and best expressed of the lower marine terraces on both sides of the fault zone. North of Airport Creek on the southwest side of the fault and on the entire northeast side of the fault, the Tripod terrace is the second emergent terrace. Locally, within and adjacent to the fault zone on the southwest side, the Tripod terrace is the third highest terrace.

The Tripod terrace northeast of the San Simeon fault zone maintains a relatively consistent elevation of 23 to 26 m from Little Pico Creek north to Arroyo del Puerto (Fig. 5). North of Arroyo del Puerto, the configuration and elevation of the original terrace are difficult to estimate due to subsequent fluvial erosion and burial by extensive eolian deposits. A narrow bedrock bench at an elevation of approximately 23 m directly northeast of the fault zone south of the north fork of Airport creek occurs at a comparable elevation, but because it has been stripped of deposits, it is not possible to determine if it is a marine or fluvial strath terrace surface. The clear lack of deformation of the older Oso terrace on the northeast side of the fault zone indicates that the younger Tripod terrace probably maintained a relatively uniform elevation prior to fluvial erosion and has not experienced broad downwarping into the fault zone as postulated by Weber (1983).

Upwarping of the Tripod terrace into the fault zone is observed on the southwest side of the fault. As illustrated on Figures 5 and 6, the terrace rises sharply from an elevation of 25 m in the vicinity of Adobe Creek to 37 m as it approaches the westernmost active strand of the fault zone. In the area bounded by the two primary strands of the fault zone, the terrace has an elevation of approximately 38 m.

Oso Terrace (Q4). The Oso terrace as originally mapped by Weber (1983) was limited to a series of thin, discontinuous patches of terrace deposits lying north of the southern strand of the Arroyo del Oso fault at elevations between 43 and 61 m. Remnants of this terrace are more prevalent than shown by Weber (1983) and are clearly present on both sides of the San Simeon fault zone along its southern onshore reach (Fig. 5). Geomorphic preservation and position of the Oso terrace on both sides of the fault is similar in that the narrow, laterally discontinuous remnants are bordered by broader, more laterally continuous and well expressed terraces.

The location and elevation of the shoreline angle for the Oso terrace on the northeastern side of the fault zone between the northern branch of Airport and Little Pico creeks is well constrained by exposures in soil pits, exploration pits, and gullies. Terrace remnants occur as thin (generally less than 200 m wide), discontinuous patches and maintain a relatively uniform elevation. The

shoreline angle elevation ranges from 32 to 35 m in this region (Figs. 5 and 6).

On the southwestern side of the fault zone, deformation of the Oso terrace is similar to deformation of both the older La Cruz and the younger Tripod and San Simeon terraces (Fig. 5). The shoreline angle lies at an elevation of 37 ± 1 m northwest of Oak Knoll Creek and is warped to an elevation of at least 40 ± 1 m directly west of the fault zone. The shoreline angle lies at a maximum elevation of 47 ± 2 m in the area between the two active fault strands.

La Cruz Terrace (Q5). The highest marine terrace mapped in detail in the San Simeon area during this study is the La Cruz terrace. This terrace includes parts of the Cambria and undifferentiated terraces on the northeastern side of the fault and parts of, but not all of, the La Cruz terrace on the southwestern side of the fault as mapped by Weber (1983).

The elevation of the shoreline angle for the La Cruz terrace is, in general, less well constrained than the elevations of shoreline angles of lower terraces. Northeast of the fault zone, the terrace forms a broad, well-expressed geomorphic surface (Fig. 6). A series of three soil pits excavated on this surface near the Hearst private airstrip and gully exposures indicate that the terrace wave-cut platform is veneered entirely by fluvial deposits, which have a higher percentage of silt to sand than marine deposits. Although the terrace appears to be stripped of marine deposits, the lateral continuity and broad, relatively uniform elevation of the terrace suggests that it has not been significantly lowered by fluvial erosion. Drill hole data and natural exposures of bedrock indicate that there is a small step in bedrock (less than 5.2 m) at the back of this terrace that lies beneath and subparallel to the airstrip (Plate 1). The step may be due to faulting as postulated by Weber (1983), but more likely represents a shoreline angle at an elevation of 53 ± 2 m.

Reconnaissance mapping indicates that the elevation of the shoreline angle for the next higher terrace above the La Cruz terrace on the northeast side of the fault zone by the airstrip is probably less than 67 m. The La Cruz and next higher terrace may have formed during sea level highstands that were closely spaced in time, thus explaining the small amount of vertical separation. Directly north of Oak Knoll, this shoreline angle was not clearly defined by field exposures or drilling. Available data suggest that there may be a shoreline angle at an elevation of greater than or equal to 56 m. This terrace appears to be part of a single, widely dissected, irregular geomorphic surface that lies at an elevation of approximately 61 m in the area between the San Simeon and Oceanic fault zones. It is likely that this geomorphic surface represents a composite terrace of multiple wave-cut platforms that have been significantly modified by fluvial erosion. Because of these complexities as well as possible tectonic influences arising from the proximity to the intersection of two major fault zones, it is difficult to differentiate clearly and date individual marine platforms in this area.

The shoreline angle elevation of the La Cruz terrace between Arroyo del Puerto and Little Pico Creek is estimated from projections of wave-cut platform exposures whose elevations are estimated from a U.S. Geological Survey 7½-minute quadrangle (contour interval = 40 ft (12 m)). As such, the uncertainty is considerably greater than for shoreline angle elevations measured in areas of better topographic control and where there is additional subsurface information (Fig. 6).

Smaller, more discontinuous remnants of the La Cruz terrace are preserved on the southwestern side of and within the San Simeon fault zone. There are limited natural exposures of the deposits overlying these platforms, and in areas where subsurface data (either drill hole or test pit data, Plate 1) were obtained, the surface appears to be largely stripped. However, small patches of marine deposits were observed in a gully exposure between Adobe and Oak Knoll creeks (Fig. 6). In the gully exposures directly south-southeast of Oak Knoll, the La Cruz terrace is buried by thick eolian deposits with a well developed soil profile.

The elevations of the shoreline angle for these remnants follows a similar pattern to the lower terraces, gradually rising from an elevation of 53 ± 3 m near Oak Knoll to 58 ± 2 m in the Adobe Creek area (Fig. 5). The highest terrace remnant occurs between the two active strands of the fault at an elevation of 79 ± 6 m. High surfaces within and southwest of the fault zone on the southeast side of Oak Knoll Creek (Plate 1) probably correlate to the La Cruz terrace, but have been stripped of all deposits except for a thin (1 m) cover of colluvium.

Correlation and Estimated Ages of Marine Terraces

Datable materials from the San Simeon area are restricted to: (1) a bone sample recovered from marine gravel overlying the San Simeon Point (Q1) marine platform, (2) samples of charcoal for radiocarbon dating, and (3) samples of silty clay from estuarine deposits underlying the San Simeon terrace (Q2) for thermoluminescence dating.

Due to the limited amount of datable materials and the fact that dated samples were from terraces on the southwestern side of the fault, other less direct dating techniques also were employed to correlate and date terraces across the San Simeon fault zone. These included:

1. Lateral correlation of the Tripod terrace to the well dated (Muhs and others, 1988; Kennedy and others, 1988; Stein and others, 1989; this study) Cayucos terrace as mapped by Weber (1983).

2. Comparison of relative soil profile development for terraces on both sides of the fault zone (see Rockwell and others, this volume), and comparison of soils in the San Simeon area to the soil developed on the previously dated Cayucos terrace and to a well established chronosequence at Punta Banda in Baja California (T. Rockwell, written comm.).

3. Comparison of geomorphic expression of and relative altitudinal spacing between terraces within terrace sequences on either side of the fault and adjacent to and within the most recently active strands of the fault zone.

Ages Based on Numerical and Calibrated Dates. A highly-weathered mammal bone fragment (sample KH-42-A, Table 2) was collected from marine gravel 1.2 m above the San Simeon Point (Q1) marine terrace on the southwest side of San Simeon Point (Fig. 5). Uranium-series analysis of this sample yielded concordant U/Th and U/Pa ages of 46 ± 2 ka and 49 ± 4 ka, respectively, providing a minimum age of approximately 46 ka for this terrace. The concordancy of these ages indicates that the bone has been a relatively closed system since uranium was introduced into the bone (Ku, written comm., 1987). Major highstands that predate these ages, occurred at about 60 ka (early stage 3), 80 ka (substage 5a) 105 ka (substage 5c) and 120 ka (substage 5e) (Table 1).

Samples for radiocarbon and thermoluminescence analysis were also collected from estuarine sediments underlying the San Simeon (Q2) terrace approximately 350 m south of the mouth of Oak Knoll Creek. A marine cobble lag, laterally continuous with marine deposits of the San Simeon terrace, overlies the estuarine sediments. These sediments fill an older fluvial channel of Oak Knoll Creek that was probably incised during a previous sea-level lowstand. Aggradation and deposition of the estuarine sediments likely occurred during the rise to the sea-level highstand that produced the San Simeon (Q2) terrace. Radiocarbon analysis of detrital charcoal (sample ^{14}C-KH-5c, Table 3) suggests an age beyond the limits of the radiocarbon method (>40,480 ± 1,080 yr B.P.) for the estuarine deposits. Two samples of clay and silty clay (TL-1a and TL-2a, Table 3) collected from the same deposits and submitted for thermoluminescence analyses yielded TL ages of 78 ± 12 ka and 96 ± 19 ka, respectively (G. Berger, written comm., 1987). The weighted mean age of these two samples, which were collected from the same strata, is 83 ± 10 ka. These ages suggest that the San Simeon (Q_2) terrace correlates to isotope substage 5a (80 ka), since stratigraphic relationships dictate that the estuary sediments pre-date the marine terrace.

Lateral Correlation to the Cayucos Terrace. Weber (1983) concluded, based on mapping of marine terraces between San Simeon and Cayucos approximately 35 km to the south, that the wave-cut platforms of the first emergent terrace at Cayucos and the Tripod (Q_3) terrace in the San Simeon area are laterally continuous and equivalent in age. The Cayucos terrace has been demonstrated by several dating techniques to be approximately 120 ka (Veeh and Valentine, 1967; Muhs and others, 1988; Kennedy and others, 1988; Stein and others, 1989; samples 505p, C-5e, and LACMNH 10731, Table 2). Weber (1983) cited minor problems of terrace cover and platform irregularity in mapping the terrace between Cambria and Point Estero, but stated that the terrace surface is definitely a single

continuous landform from the Cayucos terrace at Cayucos to the Tripod platform near Cambria. Weber (1983) noted that the terrace may be displaced by the Cambria fault based on an apparent 3-m step in the elevation of the terrace near Ellysly Creek, but he did not cite this as a difficulty in terrace correlation. We did not verify the lateral continuity of this terrace or evaluate displacement on the Cambria fault during our study.

Although the Tripod terrace as mapped by Weber (1983) is fairly continuous between Cayucos and San Simeon, the terrace has been modified by fluvial incision across the mouths of a few relatively large streams, including Ellysly Creek, Santa Rosa Creek, and San Simeon Creek. The fluvial erosion combined with the thick dune cover on the lower terraces in the vicinity of San Simeon Creek and Cambria, results in more uncertainty in the correlation than expressed by Weber (1983). However, we consider the correlation of the Tripod and Cayucos terraces as described by Weber to be reasonable.

Correlation and Estimated Ages Based on Soil Studies. In conjunction with trenching and Quaternary mapping investigations in the San Simeon study area, soil geomorphological techniques (Rockwell, written comm.) were employed to 1) establish the correlation of marine terraces across the San Simeon fault zone; and 2) estimate the ages of the displaced marine terraces. In order to develop a soil chronosequence for the flight of marine terraces, a series of 17 soil profiles were described and sampled in backhoe pits and cleared natural exposures according to Soil Survey Staff (1975) criteria. Six numerical parameters of relative soil development were assessed: 1) the Soil Profile Development Index (SPDI) (Harden, 1982); 2) Maximum Horizon Index (MHI) (Rockwell, 1983); 3) the volume of secondary clay in the profile; 4) the Clay Film Index (CFI) (Rockwell and others, 1985); 5) the maximum and average ratio of clay in the Bt horizon to that in the A horizon; and 6) the Color Index (Rockwell and others, 1985). Two additional parameters, the shape of the clay versus depth curve and position of secondary clay accumulation in the profiles and thickness of marine deposits on individual platforms also were used in correlating and dating the marine terraces across the San Simeon fault zone.

Based on these studies, the second, third, and fourth marine terraces in the uplifted block on the southwestern side adjacent to and within the fault zone correlate to the first, second and third terraces in the sequence northeast of the fault zone. These correlations are in agreement with correlations of terrace sequences across the fault zone based on geomorphic expression and relative altitudinal spacing.

Three approaches were used to estimate ages of the soils in the San Simeon area. Initially, soil-profile development in the San Simeon area was compared to three soil profiles exposed in soil pits excavated in the 120 ka Cayucos terrace. This approach proved unsuccessful in that significant differences in the parent material of the soils in the two areas do not allow for a direct correlation.

The second approach involved comparing soils from the San Simeon area to a well-dated soil chronosequence at Punta Banda in Baja California just south of the Mexico-United States border (Rockwell and others, 1987). Although there are slight differences in climate between the two areas, the strong influence of a similar marine environment coupled with similarities in parent material, slope, and topographic position allow for a reasonable correlation between the two areas. Although many soil properties allow for a correlation of the 120 ka Punta Banda terrace with either the Tripod (Q_3) or San Simeon terraces (Q_2), the best correlation is with the Tripod (Q_3) terrace (Rockwell, written comm.).

The third approach used to estimate soil ages is to compare the relative degree of soil development as indicated by two parameters (Soil Profile Development Index (SPDI) and Clay Volume (CV)) measured for individual terraces within the sequences (Rockwell, written comm.). Similarities in these values for the San Simeon (Q_2) and Tripod (Q_3) terraces suggest they may be relatively close in age, whereas the marked differences in these values between the Tripod (Q_3) and Oso (Q_4) terraces suggests a significantly greater difference in age. Based on these observations, coupled with the correlation of the Tripod soil with the 120 ka Punta Banda soil, the San Simeon (Q_2), Tripod (Q_3), and Oso (Q_4) terraces are interpreted to correspond to high stands of sea at about 80 or 105, 120, and 210 ka, respectively.

Age Estimates Based on Geomorphic Expression. Within the terrace sequences developed on both sides of the San Simeon fault zone, individual terraces can be delineated roughly by width, continuity, and degree of dissection. Similarities in the geomorphic expression of individual terraces and sequences of terraces across the fault zone support terrace correlations based on soils and altitudinal terrace spacing.

In general, the Tripod terrace is the widest and most laterally continuous terrace on both sides of the fault. The San Simeon terrace on the southwestern side of the fault zone in the vicinity of Oak Knoll south to Point San Simeon approaches the Tripod terrace in width, but north of Oak Knoll the terrace is generally confined to a narrower strip along the coast (Weber, 1983). Northeast of the fault zone, the Simeon terrace occurs as narrow discontinuous remnants along the present coastline. The San Simeon Point terrace is also a narrow discontinuous terrace, but it appears to be locally restricted to the coastline surrounding Point San Simeon on the southwestern side of the fault.

The next higher terrace above the broad Tripod terrace on both sides of the fault zone occurs only as narrow discontinuous remnants. These remnants, mapped as the Oso terrace, are bordered by significantly wider terraces both above and below. The higher terrace, the La Cruz terrace, southwest of the fault, is a series of small remnants (Fig. 5). However, the terrace as mapped further to the north by Weber (1983) is

considerably broader. The dissection and stripping of the surface on the southwestern side of the fault is likely to be a result of greater fluvial erosion in the vicinity of Oak Knoll Creek.

Elsewhere along the coast of California and Baja California, the most widespread and well-developed Pleistocene terraces are the ~120 ka and ~80 ka terraces (Lajoie and others, 1979; Muhs and others, 1988). In the San Simeon area, the Tripod (Q_3) and San Simeon (Q_2) terraces would best correlate to the ~120 ka and ~80 ka high stands, respectively, based on relative position, lack of dissection and preservation. This would suggest that the San Simeon Point terrace (Q_1) could represent the ~60 ka high stand of sea reported from Barbados (James and others, 1971) and New Guinea (Bloom and others, 1974).

Terrace Altitudinal Spacing and Uplift Rates.

Spacings of terraces within a flight depend partly on the altitudes of formation of terraces, the intervals of time between consecutive sea-level highstands, the rates of uplift, and erosion or lack of preservation of intermediate terraces.

Based on geomorphic expression, soils studies, and lateral correlation to the Cayucos terrace, it is likely that the Tripod (Q_3) terrace is approximately 120 ka. Using the present elevations of the terraces, estimated paleo-sea levels summarized in the last column of Table 1, an age of 120 ka for the Tripod terrace, and assuming there are no missing terraces in the sequences on either side of the fault, inferred uplift-rate graphs have been made for the terrace sequences on both sides of and within the San Simeon fault zone (Fig. 7).

Both the inferred uplift-rate graphs and the predictive uplift graphs for sequences of terraces in the regions on both sides of, but away from the San Simeon fault zone yield uniform and similar long-term rates of uplift. In the vicinity of Adobe Creek on the southwest side of the fault zone the long-term average uplift rate is 0.17 ± 0.02 m/ka (Fig. 7A). On the northeast side of the fault zone near Broken Bridge Creek, the long-term uplift rate is 0.16 ± 0.01 m/ka (Fig. 7C). The goodness of fit exhibited by these plots indicates that the correlations of terraces across the fault zone as well as age estimates based on correlation to the New Guinea (Bloom and Yonekura, 1985) and California-Baja California, Mexico (Muhs and others, 1988) sea-level curves are reasonable.

The spacing between terraces adjacent to and within the fault zone between Oak Knoll Creek and San Simeon Point is not consistent with a uniform rate of uplift. The greatest discrepancies and uncertainties noted are with respect to the San Simeon (Q_2) and San Simeon Point (Q_1) terraces. As illustrated in the inferred uplift-rate graphs in Figure 7B the terrace spacing for the sequence of terraces at San Simeon Point suggests that there has not been a constant rate of uplift in this region during the past 120,000 years. The best fit is obtained in Figure 7B-a where it is assumed that the San Simeon Point (Q_1), and San

Simeon (Q_2) terraces are ~80 ka and ~105 ka, respectively. This gives a long-term average uplift of 0.24 m/ka. However, even in this interpretation the uplift rate during the past 120,000 years has varied considerably from an average of 0.16 m/ka for the past 80 ka to 0.48 m/ka for the period between 80,000 and 105,000 years. Also, this correlation is not consistent with the age assignment of 80 ka for the Q_2 terrace away from and on both sides of the fault zone based on terrace altitudinal spacing and geomorphic expression.

An alternative interpretation is that the Q_1 and Q_2 terraces are ~60 ka and ~80 ka, respectively. The present shoreline angle elevations of these terraces, however, are considerably greater than would be expected assuming a uniform uplift rate based on the Tripod (Q_3) terrace. Assuming the correlations are correct and the paleo-sea-level estimates for these two highstands are accurate, the inferred uplift-rate graph (Fig. 7B-b) requires that rapid uplift in the past 60,000 years was preceded by a period of subsidence between 60,000 and 80,000 years ago and a period of no uplift between 80,000 and 120,000 years ago. That there should be changes in uplift rates within and adjacent to an active fault zone such as the San Simeon fault zone is not unreasonable, but the magnitude of the reversal from rapid uplift (0.53 m/ka) to subsidence (-0.2 m/ka) exhibited by the inferred uplift-rate graph shown in Figure 7B-b is such that this does not seem likely. The rapid uplift required by this graph during the past 60,000 years is largely a function of the estimated paleo-sea level for the ~60 ka high stand (Bloom and Yonekura, 1985; Chappell and Shackleton, 1986). Hypothetical raising of the paleo-sea level of the early ~60 ka high stand by approximately 10 m gives a more reasonable fit, but still requires more rapid uplift during the past 60,000 years and a period of no uplift between 80,000 and 120,000 years.

Therefore, although it can be inferred from each of the alternative interpretations that uplift during the past 120,000 years adjacent to and within the fault zone at San Simeon Point has not been constant, the data do not allow for preferred estimates of the ages for the lower terraces or history of uplift at this locality.

SAN LUIS OBISPO STUDY AREA

A flight of elevated marine terraces is present between Morro Bay and the northeastern margin of the Santa Maria Valley (Fig. 3). Marine terraces in this region were first described by Fairbanks (1904) who recognized sequences of elevated terraces along the coast at several locations between Morro Bay and Mallagh Landing. In the early 1980's personnel from the U.S. Geological Survey conducted reconnaissance mapping and sampled fossils from the lowest terraces (Kennedy, unpublished data). Detailed studies of marine terraces, however, were limited to very localized areas such as the Diablo Canyon Power Plant site (Pacific Gas and Electric Company, 1973) and the coastal region between Morro Bay and Point Buchon (Cleveland, 1978).

In this study, we have mapped in detail the marine terraces throughout the entire coastal region between Morro Bay and the Santa Maria Valley, and have collected and dated numerous fossil samples from the two lowest terraces in the sequence. Mapping of these terraces provides new data for evaluating the location and activity of faults and folds in this region. In addition, regional patterns of uplift based on the elevations of emergent marine terraces have been useful in defining regional structural blocks and in evaluating tectonic models for the region (Lettis and others, this volume [b]).

Description of Marine Terraces

The distribution and preservation of marine terraces varies considerably within the coastal region between Morro Bay and the northern Santa Maria Valley. Maps showing the distribution of marine terraces are presented on Plates 2 and 3. Longitudinal profiles showing elevations and alternative interpretations of regional correlations of marine terraces from Morro Bay to the northern Santa Maria Valley are presented on Plate 4. Inferred uplift-rate graphs at several locations along this coastal reach are also presented on Plate 4.

The terraces are well expressed in a relatively narrow strip along the coast between Morro Bay and Avila Beach (Plate 2). In this area, remnants of at least twelve marine terraces ranging in elevation from 4 $\pm$ 1 to 247 $\pm$ 6 m have been preserved. From Avila Beach south to Pismo Beach, the lowest two marine terraces are nearly continuous, but many intermediate and higher marine terraces are dissected and only locally preserved. South of Pismo Beach, lower terraces are buried beneath a thick mantle of eolian sand and alluvium in the Arroyo Grande and Nipomo Mesa areas, and only the older terraces can be mapped (Plate 3). In this area, however, there is a relatively complete sequence of older terraces. In contrast to the sequence of terraces from Morro Bay to Pismo Beach, which parallel the present coastline, marine terraces south of Pismo Beach diverge from the present coastline to the southeast and occur as far as 21 km inland in the southern part of the mapped area near State Highway 166 (Plate 3). South of this area, between Suey Creek and the confluence of the Cuyama and Santa Maria rivers, terrace deposits of probable marine origin are present at elevations of approximately 88 m and 110 m. These deposits suggest that high terraces were formed even farther inland along the northeastern boundary of the Santa Maria Valley and that much of the Santa Maria Valley was inundated during the middle Pleistocene.

Q_1 Terrace. The Q_1 terrace is the youngest and lowest terrace present between Morro Bay and Shell Beach. It is present along most of this reach of coastline except in the San Luis Hill area south of the San Luis Bay fault, where uplift rates have not been high enough to preserve the terrace. The Q_1 platform is typically veneered by a thin (1 to 2 m) deposit of marine sand and gravel overlain by locally thick (up to 30 m) deposits of alluvium, colluvium, and/or eolian sand. At its northernmost exposure in Montaña de Oro State Park the

elevation of the shoreline angle of the Q_1 terrace is 14 ± 2 m. Between Islay Creek and Olson hill the terrace maintains a relatively uniform elevation, ranging from 9 ± 2 m to 12 ± 2 m. In the vicinity of Olson Hill north of Deer Canyon, the Q_1 terrace appears to step down between 1.5 and 4.6 m across the postulated traces of the Olson fault. The elevation of the Q_1 terrace gradually decreases from 8 ± 1 m at the mouth of Deer Canyon to 5 ± 1 m at Pecho Creek. These data suggest that the Q_1 terrace may be tilted to the south about 3 m between the Olson and San Luis Bay faults. The most pronounced warping occurs in the vicinity of Pecho Creek. Terrace Q_1 is not present on the downthrown side of the San Luis Bay fault from Rattlesnake Canyon to the roadcut exposure of the San Luis Bay fault near Avila Beach (Lettis and others, this volume [b]), except for a small questionable remnant at an elevation of approximately 4 m at Point San Luis. Alternatively, the small 4 m high terrace at San Luis Point is a modern storm terrace or a remnant of the ~105 ka marine terrace. From Avila Beach to Shell Beach, the Q_1 terrace maintains a relatively uniform elevation of about 6 m. The Q_1 terrace is not clearly displaced by the Wilmar Avenue fault. However, the terrace is either absent on the southwest (downdropped) side of the fault or is present as a small terrace remnant at a much lower elevation of approximately 1.2 m directly southwest of the main fault trace exposed in the Pismo Beach sea cliff. These relationships suggest that the terrace has been deformed across the Wilmar Avenue fault.

<u>Q_2Terrace</u>. The Q_2 terrace is the most laterally continuous and generally the widest terrace between Morro Bay and Pismo Beach. The only section where Q_2 is poorly preserved occurs between Point San Luis and Avila Beach. Thin (1 to 2 m) deposits of marine gravel typically overlie the Q_2 wave-cut platform and these deposits are, in turn, overlain by locally thick (15 to 30 m) alluvial, colluvial, and eolian sediments. The elevation of the Q_2 terrace shoreline angle, which is well constrained by borehole data along most of the coast, maintains a relatively uniform elevation of approximately 32 ± 3 m between Islay Creek and the coastal region adjacent to Green Peak. The Q_2 platform steps down to the southwest between 4 and 6 m across the postulated Olson fault. Between the Olson fault and Pecho Creek the shoreline angle elevation of the Q_2 terrace is about 19 to 20 m. South of Pecho Creek warping of the terrace in the hanging wall of the San Luis Bay fault is suggested by the decrease in the elevation of the shoreline angle to about 16 m. The Q_2 terrace shoreline angle abruptly steps down from 16 ± 1 to 13 ± 1 m across the San Luis Bay fault at Rattlesnake Creek and stays at about 13 ± 1 m to the Port San Luis harbor office. At the Avila Beach exposure of the San Luis Bay fault (Lettis and others, this volume [b]), the elevation of the Q_2 terrace shoreline angle on the upthrown side of the fault is 20 ± 1 m. The Q_2 platform remains at about 20 ± 1 m and forms a broad, well preserved and laterally continuous terrace between Avila Beach and Pismo Beach. The Q_2 terrace is displaced as much as 6 m across the Wilmar Avenue fault

assuming that the wave-cut platform adjacent to the main fault on the downthrown side is the Q_2 terrace. Alternatively, the wave-cut platform on the downthrown side is the younger Q_1 terrace and cumulative net vertical separation of the Q_2 terrace across the fault zone is approximately 4 m. The strandline of the Q_2 terrace, which is generally subparallel to and within 100 m of the present coastline to the north, diverges from the coastline in the vicinity of Pismo Beach and can be traced for less than 1.6 km south of Pismo Creek. Disruption of the terrace by the Wilmar Avenue fault and burial of the terrace by extensive dune deposits in the Arroyo Grande and Nipomo Mesa areas make it difficult to map the terrace further to the southeast.

Q_3Terrace. Unlike the lower two terraces, the third terrace in the sequence is dissected and only locally present. It is well preserved and relatively continuous north of Coon Creek in Montaña de Oro State Park where it occurs at elevations ranging from 46 $\pm$ 3 m to 51 $\pm$ 2 m. Between Point Buchon and Point San Luis remnants of the Q_3 terrace are also present, but are buried by a thick wedge of colluvium and alluvium. Subsurface excavations and boreholes indicate that the terrace is present in the vicinity of Diablo Canyon and north of Olson Hill at slightly lower elevations of 42 to 44 m and 36 to 38 m, respectively.

Platform cutting and cliff retreat during the formation of the Q_2 terrace appears to have destroyed all evidence of the third terrace (Q_3) in the region of Point San Luis between the Olson fault and the town of Avila Beach. Small remnants of the Q_3 terrace are present in the region between Mallagh Landing and Shell Beach, but due to the thick wedge of colluvium that has formed at the base of the steep range front in this area, the extent and elevation of the terrace is known only in areas where boreholes have been drilled. The Q_3 terrace may be present in the Shell Beach area as well. Based on geomorphic expression, there appears to be at least one shoreline angle higher than the Q_2 terrace along the base of the range front near Shell Beach. Due to the thickness of alluvial fan deposits and colluvium in this area, there are no natural exposures of the wave-cut platform and the elevation of the shoreline angle is only known to be less than about 61 m. To the south the Q_3 terrace is exposed near the "Farmboy" quarry in Pismo Beach. Further to the south the Q_3 terrace is buried by the extensive dune field in the Arroyo Grande and Nipomo Mesa region.

Higher Terraces. In general, most terraces higher than Q_3 terrace are laterally discontinuous and only moderately to poorly preserved as illustrated on Plates 2 and 3. Relatively complete sequences of older terraces are preserved in only two regions of the San Luis Obispo study area, in the coastal region between Morro Bay and Point Buchon (Montaña de Oro State Park) and in the area between Pismo Beach and Arroyo Grande.

Terrace remnants in Montaña de Oro State Park occur at elevations up to 247 m. The wave-cut platforms of the higher terraces are commonly well preserved and overlain by a veneer of marine gravel and eolian sand, alluvium, and/or colluvium. Along the steep rugged coastline between Point Buchon and Green Peak, however, sea cliff retreat during the most recent sea-level highstands and erosion due to hillslope processes have destroyed most of the higher terraces.

Higher terrace remnants are present also in the Point San Luis area between Green Peak and San Luis Obispo Creek. In general the terrace remnants in this area are preserved as dissected erosional benches that usually have been stripped of overlying marine deposits. Correlation of these terrace remnants is complicated by deformation associated with the San Luis Bay fault and possibly the Olson fault (see following discussion of terrace correlation and age estimates).

Evidence of higher terraces is not observed along most of the steep range front between Mallagh Landing and Pismo Beach. It is likely that any terraces in this area were destroyed during the Q_2 terrace sea-level high stand. Several remnants of one of the higher terraces, however, are preserved at elevations of approximately 134 to 137 m along the coast between Shell Beach and Pismo Creek. These terrace remnants are overlain by both marine deposits and colluvium.

In the Pismo Beach to Arroyo Grande area, a relatively complete sequence of higher terraces is preserved. Wave-cut platforms are developed largely on the Pliocene Squire Member of the Pismo Formation between Pismo Creek and Arroyo Grande Creek. The Squire Member consists of poorly to moderately consolidated, clean, well-sorted, arkosic sandstone that was originally deposited in a nearshore marine environment. As such, it is sometimes difficult to differentiate between sandstone of the Squire Member and Quaternary marine sediments and alluvial deposits derived primarily from the Squire Member. Pholad borings were observed locally on the wave-cut platforms as indicated on Plate 3, but the common occurrence of bioturbation and soft sediment deformation within sandstone beds of the Squire Member requires caution in the interpretation of such features. Urban development in this area has provided numerous cuts and exposures. However, in addition to extensive excavation, considerable amounts of fill have been placed in developed areas, and the original deposits and bedrock, therefore, are commonly buried or removed as a result of these operations. In areas outside of developments, exposures are very limited, being masked by thick deposits of colluvium and older alluvium (Qoa).

South of Arroyo Grande Creek, wave-cut platforms are developed chiefly on Obispo Formation and Franciscan Complex rocks. Although buried by extensive older alluvium (Qoa) and colluvium, particularly along the flanks of Picacho hill, numerous exposures of the wave-cut platforms and overlying marine deposits were observed in gullies

in the area between Picacho hill and Los Berros Creek. Wave-cut platforms formed on tuff of the Obispo Formation in this area are characterized by abundant pholad borings. Pholad borings were not observed on wave-cut platforms developed on Franciscan Complex rocks, but overlying deposits of well rounded pebble and cobble gravel in a clean, well sorted sand matrix are clearly marine in origin; pholad-bored cobbles are common within these deposits. The elevation of the shoreline angles of one of the highest terraces is well constrained at several locations and increases about 12 m in elevation from 104 m east of Picacho hill to 117 m near Los Berros Creek. A northward tilt is also observed in the next lower terrace. Due to possible faulting and deformation in the Picacho hill area, the lateral correlations and ages of wave-cut platforms at elevations below this terrace (less than 91 m elevation) are uncertain.

The location and elevation of the shoreline angles of the two lowest terraces mapped in this area are inferred from sparse subsurface water-well data, and as such are poorly constrained. Due to limited access in the area northwest of Los Berros Creek and southwest of U.S. 101 near Picacho hill (Plate 3), data on the location and elevation of the intermediate shoreline angles are sparse. Thick fluvial deposits exposed along U.S. 101 north of the intersection of the highway and Los Berros Creek and in gravel borrow pits west of this area may have been deposited along an ancestral Los Berros Creek graded to a marine terrace at an elevation of less than or equal to 88 m.

Marine platforms and deposits were also observed in Nipomo Valley northeast of the Nipomo Mesa. Southeast of Nipomo, the location and elevation of the shoreline angles of two of the higher terraces at elevations of approximately 113 m and 90 m are fairly well constrained due to the presence of more numerous exposures of the wave-cut platforms and overlying marine deposits. Extensive erosion and stripping of these platforms in the northwestern part of the valley, however, make evaluation of the elevations and locations of these shoreline angles in this area more difficult. Marine terraces higher than the 113 m terrace may be present in the foot-hills of the San Lucia Range, but due to limited time were not mapped during this study. Terraces lower (younger) than the 90 m terrace are also likely to be present in the area southeast of U.S. 101 beneath the extensive sand dunes that blanket the Nipomo Mesa. Scattered water wells in this area and exposures along the bluffs of the southern end of the Nipomo Mesa indicate that the elevation of the top of bedrock drops abruptly southeast of U.S. 101. This down-to-the-southwest step in the top of bedrock may be the result of marine erosion or displacement across the postulated extension of the Wilmar Avenue fault, or a combination of both.

Estimated Ages of Marine Terraces

The ages of the lower two terraces (terraces Q_1 and Q_2) between Point Buchon and Pismo Beach are constrained by uranium-series ages on coral and vertebrate bone samples, data on amino-acid racemization of mollusks and paleoclimatic analyses of invertebrate faunal assemblages. The dating results

for samples collected from the Q_2 terrace at several sites along the coast from Point San Luis to Pismo Beach provide the best age control for an individual terrace in the study area. These ages, which are summarized in Table 2, indicate that the Q_2 terrace is approximately 120,000 years old and correlative with marine oxygen isotope substage 5e. Seven of the samples collected (Samples 520p, 522p, 523p, 525p, KIK-42, W87-10, and W87-135) provided consistent results using more than one dating technique. Discordant results were obtained for two samples (G86-100 and W87-89) from this terrace based on faunal assemblages and amino acid racemization ratios. The interpretation of the faunal assemblage data in both cases, however, indicates an age of approximately 120 ka and these data are judged to be more reliable than the age-estimates based on amino acid racemization ratios. An anomalous uranium-series age of 112 $\pm$ 4 ka, suggesting a correlation with isotope substage 5c, was obtained from a coral sample collected at an elevation of 27 $\pm$ 1 m from the wave-cut platform of the Q_2 terrace directly west and slightly south of Diablo Canyon (sample W87-135, Table 2). This date appears to be too young based on the following observations:

1. The uranium concentration ratio for this coral sample is anomalously high, which suggests that it may have been contaminated by secondary, continental uranium-bearing water (D. Muhs, pers. comm., 1988). This could yield an inaccurate younger age.

2. The faunal assemblage associated with the coral has a warm-water aspect, which is typically associated with ~120 ka terrace deposits rather than ~105 ka terrace deposits.

3. Paleoclimatic analyses and uranium-series ages for samples collected elsewhere on the Q_2 terrace (Table 2) indicate that this terrace is ~120 ka.

4. An uplift rate based on a correlation of the Q_2 terrace with the ~105 ka high sea stand is anomalously high relative to rates calculated from other terraces in the sequence.

Coral collected from the Q_2 terrace at Mallagh Landing (sample SLO-6) yielded an anomalous age of 99 $\pm$ 2, suggesting a correlation to the ~105 ka high stand. The uranium-ratios for this sample indicate no signs of secondary contamination or other open-systems effects. However, the faunal assemblage analysis and amino acid racemization results for fossils collected at the nearby 520P locality on the same terrace suggest that the terrace is ~120 ka (correlative to marine oxygen isotope substage 5e) and that the 99 $\pm$ 2 age is too young.

Six uranium-series ages have been obtained for samples of marine and terrestrial mammal teeth and bones collected from deposits overlying the lowest marine platform (Q_1). These ages, which range from approximately 49 to 82 ka (Table 2) are considered to be minimum values. However, because the maximum numerical ages are around 80 ka, a correlation to the ~80 ka high sea

stand seems more plausible than a correlation to the 105 ka high sea stand. This interpretation is consistent with evidence from other areas along the California coast (Lajoie and others, 1979; Muhs and others, 1988) that indicate that the ~105 ka terrace is rarely preserved and that a couplet of low, well preserved, broad terraces generally correlate to the ~80 ka and ~120 ka high stands. The studies on San Nicolas Island (Muhs and others, 1987) and at Punta Banda (Rockwell and others, 1987) suggest that the ~105 ka high stand was of relatively short duration and that platform cutting and sea cliff retreat at ~80 ka removed the ~105 ka terrace in most areas before uplift could result in terrace emergence and preservation.

Near Mallagh Landing, two samples (SLO-4 and SLO-5) of coral from the Q_1 terrace gave ages of 96 ± 2 and 93 ± 2 ka. The $^{234}U/^{238}U$ ratio for these samples, however, suggests that the samples probably assimilated secondary uranium and therefore, these ages are considered unreliable (Muhs, personal comm., 1990).

A vertical succession of all three (~80, ~105, ~120 ka) terraces has not been clearly demonstrated in the study area. In the area between Crowbar Canyon and Point Buchon, a possible intermediate terrace between terraces Q_1 and Q_2 is represented by a small stripped bedrock bench (Q_{1a}?) at an elevation of 23 ± 2 m. Because of the lack of associated marine deposits, the very limited extent of this terrace, and a possible relationship to a landslide, it is uncertain if this bedrock bench is a terrace representing a separate high stand. If this is a marine terrace, it could correlate in stratigraphic succession to the ~105 ka high stand.

There are no uranium-series ages or faunal assemblage data available for independent age determination of the higher terraces. However, the ages of the lower two terraces (~80 ka and ~120 ka) do provide local calibration of the terrace sequence for correlation with the paleo–sea-level curves. For terraces younger than or equal to approximately 330,000 years, we estimated terrace ages by correlating shoreline angle elevation and terrace spacing to the paleo–sea-level data summarized in Table 1.

The ages of older terraces, which are laterally discontinuous, are less well constrained due to uncertainties in lateral correlations and height of paleo-sea level during their formation. In some areas, alternative interpretations of terrace correlations (see following discussion) yield different ages for the higher terrace remnants. Due to the problems of correlation, the ages of terraces older than about 330,000 years as indicated on the longitudinal profiles (Plate 4) are assumed to be accurate to within only one major glacio-eustatic cycle (approximately ± 100,000 years).

Correlation of Marine Terraces and Estimated Uplift Rates

A longitudinal profile showing our preferred interpretation (Model A) of the ages and correlations of marine terraces in the San Luis Obispo study area is presented on Plate 4. Due to uncertainties in the ages and correlations

of higher terraces across several of the faults along the southwestern margin of San Luis Range, we have provided an alternative interpretation (Model B) for the region between Green Peak and Mallagh Landing. In the following sections we discuss the evidence favoring the various alternatives and the estimated long-term uplift rates based on these interpretations.

Montaña de Oro State Park - The higher terraces throughout the coastal region from Morro Bay to Point Buchon are interpreted to be essentially flat lying. This interpretation is supported by the apparent lateral continuity and geomorphic expression of the Q_7 terrace throughout this area. Remnants of this terrace, which generally occur at elevations of approximately 110 $\pm$ 3 m are better preserved and broader than any other higher terrace remnants, and they are overlain by similar terrace deposits. An inferred uplift-rate graph based on this interpretation gives a long-term average uplift rate of approximately 0.24 m/ka for the Montaña de Oro area between Islay Creek and Hazard Canyon.

Point Buchon to Green Peak - The ages and correlations of marine terraces in the area between Point Buchon and the Olson fault near Green Peak yield a long-term average rates of uplift ranging from 0.19 $\pm$ 0.03 to 0.20 $\pm$ 0.02 m/ka.

Green Peak to San Luis Obispo Creek - Evaluating the ages and correlations of higher terraces in the coastal region between Green Peak and San Luis Obispo Creek is complicated by deformation associated with the San Luis Bay fault and possibly the postulated Olson fault. The lower two terraces (Q_1 and Q_2) are disrupted by both the Olson and San Luis Bay faults.

The sequence of higher terraces appears to be disrupted across the San Luis Bay fault between San Luis Hill and the Irish Hills. On the southwest side of the fault the elevation of the Q_2 terrace, which encircles much of the coastal portion of San Luis Hill, indicates that the rate of uplift during the past 120,000 years has been approximately 0.06 $\pm$ 0.03 mm/yr. Ages for the highest surfaces on San Luis Hill based on this uplift are in excess of 3 million years. It is more likely, given the distribution and elevation of the Squire Member of the Pismo Formation, which is estimated to be 2.8 to 3.0 Ma, in the vicinity of San Luis Hill, that these higher surfaces are younger and that there has been a change from a higher to a lower rate of uplift of San Luis Hill since their formation. This change in uplift rate may indicate that activity on the San Luis Bay fault was initiated in the mid- to late Pleistocene. The lack of terraces of intermediate height and age between the 120 ka terrace and these higher stripped remnants makes it difficult to evaluate this hypothesis or to assign ages to the older terrace remnants on San Luis Hill.

The correlation and ages of the higher marine terraces in the vicinity of the Olson fault is also problematic. The highly eroded, stripped and discontinuous nature of these terrace remnants allows for the possibility that the fault extends inland from the zone of apparent deformation of the lowest terraces at the coast,

but does not clearly define the location of the fault. One possible interpretation is that the Olson fault extends inland towards the San Miguelito fault and disrupts the entire flight of older terraces as indicated in Model B (Plate 4). A more likely scenario is that the Olson fault is located at the base of the range front near the shoreline angle of the Q_2 terrace, and there is no brittle deformation of the higher marine terraces across this fault as indicated in Model A (Plate 4). The latter model is consistent with the interpreted deformation of the San Luis/Pismo structural block in which a northeast-trending monoclinal flexure centered approximately along the San Luis Obispo Creek occurs between the Irish Hills subblock, rising at about 0.18 to 0.24 m/ka, and the Edna subblock, rising at about 0.13 m/ka.

Models A and B imply different ages for the older terrace remnants in the Irish Hills between the Olson fault and San Luis Obispo Creek. In Model A the higher terraces are laterally correlated with the terrace sequence along the coast between Point Buchon and Green Peak implying an uplift rate of approximately 0.20 ± 0.02 m/ka. The uplift rate at the coast based on the elevation of the Q_2 terrace is affected by deformation along the Olson and San Luis Bay faults and is significantly lower, ranging from 0.14 to 0.09 m/ka. These rates reflect brittle deformation on the two faults as well as associated downwarping in the hanging wall of the San Luis Bay fault.

In Model B, it is assumed that the Olson fault extends inland and disrupts the entire terrace sequence. The ages of the older terraces in the Irish Hills south of the Olson fault are based primarily on lateral correlation to the more complete sequence of terraces in the Pismo Beach area. In this interpretation the long-term uplift rate decreases from approximately 0.18 to 0.20 m/ka on the upthrown side of the Olson fault to 0.14 m/ka in the region between the faults, to as low as 0.09 m/ka adjacent to the San Luis Bay fault near Rattlesnake Creek where fault-related warping has occurred.

<u>San Luis Obispo to Arroyo Grande</u> - Correlation of the lower five terraces between Wild Cherry Canyon and Pismo Beach is interpreted to be the same in both Models A and B. The elevations of these terraces do not vary across either the San Miguelito or Pismo faults, indicating that these faults have not been active since before middle to late Pleistocene time.

Higher terrace remnants on both sides of the San Miguelito fault also occur at similar elevations. The interpreted ages of these higher terrace remnants do vary between the two models. In Model A (Plate 4), the highest terraces correlate with the terraces at similar elevations along the coast to the northwest suggesting long-term uplift rates of about 0.20 ± 0.02 m/ka. Terraces of comparable age occur at much lower elevations in the Pismo Beach area where the long-term rate of uplift is estimated to be approximately 0.13 m/ka. This decrease in uplift occurs at the approximate boundary between topographic subblocks of the range and may indicate a structural boundary, monoclinal flexure, or change in fault dip along block bounding faults

in the general vicinity of San Luis Obispo Creek.

Alternatively, as shown in Model B, long-term uplift of the region on the downthrown side of the Olson fault is 0.14 ± 0.02 m/ka. In this model there is a regional south-to-southeast-directed tilt exhibited by the older terraces between the Olson fault and Mallagh Landing, but no abrupt steps or flexures.

In both Models A and B the uplift rates indicated by the elevations of the younger terraces in the sequence (Q_1 to Q_5) suggest lower rates (0.12 ± 0.02 m/ka) in the coastal region between Wild Cherry Canyon and Mallagh Landing. This decrease is likely related to deformation in the hanging wall of the San Luis Bay fault.

As stated previously, a relatively complete set of terraces is preserved in the Pismo Beach to Arroyo Grande region. Inferred uplift-rate and predicted uplift data for this terrace sequence indicate that the rate of uplift in this region throughout at least the past 500,000 to as long as 700,000 years has been approximately 0.13 ± 0.02 m/ka. The high degree of correlation indicated by the inferred uplift-rate graph (Plate 4) suggests that the inferred ages of these terraces are reasonable.

Arroyo Grande to Nipomo Valley - Correlation and dating of marine terraces south of Arroyo Grande Creek is complicated by the extensive eolian cover that buries most of the younger terraces in the sequence and by possible deformation related to the Wilmar Avenue fault. Two extensive and laterally continuous terraces at elevations of approximately 110 m ± 7 m and 85 m ± 7 m are present in the region between Arroyo Grande Creek and the southern end of the Nipomo Valley. Correlation of these terraces to the terrace sequence in the Pismo Beach area provides the only means of estimating their ages and the long-term uplift rate for the region. Geomorphically the two terraces are similar to terraces Q_7 and Q_9 in the Pismo Beach area. Correlation of these terraces (Model A) requires a zone of cross-structural monoclinal flexure in the vicinity of Arroyo Grande Creek between the Edna and Newsom Ridge subblocks of the San Luis/Pismo structural block. The northward tilt of the terrace sequence between Arroyo Grande Creek and Los Berros Creek is compatible with this hypothesis. According to this model the rate of long-term uplift increases from approximately 0.13 m/ka in Pismo Beach to 0.14 m/ka south of Arroyo Grande Creek to 0.15 m/ka in the vicinity of Los Berros Creek and throughout the Nipomo Valley. The higher rate of uplift in the region south of Arroyo Grande Creek also is consistent with relative differences in the general elevation of the range (see Lettis and others, this volume [a]).

ESTIMATED SEA LEVEL AT ~80 ka

Given the available elevation and age control for the lowest two emergent terraces along the coast between Morro Bay and Pismo Beach, we can estimate the paleo-sea level during the 80 ka high stand. Assuming a +6 m sea level at

120 ka and a constant rate of uplift, the elevations of the Q_1 (80 ka) and Q_2 (120 ka) terraces in this area suggest that the sea level during the ~80 ka high stand was -4 ± 1 m (relative to the present sea level). This value is considerably closer to modern sea level than estimates for equivalent terraces in New Guinea (-19 ± 5 m, Chappel and Shackleton, 1986), Bermuda (-20 to - 15 m; Harmon and others, 1981) and Barbados (-15 ± 3 m; Matthews, 1973). Our estimate, however, is in general agreement with a revised estimate of -7 m for the ~80 ka terrace on New Guinea (Bloom and Yonekura, 1985), with estimates of -5 ± 2 m (Muhs and others, 1988) for the elevation of the ~80 ka high stand in other coastal California and Baja California, Mexico locations, and with recent studies in Bermuda (Vacher and Hearty, 1989), the Mediterranean area (Hearty and others, 1986), and the Atlantic Coastal Plain (Szabo, 1985) that also indicate sea level was higher, in some cases close to the present level, during the 80 ka high stand.

CONCLUSIONS

Detailed mapping of marine terraces in the San Simeon and San Luis Obispo study areas provides new data for assessing the locations, style, and rates of Quaternary deformation in the region. In the San Simeon study area, sequences of four and five terraces have been mapped to the northeast and southwest, respectively, of the southern onshore reach of the San Simeon fault zone. From youngest to oldest, they are the San Simeon Point (Q_1), San Simeon (Q_2), Tripod (Q_3), Oso (Q_4), and La Cruz (Q_5) terraces. They are interpreted to correlate with marine oxygen-isotope stages 3 or 5a (60 or 80 ka), 5a or 5c (80 or 105 ka), 5e (120 ka), 7 (210 ka), and 9 (330 ka). Estimated ages and correlation of terraces across the San Simeon fault zone are based on lateral correlation of the Tripod terrace to the well-dated 120 ka Cayucos terrace, comparison of relative soil profile development, and comparison of geomorphic expression and terrace altitudinal spacing. Comparison of the relative altitudinal spacing of terraces in the San Simeon area to paleo-sea-level data established in other areas indicates uplift rates of 0.17 ± 0.02 m/ka southwest, and 0.16 ± 0.01 m/ka northeast of the fault and approximately 0.24 m/ka for uplifted and warped areas within and adjacent to the fault zone. A discussion of estimated horizontal and vertical displacements of the terrace strandlines used to evaluate the style of deformation and to estimate a Pleistocene slip rate for the San Simeon fault zone is provided in a companion paper by Hanson and Lettis (this volume).

In the coastal region between Morro Bay and the northeastern margin of the Santa Maria Valley (San Luis Obispo study area), a sequence of at least twelve elevated marine terraces is locally present. The lowest two terraces in this sequence (Q_1 and Q_2) are correlated to marine oxygen isotope substages 5a (~80 ka) and 5e (~120 ka), respectively, based on uranium-series ages on coral and vertebrate bone samples, amino acid racemization analyses, paleoclimatic analyses of invertebrate faunal assemblages, and on comparison of

geomorphic and terrace altitudinal spacing to other dated terrace sequences. Based on interpreted ages and terrace spacing between the lowest two emergent terraces along the coast from Morro Bay to Pismo Beach, we estimate paleo-sea level during the 80 ka high stand was -4 ± 1 m (relative to the present level). This value is considerably closer to modern sea level than estimates for equivalent terraces in New Guinea, Barbados, and Haiti (Chappell and Shackleton, 1986; Matthews, 1973; Dodge and others, 1983), but is in good agreement with a revised estimate in New Guinea (Bloom and Yonekura, 1985) and recent studies along the coast of southern California and Baja California, Mexico (Muhs and others, 1988; Muhs, in press).

Dating of the lowest two terraces in the Morro Bay to Pismo Beach region provides local calibration for correlation of the higher terraces in the sequence with the paleo–sea-level curves developed from data worldwide. For terraces equal to or younger than about 330 ka, we have estimated terrace ages by correlating shoreline angle elevations and terrace spacing using two different graphical techniques (inferred uplift-rate graphs and predicted uplift graphs). The ages of older terraces in the San Luis Obispo study area are less well constrained due to uncertainties in lateral correlations and elevations of paleo-sea level during their formation. Alternative interpretations (Plate 4) of terrace correlations in some areas yield different ages and, therefore, different long term uplift rates. The implications of the differing estimates for assessing regional patterns of Pleistocene uplift and deformation within and adjacent to the San Luis/Pismo structural block are discussed in Lettis and others (this volume [b]).

The spatial and temporal distributions of marine terraces along the south-central coast have been used to: (1) delineate a series of elongate, west-northwest-trending structural blocks (Weber and others, 1987; Hanson and others, 1989); (2) assess the deformational history within and bordering these blocks (Kelson and others, 1987; Mezger and others, 1987; Lettis and others, this volume [b]); and (3) assess Pleistocene slip rates for individual faults (Hanson and Lettis, this volume; Lettis and others, this volume [b]; Lettis and Hall, this volume).

The south-central coastal region is similar to most areas of the Pacific coast of the United States, where the lowest elevation terraces at most localities record the sea level high stands of the last interglacial. Late Pleistocene uplift rates within this region, which are based on the present elevation of the ~120 ka marine terrace (Fig. 8), range from 0.06 to 0.24 m/ka for the uplifting structural blocks to ≤ 0 m/ka for the intervening subsiding regions. These rates are comparable to uplift rates for other fault bounded structural blocks within regions dominated by right lateral crustal displacements in coastal California that are on the order of 0.1 to 0.3 m/ka (Lajoie and others, 1979; Ku and Kern, 1974; Muhs and Szabo, 1982; Muhs, 1987). These rates are less by a factor of 3 or more than uplift rates in the

Santa Cruz coastal region adjacent to the restraining bend along the San Andreas fault which ruptured during the oblique-right-lateral 1989 Loma Prieta earthquake (Anderson, 1990). These rates are considerably less than maximum uplift rates of 3 to 5 m/ka, which are reported for the coastal region directly south of the Mendicino Triple Junction (Merrits and Bull, 1989) and 5 to 7 m/ka for the region of intense crustal shortening in the Transverse Ranges (including Ventura) (Lajoie and others, 1982; Sarna-Wojcicki and others, 1987), respectively.

ACKNOWLEDGMENTS

This research was supported by Pacific Gas and Electric Company as part of the Long Term Seismic Program for the Diablo Canyon Power Plant. The research has benefitted substantially from discussion and suggestions provided by Gerald Weber, who introduced us to marine terraces in the San Simeon area, and Thomas Rockwell (University of California, San Diego), who conducted the soils chronosequence studies in the San Simeon area and assisted in various other dating analyses. Thanks are also due to Daniel R. Muhs (U.S. Geological Survey), George L. Kennedy (Los Angeles County Museum of Natural History), T.L. Ku (University of California, San Diego), J.F. Wehmiller (University of Delaware) and Glenn Berger (University of Western Washington) for their helpful discussions and their dating results. We are grateful to Daniel R. Muhs (U.S. Geological Survey) and A.L. Bloom (Cornell University) for their constructive reviews of our manuscript. We also wish to thank the numerous owners who graciously allowed us access to their properties. In particular, we wish to thank Harlan Brown, the manager of the Hearst Ranch in the San Simeon area, Frank Mello, manager of the Marré Property south of Diablo Canyon, and various members of the Williams and Wineman families in the Nipomo area.

REFERENCES

Anderson, R.S., 1990, Evolution of the northern Santa Cruz Mountains by advection of crust past a San Andreas Fault bend: Science, v. 249, p. 397-401.

Bender, M.L., Fairbanks, R.G., Taylor, F.W., Matthews, R.K., Goddard, J.G., and Broecker, W.S., 1979, Uranium-series dating of the Pleistocene reef tracts of Barbados, West Indies: Geological Society of America Bulletin, Part I, v. 90, p. 577-594.

Berger, G., 1988, Dating of Quaternary events by luminescence, in Easterbrook, D.V., *ed.*, Quaternary sediments: Geological Society of America Special Paper 227, p. 13-50.

Bloom A.L., Broecker, W.S., Chappell, J.M.A., Matthews, R.K., and Mesolella, K.J., 1974, Quaternary sea level fluctuations on a tectonic coast: New $^{230}Th/^{234}U$ dates from the Huon Peninsula, New Guinea: Quaternary Research, v. 4, p. 185-205.

Bloom A.L., and Yonekura, N., 1985, Coastal terraces generated by sea-level change and tectonic uplift: in Waldenberg, M.J, *ed.*, Models in Geomorphology, Allen and Unwin, p. 139-154.

Bradley, W.C., and Griggs, G.B., 1976, Form, genesis, and deformation of central California wave-cut platforms: Geological Society of America Bulletin, v. 87, p. 433-449.

Broecker, W.S., Thurber, D.L., Goddard, J., Ku, T.-L., Matthews, R.K., and Mesolella, K.J., 1968, Milankovitch hypothesis supported by precise dating of coral reefs and deep-sea sediments: Science, v. 159, p. 297-300.

Bull, W.B., 1985, Correlation of flights of global marine terraces: in Morisawa, M., and Hack, J., *eds.*, Tectonic Geomorphology, Proceedings of the 15th Annual Binghamton Geomorphology Symposium, Allen and Unwin, p. 129-152.

Cleveland, G.B., 1978, Geologic map of the Pt. Buchon area, San Luis Obispo County, California, with Summary comments: California Division of Mines and Geology Open-File Report 78-17 LA, 6 p.

Chappell, J., 1983, A revised sea-level record for the last 300,000 years from Papua, New Guinea: Search, v. 14, no. 3-4, p. 99-101.

Chappell, J., 1987, Late Quaternary sea-level changes in the Australian region: in Tooley, M.J., and Shennan, I., *eds.*, Sea-level changes: Institute of British Geographers Special Publication Series, v. 20, p. 296-331.

Chappell, J., and Shackleton, N.J., 1986, Oxygen isotopes and sea level, Nature, v. 324, p. 137-140.

Chappell, J, and Veeh, H.H, 1978, Late Quaternary tectonic movements and sea-level changes of Timor and Atauro Island: Geological Society of America Bulletin, v. 89, p. 356-368.

Cronin, T.M., Szabo, B.J., Ager, T.A., Hazel, J.E., and Owens, J.P., 1981, Quaternary climates and sea levels of the U.S. Atlantic coastal plain: Science, v. 211, p. 232-239.

Curray, J.R., 1965, Late Quaternary history, continental shelves of the United States: in Wright, H.E., and Frey, D.G., (eds.), The Quaternary of the United States, Princeton University Press, Princeton, New Jersey, p. 723-735.

Edwards, R.L., Chen, J.H., Ku, T.-L., and Wasserburg, G.J., 1987, Precise timing of the last interglacial period from mass spectrometric determination of Thorium-230 in corals: Science, v. 236, p. 1547-1553.

Envicom, 1977, Fault investigation, Hearst Ranch environmental data base: unpublished report for the Hearst Corporation.

Fairbanks, H.W., 1904, Description of the San Luis quadrangle: Geologic Atlas of the United States, San Luis Folio, California, no. 101, U.S. Geological Survey.

Hall, C.A., Jr., 1975, San Simeon-Hosgri fault system, coastal California: econonmic and environmental implications: Science, V. 190, no. 1221, p. 1291-1294.

Hall, C.A., Jr., Ernest W.G., Prior S.W., and Wiese S. W., 1979, Geologic map of the San Luis Obispo-San Simeon Region, California: U.S. Geological Survey Miscellaneous Investigations Series, Map I-1097, Scale 1:48,000.

Hamilton, D.H., 1984, The tectonic boundary of coastal central California: unpublished Ph.D. thesis, Stanford University, California, 290 p.

Hanks, T.C., Bucknam, R.C., Lajoie, K.R., and Wallace, R.E., 1984, Modification of wave-cut and faulting-controlled landforms: Journal of Geophysical Research, v. 89, p. 5771-5790.

Harden, J.W., 1982, A quantitative index of soil development from field descriptions — examples from a chronosequence in central California: Geoderma, v. 28, no. 1, p. 1-28.

Harmon, R.S., Ku T-L., Matthews, R.K., and Smart, P.L., 1979, Limits of U-series analysis: Phase 1 results of the uranium-series intercomparison project: Geology, v. 7, p. 405-409.

Harmon, R.S., Schwarcz, H.P., and Ford, D.C., 1978, Late Pleistocene sea level history of Bermuda: Quaternary Research, v. 9, p. 205-218.

Harmon, R.S., Land, L.S., Mitterer, R.M., Garrett, P., Schwarcz, H.P., and Larson, G.J., 1981, Bermuda sea level during the last interglacial: Nature, v. 289, p. 481-483.

Inman, D.L., and Nordstrom, C.E., 1971, On the tectonic and morphologic classification of coasts: Jour. Geol., v. 79, no. 1, p. 1-21.

James, N.P., Mountjoy, E.W., and Omura, A., 1971, An early Wisconsin reef terrace at Barbados, West Indies and its climatic implications: Geological Society of America Bulletin, v. 82, p. 2011-2018.

Kennedy, G.L., Wehmiller, J.F., and Muhs, D.R., 1988, Late Pleistocene climatic change: evidence from coastal San Luis Obispo County, central California: American Quaternary Association Program and Abstracts, p. 126.

Ku, T.-L., and Kern, J.P., 1974, Uranium-series age of the upper Pleistocene Nestor terrace, San Diego, California: Geological Society of America Bulletin, v. 85, p. 1713-1716.

Ku, T.-L., Ivanovich, M. and Luo, S., 1990, U-series dating of last interglacial high sea stands: Barbados revisited: Quaternary Research, v. 33, p. 129-147.

Ku, T.-L., Kimmel, M.A., Eastan, W.H., and O'Neil, T.J., 1974, Eustatic sea-level 120,000 years ago on Oahu, Hawaii: Science, p. 959-962.

Labeyrie, J., Lalon, C., Monaco, A., and Thommeret, J., 1976, Chronologie des niveaux eustatiques sur la cote du Roussillon de - 33000 ans BP a nos jours: Acad. Sci. Paris, D., v. 282, p. 349-352.

Lajoie, K.R., 1986, Coastal tectonics: in Wallace, R.E., *ed.*, Active Tectonics, National Academy Press, Washington, D.C., p. 95-124.

Lajoie, K.R., Weber, G.E., Mathieson, S.A., and Wallace, J., 1979, Quaternary tectonics of coastal Santa Cruz and San Mateo Counties, California, as indicated by deformed marine terraces and alluvial deposits: in Weber, G.E., Lajoie, K.R., and Griggs, G.B., *eds.*, Coastal Tectonics and Coastal Geologic Hazards in Santa Cruz and San Mateo Counties, California, Geological Society of America Guidebook.

Lajoie, K.R., Sarna-Wojcicki, A.M., and Ota, Y., 1982, Emergent Holocene marine terraces at Ventura and Cape Mendocino, California — indicators of high tectonic uplift rates (abs.): Geological Society of America, Abstract with Programs, 78th Annual Meeting, Cordilleran Section, p. 178.

Marshall, J.F., and Thom, B.G., 1976, The sea level in the last interglacial: Nature, v. 263, p. 120-121.

Martinson, D.G., Pisias, N.G., Hays, J.D., Imbrie, J., Moore, T.C., and Shackleton, N.J., 1987, Age dating and the orbital theory of the Ice Ages: development of a high resolution 0-300,000 year chronostratigraphy: Quaternary Research, v. 27, p. 1-29.

Matthews, R.K., 1973, Relative elevation of late Pleistocene high sea level stands: Barbados uplift rates and their implications: Quaternary Research, v. 3, p. 147-153.

Merrits, D. and Bull, W.B., 1989, Interpretating Quaternary uplift rates at the Mendicino triple junction, northern California, from uplifted marine terraces: Geology, v. 17, p. 1020-1024.

Mesolella, K.J., Matthews, R.K., Broecker, W.S., and Thurber, D.L., 1969, The astronomical theory of climatic change: Barbados data: Journal of Geology, v. 77, p. 250-274.

Muhs, D., (in press), The last interglacial/glacial transition in North America: Evidence from uranium-series dating of coastal deposits: in Clark, P. and Lea, P. (eds.), The Last Interglaciation/Glaciation Transition in North America, Geological Society of America Special Paper, in press for 1991.

Muhs, D.R., Kennedy, G.L., and Miller, G.H., 1987, New uranium-series ages of marine terraces and late Quaternary sea level history, San Nicolas Island, California: Geological Society of America, abstract with Programs, v. 19, no. 7, p. 780-781.

Muhs, D.R., Kennedy, G.L., and Rockwell, T., 1988, Uranium-series ages of corals from marine terraces, Pacific Coast of North America: implications for the timing and magnitude of late Pleistocene sea-level changes: American Quaternary Association, Program and Abstracts, p. 140.

Muhs, D.R., and Szabo, B.J., 1982, Uranium-series age of the Eel Point terrace, San Clemente Island, California: Geology, v. 10, p. 23-26.

Neumann, A.C., and Moore, W.S., 1975, Sea level events and Pleistocene coral ages in the northern Bahamas: Quaternary Research, v. 5, p. 215-224.

Pacific Gas and Electric Company, 1973, Section 2.5, Geology and Seismology, Final Safety Analysis Report, Units 1 and 2, Diablo Canyon Site: U.S. Atomic Energy Commission Docket Nos. 50-275 and 50-323.

Pacific Gas and Electric Company, 1974, Geology of the southern Coast Ranges and the adjoining offshore continental margin of California, with special reference to the geology in the vicinity of the San Luis Range and Estero Bay: Appendix 2.5D, FSAR, Diablo Canyon Nuclear Power Plant, AEC Docket Nos. 50-275 and 50-323.

Pacific Gas and Electric Company, 1975, Appendix 2.5E, Final Safety Analysis Report for Diablo Canyon Nuclear Power Plant: U.S. Atomic Energy Commission Docket Nos. 50-275 and 50-323.

Pillans, B., 1983, Upper Quaternary marine terrace chronology and deformation, south Taranak, New Zealand: Geology, v. 11, p. 292-297.

Rockwell, T.K., Johnson, D.L., Keller, E.A., and Dembroff, G.R., 1985, A late Pleistocene-Holocene soil chronosequence in the central Ventura Basin, Southern California, U.S.A.: in K. Richards, R. Arnett, and S. Ellis (eds.), Geomorphology and Soils, George Allen and Unwin, p. 309-327.

Rockwell, T.K., 1983, Soil chronology, geology, and neotectonics of the north-central Ventura Basin, California [unpublished Ph.D. dissertation]: Santa Barbara, California, University of California, 424 p.

Rockwell, T.K., Hatch, M.E., and Schug, D.L., 1987, Late Quaternary rates: Agua Blanca and borderland faults: U.S. Geological Survey Final Technical Report for Contract No. 14-08-0001-22012, 122 p.

Sarna-Wojcicki, A.M., Lajoie, K.R. and Yerkes, R.F., 1987, Recurrent Holocene displacement on the Gavon Canyon fault--a comparison of fault movement history with calculated average recurrence intervals: U.S. Geological Survey Professional Paper 1339, p. 125-135.

Schubert, C., and Szabo, B.J., 1978, Uranium-series ages of Pleistocene marine deposits on the islands of Curacao and La Blanquilla, Caribbean Sea: in MacGillavry, H.J., and Beets, D.J., *eds.*, Caribbean Geologic Conference Proceedings, Geologie en Mijmbouw, v. 57, p. 325-332.

Shackleton, N.J., 1987, Oxygen isotopes, ice volume, and sea level: Quaternary Science Review, v. 6, p. 183-190.

Shackleton, N.J., and Opdyke, N.D., 1973, Oxygen isotope and paleomagnetic stratigraphy of equatorial Pacific core V28-238: Oxygen isotope temperatures and ice volumes on a 10^5 year and 10^6 year scale: Quaternary Research, v. 3, p. 39-55.

Silvester, R., 1960, Stablization of sedimentary coastlines: Nature, v. 188, p. 467-469.

Silvester, R., 1970, Development of crenulate shaped bays to equilibrium: Proceedings American Society of Civil Engineers 96 (WW2), p. 275-287.

Silvester, R., 1976, Headland defense of coasts: in American Society of Civil Engineers, Proceedings 15th Coastal Engineering Conference, Chapter 82, p. 1394-1406.

Silvester, R., and Ho., S.K., 1972, Use of crenulate shaped bays to stablize coasts: in American Society of Civil Engineers, Proceedings 13th Coastal Engineering Conference, Chapter 74, p. 1347-1365.

Soil Survey Staff, 1975, Soil taxonomy – a basic system of soil classification for making and interpreting soil surveys: Washington, D.C., U.S. Department of Agriculture Handbook 436, 754 p.

Stearns, C.E., 1984, Uranium-series dating and the history of sea level: in W.C. Mahaney (ed.), Quaternary Dating Methods, Elsevier, New York, p. 53-66.

Stein, M., Chen, J.H., Wasserburg, G.J. and Lajoie, K.R., 1989, Mass spectrometric determination of ^{234}U-^{230}Th Ages in solitary corals from the California coast (abs.): EOS Transaction, American Geophysical Union, v. 70, no. 43, p. 1148.

Szabo, B.J., 1979, Uranium-series age of coral reef growth on Rottuest Island, western Australia: Marine Geology, v. 29, p. M11-M15.

Szabo, B.J., Ward, W.C., Weidie, A.E., and Brady, M.J., 1978, Age and magnitude of the late Pleistocene sea-level rise on the eastern Yucatan Peninsula: Geology, v. 6, no. 12, p. 713-715.

Thomson, J., and Walton, A., 1972, Redetermination of chronology of Aldabra Atoll by $^{230}Th/^{234}U$ dating: Nature, v. 240, p. 145-146.

Thurber, D.L., Broecker, W.S., Blanchard, W.S., and Protratz, H.A., 1965, Uranium-series ages of Pacific atoll coral: Science, v. 149, p. 55-58.

Veeh, H.H., 1966, $^{230}TH/^{238}U$ and $^{234}U/^{238}U$ ages of Pleistocene high sea-level stand: Journal of Geophysical Research, v. 71, no. 14, p. 3379-3386.

Veeh, H.H., and Chappell, J., 1970, Astronomical theory of climatic change: Support from New Guinea: Science, v. 167, p. 862-865.

Veeh, H.H., and Valentine, J .W., 1967, Radiometric ages of Pleistocene fossils from Cayucos, California: Geological Society of America Bulletin, v. 78, p. 547-550.

Ward, W.T., 1985, Correlation of east Australian Pleistocene shorelines with deep-sea core stages: a basis for a coastal chronology: Geological Society of America Bulletin, v. 96, p. 1156-1166.

Weber, G.E., 1983, Geologic investigation of the marine terraces of the San Simeon region and Pleistocene activity of the San Simeon fault zone, San Luis Obispo County, California: U.S. Geological Survey Technical Report 66.

Yasso, W.E., 1965, Plan geometry of headland-bay beaches: Journal of Geology, v. 73, p. 702-714.

TABLE 1. ESTIMATED ~~MATERIALS~~ AGES AND ELEVATIONS OF PALEOSEA-LEVELS DURING THE PAST 700,000 YEARS

Shackleton and Opdyke (1973)		Merritts and Bull (1989)[10]		Chappell, (1983); Chappell and Shackleton (1986) (New Guinea)		Bloom and Yonekura (1985) (New Guinea)		Bender and others (1979) (Barbados)		Muhs and others (1987, 1988) (Califonria)		Ages and Paleo-Sea Level Estimates Used for This Study	
Stage[1]	Estimated Age[2] (ka)	Age (ka)	Paleo-sea Level[4] (m)	Age (ka)	Paleo-sea Level[4] (m)	Age[3] (ka)	Paleo-sea Level[4,8] (m)	Age (ka)	Paleo-sea Level[4] (m)	Age (ka)	Paleo-sea Level[4] (m)	Age[6] (ka)	Paleo-sea Level[4] (m)
1	0 - 13	6	0	6	0	6	-4						
2	13 -22	29	-44	17 28	-130 -44 ± 2	28	-35					18 to 20	-120 to -160[7]
3	32 -64	40 45 53 59	-41 -45 -30 -28	40 45 59	-41 ± 4 -46 -28 ± 3	40 50-40 60	-38 -46 -24					~60	-24
4	64 - 75	72	-36	72	-36								
5 5a 5c 5e	75 - 128	81 96 100 118 124	-19 -26 -9 0 6	81 96 106 124	-19 ± 5 -24 -9 ± 3 +6	82 105 124	-7 0 +6	82[3] 105[3] 125[3]	-16 -16 to -19 +6	80 105 120	-5 ± 2 -2 ± 2 +6	~80 ~105 ~125	-5 ± 2 -2 ± 2 +6 ± 2
6	128 - 195	172	-50	135	-130								
7	195 - 251	200 212 240	-7 -7 -10					108 200 220	0 0 +2			~210	-3 ± 4
8	251 - 297	286 305	-46 -27					286 305	-46 -27				
9	297 - 347	330	+4					280 300 320	+30[9] -30			~330	+4 ± 4
10	347 - 367												

TABLE 1. (continued)

Shackleton and Opdyke (1973)		Merritts and Bull (1989)[10]		Chappell, 1983; Chappell and Shackleton (1986) (New Guinea)		Bloom and Yonekura (1985) (New Guinea)		Bender and others (1979) (Barbados)		Muhs and others (1987, 1988) (Califonria)		Ages and Paleo-Sea Level Estimates Used for This Study	
Stage[1]	Estimated Age[2] (ka)	Age (ka)	Paleo-sea Level[4] (m)	Age (ka)	Paleo-sea Level[4] (m)	Age[3] (ka)	Paleo-sea Level[4,8] (m)	Age (ka)	Paleo-sea Level[4] (m)	Age (ka)	Paleo-sea Level[4] (m)	Age[6] (ka)	Paleo-sea Level[4] (m)
11	367 - 440							undated				430	0 ± 10
12	440 - 472												
13	472 - 502							460 490 520	+13 -7 0			480	0
14	502 - 542												
15	542 - 592							590	-7			560	0
16	592 - 627												
17	627 - 647							640	-22			630	0
18	647 - 688												
19	688 - 706											700	0
20	706 - 729												
21	729 - 782											755	0

TABLE 1. (continued)

Notes:

[1]Odd numbered stages represent periods of low northern hemisphere ice volume (eustatic highstands) as recognized by oxygen-isotope rates of marine sediment; even numbered stages represent periods of high northern hemisphere ice volume (eustatic lowstands).

[2]Ages are estimated on the basis of depth in core V28-238 using a uniform sedimentation rate of 1.71×10^{-3} cm per year, calibrated by the presence of Brunhes-Matuyama magnetic epoch boundary, age 700,000 yr. at 1200 cm.

[3] Average ages of Pleistocene reef tracks in Barbados based on uranium-series dates (^{230}Th/U and ^{4}He/U methods) (Mesolella and others, 1969; Bender and others, 1979); recent mass spectrometric determination of ^{230}Th yields ages of ~87 ka, ~112 ka and ~122 to 129 ka (Edwards and others, 1987) for terraces produced during high stands of the last interglacial. Ku and other (1990) give ages of 81 ± 2 ka, 105 ± 1 ka, and 120 ± 2 ka for these terraces based on a redetermination of uranium-series ages.

[4]Paleo-sea-level elevations relative to present mean sea level; paleo sea-level for terraces correlated to marine oxygen isotope Stage 5 are based on data from paleo sea-level curves established for marine terraces elsewhere along the California coast (Muhs and others, 1987; 1988).

[5]Ages are estimated on the basis of depth in core V19-30; the timescale developed for this core is based on sedimentation rates calibrated by radiometric age determinations of marine sediments and coral terraces; this record was refined by orbital procession, obliquity, and eccentricity functions.

[6]Ages for terraces correlated to Stage 5 are based primarily on radiometrically dated terraces elsewhere in California and Baja California, Mexico, (Muhs and others, 1987; 1988) and revised ages presented by Ku and others (1990); ages for Stages 7 and 9 are based on data from New Guinea as presented by Chappell (1983) and tabulated by Bull (Merritts and Bull, 1989) and on high resolution chronostratigraphy based on oxygen-isotope records for the past 300 ka according to Martinson and others (1987).

[7]Based on Curray, 1965; Shackleton and Opdyke, 1973; Broecker, 1978; Chappell and Shackleton, 1986; and Chappell (1987).

[8]Maximum error estimates for paleo-sea-level ranges ± 25 m for 300,000 year-old terraces to ± 50 m for 640,000 year-old terraces.

[9]Bender and others (1979) regard this value as unrealistic.

[10]Tabulated by Bull from Chappell and Shackleton (1986), Chappell (1983), and Chappell (1986, personal communication to Bull).

TABLE 2. SUMMARY OF AGE ESTIMATES FOR FOSSIL SAMPLES BASED ON FAUNAL ASSEMBLAGE, AMINO ACID RACEMIZATION, AND URANIUM-SERIES DATING TECHNIQUES

Study Sample Number	Location (latitude, longitude)	Geomorphic Position (WCP[1] elevation)	Material Dated	Faunal Assemblage[2] (Interpreted Substage)	Amino Acid Racemization[3] (Interpreted Age ka)	U-Series[4] (ka)	Comments
500p	Shell Beach (Shelter Cove) (35° 09' 12"N 120° 39' 49"W)	Q_2 (22 m)	shell hash	NES (5a or 5c)	75 ± 15	N.A.	Composite sample from two closely spaced sites; shell hash 0.5-1 m thick overlying WCP
SLO-4	Mallagh Landing (35° 10' 31"N 120° 43' 15"W)	Q_1 (~4m)	coral from shell hash	ND	ND	96 ± 2	$^{234}U/^{238}U$ ration indicates sample probably assimilated secondary uranium; age is thus considered unreliable
SLO-5	Mallagh Landing (35° 10' 30"N, 120° 43' 10"W)	Q_1 (~ 4m)	coral from shell hash	ND	N.D.	93 ± 2	$^{234}U/^{238}U$ ratio indicates sample probably assimilated secondary uranium; age is thus considered unreliable
503p	Shell Beach (Sunset Palisades) (35° 10' 02"N, 120° 41' 34"W)	Q_1 14 ft (4.3 m)	shell coquina	NES (5a or 5c)	N.D.	N.A.	Shell coquina overlying WCP, 10-15 cm thick, moderately consolidated
520p	Mallagh Landing (35° 10' 31"N, 120° 43' 07"W)	Q_2 (13-15 m)	shell hash	SES? (5e?)	125 ± 5	N.A.	Shell hash 0.5 m thick overlying cobbles on WCP
SLO-6	Mallagh Landing (35° 10' 31"N, 120° 43' 07"W)	Q_2	coral from shell hash	N.D.	N.D.	99 ± 2	Uranium concentration is high; U-series age is not consistent with results for Sample 520p from the same terrace
522p	Pirate's Cove (east of Mallagh Landing) (35° 10' 32"N, 120° 42' 40"W)	Q_2 (13.4 m)	fossiliferous sand	SES (5e)	125 ± 5	N.A.	Fossiliferous sand 0.3 m thick

TABLE 2. (continued)

523p	Pismo Beach (Harbor View Avenue) (35° 08' 44"N, 120° 38' 48"W)	Q_2 (4 m)	fossiliferous sand	SES (5e)	125 ± 5	N.A.	Fossil horizons 0.3-0.6 m thick; collected 2.4 m above WCP on down-thrown side of Wilmar Avenue fault
524p	~0.15 km west of mouth of Pecho Creek (35° 10' 44"N, 120° 47' 36"W)	Q_1 (3 - 3.4 m)	whale rib	N.A.	N.A.	Th 49 ± 1 Pa 51 ± 4	Collected from marine gravel ~ 0.6 m above WCP
525p	Shell Beach (35° 09' 39"N, 120° 40' 35"W)	Q_2 (16.4 - 18 m)	fossil hash	SES (5e)	125 ± 5	N.A.	Fossil hash 1 m thick overlying WCP. Collected from boreholes 110 and 114.
KIK-42	Shell Beach (Shelter Cove) (35° 09' 10"N 120° 39' 36"W)	Q_2 (19 m)	coquina	SES (5e)	125 ± 5	N.A.	Coquina 3.5 m thick overlying WCP; WCP is laterally continuous; USGS fossil locality M7498
KIK-44	Pirate's Cove (east of Mallagh Landing) (35° 10' 10"N, 120° 42' 33"W)	Q_1 (6.1 m)	fossiliferous pebble conglomerate	NES (5a or 5c)	75 ± 15	N.A.	Fossiliferous conglomerate 20 cm thick overlying WCP, at SLA
G86-100	Point San Luis (35° 09' 45"N, 120° 45' 58"W)	Q_2 (12.2 m)	fossil hash	SES (5e)	75 ± 15[5]	N.A.	Amino acid and faunal assemblage results are discordant
W87-10	Point San Luis, (NW side of road) (35° 09' 38"N, 120° 45' 19"W)	Q_2 (13.4 m)	coral from fossiliferous sand	SES (5e)	N.D.	Th 117 ± 3	Collected from 2.6 m thick marine sandy gravel approximately 1.1 to 3.7 m above WCP
W87-61	Irish Canyon (35° 10' 59"N, 120° 48'W)	Q_1 (4.9 m)	horse dentary	N.A.	N.A.	Th 62 ± 2 Pa 66 ± 4	Collected from alluvium 30 cm above WCP
W87-62	Irish Canyon (35° 11' 01"N, 120° 48' 04"W)	Q_1 (4.9 m)	Bison dentary	N.A.	N.A.	Th 51 ± 2 Pa 43 ± 3	Collected from alluvium 10 cm above WCP

TABLE 2. (continued)

W87-89	San Luis Obispo Bay (35° 10' 12"N, 120° 45' 20"W)	Q_2 (at SLA) (12.8 m)	fossiliferous sand	SES (5e)	75 ± 15[5]	N.A.	Amino acid and faunal assemblage results discordant
KH-42-A	San Simeon Point (35° 38' 30"N, 120° 12' 30"W)	San Simeon Point Terrace Q_1 (8.9 m)	mammal bone fragment	N.A.	N.A.	Th 46 ± 2 Pa 49 ± 4	Collected from marine gravel 1.2 m above WCP near SLA
LM-100	~0.6 km northwest of the mouth of Crowbar Canyon Creek (35° 13' 39"N, 120° 52' 24"W)	Q_1 (5.5 m)	large mammal bone fragment	N.A.	N.A.	Th 76 ± 3 Pa 76 ± 4	Collected from marine sand approxi-mately 1.2 m above WCP.
W87-101	Near mouth of Pecho Creek (35° 10' 43"N, 120° 47' 31"W)	Q_1 (4.6 m)	marine mammal tooth	N.A.	N.A.	Th 83 ± 3 Pa 109 +57,-25	Sloth, horse and camel bones collected from same site
W87-103	Approximately 1 km northwest of the mouth of Deer Creek (35° 11' 34"N, 120° 49' 17"W)	Q_1 (7 m)	whale rib	N.A.	N.A.	Th 63 ± 2 Pa 58 ± 3	
W87-135 (SLO-7)	Diablo Canyon Power Plant (35° 12' 22"N, 120° 51' 05"W)	Q_2 (26 m)	coral from fossiliferous sand	SES? (5e?)	N.A.	Th 112 ± 4	Fossiliferous cobbly sand, 25-50 cm thick. Uranium concentration is high
LM-74	~1.6 km northwest of mouth of Crowbar Canyon Creek (35° 14' 02"N, 120° 52' 52"W)	Q_1 (5.8 m)	fossiliferous sand	NES (5a or 5c)	75 ± 15	N.A.	USGS locality M7280 and LACMNH locality 5640

TABLE 2. (continued)

LM-124	Pecho Ranch NE of Lion Rock (35° 13' 09"N, 120° 52'W)	Q_1 (8.5 - 9)	fossiliferous sand	NES (5a or 5c)	N.A.	N.A.	USGS locality M7285 and LACMNH locality 5639
C-5e	Cayucos (35° 26' 51"N, 120° 55' 21"W)	Cayucos Terrace (4 m)	whale rib	N.A.	N.A.	Th 124 ± 4 Pa 108 +21,-14	Sample from basal marine deposits directly overlying WCP of first emergent terrace
LACMNH #10731	Cayucos (35° 26' 58"N 120° 54' 48"W)	Cayucos Terrace (4 m)	coral from shell hash	SES (5e)	125 ± 5	Th 117 ± 3	Sample collected by G. Kennedy
M5922	Cayucos	Cayucos Terrace	shells	SES (5e)	N.A.	N.A.	Sample from LACMNH collection

[1]WCP - wave-cut platform
SLA - shoreline angle
[2]Faunal determinations by G.L. Kennedy, Los Angeles County Museum of Natural History, written communication, 1986-1987
NES - northern extralimital species present
SES - southern extralimital species present
[3]Amino acid racemization analyses and interpreted ages of shell samples are from J.F. Wehmiller, Department of Geology, University of Delaware (written communication, 1987)
[4]U-Series ages of coral are from D.R. Muhs, U.S. Geological Survey (written communiction, 1989; personal communication, 1990). U-series ags of bone and teeth are from T.L. Ku, University of Southern California (written communication, 1987).
[5]Terrace equivalent to terrace at W87-10; amino acid racemization age estimate probably incorrect, low allo/iso ratio suggests leaching.

ka - 1000 years
N.D. - not dated
N.A. - not applicable
USGS - U.S. Geological Survey
LACHMNH - Los Angeles County Museum of Natural History

TABLE 3. SUMMARY OF RADIOCARBON AND THERMOLUMINESCENCE AGE ESTIMATES

Sample Number (analysis)	Location (latitude, longitude)	Geomorphic Position	(ka B.P.)	Comments
^{14}C-KH-5c[1] (radiocarbon)	San Simeon 35° 39' N 121° 12' 30" W	Estuarine deposits underlying San Simeon marine terrace (Q_2) south of Oak Knoll Creek	>40,480 ± 1,080 yr B.P. (infinite)	Detrital charcoal
TL1a[2] (thermoluminescence)	San Simeon 35° 39' N 121° 12' 30" W	Estuarine deposits underlying San Simeon marine terrace (Q_2) south of Oak Knoll Creek	78 ± 12[3]	Organic-rich silty clay from same estuarine deposits as ^{14}C-KH-5c radiocarbon sample. Sample TL-1a, which is clay-rich, is probably more reliable sample than sample TL-1b, which contains more silt.
TL-2a[2] (thermoluminescence)	San Simeon 35° 39' N 121° 12' 30" W	Estuarine deposits underlying San Simeon marine terrace (Q_2) south of Oak Knoll Creek	96 ± 19[3]	Sample T1-2a is from the same strata as TL-1a.
TL-5b[2] (thermoluminescence)	San Simeon State Park Beach Exposure (35° 38' 25" N) 121° 11' 38" W	Estuarine deposits overlying late Pliocene/Pleistocene Careaga? Formation	193 ± 47	

Notes:

[1]Laboratory number - Beta-22313 ETH-3217, Beta Analytic Inc., University Branch, P.O. Box 248113, Coral Gales, Florida 33124; sample analyzed using AMS (Accelerator Mass Spectrometry) technique at ETH (Eidenossiche Technische Hochschule) University of Zurich, Switzerland.

[2]Thermoluminescence ages are from Glenn Berger, Department of Geology, Western Washington University, Bellingham, Washington (written communication, 1987). These ages are based on a partial bleach method as described by Berger (1988).

[3] The weighted man average age of these two samples, which were collected from the same strata is 83 ± 10 ka.

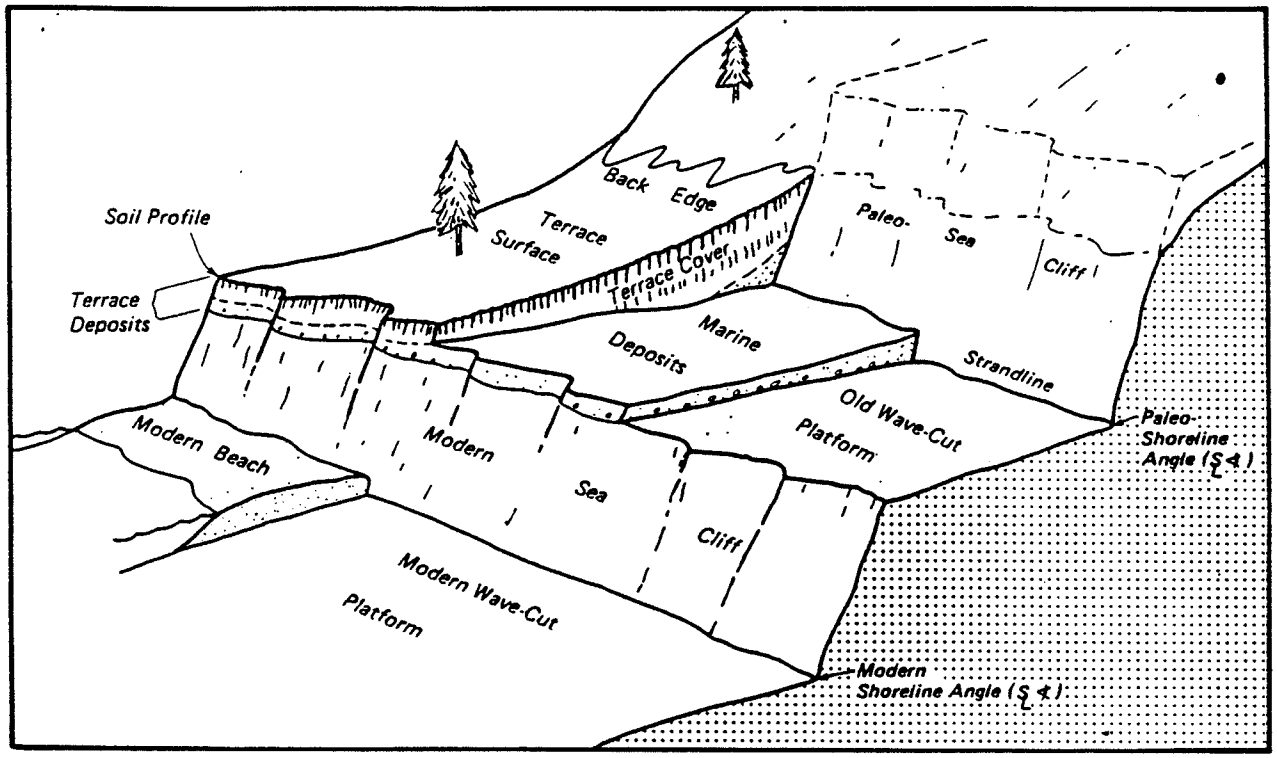

Figure 1. Schematic diagram illustrating the spatial relationships of major elements of marine terraces. (modified from Weber, 1983).

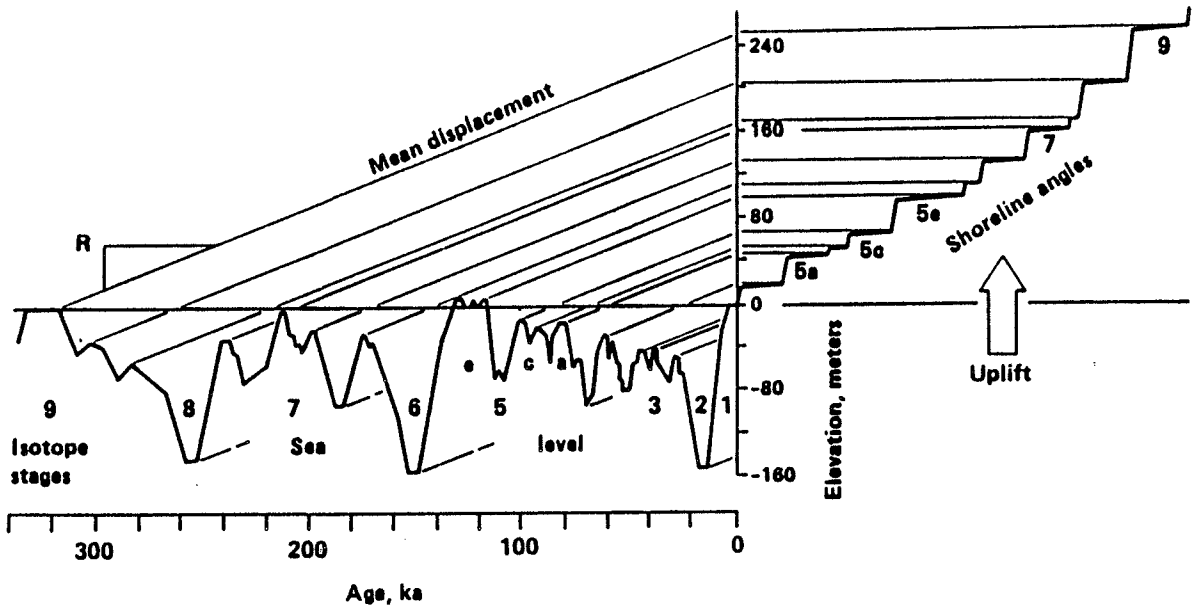

The slope (R) of the line drawn between the peak of sea level highstand and the abcissa is the uplift rate. If the uplift rate is constant, the uplift lines are parallel. The sea level curve is modified from Chappell (1983) and oxygen isotope stages and substages are from Shackleton and Opdyke (1973), (modified from Lajoie, 1986).

Figure 2. Diagram showing the relationship between sea level fluctuations and emergent marine terrace elevations on a rising coastline

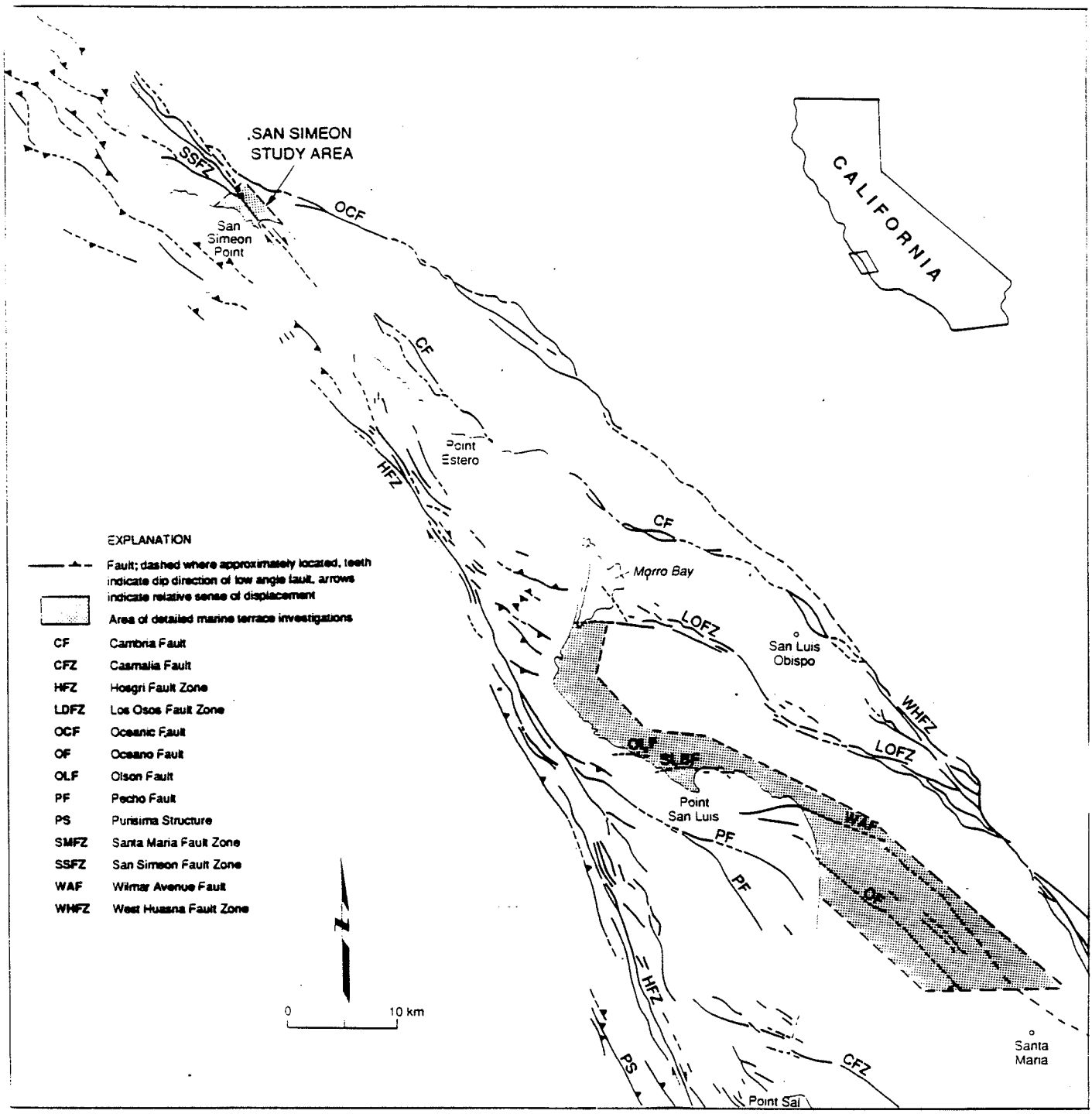

Figure 3. Map showing locations of detailed marine terrace investigations along the south-central coast of California.

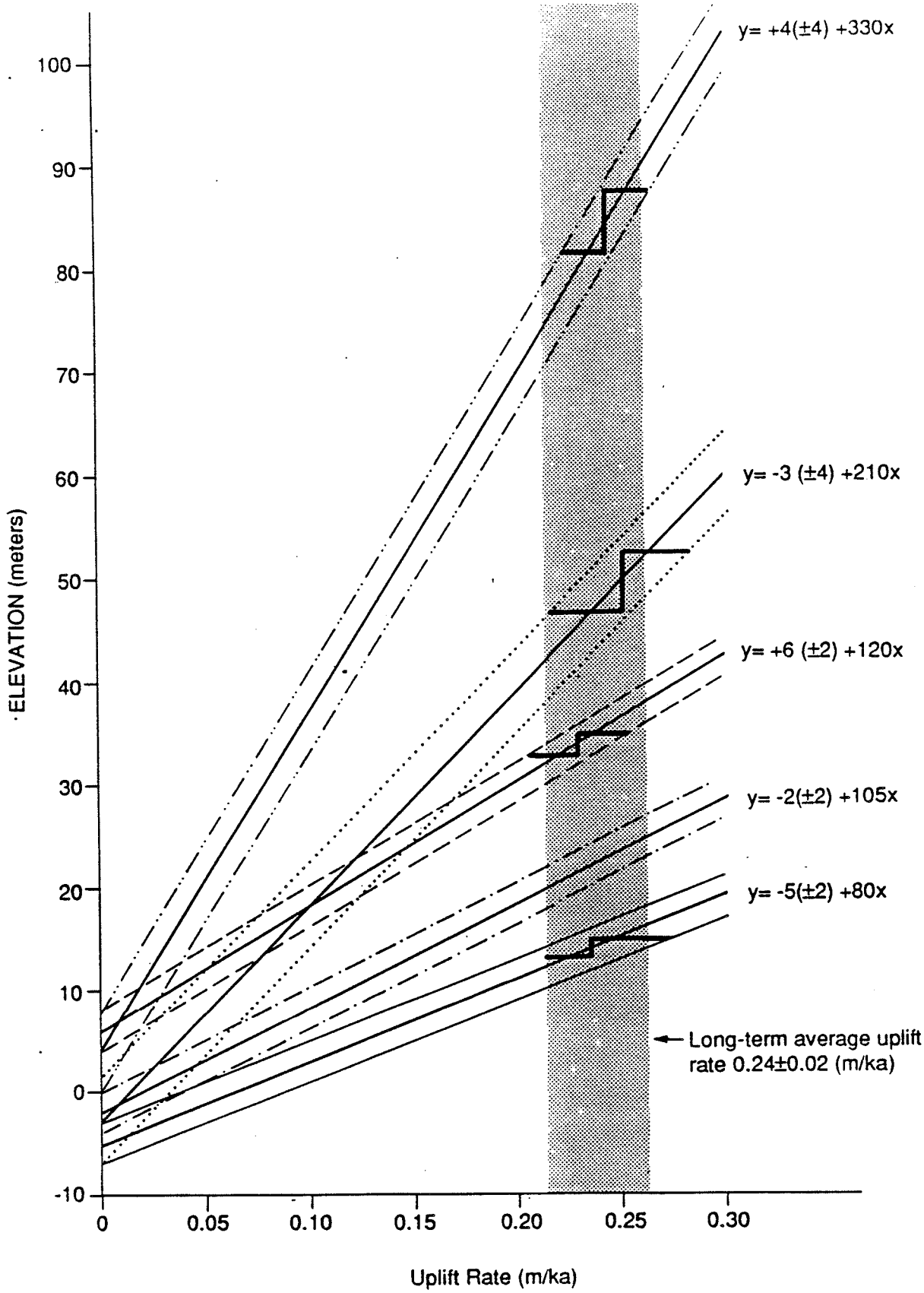

Figure 4. Example of a predicted uplift - graph showing estimated average long-term uplift rate for a flight of marine terraces at Montaña de Oro State Park, San Luis Obispo study area.

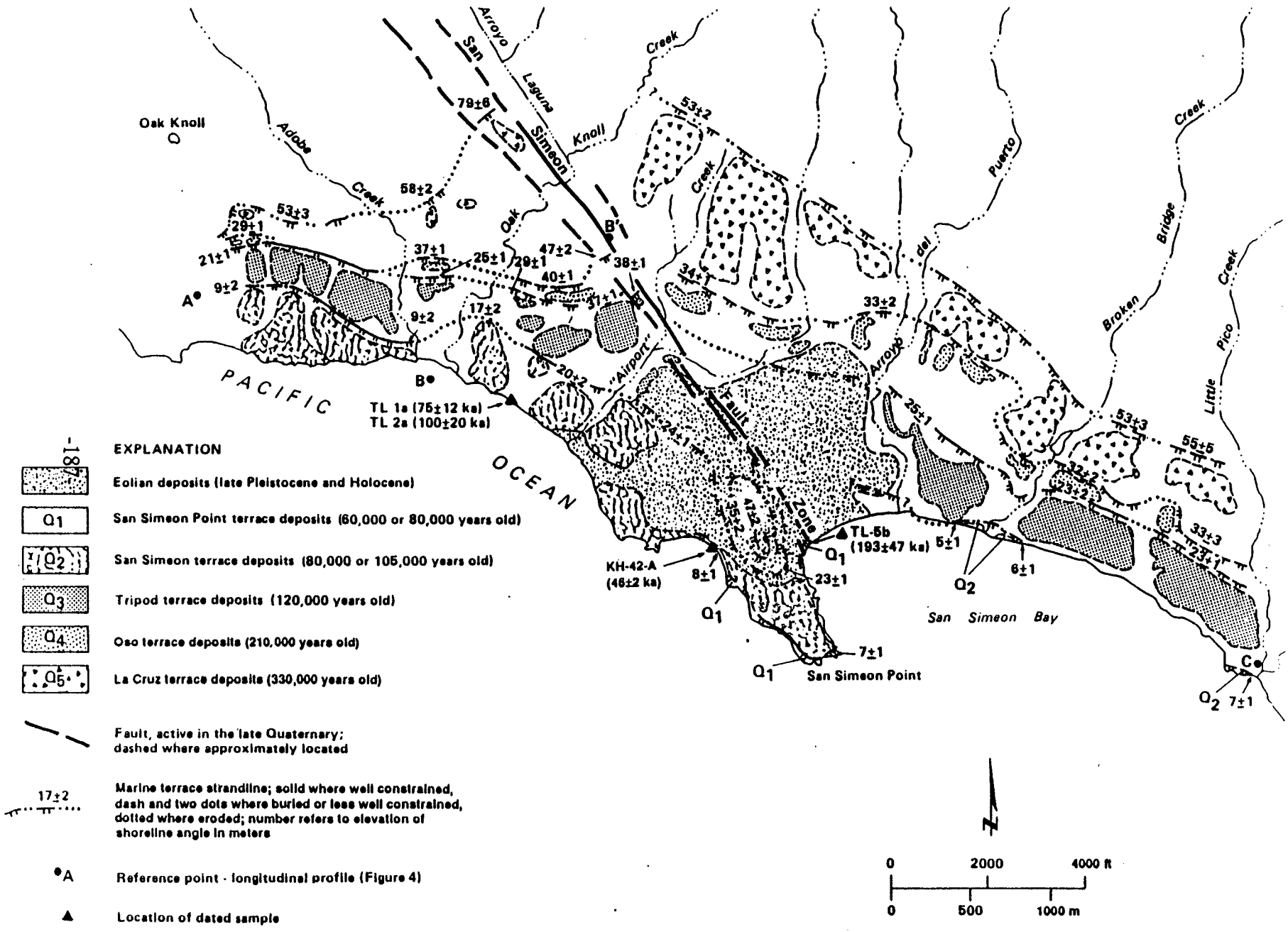

Figure 5. Geologic map of marine terraces along the southern onshore reach of the San Simeon fault zone.

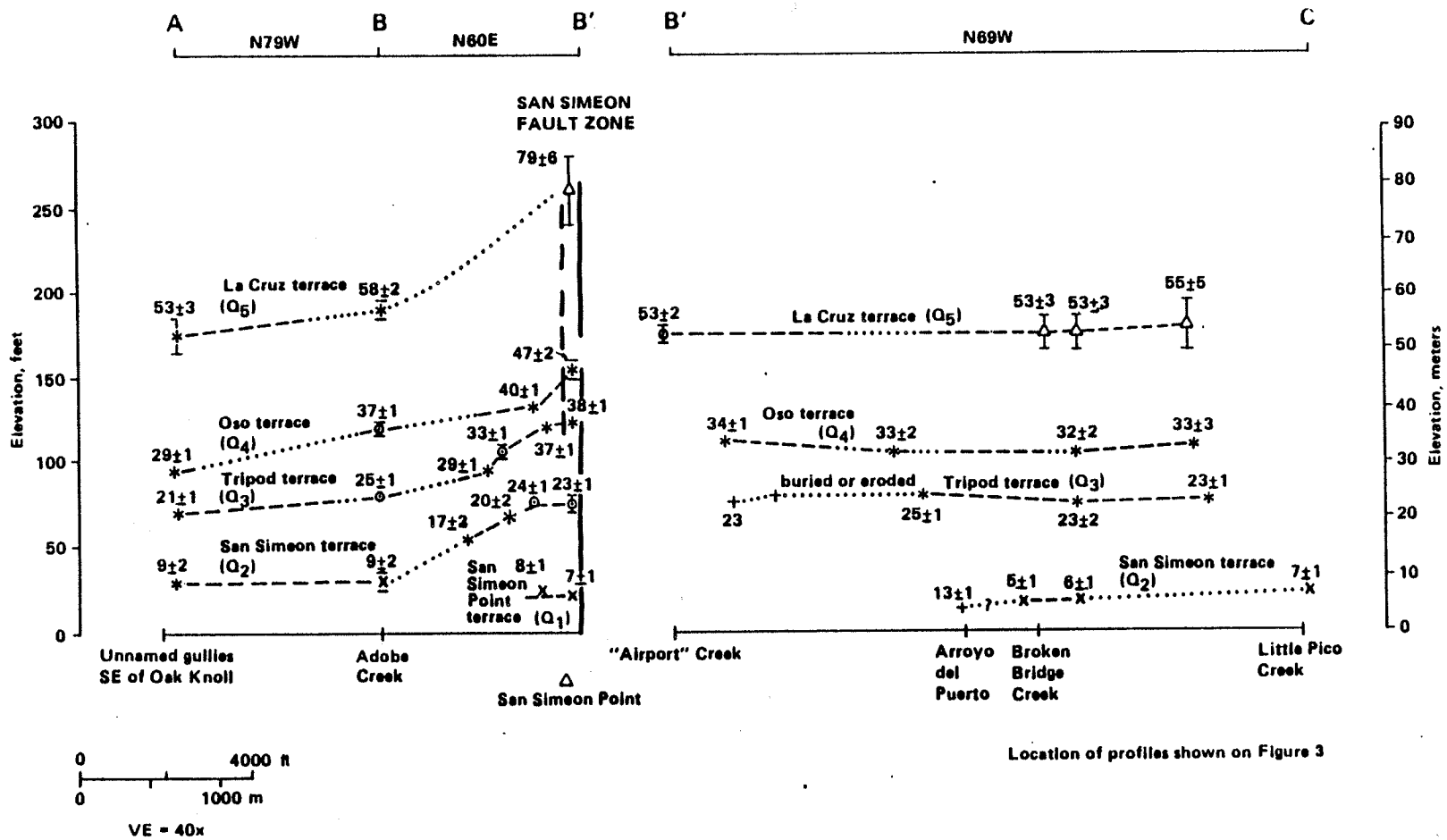

EXPLANATION

Lines

- ——— ⚟ with well exposed wave cut platform (WCP)
- - - - - ⚟ without well expressed wave cut platform
- ····· Eroded ⚟

General note: Error bars are shown except where symbol is larger than error.

Symbols

- ⚟ Shoreline angle
- x ⚟, elevation based on surveying of exposed ⚟ (meters)
- ⊙ ⚟; elevation based on drill hole projections (meters)
- * ⚟; elevation based on projection of surveyed wcp exposed in seacliff, stream cut or soil pit (meters)
- △ ⚟; elevation estimated from bedrock outcrops plotted on USGS 7.5' topographic quadrangle map (meters). Contour interval 40 feet
- + Elevation of bedrock surfaces (meters)

Figure 6. Longitudinal profile of marine terraces along the southern onshore San Simeon fault zone.

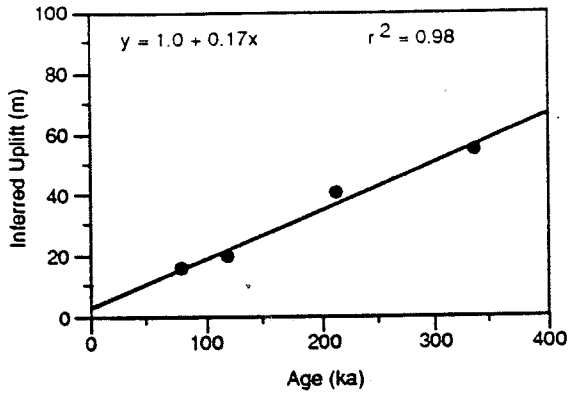

A) Adobe Creek Area (Southwest of San Simeon Fault Zone)

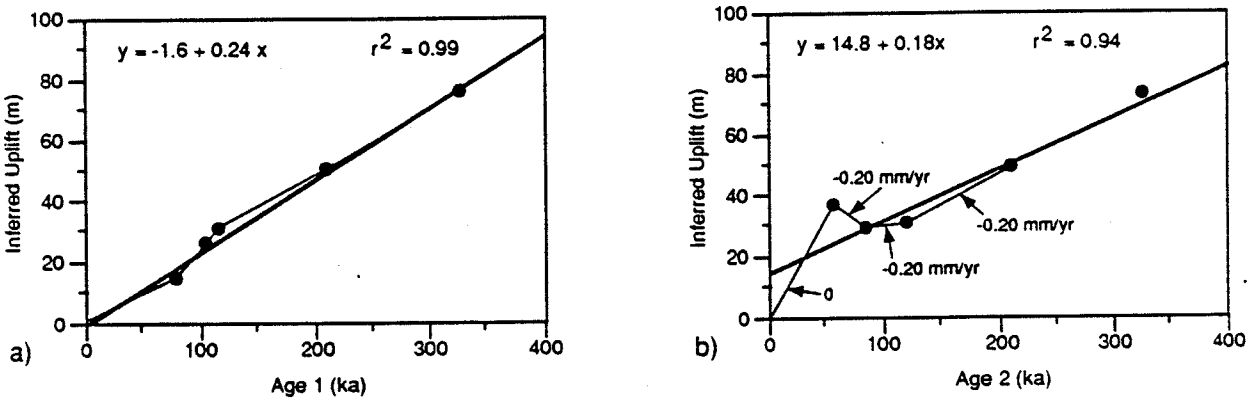

B) San Simeon Point (Adjacent to and within the San Simeon Fault Zone)

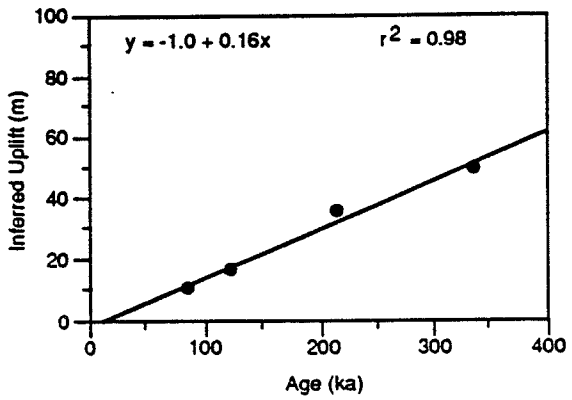

C) Broken Bridge Creek Area (Northeast of San Simeon Fault Zone)

Figure 7. Inferred uplift-rate graphs, San Simeon study area.

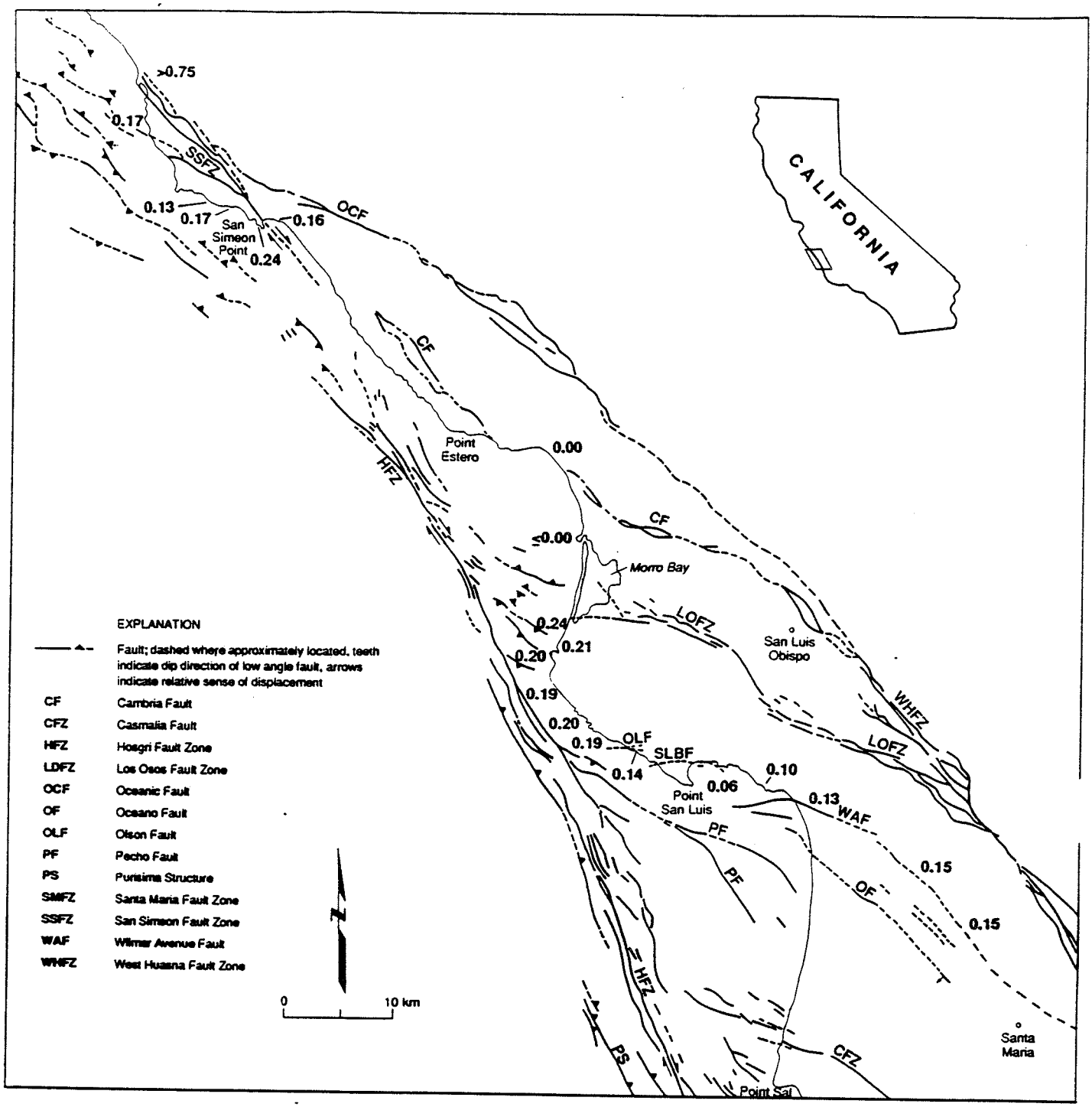

Figure 8. Map showing uplift rates, south-central coast of California.

ESTIMATED PLEISTOCENE SLIP RATE FOR THE SAN SIMEON FAULT ZONE, SOUTH-CENTRAL COASTAL CALIFORNIA

by

Kathryn Hanson
Geomatrix Consultants, Inc., San Francisco, California

and **William R. Lettis**
William Lettis and Associates, Lafayette, California

ABSTRACT

The San Simeon fault zone disrupts a flight of emergent marine terraces and laterally deflects a series of drainages near San Simeon Point along the coast of south-central California. Detailed studies of the offset marine terraces and deflected drainages provide data that we use to estimate the late Pleistocene slip rate for this fault zone. We map four and five marine terraces to the northeast and southwest, respectively, of the southern onshore reach of the San Simeon fault zone. These terraces correlate to marine oxygen-isotope stages 3 or 5a (60 or 80 ka), 5a or 5c (80 or 105 ka), 5e (120 ka), 7 (210 ka), and 9 (330 ka). The marine terrace strandlines are right laterally offset by the San Simeon fault zone along two or possibly three primary fault traces within a zone of shearing and warping up to 500 meters wide. Estimated slip rates based on the present locations of strandlines for the San Simeon (5a or 5c), Tripod (5e), and Oso (7) terraces, and paleogeographic reconstructions of the shoreline configurations during their development, range from about 0.4 to 11 mm/yr with the best constrained values ranging from 1 to 3 mm/yr. Slip rates based on deflections and apparent offset of drainages across the primary active traces of the San Simeon fault zone are in agreement with the 1 to 3 mm/yr values estimated from the marine terrace study.

INTRODUCTION

The San Simeon Fault Zone trends N35°W along the coast of central California from the latitude of Lopez Point on the north to the latitude of Point Estero on the south, a distance of about 90 km (Fig. 1). To the north and south, the fault zone is aligned with the San Gregorio and Sur-Serra Hill fault zones and the Hosgri fault zone, respectively. The regional alignment of these fault zones together with regional stratigraphic correlations (Hall, 1978; Graham and Dickenson, 1976; 1978a, 1978b) suggest that they are components of a single right-slip fault system. However, these fault zones lie primarily offshore where it is difficult to characterize their Quaternary behavior. The San Gregorio fault zone locally comes onshore at Seal Cove and Año Nuevo where detailed paleoseismic studies indicate the fault is characterized by late Quaternary right-slip (Weber and Lajoie, 1979a,b). The Sur fault zone locally comes onshore at Point Sur where reconnaissance studies indicate right-slip activity (Hall, 1989). The Hosgri fault zone is not present

onshore. Offshore geophysical, geological, and seismological studies conducted by Pacific Gas and Electric Company (PG&E, 1988) indicate that the fault is a high-angle, strike slip fault. Earlier geophysical and structural modeling studies by Crouch and others (1984), Hamilton (1984), Hamilton and Willingham (1977, 1978), McCulloch (1987), and Davis and McIntosh (1987), variously interpreted the Hosgri fault to be a thrust fault, high-angle transtensional fault, or an inactive basin-margin normal fault.

The San Simeon fault zone is locally exposed onshore for about 20 km from San Simeon Bay to north of Ragged Point (Figs 1 and 2). This onshore reach of the fault zone provides the best opportunity to assess through geologic investigation the style and rate of late Quaternary deformation along the coastal fault system. Geologic studies by Hall (1976), Hall and others (1979), and Weber (1983) indicate that the fault zone in this area progressively broadens northward from a relatively narrow, well constrained zone about 120 m wide at San Simeon Bay to a series of branching fault traces in a zone over 5 km wide at the latitude of Ragged Point (Fig 2b). Within this branching zone, three primary fault strands are present, the eastern and western traces of the "San Simeon fault zone," and the more westerly trending Arroyo del Oso fault. These traces are approximately coincident with the Arroyo Laguna, San Simeon, and Arroyo del Oso faults, respectively, as mapped by Hall (1976), Hall and others (1979), and Weber (1983).

In the region from San Simeon Bay to Ragged Point, the San Simeon fault zone traverses a flight of well developed and preserved emergent marine terraces. The marine terraces are late Pleistocene in age and provide an excellent strain gauge for evaluating the style and rate of late Quaternary deformation along the fault zone. The presence of these terraces on both sides of the San Simeon fault zone indicates that there has been broad regional Pleistocene uplift. Local differential uplift along the San Simeon fault zone also has produced a northeast-facing 30- to 65-m-high escarpment that is best developed along Arroyo Laguna (Fig. 2b). In addition to this linear escarpment, the fault zone is well expressed geomorphically by a series of linear stream drainages, springs, linear topographic scarps, side-hill benches, sag ponds, pressure ridges, deflected stream channels and stream valleys, vegetation and tonal lineaments, captured and beheaded streams, underfit stream valleys, and ponded alluvium. Many of these features, including deflected drainages, pressure ridges and sag ponds are commonly associated with strike-slip faulting. Because these features are developed in and across late Pleistocene marine terraces, they clearly indicate late Pleistocene or Holocene fault activity. In this study, we assess the style of faulting and quantify the amount of cumulative offset of some of these features, in particular, marine terrace strandlines and deflected drainage channels. These offset late Pleistocene and Holocene features provide a means of assessing the style and rate of slip along the San Simeon fault zone.

PREVIOUS STUDIES

The onshore reach of the San Simeon fault zone was initially identified and mapped by Taliaferro (1943), who referred to it as the

Arroyo Laguna fault. Pacific Gas and Electric Company (1974, 1975) later mapped parts of the fault zone and assigned the name San Simeon fault. The most detailed geologic mapping of pre-Quaternary stratigraphy and structure in the San Simeon area is provided by Hall (1976) and Hall and others (1979).

During the mid- to late-1970s and the early 1980s, the San Simeon fault zone was interpreted to be an integral component of a major through-going coastal fault system that also included the San Gregorio, Sur-Serra Hill and Hosgri faults (Silver, 1974, 1978; Graham and Dickinson, 1976, 1978a, 1978b; Hall, 1978; Leslie, 1980a, 1980b, and 1981). The lack of good quality, near-shore geophysical data at that time precluded resolution of the structural and genetic complexities of all the branching and en echelon faults within this complex system. Hall (1975), and later McCulloch and others (1977), concluded that the San Simeon fault is part of the Hosgri fault zone and showed an en echelon offset between the two faults in the offshore area south of San Simeon Point. Leslie (1980a, 1980b, and 1981) also interpreted that the two faults are connected, based on high resolution seismic reflection data in nearshore areas south of San Simeon Bay and on the aeromagnetic data of McCulloch and Chapman (1977). However, other investigators (Hoskins and Griffiths, 1971; Wagner, 1974; Hamilton, 1984) considered the San Simeon and Hosgri faults to be distinct structures and interpreted the Hosgri fault trace to extend in the offshore several kilometers west of San Simeon Point to the latitude of Ragged Point rather than merging with or stepping onshore to the San Simeon fault as proposed by Hall (1975).

The northward extension of the San Simeon fault zone and lateral continuity with faults in the Monterey Bay area also has been the subject of extensive study. Citing evidence for possible correlation of offset geologic features, Graham and Dickinson (1978a, 1978b) postulated that the San Gregorio fault is continuous, via a portion of the Sur fault zone, with the San Simeon-Hosgri fault zone. As indicated by Silver (1978), most of the geologic, seismic, and magnetic evidence favors, or at least allows for, the continuity between the Sur and San Simeon faults. McCulloch (1987), however, suggests that the two faults do not directly connect, and instead shows two intervening faults that bend to the west around Point Sur. More recently, marine terrace investigations in the Monterey to Point Sur area by McKittrick (1988) indicate that the Sur-Serra Hill fault has not experienced activity in the late Quaternary, but that the Rocky Creek fault, a branch of the Sur fault, is active and may, in part, connect the San Simeon and San Gregorio faults.

Estimates of Pleistocene and Neogene slip along the San Gregorio-Hosgri fault system differ substantially. Silver (1974) proposed 80 to 90 km of Neogene right-lateral slip along the San Gregorio fault based on offset basement terraces using offshore geophysical data in the Monterey Bay region. A similar value of 80 to 100 km of post-Miocene right-lateral offset on the San Simeon-Hosgri fault was proposed by Hall (1975). In a subsequent report, Hall (1978) hypothesizes that there has been 80 to 95 km of right-slip along the San Simeon-Hosgri fault zone since the Pliocene (during the past 5 Ma). Graham (1976) and Graham and Dickinson (1978a) propose that up to 115 km of right-

lateral offset has occurred on the San Gregorio-Hosgri fault system since late-Miocene time based on several pairs of apparently offset features. Greene (1977) suggests about 110 km of right lateral slip along offshore faults extending across Monterey Bay, with 40 km of this slip assigned to the San Gregorio fault. Clark and others (1984) postulate about 150 km of right-slip on the San Gregorio fault since late Miocene time based on similarities in basement and Tertiary sedimentary rocks in the Point Reyes area, Santa Cruz Mountains, and Monterey area.

In contrast to the above estimates, other authors have argued for lesser amounts of Neogene displacement on the San Gregorio-Hosgri fault zone. Hamilton and Willingham (1977, 1978, and 1979) propose that cumulative post-middle Miocene right-lateral slip on the Hosgri fault is on the order of 10 to 15 km or less, on the basis of comparison of stratigraphic sections on both sides of the fault in San Luis Obispo Bay. Hamilton (1984) concluded that displacement along the San Gregorio-Hosgri fault system in the past 5 million years has amounted to about 5 km of right-lateral displacement. The major parts of the system, according to Hamilton (1984), have an earlier history of movement as part of a late Paleogene "proto-San Andreas" fault system, which underwent around 250 km of right slip along a combined San Andreas-San Gregorio trace at the north, with the amount of slip distributed southward on several fault strands including about 100 km along a San Simeon/Hosgri fault strand. Based on interpretations of field relations between Monterey Bay and Point Sal and on correlations of stratigraphic sections on opposite sides of the San Simeon-Hosgri fault, Seiders (1979) suggested that there has been less than 30 km of post-late Miocene and less than 50 km of post-Oligocene offset.

Evidence for Quaternary activity along the San Simeon fault zone has been reported by several workers in the San Simeon area (Pacific Gas and Electric Company, 1974; Hall, 1975; Envicom, 1977; Weber and others, 1981; Weber, 1983; and Manson, 1985). Pacific Gas and Electric Company (1974) concluded that the San Simeon fault exhibits probable Pleistocene right-lateral strike-slip movement of as much as 460 m near San Simeon based on deflected drainages, but that the fault apparently does not displace sand dune deposits of late Pleistocene or early Holocene age near San Simeon Bay. Pacific Gas and Electric Company (1974) also noted that one westerly trending, north-dipping reverse fault that splays from the San Simeon fault zone disrupts the youngest, lowest marine terrace and therefore has experienced movement in the past 130 ka. Hall (1975) interpreted that at least two traces of the San Simeon fault zone have experienced activity during the past 130 ka based on offset marine terrace deposits, and that there has been 150 to 450 m of right-lateral offset along one trace of the fault zone based on offset drainages. Envicom (1977) concluded that the most recent movement on the two most active traces of the San Simeon fault zone is post-130 ka but pre-Holocene in age, on the basis of trenching, drilling, and mapping studies on the Hearst Ranch property. Prior to this study and trenching investigations by Hall and others (this volume), the most comprehensive study of the Pleistocene geology of the San Simeon

coastal area was provided by Weber (1983). Based on mapping of marine terraces between Cayucos and Cape San Martin, and a preliminary correlation of flights of marine terraces across the San Simeon fault zone, Weber (1983) estimated a Pleistocene slip rate of between 5 to 19 mm/yr of right-lateral strike-slip movement, with a preferred estimate of 8 to 10 mm/yr for the past 350 to 400 ka. Weber and others (1981), and Weber (1983) concluded that displacement of unconsolidated dune sands at San Simeon Bay by small secondary faults within the zone indicates late Pleistocene and probable Holocene activity on the fault. A similar conclusion was reached by Manson (1985), who classified the Arroyo Laguna fault a Special Studies zone according to provisions of the Alquist-Priolo Act of California.

SLIP RATES BASED ON DISPLACED MARINE TERRACES

Emergent marine terraces are useful strain gauges to evaluate late Quaternary tectonic deformation. Marine terraces are wave-cut platforms commonly covered with a veneer of sediment, which form in the intertidal and nearshore zone of marine abrasion, that have been subsequently exposed by eustatic sea level lowering and/or tectonic uplift. Detailed geochronological studies on many coastlines indicate that flights of marine terraces higher than present sea level are the geologic record of periodic glacio-eustatic sea-level highstands superimposed on a rising coastline (Broecker and others, 1968; Mesolella and others, 1969; Matthews, 1973). Marine terrace strandlines, the initially level intersection between the emergent wave-cut platform and the relict sea cliff, ideally can be used to evaluate vertical and horizontal displacement across a fault zone (Weber and Lajoie, 1979a; Lajoie and others, 1979; Weber and Cotton, 1981; Weber, 1983; Lajoie, 1986). Using marine terrace strandlines to estimate lateral fault offset accurately, however, requires an understanding of the geometry or paleogeography of the coastline at the time the strandline was formed.

In the San Simeon area, depositional and erosional processes have locally obscured large areas of the marine terrace sequence. An extensive eolian complex veneers the lower terraces in the vicinity of San Simeon Point. Fluvial dissection and deposition have likewise destroyed or obscured many of the higher, older terraces. In order to constrain paleogeographic conditions at the time of their formation and to delineate the present locations and elevations of older marine strandlines, we conducted detailed mapping augmented by extensive drilling and shallow geophysical surveys along the southern onshore reach of the San Simeon fault where the zone of late Quaternary deformation is constrained to a narrow zone (Fig. 2b).

Flights of four and five marine terraces are present to the northeast and southwest, respectively, of the southern onshore reach of the fault zone near San Simeon Bay. From youngest to oldest, these terraces are designated the San Simeon Point (Q_1), San Simeon (Q_2), Tripod (Q_3), Oso (Q_4), and La Cruz (Q_5) terraces. These five terraces are correlated across the San Simeon fault and are interpreted to represent marine oxygen-isotope stages 3 or 5a (60 or 80 ka), 5a or 5c (80 or 105 ka), 5e (120 ka), 7 (210 ka),

and 9 (330 ka) based on terrace spacing, relative degree of preservation and soil-profile development, and lateral correlation to a dated marine terrace near Cayucos (PGE, 1988; Hanson and others, this volume). The distribution of Quaternary marine terraces in this area and a longitudinal profile illustrating the elevations of shoreline angles of the strandlines on both sides of the fault zone are shown on Figures 3 and 4, respectively.

Based on detailed mapping of the extent and elevations of marine terrace strandlines, we conclude that late Pleistocene deformation is concentrated along two or possibly three primary traces of the San Simeon fault zone. The marine terraces are right laterally offset across the main active traces of the San Simeon fault zone. In addition, the terraces west of the fault zone are upwarped and elevated relative to the terraces east of the fault zone, indicating that vertical separation has also occurred on the fault zone (Fig. 4). Analysis of the components of horizontal to vertical maximum displacement of the marine terrace strandlines (see later discussion) yields horizontal to vertical (H:V) slip ratios ranging from 8:1 to greater than 50:1, indicating that the San Simeon fault zone is behaving predominantly as a strike-slip fault in the present tectonic setting. The H:V is even greater if the rate of uplift southwest of the zone of upwarping adjacent to the main fault (0.17 m/ka) is compared to the rate of uplift (0.16 m/ka) northeast of the fault. Paleoseismic indicators observed in trench exposures also document the predominantly strike-slip behavior of the deformation along the main traces of the fault zone (Hall and others, this volume).

Upwarping of the terrace strandlines west of the main traces of the fault suggests that one or more low-angle, southwest-vergent faults may splay from the main high angle fault traces. We did not observe evidence of surface faulting, however, along the flexural hinge of the upwarped region suggesting that the postulated low-angle thrust faults are concealed or "buried" and are manifest at the surface primarily as fold deformation. Similar upwarping or folding of strata in association with low-angle upward-diverging fault splays is observed on seismic reflection profiles across many known strike-slip faults (Christie-Blick and Biddle, 1985) as well as the Hosgri fault zone to the south (Pacific Gas and Electric, 1988) and the San Gregorio fault zone to the north (Fig. 5). In the case of the San Gregorio fault zone near Año Nuevo (Fig. 5) and the San Simeon fault zone near Piedras Blances (Fig. 2b) low-angle, dip slip fault strands that subparallel the high-angle strike-slip strands also displace late Quaternary marine terraces (Weber and Lajoie, 1979a, 1979b).

The present configuration of the coastline across the San Simeon fault zone at San Simeon Bay consists of a large (approximately 600 m long) headland (San Simeon Point) to the southwest and an embayment (San Simeon Bay) to the northeast. This shoreline geometry gives an apparent left separation across the fault. Weber (1983) noted that comparable headland/bay configurations may have been present at San Simeon along paleo-shorelines during previous highstands and that a lack of recognition of these paleo-shoreline configurations would result in a substantial underestimation of lateral slip along the fault zone if slip estimates were based solely on

the present locations of marine terrace strandlines. Because of the significance of a headland/bay configuration for estimating lateral offset of a strandline, we describe below the development, geometry and potential dimensions of headland/bay shoreline configurations at San Simeon and the implications of these paleo-shoreline configurations for estimating slip on the San Simeon fault zone.

Factors Governing the Development and Size of Headland-Bay Beach Shorelines

Model simulations by Silvester (1960) and empirical studies of natural bays by Yasso (1965) show that crenelate-shaped bays occur along coastlines between headlands where waves approach the coast obliquely. Waves arriving at the shoreline of a crenelate-shaped bay both diffract and refract into the shadow zone of the upcoast headland, producing a log-spiral shape for the bay (Yasso, 1965; Silvester and Ho, 1972) (Fig. 6a). At all stages of development, the coast between two successive headlands or in the lee of and downcoast from a single prominent headland consists of a tangential zone downcoast and a logarithmic spiral section upcoast that defines the curved waterline within the bay (Yasso, 1965; Silvester, 1976). The degree of indentation is dictated by a number of variables, namely, the obliquity of the predominant waves (B) to the headland alignment, the spacing (b) between headlands, and the supply conditions of sand from upcoast or from river mouths within the bay (Silvester, 1976). As illustrated in Figure 6a, the angle B between the incoming wave crests and the headland alignment is similar to the angle between the tangential coastline and the headland alignment (Silvester and Ho, 1972). Progressive indentation of the bay is achieved by the lengthening of the beach line to the headland alignment (limit of encroachment, Fig. 6a).

These relationships provide a framework for evaluating the paleogeography of headland/bay configurations along elevated and eroded strandlines. In paleogeographic reconstructions of such strandlines many of the variables that affect the development of a headland/bay configuration, particularly along a major fault zone, may be uncertain or poorly constrained such as: (1) the obliquity of the predominant waves, (2) the sand budget from upcoast and within the bay, (3) the effects of fault displacement, (4) the effects of lithologic variations on resistance and erodibility, and (5) the length of time the system operated at a given level (i.e. the approach to equilibrium conditions). Many of these variables however, relate to the probability that a headland/bay configuration will initially develop and subsequently to the degree to which the system reaches equilibrium. Empirical studies of natural bays (Yasso, 1965; Silvester and Ho, 1972) suggest that the curved portion of the bay is defined by a logarithmic spiral at all stages of development. Therefore, if interpretation of available data allows for the possibility that a headland was present, the relationships cited above can be used to assess the dimensions of possible headland/bay configurations. In particular, these relationships provide a basis for estimating the size of a paleo-headland given some constraints on the possible width or size of the associated bay that may have been present. Yasso (1965) noted that in the case of each natural bay he studied, the center of

the best fit log spiral is in close proximity to the headland and that the radius of curvature in plan view increases with distance from the headland (Fig. 6b). It follows from this observation and the relationships described above that the length of a headland will generally not exceed the width of the bay. Therefore, given some constraints on the width of a paleo-bay, it is possible to estimate the maximum length of a headland that may have been present.

The shape and dimensions of a headland/bay shoreline can be influenced by the presence of a fault zone such that the headland/bay geometric relationships described above would not be valid. For instance, fault-line erosion during periods of lowered sea-level could result during a subsequent high stand in the development of a long, narrow bay in which the length of the headland greatly exceeds the width of the bay. Observations of drowned valleys formed behind headlands along the San Andreas fault in the Point Reyes area north of San Francisco, however, suggest that this generally does not occur. The present shoreline configuration of two fault-controlled bays, Bolinas and Bodega bays, generally conform to log-spiral shaped curves. In these bays, the log spiral-shaped curve is defined by a large sand spit that blocks lagoons formed in the drowned valleys behind the spits (Fig. 7). Relict fault-controlled embayment or lagoons would be characterized by low-energy, fine-grained deposits. We do not observe these deposits on any of the marine terraces adjacent to the San Simeon fault zone. Rather, the marine terraces are characterized by a veneer of high-energy, near-coastal, gravelly, fine to coarse sand deposits, The absence of fine grained deposits indicate that a narrow, fault-controlled, embayment similar to Bolinas Bay, was not present along the San Simeon fault zone at any time during the late Pleistocene. In the case of the present San Simeon Bay, the very linear southwestern margin of the bay along the San Simeon fault zone appears to be fault controlled and is also likely to be the result of fault-line erosion during previous periods of lowered sea level. The general shape of the bay, however, conforms to a log-spiral curve such that the headland length/bay width relationship is applicable to the present configuration.

Paleogeographic Reconstructions

Several processes have been involved in the development of the San Simeon Point headland. Greater uplift of the region within and adjacent to the fault on its southwestern side initially created an irregular shoreline and favored the development of a headland in the uplifted area. The longevity of a headland in this environment is influenced by: (1) continued right-lateral slip along the fault and wave erosion, which act to reduce the length of the headland; and (2) progressive development of an associated bay due to wave erosion on the leeward side of the headland. It is unlikely that a headland would persist for a long time without a significant difference in erodibility of units across the fault. San Simeon Point is underlain by resistant interbedded chert and diatomaceous siltstone of the Monterey Formation. In contrast, bedrock within the fault zone, the Careaga Formation (?), consists of moderately consolidated fossiliferous sandstone and siltstone of probable Pliocene or early Pleistocene age (see Hall and others, this volume). On the northeast side

of the fault, bedrock consists of Franciscan mélange. Differences in the erodibilities of these lithologies likely enhance the persistence of the San Simeon Point headland as a prominent geomorphic feature.

Paleogeographic reconstructions based on the configurations of marine terrace strandlines (Fig. 8) show that development of a large headland at San Simeon Point is relatively recent (post-120 ka). During development of the Oso terrace (approximately 210 ka), a small island approximately 3.3 kilometers offshore was present in the general vicinity of San Simeon Point. A small headland underlain by more resistant Franciscan metavolcanic rocks may have been present on the shoreline southwest of the San Simeon fault zone during this time. The maximum size of this headland can be estimated by comparison of the geometry of the Oso (Q_4) terrace to the geometry of modern headland/bay beach shorelines, whose crenelate shaped bays can be defined by a logarithmic spiral equation (Yasso, 1965; Silvester and Ho, 1972). The location of the Oso (Q_4) terrace strandline is well constrained on both sides of the San Simeon fault zone. The strandline geometry suggests that if a headland/bay coastline configuration occurred, the bay must have been less than 250 meters wide. Empirical and modeling data on the configurations and dimensions of modern headland/bay beach shorelines described previously, suggest that the length of a possible adjacent Oso terrace headland would be 250 meters or less, the width of the bay.

Stratigraphic relationships observed in soil test pits on the northeast side of the fault zone also suggest that a large headland was not present during development of the Oso terrace. Coarse pebble- to cobble-gravel marine deposits exposed on the Oso wave-cut platform in these pits Fig. 9a; Plate 1, Hanson and others, this volume) are more indicative of an open coastal depositional environment, rather than that of a quiet bay or lagoon that would have been present if there had been a large headland during development of the Oso terrace.

Although it is difficult to reconstruct the exact paleography of the Tripod coastline, certain strandline features are well preserved. San Simeon Point was also the site of an island during the development of the Tripod terrace, approximately 120 ka (Fig. 8). The Tripod island was larger and closer (approximately 1.3 km) to the Tripod coastline than the Oso island. Consequently, the island may have significantly influenced the distribution of wave energy and long shore currents that carved the Tripod coastline. The location of the Tripod (Q_3) terrace strandline is also moderately well constrained within and southwest of the fault zone. Extensive fluvial modification of the Tripod terrace, however, has largely obscured the strandline on the northeast side of the fault zone. As a result, there are considerably fewer geometric constraints on the size and shape of possible headland/bay beach configurations. Although existing subsurface data allow for a headland/bay shoreline configuration comparable to the present San Simeon Point headland/bay, the presence of a significant island offshore from the Tripod shoreline may have hindered development of such a headland. In addition, unlike the present headland that formed as a result of differential erosion of bedrock lithologies across the San Simeon

fault, similar lithologies are present on both sides of the San Simeon fault zone where the Tripod strandline crosses the fault zone. In general, the Tripod shoreline developed on Franciscan Complex rocks, chiefly greywacke and mélange. Geologic relationships, therefore, argue against the presence of a large headland along the Tripod coastline comparable in size to the modern San Simeon Point headland (600 m). On the northeast side of the fault, the Tripod wave-cut platform is probably represented by a narrow bedrock bench near the Airport Creek trenching site (Figure 9b). The lack of deposits on this bench, however, makes it difficult to assess whether the bench is a wave-cut platform or a fluvial strath terrace. Assuming that the bench is a remnant of the Tripod wave-cut platform, we can estimate the size and configuration of the headland that may have developed during Tripod time. The width of the possible bay that may have formed on the northeast side of the fault is approximately 360 meters. Based on the arguments presented previously, maximum headland length would not likely exceed this value.

A headland comparable to San Simeon Point probably first developed during San Simeon time (80 or 105). The shape of the San Simeon strandline southwest of the fault, which is well constrained by borehole data, subparallels the modern headland coastline (Fig. 9c). The boring data allow for a headland ranging from 350 m to approximately 840 m long. The exact location and configuration of the associated bay beach on the northeast side of the fault is less well known. Directly northeast of the fault zone, within 220 meters of the coastline, boreholes extend to depths of -7.6 meters and <-9.7 meters below sea level without encountering bedrock. We infer from these data that there has been fluvial erosion in this area subsequent to the formation of the San Simeon wave-cut platform. Farther to the east, the San Simeon terrace is clearly present along the coastline between Arroyo del Puerto and Broken Bridge Creek and may extend north of Arroyo del Puerto along the queried strandline shown on Figure 9c. Due to the uncertainties in the location of the San Simeon strandline west of Arroyo del Puerto, it is difficult to define the exact location of the curved part of the bay that would have developed behind the San Simeon headland during the development of the San Simeon terrace. The strandline may curve toward San Simeon Point from Arroyo del Puerto or from some point farther north in the area of fluvial incision. The latter hypothesis is more likely in that the total slip on the fault since the development of the older Oso strandline (210 ka) appears to have been less than 550 m (see following discussion) and the first hypothesis would require considerably greater offset.

Estimated Slip Rates

We have estimated late Quaternary slip rates for the San Simeon fault zone based on the offset Oso, Tripod and San Simeon marine terraces (Table 2). The Oso (Q_4) terrace provides the best constrained slip rate based on mapping of marine terrace strandlines. The location and elevation of the Oso strandline on both sides of the fault zone are tightly constrained by field mapping and by subsurface data from boreholes, soil pits and exploration pits (Fig. 9a). Correlation of the terrace remnants on both sides of the fault is supported by relative soil profile

development, geomorphic expression, and correlation of shoreline-angle elevation/ altitudinal spacing to other dated paleosea-level curves (Hanson and others, this volume).

Estimates of lateral offset of the Oso strandline range from 150 to 550 m (Fig. 9a). The minimum value is less well constrained than the maximum value due to the degree of fluvial incision and erosion of the Oso terrace northeast of the fault zone. The shape of the strandline on the northeast side of the fault zone beyond the piercing point indicated on Figure 9a is constrained in part by an outcrop of higher bedrock (39 m) that is present on the hillslope north of Airport Creek. The steepness of the hillslope below this outcrop suggests that it is also underlain by bedrock that would lie at elevations above the elevation of the Oso terrace (34 meters). The projected trend of the strandline, therefore, probably lies southward of the 34-meter contour indicated on Figure 9a. Although the Oso strandline on the northeast side of the fault zone may appear to project to a piercing point adjacent to the strandline southwest of the fault zone, thus indicating little or no offset of the strandline, lithologic variations across the fault zone suggest this would not be the case. Metavolcanic bedrock underlying the Oso strandline southwest of the fault is more resistant than either sheared bedrock within the fault zone or Franciscan Complex bedrock northeast of the fault zone. This would likely favor the development of at least a small headland along the Oso shoreline. This in turn would lead to the formation of a log-spiral shaped waterline on the northeast side of the fault zone. The projection shown on Figure 9a, which gives a minimum value of 150 m, reflects this interpretation.

The maximum value for the offset of the Oso strandline is also based on the assumption that a headland may have been present on the southwest side of the fault during formation of the Oso terrace. The maximum size of this headland (250 m) was estimated by comparison of the configuration of the Oso strandline to the configurations of modern headland/bay beach shorelines described above. This value (250 meters) added to the present 300-meter separation of the two piercing points on either side of the fault yields a maximum offset of 550 meters (Fig. 9a). Using values of 150 to 550 meters for the amount of lateral offset and a preferred age of 210 ka for the Oso terrace yields a slip rate ranging from 0.7 to 2.6 millimeters per year.

Estimates of lateral offset for the Tripod terrace are not as well constrained as for the Oso terrace. The Tripod terrace has been extensively modified by fluvial erosion and deposition northeast of the fault zone precluding accurate mapping of the Tripod strandline. A maximum lateral offset is estimated by assuming that a headland was present southwest of the fault zone during Tripod time. Using the geometric constraints for headland/bay beach configurations described previously, we estimate that the length of this headland would not have exceeded 360 m, the width of the associated bay (Fig. 9b). Adding a 360-m headland to the apparent offset of 570 m shown on Figure 9b gives a maximum lateral offset of 930 m. This value divided by the preferred age of the Tripod terrace of 120 ka gives a slip rate of 7.8 millimeter per

year, which exceeds the better-constrained range of slip rate based on offset of the Oso terrace (Table 2). This estimate, therefore, is considered to be high. Also, it is unlikely that a large headland developed west of the fault zone during Tripod terrace time. Unlike the present San Simeon Point headland, which is underlain by very resistant Monterey chert, there is little or no contrast between bedrock lithologies in the vicinity of the Tripod strandline where it crosses the fault. A minimum value of lateral offset of 100 meters is obtained if it is assumed that the narrow bedrock bench at an elevation of 23 m northeast of the fault zone in the vicinity of the Airport Creek trench locality (Fig. 9b) is a stripped remnant of the Tripod terrace and that there was no headland during formation of the Tripod terrace. Using an age of 120 ka for the Tripod terrace yields a minimum slip rate of 0.8 millimeter per year (Table 2).

The paleogeographic reconstruction of the San Simeon terrace, like the Tripod terrace, is complicated by fluvial modification of the terrace surface and the presence of thick eolian deposits northeast of the fault zone. The location of the strandline piercing point on the southwest side of the fault is moderately well constrained by borehole data (Fig. 9c). Tightly spaced borings along the access road north of the Borrow Pit trench site provide a northernmost limit for the possible location of the strandline on the southwest side of the fault zone. On the northeast side of the fault zone the terrace is clearly observed along the coastline between Arroyo del Puerto and Broken Bridge Creek and may extend further to the northwest as shown on Figure 9c based on indirect geomorphic and subsurface borehole and geophysical data. We estimate a maximum value of lateral offset of approximately 900 meters assuming a maximum headland length and a shoreline configuration that did not extend northwest of Arroyo del Puerto, but rather wrapped into the fault zone mimicking the curve of the present shoreline (Fig. 9c). In this interpretation, the offshore portion of the strandline would have been eroded by fluvial and possibly subsequent marine erosion. Assuming a 900 meter offset and an age of 80 ka, we calculate an estimated maximum slip rate of 11 millimeters per year (Table 2). This value also greatly exceeds the better constrained slip rates based on the Oso terrace. It seems more likely that the San Simeon strandline extends northwest of the Arroyo del Puerto area, possibly along the alternate strandline configuration shown on Figure 9c. Due to the uncertainties in the actual northwestern extent of the strandlines on both sides of the fault zone, the data are insufficient to estimate a reasonable minimum slip rate.

An alternative approach for estimating net slip on the San Simeon fault is to convert the well constrained vertical separation of marine terrace strandlines across the fault into cumulative lateral offset using the plunge of slickensides and mullions on the fault plane as the assumed slip direction. The benefit of this technique is that it uses the vertical separation of terrace strandlines, which are much more tightly constrained than their lateral offset, and because the initial elevation of the strandline generally approximates former mean sea level and is not significantly affected by paleogeography. On the other hand, this technique assumes that slickensides are reliable as an indicators of long-term slip vectors, which may not be

the case. Lateral slip rates calculated using this technique from vertical displacements of the San Simeon (Q_2), Tripod (Q_3) and Oso (Q_4) (Fig. 9) terraces are 1.2 to 2.9 millimeter per year, 0.7 to 1.2 millimeter per year and 0.4 to 0.8 millimeter per year, respectively.

Slip Rates Based on Drainage Deflections

Previous workers (Pacific Gas and Electric Company, 1974, 1975; Hall, 1975; Weber, 1983; Hamilton, 1984) observed that numerous stream channels are deflected by various strands of the onshore San Simeon fault zone. Oak Knoll Creek is a major drainage that perpendicularly crosses the San Simeon fault zone along the southern part of its onshore reach. Although the present active channel exhibits a left deflection across the main active fault zone, the margins of the valley, which are incised into bedrock, exhibit an apparent 100 to 175 meters of right separation (n_1, Fig. 10). Incision of Oak Knoll Creek post-dates formation of the La Cruz terrace that is interpreted to be 330 ka. Therefore, right deflection of the Oak Knoll drainage suggests a minimum slip rate of 0.3 to 0.5 mm/yr. Between Oak Knoll Creek and Arroyo de la Cruz, two small drainages both exhibit apparent right-lateral deflection of approximately 360 meters across the main trace of the fault (n_{2a} and n_{2b}, Fig. 10). These drainages are incised into elevated surfaces mapped by Weber (1983) as the Oak Knoll and Cinnabar marine terraces. The ages of these surfaces are not precisely known, but based on their present elevations with respect to the approximately 330 ka (correlative to marine oxygen isotope stage 9) La Cruz terrace, they are estimated to be at least 430,000 and 480,000 years old (correlative to marine oxygen isotope stages 11 and 13; see Table 1, Hanson and others, this volume for estimated ages), respectively. Using these ages and the 360-meter deflections along the fault suggests a minimum right-lateral slip of approximately 0.8 to 1.1 millimeter per year for this strand of the fault.

Higher slip rates are suggested by deflections of streams along the two most active traces of the fault zone north of Arroyo de la Cruz. Along the western trace a minimum deflection of 360 meters (n_6, Fig. 10) is observed for an unnamed creek north of Arroyo de los Chinos. Along the eastern trace, Arroyo Hondo is deflected 400 meters (n_8, Fig. 10). Both of these streams are incised into a surface equivalent to or younger than the Oak Knoll terrace as mapped by Weber (1983). The Oak Knoll terrace is estimated to be correlative to marine oxygen isotope stage 11 (~430 ka) or stage 13 (~480 ka). Based on these data, minimum slip rates for the western and eastern traces are 0.75 and 0.83 mm/yr, respectively, or 1.6 mm/yr for the fault zone. In this area, geomorphic relations also suggest that stream capture has occurred during the evolution of the drainage network. The lower reach of Arroyo de los Chinos appears to have previously followed a more northerly direction based on the presence of an extensive alluvial fan near Breaker Point at the mouths of what currently are small, beheaded arroyos. This fan appears to require a larger source area than that presently provided by the two unnamed creeks south of Arroyo Hondo. Also, the present stream along one of these drainages (n_6, Fig. 10) is clearly underfit with respect to the size of the channel

margins. Assuming that capture occurred, the stream has been deflected about 500 meters in the past 320 to 500 ka, which suggests a minimum slip rate of about 1 to 1.6 mm/yr along this trace.

Maximum lateral slip can be broadly constrained by assuming that the large Arroyo de la Cruz channel reflects actual fault offset on the major fault strand(s) of the San Simeon fault zone (n_3, Fig. 10). The channel is deflected roughly 3,000 m and is incised into the oldest marine terrace in the area (≥ 480 ka), suggesting a maximum slip rate of about 6 mm/yr (Table 1).

Right-lateral strike slip displacement along the San Simeon fault zone is also suggested by the apparent 1 to 2 kilometer right deflection of a large canyon, the Mill Creek submarine canyon, in the offshore region 29 km northwest of Ragged Point (Fig. 11). The age of this canyon is poorly constrained but may be late Pliocene or younger suggesting a long-term slip rate of approximately 1 mm/yr.

CONCLUSIONS

Detailed mapping of elevated marine terraces along the southern onshore San Simeon fault zone provides new data for characterizing the late Quaternary sense of slip and slip rate of this fault zone. The right slip behavior of the fault zone, which is strongly suggested by right-deflection of several drainages along its onshore reach and the Mill Creek submarine canyon offshore, is further substantiated by estimated components of slip based on paleogeographic reconstructions of Pleistocene marine terrace strandlines. Estimated values of horizontal and vertical separation of the San Simeon (80 ka), Tripod (120 ka), and Oso (210 ka) terraces indicate ratios of horizontal to vertical separation across the main active traces ranging from 8:1 to greater than or equal to 50:1 (Table 1). However, the rate of uplift on the southwest side of the fault zone beyond the zone of upwarping adjacent to the active traces (17 m/ka) is comparable to the rate of uplift (0.16 m/ka) northeast of the fault, indicating that the component of vertical slip across the entire fault zone is negligible.

Rates of vertical separation across the San Simeon fault zone may have increased over the past 200,000 years (Table 1). Data are not sufficient, however, to resolve if this apparent increase represents a temporal increase in the rate of vertical slip or is the result of spatial variation in uplift along strike of the fault zone. Uplift data for terraces adjacent to and within the fault zone in the vicinity of San Simeon Point suggest that a temporal increase in the rate of vertical slip is most likely. Comparison of the altitudinal spacing of these terraces to

dated terraces elsewhere in the world indicate that uplift of San Simeon Point during the past 120,000 years has not been constant and may have been considerably higher during some of that interval of time (Hanson and others, this volume). The increased vertical uplift in the vicinity of San Simeon Point may be related to increased activity on branching "buried" thrust faults associated with the main fault zone that may not be continuous along the entire fault zone.

We estimate Pleistocene slip rates for the primary active onshore traces of the San Simeon fault zone based on interpreted offset of both elevated marine terraces and deflection of drainage channels. A summary of the slip rates calculated using these data is provided in Table 2. The values range from about 0.4 to 11 mm/yr, with the best constrained data suggesting a range in slip rate from 1 to 3 mm/yr. Based on this estimated long-term average slip rate, the San Simeon fault is comparable to other major strike-slip faults in California, including the Hayward, Calaveras, and Rogers Creek fault zones.

ACKNOWLEDGEMENTS

This research was supported by Pacific Gas and Electric Company as part of the Long Term Seismic Program for the Diablo Canyon Power Plant. A special thanks to Dr. Gerry Weber, who shared with us his ideas and mapping experience in the San Simeon area and to Lili Mezger, who assisted in the mapping and drilling aspects of our field study. We also wish to thank Drs. Douglas Hamilton and N.T. Hall for their useful input to discussions, and Dwight Hunt, who provided additional field data on stream deflections along the northern part of onshore San Simeon fault zone. Geophysical interpretation of the seismic reflection profile across the San Gregorio fault zone was provided by Dick Willingham and Gerald Shiller under the direction of Jan Reitman for the Pacific Gas and Electric Company Long Term Seismic Program. We would also like to express our appreciation to Harlan Brown, Manager of the Hearst Ranch, for his patience and assistance in providing access throughout the study area. In conclusion we thank N. Timothy Hall for his careful and constructive review of an early draft of this manuscript.

REFERENCES

Broecker, W.S., Thurber, D.L., Goddard, J., Ku, T.-L., Matthews, R.K., and Mesolella, K.J., 1968, Milankovitch hypothesis supported by precise dating of coral reefs and deep-sea sediments: Science, v. 159, p. 297-300.

Christie-Blick, N., and Biddle, K. T., 1985, Deformation and basin formation along strike-slip faults, in Biddle K. T., and Christie-Blick, N., (eds.), Strike-slip Deformation, Basin Formation, and Sedimentation: Society of Economic Paleontologists and Mineralogists Special Publication 37, p. 1-34.

Clark, J.C., Brabb, E.E., Greene, H.G., and Ross, D.C., 1984, Geology of Point Reyes Peninsula and implications for San Gregorio fault history: in Crouch, J.K., and Bachman, S.B. (eds.), Tectonics and Sedimentation Along the California Margin; Pacific Section S.E.P.M., v. 38, p. 67-86.

Crouch, J., and Bachman, S.B., and Shay, J.T., 1984, Post-Miocene compressional tectonics along the central California margin: in Crouch, J., and Bachman, S.B., eds., Tectonics and Sedimentation Along the California Margin; Pacific Section, S.E.P.M., v. 38, p. 37-54.

Davis, T., and McIntosh, K.D., 1987, A retrodeformable structural solution across the southern Coast Ranges and implications for seismically active structures (abs.): Geological Society of America, Cordilleran Section Meeting Abstracts with Program, v. 19, no. 6, p. 447.

Envicom, 1977, Fault investigation, Hearst Ranch environmental data base: unpublished report for the Hearst Corporation.

Graham, S.A., 1976, Tertiary sedimentary tectonics of the central Salinan block of California: unpublished Ph.D. thesis, Stanford University, California, 510 p.

Graham, S.A. and Dickinson, W.R., 1976, The San Gregorio fault as a major right-slip fault of the San Andreas fault system (abs.): Geological Society of America Abstracts with Programs, v. 8, p. 890.

Graham, S.A., and Dickinson, W.R., 1978a, Evidence for 115 kilometers of right slip on the Gregorio-Hosgri fault trend: Science, v. 199, p. 179-81.

Graham and Dickinson, 1978b, Apparent offsets of on-land geologic features across the San Gregorio-Hosgri fault trend: in Silver, E.A. and Normack, W.R., (eds), San Gregorio-Hosgri Fault Zone, California: California Division of Mines and Geology, Special Report 137, p. 13-23.

Greene, H.G., 1977, Geology of the Monterey Bay region: U.S. Geological Survey Open-File Report 77-718, 347 p.

Hall, C.A., Jr., 1975, San Simeon-Hosgri fault system, coastal California: economic and environmental implications: Science, v. 190, no. 4221, p. 1291-1294.

Hall, C.A., Jr., 1976, Geologic map of the San Simeon-Piedras, San Luis Obispo County, California: U.S. Geological Survey Miscellaneous Field Studies Map MF-784, scale 1:24,000.

Hall, C.A., Jr., 1978, Origin and development of the Lompoc-Santa Maria pull-apart basin and its relation to the San Simeon-Hosgri strike-slip fault, western California: in Silver, E.A., and Normack, W.R. (eds.), San Gregorio-Hosgri Fault Zone, California, California Division of Mines and Geology Special Report 137, p. 25-31.

Hall, C.A., Jr., 1989, San Gregorio-San Simeon-Hosgri fault, Point Sur, California (abs.): Program, 64th Annual Meeting, Pacific Section AAPG-SEPM.

Hall, C.A., Jr., Ernest W.G., Prior S.W., and Wiese S. W., 1979, Geologic map of the San Luis Obispo-San Simeon region, California: U.S. Geological Survey Miscellaneous Investigations Series, Map I-1097, Scale 1:48,000.

Hamilton, D.H., 1984, The tectonic boundary of coastal Central California: Ph.D. dissertation, Stanford University, 290 p.

Hamilton, D.H., and Willingham, C.R., 1977, Hosgri fault zone: structure, amount of displacement, and relationship to structures of the western Transverse Ranges (abs): Geological Society of America Abstracts with Program, v. 9, no. 4, p. 429.

Hamilton, D.H., and Willingham, C.R., 1978, Evidence for a maximum of 20 km of Neogene right slip along the San Gregorio fault zone of central California (abs.): Transactions, American Geophysical Union, v. 59, no. 12, p. 1210.

Hamilton, D.H., and Willingham, C.R., 1979, The coastal boundary zone of central California (abs.): Geological Society of America, Abstracts with Programs, Cordilleran Section Meeting, v. 11, no. 3, p. 81.

Hoskins, E.G. and Griffiths, J.R., 1971, Hydrocarbon potential of northern and central California offshore: in Cram, I.H. (ed.), Future petroleum provinces of the United States — Their Geology and Potential: American Association of Petroleum Geologists Memoir 15, p. 212-228.

Lajoie, K.R., 1986, Coastal Tectonics: in Wallace, R.E. (ed.), Active Tectonics, National Academy Press, Washington, D.C., p. 95-124.

Lajoie, K.R, Weber, G.E., Mathison, S.A. and Wallace, J., 1979, Quaternary tectonics of coastal Santa Cruz and San Mateo Counties, California, as indicated by deformed marine terraces and alluvial deposits: in Weber, G.E., Lajoie, K.R. and Griggs, G.B. (eds.), Coastal Tectonics and Coastal Geologic Hazards in Santa Cruz and San Mateo Counties, California, Geological Society of America Guidebook.

Leslie, R.B., 1980a, Continuity and tectonic implications of the San Simeon-Hosgri fault zone, Central California: unpublished Masters Thesis, University of California at Santa Cruz, California.

Leslie, R.B., 1980b, Acoustic reflection profiles, Yankee Point to Estero Bay, April, 1979, Cruise of the R/V Scammon, central California offshore: U.S. Geological Survey Open-File Report 80-352.

Leslie, R.B., 1981, Continuity and tectonic implications of the San Simeon Hosgri fault zone, central California: U.S. Geological Survey Open-File Report 81-430.

Manson, M., 1985, San Simeon fault zone and Cambria fault, San Luis Obispo County, California: California Division of Mines and Geology Fault Evaluation Report FER-170, p. 12.

Matthews, R.K., 1973, Relative elevation of late Pleistocene high sea level stands: Barbados uplift rates and their implications: Quaternary Research, v. 3, p. 147-153.

McCulloch, D.S., 1987, Regional geology and hydrocarbon potential of offshore Central California: U.S. Geological Survey Professional Paper (in press), 127 pp.

McCulloch, D.S., and Chapman, R.H., 1977, Maps showing residual magnetic intensity along the California coast, Lat. 37°30'N to 34°30'N: U.S. Geological Survey Open-File Report 77-79, 14 sheets.

McCulloch, D.S., Clarke, S.H., Jr., Field, M.E., Scott, E.W., and Utter, P.M., 1977, A summary report of the regional geology, petroleum potential, and environmental geology in the area of proposed lease sale 53-A, central and northern California outer continental shelf: U.S. Geological Survey Open-file Report 77-593, part A, 39 p.

McKittrick, M.A., 1988, Late Quaternary deformation of marine terraces, Monterey Peninsula, California (abs.): Geological Society of America Abstracts with Programs, v. 20, no. 3, p. 214.

Mesolella, K.J., Matthews, R.K., Broecker, W.S., and Thurber, D.L., 1969, The astronomical theory of climatic change: Barbados data: Journal of Geology, v. 77, p. 250-274.

Pacific Gas and Electric Company, 1974, Geology of the southern Coast Ranges and the adjoining offshore continental margin of California, with special reference to the geology in the vicinity of the San Luis Range and Estero Bay: Appendix 2.5D, FSAR, Diablo Canyon Nuclear Power Plant, AEC Docket Nos. 50-275 and 50-323.

Pacific Gas and Electric Company, 1975, Appendix 2.5E, Final Safety Analysis Report for Diablo Canyon Nuclear Power Plant: U.S. Atomic Energy Commission Docket Nos. 50-275 and 50-323.

Pacific Gas and Electric Company, 1988, Diablo Canyon power plant long term seismic program report: Pacific Gas and Electric Company, San Francisco, California.

Seiders, V.M., 1979, San Gregorio-Hosgri fault zone south of Monterey Bay, California: A reduced estimate of maximum displacement: U.S. Geological Survey Open-File Report 79-385, 10 p.

Silver, E.A., 1974, Structural interpretation from free-air gravity on the California continental margin, 35° to 40°N (abs.): Geological Society of America Abstracts with Programs, v. 6, no. 3, p. 253.

Silver, E.A., 1978, The San Gregorio-Hosgri Fault Zone: An Overview: in Silver, E.A., and Normark, W.R. (eds.), San Gregorio-Hosgri Fault Zone, California: California Division of Mines and Geology Special Report 137, p. 1-2.

Silvester, R., 1960, Stabilization of sedimentary coastlines: Nature, v. 188, no. 4749, p. 467-469.

Silvester, R., 1976, Headland defense of coasts: Proceedings of the 15th Coastal Engineering Conference, Honolulu, Hawaii, p. 1394-1406.

Silvester, R., and Ho, S.-K., 1972, use of crenelate shaped bays to stabilize coasts: Proceedings of the 13th Coastal Engineering Conference, v. 2, p. 1347-1365.

Taliaferro, N.L., 1943, Geologic history and structure of the central Coast Ranges of California: in Jenkins, O.P., ed., Geologic Formations and Economic Development of the Oil and Gas Fields of California, California Department of Natural Resources, Division of Mines, Bulletin No. 118, p. 119-163.

Wagner, H.C., 1974, Marine geology between Cape San Martin and Point Sal, south-central California offshore: U.S. Geological Survey Open-file Report, 17 p.

Weber, G.E., 1983, Geologic investigation of the marine terraces of the San Simeon Region and Pleistocene activity of the San Simeon fault zone, San Luis Obispo County, California: U.S. Geological Survey Technical Report 66.

Weber, G.E. and Cotton, W.R., 1981, Geologic investigation of recurrence intervals and recency of faulting along the San Gregorio fault zone, San Mateo County, California: U.S. Geological Survey Open-File Report 81-263.

Weber, G. E., and Lajoie, K. R., 1979a, Late Pleistocene rates of movement along the San Gregorio fault zone, determined from offset of marine terrace shoreline angles: in Weber, G. E., Lajoie, K. R., and Griggs, G. B., (eds.), Coastal Tectonics and Coastal Geologic Hazards in Santa Cruz and San Mateo Counties, California, Field Trip Guide for Cordilleran Section of the Geological Society of America, 75th Annual Meeting, p. 101-111.

Weber, G. E., and Lajoie, K. R., 1979b, Evidence for Holocene movement on the Frijoles fault near Point Año Nuevo, San Mateo County, California: in Weber, G. E., Lajoie, K. R., and Griggs, G. B., (eds.), Coastal Tectonics and Coastal Geologic Hazards in Santa Cruz and San Mateo Counties, California, Field Trip Guide for Cordilleran Section of the Geological Society of America, 75th Annual Meeting, p. 92-100.

Weber, G.E., Oshiro, L.K., Brown, D.F., McCrory, P.A., 1981, Evidence for Late Pleistocene or Holocene faulting Along the San Simeon Fault Zone at San Simeon Bay, San Luis Obispo County, California (abs.): Geological Society of America Abstracts with Program 1981, v. 12, no. 2, p. 113.

Yasso, W.E., 1965, Plan geometry of headland-bay beaches: Journal of Geology, v. 73, p. 702-714.

TABLE 1

COMPONENTS OF SLIP BASED ON DISPLACED MARINE TERRACES

	Vertical Separation(V) (meters)	Vertical Slip Rate (mm/yr)	Horizontal Displacement(H) (meters)	Slip Rate (mm/yr)	(H:V)
San Simeon Terrace (80 ka) or (105 ka)	16 to 20	0.20 to 0.25 0.15 to 0.19	? to 900	? to 8.6	? to 56:1
Tripod Terrace (120 ka)	10 to 13	0.08 to 0.11	100 to 930	0.8 to 7.8	8:1 to 93:1
Oso Terrace (210 ka)	11 to 15	0.05 to 0.07	150 to 550	0.7 to 2.6	10:1 to 50:1

TABLE 2

ESTIMATED SLIP RATES -
SAN SIMEON FAULT ZONE

	San Simeon Terrace (80 ka)	Tripod Terrace (120 ka)	Oso Terrace (210 ka)
Marine Terrace Investigation			
A. Strandline piercing points based on mapping	? to 11.2 mm/yr	0.8 to 7.8 mm/yr	0.7 to 2.6 mm/yr*
B. Horizontal component of slip calculated from vertical separation of terrace (Table 1) and 5°-7° plunge of slickensides observed along the fault in trenches	1.2 to 2.9 mm/yr	0.7 to 1.2 mm/yr	0.4 to 0.8 mm/yr

	Minimum	Maximum
Geomorphic Expression		
A. Drainage displacement	1.0 to 2.0 mm/yr	6 mm/yr

* best constrained data

LIST OF FIGURES

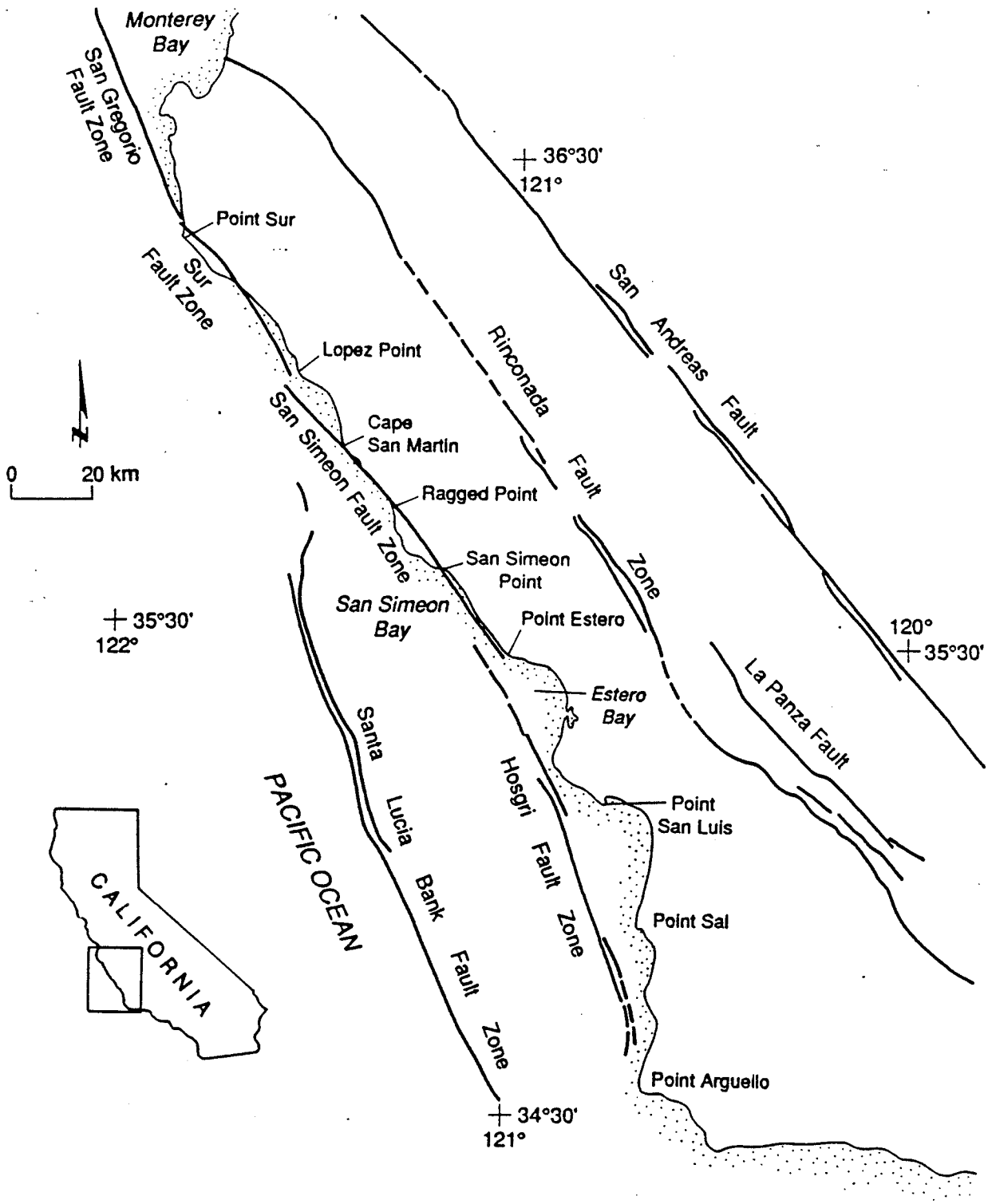
Monterey Bay
San Gregorio Fault Zone
Point Sur
Sur Fault Zone
Lopez Point
Cape San Martin
Ragged Point
San Simeon Fault Zone
San Simeon Point
San Simeon Bay
Point Estero
Estero Bay
Point San Luis
Point Sal
Point Arguello
Rinconada Fault Zone
San Andreas Fault
La Panza Fault
Hosgri Fault Zone
Santa Lucia Bank Fault Zone
PACIFIC OCEAN
CALIFORNIA
36°30'
121°
35°30'
122°
120°
35°30'
34°30'
121°
0
20 km

Figure 1.

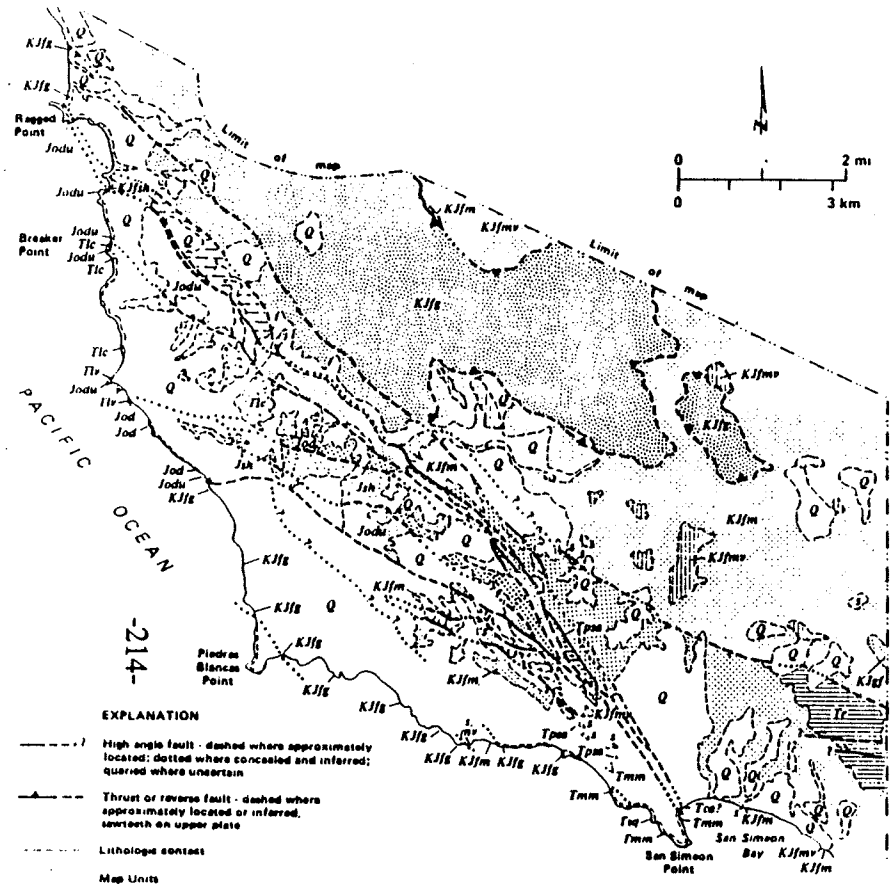
Ragged Point
Breaker Point
Piedras Blancas Point
San Simeon Point
San Simeon Bay
PACIFIC OCEAN
Limit of map
0 2 mi
0 3 km
EXPLANATION
High angle fault - dashed where approximately located; dotted where concealed and inferred; queried where uncertain
Thrust or reverse fault - dashed where approximately located or inferred, sawteeth on upper plate
Lithologic contact
Map Units
Q Quaternary deposits - includes alluvial, fluvial, eolian, marine and landslide deposits
Tca Cerasoa Sandstone (Pliocene)
Tsq Sisquoc Formation (Pliocene)
Tmm Monterey Formation (Miocene)
Tpsa Point Sal Formation (Miocene)
Tr Rincon Shale (lower Miocene-Oligocene)
Tlc/Tlv Lospe Formation (Oligocene)
Franciscan Complex Rocks (Cretaceous or Jurassic):
KJfg Graywacke
KJfmv Metavolcanic rocks
KJfm Mélange
KJfsh Shale
Jsh Unnamed shale
Ophiolite (Jurassic):
Jod Dike and sill complex
Jodu Diorite and ultramafic rocks
Serpentinite
Note: Exposures of bedrock along the coast are too small to be shown at this scale; selected outcrops are indicated

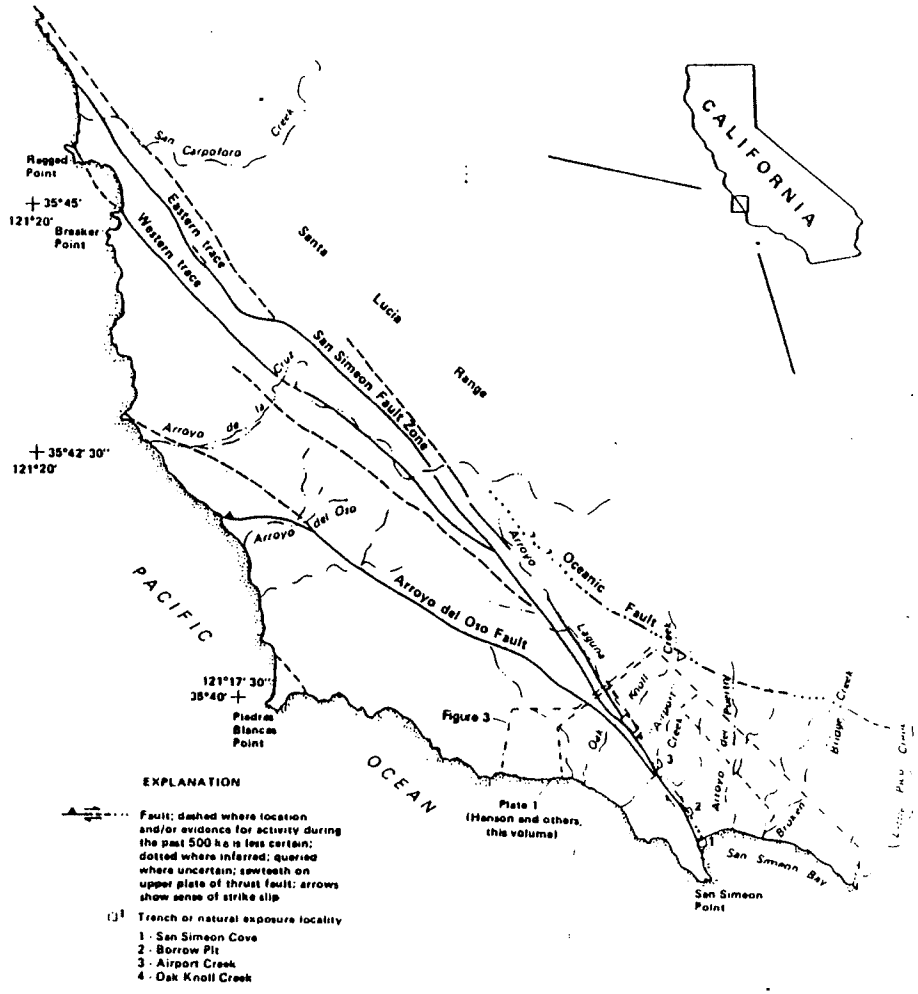
CALIFORNIA
Ragged Point
Breaker Point
35°45'
121°20'
35°42'30"
121°20'
121°17'30"
35°40'
Piedras Blancas Point
San Simeon Point
San Simeon Bay
PACIFIC OCEAN
Santa Lucia Range
Eastern trace
Western trace
San Simeon Fault Zone
Arroyo del Oso Fault
Oceanic Fault
Figure 3
Plate 1 (Hanson and others, this volume)
EXPLANATION
Fault; dashed where location and/or evidence for activity during the past 500 ka is less certain; dotted where inferred; queried where uncertain; sawteeth on upper plate of thrust fault; arrows show sense of strike slip
Trench or natural exposure locality
1 - San Simeon Cove
2 - Borrow Pit
3 - Airport Creek
4 - Oak Knoll Creek

Figure 2.

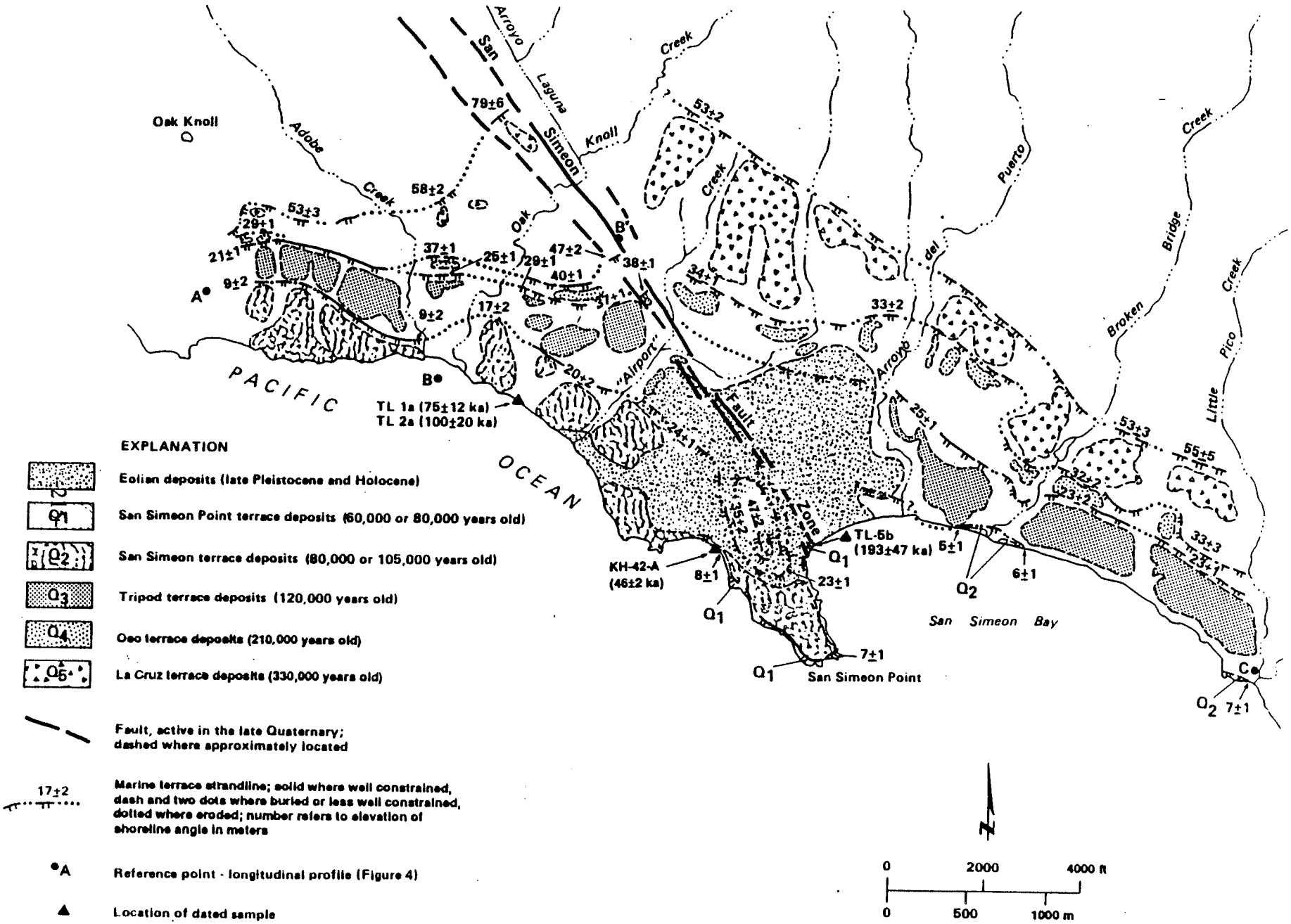
Oak Knoll
Adobe Creek
San Simeon Fault Zone
Arroyo Laguna
Oak Knoll Creek
Arroyo del Puerto
Broken Bridge Creek
Little Pico Creek
"Airport"
PACIFIC OCEAN
San Simeon Bay
San Simeon Point
TL 1a (75±12 ka)
TL 2a (100±20 ka)
KH-42-A (46±2 ka)
TL-5b (193±47 ka)
79±6
58±2
53±3
29±1
21±1
9±2
37±1
25±1
29±1
47±2
40±1
31±1
38±1
17±2
20±2
34±1
53±2
33±2
24±1
25±1
35±2
47±2
53±3
55±5
32±2
23±2
33±3
23±1
8±1
23±1
5±1
6±1
7±1
7±1
A
B
B'
C
Q1
Q2
EXPLANATION
Eolian deposits (late Pleistocene and Holocene)
San Simeon Point terrace deposits (60,000 or 80,000 years old)
San Simeon terrace deposits (80,000 or 105,000 years old)
Tripod terrace deposits (120,000 years old)
Oso terrace deposits (210,000 years old)
La Cruz terrace deposits (330,000 years old)
Fault, active in the late Quaternary; dashed where approximately located
Marine terrace strandline; solid where well constrained, dash and two dots where buried or less well constrained, dotted where eroded; number refers to elevation of shoreline angle in meters
Reference point - longitudinal profile (Figure 4)
Location of dated sample
0 2000 4000 ft
0 500 1000 m

Figure 3.

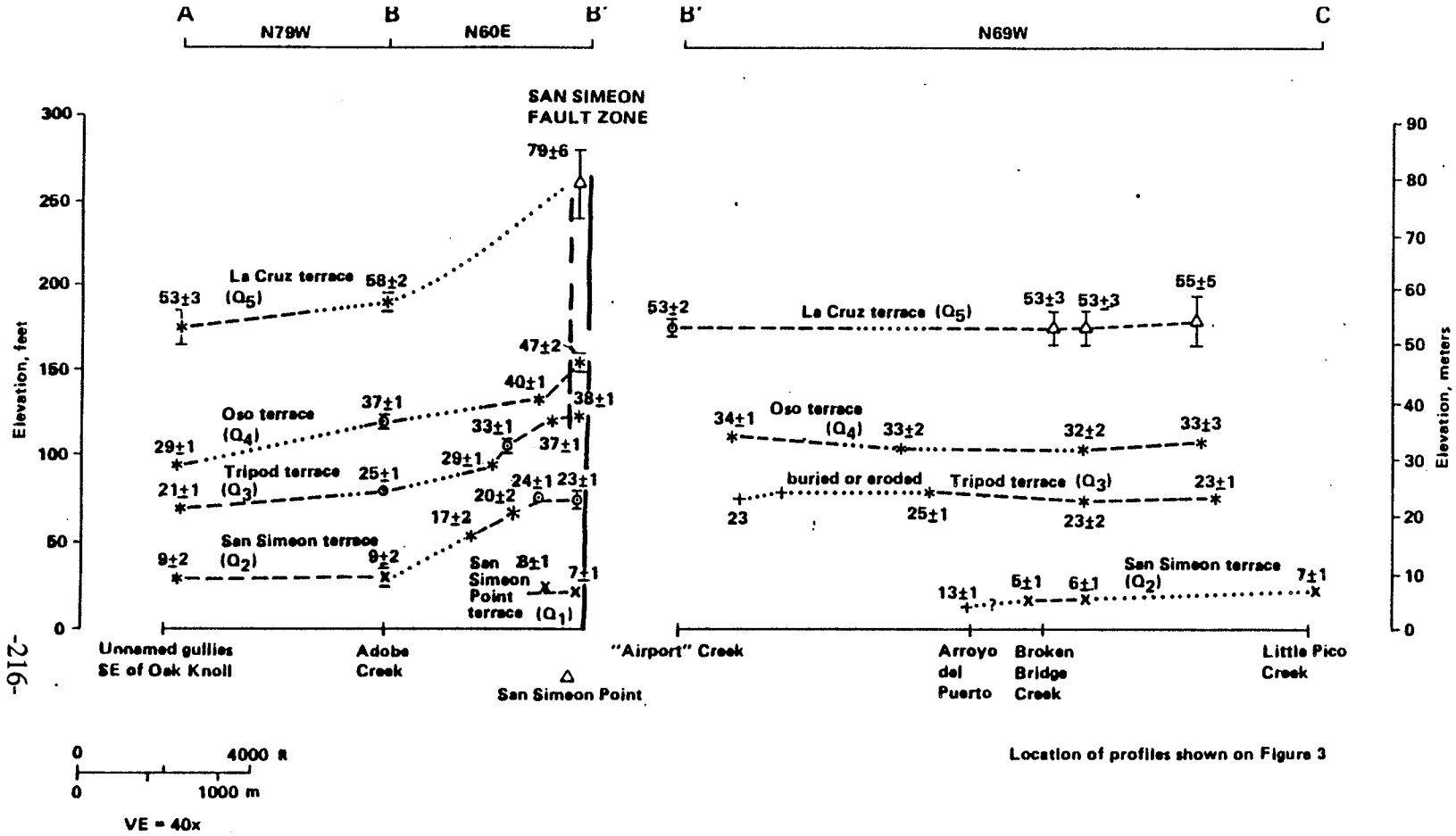

EXPLANATION

Lines

- ——— ⦣ with well exposed wave cut platform (WCP)
- - - - - ⦣ without well expressed wave cut platform
- ····· Eroded ⦣

General note: Error bars are shown except where symbol is larger than error.

Symbols

- ⦣ Shoreline angle
- x ⦣, elevation based on surveying of exposed ⦣ (meters)
- ⊙ ⦣; elevation based on drill hole projections (meters)
- * ⦣; elevation based on projection of surveyed wcp exposed in seacliff, stream cut or soil pit (meters)
- △ ⦣; elevation estimated from bedrock outcrops plotted on USGS 7.5' topographic quadrangle map (meters). Contour interval 40 feet
- + Elevation of bedrock surfaces (meters)

Figure 4.

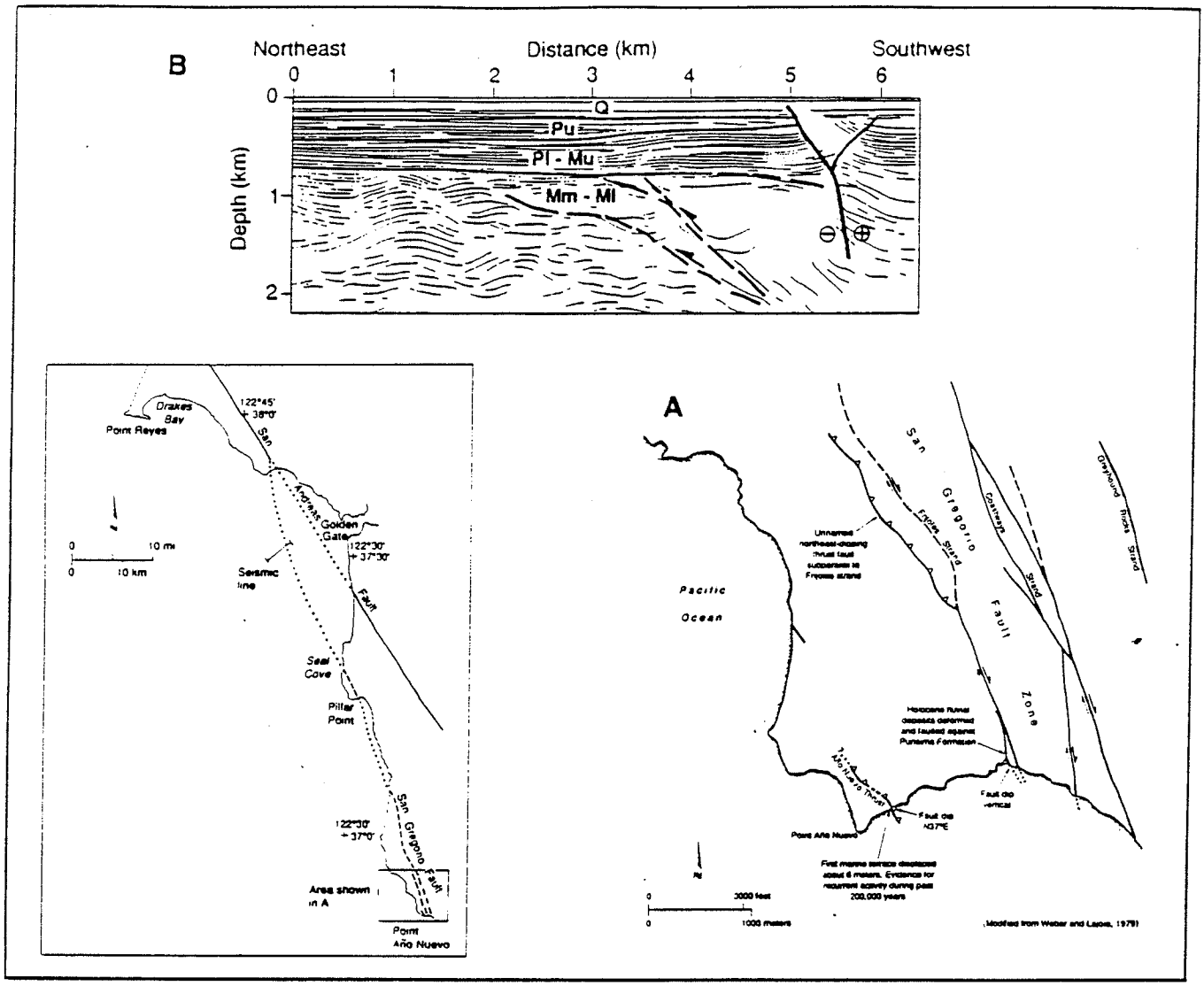
B
Northeast
Distance (km)
Southwest
0
1
2
3
4
5
6
Depth (km)
Q
Pu
Pl - Mu
Mm - Ml
Drakes Bay
Point Reyes
San Andreas
Golden Gate
Seismic line
Fault
Seal Cove
Pillar Point
San Gregorio Fault
Area shown in A
Point Año Nuevo
A
Pacific Ocean
San Gregorio Fault Zone
Greyhound Rocks Strip
Unnamed northeast-dipping thrust fault subparallel to Frijoles strand
Holocene fluvial deposits deformed and faulted against Purisima Formation
Fault dip vertical
Fault dip N37°E
Point Año Nuevo
First marine terrace displaced about 6 meters. Evidence for recurrent activity during past 200,000 years
3000 feet
1000 meters
(Modified from Weber and Lajoie, 1979)

Figure 5.

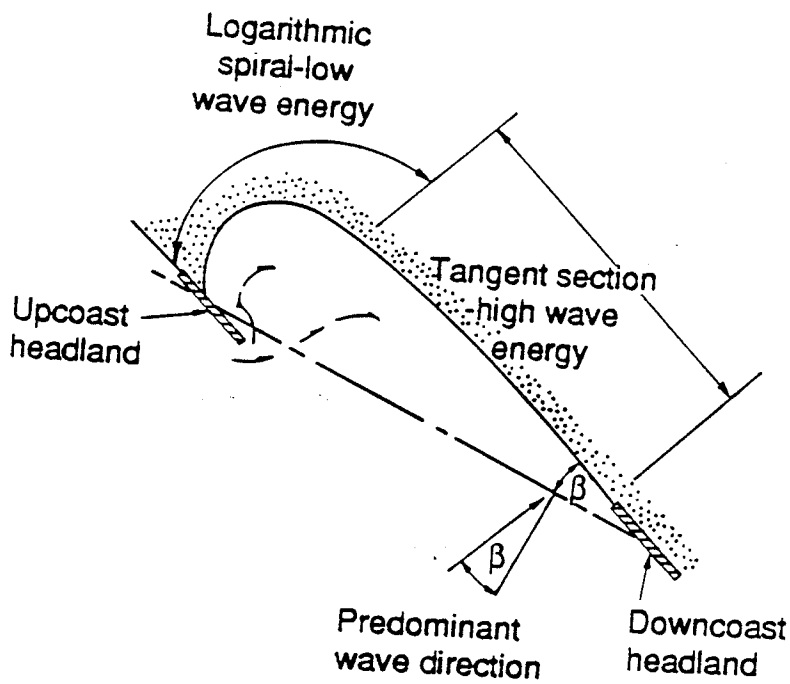

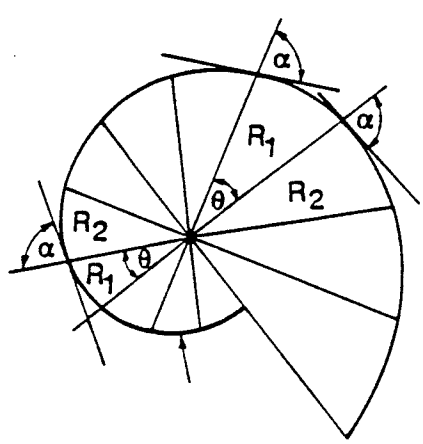

$$\frac{R_2}{R_1} = e^{\theta \cot \alpha}$$

Figure 6.

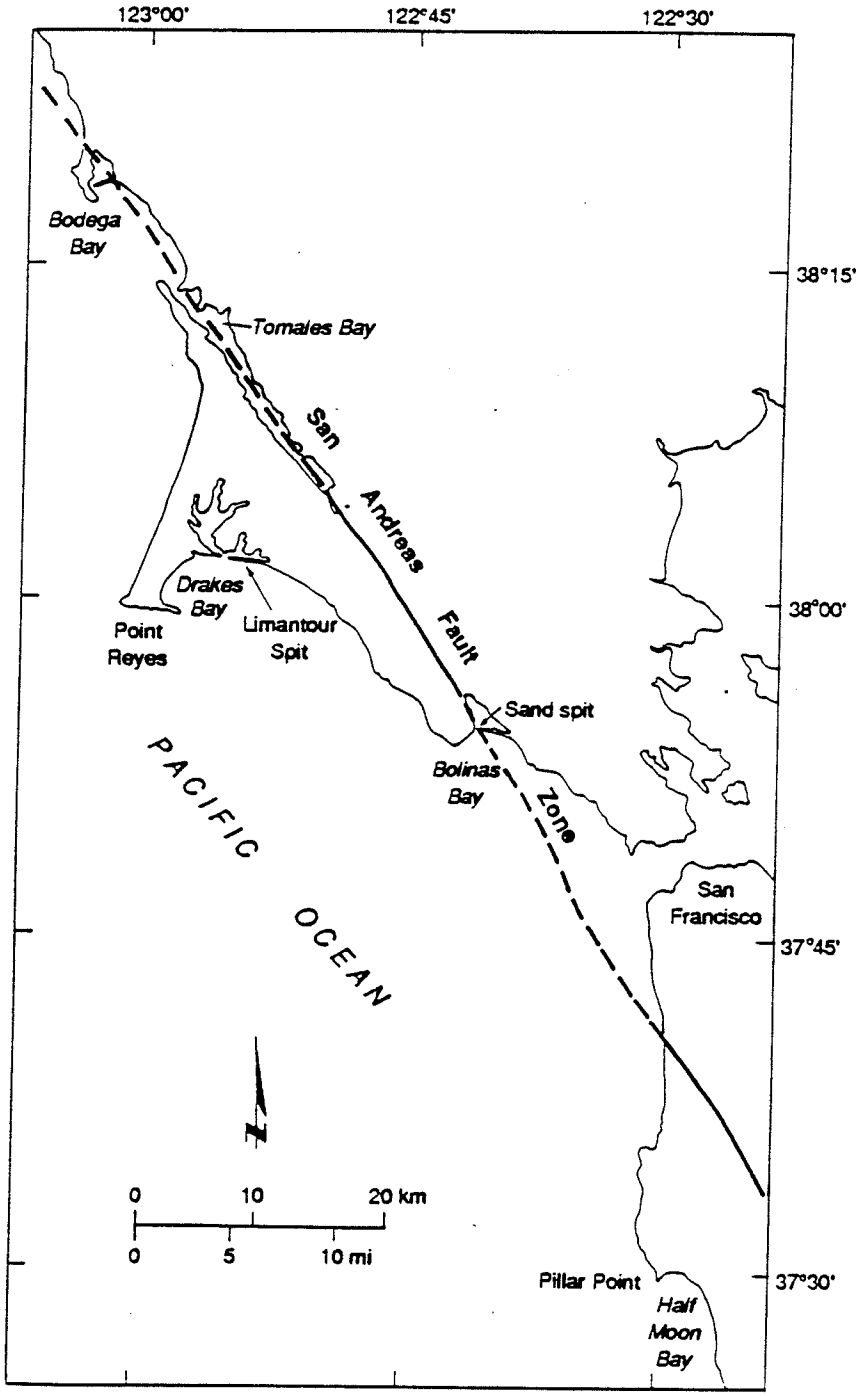
123°00'
122°45'
122°30'
38°15'
38°00'
37°45'
37°30'
Bodega Bay
Tomales Bay
San Andreas Fault Zone
Drakes Bay
Point Reyes
Limantour Spit
Sand spit
Bolinas Bay
PACIFIC OCEAN
San Francisco
Pillar Point
Half Moon Bay
N
0 10 20 km
0 5 10 mi

Figure 7.

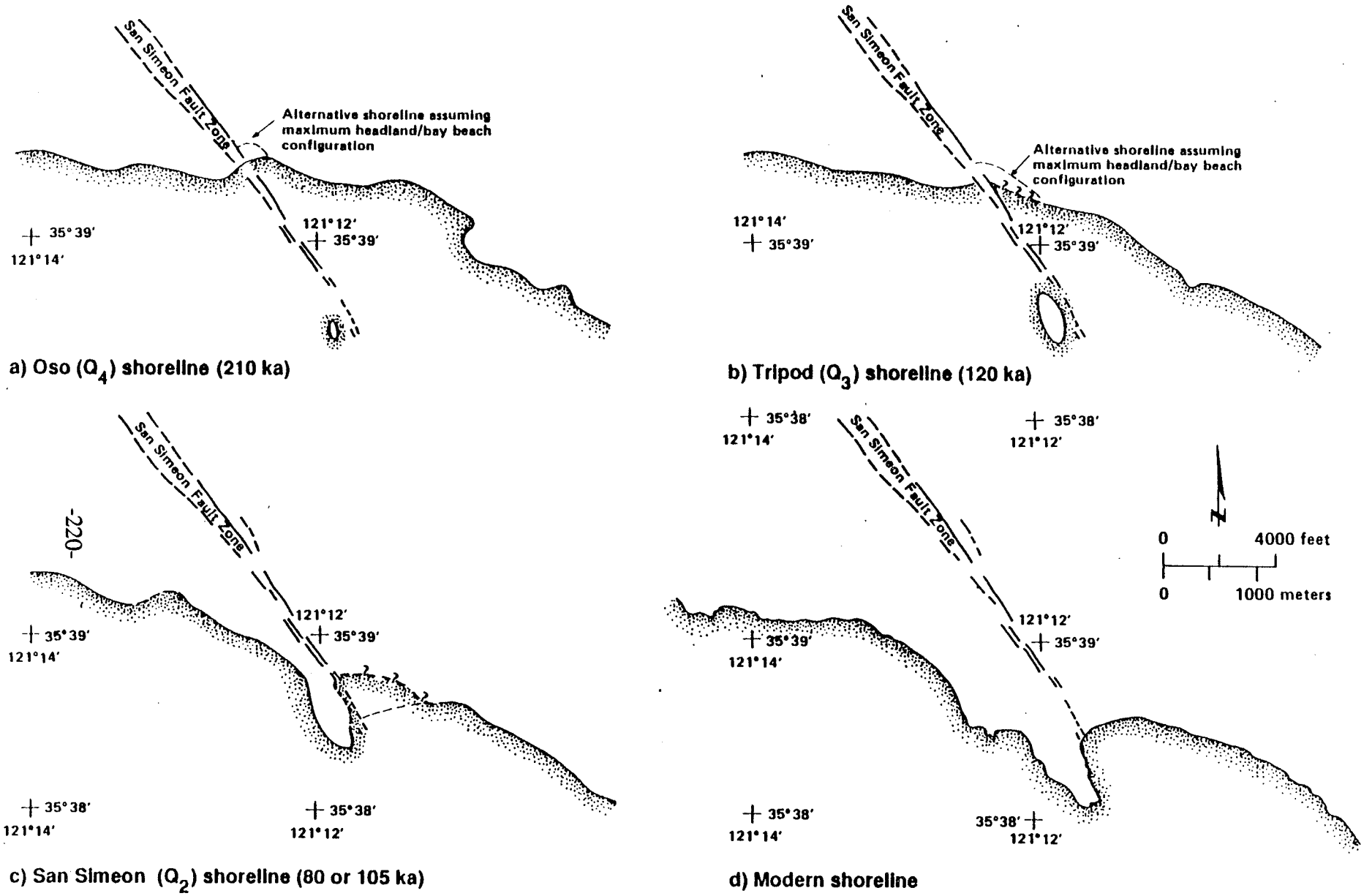
San Simeon Fault Zone
Alternative shoreline assuming maximum headland/bay beach configuration
35°39′
121°14′
121°12′
35°39′
a) Oso (Q_4) shoreline (210 ka)
San Simeon Fault Zone
Alternative shoreline assuming maximum headland/bay beach configuration
121°14′
35°39′
121°12′
35°39′
b) Tripod (Q_3) shoreline (120 ka)
San Simeon Fault Zone
121°12′
35°39′
35°39′
121°14′
35°38′
121°14′
35°38′
121°12′
c) San Simeon (Q_2) shoreline (80 or 105 ka)
35°38′
121°14′
35°38′
121°12′
San Simeon Fault Zone
N
0
4000 feet
0
1000 meters
121°12′
35°39′
35°39′
121°14′
35°38′
121°14′
35°38′
121°12′
d) Modern shoreline

Figure 8.

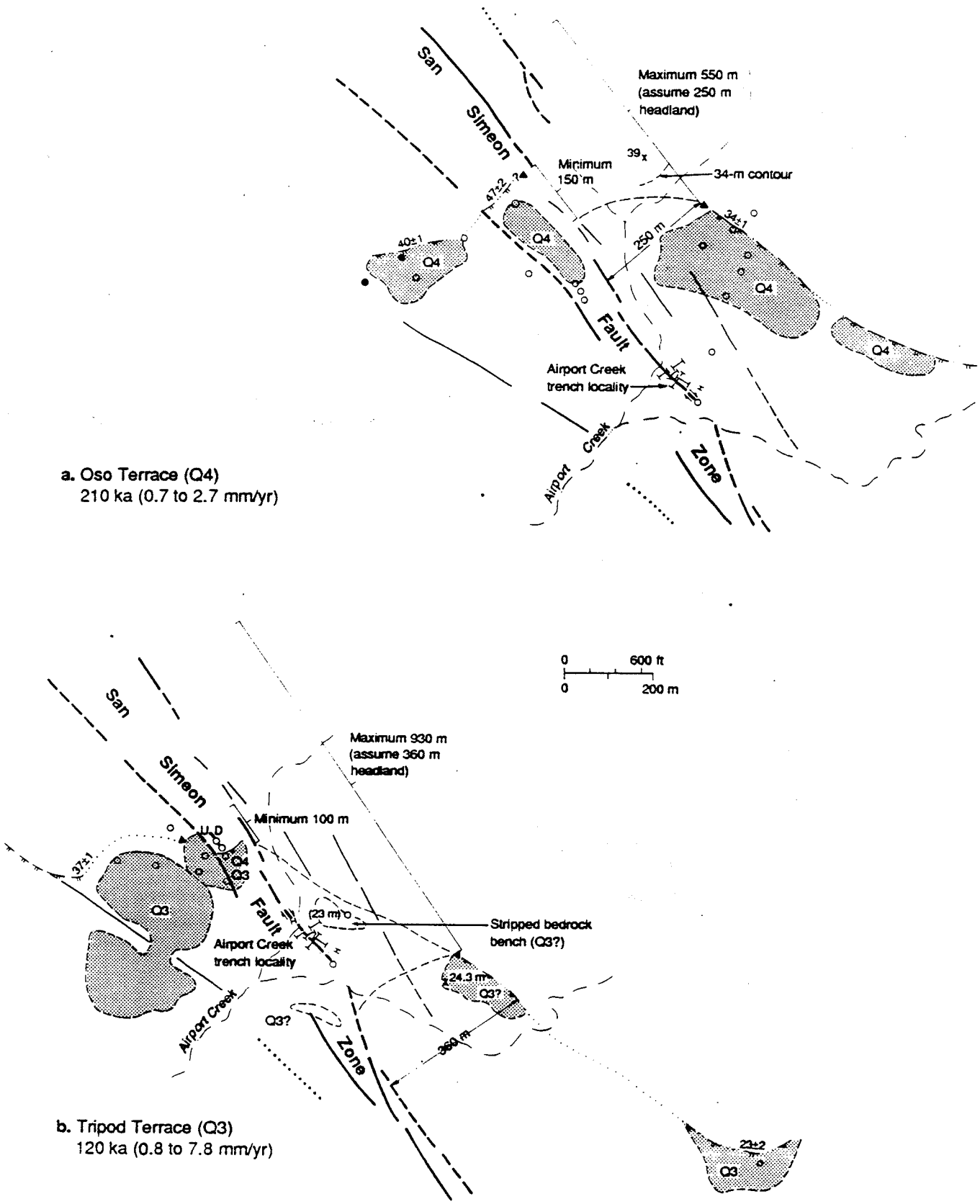

Figure 9. Estimates of late Pleistocene slip rates of the San Simeon fault zone based on offset marine terrace strandlines.

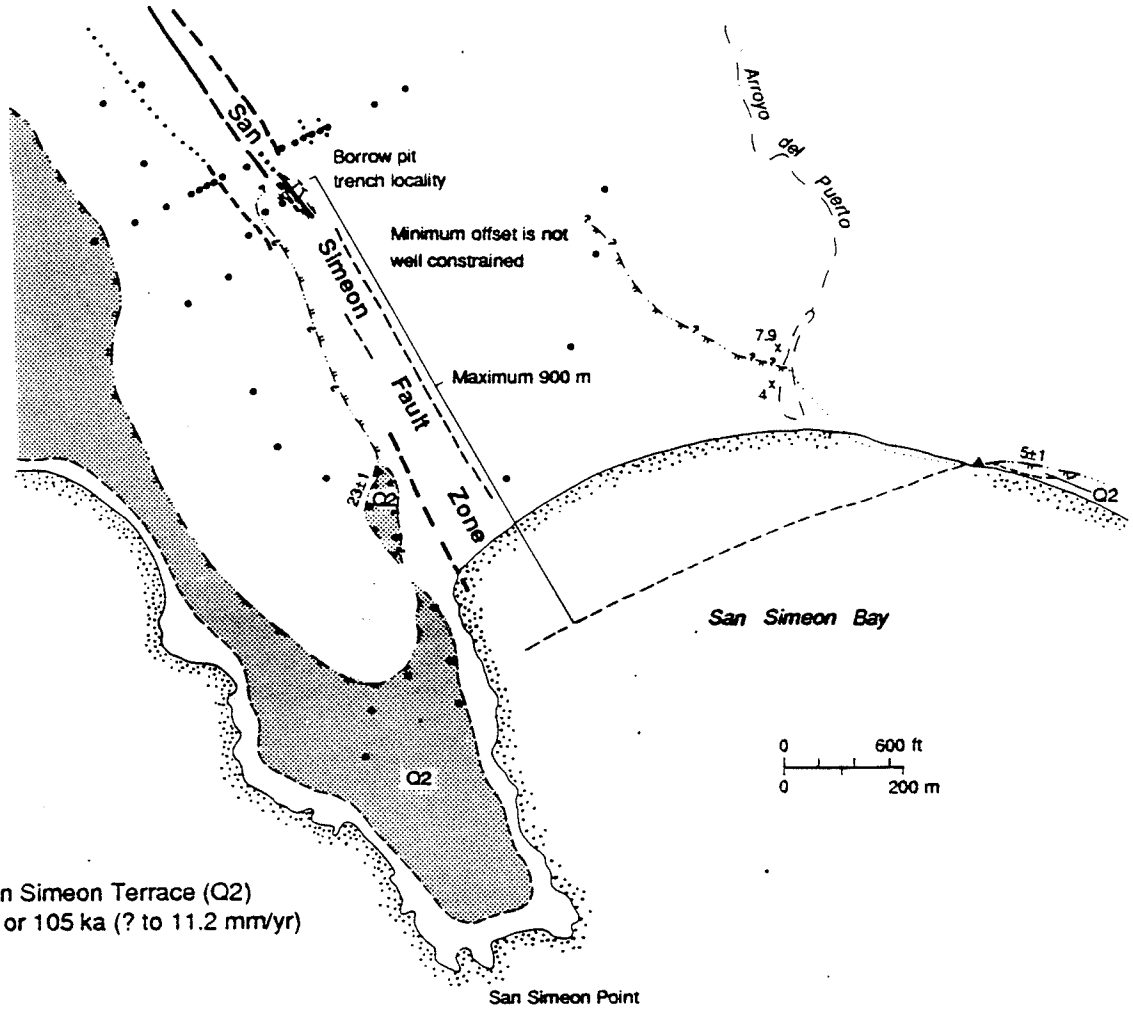

c. San Simeon Terrace (Q2)
80 or 105 ka (? to 11.2 mm/yr)

EXPLANATION

Late Pleistocene or Holocene fault; dashed where approximately located, dotted where inferred; arrows indicate relative sense of displacement

Lineament, dashed where less distinct

5±1 Strandline; solid where well constrained; double dot where buried or less well constrained, dotted where eroded; queried where uncertain; elevation of shoreline angle (meters); terrace remnants are indicated by stippled pattern

Postulated projections(s) of strandline

Exploration or soil test pit

Boring

Trench

4 Bedrock outcrop; elevation (meters)

See Plate 1 (Hanson and others, this volume) for detailed geologic map

Figure 9 (continued)

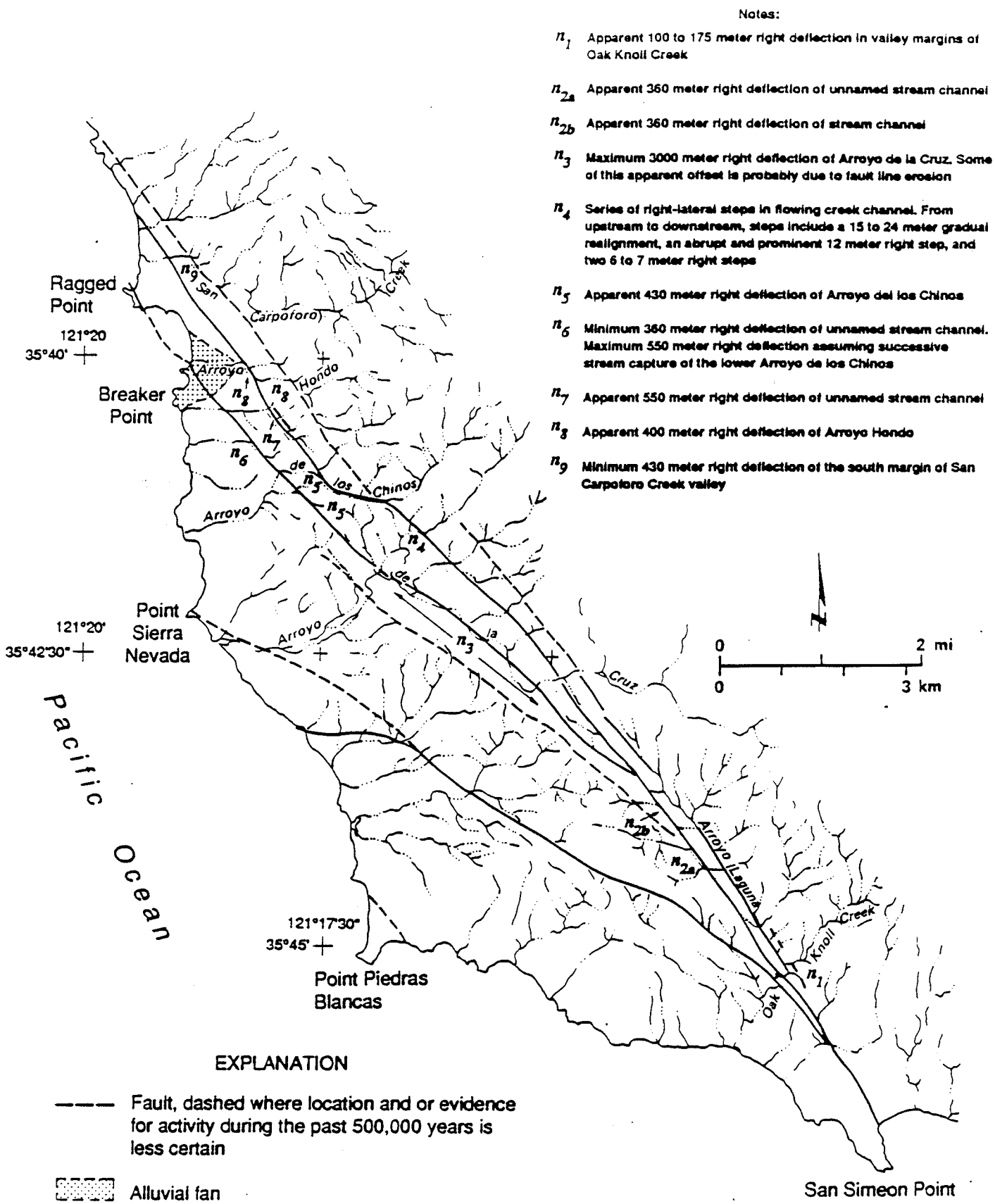

Figure 10. Map of drainage pattern in the San Simeon region showing possible stream deflections across traces of the San Simeon fault zone.

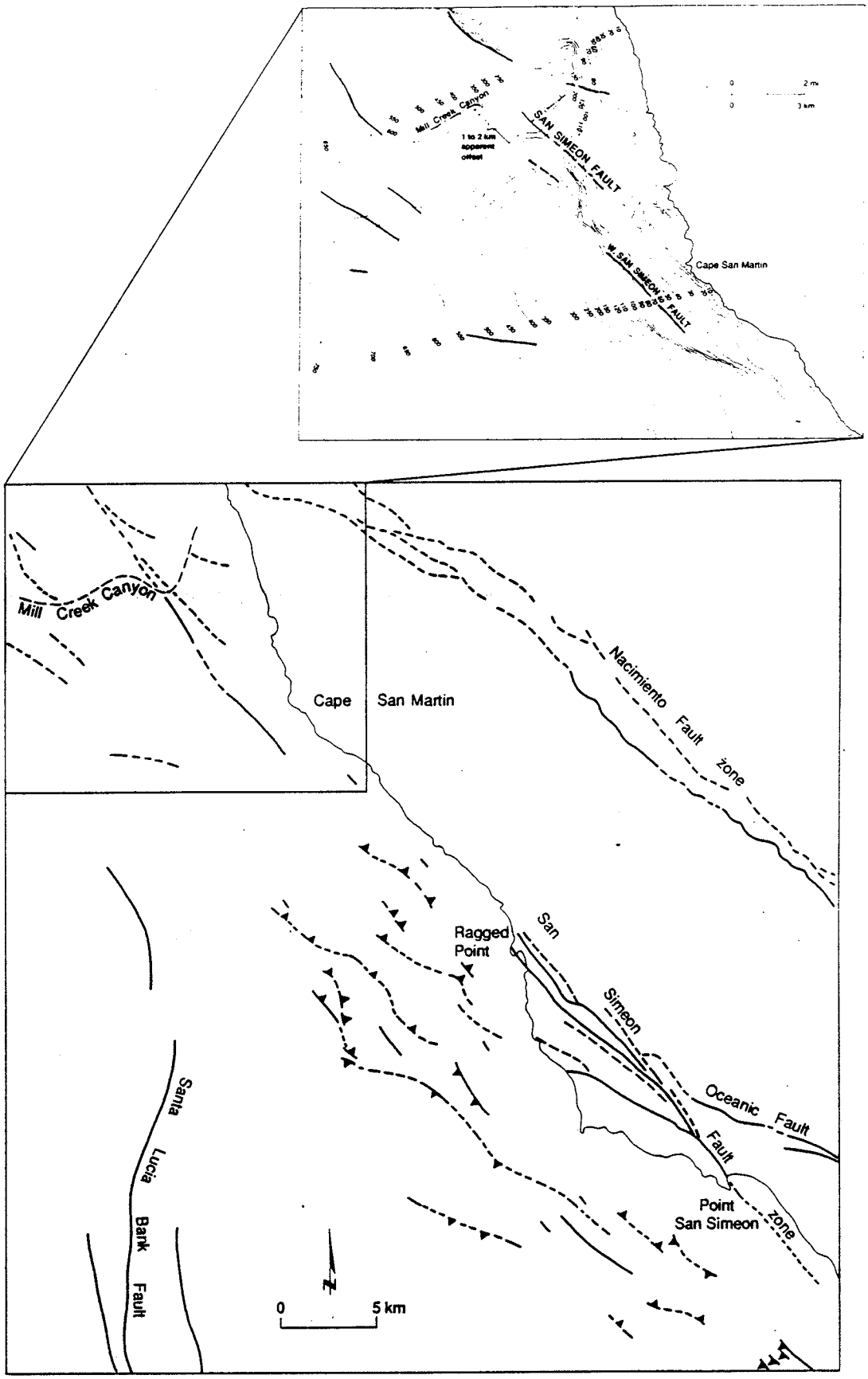

KEY

Fault; dashed where approximately located; teeth indicate dip direction of low angle fault

Figure 11. Map showing apparent right deflection of the Mill Creek submarine canyon across the San Simeon fault zone.

HOLOCENE BEHAVIOR OF THE SAN SIMEON FAULT ZONE, SOUTH-CENTRAL COASTAL CALIFORNIA

N. Timothy Hall
Geomatrix Consultants, Inc., San Francisco, California 94105

T. Dwight Hunt
Earth Sciences Associates, Palo Alto, California

and **Patrick R. Vaughan**
Rogers Johnson and Associates, Santa Cruz, California

ABSTRACT

Detailed geologic investigations that included mapping, geomorphic analysis, drilling, and logging of natural and trench wall exposures were performed to characterize the Holocene behavior of the southeastern onshore reach of the San Simeon fault near San Simeon, California. Our field investigations revealed that the San Simeon fault consists of two and possibly four or more major strands that define a southeast-tapering zone that is about 400 m wide at Oak Knoll Creek, narrowing to about 120 m at San Simeon Cove, 2.6 km to the south-east. Geologic and soils data from four sites within this fault reach show that the primary San Simeon fault traces are northwest-trending, vertical to near-vertical, right-slip faults that have subhorizontal striae and slickensides. The ratio of strike slip to dip slip on primary traces is ≥ 10:1 at the Borrow Pit site and about 8:1 to 10:1 at Airport Creek. These faults have undergone multiple slip events during the Holocene. We estimate a slip rate for the fault zone of 0.9 to 3.4 mm/yr, with a preferred value of 1.0 to 1.4 mm/yr. Because our studies are confined to one major strand within the fault zone, this estimate is likely a minimum value for the fault zone as a whole. Two fault strands, one at Oak Knoll Creek and the other at Airport Creek, yield net slip estimates of 1 to 2 m per event. Based on estimates of both slip rate and net slip per event, recurrence frequencies for the San Simeon fault are estimated to fall within the range of 265 to 2000 years, with preferred values between approximately 600 and 1800 years. Evidence at Airport Creek suggests that slip events have not occurred at uniform intervals.

INTRODUCTION

The San Simeon fault zone is a northwest-trending, predominantly strike-slip fault that trends subparallel to the central California coast. It is recognized from near Lopez Point on the north to Point Estero on the south, for a distance of 97 km. The fault extends onshore for about 20 km, from near Ragged Point to San Simeon Point (Fig. 1A). This paper presents results of detailed geologic mapping and logging of natural and trench wall exposures to evaluate the Holocene behavior of the San Simeon fault zone. Quaternary slip rates for the San Simeon fault based on offset marine terraces and stream channels in this same area are

presented in a companion paper by Hanson and Lettis (this volume).

The onshore reach of the San Simeon fault zone is structurally complex, consisting of several branching and anastomosing faults (Fig. 1B). The onshore reach of the fault was mapped by Taliaferro (1943), who referred to it as the Arroyo Laguna thrust zone; by Earth Sciences Associates (1974, 1975); by Hall (1976); and by Hall and others (1979). The name San Simeon fault was assigned by Earth Sciences Associates (1974); the Arroyo del Oso fault, a prominent westward splay, was named by Hall (1976). Our field investigation identified three primary fault traces, the eastern and western traces of the San Simeon fault and a prominent westward splay, the Arroyo del Oso fault (Fig. 1B). Regional mapping by Hall and others (1979) and local detailed mapping conducted during this study indicate that faults within the San Simeon fault zone bound and tectonically dismember an imbricated zone of ophioilitic rocks within a terrain of Franciscan Complex rocks. Within and to the southwest of the fault zone, the ophiolite and Franciscan units are, in part, overlain by or in fault contact with Tertiary marine sedimentary rocks of the Lospe, Rincon, Point Sal, Monterey, and Careaga formations. Correlative Tertiary rocks in the San Simeon area are absent northeast of the fault zone. Bedrock here consists almost entirely of Franciscan Complex units containing local pods of other Mesozoic basement rocks. Bedrock in the San Simeon region is overlain by marine terrace deposits, alluvium, and dunes of Quaternary age (Fig. 1A).

Within the past decade and a half, several investigators have focused on the activity of the San Simeon fault. Envicom Corporation (1977) performed detailed mapping and exploratory work that included trenching and magnetometer surveys of the southeastern half of the onshore reach of the fault zone. Weber (1983) mapped the Pleistocene marine terraces in detail and tentatively correlated individual terrace surfaces across various strands within the San Simeon fault zone. Using age estimates of the various faulted terraces and the fault-related geomorphic features along individual segments, Weber (1983) classified each fault as "recently active and late Pleistocene," "early to middle Pleistocene," or "pre-Pleistocene." Weber and others (1981) and Weber (1983) noted less than 0.3 m of apparent normal fault separation in weakly cemented dune sands estimated to be 5000 to 15,000 years old on a major strand of the San Simeon fault exposed in the sea cliff at San Simeon Bay. Manson (1985) reviewed previous geologic investigations of the fault zone, examined air photos, and made field observations to evaluate which, if any, fault segments met the criteria of "sufficiently active and well defined" to be zoned by the California State Geologist under the Alquist-Priolo Special Studies Zones Act (see Hart, 1985). Manson (1985) found geomorphic features suggestive of recent right-lateral displacement along two major components of the southern onshore reach of the fault zone. He concluded that they meet the criteria for Alquist-Priolo zoning. The Holocene traces of the San Simeon fault between Arroyo de la Cruz and San Simeon Bay and an eastern strand that is partly coincident with Arroyo Laguna (the Arroyo Laguna fault of Hall, 1976) between Oak Knoll Creek and San Simeon Bay were shown on an Official Map of Special Studies Zones, San Simeon quadrangle, by the California Division of Mines and Geology (1986).

Onshore, the San Simeon fault zone lies within a broad coastal region of rolling

uplands and benchlands dominated by a flight of elevated Pleistocene marine terraces. Hanson and Lettis (this volume), who mapped these terraces in detail, estimated fault slip rates based on the present locations of elevated and deformed strandlines. In addition to offset terrace strandlines, the fault zone is well expressed geomorphically by a series of linear stream drainages, springs, linear scarps and ridges, sidehill benches and swales, deflected stream channels and stream valleys, vegetation and tonal lineaments, and anomalous drainage patterns that include captured and beheaded streams, underfit stream valleys, and ponded alluvium. These geomorphic features and bedrock mapping reveal that the San Simeon fault zone is about 120 m wide at San Simeon Cove, widening to the northwest through the development of successive splays that trend more westerly than the N35°W strike of the primary east boundary trace of the zone (Fig. 1B). Based on geomorphic expression and trenching, at least two and possibly four major strands define a zone that is approximately 400 m wide at Oak Knoll Creek, which lies 2.6 km northwest of San Simeon Cove.

Because of the complexity of the onshore reach of the San Simeon fault zone, we concentrated our field investigations along the narrower, better-constrained southern part of the onshore zone between San Simeon Cove and Oak Knoll Creek. Our studies included identification and characterization of fault traces by interpretation of aerial photographs, detailed mapping of bedrock and Quaternary deposits, logging of natural exposures, trenching and drilling, and analysis of shallow seismic refraction profiles. The southern onshore reach of the fault zone is buried by colluvium, extensive thick dune sand, and stream terrace deposits. The most recently active strands are expressed as discontinuous linear vegetation and tonal contrasts in the dune areas, by linear bedrock ridges, and by springs and boggy areas. To evaluate the origin of the geomorphic features and to assess fault geometry and behavior, we logged natural exposures and trench excavations at four localities along this reach of the fault zone: the San Simeon Cove, Borrow Pit, Airport Creek, and Oak Knoll Creek sites (Fig. 2). Data from the four sites are summarized and interpreted below.

SAN SIMEON COVE

The San Simeon fault zone intersects the coastline at a cove in the northwestern corner of San Simeon Bay (Fig. 2). San Simeon Bay is separated from the Pacific Ocean by San Simeon Point, a headland that, on the southwestern side of the fault, is composed of resistant beds of the Monterey Formation. Based on available sea cliff exposures and limited hand excavations, we interpret the fault zone to enclose a fossiliferous, pebbly, shallow marine sandstone that Hall (1976) tentatively correlated with the Careaga Formation of Pliocene and Pleistocene age in the onshore Santa Maria basin (Fig. 3). Detailed logging of these exposures documents that to the west the fossiliferous beds are in fault contact with sheared and contorted chert and diatomaceous shale of the Monterey Formation. Both the Careaga and the Monterey formations are beveled by the wave-cut platform of the San Simeon Point marine terrace (terrace Q_1 of Hanson and Lettis, this volume), which they estimate to be 60,000 or 80,000 years old (marine oxygen isotope stages 3 or 5a, respectively). This abrasion platform is about 2.5 m higher on the more resistant southwestern side of the fault, strongly suggesting late Quaternary

activity on the western margin of the fault zone. Because thick colluvium derived from overlying dune sand obscures the fault near the base of the sea cliff, we did not observe this fault directly. Weber (1983) reports that this fault and another that cuts the Careaga beds both displace "bedding-like" structures (probably lamellar B horizons) within the overlying late Pleistocene-Holocene dune sand. According to Weber (1983) and Weber and others (1981), these small faults trend to the northwest, dip 60+° northeast, and have apparent normal separation.

Faults are visible on either side of a small prominence composed of Careaga Formation exposed at San Simeon Cove (Fig. 3). On the southwest side of the prominence, branching and anastomosing cemented shears cut the Careaga Formation but not the overlying marine terrace platform. The most prominent of these shears strikes N28°W and dips 53° NE. On the northeast side of this prominence, Careaga beds are overlain by tilted estuarine deposits that show a thermoluminesence age of 197,000 ± 48,000 years (Table 1). Here, the Careaga Formation, the estuarine beds, the overlying San Simeon Point terrace platform, and the basal marine terrace deposits are cut by a small fault. A distinctive oxidized sandy layer within the basal marine terrace deposits exhibits a vertical separation of 7.6 mm across this fault, indicating minor slip in the late Quaternary.

East of the prominence, the Careaga Formation probably is faulted against rocks of the Franciscan Complex, which outcrop at the mouth of Arroyo del Puerto Creek (Fig. 1B), but this contact is not exposed along San Simeon Beach (Fig. 3). This fault, which may be exposed at the Borrow Pit site to the northwest, will be described in the following section. Pleistocene activity on this eastern trace is indicated by probable displacement of the marine terrace Q_1 wave-cut platform that is developed across the top of the Careaga Formation and by displacement of the Q_2 or Q_3 terrace of Hanson and Lettis (this volume) that is developed across Franciscan rocks at the Borrow Pit site. The San Simeon Point terrace platform steps down an undetermined amount to the east across this poorly located fault trace. The platform is not visible along San Simeon Beach south and east of the outcrop of Careaga Formation, suggesting that (1) the terrace is obscured by dune sand and/or colluvium; (2) fluvial incision during the late Pleistocene sea-level lowstand (marine oxygen isotope stage 2) destroyed the Q_1 terrace locally; and/or (3) the rate of uplift northeast of the San Simeon fault zone was not great enough to elevate and preserve this terrace above sea level.

The San Simeon fault zone extends offshore to the southeast from the sea cliff exposure into San Simeon Bay (Fig. 2). Rock samples collected by a diver-geologist show that on the floor of San Simeon Bay, Monterey Formation and Franciscan Complex rocks are separated by a strip of sandy bottom, perhaps developed on a less-resistant fault slice of the Careaga Formation or perhaps along a submerged fluvial channel. The distribution of submarine rock outcrops indicates that the approximate N35°W trend of the San Simeon fault zone observed onshore extends offshore for at least 2 km southeast of San Simeon Point.

BORROW PIT SITE

During the initial phases of mapping, we discovered that a major eastern strand of the San Simeon fault zone was partially exposed

in a small excavation for sand. The excavation, informally named the Borrow Pit site, is about 600 m northwest of San Simeon Bay (Fig. 2) within an eolian dune complex that covers late Pleistocene marine terraces. The trace exposed at this site is characterized by a clay-rich zone of fault gouge as much as 1.5 m wide. Locally it contains exotic boulders and cobbles derived from Franciscan Complex rocks and from deeply weathered basal marine terrace deposits. Shears and clay gouge within unconsolidated to moderately consolidated late Pleistocene or younger dune sand indicated that this site might contain a decipherable late Quaternary paleoseismic record.

We excavated five trenches at the Borrow Pit site (Fig. 4), four of which exposed a marine terrace platform interpreted to be about 80,000 or 120,000 years old (terrace Q_2 or Q_3 of Hanson and others, this volume). These trenches revealed one major fault and possibly a second zone of faulting, both of which exhibit apparent down-on-the-west displacement of the late Pleistocene dune sand against rocks of the Franciscan Complex. Trenches T-1, T-2, and T-3 intersected a fault we informally named the eastern Borrow Pit fault (Fig. 5). This fault is marked by a prominent vertical to subvertical sheet of gouge that separates dune sand on the west from marine terrace deposits overlying the wave-cut platform and from the underlying Franciscan bedrock on the east. At the deepest levels of exposure in trenches T-1 and T-2, the strike and dip of the fault are N36°W, 81°SW and N39°W, 87°SW, respectively. Prominent slickensides on the fault plane plunge 4° to 6° southeast.

Trench T-3, which is outside the excavated area of the Borrow Pit, has an unmodified section of dune sand above a wave-cut platform that bevels Franciscan greenstone. Here strike of the eastern Borrow Pit fault shifts clockwise from N36°W at the base of the trench to N22°W in the dune sand near the surface (Fig. 5). This upward clockwise rotation of strike, coupled with well-developed subhorizontal slickensides and grooves on the fault plane that plunge 2° to 5° southeast, confirm that its most recent activity was essentially pure dextral slip. Late Quaternary and possibly Holocene activity on the eastern Borrow Pit fault exposed in trench T-3 is suggested by (1) faulting within the dune sand; (2) a thickened zone of topsoil developed on the fault trace, which may be indicative of eluviation promoted by recent ground disturbance; and (3) the apparent down-on-the-west vertical separation of the base of the topsoil (A, AB, and E horizons) and the base of the Bt horizon across the fault (Fig. 5).

Geologic relationships exposed in trenches T-2, T-2A, and T-4 indicate that another, more westerly fault trace, also with down-on-the-west vertical separation, may exist within the San Simeon fault zone (Fig. 5). Although we did not locate the fault surface, we informally call this the western Borrow Pit fault. In trench T-2, saturated Franciscan siltstone is exposed at an estimated depth of 7 m below the original ground surface. This siltstone cannot be traced west of a small failure in the trench wall. To the west are fractured, weakly consolidated clayey sands that have locally dislocated lamellar B horizons. These minor breaks could be tectonic, or they could be the result of former slope failures or differential compaction. A hand-auger hole excavated in the bottom of trench T-2A encountered dry silt and silty sand to a depth of approximately 13 m below the original

ground surface. Although the absence of Franciscan Complex rocks to the west might be explained by an erosional feature such as a buried surge channel or a fluvial channel developed along the San Simeon fault zone, the lack of both groundwater and Franciscan bedrock in this hole strongly suggests that a fault exists between trenches T-2 and T-2A. Flight-auger data described below also support the existence of a fault west of trench T-2.

Flight-auger data from the downthrown western block indicate that the dune sand overlies fossiliferous marine sands and that Franciscan Complex rocks, if present, must be at least 40 m below the ground surface. Borehole DH-21, which is located 10 m southwest of trench T-2A, encountered fossiliferous marine sands 4.5 m below the elevation of the bottom of the hand-auger hole (Figs. 4 and 6). We tentatively have correlated these sands with the Careaga Formation, which is exposed 0.6 km away at San Simeon Bay. We are reasonably confident that these marine fossils are from the Careaga Formation and not from marine terraces, because the fossil materials from the drill holes represent no living species.[1] Additionally, no marine invertebrate fossils have been observed in any marine terrace deposits in the San Simeon region despite extensive mapping by Weber (1983) and by Hanson and others (this volume).

A cross section through Borrow Pit trenches T-2 and T-2A illustrates their stratigraphic relationships (Figure 6, section B-B'). Section A-A' on this figure is drawn perpendicular to the trend of the San Simeon fault zone and approximately 120 m northwest of the Borrow Pit site. This section, which synthesizes mapping, trenching, drilling, and shallow seismic refraction data, shows a complex fault zone approximately 180 m wide that contains at least six strands. Apparent vertical separations across these strands are both down-on-the-east and down-on-the west. Consequently, trenches at the Borrow Pit site exposed only a fraction of the San Simeon fault zone to direct observation.

The two fault traces at the Borrow Pit site may correspond to the inferred eastern fault at San Simeon Cove that separates Careaga Formation on the west from Franciscan Complex rocks on the east. Stratigraphic relationships exposed in the cliff at San Simeon Cove (Fig. 3) and the findingssummarized in cross sections A-A' and B-B' (Fig. 6) indicate that beds of the Careaga Formation occupy a fault slice between a block of Monterey Formation on the west and Franciscan Complex rocks on the east. The borehole data also indicate that the base of the Careaga Formation in the fault slice rises to the northwest, a structural relationship consistent with the observed southeast-plunging slickensides on a dextral fault. The down-on-the-west vertical separations observed on the Borrow Pit faults, however, are inconsistent with the plunge of the slickensides. This discrepancy might be explained by various processes, including "scissoring" of vertical slip components within the fault zone, a recent change in the style of slip on the fault, former differential erosion along the fault zone, or juxtaposing blocks that have experienced different amounts of erosion.

Trenching and drilling at the Borrow Pit site confirmed that (1) the San Simeon fault zone consists of multiple splays that manifest both down-on-the-east and down-on-the-west apparent vertical separations; (2) the most recent activity on one major strand, the eastern Borrow Pit fault, was essentially pure right slip; (3) this faulting cuts dune

sand of late Pleistocene age; and (4) this faulting also disrupts the topsoil developed on the dune sand, indicating activity during the Holocene.

AIRPORT CREEK SITE

The Airport Creek site is located within the San Simeon fault zone about 900 m northwest of the Borrow Pit site (Fig. 2). Two geomorphic features indicate possible Holocene faulting at the site: a local 1.8 m right deflection of the Airport Creek channel margins, and a subtle topographic trough bounded by low scarps in unconsolidated materials on the southeast side of the creek (Fig. 7). Based on this surface evidence and on trenches excavated by Envicom (1977) that show deformed terrace deposits, we excavated seven trenches and two exploratory pits (one of which is outside the limits of Figure 7) at the site to evaluate the faulting that occurred during the late Pleistocene and Holocene. Four of the trenches, T-1, T-2, T-4, and T-5, crossed a major trace of the San Simeon fault that has apparent down-on-the-east vertical separation. Simplified logs of these four trenches plus trench T-3 are presented in Figure 8, a detailed log of T-1 is presented in Plate 1.[2] The discussions that follow focus on the distribution of Quaternary deposits at the Airport Creek site, on the record of faulting preserved in these deposits, and on the inferences that can be drawn from the right-laterally deflected channel of Airport Creek. This information will be used to estimate slip rate, slip per event, and recurrence frequency for ground-rupturing earthquakes on the San Simeon fault.

Stratigraphy

For simplification, we have grouped the earth materials exposed in the Airport Creek trenches into three categories--Quaternary units, shear-zone units, and bedrock units (Fig. 8). Oldest are the bedrock units of presumed Mesozoic age. These include deeply weathered and sheared siltstone exposed west of the faults in trenches T-1, T-2, and T-5. Based on the lithologic descriptions provided in Hall and others (1979), this siltstone may be part of the unnamed shale of Upper Jurassic age, the Toro Formation of Upper Jurassic and Lower Cretaceous age, or the Franciscan Complex. North of Airport Creek, Franciscan greenstone is exposed west of the fault in trench T-4. East of the fault, bedrock was exposed only in trench T-3, where it consists of sheared interbedded siltstone and sandstone of unknown, but possibly Franciscan, affinities.

Next oldest are the highly deformed materials in the shear zones. These materials include clay-rich fault gouge (resembling Franciscan melange matrix) and highly deformed, older fluvial units. The deformed fluvial units probably represent deposits of various ages. Fluvial gravels exposed in trench T-4, for example, contain abundant ultramafic clasts. Based on descriptions by Hall and others (1979), we tentatively correlate these gravels with the Lospe Formation of Oligocene age. Highly deformed fluvial sediments observed adjacent to faults and within shear zones in the other Airport Creek trenches appear to be much younger, however.

The third major category includes alluvium, colluvium, marine terrace deposits, and soils of Quaternary age. The presumed oldest sediments within this category are marine terrace deposits observed in the southwestern parts of trenches T-2 and T-5, where they cap both bedrock and shear-zone units (Fig. 8). These deposits consist mostly of

deeply weathered sands that overlie gravelly sands containing scattered pholad-bored cobbles along the contact with bedrock. This stratigraphic sequence may represent basal marine terrace deposits that subsequently were buried by dune sand. This unit may have been reworked in part; it is sheared and deformed extensively near the faults. Older alluvium of late Pleistocene age, which is the next younger of the Quaternary units, consists predominantly of coarse-grained fluvial deposits (sands and gravels) that are exposed in trenches T-2, T-3, T-6, and T-7 (Figs. 8 and 9). Radiocarbon ages from these deposits generally range from about 25,000 to 35,000 years B.P. (samples ^{14}C-4, -22, and -25, Table 1). Younger alluvium of Holocene age consists of clay, silt, and silty sand deposited by Airport Creek that disconformably overlie the late Pleistocene alluvium. This unconformity shows clearly in trench T-6 (Fig. 9). The younger alluvium, which was recognized in all but trench T-7, appears to have been partially ponded against the elevated western block of the fault. Radiocarbon ages of 9000 to 11,000 years B.P. (samples ^{14}C-1, -2, -3, -8, and -10, Table 1) indicate that the young alluvium was deposited during a time of rising sea level after the late Wisconsinan lowstand, which began approximately 18,000 to 20,000 years ago. The youngest Quaternary unit consists of the topsoil developed across the Airport Creek site.

Sheared gravelly clays that are cut by the fan of northeast-verging shears in the upper part of trench T-2 yielded a radiocarbon age of 13,790 $\pm$ 260 years B.P. (sample ^{14}C-9, Table 1). We correlate this deposit with the deformed clayey gravels that mantle the shear-zone units west of the primary fault in trench T-5. Because these two deposits are bounded by faults, their assignment to either the older or the younger alluvium is speculative. They are lithologically similar to the sheared gravelly clay of probable fluvial origin located at the base of trench T-5 in a zone of minor faulting east of the primary fault. This latter deposit gave a radiocarbon age of 10,670 $\pm$ 260 years B.P. (sample ^{14}C-10, Table 1). We therefore tentatively assign these three deposits to the younger alluvial unit that was deposited by Airport Creek.

Style of Faulting

The faulting exposed in Airport Creek trenches T-1, T-2, T-4, and T-5 consists of two or three distinct strands that occur within 9- to 12-m-wide zones of highly sheared materials (Fig. 8). In trenches T-1, T-2, and T-5, at least one fault strand cuts the base of the topsoil (A horizon), demonstrating Holocene activity on the San Simeon fault. We believe that the strand indicated by the heavy dashes on Figure 8 is the primary fault exposed at the Airport Creek site. Note that the apparent vertical separation on this fault is down-on-the-east, which is consistent with southeast-plunging grooves and striae. If this fault is continuous along trend to the southeast, it probably is one of the traces located east of the crest of the hill at the Borrow Pit site (section A-A', Fig. 6). The western fault exposed in trenches T-1, T-2, T-4, and T-5 separates bedrock on the west from the zone of shearing on the east. This fault clearly is associated with a minor apparent down-on-the-west step at the top of the Bt horizon in trench T-5, where bedrock is essentially at the surface, but it cannot be traced to the surface through sediments of late Pleistocene or Holocene age in the other three trenches. We attribute the apparent down-on-the-west separation across the western fault in trench T-5 to differential weathering of the parent materials.

The structural expression of the youngest faulting varies greatly from trench to trench, ranging from a nearly horizonal single trace in trench T-4 and a nearly vertical single trace in trench T-1, to multiple west-dipping traces in trenches T-2 and T-5. Except for the vertical fault of trench T-1, the apparent sense of slip on faults in the Airport Creek trenches, as determined by stratigraphic separations, is up toward the northeast, perhaps reflecting a local component of compression across the San Simeon fault. However, because the relationship between fault dip and slope steepness is consistent on the west side of the fault, and because striae having a high angle of rake were not observed in trench exposures of the fault surface, the observed northeast vergence may partly reflect gravitational creep. The strike of the fault also varies, ranging from N25°W to N41°W. Grooves and striae on the primary fault plane plunge 2° to 11° southeast, indicating that the most recent movement was predominantly strike slip.

Slip Per Event

After the younger alluvial unit was deposited, Airport Creek downcut 3 to 4.5 m into these early Holocene deposits, creating a well-preserved, paired fluvial terrace. We estimate the age of this surface to fall within the range of 5000 to 7725 years (see discussion below). The steep walls of this incised channel are right-laterally deflected 1.8 m where they cross the active fault. The inset on Figure 7 shows details of the right-deflected active channel of Airport Creek between trenches T-1 and T-4. Although the creek changes direction near the fault, both channel walls display a consistent 1.8 m of right-lateral displacement. Examination of the steep channel walls and logging of the fault exposed in the southeastern wall indicate that the channel deflection is of tectonic origin and not caused by differences in erodability of materials on opposite sides of the fault. We believe that the displacement of the channel walls, although not constrained by radiocarbon ages, probably occurred during the late Holocene. We base this inference on several observations. First, the channel walls are very steep, even though they are developed in young, poorly consolidated sediments, suggesting that downcutting has occurred recently. Second, the channel downcut several centimeters in the four years during which we made observations in this area. Third, although we have no date for the lower terrace that formed on the upstream side of the channel deflection and therefore cannot date the most recent slip event (Fig. 7), the absence of soil development suggests that this terrace is historical or slightly older (< 1000 years). We interpret that the channel deflection probably occurred during one, or at most two, slip events on the fault trace. Because Airport Creek appears to be actively downcutting through weakly consolidated terrace deposits, a consistent 1.8 m of right deflection of both channel walls probably would not be preserved if it represented the cumulative effect of multiple small slip events occurring throughout thousands of years. In the next section we document an event involving a slip of 1.2 m recorded at the Oak Knoll Creek site, which supports the reasonableness of 1- to 2-m slip events within the San Simeon fault zone.

Slip Rate

The Airport Creek site yielded information that enabled us to evaluate the sense of slip, timing of most recent slip, and slip per event for a major fault within the San Simeon fault zone. The evidence presented above indicates that the major strand at the Airport Creek site is a right-slip fault having a minor down-on-the-east vertical component. Right-

lateral strike slip of 1.8 m has occured during the late Holocene following incision of Airport Creek into its early to middle Holocene terrace deposits. The rate of slip on this fault can be estimated from the dislocated southern margin of the early Holocene terrace surface (Fig. 7), from offset younger alluvium, and from a geometric analysis of vertically separated soil horizons exposed in trench T-1 (Fig. 10). These potential strain indicators are discussed below.

The upper surface of the younger alluvium forms a terrace that is broader northeast than it is southwest of the fault. The southern margin of this terrace is a poorly constrained piercing point that intersects the primary fault at Airport Creek from the east at a low angle near Envicom trench 5 and from the west between trenches T-1 and T-5 (Fig. 7). We estimate the amount of right separation of this terrace margin to be about 12 ± 5 m. The age of the terrace margin also is poorly constrained. The youngest radiocarbon age for the alluvium beneath the terrace is 8950 ± 260 years B.P. (sample ^{14}C-8, Table 1) found 2.45 m below the surface (Fig. 10). If sediment accumulated against the east side of the fault at a relatively uniform rate, the sedimentation rate derived from the sediment thicknesses separating samples ^{14}C-1, -2, and -8 (Fig. 10) falls within the range of 1 to 2 mm/yr. The age of the terrace surface therefore may be about 6500 to 7725 years. If the rate of sedimentation decreased toward the top of the terrace, as suggested by two buried B horizons above sample ^{14}C-8, the terrace surface probably is younger. We estimate that the Airport Creek terrace is similar in age to the Oak Knoll Creek terrace (terrace Qt_5; Hanson and others, this volume) that is found in the next drainage to the north (Fig. 2). Based on particle size data, soil development indices, and radiocarbon ages, we estimate the Oak Knoll Creek terrace surface to be about 5000 to 5500 years old. From the age range for the Airport Creek terrace (5000 to 7725 years), we estimate a slip rate of between 0.9 and 3.4 mm/yr. We emphasize that the slip rate estimate based on the Airport Creek terrace margin is poorly constrained by the available data.

The clayey gravels and gravelly clays exposed in trenches T-2, T-5, and T-6, which we correlated and assigned to the younger alluvium, provide another opportunity for estimating the slip rate. The deposits have radiocarbon ages that range from 10,670 ± 260 years B.P. to 13,790 ± 260 years B.P. (samples ^{14}C-9 and -10, Table 1) and are considered basal components of the Airport Creek terrace. Based on the known distribution of these deposits east of the primary fault in trenches T-2 and T-5 and their distribution to the west in trench T-5, we estimate that they are offset between 16 m and 28 ± 2 m. From these data we estimate a slip rate of between 1.1 and 2.9 mm/yr.

To develop additional estimates of slip rate at the Airport Creek site, we focused on trench T-1. This trench was excavated into the essentially horizontal Airport Creek terrace, where the fault plane appears not to have been rotated downslope by local surficial creep (Fig. 10). In this trench we observed and radiocarbon-dated a generally fine-grained and flat-lying sequence of fluvial deposits that to varying degrees have been modified by pedogenic processes. Figure 10 is a detailed soils log that shows the San Simeon fault strand exposed in the northwest wall of trench T-1 and indicates the locations of radiocarbon-dated samples. Here the fault is a single subvertical strand that trends N40°W and has well-defined

slickensides that plunge 6° to 7° southeast. Near the surface, the fault increases in width as it separates into several splays. The progressive decrease of vertical separations upsection in trench T-1 provides strong evidence that multiple slip events have occurred on the fault during the Holocene.

To estimate slip rates from the vertical separations and unit thicknesses observed in trench T-1, we use a geometric approach based on the following assumptions.

- The fault is a predominantly vertical right-slip fault that has a minor component of dip slip defined by the 6° to 7° SE plunge of the observed slickensides. The ratio of right slip to dip slip falls within the range of 8:1 to 10:1 and characterizes the long-term style of slip on this fault.

- The amount of slip per event on this fault is on the order of 1 to 2 m. This assumption is based on the arguments presented above regarding the right deflection of the Airport Creek channel and on a slip event documented at the Oak Knoll Creek site described below.

- The beds that constitute the Holocene Airport Creek terrace are essentially flat and are deformed only locally at the fault. The true vertical separation of a given layer can be calculated by projecting its elevations from either block into the fault from a distance of 1 to 2 m or more.

Using the observed vertical separation of 1.15 to 1.20 m for the base of unit 7 and an age of 8950 ± 260 radiocarbon years B.P. from sample ^{14}C-8 (Fig. 10), the total horizontal slip on the fault since deposition of the base of unit 7 is given by:

(1) tan (83° to 84°) (1.15 to 1.20 m) = 9.37 to 11.42 m

The estimated average horizontal slip rate since the deposition of unit 7 therefore is 1.0 to 1.3 mm/yr. Similarly, we can use the observed vertical separation of 1.25 to 1.4 m for the base of unit 8 and an estimated age for this horizon of 9240 to 9910 years, which is based on a calculated sedimentation rate between radiocarbon samples ^{14}C-2 and ^{14}C-8 (Fig. 10). Then the total horizontal slip on the fault since deposition of the base of unit 8 is given by:

(2) tan (83° to 84°) (1.25 to 1.40 m) = 10.18 to 13.32 m

The average horizontal slip rate since deposition of the base of unit 8 is 1.0 to 1.4 mm/yr, values consistent with those calculated for unit 7.

Recurrence Interval

Using the range of slip rates estimated from the vertical separations observed in trench T-1 (1.0 to 1.4 mm/yr), from the displaced Airport Creek terrace margin (1.0 to 3.4 mm/yr), and from the offset basal gravelly deposits of the Airport Creek terrace (1.1 to 2.9 mm/yr), plus our estimate of net slip per event of 0.9 or 1.8 m, we can constrain a likely average interval between slip events:

0.9 m/event @ 0.9 mm/yr = 1000-yr interval

0.9 m/event @ 3.4 mm/yr = 265-yr interval

1.8 m/event @ 0.9 mm/yr = 2000-yr interval

1.8 m/event @ 3.4 mm/yr = 529-yr interval

These calculations suggest that ground-rupturing events on the San Simeon fault where it is exposed at the Airport Creek site should recur approximately every 265 to 2000 years. The average minimum slip rate from our studies is 1.0 mm/yr, while the maximum value, as constrained by the geomtric analysis of the soils in trench T-1, is 1.3 to 1.4 mm/yr. These values (1.0 to 1.4 mm/yr) provide our best estimate for the Holocene slip rate. From these values the recurrence interval for this fault can be further constrained to a range of 643 to 1800 years.

Discussion

The slip rate estimates based on observed vertical separation and plunge of slickensides are reliable only if the slickensides represent the true sense of slip for all events since deposition of the units shown in the soils log (Fig. 10) and if the beds are flat-lying. If, however, the fluvial terrace deposits in trench T-1 initially dipped 2° to the northwest, then the actual vertical separation during a slip event would be a third greater than for flat beds. A 1° to 2° slope to the northwest, which unfortunately lies within the limits of our measurements, would produce an overestimation of both the slip rate and the number of events that occurred during a given interval.

A long-term check on the reasonableness of our preferred Holocene slip rate for the San Simeon fault at Airport Creek is provided by displaced strandlines of marine terraces. For example, the 120,000-year-old marine terrace (terrace Q_3 of Hanson and Lettis, this volume) is 10 to 13 m higher west of the fault, which yields an average late Quaternary vertical slip rate of 0.08 to 0.11 mm/yr. The horizontal rate of slip, if calculated from the observed vertical slip using the 6° to 7° southeast plunge of slickensides observed in trench T-1, is 0.7 to 1.1 mm/yr, a value reasonably consistent with the rate of vertical separation calculated from trench T-1. Hanson and Lettis (this volume) provide a thorough discussion of slip on the San Simeon fault during the Pleistocene based on deformed marine and fluvial terraces.

Although the above calculations help in modeling recent behavior of the San Simeon fault, conclusions based on them must be regarded as preliminary. More reliable estimates of Holocene slip rates for the San Simeon fault require a better understanding of the three-dimensional distribution of the beds that comprise the Airport Creek terrace. Even though the modern soil profile was disrupted by the most recent slip event on the primary fault, the lack of significant vertical separation in the modern soil profile (X in Figure 10) and the absence of a prominent step in the terrace surface both suggest that the fault may not have moved more than once or twice during the past few thousand years. Considering our estimate of the late Holocene age of last slip based on the offset of the apparently youthful canyon walls of Airport Creek, this incongruity indicates that a clustering of slip events may have occurred in the mid-Holocene, creating the vertical separation of units 4 through 11 (Fig. 10) and producing a scarp that may have existed during deposition of units 4 and 5. Units 1, 2, and 3, which show little disruption from faulting, may have formed during an interval of quiescence on the fault. The apparently young deflection in the Airport Creek

channel therefore may signal the onset of another period of activity on the San Simeon fault. We can niether resolve this apparent incongruity nor evaluate these speculations without additional information. Furthermore, because the active fault observed at Airport Creek is a single trace, its estimated slip rate probably represents a minimum value for the San Simeon fault zone. Likewise, the recurrence interval calculated for the fault at Airport Creek may underestimate the occurrence of ground-rupturing events within the broader fault zone.

OAK KNOLL CREEK SITE

Oak Knoll Creek crosses the San Simeon fault zone orthogonally. Its intersection with the fault is marked by a prominent deflection of the active channel (Fig. 2; Hanson and Lettis, this volume) and by right-deflected, deformed fluvial terrace deposits (Bickner and Vaughan, 1987; Hanson and Lettis, Plate I, this volume). We excavated six trenches at the Oak Knoll Creek site to identify the locations of the primary traces of the San Simeon fault and to assess their late Quaternary kinematic behavior. Trenches T-1, T-2, T-2A, and T-3 were excavated to depths of 4.5 m or more in the semiconsolidated Holocene deposits of fluvial terrace Qt_5. This terrace was radiocarbon-dated at 5500 to 7900 years by Hanson and others (this volume). Trenches T-1, T-2, and T-2A, described in detail below, intersected an active strand of the San Simeon fault. Initially, we intended to extend trench T-3 an additional hundred meters or more to the northeast to detect other potentially active, more easterly strands. However, unstable trench walls and homogenous, poorly stratified overbank deposits required an alternative approach. We excavated trenches T-4 and T-5 south of the creek in a hillside area of shallow bedrock overlain by a thin veneer of alluvial and colluvial materials (Fig. 11). Trench T-5 revealed a sheared contact between Franciscan greenstone and colluvium, also described below.

Figure 12A is a diagrammatic oblique view of the Oak Knoll Creek site that shows the approximate relative positions of trenches T-1, T-2, T-2A, and T-3; the active strand observed in trenches T-1 and T-2; and the projected position of the more easterly strand encountered in trench T-5. Detailed logging along the north wall of trench T-2 revealed a vertical fault having a strike of N26°W at 4.5 m below the ground surface (Fig. 13). At a depth of 1.5 m, the strike of the fault plane rotates clockwise to N14°W, suggesting right slip. A distinctive sand bed, which has a thickness that changes abruptly across the fault, lies at a depth of 1.5 to 2.1 m below the Qt_5 surface in trench T-2. A second trench (T-2A), hand-excavated parallel to the fault, provided a three-dimensional view of the sand bed and was used to measure variations in bed thickness for an isopach map. The equal-thickness contours yielded excellent piercing points on the fault, from which we were able to measure vertical and lateral components of fault displacement (Fig. 12B). Radiocarbon samples collected from above and below the sand bed indicate that this component at the Qt_5 terrace was deposited between 6250 $\pm$ 170 and 5540 $\pm$ 120 radiocarbon years B.P. (samples ^{14}C-28 and -29, Table 1). Detailed analysis of the fault exposed in trenches T-2 and T-2A indicates that its most recent slip has the following characteristics:

(1) The horizontal right-slip component is 1.2 $\pm$ 0.03 m.

(2) The vertical-slip component (east side up) is 0.2 m.

(3) The net slip is 1.23 ± 0.04 m.

(4) Poorly defined slickensides and grooves on the fault plane indicate that the slip vector plunges 10° to 15° to the north (11°N plunge best fits the observed horizontal and vertical slip components).

(5) Slip occurred within the past 5540 ± 120 radiocarbon years B.P.

Whether this slip occurred during one or more than one event cannot be resolved by the present data. However, the amount of vertical separation between correlative layers measured across the fault remains constant to the bottom of the trench. This indicates that the upper 4.5 m of the Oak Knoll Qt_5 terrace deposits have undergone similar amounts of displacement and supports a single-event hypothesis. Although faulting is not expressed on the Qt_5 terrace surface, the fault dislocates the base of the A horizon, suggesting that latest slip might be considerably younger than 5540 ± 120 radiocarbon years B.P. The absence here of clear evidence for multiple events contrasts with the paleoseismic record observed at the Airport Creek site. Although the fault exposed in the Oak Knoll Creek Qt_5 terrace deposits has documented Holocene activity and clear geomorphic expression in the form of sidehill benches in the canyon wall south of the terrace (Fig. 11), its down-on-the-west vertical separation and lack of evidence for multiple slip events suggest that it is not the same fault as the one exposed at the Airport Creek site.

As mentioned above, we shifted our search for major traces of the San Simeon fault zone at Oak Knoll Creek up the hillside to the southeast because trenches excavated in the Holocene fluvial terrace deposits were prone to failure. Trenches T-4 and T-5 were positioned to intersect potential southeastern extensions of the faults associated with vegetation and tonal lineaments (Hanson and others, this volume); the deformed fluvial terraces of Oak Knoll Creek (Fig. 11; Bickner and Vaughan, 1987); and the prominent northeast-facing escarpment along Arroyo Laguna north of Oak Knoll Creek (Fig. 2). Trench T-4 exposed a locally pebbly sandstone of unknown age that is lithologically distinct from Franciscan graywacke. This sandstone is overlapped on the west by undeformed fluvial and colluvial deposits and is capped by an unfaulted soil (Fig. 14). Trench T-5 encountered a ridge of internally sheared Franciscan greenstone buried within subhorizontal beds of alluvium and colluvium. Approximately 120 m southeast of trench T-5, the ridge of Franciscan greenstone forms a low outcrop. In trench T-5, shears are prominent along the northeastern margin of this ridge, but these shears do not appear to cut the overlying soils (Fig. 14).

The trenches excavated at Oak Knoll Creek apparently did not cross major Holocene traces of the San Simeon fault. The trenches may have been located within an en echelon step in the fault trace so as to miss active fault strands. Recently active strands also may occur beneath the isolated knob that lies in the gap between trenches T-3 and T-4. Alternatively, a pure strike-slip fault might have been overlooked in the homogeneous flat-lying stratigraphy of Oak Knoll Creek fluvial terrace Qt_5, although we believe this is unlikely. Compared with the faults exposed at the Borrow Pit and Airport Creek sites, the fault that was exposed in Oak Knoll Creek trenches T-1, T-2, and T-2A appears to be a relatively minor feature.

SUMMARY

The southeastern end of the onshore reach of the San Simeon fault zone near San Simeon, California, is characterized by complex deformation consisting of multiple fault traces that form a zone 120 m wide or wider. The major traces exposed at the Borrow Pit and Airport Creek sites are vertical to near-vertical, right-slip faults having minor components of both down-on-the-west and up-on-the-west dip slip. Based on the plunge of slickensides, the ratio of strike slip to dip slip is at least 8:1 to 10:1. These active faults have experienced multiple slip events in the Holocene. Estimates of slip rate for the fault trace at Airport Creek range from 0.9 to 3.4 mm/year, with preferred values of 1.0 to 1.4 mm/yr. These must be considered minimum values for the San Simeon fault zone as a whole. The offset channel of Airport Creek and the well-documented minor fault at Oak Knoll Creek indicate that slips of 1 to 2 m per event may typify the San Simeon fault. Based on estimates of both slip rate and slip per event, recurrence frequencies for the San Simeon fault may be about 600 to 1800 years for a 1- to 2-m event, although evidence at Airport Creek suggests that slip events may not occur at uniform intervals.

ACKNOWLEDGEMENTS

We are grateful for discussions with many individuals regarding the Holocene history of the onshore San Simeon fault. P.A. Frame and F.R. Bickner assisted in interpreting and logging the trenches. F.R. Bickner, K.L. Hanson, and T.K. Rockwell contributed soils stratigraphic analysis to the geologic logs. Thoughtful evaluations of the trench logs and their interpretations were provided by F.H. Swan and W.R. Lettis. G.L. Kennedy, Natural History Museum of Los Angeles County, identified the invertebrate fossils. The manuscript was reviewed by J. Sims of the U.S. Geological Survey and E. Hart of the California Division of Mines and Geology. We especially appreciate the cooperation of H. Brown, Manager of the Hearst Ranch, who facilitated our access to the trenching sites. This research was supported by the Pacific Gas and Electric Company.

REFERENCES

Bickner, F.R., and Vaughan, P.R., 1987, Evidence for Holcene activity of the San Simeon fault from deformed fluvial terraces near San Simeon, coastal central California: Geological Society of America Abstracts with Programs, v. 19, no. 6, p. 359.

California Division of Mines and Geology, 1986, Official Map of Special Studies Zones: San Simeon Quadrangle, scale 1:24,000.

Earth Sciences Associates, 1974, Geology of the southern Coast Ranges and the adjoining offshore continental margin of California, with special reference to the geology in the vicinity of the San Luis Range and Estero Bay: Appendix 2.5D to Final Safety Analysis Report for Diablo Canyon Nuclear Power Plant, U.S. Atomic Energy Commission Docket Nos. 50-275 and 50-323.

Earth Sciences Associates, 1975, Section 2.5, Geology and seismology, in Final Safety Analysis Report, Units 1 and 2, Diablo Canyon Site, San Luis Obispo County, California: U.S. Atomic Energy Commission Docket Nos. 50-275 and 50-323.

Envicom Corporation, 1977, Fault investigation section, Hearst Ranch environmental data base; Sherman Oaks, California: unpublished consulting report prepared for the Hearst Corporation, 30 p., 1 plate.

Hall, C.A., Jr., 1976, Geologic map of the San Simeon-Piedras Blancas region, San Luis Obispo County, California: U.S. Geological Survey Miscellaneous Field Studies Map MF-784, scale 1:24,000.

Hall, C.A., Jr., Ernst, W.G., Prior, S.W., and Wiese, J.W., 1979, Geologic map of the San Luis Obispo-San Simeon Region, California: U.S. Geological Survey Map I-1097, scale 1:48,000.

Hanson, K.L., and Lettis, W.R., this volume, Estimated Pleistocene slip rate for the San Simeon fault zone, south-central coastal California.

Hanson, K.L., Wesling, J.R., Lettis, W.R., Kelson, K.I., and Mezger, L., this volume, Correlations, ages, and uplift rates of Quaternary marine terraces, south-central coastal California.

Hart, E.W., 1985, Fault-rupture hazard zones in California: California Division of Mines and Geology Special Publication 42 (revised), 24 p.

Manson, M.W., 1985, San Simeon fault zone and Cambria fault, San Luis Obispo County, California: California Division of Mines and Geology Fault Evaluation Report FER-170 (unpublished).

Pacific Gas and Electric Company, 1988, Final report of the Diablo Canyon Long Term Seismic Program: U. S. Nuclear Regulatory Commission Docket Nos. 50-275 and 50-323.

Pacific Gas and Electric Company, 1989, Hosgri fault zone, tabulation of observations: Diablo Canyon Long Term Seismic Program, Response to Question 43j, U. S. Nuclear Regulatory Commission Docket Nos. 50-275 and 50-323.

Taliferro, N.L., 1943, Geologic history and structure of the central Coast Ranges, California: California Division of Mines and Geology Bulletin 118, p. 119-163

Weber, G.E., 1983, Geologic investigation of the marine terraces of the San Simeon region and Pleistocene activity of the San Simeon fault zone, San Luis Obispo County, California: U.S. Geological Survey Final Technical Report, contract 14-08-0001-18230, 66 p., 5 plates.

Weber, G.E., Oshiro, L.K., and Brown, D.F., 1981, Evidence for late Pleistocene or Holocene faulting along the San Simeon fault zone at San Simeon Bay, San Luis Obispo County, California: Geological Society of America Abstracts with Programs, Cordilleran Section, v. 13, no. 2, p. 113.

1.As reported by George L. Kennedy, invertebrate paleontologist, Natural History Museum of Los Angeles County, 1986.

TABLE 1

SUMMARY OF RADIOCARBON AND THEMOLUMINESCENCE AGE ESTIMATES, SAN SIMEON FAULT

Results of Radiocarbon Analyses[1]

Sample Number	Site[2]	Trench	AMS[3] (years B.P.)	Conventional (years B.P.)		Comments
				^{14}C	^{13}C Adjusted	
^{14}C-1	AC	T-1	11,150 ± 115	---	---	Detrital charcoal; Beta - 18,244
^{14}C-2	AC	T-1	10,690 ± 130	---	---	Detrital charcoal; Beta - 22,700
^{14}C-3	AC	T-1	9760 ± 180	---	---	Detrital charcoal; Beta - 18,856
^{14}C-4	AC	T-2	35,160 ± 560	---	---	Charcoal; Beta - 18247
^{14}C-8	AC	T-1	8950 ± 260	---	---	Charcoal, low beam current - not corrected for ^{13}C; Beta - 22,701
^{14}C-9	AC	T-2	13,790 ± 260	---	---	Detrital charcoal; Beta - 18,857
^{14}C-10	AC	T-5	---	10,670 ± 260	10,670 ± 260	Detrital charcoal; Beta - 18,249 (formerly #9/22/86-2)
^{14}C-22	AC	T-7	33,190 ± 530	---	---	Detrital charcoal; stratigraphically higher than ^{14}C-25; Beta - 22,702
^{14}C-25	AC	T-6	24,790 ± 1400	---	---	Charcoal; stratigraphic relationships suggest age is too young. Low beam current, not corrected for ^{13}C; Beta - 22,314
^{14}C-28	OKC	T-2	5540 ± 120	---	---	Detrital charcoal; Beta - 18,859
^{14}C-29	OKC	T-2	6250 ± 170	---	---	Detrital charcoal; Beta - 18,860

TABLE 1 (continued)

Results of Thermoluminescence Analyses[4]

Sample Number	Site[2]	Trench	TL Age (ka)	Lithology	Comments
TL-3a	AC	T-1	4.73 ± 0.96	silty organic clay	Age judged reliable by lab.[5]
TL-4a	OKC	T-2	16.3 ± 3.1	clayey silt or silty organic clay	Age judged reliable by lab.[6]
TL-5b	SSC	sea cliff exposure (Figure 3)	197 ± 47	estuarine clay	Age judged less reliable than TL-3a and TL-4a.

[1]Radiocarbon analyses performed by Beta Analytic, Inc., P.O. Box 248113, Coral Gables, Florida 33124.

[2]Site designations: AC = Airport Creek, BP = Borrow Pit, OKC = Oak Knoll Creek, SSC = San Simeon Cove.

[3]AMS = Accelerator Mass Spectrometry.

[4]Thermoluminescence analyses performed by G.W. Berger, Department of Geology, Western Washington University, Bellingham, Washington 98225.

[5]This age is not consistent with radiocarbon samples ^{14}C-1, -2, -3, and -8, which indicate a range of ages from 11,150 ± 115 to 8950 ± 260 years B.P. for the younger alluvium of Airport Creek trench T-1.

[6]This age is not consistent with radiocarbon samples ^{14}C-28 and -29, which indicate ages of 6250 ± 150 to 5540 ± 120 years B.P. for the alluvium of Oak Knoll Creek terrace Qt_5.

TABLE 1
CHARACTERISTICS OF FAULT SEGMENTS ALONG THE LOS OSOS FAULT ZONE
(FAULT SEGMENTS SHOWN ON FIGURE 2.)

Fault Segment	Topographic Segmentation	Range-front Character	Geomorphic Expression	Recency of Slip	Late Quaternary Slip Rate mm/yr	Length	Characteristics At Segment Boundary
Estero Bay	Poorly defined; deeply eroded bedrock platform with several NW-trending linear ridges.	Borders NE flank of "59-meter ridge." Northern trace unknown.	Onshore trace marked by several NE-facing scarps, tonal lineaments and linear drainages. Offshore extension constrained by linear bedrock/unconsolidated Quaternary sediment contact.	Not well constrained. May displace post-late Wisconsinan sediment.	Not well constrained.	13 ± 2 km	Northwest—inferred to intersect Hosgri fault in Estero Bay. Southeast—segment bends 15° to 25° to more northwesterly trend along southern margin of Morro Bay basin and ends at northwestern margin of Irish Hills subblock.
Irish Hills	Coincident with Irish Hills subblock.	Well-defined range-front fault. Range front linear, steep, moderately dissected.	Well-defined scarps, spring lines, and lineaments. Tectonically impounds Pleistocene and Holocene (?) alluvium.	Multiple late Pleistocene and Holocene events.	Vertical 0.2 to 0.4. Net = 0.25 to 0.5 (60° dip); 0.4 to 0.8 (30° dip)	18 ± 2 km	Northwest— segment ends at Morro Bay basin coincident with en echelon or branching fault relationship or bends to more westerly trend to project into Estero Bay segment (see above). Southeast—1 to 2 km en echelon right step to Lopez Reservoir segment. Coincident with SE termination of Irish Hills subblock, 2 to 4 km right step in range front, and possible intervening basin of subsidence.

Table 1
(continued)

Fault Segment	Topographic Segmentation	Range-front Character	Geomorphic Expression	Recency of Slip	Late Quaternary Slip Rate mm/yr	Length	Characteristics At Segment Boundary
Lopez Reservoir	Coincident with Edna subblock.	Poorly defined range-front fault along NW part. Range front deeply dissected. Fault crosses rolling foothills along SE part.	Poorly defined lineaments. Tectonically impounds Pleistocene and Holocene (?) alluvium.	Displaces early (?) Pleistocene alluvium. Late Pleistocene and Holocene activity suggested by ponded allurium but not documented by displaced strata.	Vertical = < 0.1	17 ± 2 km	Northwest—1 to 2 km en echelon right step to Irish Hills subblock (see above). Coincident with NW termination of Edna subblock. Southeast—poorly defined. Coincident with SE termination of Edna subblock.
Newsom Ridge	Subparallel to and within Newsome Ridge subblock.	Intra-range fault; range deeply dissected.	No topography indicative of Quaternary faulting. Trace may be defined, in part, by linear drainage.	Quaternary displacement not observed.	Vertical = < 0.1 Probably not active.	8 ± 2 km	Northwest—poorly defined (see above). Lies along projection of Lopez Reservoir segment. Southeast—intersects West Huasna fault zone near Twitchell Reservoir.

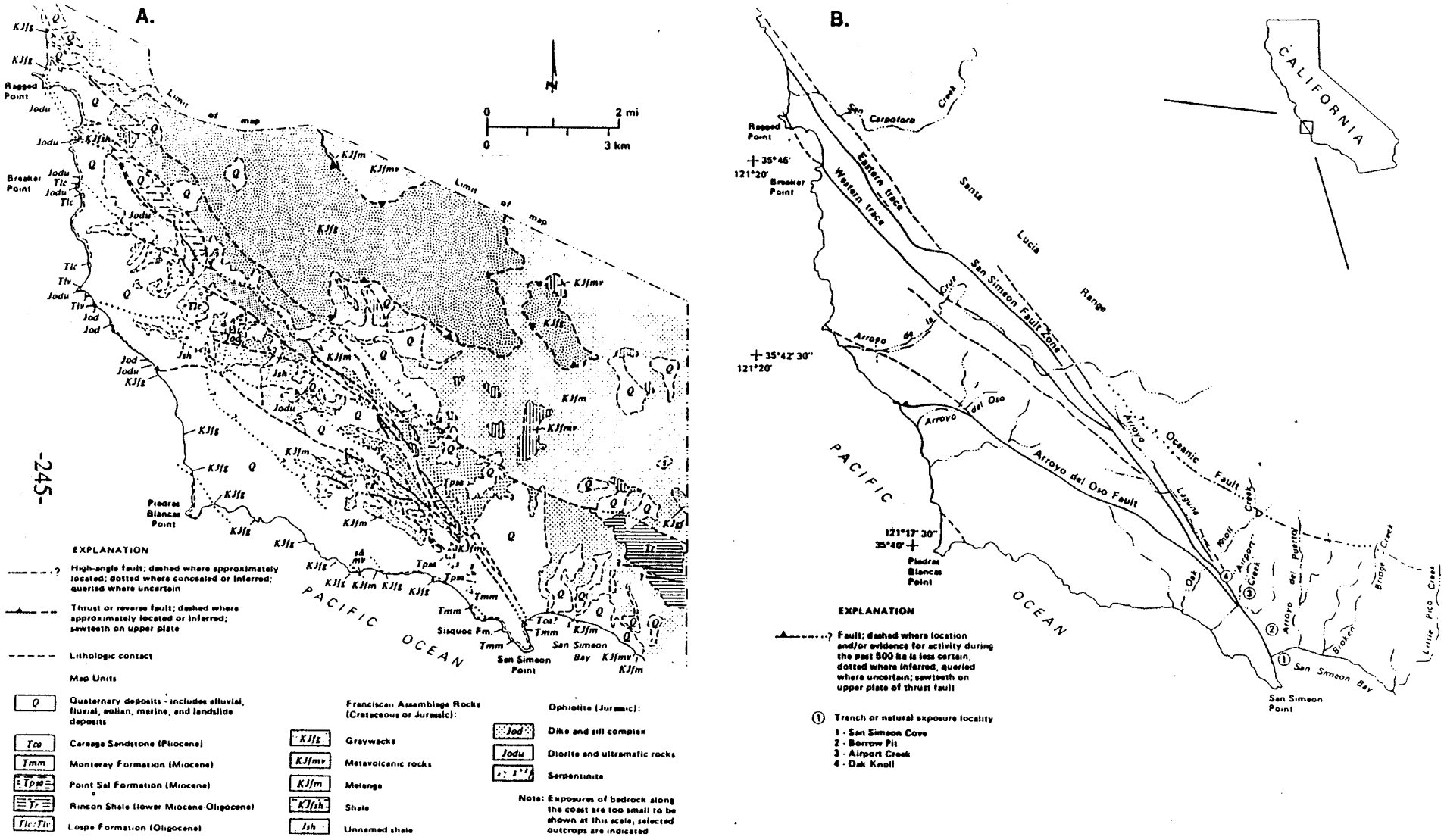

Figure 1. A. Generalized geologic map of the onshore San Simeon fault zone (modified from Hall and others, 1979).
B. Map showing major traces and location of study areas within the San Simeon fault zone.

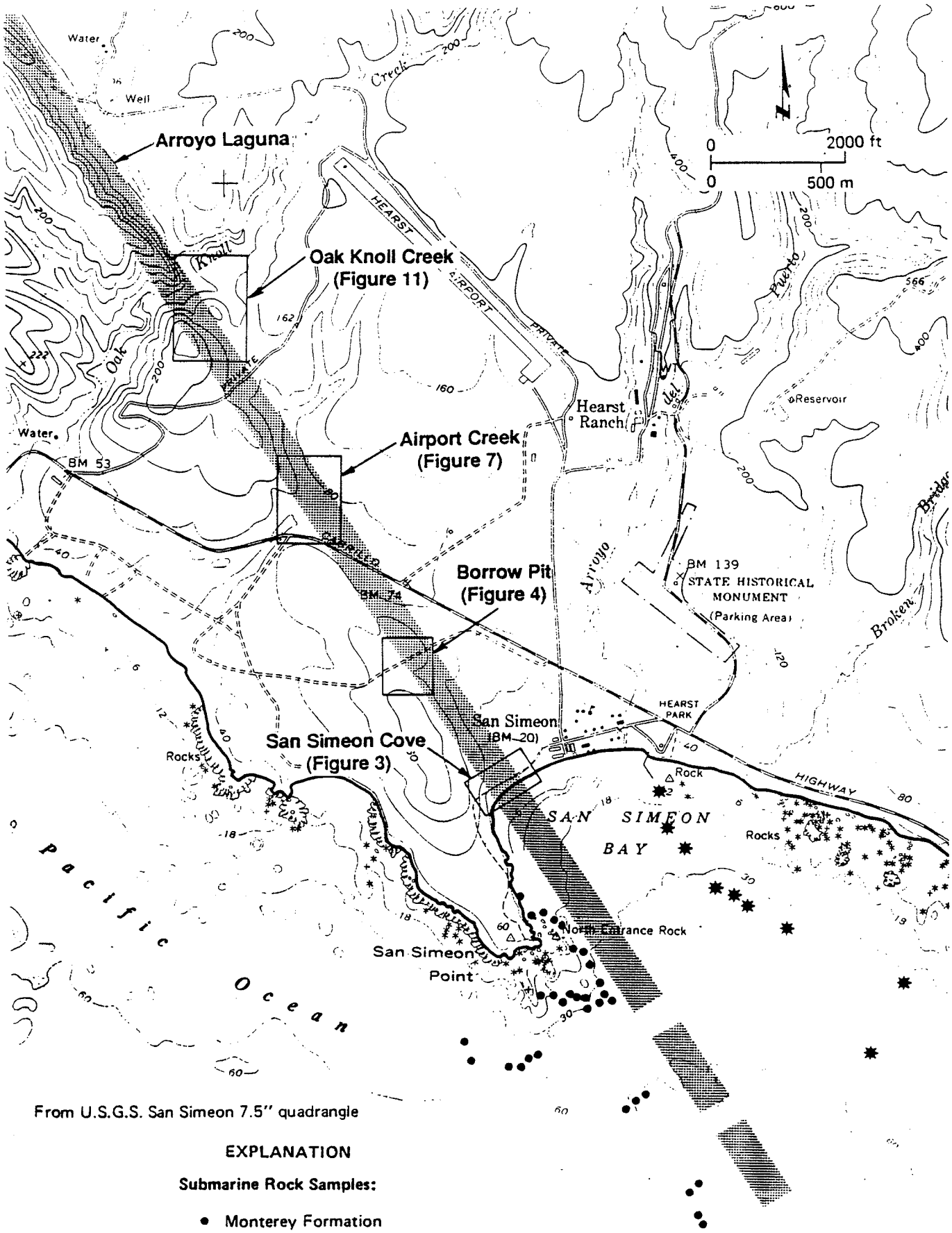

From U.S.G.S. San Simeon 7.5" quadrangle

EXPLANATION

Submarine Rock Samples:

- Monterey Formation
- Franciscan Complex

Approximate trend of the San Simeon fault zone

Figure 2. Map showing study areas and locations of submarine rock samples along the San Simeon fault zone.

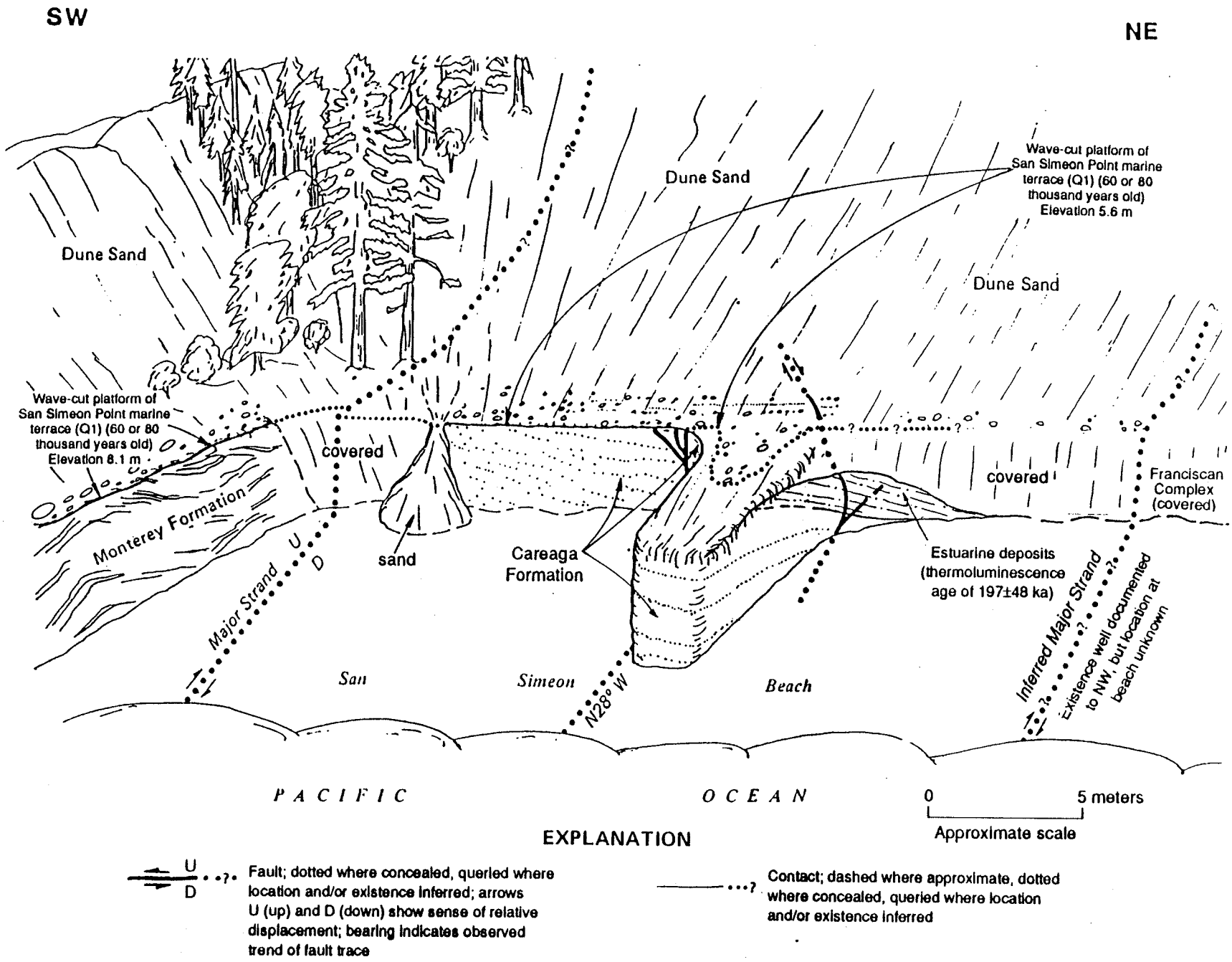

Figure 3. Gull's eye view of San Simeon fault zone at San Simeon Cove.

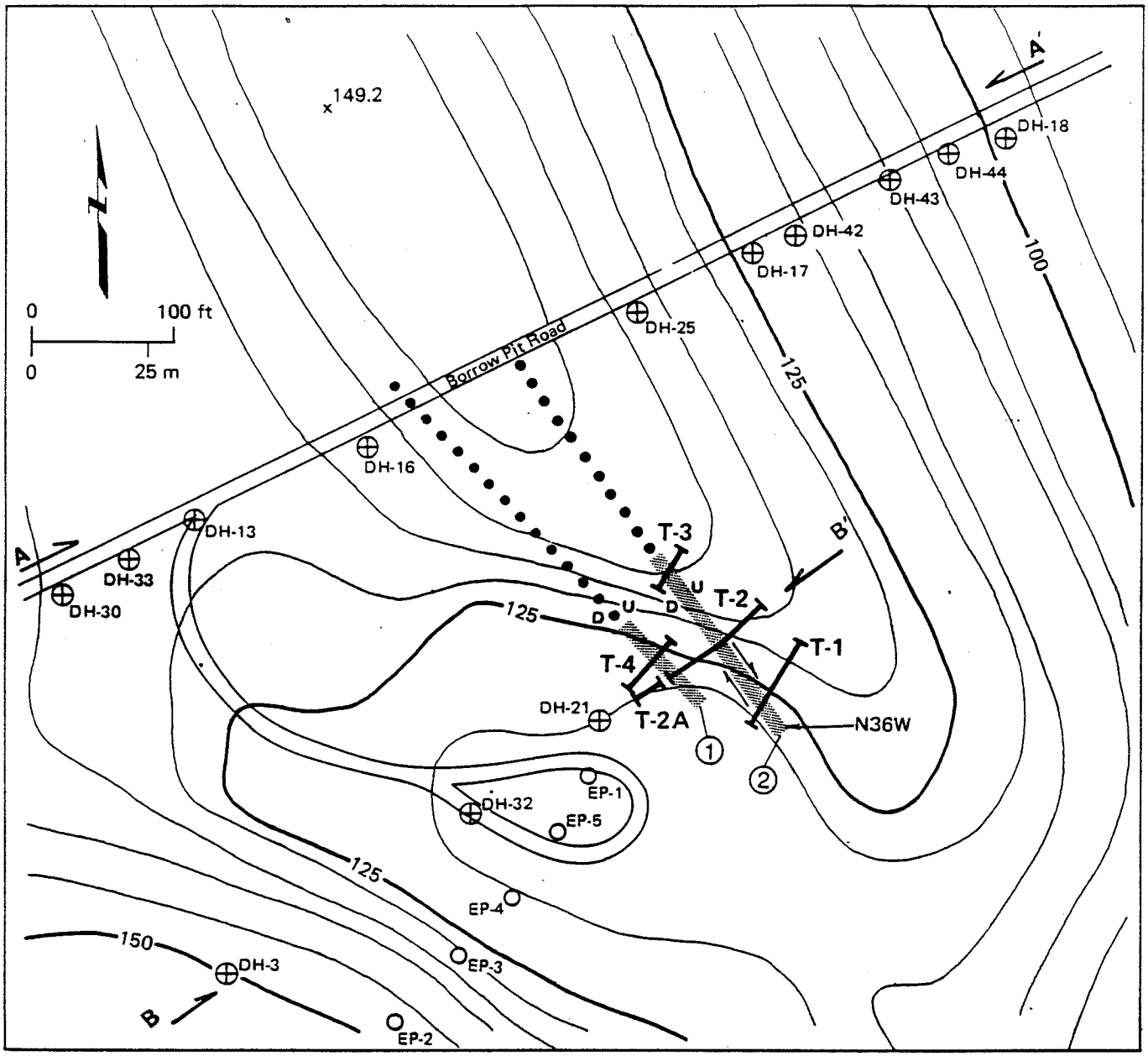

EXPLANATION

30"-wide backhoe trench

DH-16 — 5"-diameter flight-auger hole

EP-1 — 30"-wide backhoe exploratory pit

A — A' — Line of cross section (Figure 6)

125 — Topographic contour showing elevation in feet; contour interval 5'

N48W — Trace of fault exposed in trenches; dotted where concealed and extended by auger-hole data; arrows show sense of slip; bearing indicates observed trend of fault trace

① — Western Borrow Pit trace (inferred)

② — Eastern Borrow Pit trace

Figure 4. Map of Borrow Pit site showing locations of trenches, auger holes, and exploratory pits.

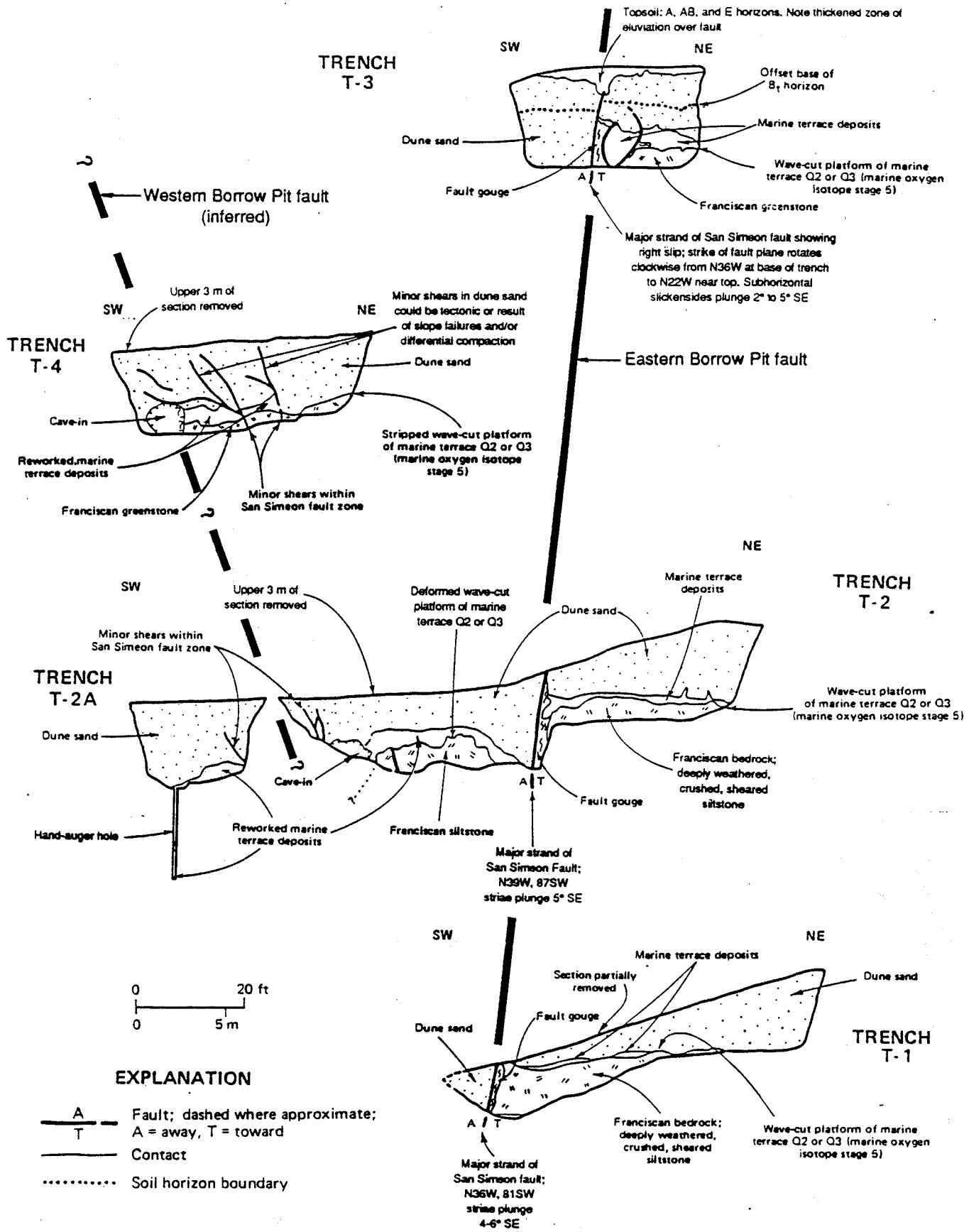

Figure 5. Simplified logs of Borrow Pit trenches showing major strand of San Simeon fault (view to NW)

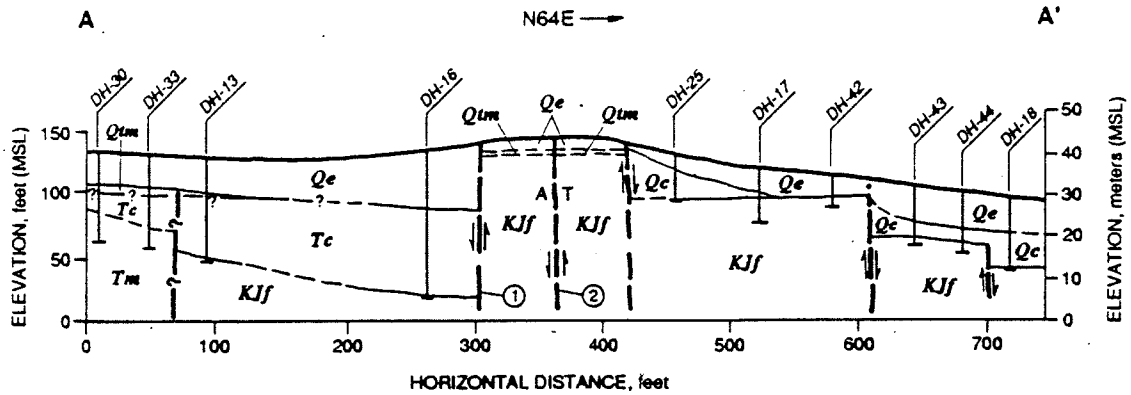

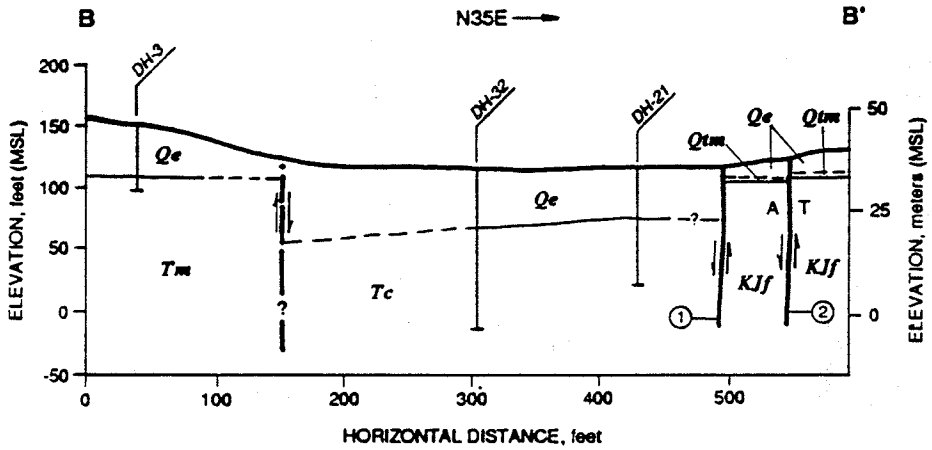

EXPLANATION

Qtm	Quaternary marine terrace deposits
Qe	Quaternary eolian deposits
Qc	Quaternary colluvium
Tc	Careaga Formation
Tm	Monterey Formation
KJf	Franciscan Complex

Fault; dashed where approximately located, dotted where concealed, queried where uncertain; A/T (away/toward) and arrows indicate apparent relative direction of displacement

DH-30 — 5"-diameter flight-auger hole

① — Western Borrow Pit fault

② — Eastern Borrow Pit fault

For locations of cross sections, see Figure 4.

Figure 6. Cross sections through the Borrow Pit site showing multiple strands within the San Simeon fault zone. Section A - A' is drawn along the Borrow Pit Road; section B - B' is drawn across the trenching site.

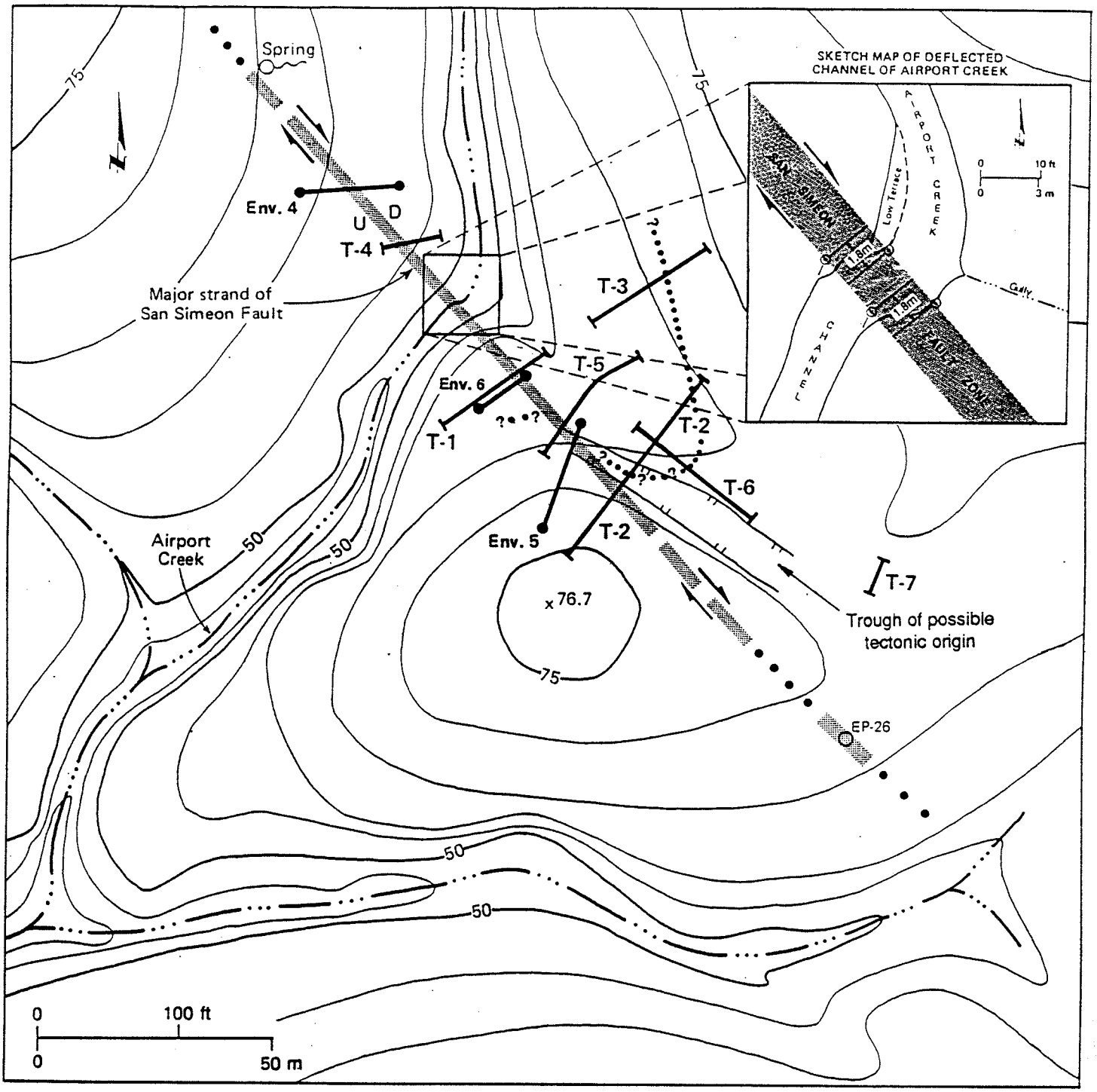

EXPLANATION

T-4 — 30"-wide backhoe trench

Env. 4 — Backhoe trench excavated by Envicom in 1977

EP-26 — 30"-wide backhoe exploratory pit

50 — Topographic contour showing elevation in feet; contour interval 5'

U D — Trace of fault exposed in trenches; dashed where approximate, dotted where concealed; U=up, D=down; arrows indicate relative sense of horizontal displacement

? — Approximate limit of Holocene fluvial terrace surface; queried where poorly constrained

Figure 7. Map of Airport Creek site showing locations of trenches, exploratory pits, and deflected channel.

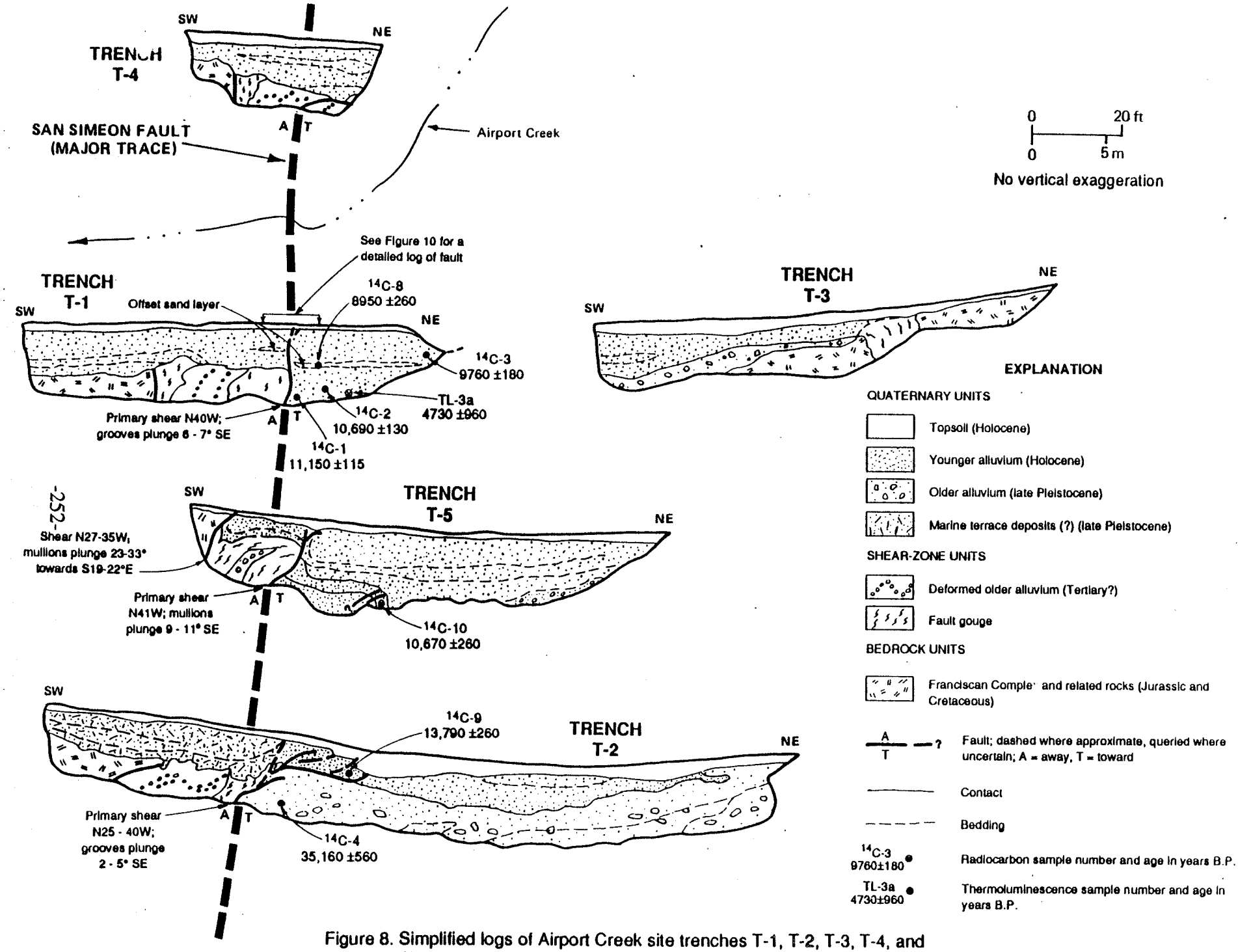

Figure 8. Simplified logs of Airport Creek site trenches T-1, T-2, T-3, T-4, and T-5 showing a major strand of the San Simeon fault (view to NW).

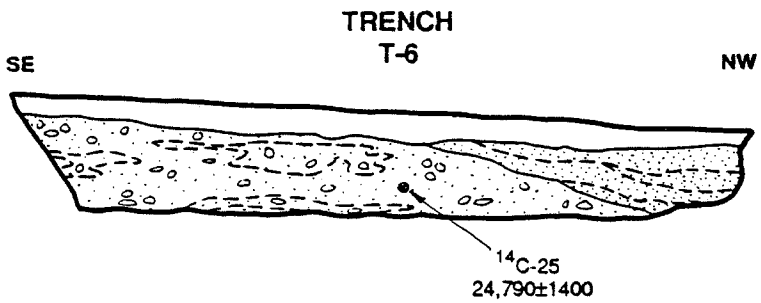

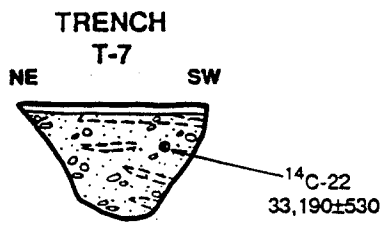

EXPLANATION

QUATERNARY UNITS

- Topsoil (Holocene)
- Younger alluvium (Holocene)
- Older alluvium (late Pleistocene)
- Contact
- Bedding in alluvial units
- ^{14}C-22 33,190±530 — Radiocarbon sample number and age in years B.P.

0 — 20 ft
0 — 5 m
No vertical exaggeration

Figure 9. Simplified logs of Airport Creek site trenches T-6 and T-7 showing disconformable contact between younger and older alluvium.

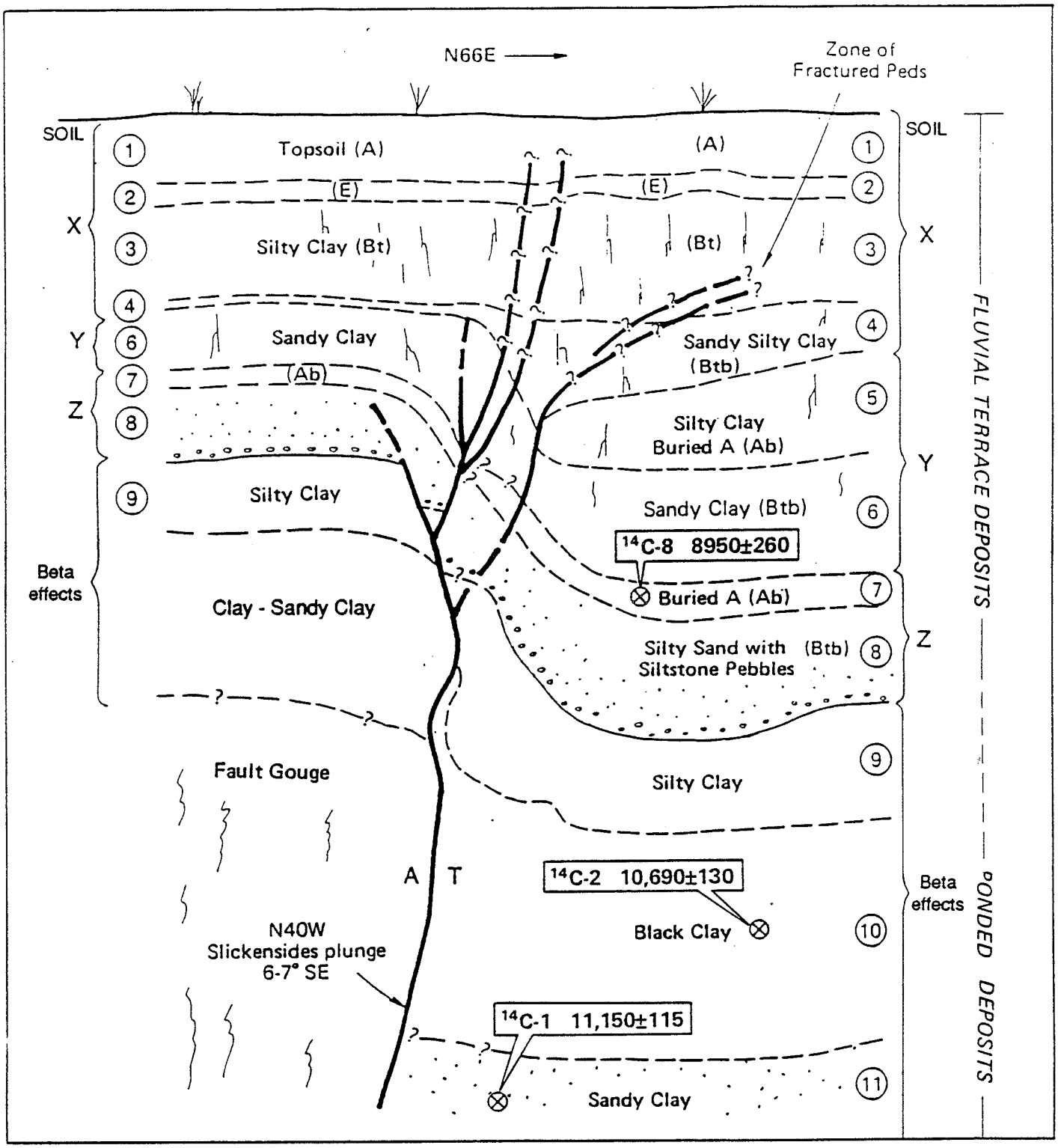

EXPLANATION

X	Modern soil
Y, Z	Buried paleosols
A T	Fault; dashed where approximately located, queried where uncertain; A/T (away, toward) indicate apparent relative sense of displacement
	Contact; dashed where approximately located, queried where uncertain
⊗	Radiocarbon sample; age in years B.P.

0 2 ft
0 1 m
No vertical exaggeration

Figure 10. Detailed log of San Simeon fault strand exposed in NW wall of Airport Creek trench T-1.

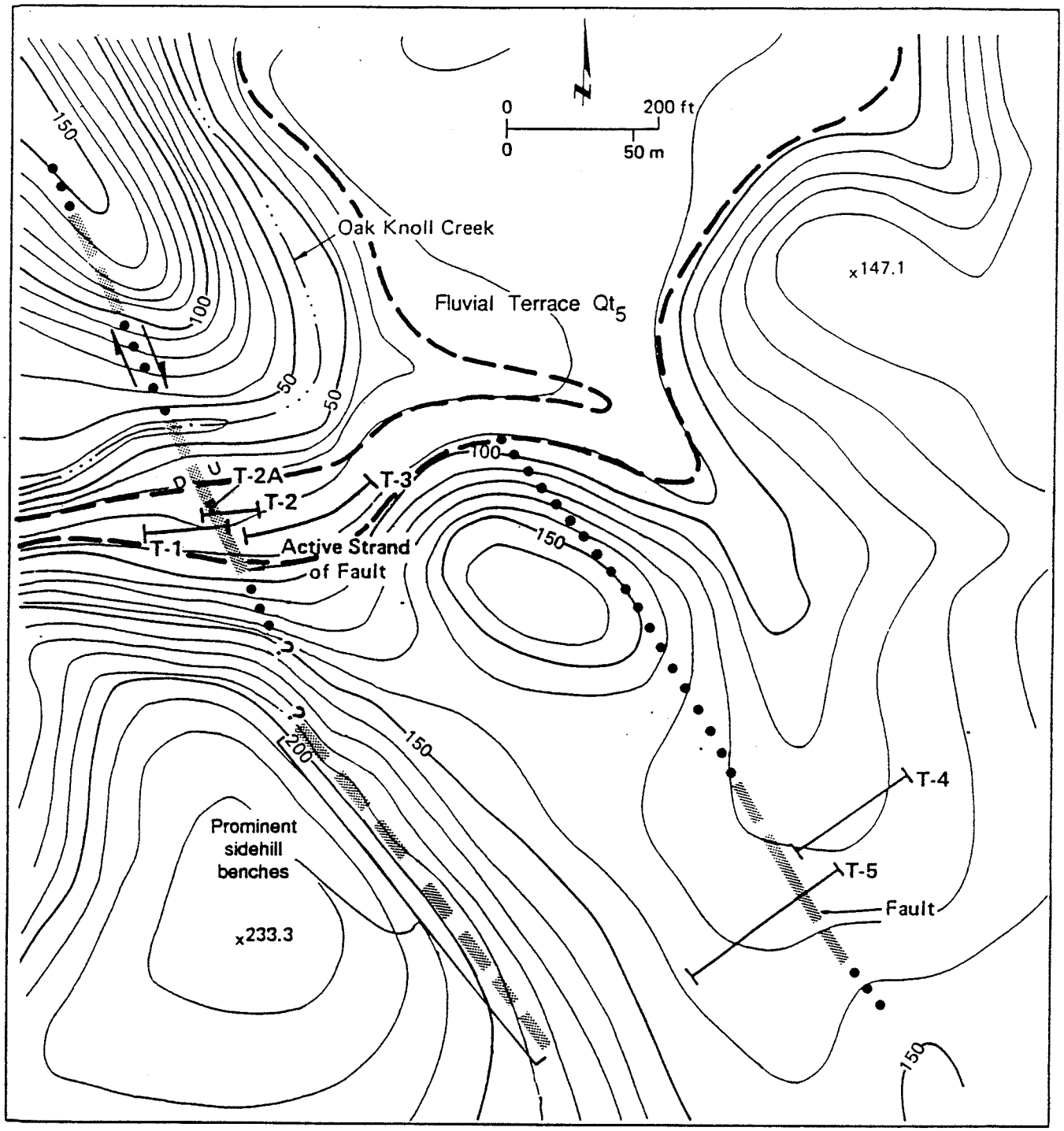

EXPLANATION

30"-wide backhoe trench

150 Topographic contour showing elevation in feet; contour interval 10'

Limits of fluvial terrace Qt_5

U D •?• Trace of fault exposed in trenches; dashed where approximate, dotted where concealed or inferred, queried where connection uncertain; U = up, D = down; arrows indicate sense of horizontal displacement

Figure 11. Map of Oak Knoll Creek site showing locations of trenches.

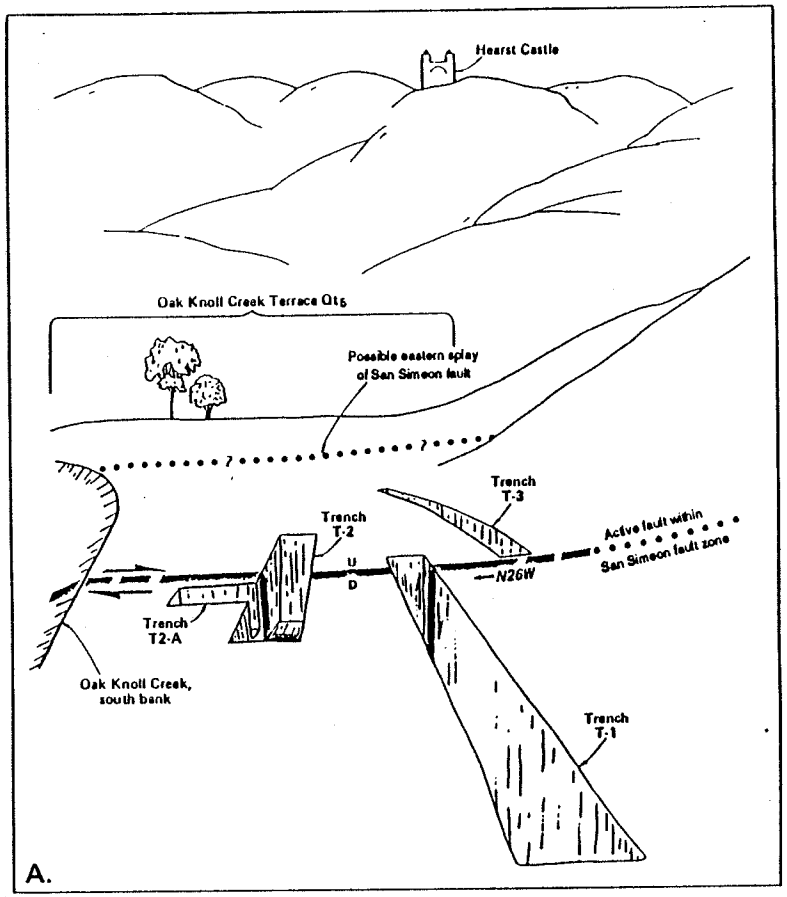

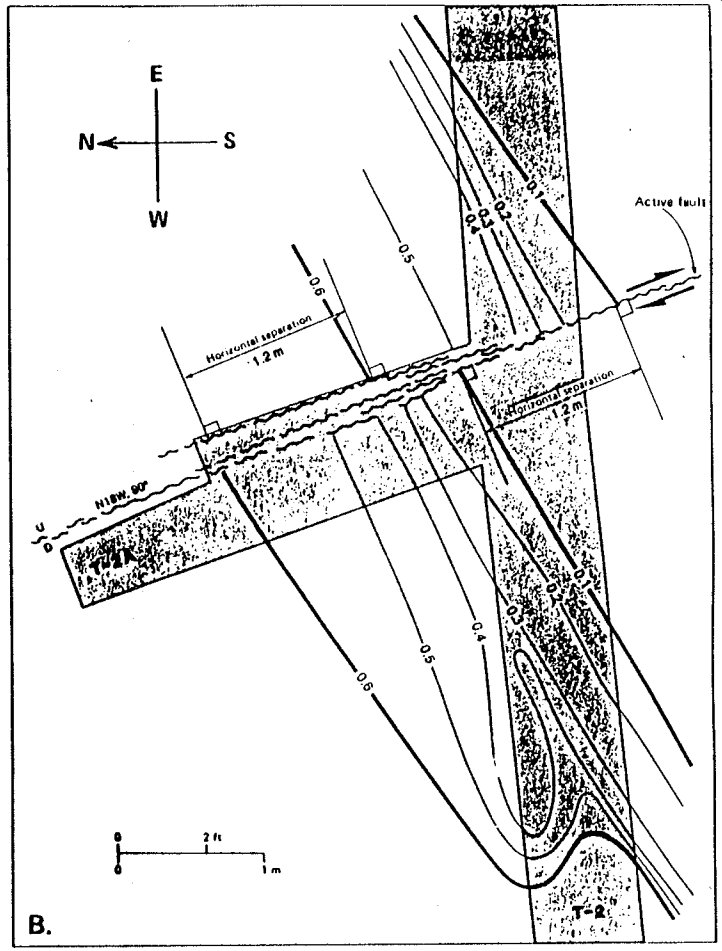

EXPLANATION

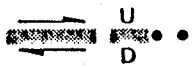

Trace of fault exposed in trenches; dashed where approximate, dotted where concealed; U=up, D=down; arrows indicate relative direction of displacement

N26W — Trend of fault

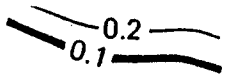

Isopachs (lines of equal thickness) on clayey sand marker horizon (unit ⓐ of Fig. 13); contour interval 0.1 ft. Heavy contours used as piercing points

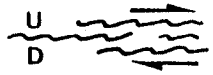

Fault; U=up, D=down; paired arrows indicate relative sense of displacement

N18W, 90° — Orientation of fault at elevation of clayey sand marker horizon

Figure 12. A. Sketch showing an active fault within the San Simeon fault zone exposed in trenches on Oak Knoll Creek fluvial terrace Qt_5.
B. Isopach of clayey sand marker horizon showing right-lateral separation across active San Simeon fault trace.

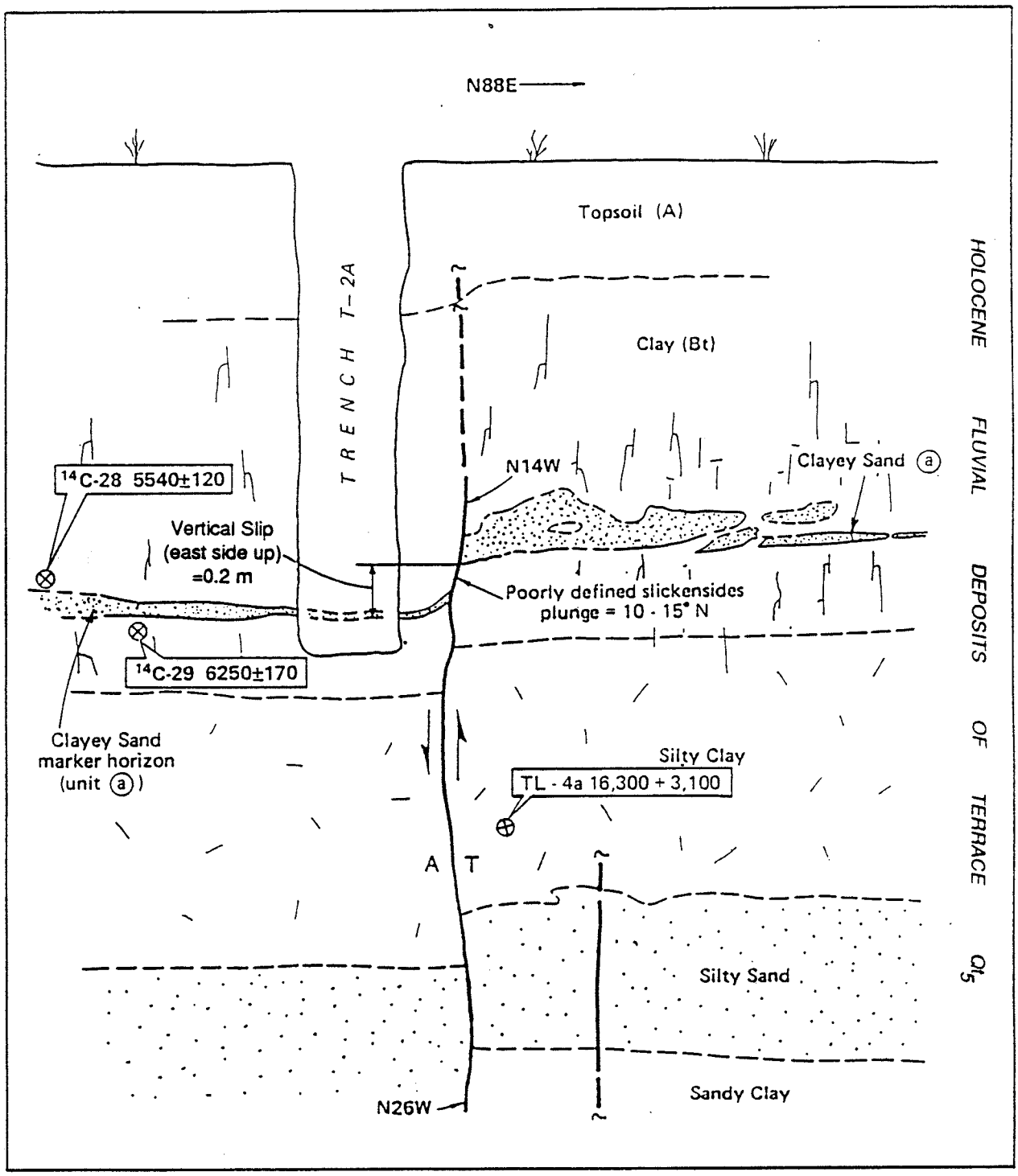

EXPLANATION

A T — Fault; dashed where approximate, queried where uncertain; A/T (away/toward); arrows indicate apparent relative direction of displacement

Contact; dashed where approximate

⊗ ^{14}C — Radiocarbon sample; age in years B.P.

⊗ TL — Thermoluminescence sample; age in years B.P.

0 — 2 ft.
0 — 1 m

Figure 13. Detailed log of north wall of Cold Knoll Creek trench T-2 showing an active fault within the San Simeon fault zone.

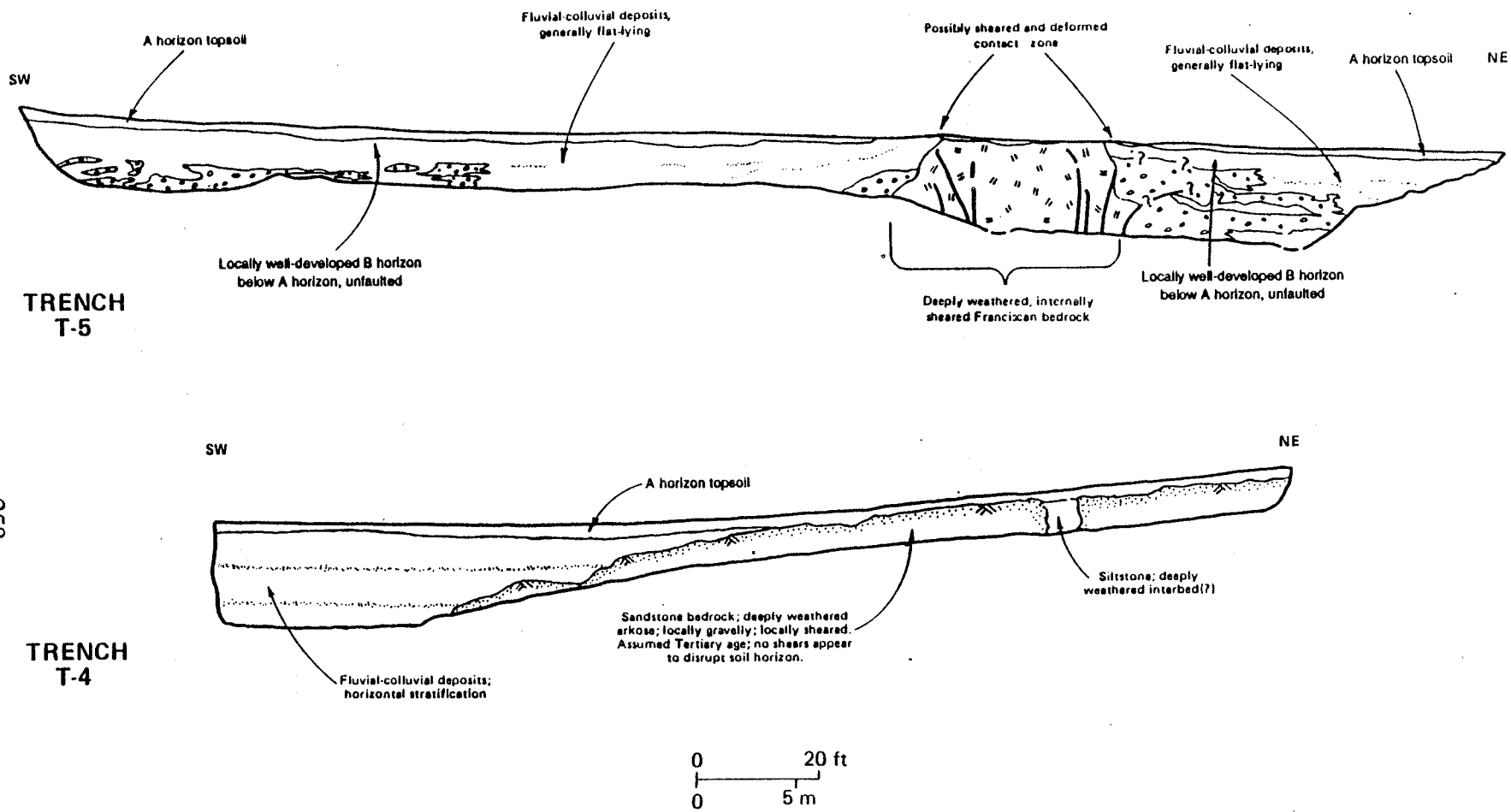

EXPLANATION

——— — —?— Fault; dashed where approximate; queried where inferred

——— — —?— Contact; dashed where approximate; queried where inferred

Figure 14. Simplified logs of Oak Knoll Creek trenches T-4 and T-5.

QUATERNARY DEFORMATION OF THE SAN LUIS RANGE, SAN LUIS OBISPO COUNTY, CALIFORNIA

W.R. Lettis and K.I. Kelson
William Lettis & Associates, Lafayette, California

J.R. Wesling, M. Angell, K.L. Hanson, and N.T. Hall
Geomatrix Consultants, San Francisco, California

ABSTRACT

The San Luis Range is a prominent west-northwest-trending topographic and structural high that is one of a series of elongated structural blocks bordered by west-northwest-trending reverse faults within the Los Osos/Santa Maria (LOSM) domain. We conducted geomorphic, geologic, and geophysical investigations to characterize the geometry and late Quaternary behavior of faults and folds within and bordering the range.

Major geologic structures within the San Luis Range include the Pismo syncline and the San Miguelito, Edna, and Pismo faults. Quaternary deposits and landforms within and along the margins of the range indicate that none of these structures has had deformation in at least the past 500,000 years. Elevations and ages of marine terraces indicate that the San Luis Range is uplifting, at rates of between 0.12 m/ka and 0.24 m/ka, as a relatively rigid crustal block with little to no internal deformation.

The northeastern margin of the range is bordered by the Los Osos fault zone, a southwest-dipping reverse fault that separates the uplifting San Luis Range from the subsiding or southwest-tilting Cambria block to the northeast. The fault zone has had recurrent late Pleistocene and Holocene displacement at a long-term slip rate of 0.2 to 0.4 mm/yr. Uplift of the range has been accommodated, in part, by displacement along this fault zone.

The southwestern margin of the San Luis Range is bordered by a complex system of late Quaternary reverse faults that separates the San Luis Range from the subsiding onshore Santa Maria Valley to the southwest. The zone includes the Wilmar Avenue, San Luis Bay, Olson, Pecho, and Oceano faults, which dip moderately to the northeast. The cumulative net dip-slip rate of displacement for this system of faults ranges from about 0.2 mm/yr to about 0.3 mm/yr. This rate is partitioned among the major faults within the system, with slip rates on individual faults generally ranging from 0.04 to 0.11 mm/yr.

Because the San Luis Range is a major structural element within the LOSM domain, we infer that crustal shortening in the domain is accommodated primarily by reverse faulting along the margins of structural blocks and by uplift, subsidence, or tilting of the blocks. The west-northwest structural grain and tectonic style within the LOSM domain is unique in the south-central coastal California region, and is transitional between the west-trending

structural grain of the western Transverse Ranges and the north-northwest-trending grain of the Santa Lucia and San Rafael Ranges. We interpret that Quaternary deformation within the domain is related to renewed clockwise rotation of the western Transverse Ranges and compression of the domain against the relatively stable Salinian crust that underlies much of the Santa Lucia and San Rafael ranges to the northeast.

INTRODUCTION

The San Luis Range is a prominent west-northwest-trending topographic and structural high that lies in the central part of the Los Osos/Santa Maria tectonic domain (Lettis and others, 1989). This triangular-shaped domain lies between the offshore Santa Maria basin on the west, the western Transverse Ranges on the south, and the Santa Lucia and San Rafael mountains on the northeast (Fig. 1). Physiographically, the domain consists of a series of west-northwest-trending topographic lowlands and uplands, the more prominent of which include the Los Osos, Santa Maria, San Antonio-Los Alamos, and Lompoc valleys, and the Irish, Casmalia, Solomon, and Purisima hills. In general, topographic uplands within the domain coincide with uplifting structural blocks; whereas lowlands coincide with subsiding, tilting, or static structural blocks. In the offshore to the west, geophysical data indicate that the geomorphic character of the province continues to but not across the Hosgri fault zone: near-surface bedrock platforms occur along the offshore projections of the Irish and Casmalia Hills, and sediment-filled basins occur along the offshore projections of the Santa Maria and Los Osos Valleys (PG&E, 1988). West of the Hosgri fault zone, the offshore Santa Maria Basin is characterized by regional subsidence and north-northwest-trending basins and bathymetric highs.

Because the San Luis Range is a major structural feature within the LOSM domain, investigation of the Quaternary deformation of the range is important for assessment of the current regional tectonic setting. The range is bordered on the northwest by the Hosgri fault zone, on the east by the West Huasna fault (Hall, 1973a; Hall and others, 1979), on the northeast by the Los Osos fault zone (Lettis and others, this volume), and on the southwest by the diffuse zone of faulting and fault-related folding described in this paper.

FIELD INVESTIGATIONS

Beginning in early 1986, we conducted geomorphic, geologic, and geophysical investigations of the San Luis Range to characterize the geometry and late Quaternary behavior of faults and folds within and bordering the range. Geomorphic investigations of the northeastern and southwestern margins of the block included identification of geomorphic features suggestive of late Quaternary faulting via field mapping and interpretation of black-and-white, color-infrared, and low-sun-angle aerial photographs. Selected geomorphic features were investigated by detailed geologic mapping, drilling, and trenching to provide site-specific data on fault location, geometry, sense of displacement, recency, and recurrence. As described by Hanson and others (this volume), marine terraces were mapped along the northwestern, western and

southwestern margins of the San Luis Range to evaluate long-term uplift rates and the sense and recency of fault displacements. In addition, we logged numerous natural and trench exposures and drilled over two hundred boreholes to assess the geometry and behavior of several fault traces and to assess deformation of late Quaternary marine terraces.

To evaluate the possible offshore continuation of structures asociated with the San Luis Range and their relationships to the Hosgri fault zone, we analyzed an extensive suite of geophysical data in the region including Estero and San Luis Obispo Bays. In addition to locating possible fault traces, these investigations were aimed at characterizing fault geometry, sense of displacement, recency, and associated deformation. The investigations consisted of acquiring and interpreting deep common-depth-point and shallow high-resolution seismic reflection data, analyzing gravity and magnetic data, and analyzing bathymetric and outcrop patterns from side-scan sonar data. A detailed discussion of these data is presented in a report by Pacific Gas and Electric Company (PG&E) to the U.S. Nuclear Regulatory Commission (PG&E, 1988).

RESULTS

Structures within the San Luis Range

Based on topographic expression and late Pleistocene uplift rates, the San Luis Range consists of four distinct subblocks: the Estero Bay, Irish Hills, Edna, and Newsom Ridge subblocks (Fig. 2). The Irish Hills subblock is characterized by relatively high relief and crest elevations of 425 to 550 m. The Edna subblock has low relief and crest elevations of 180 to 240 m. The Newsom Ridge subblock is comparable to the Irish Hills subblock in relief and maximum crest elevations. The Estero Bay subblock, which lies offshore, is characterized by a bedrock platform containing a series of northwest-trending, discontinuous sea-floor ridges. This platform may be a deeply-eroded offshore continuation of the Irish Hills subblock, with the present coastline between Morro Bay and Pt. Buchon representing an erosional escarpment produced by present and former sea-level highstands. Alternatively, the difference in elevation from onshore to offshore may reflect different rates of uplift between two subblocks.

The elevations and ages of marine terraces within the San Luis Range indicate that Quaternary rates of uplift have varied among coastal areas and that relative differences in uplift between areas have persisted throughout much of the Pleistocene. In general, uplift rates are highest within the Irish Hills subblock, which has risen at a long-term rate of 0.19 $\pm$ 0.02 m/ka to possibly as much as 0.24 $\pm$ 0.02 m/ka (Hanson and others, this volume). Based on elevations and ages of marine terraces, the southwestern flank of the Edna subblock has been uplifted at an average rate of 0.12 $\pm$ 0.01 m/ka for at least the past 120 ka and likely for the past 500 ka, and the southwestern flank of the Newsom Ridge subblock has been uplifted at an average late Quaternary rate of 0.13 to 0.15 m/ka. Differences in late Pleistocene uplift rates among subblocks are consistent with differences in topographic expression, which may reflect longer-term uplift rates. These relations suggests that the subblocks may be structurally controlled. However, different uplift rates

may also reflect variations in the style or amount of local deformation associated with faulting along the southwestern margin of the structural block.

Major geologic structures within the San Luis Range include the Pismo syncline and the San Miguelito, Edna, and Pismo faults (Fig. 2) (Hall, 1973a, 1973b, 1981, 1982; Hall and Corbato, 1967; Hall and Prior, 1975; Hall and others, 1979). We investigated the deformational history and recency of activity of these structures to address the presence or absence of Quaternary deformation within the San Luis Range. Our investigations reveal that none of these structures has had deformation over at least the past 500 ka.

Pismo Syncline - The Pismo syncline is the dominant structural element within the San Luis Range (Fig. 2). It is an open, doubly-plunging syncline composed of numerous small folds with subparallel axial traces (Hall, 1973a, 1973b; Hall and others, 1979). The primary axial trace of the Pismo syncline trends about N60W from east of the town of Arroyo Grande, through the Irish Hills, and to the coastline near the mouth of Islay Creek (Fig. 2). The hinge line of the Pismo syncline plunges about 5 degrees to the southeast near Avila Beach, and 4 to 10 degrees to the northwest near Arroyo Grande (Hall, 1973a).

Based on stratigraphic relations of the Neogene Monterey and Pismo Formations, folding of the Pismo syncline began in the late Miocene or early Pliocene and ceased after the late Pliocene (Hall, 1973a, 1973b; Hall and others, 1979). The areal extent and coarsening-upward stratigraphy of the Pismo Formation indicate that depocenters became progressively shallower and more restricted during the Pliocene, suggesting gradual uplift of the region. Emergent Quaternary marine terraces provide minimum age-constraints on deformation associated with the Pismo syncline. The marine terrace sequence between Morro Bay and Point Buchon, which represents at least the past 500 ka, is undeformed across the axial trace of the syncline (Fig. 3; Hanson and others, this volume). These data indicate that deformation of the Pismo syncline ceased prior to 500 ka and that the former synclinal depocenter now occupies the core of an uplifting range.

San Miguelito Fault - The San Miguelito fault is a 9-km-long, west-northwest-trending zone of anastomosing faults that lies near the southwestern margin of the Pismo syncline (Fig. 2). The fault juxtaposes Miocene and Pliocene volcanic and sedimentary rocks on the northeast against Mesozoic basement rocks on the southwest, and is interpreted as a high-angle, generally northeast-dipping fault zone with predominantly normal dip-slip displacement (Hall, 1973a, 1981). Stanley and Surdam (1984) argue that deposition of upper Miocene and lower Pliocene members of the Pismo Formation pre-dates significant movement along the San Miguelito fault. Disrupted upper Pliocene rocks of the Pismo Formation show that movement along the San Miguelito fault continued during the late Pliocene (Hall, 1973a; 1981).

Detailed bedrock and marine-terrace mapping (Kelson and others, 1987; Clark and others, 1988; Hanson and others, this volume) and trenching studies address the recency of activity of the San Miguelito fault. Along the northwestern projection

of the San Miguelito fault (as mapped by Hall, 1973b, 1982, and Hall and others, 1979), detailed mapping revealed intense folding and some localized shearing, but no mappable fault traces. A sequence of emergent, middle to late Quaternary marine terraces are undeformed across the northwestern projection of the San Miguelito fault (Fig. 3).

The San Miguelito fault crosses a sequence of high marine terrace remnants developed on the southwestern flank of the San Luis Range. These terrace remnants consist primarily of wave-cut platforms stripped of their marine deposits. Although elevations of the terrace strandlines have measurement uncertainties of $\pm$ 6 m, the lateral and vertical distribution of the terraces is not substantially different across the fault. The terrace remnants are at least 500 ka and are probably significantly older. Even a low slip rate along the San Miguelito fault would have produced significant cumulative offset (vertical or lateral) of the terrace sequence. The absence of significant offset, therefore, suggests that the fault has been inactive during the late Quaternary.

The southeastern onshore end of the San Miguelito fault, as mapped by Hall (1973a), intersects the coastline near Mallagh Landing (Fig. 4). Five late Quaternary marine terraces cross the trend of the fault in this area (Kelson and others, 1987; Hanson and others, this volume). Although a large landslide locally obscures the relationship between the fault and the lower terraces, shoreline-angle elevations on both sides of the fault indicate that there is no vertical displacement of the wave-cut platforms (Fig. 4). The lowest two platforms are estimated as 80 ka and 120 ka, and the entire sequence probably spans more than 500 ka (Hanson and others, this volume). These data provide additional evidence that the San Miguelito fault has had no displacement over the past 120 ka, and probably has had no movement for at least 500 ka.

Edna Fault - The northwest-trending Edna fault, as mapped by Hall (1973a) and Hall and others (1979), borders the northern limb of the Pismo syncline for a distance of about 40 km (Fig. 2). These workers interpreted the Edna fault as a 1.5 to 2.4-km-wide zone of high-angle, down-to-the-southwest normal faulting, although individual strands exhibit different amounts and senses of displacement. The irregular traces of major strands suggests that little (if any) strike-slip movement has occurred. Schematic geologic cross-sections by Hall and Surdam (1967) and Hall (1973a) imply that the total amount of vertical separation may be nearly a thousand meters along the central part of the fault zone. Hall (1973a) shows Pliocene and Pleistocene units displaced by the Edna fault. The southeastern and northwestern ends of the Edna fault, as mapped by Hall (1973a), are truncated by the Los Osos fault zone (Lettis and Hall, this volume).

Detailed bedrock mapping and trenching indicate that the northwestern end of the fault is a sheared depositional contact concealed by Quaternary marine terraces and/or eolian deposits. However, marine, colluvial, and eolian deposits overlying marine wave-cut platforms more than 500 ka are displaced locally by several discontinuous, northwest-trending shears (Hanson and others, this volume). The variable senses of displacement along the shears and the numerous, large rotational block and

debris landslides in the area suggest that the shears are a result of extensional deformation in the headwall area of a large landslide complex. Along the northwestern projection of the fault, shoreline angles of emergent Quaternary marine terraces are undisplaced (Cleveland, 1978; Hanson and others, this volume), suggesting that the Edna fault has had no late Quaternary movement.

Pismo Fault - Hall (1973a) mapped the 5.6 km-long, northwest-trending Pismo fault between the towns of Arroyo Grande and Shell Beach (Fig. 2). The southwest-dipping, high-angle, dip-slip fault disrupts lower Miocene to Pliocene marine rocks but not Quaternary sediments (Hall, 197-3a). Detailed marine terrace mapping indicates that the 120 ka marine terrace is undeformed across the projection of the fault (Hanson and others, this volume; Fig. 5). In addition, the fault as mapped by Hall (1973a) crosses but does not displace three higher emergent marine terraces that are up to at least 430 ka (Hanson and others, this volume). Thus, the Pismo fault has been inactive during the middle and late Quaternary.

Northeastern Margin of the San Luis Range: The Los Osos Fault Zone

The northeastern margin of the San Luis Range is bordered by the Los Osos fault zone, a southwest-dipping reverse fault that has a complex history of strike-slip and dip-slip displacement (Lettis and Hall, this volume). The fault zone, which is a 2-km-wide system of discontinuous, subparallel, and en echelon fault traces, extends from an intersection with the Hosgri fault zone in Estero Bay to an intersection with the West Huasna fault southeast of San Luis Obispo, a distance of 55 to 60 km (Fig. 2). The fault zone is one of a series of west-northwest-trending reverse faults within the Los Osos/Santa Maria structural domain that border uplifted structural highs. In particular, the Los Osos fault zone separates the San Luis Range from the relatively stable or southwest-tilted Cambria structural block to the northeast (Fig. 2).

As mapped by Hall and others (1979), the Los Osos fault zone consists of many fault traces that generally bound tabular bodies of serpentinite within the Franciscan Complex. Late Cenozoic activity along several of these fault traces is indicated by displacement of the Tertiary Pismo Formation and the Pliocene to Pleistocene Paso Robles Formation. Lettis and Hall (this volume) show that late Quaternary activity occurs on traces of the Los Osos fault zone previously unmapped by Hall and others (1979).

The Los Osos fault zone is divided into four segments based on differences in behavioral characteristics (e.g., recency of activity, slip rate); spatial coincidence with topographic subblocks of the San Luis Range; en echelon separation of fault traces; intersection with known or inferred branching or crossing structures (e.g., faults, subsiding basins); and geomorphic expression as a range-front or intra-range fault. From northwest to southeast, Lettis and Hall (this volume) propose naming the segments the Estero Bay, Irish Hills, Lopez Reservoir, and Newsom Ridge segments.

The Irish Hills segment, which is 17 to 21 km long, exhibits the strongest expression of Holocene activity and is a well-defined range-front fault. Detailed mapping of marine terraces and trenching of fluvial

deposits suggest this segment has had recurrent late Pleistocene and Holocene displacement at a long-term slip rate of 0.2 to 0.4 mm/yr. The adjacent Lopez Reservoir segment is a 15- to 19-km-long, poorly defined range-front fault that displaces older Quaternary alluvium. Detailed mapping and trenching indicate no late Pleistocene or Holocene activity. The Newsom Ridge segment is an 8-km-long, intra-range fault that has poor geomorphic expression and that apparently does not displace Quaternary deposits. The Estero Bay segment is 11 to 15 km long and lies offshore. This fault segment is poorly imaged on seismic reflection data and is weakly expressed in seafloor bathymetry, suggesting a low rate of late Quaternary activity. Additional details concerning the structural and paleoseismic characteristics of segments of the Los Osos fault zone are presented by Lettis and Hall (this volume).

The elevations and ages of marine terraces between Morro Bay and Point Buchon indicate that the Irish Hills subblock of the San Luis Range has a late Pleistocene uplift rate of 0.19 $\pm$ 0.02 mm/yr to 0.24 $\pm$ 0.02 mm/yr (Hanson and others, this volume). This uplift has been accommodated, in part, by displacement along the Los Osos fault zone. Thus, the fault zone is an important structural element that accommodates regional northeast-southwest Quaternary crustal shortening in the Los Osos/Santa Maria domain. The fault separates the uplifted San Luis Range from the subsiding or southwest-tilted Cambria block and appears to accommodate relative motion between these blocks. If data from this area are representative of the style of deformation for the domain as a whole, late Quaternary crustal shortening in the domain is occurring by reverse displacement on northwest-trending faults, and by uplift, subsidence, and tilting of rigid crustal blocks.

Southwestern Margin of the San Luis Range

The southwestern margin of the San Luis Range is bordered by a complex zone of late Quaternary reverse faults that separates the San Luis Range from the subsiding onshore Santa Maria Valley to the southwest (Fig. 2). The zone is 4 to 6 km wide, may be over 60 km long, and consists of several faults that generally strike west-northwest and dip moderately to the northeast. Major structures within this zone include the Wilmar Avenue, San Luis Bay, Olson, Pecho, and Oceano faults, all of which were identified during our investigations. The net dip-slip rate of displacement for this zone ranges from about 0.2 mm/yr to about 0.3 mm/yr. This rate appears to be partitioned among the structures within the zone, with major faults exhibiting similar late Quaternary slip rates.

Because each of these faults lies partially or wholly offshore, and because onshore reaches have poor geomorphic expression or are buried beneath extensive alluvial and eolian deposits, structural and behavioral fault characteristics have been identified via several direct and indirect methods. The locations, displacements, and slip rates for the Olson, San Luis Bay, and Wilmar Avenue are based on disruptions of late Quaternary marine terraces (Hanson and others, this volume). Terrace mapping data are supported by shallow borehole data, logs of natural and artificial exposures, analysis of water and oil well data, and analysis of onshore and offshore

geophysical data. Characteristics of the principal structures along the southwestern margin of the San Luis Range are given below.

Wilmar Avenue Fault - The Wilmar Avenue fault is a northwest-trending, northeast-dipping reverse fault along the southwestern boundary of the San Luis Range (Fig. 2). The fault has poor geomorphic expression and is exposed only at the present sea cliff near Wilmar Avenue in Pismo Beach (Fig. 6). The location of the fault is well constrained southeast of the sea-cliff exposure for a distance of about 2.3 km. The fault continues at least to Arroyo Grande and may extend along the northeastern margin of the Nipomo Mesa to the northern part of the Santa Maria Valley, a distance of 25 km. Offshore to the west of the sea-cliff exposure, the fault appears to bend to a more southwesterly trend and continue for a distance of at least 5.1 km along a well-defined bathymetric lineament. The maximum length of the Wilmar Avenue fault is approximately 30 km.

The Wilmar Avenue fault as defined here coincides with part of the Santa Maria Basin fault as shown by Gray (1980) and may include part of the Santa Maria River fault of Hall (1978a, 1978b, 1982). The locations of both of these previously mapped, concealed faults are inferred based on interpretation of water and oil well data. California Department of Water Resources (1970) depicts a vertical fault approximately at the location of the sea-cliff exposure of the Wilmar Avenue fault in Pismo Beach, but does not describe the fault. Kelson and others (1987) and Coyle and others (1987) note the presence of late Pleistocene activity on the Wilmar Avenue fault and provide preliminary displacement and slip rate data.

The fault zone exposed in the Wilmar Avenue sea cliff is approximately 4 $\pm$ 2 m wide and contains shears that range in strike from N40W to east-west and dip from 45 to 70 degrees to the northeast. The fault juxtaposes Oligocene to lower Miocene Rincon and Obispo Formations over the Pliocene Squire Member of the Pismo Formation. Slickensides and mullions on the southeasternmost fault plane are subparallel to fault dip. These striae and the presence of older bedrock overlying younger bedrock indicate predominantly reverse displacement.

The marine wave-cut platform exposed in the sea cliff near Wilmar Avenue is interpreted to be 120 ka (Fig. 5). This platform has a net vertical separation of 6.4 m across the fault (Fig. 7). However, the platform on the downthrown side of the main fault may have been partially reoccupied by a later sea-level stand; if so, the cumulative net vertical separation of the 120 ka platform across the fault zone is approximately 4.3 m. Based on a range in fault dip of 45 to 70 degrees and a range in vertical separation of 4.3 to 6.4 m, the Pismo Beach reach of the Wilmar Avenue fault has an average late Pleistocene net slip rate of 0.04 to 0.08 mm/yr.

Distinct beds within the terrace deposits overlying the 120 ka platform exposed in the sea cliff near Wilmar Avenue show progressively lower amounts of vertical separation up section across a subsidiary fault to the southwest of the main trace (Fig. 7). This decrease may be a result of distributed shearing within the terrace deposits, or, more likely, of multiple

syndepositional faulting events. The bedrock-parallel attitude of this strand and its opposite sense of vergence from the primary fault plane suggest that the southern strand is probably a flexural slip fault related to formation of a footwall syncline (Fig. 7). Because the syncline appears to be related to slip on the primary fault strand, growth of the syncline probably is related to slip on the subsidiary fault. Therefore, episodic slip on the southern flexural-slip fault probably reflects similarly episodic slip on the primary Wilmar Avenue fault strand.

To the west of the Wilmar Avenue sea cliff exposure, the fault extends at least 5.1 km into San Luis Obispo Bay (Fig. 1). Based on seismic reflection and seafloor sampling data, the fault does not extend westward to the Hosgri fault zone or merge with the Oceano, San Luis Bay, or Pecho faults (PG&E, 1988). Seafloor samples from the area north of the fault consist of Miocene Obispo Formation and Oligocene Rincon Formation. South of the fault, bedrock outcrops are sparse and the seafloor is mantled with Quaternary sediments, which suggests that the area south of the fault is underlain by the poorly resistant, semiconsolidated sandstone of the Pliocene Squire Member of the Pismo Formation. These relations are similar to rock types exposed at the coastline.

Approximately 2 km southeast of the Wilmar Avenue sea-cliff exposure, the location of the Wilmar Avenue fault is constrained by the distribution of marine platforms and by quarry, trench, and ditch exposures in the Farmboy Quarry area (Fig. 6). These trenches exposed unfaulted late Quaternary alluvium and colluvium overlying vertical to overturned beds of the Pliocene Squire Member of the Pismo Formation, which contained a complex system of minor shears and fractures (Fig. 8). Minor displacements of the 120 ka marine platform by low- and high-angle faults are exposed in the quarry walls. The trench and quarry exposures indicate that the hanging wall block is characterized by an overturned anticline and considerable amounts of complex, small-scale brittle deformation. As shown on Figure 8, one high-angle fault that displaces the 120 ka platform has an up-to-the-west sense of displacement. This fault probably merges with the main up-to-the-east reverse fault in the subsurface and thus probably is a hanging-wall "backthrust".

Bedding in the Squire Member exposed in a drainage ditch about 100 m south of the quarry is essentially horizontal and is overlain by marine deposits associated with the 120 ka platform (Fig. 8). Bedding attitudes within the Squire Member exposed in the quarry walls and the drainage ditch suggest that the surface projection of the Wilmar Avenue fault lies between these exposures and is approximately coincident with U.S. Highway 101. Folding associated with the Wilmar Avenue fault in this area consists of primarily anticlinal deformation located in the hanging-wall block, and hence constrasts with development of the footwall syncline exposed at the sea-cliff exposure near Wilmar Avenue.

Detailed mapping of marine terraces and borehole data also suggest that the surface projection of the Wilmar Avenue fault lies beneath U.S. Highway 101. Vertical separation of the 120 ka wave-cut platform across the fault is between 4.3 to 6.4 m (Fig. 8), based on assumed slopes of 1 and

2 degrees to the southwest for the wave-cut platform. These values of vertical separation are comparable to the separation of the 120 ka platform in the Wilmar Avenue sea-cliff exposure. Assuming fault dips of 45 to 70 degrees, we estimate an average late Pleistocene net slip rate of 0.04 to 0.08 mm/yr.

Southeast of the Farmboy Quarry area, numerous photogeologic lineaments and disruptions of the marine terrace sequence indicate that deformation associated with the Wilmar Avenue fault occurs over a zone up to 0.6 km wide. However, because of extensive eolian deposits, fluvial erosion, parallelism of the fault trend and marine strandlines, and limited land access, assessment of the characteristics of the fault is difficult. South of the town of Nipomo, the trace of the Wilmar Avenue fault is inferred by the alignment of several subtle geomorphic and geologic features, including a straight segment of Nipomo Creek and a postulated Tertiary basin margin. This basin margin is inferred on the basis of field mapping and water well data that indicate a 37 m down-on-the-south change in elevation of the top of Franciscan Complex across the projected trend of the Wilmar Avenue fault. This change may represent a shoreline angle and/or displacement along the Wilmar Avenue fault.

San Luis Bay Fault - The San Luis Bay fault is a generally west-trending reverse fault that displaces and locally warps late Quaternary marine terraces near the community of Avila Beach (Fig. 9). The fault, which was identified during detailed mapping of marine terraces in early 1987, is poorly expressed geomorphically and is observed in only one location, a roadcut and sea-cliff exposure about 0.3 km west of Avila Beach (Fig. 10). The behavior and geometry of the fault are interpreted primarily from detailed investigation of this exposure, analysis of deformed marine platforms onshore (Hanson and others, this volume), and supported by interpretation of offshore geophysical data (PG&E, 1988).

The San Luis Bay fault exposed in the roadcut and seacliff near Avila Beach is a zone of shearing whose northern strand strikes approximately east-west and is about 1 m wide. The fault dips about 15 to 45 degrees to the north and becomes progressively steeper down dip. Mullions within the fault zone trend roughly N17E and suggest predominantly dip-slip displacement on the fault. Up-to-the-north reverse displacement is indicated by the juxtaposition of rocks of the Franciscan Complex over the Pliocene Squire Member of the Pismo Formation. The fault displaces the 120 ka marine terrace and younger overlying colluvial deposits. Based on elevations of the 120 ka strandline on both sides of the fault, there is 5 to 8.5 m of cumulative post-120 ka vertical separation across the fault zone in the vicinity of Avila Beach (Fig. 4).

At the mouth of San Luis Obispo Creek, late Quaternary fluvial terrace deposits are displaced by a strand of the San Luis Bay fault (Fig. 11). The base of these deposits, which yielded a radiocarbon age of 21,040 $\pm$ 850 yr BP, shows approximately 20 cm of apparent vertical separation on a fault that strikes N87W and dips 38 $\pm$ 5 degrees northeast. Slickensides on the fault plane indicate essentially pure dip slip.

The San Luis Bay fault is interpreted to continue west from the Avila Beach expo-

sure through a large topographic saddle between San Luis Hill and the Irish Hills (Fig. 9). West of the topographic saddle, detailed field mapping, drilling, and surveying suggest that the two lowest marine terraces are disrupted by faulting and/or tight monoclinal folding near the mouth of Rattlesnake Canyon (Fig. 4). Close to the fault, there is 1.0 to 4.6 m of vertical separation of the 120 ka strandline. However, over a zone approximately 1500 m wide, there is about 7.0 to 7.4 m of vertical separation of this strandline as a result of faulting and down-to-the-south warping. The 80 ka strandline lies at an elevation of 4.6 m on the upthrown block, but is not present on the downthrown side of the fault (Fig. 4). If this difference in elevation is a result of tectonic deformation (rather than erosion), then the 80 ka strandline has a minimum vertical separation of 4.6 m.

Based on data from the Rattlesnake Canyon area and the Avila Beach exposure, the estimated post-120 ka rate of vertical separation ranges from 0.04 to 0.07 mm/yr. Based on a range in fault dip from 40 to 70 degrees, these data yield a range in average slip rate of 0.04 to 0.11 mm/yr. This range is comparable to that estimated for the Wilmar Avenue fault and suggests a low degree of activity.

West of Rattlesnake Canyon, the San Luis Bay fault probably extends into the offshore area between the coastline and the Hosgri fault. Within 2.5 km of the east trace of the Hosgri fault zone, several geophysical lines image what is probably a reverse fault in bedrock that dips steeply (approximately 70 degrees) to the northeast. This fault reaches the sea floor and cuts rocks interpreted to be of Miocene age. Available stratigraphic data do not permit evaluation of the activity of this offshore fault during the Quaternary. Bathymetric data and sea floor samples permit, but do not require, connection of this unnamed fault with the San Luis Bay fault.

The San Luis Bay fault may extend offshore to the southeast from the Avila Beach exposure along the northern margin of San Luis Obispo Bay. Detailed mapping of marine terraces and bedrock geology between Avila Beach and Pismo Beach revealed an unbroken flight of marine terraces and indicates that if the fault extends to the southeast, it remains offshore southeast of Avila Beach. Bathymetric data, seafloor samples, and structural data collected by diver geologists suggest that the fault dies out within about 4 km southeast of the Avila Beach exposure and is not directly continuous with the Wilmar Avenue fault. Thus, the available evidence supports the interpretation that the San Luis Bay fault and the Wilmar Avenue fault do not directly connect, but have an en echelon geometry as individual structural elements along the southwestern margin of the San Luis Range.

<u>Olson Fault</u> - The Olson fault is a west-trending fault that intersects the coastline about 6.4 km northwest of Point San Luis (Fig. 9). The fault was identified during detailed mapping of marine terraces in 1987 and is interpreted to be the northeasternmost element of the zone of faults along the southwestern margin of the San Luis Range. The presence of the fault is inferred on the basis of abrupt down-on-the-south changes in elevations of lower marine wave-cut platforms. The fault is

not exposed onshore and it has no geomorphic expression. Based on analogy with other faults along the southwestern margin of the San Luis Range, tectonic and kinematic evidence indicating regional compression rather than extension, and offshore stratigraphic relationships, we interpret the Olson fault to dip moderately to steeply to the north and to be characterized by reverse slip.

Detailed field mapping, drilling, and surveying in the vicinity of Olson Hill suggest that the two lowermost marine platforms are disrupted by the Olson fault (Fig. 4). From these data, we estimate 1.5 to 4.6 m of down-to-the-south vertical separation for the 80 ka marine platform, and 4.1 to 6.4 m of vertical separation for the 120 ka marine platform. Thus, the rate of vertical separation ranges from 0.03 to 0.05 mm/yr.

Evaluating the potential offshore continuity of the Olson fault, and its relationship to the Hosgri fault is difficult in large part because of the extremely low rate of slip. Based on diver-geologist data, a 2-km reach of the fault is expressed in the offshore next to the coastline as a discordant contact between rocks of the Franciscan Complex in the hanging wall block and the Squire Member of the Pismo Formation in the footwall block. Further offshore, geophysical evidence for the northwestern extension of the Olson fault is uncertain to nonexistent.

Assessment of possible late Quaternary displacement on the Olson fault east of Olson Hill is problematic because marine platform remnants older than 120 ka are discontinuous and highly eroded. Correlation of platform remnants across the eastern projection of the Olson fault is difficult because the remnants typically are stripped of potentially dateable marine deposits and are not physically continuous across possible fault projections. One possible interpretation of the marine platform correlation suggests that the Olson fault extends inland along the base of the range front and does not disrupt the sequence of higher platforms (Fig. 4). Alternatively, the Olson fault may project to the southeast and displace marine platforms higher than the 120 ka platform with down-to-the-south displacement (Hanson and others, this volume).

We consider the Olson fault to be a minor, local, late Tertiary-Quaternary reactivation of favorably oriented elements within a structurally complex and extensively sheared contact zone between rocks of the Franciscan Complex and the Cretaceous sandstone unit of Hall and others (1979). The Olson fault is possibly a zone of en echelon minor faults that may coalesce at depth, whose attitude and expression is dictated by pre-existing shears. By analogy with other components along the southwestern margin of the San Luis Range and from poorly imaged seismic reflection data, we infer that the Olson fault is a high-angle, north- to northeast-dipping reverse fault. Although the age of most recent rupture is uncertain, the absence of geomorphic expression strongly suggests little or no Holocene activity.

<u>Pecho Fault</u> - The northwest-trending Pecho fault lies entirely offshore west and south of Point San Luis (Fig. 2). The fault is interpreted from offshore geophysical data to dip steeply to the northeast and to have up-to-the-north reverse displacement. To the northwest, the fault merges with or

terminates against the Hosgri fault zone about 10 km west of Point San Luis. To the southeast, the fault branches into two traces in southern San Luis Obispo Bay, both of which appear to die out before intersecting the coast in the Santa Maria Valley area. The total fault length is 22 km including the northern trace and 19 km including the southern trace.

The Pecho fault is expressed geomorphically as a northwest-trending seafloor scarp that extends at least 5.1 km southeast from near the Hosgri fault zone into San Luis Obispo Bay. The scarp is an irregular, southwest-facing scarp in the Franciscan Complex or middle Tertiary bedrock that exhibits average relief of 2 to 3 m and maximum relief of 11 m. The scarp cannot be used to establish the timing of most recent fault activity because it is located in an area that lacks post-late Wisconsin sediments. Seismic reflection data show that a linear trend of terminated reflectors, warped reflectors and zones of disruption occurs along the Pecho fault trace.

Evidence of Quaternary movement along the Pecho fault is observed along the southeastern end of its northern trace in San Luis Obispo Bay. Sedimentary rocks interpreted to be of Wheelerian age (early Pleistocene) are separated about 17 m by what appears to be a vertical fault on seismic reflection profiles. Assuming that the fault dips steeply northeast similar to other faults along the southwestern margin of the San Luis Range, this vertical component of slip suggests a net dip-slip rate of about 0.02 mm/yr. The overlying late Wisconsin unconformity as well as post-late Wisconsin sediments are not displaced in this area. Near the junction of the northern and southern traces of the Pecho fault, geophysical records show that the late Wisconsin unconformity may be elevated up to 6 m across the northern trace, which suggests that slip may have occurred on the northern trace of the Pecho fault in the past 18 ka (PG&E, 1988).

Oceano Fault - The Oceano fault is a 20-km-long northwest-trending reverse fault recognized in the Nipomo Mesa area and in the offshore region west of the town of Oceano (Fig. 2), based on interpretation of onshore and offshore seismic reflection data (PG&E, 1988). The N45W to N50W trend of the structure projects to a previously recognized subsurface fault (California Department of Water Resources, 1970), and to a structure observed in geophysical data in the offshore region 1.8 km northwest of the coastline. The offshore structure follows a more east-southeast trend and appears to terminate in San Luis Obispo Bay approximately 3.3 km from the coastline.

Onshore, the Oceano fault is not exposed or geomorphically expressed. Thick eolian and alluvial deposits and extensive fluvial erosion in the Santa Maria Valley have buried and/or obscured the onshore fault trace. Based on seismic reflection data from the central part of the Nipomo Mesa, the Oceano fault dips 40 to 50 degrees to the northeast. The fault clearly displaces the unconformity on the top of the Franciscan Complex and displaces overlying Tertiary strata. Deformation associated with the fault has occurred as brittle failure and warping on the hanging wall or as a monoclinal flexure. Seismic reflection and oil well data (PG&E, 1988) suggest that the apparent vertical separation

of the top of Franciscan basement in the central part of the Nipomo Mesa is about 122 to 183 m. Along trend to the southeast, the Oceano fault is imaged as a smaller southwest-facing monoclinal flexure with about 43 m of apparent vertical separation of the top of Franciscan basement. This southeasterly decrease in the vertical separation suggests that the fault probably dies out in the northern Santa Maria Valley.

Estimates of the slip rate along the onshore reach of the Oceano fault are based on vertical separation of marine deposits of probable Pliocene or possibly early Pleistocene age. Oil well data suggest that in the Nipomo Mesa area the vertical separation of the top of the Foxen Formation is between 77 and 126 m (Hanson and others, this volume). Assuming an age of 1 to 2 ma for this unconformity, and a fault dip of between 40 and 65 degrees, yields a net slip rate of 0.04 to 0.20 mm/yr for the fault in the Nipomo Mesa area. Data from water wells along the coastline suggest that the top of the Foxen Formation has about 27 m of vertical separation (Hanson and others, this volume). Assuming the same age and fault dip ranges yields a net post-Pliocene slip rate of 0.01 to 0.04 mm/yr for the Oceano fault at the coast.

Offshore geophysical data suggest that the Oceano fault displaces beds of probable Pleistocene age overlying a late Pliocene (?) unconformity (PG&E, 1988). Along the western end of the Oceano fault, the late Wisconsin (18 ka) unconformity is not disrupted, suggesting that the fault has not been active in the late Pleistocene and Holocene.

DISCUSSION

The San Luis Range is one of a series of west-northwest-trending, elongated structural blocks within the Los Osos/Santa Maria (LOSM) domain. Our studies indicate that these blocks typically are bordered by west-northwest-trending reverse faults (Fig. 1). The structural grain of and tectonic style within the LOSM domain are unique to the south-central coastal California region. The west-northwest-trending grain of the domain is transitional between the east-west-trending western Transverse Ranges to the south and the north-northwest-trending Santa Lucia and San Rafael ranges to the northeast. To the west, the west-northwest-trending reverse faults and structural blocks of the LOSM domain terminate against the north-northwest-trending Hosgri and San Simeon fault zones. The pattern and development of structures in the offshore Santa Maria Basin west of the Hosgri and San Simeon fault zones contrasts sharply with those in the LOSM domain. The offshore basin is characterized by gradual block subsidence, scattered faults, and broad, late Cenozoic folds that are subparallel to the Hosgri and San Simeon fault zones and oblique to the structures within the LOSM.

Many of the blocks within the LOM domain contain geologic evidence of Tertiary fold deformation (Hall, 1973a; Hall and Prior, 1979; Blake and others, 1978). Our investigations of Quaternary deposits and landforms within and along the margins of the San Luis Range indicate that fold deformation ceased prior to 500,000 years ago and probably 1 million years ago. Marine terrace elevations determined by Hanson and others (this

volume) indicate that the San Luis Range has undergone late Quaternary uplift as a relatively rigid crustal block with little to no internal deformation of the block. We informally name this block the San Luis/Pismo (SLP) structural block.

Quaternary uplift of the SLP block occurred primarily via reverse faulting along the block margins. The northeastern margin is bordered by the northeast-vergent Los Osos fault zone (Lettis and others, this volume). The southwestern margin is bordered by the southwest-vergent Wilmar Avenue, San Luis Bay, Olson, Oceano, and Pecho faults, a described in this paper. Minor amounts of tilting have occurred between these latter faults. This tilting, combined with the lateral discontinuity of the fault traces, suggest that this margin of the block is a complex, diffuse zone that contrasts with the comparatively discrete Los Osos fault zone along the northwestern margin of the block. The lack of emergent marine terraces and substantial sedimentation within the Santa Maria Valley suggest that the zone of faulting along the southwestern margin of the block represents a zone of transition between uplift of the range and subsidence of the valley. Based on the distribution of marine terraces, the Santa Maria Valley and Cambria structural blocks, which border the SLP block on the southwest and northeast, respectively, have subsided or remained static since at least the middle Pleistocene. From these data, we infer that crustal shortening in the LOSM domain is accomodated by rigid uplift, subsidence, or tilting of structural blocks along reverse faults at block margins.

Regional Tectonic Environment

Deformation within the Los Osos/Santa Maria domain is ultimately driven by transpressive dextral shear arising from relative motion between the Pacific and North American plates. The plate boundary is a broad, heterogeneous zone of dextral strike-slip and north-northeast to south-southwest-directed compressive deformation centered along the San Andreas fault (Crowell, 1962; Dickinson and Snyder, 1979) and extending in width from the western Great Basin to the continental slope (McCulloch, 1987). Within this broad zone, movement of large crustal blocks, such as rotation of the western and central Transverse Ranges (Hornafius and others, 1986) and extension within the Basin and Range province, has locally influenced the pattern and style of deformation. As described below, we interpret that rotation of the western Transverse Ranges, in particular, has influenced contemporary deformation within the Los Osos/Santa Maria domain.

Recent plate-motion models suggest the North America-Pacific plate boundary at the latitude of central California is continuing to experience transpressional or pure translational right shear. The NUVEL-1 plate-motion model estimates relative motion between these plates to be about 48 mm/yr towards N35°W (DeMets and others, 1987; Gordon and others, 1987). This predicted motion is approximately 6 to 8 mm/yr slower than, but in the same general direction as, that predicted by the RM2 model of Minster and Jordan (1978). Saucier and Humphreys (1988) estimate the relative motion to be about 53 mm/yr toward approximately N46°W. The model of Pollitz (cited in Mount and Suppe, 1987),

which does not incorporate Basin and Range extension, estimates relative motion of 44 mm/yr towards N30°W.

Estimates of relative motions between the North American and Pacific plates based on geologic and geodetic observations are typically significantly less than those calculated by these plate motion models. Geologic and geodetic studies indicate that the San Andreas fault presently accomodates approximately 35 mm/yr of the motion between the North American and Pacific plates, in a direction N41°W (Sieh and Jahns, 1984; Kroger and others, 1987; Jordan and Minster, 1988). Additional plate motion is represented by extension within the Basin and Range province at a rate of about 10 millimeters per year, in roughly a N56°W direction (Gordon and Sauber, 1988). The combined displacement on the San Andreas fault and extension in the Basin and Range, however, does not accommodate the total amount of relative plate motion predicted by the plate motion models described above.

Vector solutions of relative plate motion using the NUVEL-1 model and the geologic data described above suggest a plate-motion deficit, termed the San Andreas discrepancy, of about 9 mm/yr in a N14°E direction (Jordan and Minster, 1988). This unaccounted plate motion may be the result of one or more of the following factors: the NUVEL-1 estimate of plate motion may be too high; the estimate of the amount and direction of extension in the Basin and Range may be incorrect; additional slip may be occurring on faults across the western United States; crustal shortening may be occurring along folds and faults; or slip may be occurring as steady, aseismic deformation within the crust. It is likely that at least part of this plate motion deficit is accommodated on right-slip faults between the continental slope and the southern Great Basin, and by compressional deformation within the plate boundary zone. The NUVEL-1 model, for example, predicts about 4 mm/yr additional northwest right slip and 4 to 10 mm/yr northeast-southwest compression normal to the San Andreas fault in central California (DeMets and others, 1987). The RM2 model predicts about 14 mm/yr NE-SW compression (Minster and Jordan, 1978).

The northwest-directed right-slip component of the San Andreas discrepency is reduced significantly by the estimated 1 to 3 mm/yr of right-lateral slip on the Hosgri-San Simeon fault system (PG&E, 1988). The remaining 1 to 3 mm/yr is likely distributed among other major northwest-trending strike-slip faults within the California continental margin, including the Santa Lucia Bank, West Huasna, Nacimiento and Rinconada faults. The northeast-directed shortening strains of the San Andreas discrepency are more difficult to resolve. Geodetic (Feigl and others, 1990) and in-situ stress measurements (Mount and Suppe, 1987; Zoback and others, 1987) suggest northeast-southwest-directed crustal shortening. The distribution and mechanism of these shortening strains is currently a topic of considerable debate. Some authors have proposed that simple fold and thrust style deformation across the southern Coast Ranges and Santa Maria Basin account for as much as 6 to 7 mm/yr of northeast-southwest convergence (Namson and Davis, 1990; Feigl and others, 1990). Although these modeling efforts represent a positive step toward

resolving the compressional component of the San Andreas discrepancy, the resulting fault-related uplift rates greatly exceed those recorded locally in the northern LOSM domain and those implied regionally by continued subsidence of the Santa Maria basin. This suggests the rates of slip proposed by these models may be greatly overestimated. Other models based on the use of balanced cross sections to determine slip rates within the offshore Santa Maria Basin (Clark and others, 1990) and the San Luis Range (PG&E, 1990), which are constrained by Quaternary uplift and geophysical data, indicate that local rates of convergence locally are less than 1 mm/yr.

Crustal Block Rotation

In addition to confirming the motion of large lithospheric plates, recent paleomagnetic investigations strongly indicate discordant motion of smaller regional crustal blocks within the North America-Pacific transform boundary zone. Paleomagnetic declination data, for example, indicate that the Transverse Ranges and parts of the Mojave region have rotated clockwise up to 100 degrees during the Neogene (Luyendyk and others, 1980, 1985; Hornafius and others, 1986; Carter and others, 1987). Since about 6 million years ago, the western Transverse Ranges have rotated 35 degrees clockwise and the San Gabriel Mountains 15 degrees counterclockwise, implying oroclinal bending of the Transverse Ranges in Pliocene and Pleistocene time (Hornafius, 1985; Hornafius and others, 1986). Luyendyk and others (1980, 1985) attribute these movements to rigid block rotations within a right shear couple, resulting in right slip on northwest-trending faults, left slip on (presently) west-trending faults, and clockwise rotation of the originally north-trending Transverse Ranges.

Hornafius and others (1986) suggest that the tectonic history of the western Transverse Ranges involved 1) clockwise rotation during the Middle Miocene (17 to 10 million years ago), and 2) oroclinal bending since 6 million years ago with additional clockwise rotation to the west and counterclockwise rotation to the east. They propose that compression along the north margin of the western Transverse Ranges may be a result of the change from a releasing to a restraining geometry as the San Andreas fault migrated eastward to align with spreading in the Gulf of California.

SUMMARY OF CONTEMPORARY TECTONIC SETTING

The LOSM domain is undergoing north-northeast directed crustal shortening between the western Tranverse Ranges to the south and the Santa Lucia and San Rafael Ranges to the northeast. Quaternary geologic and kinematic data indicate that the shortening is accomodated in the northern part of the LOSM domain primarily by rigid block uplift or subsidence along west-northwest-trending reverse faults. These data indicate that little to no folding is occurring within the structural blocks. This pattern and style of deformation appear to be incompatible with an interpretation of a simple fold and thrust style of deformation. The absence of late Quaternary folding within the San Luis Range is incompatible with the style of deformation predicted by geometric constraints of low-angle, fault-propagation or fault-bend fold models (Suppe, 1985).

We interpret that crustal shortening in the LOSM domain is related to northwestward movement of the Pacific plate relative to the North America plate, locally modified by late Cenozoic clockwise rotation of the western Transverse Ranges (Luyendyk and others, 1980, 1985; Luyendyk and Hornafius, 1983). Clockwise rotation of the western Transverse Ranges has compressed the domain against the relatively stable Salinian crust that underlies much of the Santa Lucia and San Rafael ranges to the northeast. This model requires that crustal shortening at depth is accomodated by ductile flow in the lower crust or by aseismic slip on a subducted, northeast-dipping oceanic plate that underlies the domain at depths of about 12 to 22 km (Meltzer and Levander, 1987). Above the brittle/ductile transition, crustal shortening in the northern and northwestern parts of the Los Osos/Santa Maria domain is accommodated primarily by reverse faulting along the margins of structural blocks and by uplift, subsidence, or tilting of the blocks.

REFERENCES

Blake, M.C. Jr., Campbell, R.H., Dibblee, T.W., Jr., Howell, D.G., Nilsen, T.H., Normark, W.R., Vedder, J.C., and Silver, E.A., 1978, Neogene basin formation in relation to plate-tectonic evolution of San Andreas fault system, California: The American Association of Petroleum Geologists Bulletin, v. 62, no. 3, p. 344-372.

California Department of Water Resources, 1970, Sea-water intrusion: Pismo-Guadalupe area, Bulletin No. 63-3, 5 sheets.

Carter, J.M., Luyendyk, B.P., and Terres, R.R., 1987, Neogene clockwise rotation of the eastern Transverse Ranges, California, suggested by paleomagnetic vectors: Geological Society of America Bulletin, v. 98, p. 199-206.

Clark, D.H., Hall, N.T., Hunt, T.D., and Lettis, W.R., 1988, Style and timing of slip on the San Miguelito fault, San Luis Obispo County, California (abs.): Geological Society of America, Cordilleran Section Meeting, Abstracts with Programs, v. 20, no. 3, p. 150.

Clark, D.H., Hall, N.T., Hamilton, D.H., and Heck, R.G., in press, Structural analysis of late Neogene deformation in the central offshore Santa Maria Basin, California: Journal of Geophysical Research.

Cleveland, G.B., 1978, Geologic map of the Pt. Buchon area, San Luis Obispo County, California, with summary comments: U.S. Geological Survey Open-File Report 78-17 LA, 6 p.

Coyle, J.M., Hall, N.T., Hengesh, J.V., and Lettis, W.R., 1987, Quaternary deformation along the southwestern margin of the San Luis-Pismo synform, Pismo Beach, California (abs.): Geological Society of America, Abstracts with Programs, v. 19, no. 6, p. 368.

Crowell, J.C., 1962, Displacement along the San Andreas fault, California: Geological Society of America Special Paper 71, 61 p.

DeMets, C., Gordon, R.G., Stein, S., and Argus, D.F., 1987, A revised estimate of Pacific-Noth American motion and implications for western North America plate boundary zone tectonics: Geophysical Research Letters, v. 14, p. 911-914.

Dickinson, W.R., and Snyder, W., 1979, Geometry of triple junctions related to the San Andreas transform: Journal of Geophysical Research, v. 84, p. 561-572.

Feigl, K.L., King, R.W., and Jordan, T.H., 1990, Geodetic measurement of tectonic deformation in the Santa Maria fold and thrust belt, California: Journal of Geophysical Research, v. 95, no. B2, p. 2679-2699.

Gordon, D., and Sauber, T., 1988, Geodesy by radiointerferometry: Determination and analysis of vector site motions in the southwestern United States (abs.): EOS, v. 69, no. 16, p. 331.

Gordon, R., DeMets, C., Stein, S., Argus, D., and Woods, D., 1987, A new dataset and model for current plate motions: Indian Ocean, Caribbean plate, and Pacific-North America: Geodynamics Symposium, Programs and Abstracts, p. 709.

Gray, L.D., 1980, Geology of Mesozoic basement rocks in the Santa Maria basin, Santa Barbara and San Luis Obispo counties, California: unpublished M.S. thesis, San Diego State University, San Diego, California, 78 p.

Hall, C.A., Jr., 1973a, Geology of the Arroyo Grande quadrangle, California: California Division of Mines and Geology, Map Sheet 24, scale 1:48,000.

Hall, C.A., Jr., 1973b, Geologic map of the Morro Bay South and Port San Luis quadrangles, San Luis Obispo County, California: U.S. Geological Survey Miscellaneous Field Studies Map MF-511, scale 1:24,000.

Hall, C.A., Jr., 1978a, Geologic map of Twichell Dam and parts of Santa Maria and Tepusquet Canyon quadrangles, Santa Barbara County, California: U.S. Geologic Survey Miscellaneous Field Studies Map MF-933, Scale 1:24,000.

Hall, C.A., Jr., 1978b, Origin and development of the Lompoc-Santa Maria pull- apart basin and its relation to the San Simeon-Hosgri strike-slip fault, western California: in Silver, E.A., and Normack, W.R. (eds.), San Gregorio-Hosgri fault zone, California, California Division of Mines and Geology Special Report 137, p. 25-31.

Hall, C.A., Jr., 1981, Chapter 17 - Evolution of the western Transverse Ranges microplate: Late Cenozoic faulting and basinal development: in Ernst, W.G. (ed.), The Geotectonic Development of California, Rubey Volumn, no. 1, Prentice-Hall, Inc., Englewood Cliffs, New Jersey, p. 559-582.

Hall, C.A., Jr., 1982, Pre-Monterey subcrop and structure contour maps, western San Luis Obispo and Santa Barbara Counties, south-central California: U.S. Geological Survey, Miscellaneous Field Studies Map MF-1386, 6 sheets, scale 1:62,5000, 28 p.

Hall, C.A., Jr., and Corbato, C.E., 1967, Stratigraphy and structure of Mesozoic and Cenozoic rocks, Nipomo quadrangle, Southern Coast Ranges, California: Geological Society of America Bulletin, v. 78, p. 559-582.

Hall, C.A., Jr., and Prior, S.W., 1975, Geologic map of the Cayucos-San Luis Obispo region, San Luis Obispo County, California (1:24,000): U.S. Geological Survey Miscellaneous Field Studies Map MF-686, 2 sheets.

Hall, C.A., Jr., and Surdam, R.C., 1967, The San Luis Obispo-Nipomo area, San Luis Obispo County, California: Geological Society of America Guidebook, 63rd Annual Meeting of Cordilleran Section, p. 1-26.

Hall, C.A., Jr., Ernest, W.G., Prior, S.W., and Wiese, J.W., 1979, Geologic map of the San Luis Obispo-San Simeon Region, California: U.S. Geological Survey Miscellaneous Investigations Series, Map I-1097, Scale 1:48,000.

Hanson, K.L., Wesling,J.R., Lettis, W.R., Kelson, K.I., and Mezger, L., this volume, Correlation, ages, and uplift rates of Quaternary marine terraces, south-central coastal California.

Hornafius, J. S., 1985, Neogene tectonic rotation of the Santa Ynez Range, western Transverse Ranges, California, suggested by paleomagnetic investigation of the Monterey Formation: Journal of Geophysical Research, v. 90, p. 12503-12522.

Hornafius, S.J., Luyendyk, B.P., Terres, R.R., and Kamerling, M.J., 1986, Timing and extent of Neogene tectonic rotation in the western Transverse Ranges, California: Geological Society of America Bulletin, v. 97, p. 1476-1487.

Jordan, T.H., and Minster, J.B., 1988, Measuring crustal deformation in the American West: Scientific American, v. 256, no. 8, p. 48.

Kelson, K.I., Lettis, W.R., Weber, G.E., Kennedy, G.L., and Wehmiller, J.F., 1987, Amount and timing of deformation along the Wilmar Avenue, Pismo, and San Miguelito faults, Pismo Beach, California: Geological Society of America, Cordilleran Section Meeting, Abstracts with Programs, v. 19, no. 6, p. 394.

Kroger, P.M., Lyzenga, G.A., Wallace, K.S., and Davidson, J.M., 1987, Tectonic motion in the western United States inferred from very long baseline interferometry measurements, 1980-1986: Journal of Geophysical Research, v. 92, no. B13, p. 14,151-14,163.

Lettis, W. R., Hall, N. T., and Hamilton, D. H., 1989, Quaternary tectonics of south-central coastal California (abs.): 28th International Geological Congress, Abstracts, v. 2, p. 2-285.

Lettis, W.R. and Hall, N.T., this volume, The Los Osos fault zone, San Luis Obispo County, California.

Lettis, W.R., DiSilvestro, L., Hanson, K.L., and Shiller, G.I., this volume [a], The San Simeon/Hosgri pull-apart basin: south-central coastal California.

Luyendyk, B.P., Kamerling, M.J., and Terres, R.R., 1980, Geometric model for Neogene crustal rotations in southern California: Geological Society of America Bulletin, Part I, v. 91, p. 211-217.

Luyendyk, B.P., Kamerling, M.J., Terres, R.R., and Hornafius, J.S., 1985, Simple shear of southern California during the Neogene: Journal of Geophysical Research, v. 90, p. 12,454-12,466.

Luyendyk, B.P., and Hornafius, J.S., 1983, Neogene crustal rotations, fault slip, and basin development in southern California: in Ingersoll, R.V., and Ernst, W.G., eds., Cenozoic Basin Development of Coastal California, p. 260-283.

McCulloch, D. S., 1987, Regional geology and hydrocarbon potential of offshore central California; in Scholl, D. W., Grantz, A., and Vedder, J., eds., Geology and Resource Potential of the Continental Margin of Western North America and Adjacent Ocean Basins, Beaufort Sea to Baja California: American Association of Petroleum Geologists, Cicum Pacific Earth Science, v. 6, p. 353-401.

Meltzer, A.S., and Levander, A.R., 1987, Interpretation of deep crustal reflection profiles offshore southern central California (abs.): EOS, v. 68, no. 44, p. 1365.

Minster, J.B., and Jordan, T.H., 1978, Present-day plate motions: Journal of Geophysical Research, v. 83, no. B11, p. 5331-5354.

Mount, V.S., and Suppe, J., 1987, State of stress near the San Andreas fault: Implications for wrench tectonics: Geology, v. 15, p. 1143-1146.

Namson, J.S., and Davis, T.L. 1990, in review, Susurface study of the late Cenozoic structural geology of the Santa Maria basin, western Transverse Ranges and southern Coast Ranges, California.

Pacific Gas and Electric Company, 1989, Hosgri fault zone, tabulation of observations: Diablo Canyon Long Term Seismic Program, Response to Question 43, Attachment Q43-1, U. S. Nuclear Regulatory Commission Docket Nos. 50-275 and 50-323.

Pacific Gas and Electric Company, 1990, Montage of geophysical data and interpretations, Hosgri fault zone, eastern offshore Santa Maria basin, data base, interpretational procedures, and key observations; Diablo Canyon Long Term Seismic Program report, Response to Question GSG-1, Attachment GSG Q1-A: U. S. Nuclear Regulatory Commission, Docket Nos. 50-275 and 50-323, 59 p., 29 panels.

Saucier, F., and Humphreys, E., 1988, Finite element kinematic model of southern California (abs.): EOS, Transactions of the American Geophysical Union, v. 69, p. 331.

Sieh, K.E., and Jahns, R.H., III., 1984, Holocene activity of the San Andreas fault at Wallace Creek, California: Geological Society of America Bulletin, v. 95, no. 8, p. 883-896.

Stanley, K.O., and Surdam, R.C., 1984, The role of wrench fault tectonics and relative changes of sea level on deposition of upper Mio-Pliocene Pismo Formation, Pismo syncline, California: in Surdam, R.C., ed., Stratigraphic, Tectonic, Thermal, and Digenetic Histories of the Monterey Formation, Pismo and Huasna Basin, California: Society of Economic Paleontologists and Mineralogists Guidebook No. 2, San Jose, California, p. 21-37.

Suppe, J., 1985, Principles of Structural Geology: Prentice-Hall, Englewood Cliffs, New Jersey.

Zoback, M.D., Zoback, M.L., Mount, V.S., Suppe, J., Eaton, J.P., Healy, J.H., Oppenheimer, D., Reasenberry, P., Jones, L., Raleigh, C.B., Wong, I.G., Scotti, O., and Wentworth, C., 1987b, New evidence on the state of stress of the San Andreas fault system: Science, v. 238, p. 1105-1111.

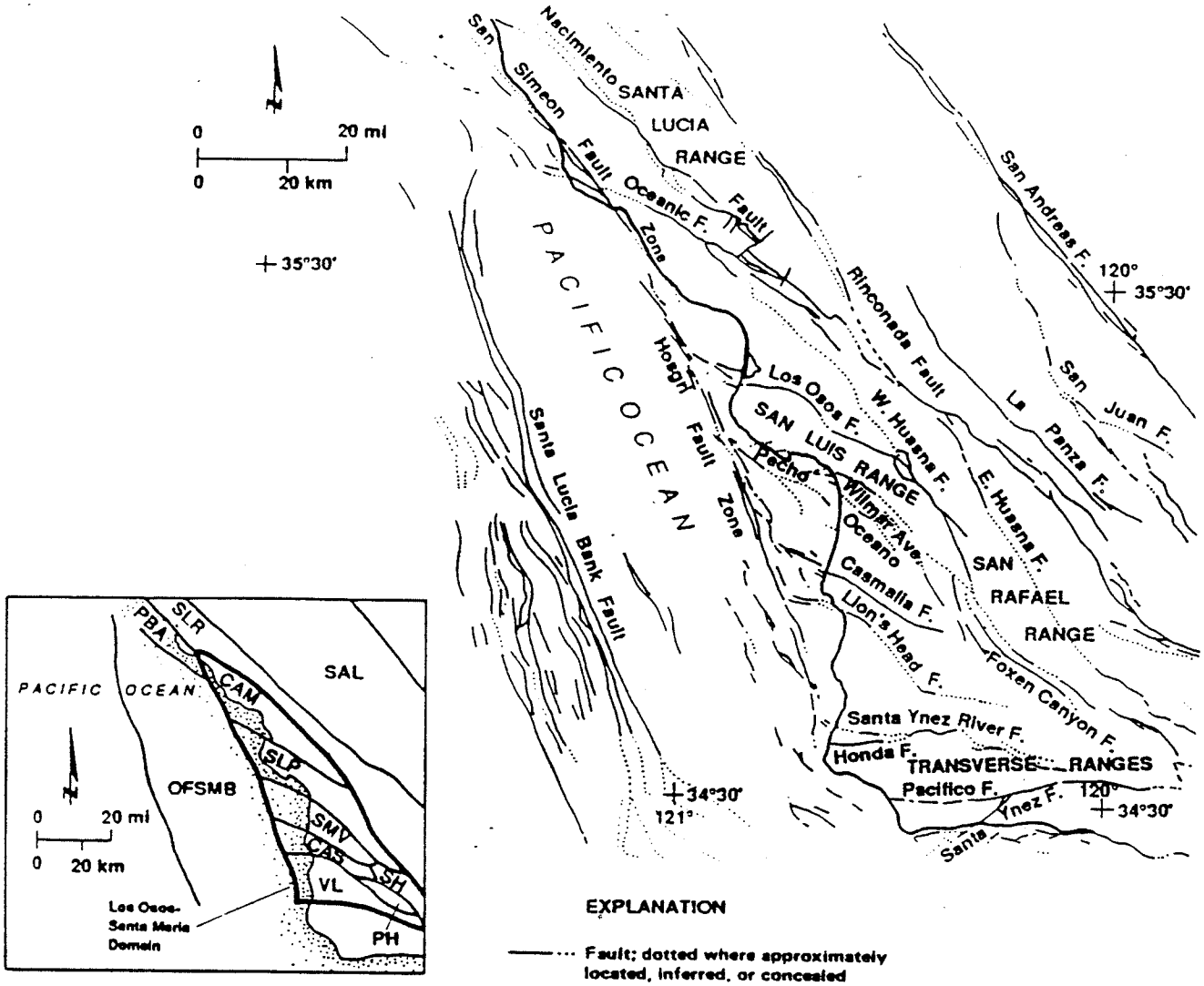

Figure 1. Map of structural blocks and faults in the south-central California coastal region. SAL = Salinian block, SLR = Santa Lucia Range block, PBA = Piedras Blancas anticlinorium, CAM = Cambria block, SLP = San Luis/Pismo block, OFSMB = Offshore Santa Maria basin block, SMV = Santa Maria Valley block, CAS = Casmalia block, VL = Vanderberg/Lompoc block, PH = Purisima Hills block, SH = Solomon Hills block.

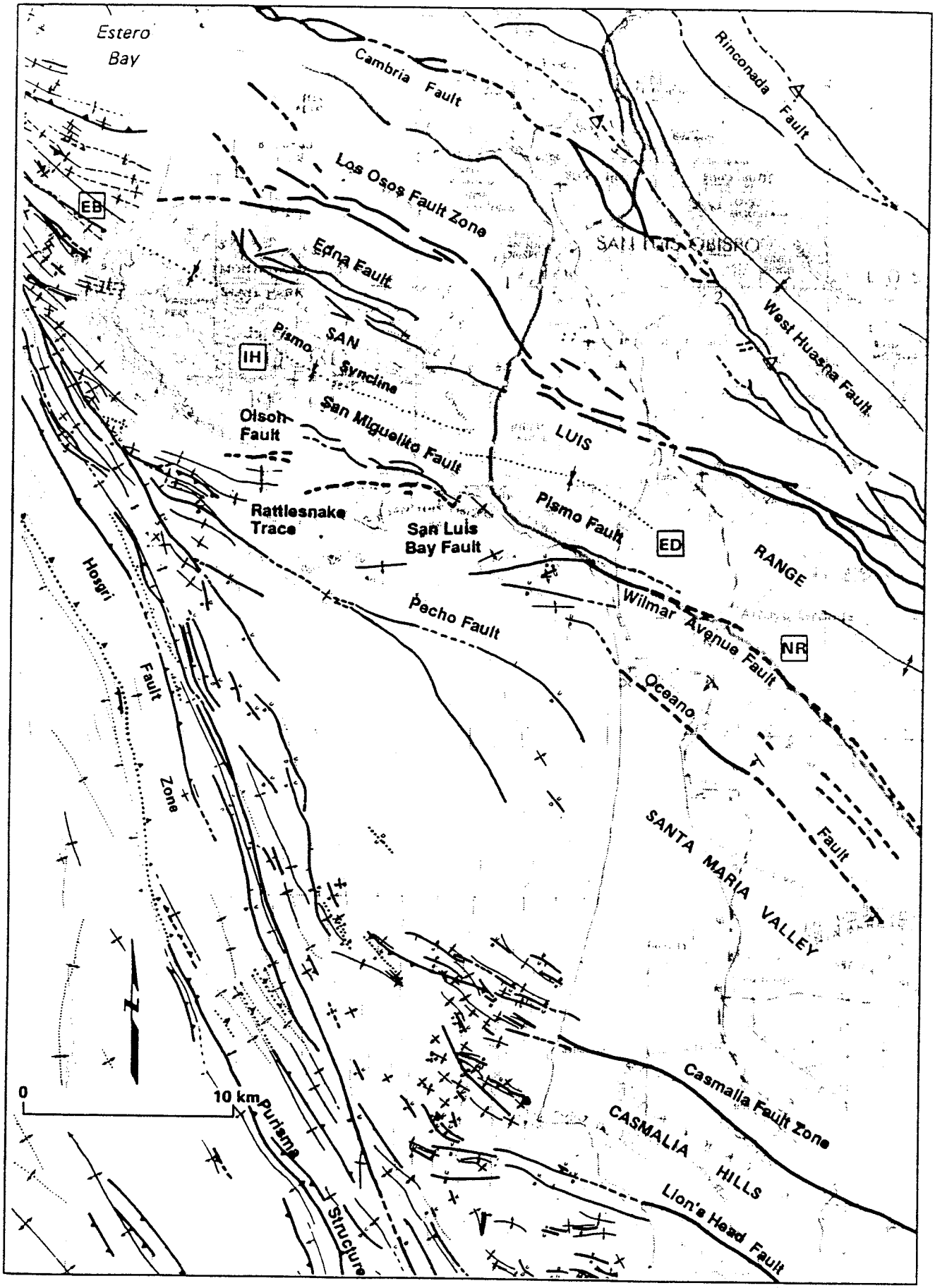

Figure 2. Map of faults and folds in the onshore and offshore regions of south-central California. Subblocks of the San Luis Range are: EB, Estero Bay; IH, Irish Hills; ED, Edna; and NR, Newsom Ridge.

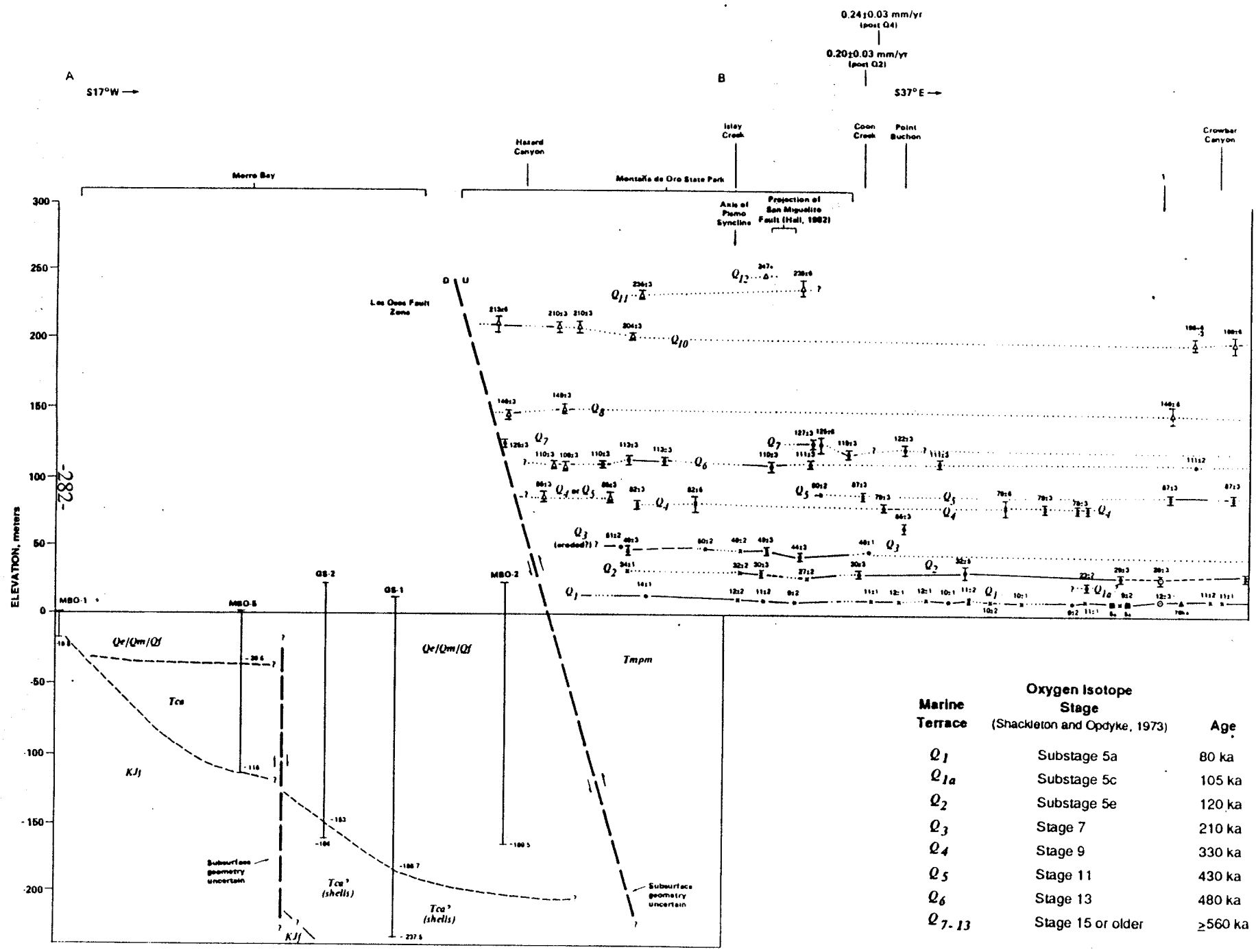

Figure 3. Longitudinal profiles of terraces between Morro Bay and Crowbar Canyon, across the Pismo Syncline and projection of the San M[illegible] ult. No vertical exaggeration. For location of profile, see Hanson et al. [illegible] (this volume)

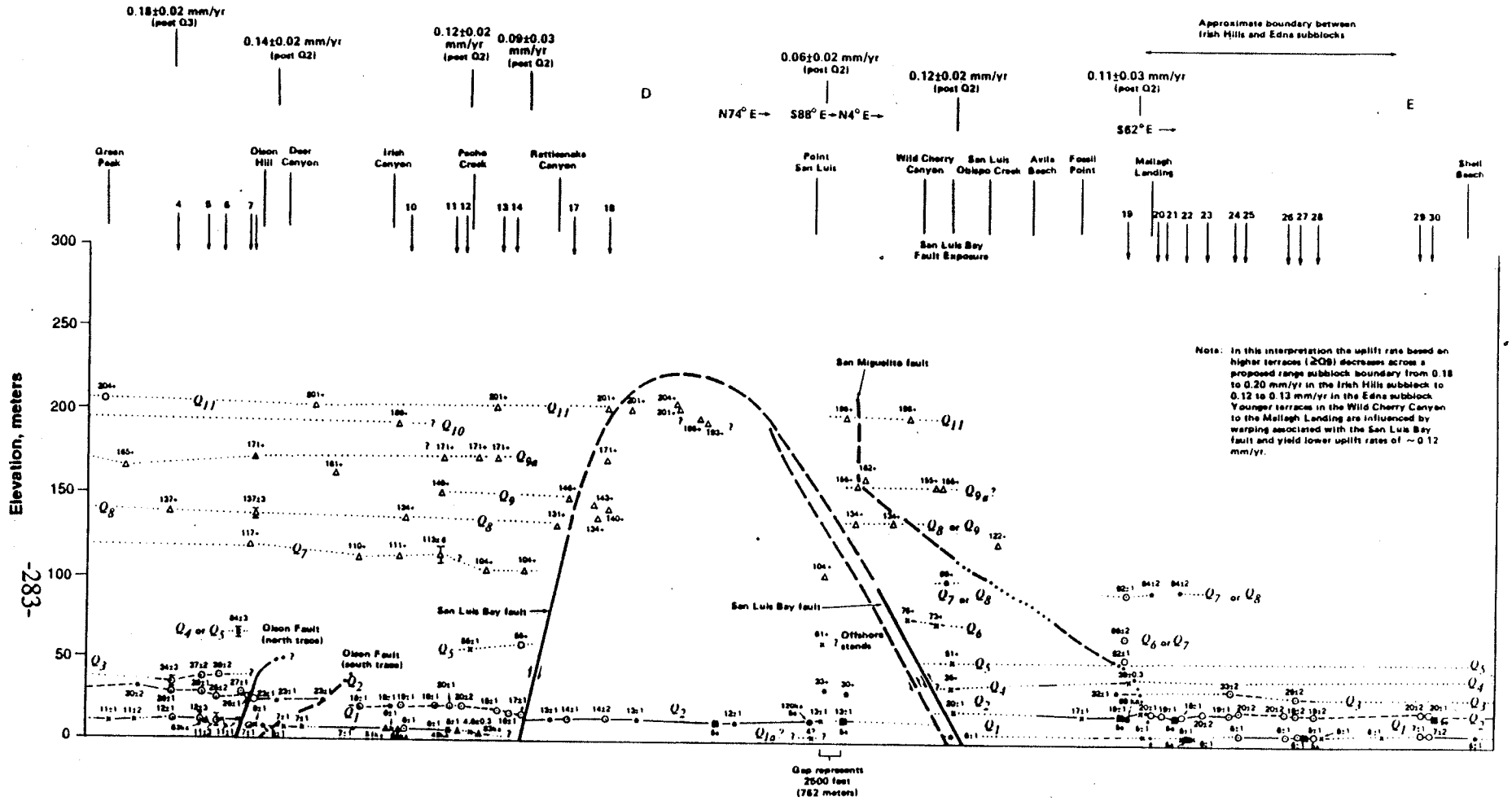

Marine Terrace	Oxygen Isotope Stage (Shackleton and Opdyke, 1973)	Age
Q_1	Substage 5a	80 ka
Q_{1a}	Substage 5c	105 ka
Q_2	Substage 5e	120 ka
Q_3	Stage 7	210 ka
Q_4	Stage 9	330 ka
Q_5	Stage 11	430 ka
Q_6	Stage 13	480 ka
$Q_{7\text{-}13}$	Stage 15 or older	≥560 ka

Figure 4. Longitudinal profiles of marine terraces between Green Peak and Shell Beach, crossing the Olson, San Luis Bay, and San Miguelito faults. No vertical exaggeration. For location of profile, see Hanson and others (this volume).

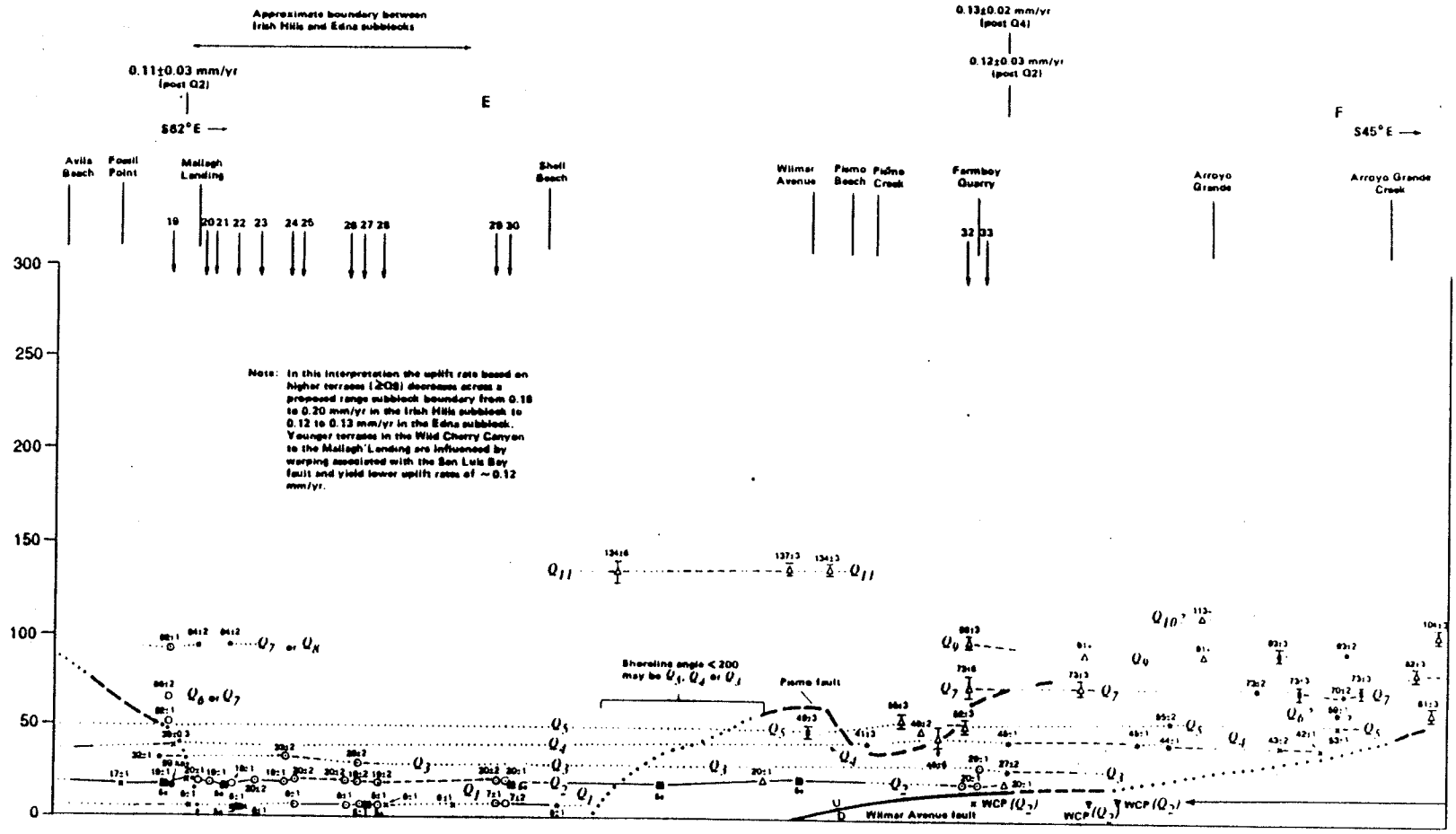

Marine Terrace	Oxygen Isotope Stage (Shackleton and Opdyke, 1973)	Age
Q_1	Substage 5a	80 ka
Q_{1a}	Substage 5c	105 ka
Q_2	Substage 5e	120 ka
Q_3	Stage 7	210 ka
Q_4	Stage 9	330 ka
Q_5	Stage 11	430 ka
Q_6	Stage 13	480 ka
$Q_{7\text{-}13}$	Stage 15 or older	>560 ka

Figure 5. Longitudinal profiles of marine terraces between Avila Beach and Arroyo Grande, crossing the San Miguelito, Pismo, and Wilmar Avenue faults. No vertical exaggeration. For location of profile , see Hanson and others (this volume).

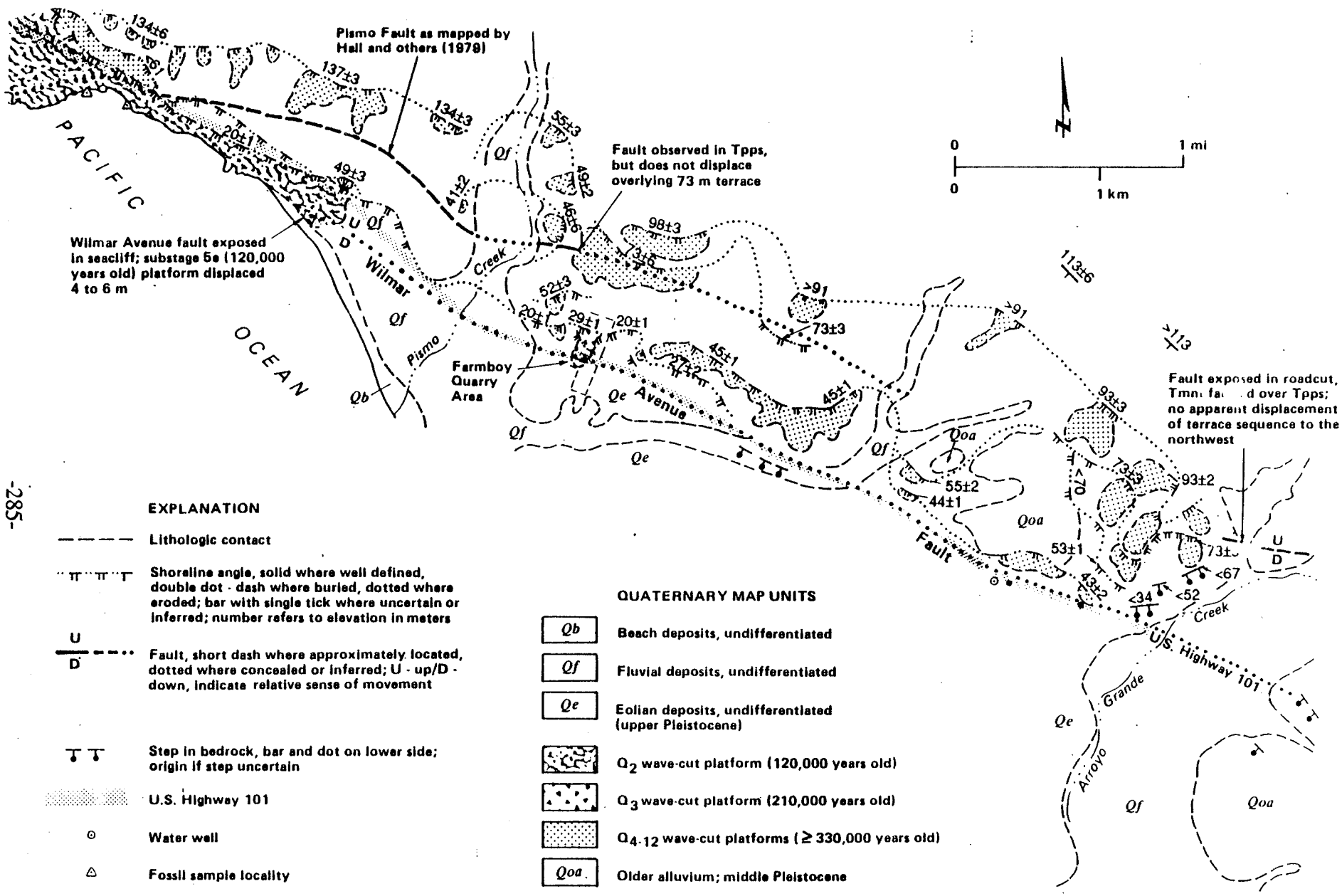

Figure 6. Map of surficial deposits and marine wave-cut platforms along the Wilmar Avenue fault between Pismo Beach and Arroyo Grande.

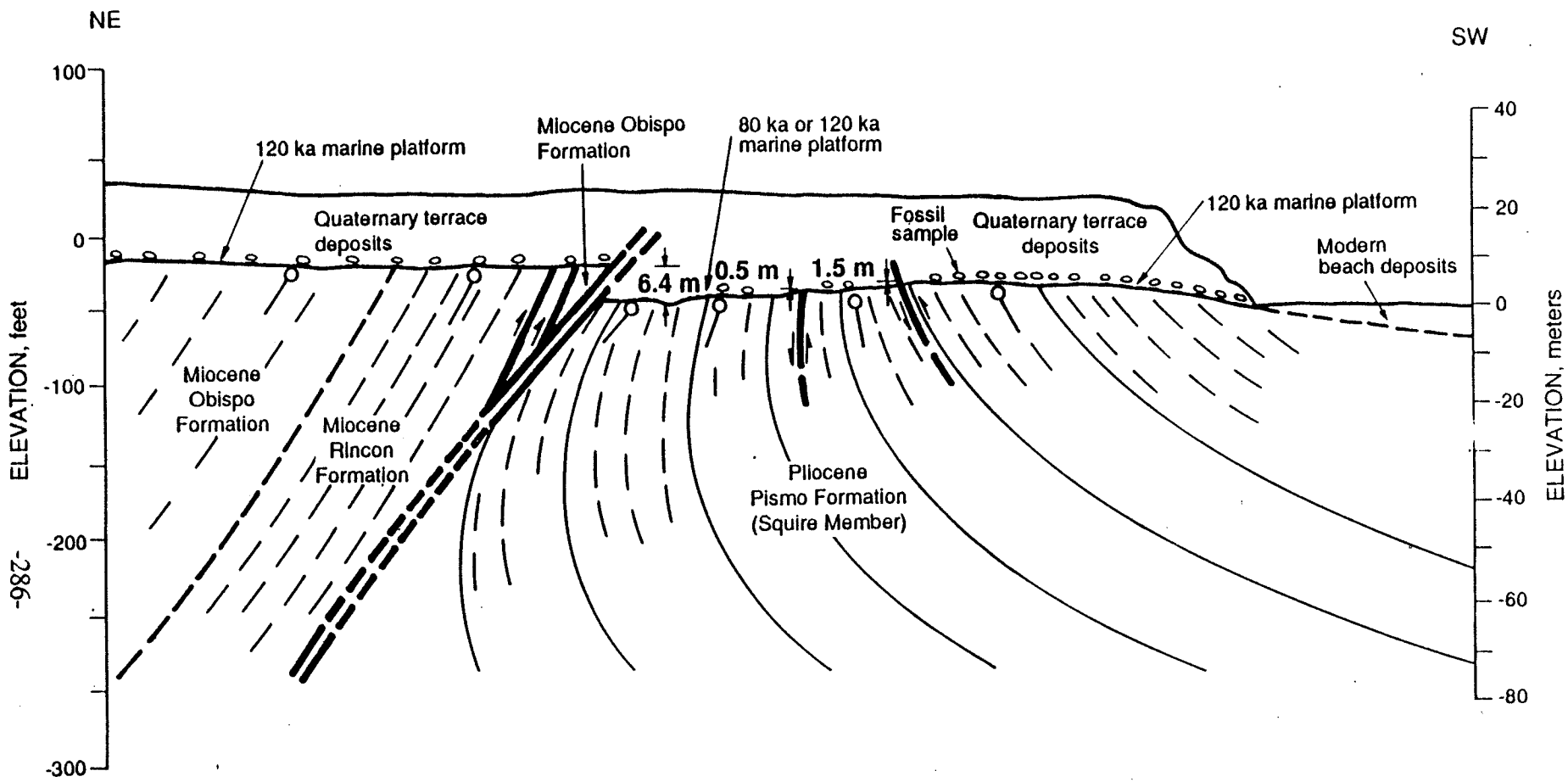

Figure 7. Schematic geologic section across the Wilmar Avenue fault exposed in the sea cliff, Pismo Beach .

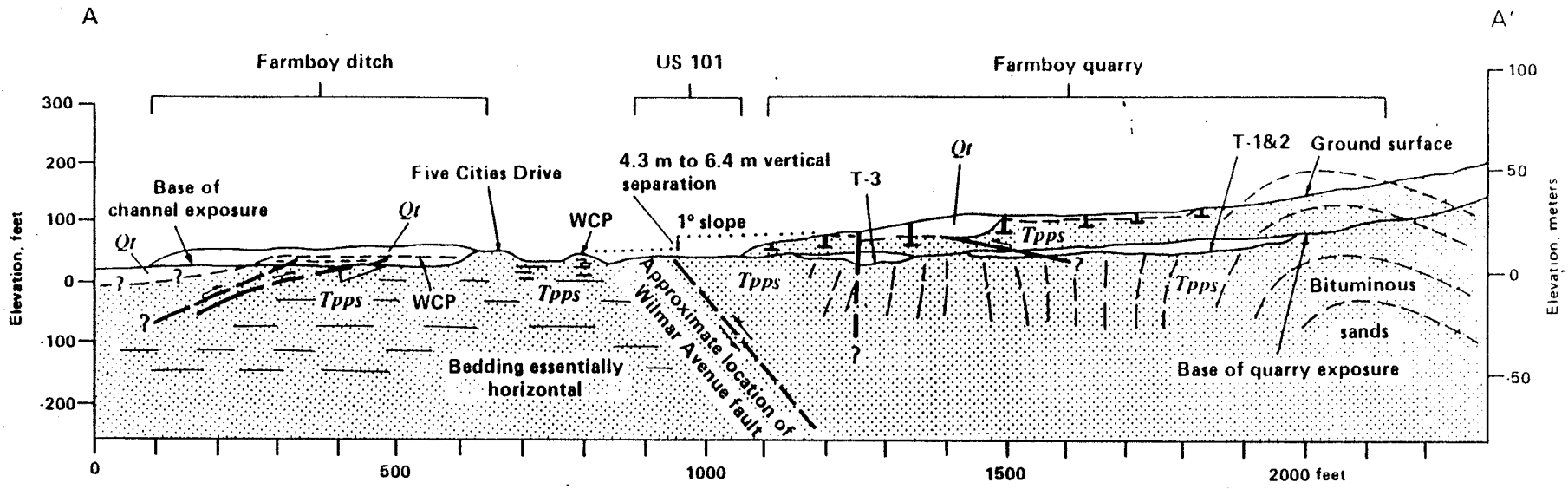

EXPLANATION

Qt	Terrace deposits
Tpps	Squire Member of Pismo Formation; dashed lines indicate bedding orientation
?	Fault; dashed where approximately located; queried where uncertain, arrows indicate relative sense of displacement
WCP	Wave-cut platform
T-1&2	Trench location
⊥	Borehole

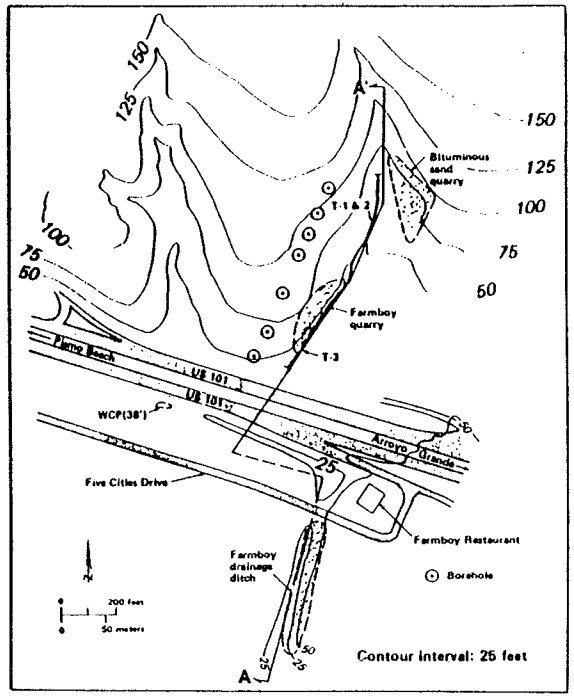

Figure 8. Geologic section across theWilmar Avenue fault in the Farmbooy Quarry area, Pismo Beach. Location of area shown on Figure 6.

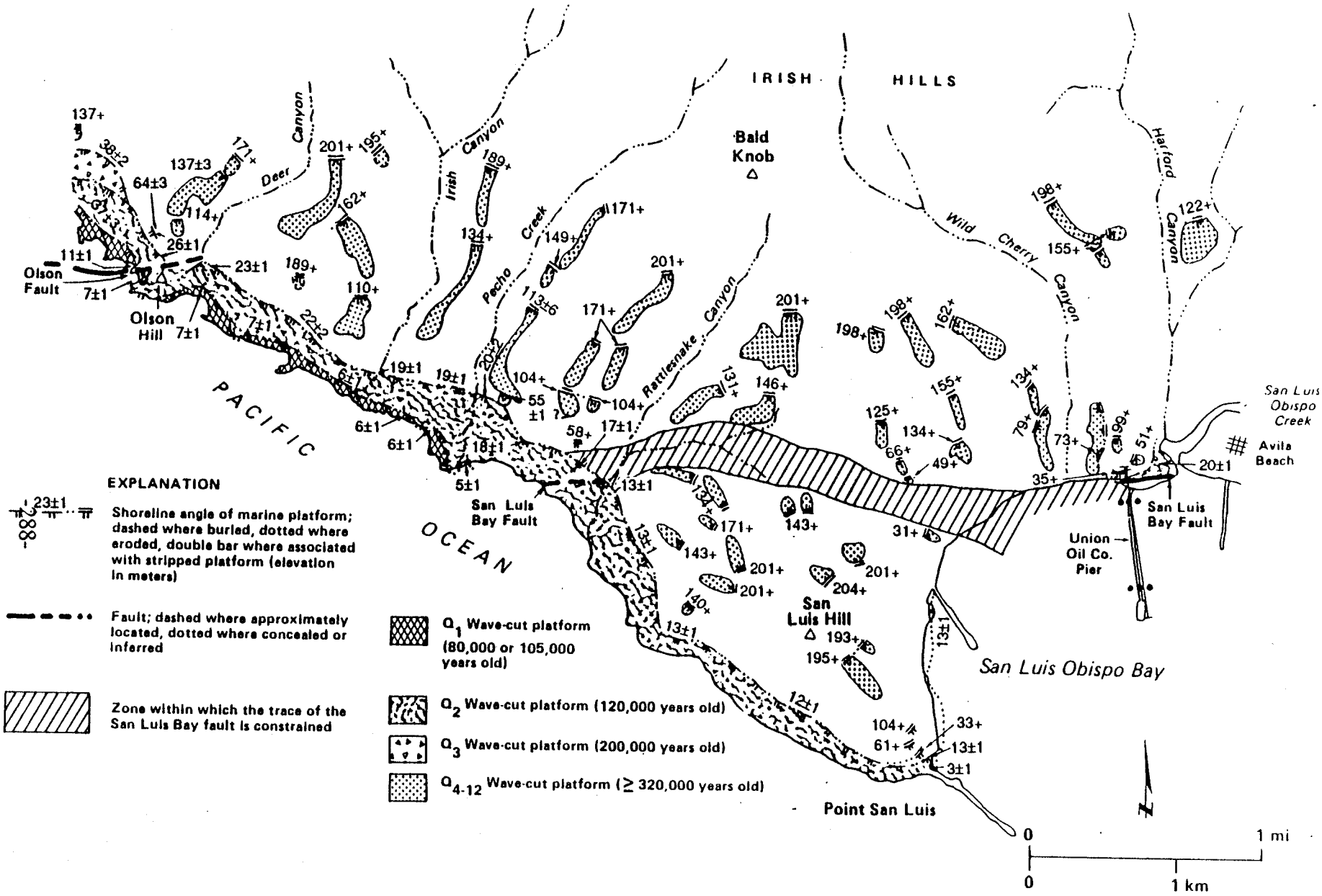

Figure 9. Map of marine wave-cut platforms in the vicinity of the San Luis Bay and Olson faults.

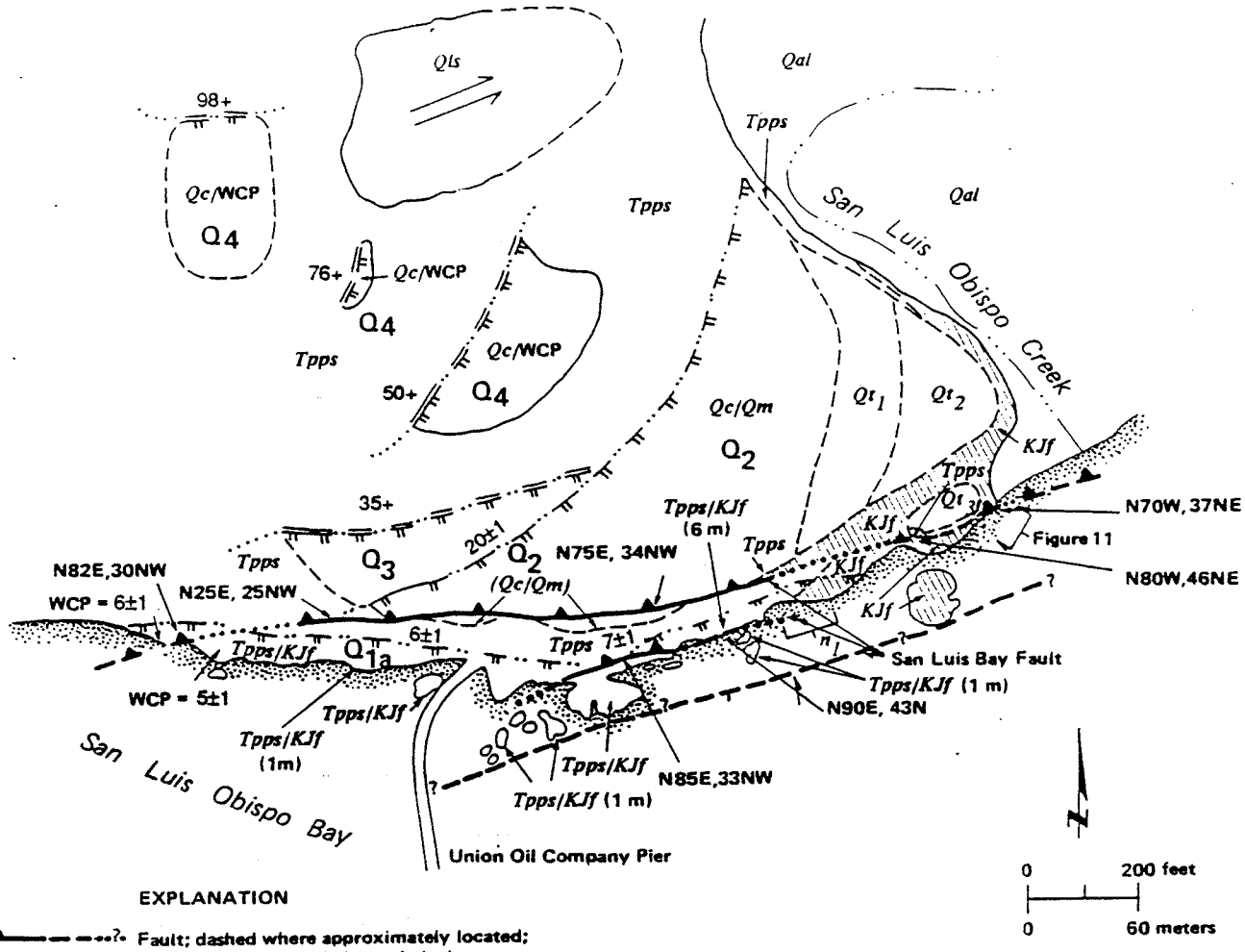

EXPLANATION

Fault; dashed where approximately located; dotted where concealed; queried where inferred; sawteeth on upthrown block of reverse fault

18±1 35+ Shoreline angle; solid where well constrained; double dot where buried, and dotted where eroded; elevation of shoreline angle shown in feet. Double bar indicates shoreline angle of stripped marine wave cut platform; minimum elevation of shoreline angle shown in meters

Lithologic contact; dashed where approximate

Q_{1a}	Marine terrace (80,000 or 105,000 years old)
Q_2	Marine terrace (120,000 years old)
Q_3	Marine terrace (200,000 years old)
Q_4	Marine terrace (≥320,000 years old)
WCP	Wave-cut platform
Tpps/KJf (1m)	Contact between Squire Member of Pismo Formation and underlying Franciscan Complex. Elevation of contact (gently north dipping) given in parenthesis (feet)

n_1 KJf exposed in seacliff. Sparse lag gravel and vertebrate bones indicated that contact with Tpps is at or near top of seacliff at an elevation of 19'-21' (outcrops largely eroded during winter of 1987-88). Top of seacliff coincident with WCP of 22-foot shoreline angle and veneered by rip rap and fill from railroad and highway construction.

Qls	Landslide	Quaternary
Qc	Colluvium	Quaternary
Qal	Modern Alluvium	Quaternary
Qt_1	Stream terrace 1 = oldest and 3 = youngest	Quaternary
Qm	Marine terrace deposits	Quaternary
Tpps	Pismo Formation - Squire Member	Tertiary
KJf	Franciscan Complex	Cretaceous and Jurassic

Figure 10. Geologic map of the Avila Beach exposure of the San Luis Bay fault.

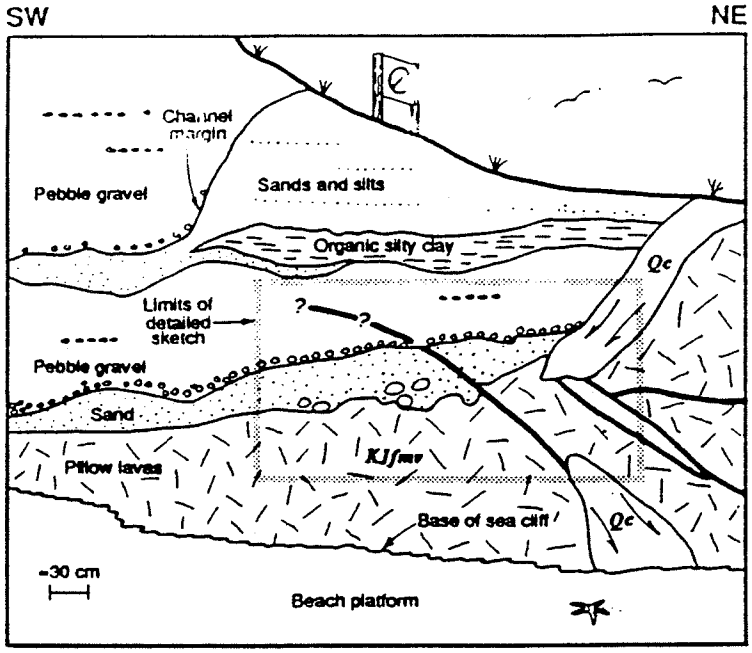

Overview

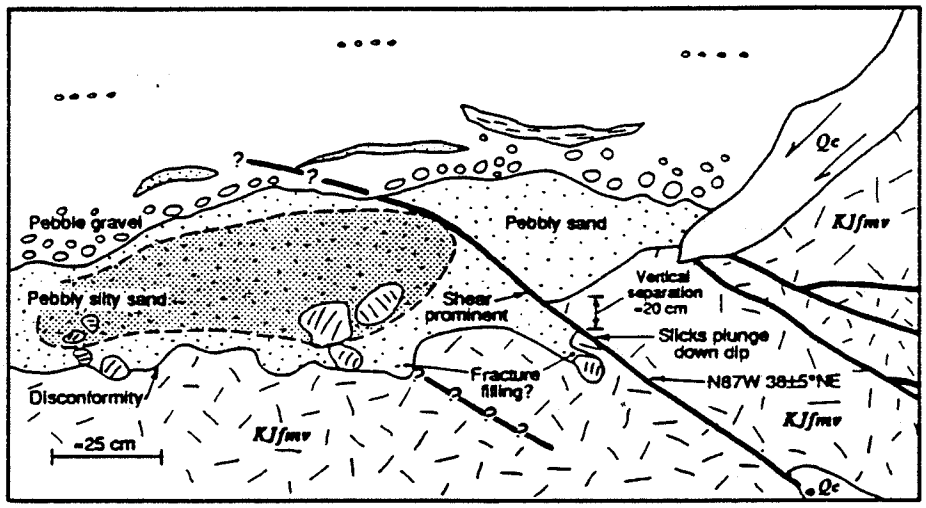

Detailed Sketch

EXPLANATION

—— —?	Fault, dashed and queried where indistinct	⊘	Cobble
——	Contact	Qc	Colluvium
⬭	^{14}C sample WL-89-1 collected in this zone; 21,040 ± 850 years B.P.	KJfmv	Franciscan pillowed greenstone

Figure 11. Sketch logs of geologic relationships exposed in the seacliff at the mouth of San Luis Obispo Creek showing a trace of the San Luis Bay fault cutting latest Pleistocene fluvial terrace deposits.

LATE QUATERNARY COASTAL DUNES OF THE SANTA MARIA AREA: A SYNOPSIS

Antony R. Orme,
Department of Geography,
University of California,
Los Angeles, California 90024

INTRODUCTION

Quaternary dunes of various ages occur at intervals along the south-central California coast. Widespread dunefields are preserved in areas that have experienced net tectonic subsidence or limited uplift during late Quaternary times, notably in the Morro Bay area, the lower Santa Maria valley and the lower Santa Ynez valley (Fig.1). Where greater tectonic uplift has occurred, relatively thin aeolian deposits are sometimes associated with marine terrace sequences, for example along the San Simeon coast.

Cooper (1967) first placed the more extensive dunes within a Quaternary sequence, recognizing Pre-Flandrian dunes, stabilized Flandrian dunes, and active Flandrian dunes. Excellent though the field observations were, his timeframe lacked good geochronologic control. Orme and Tchakerian (1986) subsequently defined physical parameters for distinguishing between four major dune phases, and Orme (1988) related these dune phases to relative sea-level changes and fluctuating sediment budgets during later Quaternary times. More recently, Orme (1990) has recognized three Holocene dune episodes overlying late Pleistocene paleodunes in the Morro Bay area, and (Orme 1990, submitted) has established a geochronologic sequence for late Quaternary aeolian, fluvial and lacustrine deposition in the Point Sal area. Johnson, Glassow and Morgan (1988) have discussed dune sequences in their study of soil geomorphology in the Vandenberg-Lompoc area towards the mouth of the Santa Ynez valley.

EARLIER PLEISTOCENE AEOLIAN DEPOSITS

Earlier Pleistocene marine and non-marine deposits, variously assigned to the 'Orcutt Sand', the 'Paso Robles Formation' and other formations, include units of medium to fine, often cross-bedded sands which appear to be of aeolian origin. An aeolian origin for some of these materials is not unreasonable in view of the exposed location of the south-central California coast as abundant clastic debris was shed from rising coastal hills and interior ranges during Pleistocene times. These deposits are, however, normally buried within stratigraphic sequences of mostly fluvial deposits. More research is needed on these complex sequences.

LATE PLEISTOCENE PALEODUNES

The earliest extensive aeolian deposits at the surface occur as variably indurated paleodunes of considerable thickness in valley locations but feathering out against marine terraces sequences on nearby uplifted coastal hills. These are designated Phase II dunes on Figure 1. In the Morro Bay area, these paleodunes feather out at 300 m against the San Luis Range (Irish Hills) but also descend across largely

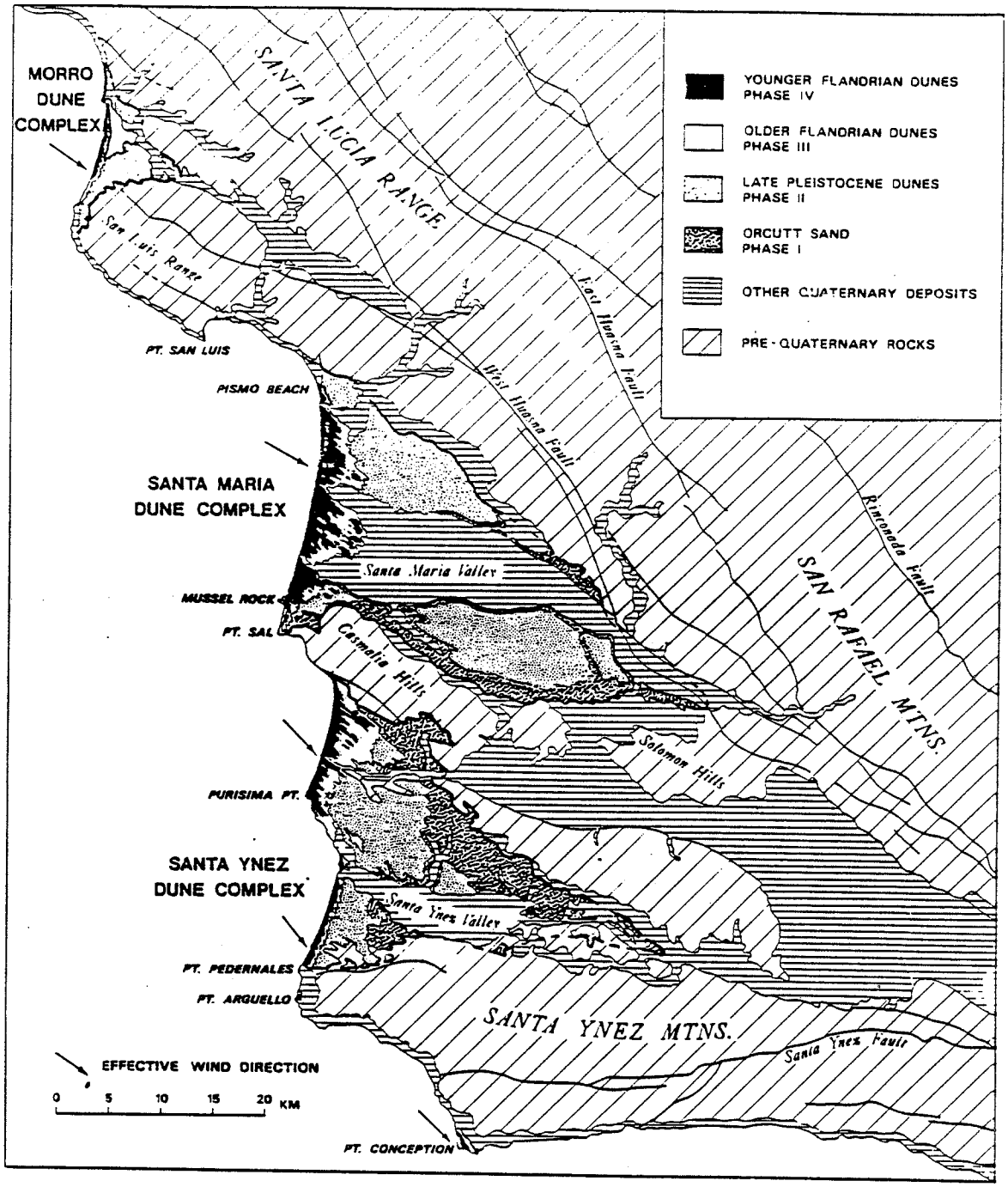

Figure 1. Late Quaternary dune phases and associated deposits along the south-central California coast (Orme and Tchakerian 1986)

buried marine terraces to below present sea level north of Hazard Canyon. They also descend below sea level in some parts of the lower Santa Maria valley but are also found locally overlying fluvial deposits.

In the Montaña de Oro area south of Morro Bay, paleodunes up to 30 m thick overlie alluvial, colluvial and raised beach deposits which in turn rest upon a raised shore platform exposed 2-4 m above present sea level at the coast. Marine and terrestrial mammal teeth and bones from these subjacent deposits in the general area have provided uranium-series ages ranging from 49 to 82 ka, which are considered to be minimum ages (Hanson and others, submitted). From this evidence it is thought that the raised shore platform and beach deposits may correlate with oxygen-isotope substage 5a around 82 ka. In the vicinity of Point Sal, extensive paleodunes are interbedded with fluvial and lacustrine sediments which have provided a number of bracketing ^{14}C ages between 20 and 30 ka (Orme 1990, submitted). At the coast, the paleodunes overlie a well-developed raised shore platform which may be of comparable age to that south of Morro Bay. In the Point Sal area, however, it is not inconceivable that the lowest emergent shore platform may be younger, perhaps oxygen-isotope stage 3 when global sea level is thought to have been around 40 m below the present. This would imply a much faster rate of uplift for the Casmalia Hills region.

Whether the underlying marine terrace sequence is correlated with oxygen-isotope stage 3 or substage 5a or even substage 5e, it seems evident that the paleodunes were emplaced during and after a falling sea level. During marine regressions, vast amounts of nearshore sediment are often stranded on emergent shelves, to be augmented by debris introduced by rivers extending across the shelf. Under these conditions, onshore winds may promote the development of thick and extensive coastal dunes and, in the unstable conditions prevailing, these dunes may climb from a relatively low sea level to well above present sea level (Orme 1988). Even as such thick sequences are emplaced, however, streams flowing seawards toward lower sea levels cut channels through the dunes or are temporarily imponded by drifting sand, with the consequent development of shallow lacustrine sedimentation. Regressive dune sequences thus tend to embrace fluvial and lacustrine sediments within their overall mass, as observed at several localities along the south-central California coast.

Late Pleistocene paleodunes are distinguishable from Holocene dunes in terms of surface morphology, grain-size distribution, grain micromorphology, weathering mineralogy, soil properties, and vegetation (where it survives). Using discriminant analysis on various grain-size parameters, the three major phases of late Quaternary dune deposition in the Santa Maria basin are readily distinguished (Fig.2, Orme and Tchakerian, 1986). The marked tail of fines in the paleodunes is primarily attributable to post-depositional weathering. Although the paleodunes discussed above are treated here as one mass subject to episodic emplacement during late Pleistocene times, with weak paleosols reflecting hiatuses of non-deposition, it is possible that more distinct phases of deposition may have occurred, but the evidence for these is presently ambiguous.

HOLOCENE DUNES

At least three, and possibly four, phases of dune development characterize the Holocene record. The first phase is somewhat conjectural but, in view of what happened later, it is hypothesized that one or more transverse dune ridges proceeded up-shelf during the Flandrian marine transgression between 17 and 5 ka.

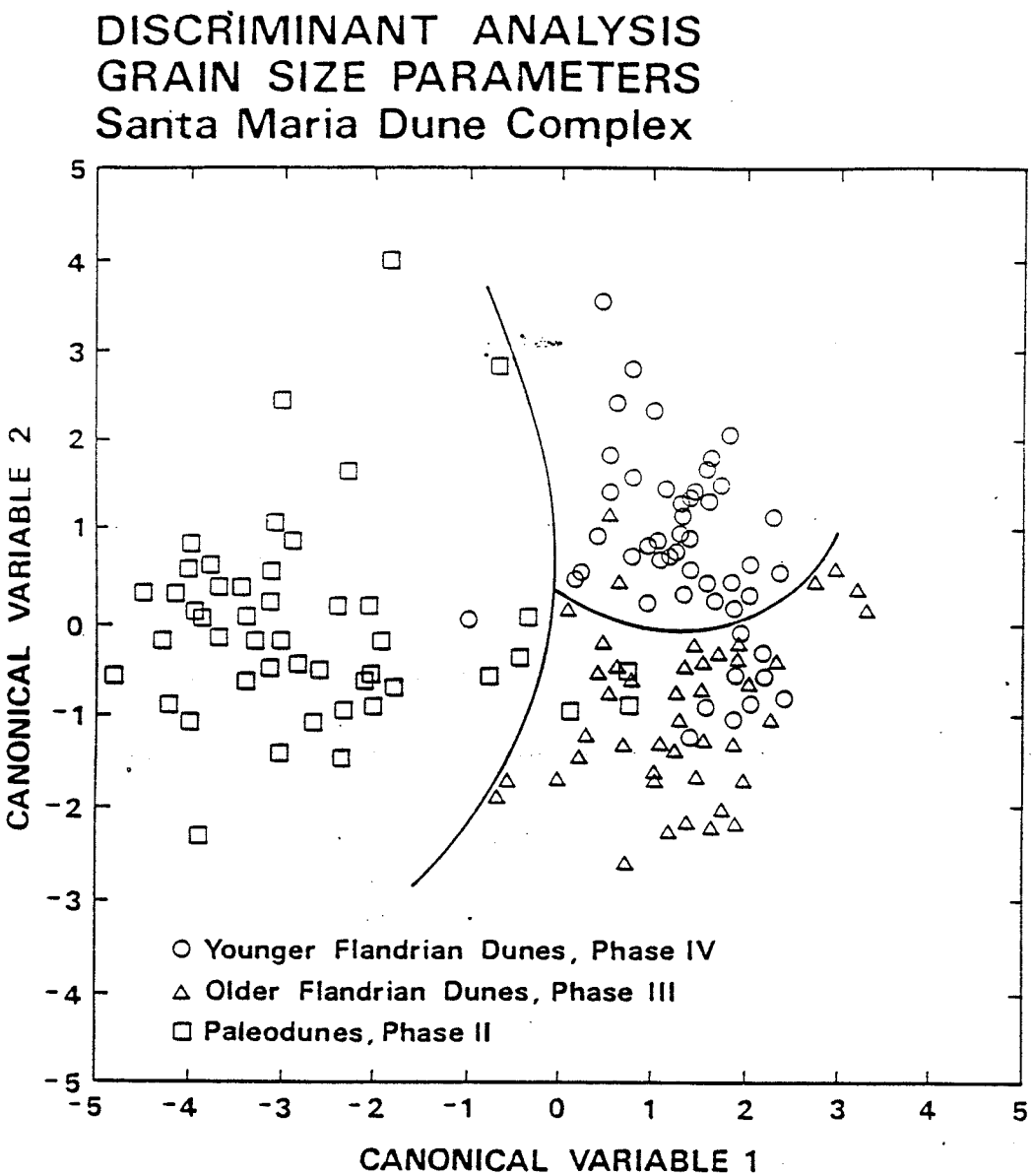

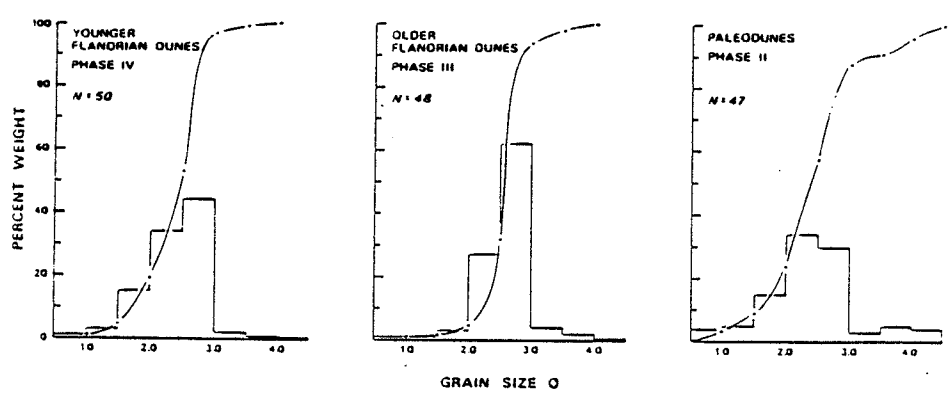

Figure 2. Grain-size characteristics of Late Pleistocene paleodunes, older Flandrian (parabolic) dunes, and younger Flandrian (transverse) dunes in the Santa Maria Dune Complex, south-central California (Orme and Tchakerian 1986).

In the relatively unstable conditions that characterize a marine transgression, nearshore marine and eroding terrestrial sediments, including paleodunes, provide abundant material for wind transport. As the transgression slows down, these new dunes overlap onto the eroded remnants of older dunes. As sand supplies are curtailed with approaching sea-level 'stability', the new dunes may be stabilized by vegetation. Commonly, however, the wind continues to function in an environment of reduced sediment availability, transverse dunes become barchanoid, and the latter are eventually flushed downwind as parabolic dunes.

Parabolic dunes are widespread along the south-central coast of California, most notably from Pismo Beach southward to the Santa Maria River and also south of Morro Bay. Parabolas of several ages are represented on the surface and in section, but it seems most likely that the initial formation of parabolic dunes began as the rate of relative sea-level rise slowed down after 7000 BP, when sea level was still some 10 m below the present. Thereafter, the downwind migration of parabolic dunes was time transgressive, so that the noses of various parabolas represent a late episode of deposition. In the Montaña de Oro area south of Morro Bay, the noses of several parabolic dunes occur along the bluff top, but the ramp over which they migrated across the underlying paleodunes has long since been removed by marine erosion. A distinct paleosol capping the paleodunes is separated from the noses of the parabolic dunes by midden materials and artifacts which have yield ^{14}C ages between 3080 and 4160 BP (Orme 1990). From this evidence, it is probable that the dune transgression began some distance seaward at an earlier time and then ceased around 3000 BP. Parabolic dunes also climbed inland over Pleistocene paleodunes in the Santa Maria basin, onlapping onto Nipomo Mesa, but their finest expression occurs near sea level between the mesa and Pismo Beach. Here, prominent parabolic dunes with crestal ridges rising to 20-30 m harbor several small lakes whose sedimentary record is expected to reveal much about the later Holocene development of the area.

In the Morro Bay area, a further major phase of parabolic-dune activity began after a widespread fire dated from a persistent charcoal seam at around 1730 BP. Whether this fire was set by lightning or by pre-Chumash hunting peoples is uncertain, but it appears to have been responsible for extensive destruction of vegetation and led to destabilization of existing dunes. Some dunes developed after this time are truly parabolic, others are more lobate - implying more sand availability and/or less distance of movement downwind. Other renewed activity in the Santa Maria and Santa Ynez valleys also produced parabolic forms, but there is presently no reason to assume that this activity was contemporaneous with that at Morro Bay. The world's coasts are replete with examples of dune reactivation attributable to natural or human-induced fire at one time or another.

The fourth and last phase of Holocene dune development appears to have commenced about 200 years ago, and is represented today by active transverse and barchanoid dunes at numerous localities along the coast. The causes are complex. Destruction of vegetation by increased fires, grazing, military activity and off-road vehicles is readily documented. At Morro Bay, modifications to the entrance channel and subsequent discharge of dredged sediment have thoroughly upset the stability of the Morro barrier system. Natural forces, notably relative sea-level rise and increased storm frequency and wind intensity, cannot be ruled out but they are difficult to distinguish amid the pervasive impact of recent human activities.

REFERENCES

Cooper, W.S. (1967) Coastal dunes of California. Geol. Soc. Amer. Mem. 104, Boulder

Hanson, K.L., Wesling, J.R., Lettis, W.R., Kelson, K.I., and Mezger, L. (submitted) Correlation and ages of Quaternary marine terraces: south-central coastal California.

Johnson, D.L., Glassow, M.A, and Morgan, T. (1988) Soil geomorphology, paleopedology, and pedogenesis in the Vandenberg-Lompoc area, Santa Barbara County, California. Soil Science Society of America, Fieldguide.

Orme, A.R. (1988) Coastal dunes, changing sea level and sediment budgets. Journal of Coastal Research, 3, 127-129

Orme, A.R. (1990) The instability of Holocene coastal dunes: the case of the Morro dunes, California. In Coastal Dunes: Form and Process (K.F.Nordstrom, N.P.Psuty, and R.W.G.Carter, eds.), New York and Chichester: John Wiley & Sons, 317-338.

Orme, A.R. (submitted) Late Quaternary deposits of the Point Sal area, California.

Orme, A.R. and Tchakerian, V.P. (1986) Quaternary dunes of the Pacific coast of the Californias. In Aeolian Geomorphology (W.G.Nickling, ed.), London & Boston, Allen & Unwin, 149-175.

THE LOS OSOS FAULT ZONE, SAN LUIS OBISPO COUNTY, CALIFORNIA

W.R. Lettis
William Lettis and Associates, Lafayette, California

and **N. Timothy Hall**
Geomatrix Consultants, San Francisco, California

ABSTRACT

The Los Osos fault zone is a west-northwest-trending reverse fault in San Luis Obispo County, California. The fault zone extends as a discontinuous en echelon zone of faults from the Hosgri fault zone in Estero Bay southeast to an intersection with the West Huasna fault zone near Twitchell Reservoir, a distance of up to 60 km. The fault zone is divided into four segments based on differences in behavioral characteristics (e.g., recency of activity, slip rate); spatial coincidence with distinct topographic range segments; en echelon separation of fault traces; intersection with known or inferred branching or crossing structures (e.g., faults, subsiding basins); and geomorphic expression as a range-front or intra-range fault. From northwest to southeast, we propose naming the segments the Estero Bay, Irish Hills, Lopez Reservoir, and Newsom Ridge segments. The Irish Hills segment, which is 17 to 21 km long, exhibits the strongest expression of Holocene activity and is a well-defined range-front fault. Detailed mapping of marine terraces and trenching of fluvial deposits suggest this segment has had recurrent late Pleistocene and Holocene displacement at a long-term slip rate of 0.2 to 0.4 mm/yr. The adjacent Lopez Reservoir segment is a 15- to 19-km-long, poorly defined range-front fault that displaces older Quaternary alluvium. Detailed mapping and trenching indicate no Holocene activity. The Newsom Ridge segment is an 8-km-long, intra-range fault that has poor geomorphic expression and appears not to displace late Pleistocene deposits. The Estero Bay segment, 11 to 15 km long, lies primarily offshore in Estero Bay. Its recency of activity is unknown. The segment is poorly imaged on seismic reflection data and is weakly expressed in seafloor bathymetry, suggesting a low rate of late Quaternary activity.

INTRODUCTION

The Los Osos fault zone lies along the northeastern margin of the San Luis Range in San Luis Obispo County, California (Fig. 1). As initially mapped by Hall and others (1979), the zone consists of many fault traces that generally bound tabular bodies of serpentinite within the Franciscan Complex (Plate 1). Locally, several of these fault traces displace late Tertiary strata of the Pismo Formation and Pliocene and Pleistocene deposits of the Paso Robles Formation, indicating late Cenozoic activity. Prior to this study, however, no late Quaternary activity was described along the Los Osos fault zone.

Earlier geologic maps of the region by Hall (1973a) and Dibblee (1974) did not identify the Los Osos fault zone. The southwest part of what we interpret to be the Los Osos fault zone coincides, in part, with the Edna fault as mapped by Hall (1973b) and Hall and others (1979). Hall (1981) interpreted this part of the fault to have experienced late Cenozoic dextral strike-slip and to be part of a larger system of late Cenozoic northwest-trending strike-slip faults that are responsible for creating the late Tertiary Santa Maria, Pismo, and Huasna "pull-apart" depositional basins. Namson and Davis (1990) constructed a retrodeformable cross section through the San Luis Range and interpreted the presence of an active regional decollement beneath the range. They did not identify nor discuss the implications of an active fault along the northeastern margin of the range.

As defined in this study, the Los Osos fault zone is one of a series of west-northwest-trending reverse faults along the south-central California coast that terminate in the offshore to the northwest against the more northerly trending Hosgri fault zone (Fig. 1). Within this coastal region, termed the Los Osos/Santa Maria Domain (PG&E, 1988; Lettis and others, 1989), the reverse faults border a series of west-northwest-trending structural blocks (Weber and others, 1987). Elevated marine terraces along several of these blocks indicate that the blocks are being actively uplifted along their bounding faults (Hanson and others, this volume). The Los Osos fault zone separates the elevated San Luis/Pismo structural block on the southwest from the relatively stable or southwest-tilted Cambria structural block on the northeast (Fig. 2) (Lettis and others, this volume). Because this block-bounding fault is a potentially significant seismic source, we conducted an extensive program of reconnaissance and detailed mapping, drilling, trenching, and geophysical profiling to evaluate its style, rate, and recency of activity.

In this paper, we describe the field program and evidence for late Quaternary activity along the Los Osos fault zone. Our field studies along the northeast margin of the San Luis/Pismo block indicate that the fault zone is a southwest-dipping reverse fault that has a complex history of strike-slip and dip-slip displacement. The fault zone is a 2-km-wide system of discontinuous, subparallel, and en echelon fault traces, extending from an intersection with the Hosgri fault zone in Estero Bay to the northwest to an intersection with the West Huasna fault south of San Luis Obispo to the southeast, a distance of 55 to 60 km (Fig. 2). We have confirmed many of the bedrock fault traces mapped by Hall and others (1979) and have identified additional traces within the fault zone. Most of the late Quaternary activity identified during this study occurs on traces of the Los Osos fault zone not previously mapped by Hall and others (1979).

FIELD INVESTIGATIONS

We conducted geomorphic, geologic, and geophysical investigations to characterize the geometry and behavior of the Los Osos fault zone. Geomorphic investigations included evaluating the relationship of the fault zone to the San Luis/Pismo structural block, assessing the character of the zone as a range-front or intra-range fault, and identifying geomorphic features along the fault trace that are indicative or suggestive of late Quaternary faulting. Geomorphic features were identified and mapped by field reconnaissance and by interpretation of conventionalblack-and-white,color-infrared, and low-sun-angle aerial photographs that

cover the entire onshore length of the fault zone at scales ranging from 1:6,000 to 1:40,000. Offshore, the geomorphic expression of the fault was evaluated by analysis of seafloor bathymetry, distribution of bedrock outcrop patterns observed from side-scan sonar, and distribution of Quaternary depositional basins imaged on high-resolution seismic reflection data.

Selected lineaments or clusters of geomorphic features then were investigated by detailed geologic mapping, drilling, and trenching to provide site-specific data on fault location, geometry, sense of displacement, recency, and recurrence. Sites of detailed investigation are shown on Fig. 3. A compilation map showing geomorphic features and geologic data along the Los Osos fault zone from Estero Bay to Arroyo Grande Creek is shown on Plate 1. Trenches were excavated at six sites that we informally named the Ellsworth, Cuesta, and Ingley sites along the Irish Hills segment of the fault zone, and the Glick, Brughelli (Airport), and Guidetti sites along the Lopez Reservoir segment (Plate 1; Fig. 3). In addition, we drilled a series of boreholes at the Ingley site to assess cumulative post-Pliocene vertical separation across the fault.

In addition to these geomorphic studies and detailed site investigations, marine and fluvial terraces were mapped in several areas adjacent to and across the Los Osos fault zone. These terrace sequences provide excellent Quaternary "strain gauges" from which we were able to evaluate long-term slip rate, sense of displacement, and recency of displacement. Fluvial terraces were mapped along San Luis Obispo Creek, Pismo Creek, and Arroyo Grande Creek (Fig. 3). These creeks established their channels prior to uplift of the San Luis/Pismo block and flow at nearly right angles across the Los Osos fault zone. Marine terraces were mapped along the coast in the Montaña de Oro State Park southwest of the Los Osos fault zone (Fig. 3). A flight of elevated terraces is well preserved at Montaña de Oro but is not present north of the fault zone in the Morro Bay area. Borehole, gravity, and magnetic data were interpreted to assess the geology beneath Morro Bay, a locally subsiding basin.

The Los Osos fault zone appears to extend westward offshore into Estero Bay (Fig. 2). To evaluate the possible offshore continuation of the fault zone and its relationship to the Hosgri fault zone, we analyzed an extensive suite of geophysical data from Estero Bay. In addition to locating possible fault traces, these investigations were aimed at characterizing fault geometry and the sense and recency of displacement. The geophysical investigations consisted of acquiring and interpreting deep common-depth-point and shallow high-resolution seismic reflection data, analyzing gravity and magnetic data, and analyzing bathymetric and outcrop patterns from side-scan sonar data. A detailed discussion of the geophysical data is beyond the scope of this paper, but the data and interpretations are presented in a report by Pacific Gas and Electric Company (PG&E) to the U.S. Nuclear Regulatory Commission (PG&E, 1988).

SEGMENTATION OF THE LOS OSOS FAULT ZONE

Identifying fault segments is important for accurately characterizing the seismic capabilities of the Los Osos fault zone. We have identified four segments along the fault zone based on differences in physical and behavioral characteristics (Table 1). From northwest to southeast, these segments are

informally named the Estero Bay, Irish Hills, Lopez Reservoir, and Newsom Ridge segments (Fig. 2) (Lettis and Hall, 1988). Physical characteristics used to differentiate segments include spatial coincidence with distinct topographic elements or geomorphically defined subblocks of the San Luis/Pismo structural block, en echelon separation of fault traces, intersection with known or inferred branching or crossing structures, and geomorphic character as a range-front fault or intra-range fault. Behavioral characteristics include recency of activity and late Quaternary slip rate.

Of the four segments identified, the Irish Hills segment is best expressed geomorphically and exhibits evidence of repeated Holocene displacement at a net slip rate on the order of 0.2 to 0.8 mm/yr for the late Pleistocene. The Lopez Reservoir and Newsom Ridge segments are poorly to moderately expressed geomorphically. Although they exhibit evidence of Quaternary displacement at a slip rate of less than 0.1 mm/yr, there is no evidence of late Holocene activity. The offshore Estero Bay segment is poorly imaged on geophysical data and weakly expressed by seafloor bathymetry, suggesting that it has a low or nonexistent rate of activity during the late Quaternary.

Table 1 summarizes the salient behavioral, geomorphic, and structural characteristics of each segment. In assessing these characteristics, it is important to recognize the varying levels of effort and types of investigation accorded each segment. The Estero Bay segment was investigated chiefly by offshore geophysical methods. The Irish Hills and Lopez Reservoir segments were investigated by reconnaissance and detailed geologic and geomorphic analyses. The Newsom Ridge segment was evaluated only by aerial reconnaissance, photo interpretation, and geomorphic analysis of regional topography. The different methodologies engender differences in the level of certainty regarding the behavior of each segment. Despite these uncertainties, we believe that these investigations support distinguishing at least two (the Irish Hills and Lopez Reservoir) and possibly four segments of the fault zone.

The Los Osos fault zone defined in this study is, in part, a range-front fault along the northeastern margin of the San Luis/Pismo structural block. Lettis and others (this volume) divide the San Luis/Pismo structural block into four range segments, or subblocks, on the basis of distinct differences in topographic expression and inferred uplift rate (Fig. 2). Because recent studies of fault segmentation show a strong spatial correlation between topographic range segments and fault rupture lengths for fault systems worldwide (Knuepfer and Coppersmith, 1987; Menges, 1987), recognizing these subblocks helps constrain the lengths and locations of fault segments along the Los Osos fault zone. From northwest to southeast, these topographic subblocks are named informally the Estero Bay subblock, which lies offshore, and the Irish Hills, Edna, and Newsom Ridge subblocks, which lie onshore. Uplift rates for these subblocks, as estimated from marine terrace investigations by Hanson and others (this volume), are shown on Fig. 2; topographic expressions for the onshore subblocks are shown on Fig. 4. The Irish Hills subblock is well defined, having an uplift rate ranging from 0.13 to 0.22 mm/yr and crest elevations ranging from 425 to 550 m. The Edna and Newsom Ridge subblocks are less well defined, having uplift rates ranging from 0.11 to 0.15 mm/yr and crest elevations

ranging from 180 to 245 m and 365 to 425 m, respectively. The offshore Estero Bay subblock is characterized by little or no uplift and consists primarily of a deeply eroded, bedrock platform that has isolated linear ridges having crest elevations up to 59 m below sea level ("59-meter-ridge," Fig. 4).

Fig. 5 is a longitudinal profile that illustrates the contrast in elevations of the range crests for the three onshore sublocks. Also profiled on Fig. 5 is the elevation of the Los Osos fault zone along the northeastern margin of the San Luis/Pismo block. The difference in elevation between the range crest and fault trace varies markedly along the Los Osos fault zone. This difference in elevation is an approximate measure of the height of the range-front escarpment and, thus, indicates whether the fault trace is a prominent range-front fault. The difference in heights of the range escarpment is used as one physical criterion for segmentation of the Los Osos fault zone. Fig. 5 shows the correlation of subblocks of the San Luis/Pismo block with the segments of the Los Osos fault zone.

The height of a range escarpment along any presumed Quaternary active fault can also be used as a relative measure of the long-term rate of vertical separation across that fault. In this respect, the difference in heights of the range escarpment suggests that the Los Osos fault zone may be segmented according to long-term behavioral characteristics. Because the Irish Hills segment is characterized by a range escarpment roughly 305 to 427 m high, we interpret it as having a relatively high long-term rate of vertical displacement associated with uplift of the Irish Hills subblock. The Lopez Reservoir segment is characterized by a low range escarpment along the Edna subblock, roughly 152 to 183 m high along its northwestern part; the segment progressively becomes an intra-range fault along its southern part. The Lopez Reservoir segment thus is interpreted as having a lower long-term rate of vertical displacement relative to the Irish Hills segment. The Newsom Ridge segment extends into the Newsom Ridge subblock and has little or no range-front relief. The absence of a range escarpment suggests little or no long-term vertical displacement on that segment.

IRISH HILLS SEGMENT

The Irish Hills segment of the Los Osos fault zone lies along the northeastern flank of the Irish Hills subblock of the San Luis/Pismo block between Morro Bay on the northwest and San Luis Obispo Creek on the southeast, a distance of 19 $\pm$ 2 km (Fig. 2). As described above, it is a well-defined range-front fault over most of its length, but is obscured by cultural features and eolian and fluvial deposits along its northwestern and southeastern sections.

Geomorphic features indicative of Quaternary faulting are well expressed along the central 8 to 10 km of the segment between the town of Los Osos on the northwest and San Luis Obispo city limits on the southeast (Fig. 2). Prominent spring lines, linear and arcuate topographic scarps, and linear tonal contrasts define numerous northwest-trending lineaments up to several kilometers in length (Plate 1). Less prominent discontinuous geomorphic features such as linear stream segments, deflected drainages, side-hill benches, stream nickpoints, and linear faceted ridge spurs also occur along this reach of the segment.

The northwestern and southeastern sections of the Irish Hills segment have poor

geomorphic expression, perhaps as a result of decreasing rates of displacement toward the ends of the segment and/or modification of surface expression by eolian and fluvial processes. Fig. 3 is a geologic map modified from Hall (1973a) and Hall and others (1979) that illustrates the surface distribution of alluvial and eolian deposits along the Los Osos fault zone. Southeast of the Irish Hills subblock, the fault crosses the floodplain of San Luis Obispo Creek, where deposition and/or erosion may have removed evidence of faulting. In addition, development of the city of San Luis Obispo has obscured large sections of the fault trace. Quaternary displacement along the southeastern part of the segment, however, is indicated by the following geomorphic and stratigraphic relationships: 1) the range front continues as a steep, linear escarpment; 2) the fault truncates a flight of elevated fluvial terraces along San Luis Obispo Creek; and 3) an internally drained basin, Laguna Lake, lies along and may have been tectonically dammed by a projected trace of the fault (Plate 1).

Near its northwestern end, the Irish Hills segment is overlain by late Pleistocene and Holocene eolian deposits that form a large "sand ramp" against the northeastern margin of the Irish Hills subblock (Plate 1; Fig. 3). No evidence of faulting was observed in the largely unconsolidated dune sand, although surface evidence of faulting may have been destroyed by subsequent eolian and/or colluvial processes. Late Quaternary deformation in this area is suggested by the following indirect geomorphic relationships: 1) the range front continues to the west as a steep, linear escarpment; and 2) the fault separates an area of Quaternary uplift, the San Luis/Pismo structural block, from an area of Quaternary subsidence beneath Morro Bay, informally termed the Morro Bay basin.

The northwestern boundary of the Irish Hills segment is poorly constrained. The segment is interpreted to end near the intersection with Los Osos Creek, coincident with the subsiding Morro Bay basin, with the intersection of two poorly constrained fault traces, and with a westerly change in trend of the northern range front of the Irish Hills subblock (Figs. 2, 7). The location of the boundary is uncertain, however, because the thick veneer of eolian sand obscures the fault trace. The Irish Hills segment may 1) terminate at the southeastern margin of the Morro Bay basin, where, on the basis of borehole and geophysical data, a more northerly trending fault is interpreted to branch into northern Estero Bay; 2) bend abruptly 15° to 25° to the west along the southern margin of the Morro Bay basin where it projects seaward into the Estero Bay segment; or 3) make a 2- to 4-km en echelon left stepover to the offshore Estero Bay segment.

The southeastern boundary of the Irish Hills segment is relatively well constrained on the basis of physical characteristics. The segment is separated from the Lopez Reservoir segment by a 1- to 2-km en echelon right stepover or a short 20° to 30° bend in the fault trace to a more north-northwesterly trend across San Luis Obispo Creek. This discontinuity coincides with a similar 2- to 4-km right step in the range front and with the southeastern termination of the Irish Hills subblock (Fig. 4). Well data in the San Luis Obispo Creek area (Plate 1) show a thickening of late Quaternary deposits near the en echelon stepover, suggesting that a small subsiding basin, informally named the San Luis basin, may occur at the stepover (Fig. 2).

Marine Terrace Investigations - Montaña de Oro State Park/Morro Bay Area

The Irish Hills segment of the Los Osos fault zone disrupts a flight of emergent marine terraces along the coast between Montaña de Oro State Park and Morro Bay. Disruption of the terrace sequence demonstrates late Quaternary activity on the fault (Plate 1; Fig. 6). These terraces were mapped in detail to provide constraints on the location of the fault within the dune complex south of Morro Bay, to evaluate the relationship of the fault to the San Luis/Pismo structural block, and to estimate long-term rates of vertical separation across the fault.

Eleven emergent marine terraces are preserved along the coast from San Luis Obispo Bay on the south to Montaña de Oro. These terraces are not present in the vicinity of Morro Bay north of the Los Osos fault. The lower two emergent terraces are well preserved and laterally continuous along the coastline. Based on 28 age dates and on comparison to marine terrace sequences worldwide, Hanson and others (this volume) interpret these two lower terraces to be 80 ka and 120 ka (marine oxygen isotope sub-stages 5a and 5e, respectively). The higher, older terraces, which are moderately to poorly preserved, occur as discontinuous remnants along the coast. Based on terrace elevations and correlation to paleosea-level highstands, these higher terraces are interpreted to range in age from about 214 ka to well over 500 ka.

The Los Osos fault zone truncates the flight of marine terraces between Montaña de Oro State Park and the town of Los Osos along the northeastern margin of the San Luis/ Pismo structural block (Figs. 6, 7). The marine terrace shoreline angles are cut into bedrock at elevations ranging from 14 m to more than 235 m. The elevation of the shoreline angles remains relatively constant laterally but shows a slight increase close to the Los Osos fault zone within a limit of resolution of $\pm$ 2 m for the Stage 5 terraces and $\pm$ 5 m for the older, higher terraces (Fig. 6). The minor rise in elevation of the marine terrace sequence toward the fault may be the result of secondary hanging-wall deformation such as backthrusting, minor tilting, or localized folding associated with the Los Osos fault zone. Such deformation, however, was not identified in the Montaña de Oro area. Alternatively, the interpreted rise in elevation of the marine terrace sequence may reflect measurement error related to the obscuring veneer of dune sand.

Morro Bay Basin

There are no emergent marine terraces in the Morro Bay area north of the Los Osos fault zone. Borehole and gravity data indicate that a deep but locally restricted basin is present in the southern Morro Bay area directly north of the fault (Fig. 8). The fault, therefore, separates the uplifted San Luis/Pismo structural block to the south from an area of local subsidence to the north, informally referred to here as the Morro Bay basin. Onshore, the Morro Bay basin is triangular in plan view and is about 6 km long and 3 to 4 km wide at the coast. Gravity data suggest that the basin extends offshore an additional 2 to 3 km to the northwest. In general, bedrock north, northeast, and southwest of the basin consists of Franciscan Complex rocks, while bedrock south of the basin consists of the lower Pliocene and upper Miocene Miquelito Member of the Pismo Formation. The basin contains fossiliferous deposits of the Pliocene and Pleistocene Careaga Sandstone overlain by up to 200 m of undifferentiated Quaternary sediment. The presence of Careaga sandstone and Quaternary sediment

in the basin suggests that subsidence was occurring during the late Tertiary and Quaternary.

The origin of the basin appears to be tectonic rather than erosional. Logs of water wells in the Morro Bay area (Yates and Wiese, 1988) show that Quaternary sediment overlies Pliocene bedrock in the basin at depths at least as great as 189 m below sea level (Figs. 8 and 9). The depth to which bedrock can be lowered by fluvial erosion is limited by sea-level lowstands. Maximum lowering of sea level in this region during the middle to late Pleistocene was on the order of 130 to 150 m below modern sea level (Chappell and Shackleton, 1986). Streams draining Morro Bay and the Los Osos Valley established gradients to the lower sea-level stands on the continental shelf and, thus, at any point upstream had an elevation higher than the corresponding sea level. Based on this reasoning, the deepest possible erosional Quaternary valley along the coastline is shallower than 150 m below present sea level. Because the base of the Quaternary section is at 189 m below present sea level, the Morro Bay basin is interpreted to have subsided at least 40 to 60 m.

Although the depth and timing of erosion are uncertain, the late Quaternary subsidence rate is estimated by subtracting the maximum potential depth of bedrock due to erosion (150 m) from the observed maximum depth of bedrock (189 m). Low sea-level stands have occurred repeatedly during the late Pleistocene, the latest approximately 18 ka ago. Using these data, the rate of late Quaternary subsidence is estimated to be at most 2.8 mm/yr.

The distribution of marine terraces north of Morro Bay also indicate that the Morro Bay basin formed, in part, by southwest-directed tectonic tilting and subsidence. Between the towns of Cayucos and Morro Bay, a single, well-developed marine terrace is preserved (Weber, 1983). Field reconnaissance indicates that the terrace ranges in elevation from 5 to 6 m near Cayucos to slightly less than 5 m near Morro Bay, suggesting a slight tilt to the south. The terrace is approximately 120 ka (substage 5e) based on Uranium-series dates, analyses of paleoclimate from faunal assemblages, and amino-acid racemization analyses (Weber, 1983; Veeh and Valentine, 1967; Hanson and others, this volume). Coincidence of the substage 5e high-stand elevation (about 6 m) with the present terrace elevation near Cayucos indicates that the coastline in this area has undergone little or no tectonic uplift or subsidence. The slight tilt of the terrace toward Morro Bay suggests a slight subsidence of the coastline in this area. Static tectonic conditions or slight subsidence of the coastline is further supported by the absence of higher, older emergent marine terraces is preserved in the Cayucos and Morro Bay region.

The location of the southwestern margin of the Morro Bay basin is constrained to within a 1-km-wide area on the basis of borehole, gravity, and field-mapping data. The margin must lie south of the southernmost borehole in the Morro Bay area (Borehole MBO-2, Figs. 8 and 9), and north-northwest of the northernmost outcrop of bedrock and marine terraces in Montaña de Oro State Park. These data suggest that a major structural boundary occurs beneath the eolian deposits along the southern margin of the Morro Bay basin. Offshore, the southwestern margin is less well-constrained by fathometric data and diver geologic mapping that indicates an abrupt east-west trending unconsolidated Quaternary segment to the

north. The boundary, coincident with the northeastern margin of the San Luis/Pismo structural block, is interpreted to be the - western extension of the Los Osos fault zone.

The north-northeastern margin of the basin is constrained by borehole data that show the distribution of Careaga Sandstone (Fig. 9). The sandstone thins northward and pinches out south of borehole MBO-1 (Fig. 8). Within the basin, the elevation of the top of Careaga Sandstone decreases abruptly across a northwest trend through the center of Morro Bay. This change in bedrock elevation may be an abrupt monoclinal flexure or a fault. If this bedrock step represents a fault, then the most likely geometry of this fault considering the regional tectonic environment is a northeast-dipping reverse or thrust fault.

Even though the tectonic process that produced the Morrow Bay basin is uncertain, the basin's proximity to the active Los Osos fault zone suggests a genetic relationship. We consider 4 possible mechanisms for local basin development that are consistent with the late Neogene to Quaternary tectonic framework: 1) extension between two en echelon strike-slip faults ("pull-apart" basins); 2) sediment ponding behind a fault scarp; 3) counter clockwise rotation of the San Luis/Pismo structural block; or 4) convergence between two opposing reverse faults ("ramp" basins).

Alternative 1 is unlikely to have produced the basin in the modern tectonic setting. A "pull-apart" mechanism requires a significant component of lateral slip on the Los Osos fault zone since late Pliocene times. Because no late Quaternary component of lateral slip was observed during this study, we believe that post-Pliocene lateral slip is minimal, and the basin is not currently operating as a "pull-apart" basin. The presence of late Tertiary sediment in the basin suggests that it may be a long-lived structural feature, and its origin may therefore predate the present reverse fault behavior of the Los Osos fault zone. It is possible that the basin formed as a "pull-apart" basin during an earlier period of strike-slip displacement and that the associated structural elements have survived this change in behavior from predominantly strike-slip to predominantly reverse displacement. In this case, the continuing subsidence of the basin requires that the current tectonic regime has somehow reactivated the former "pull-apart" basin.

Alternative 2 also is unlikely to have produced the basin because the depth to bedrock indicates that tectonic subsidence is responsible for the accumulation of at least 40 to 60 m of sediment in the Bay Morro basin. Although sediment ponding (loading) can produce isostatic subsidence, the isostatic adjustment generally (depending on the rate of sediment loading) is spread over a broad area that has gently sloping margins rather than being confined to a narrow restricted basin having relatively steep, abrupt margins.

Counter-clockwise rotation of the San Luis/Pismo block would produce localized basins at the northeastern and southwestern margins of the block. Counter-clockwise rotation would occur in a sinistral slip shear couple. Luyendyke and others (1989) propose that clockwise rotation of the western Transverse Ranges is accommodated within the onshore Santa Maria basin by left lateral slip on northwest-trending faults. However, we do not observe evidence of left slip on the Los Osos fault and sparse paleomagnetic data in the onshore Santa

Maria basin indicate, if anything, clockwise rotation of structural blocks rather than counter-clockwise rotation.

Alternative 4 is the most plausible explanation for the origin of the Morro Bay basin in the current tectonic setting given the available data and probable geometry of the northwest-trending intrabasinal fault. Borehole data indicate that the upper and lower contacts of the Careaga sandstone are vertically separated down-to-the-southwest (Figs. 8 and 9). In the region's current tectonic setting, a north-northeast-dipping reverse fault is consistent with this sense of displacement. This sense of slip and down-dip geometry is opposite to that observed along the adjacent Irish Hills segment of the Los Osos fault zone. Because we interpret that the intrabasinal fault dips to the northeast, it cannot be a branch of the Los Osos fault zone. The Morro Bay basin is interpreted to have formed as a "ramp" basin created by convergence between the southwest-verging intrabasinal fault and the north-northeast - verging Los Osos fault.

Fluvial Terrace Investigations - San Luis Obispo Creek Area

The distribution of alluvial deposits along the Los Osos fault zone strongly suggests tectonic impoundment of alluvium along streams that flow southwest across the fault zone and the uplifted San Luis/Pismo structural block. Fig. 3 illustrates the general geology and regional distribution of older and younger fluvial deposits along the fault zone based on the mapping of Hall (1973a) and Hall and others (1979). In general, younger alluvium is more extensive along the Irish Hills segment of the fault zone, while older alluvium is preserved along the Lopez Reservoir segment. This general distribution of younger and older alluvium suggests that the Irish Hills segment has a higher rate of activity and/or has been more recently active than the other onshore segments of the fault zone, and that the Lopez Reservoir segment might have had a higher rate of activity in the early and middle Quaternary than in the late Quaternary.

San Luis Obispo Creek flows southwest across the San Luis/Pismo structural block at the boundary between the Lopez Reservoir and Irish Hills segments of the Los Osos fault zone (Fig. 3). A flight of fluvial strath and fill terraces is preserved along the creek within the elevated structural block (Plate 1), suggesting that the establishment of the creek preceded uplift of the block (Killeen, 1988). The terraces, which are truncated by the Los Osos fault zone, now project up to 34 m above the Los Osos Valley floor. Based on correlation of the fluvial terraces to marine terraces near Avila Beach, Killeen (1988) interpreted the oldest terrace remnants are estimated to be on the order of 430 to 580 ka. Disruption of the terrace sequence by the fault, therefore, strongly indicates recurrent late Quaternary activity along the Irish Hills (and possibly the Lopez Reservoir) segment(s) of the fault zone. The higher terraces appear to warp down to the northeast into the fault zone, suggesting that local folding has accompanied reverse displacement on the fault.

A similar flight of elevated terraces is absent along San Luis Obispo Creek within the Los Osos Valley, suggesting an absence of late Quaternary uplift in the valley (Plate 1). Rather, aggradation of Pleistocene and Holocene deposits in the valley suggest tectonic ponding behind the rising San Luis/Pismo structural block and/or subsidence of the Los Osos Valley. The fluvial stratigraphy along San Luis Obispo Creek thus records late Quaternary up-to-

the-south vertical separation along the Irish Hills segment of the Los Osos fault zone.

Detailed Site Investigations

Detailed investigations were conducted at three sites along the Irish Hills segment of the Los Osos fault zone. These sites, informally named the Cuesta, Ingley, and Ellsworth sites (Plate 1; Fig. 3), were investigated by detailed mapping of bedrock, Quaternary deposits, and geomorphic features; drilling; seismic refraction profiling; and exploratory trenching to assess the geometry and late Quaternary behavior of this fault segment.

The Cuesta, Ingley, and Ellsworth sites are located along the geomorphically well-expressed central part of the Irish Hills segment (Plate 1; Fig. 3). The general geology of the area and the sites of detailed exploration are shown on Fig. 10. Two traces of the Los Osos fault zone mapped by Hall and others (1979) cross the southwestern part of the area and enclose a zone of serpentinite within the northeastern foothills of the Irish Hills. The other faults and fault-related features shown on Fig. 9 were identified during this investigation and are based primarily on geomorphic indicators and/or observed disruption of Quaternary deposits. Quaternary surficial deposits veneer most of the Los Osos Valley north and northeast of the fault traces mapped by Hall and others (1979). The Franciscan Complex, however, is locally exposed and underlies most of the area at shallow depth. Depth to bedrock generally increases to the northeast across the fault zone, reaching more than 23 m below the surface in boreholes on the Ingley site near Los Osos Valley Road.

Ellsworth Site. Ellsworth trench T-1 was excavated to assess fault behavior and geometry along one of the traces mapped by Hall and others (1979) within the low foothills of the Irish Hills. In the trench the fault juxtaposes older alluvium, which Hall and others (1979) map as Pliocene(?) and Pleistocene Paso Robles Formation, on the southwest against sheared serpentinite on the northeast (Fig. 11)[1]. Weakly developed slickensides on the fault plane, which dips about 75° NE, suggest predominantly vertical displacement. The older alluvium in the footwall is approximately horizontal 5 m away from the fault but progressively steepens upward to nearly vertical at the fault, suggesting that drag folding occurred during displacement. Synclinal drag folding of the older alluvium within the footwall adjacent to the northeast-dipping fault is consistent with southwest-verging reverse displacement on the fault. The base of a soil B horizon that developed in the older alluvium appears to be displaced approximately 12 cm by the exposed fault. The upper part of the soil B horizon and overlying colluvium appear to be unfaulted.

Stratigraphic relations from this trench indicate a period of southwest-verging reverse displacement on a near-vertical to northeast-dipping fault. Drag folding and vertical offset of Pliocene(?) and Pleistocene alluvium suggests that reverse displacement at this location continued into at least the early Quaternary. This sense of displacement is opposite to that generally

[1]Detailed logs of the Ellsworth trench and all other trenches described in this paper are provided in PGE (1988) and Response to Nuclear Regulatory Commission Question 43j (PGE, 1989)

expected for the Los Osos fault zone based on the geomorphic evidence and the displaced marine and fluvial terraces described above, both of which indicate late Quaternary uplift of the Irish Hills relativeto the Los Osos Valley. In addition, the older alluvium contains dacite clasts that are derived from a series of Oligocene intrusions (the Morro Rock-Islay Hill complex of Greenhaus and Cox, 1979) that crop out along the northern margin of the Los Osos Valley. The clasts indicate that mudflows or streams flowed to the south or southwest across the valley. This alluvium, however, is exposed in the foothills of the Irish Hills at up to 50 m above the modern floor of the Los Osos Valley. These relationships indicate that, although the older alluvium is within the footwall of a southwest-verging reverse fault exposed in the Ellsworth trench, it has been elevated significantly by either up-on-the-southwest range-front faulting along the valley margin, or there has been significant incision and removal of alluvium from the floor of Los Osos Valley. Several possible interpretations explain these stratigraphic relations as the result of tectonic movement on the Los Osos fault:

1. The trace of the Los Osos fault zone exposed at the Ellsworth site is inactive. Earlier southwest-vergent reverse movement ceased sometime in the middle or early Quaternary following deposition and displacement of the Pliocene-Pleistocene older alluvium (Paso Robles Formation of Hall and others, 1979).

2. The Ellsworth trace is an active backthrust in the hanging wall of the Los Osos fault zone. The primary trace lies to the north-northeast and is responsible for elevation of the range and the older alluvium that contains dacite clasts.

3. The Ellsworth trace is an active normal fault resulting from localized tension in the hanging-wall of the Los Osos fault zone. The stratigraphic relationships along this fault trace are inherited from an earlier phase of strike-slip displacement. Subsequent Quaternary dip-slip displacement has not obliterated the earlier stratigraphic separation.

A history of strike-slip displacement on the Los Osos fault zone is indicated in a series of gully exposures along Perfumo Canyon Creek about 2 km southeast of the Ellsworth trench (Plate 1). At this location, metavolcanic rocks of the Franciscan Complex are sheared extensively by multiple fault planes exposed in a zone 2 to 5 m wide. Slickensides and mullions are preserved on near-vertical, polished fault planes. The slickensides and mullions are horizontal to subhorizontal, indicating that the fault experienced strike-slip displacement at some time in the past. Evidence from the Ellsworth trench suggests that this strike-slip fault was reactivated as a high-angle fault having dip-slip displacement. This inferred earlier history of stratigraphic separation due to strike-slip displacement may be important for interpreting the stratigraphic relationships and structural history of the Los Osos fault on the Ingley and Cuesta sites, as described below.

Cuesta Site. The Cuesta site lies about 1 km northeast of the Ellsworth site at the base of the Irish Hills range front (Fig. 10). Several northeast-facing topographic scarps, alignment of springs, tonal lineaments, and stream nickpoints occur in a zone that is up

to 300 m wide and is coincident with the range front of the Irish Hills subblock. The detailed geology and the distribution of potentially fault-related geomorphic features on the Cuesta site are shown on a one-foot contour interval topographic base on Fig. 12. The surficial deposits are divided into eight units based on topographic position in a sequence of inset terraces, relative degree of clast weathering, and relative degree of soil-profile development. Older alluvium (Qoa) consists of deeply weathered clayey gravel that may correlate with the Pliocene (?) and Pleistocene Paso Robles Formation as mapped by Hall and others (1979), or may be reworked from the Paso Robles Formation. A bone sample from the older alluvium exposed in Cuesta trench T-3 yielded a discordant uranium-series date of 37.0 $\pm$ 2.6 ka, which represents a minimum age for the deposit. A charcoal sample from the same deposit yielded a date of 42,210 $\pm$ 1370 radiocarbon years B.P., which is probably beyond the effective range of conventional radiocarbon dating techniques and is therefore also a minimum age for Qoa. The younger seven inset alluvial deposits are interpreted to be late Pleistocene and/or Holocene in age. The youngest deposits (Qa_6 and Qac) consist, at least in part, of modern gully-wash deposits.

The scarps, tonal lineaments, and alignment of springs at the Cuesta site occur within older alluvium and the intermediate inset surficial deposits (Qf_1, Qf_2, and Qf_3). In addition, nickpoints are preserved in modern gully channels that are incised into the unconsolidated alluvium. These steps generally coincide with the topographic scarps and have not migrated appreciably upstream. The origin of these geomorphic features is uncertain. Some may have formed by coseismic surface displacement along the Irish Hills segment of the Los Osos fault, while others may be the result of erosional processes along a fault trace. Because the scarps and nickpoints on the Cuesta site are preserved in Quaternary alluvium, they are probably due to processes (tectonic and/or geomorphic) that remain active.

We excavated three trenches across the Cuesta scarps to assess the origin of the scarps (Fig. 12). Cuesta trench T-1, which crossed a prominent 0.5 m-high scarp near the northwestern boundary of the site, revealed very hard Franciscan ultramafic rock overlain by alluvial and colluvial units that we mapped as younger alluvium (Qf_2) (Fig. 12). Neither the buried erosional surface carved across the Franciscan bedrock nor the overlying young sediments are disrupted by faulting. The proximity of a creek to the northwestern end of this scarp suggests that it may, in part, be an erosional feature.

Cuesta trench T-2 crossed the most prominent scarp on the site near the southeastern margin of the property (Fig. 12). This arcuate, northeast-facing scarp is 1.2 to 1.8 m high and marked by several small springs and seeps. A fault striking N30W, and dipping 46NE is exposed in the trench beneath the scarp (Fig. 13). Prominent down-dip slickensides are presented on the fault plane indicating pure dip-slip during at least the last event. The fault juxtaposes highly deformed Franciscan Complex melange in the footwall on the northeast against crudely stratified, subhorizontal sedimentary deposits tentatively correlated with the Paso Robles Formation in the hanging wall on the southwest. The observed stratigraphic relationships and geomorphic expression of the fault scarp provide conflicting evidence of sense of slip.

Stratigraphic relationships indicate reverse displacement with Franciscan Complex rocks of the northeastern block displaced over the Paso Robles Formation (?). However, the northeast-facing scarp coincident with the fault trace indicates that the most recent fault activity has been normal displacement, if the scarp is a direct result of fault slip and is not related to differential erosion.

Four prominent faults were observed within the 125-m-long exposure in Cuesta trench T-3 (Fig. 14, Plate 2). Three appear to be reverse faults that dip from 45° to 72° to the northeast. One appears to be a small thrust fault that dips 15° to 20° to the southwest and is displaced slightly by one of the steeper reverse faults. All four faults occur at the southwestern margins of blocks of Franciscan Complex melange. Franciscan bedrock at the surface on the Los Osos Valley (northeast or hanging wall) side of each fault indicates that these faults are not the primary range-front structure that separates the elevated Irish Hills from the Los Osos Valley. We interpret these faults to be secondary, backthrusting (or antithetic faulting) in the hanging wall of a primary reverse or thrust fault at depth that probably intersects the surface to the north-northeast of the trench location. Each of these faults displaces older alluvium and, with the exception of the middle fault (Section B-C, Fig. 14), shows as a fracture, clay seam, and/or fissure filling that extends into the surface soil, indicating probable Holocene displacement. The surface soil is a clay-rich vertisol that lacks apparent horizons. Vertical churning of the soil due to shrink/swell phenomena, which is typical of vertisols, commonly overturns the entire soil profile every several hundred years. Preservation of nonvertical planar fault-related features (fractures, clay seams) within the soil thus indicates probable fault activity within the past few hundred years. If these are secondary faults related to a primary fault at depth, we can deduce late Holocene activity on the primary fault.

Cuesta trench T-3 provided another exposure of the dip-slip fault that lies beneath the most prominent northeast-facing scarp on the Cuesta site (Section A-B, Fig. 14) and that was also intersected in Cuesta trench T-2. The stratigraphic juxtaposition of Franciscan Complex melange over beds tentatively correlated with the Paso Robles Formation, plus a southwest-facing step of 13 cm at the base of an organic-rich A horizon soil, both suggest reverse slip on the fault. This is in contrast to the geomorphic expression of the northeast facing scarp which, if directly related to slip on the underlying fault it is most appropriately interpreted as a normal fault.

A second fault, which lacks geomorphic expression, was exposed in Cuesta trench T-3 approximately 30 m northeast of the base of the prominent scarp (Section B-C, Fig. 14). This fault has stratigraphic and structural relationships that suggest it might have undergone a reversal of slip during its evolution. Bedded alluvial deposits in the hanging wall (NE) block are deformed into a small, plunging syncline that lies below the base of the soil, suggesting that normal slip, possibly with an oblique component, occurred on the fault during and/or shortly after deposition of the alluvium. The inferred broad folding of the alluvial deposits shown on Fig. 14 and the presence of Franciscan Complex bedrock over alluvial and colluvial materials at the base of the trench, in contrast, suggest compression in the hanging wall and reverse slip on the fault sometime after deposition of the alluvium.

Approximately 75 m northeast of the base of the prominent scarp noted above, a pair of intersecting faults was exposed in trench T-3 (Section C-D, Fig. 14). The lower is a reverse fault oriented N50W, 47NE with slickensides and mullions that trend N30-35E. Like the two other reverse faults exposed farther to the southwest in this trench, this fault juxtaposes Franciscan Complex melange on the northeastern (hanging wall) block over alluvial and colluvial deposits of presumed Quaternary age in the southwestern block. The reverse fault offsets a small secondary thrust fault oriented N55W, 15SW that, in turn extends clearly into the overlying vertic soil. These relationships suggest that both faults have moved during the Holocene. An organic-rich krotovina in the southeastern trench wall is truncated by the southwest-dipping fault and provides a mean residence time (MRT) radiocarbon date of 2516 $\pm$ 10 years B.P., confirming Holocene activity for both faults. The base of the soil is lower on the hanging wall of the apparent thrust in the northwest trench wall (shown on Fig. 14) (inverse of thrust movement), but is higher on the southeast wall. Differing rates of soil development on different parent materials may account for this apparent difference in sense of movement. The apparent thrust fault flattens to the southwest and becomes indistinguishable or dies out down-dip.

The stratigraphic and structural relationships observed in Cuesta trench T-3 are similar to those described earlier for the trace of the Los Osos fault exposed in Ellsworth trench T-1. In particular, the stratigraphic sense of displacement is opposite to that expected based on scarp aspect and elevation of the Irish Hills, which imply up-on-the-southwest displacement. Some stratigraphic relationships observed in Cuesta trench T-3 may not reflect the most recent behavior of the exposed faults but may be inherited offsets from a history that included previous strike-slip behavior within the Los Osos fault zone. Because of the uncertainty that results from this apparent contradiction, the following interpretations are possible:

1. The high-angle faults represent secondary reverse faults or back-thrusts in the hanging wall of a larger, low-angle thrust fault. This model, schematically illustrated as Alternative A on Fig. 15, assumes that the observed stratigraphic relationships represent late Quaternary displacement and the northeast-facing scarps are not directly related to the underlying reverse faults. According to this interpretation, the hanging wall is experiencing active compression that might be explaced if the inferred primary Los Osos fault flatten at depth.

2. The high-angle faults represent secondary normal faults in the hanging wall of a larger, low-angle thrust fault. This model, schematically illustrated as Alternative B in Fig. 15, assumes that the observed stratigraphic separation is inherited from a former, perhaps strike-slip, style of deformation. In this interpretation, the northeast-facing scarps are a direct result of tectonic deformation in the upper plate associated with movement at depth on the primary reverse fault. In this case, localized tension in the hanging wall might be explained if the primary Los Osos fault steepens at depth.

The conflicting stratigraphic and geomorphic data can be explained if the Los Osos fault zone changes geometry at depth. In this model, a moderately dipping fault zone at depth first steepens then shallows, toward the surface. The change from a moderately dipping fault at depth to a steeply dipping fault toward the surface will produce localized compression in the hanging wall of the fault potentially producing secondary backthrusts. As these backthrusts are carried in the hanging wall onto the shallow dipping, near-surface part of the fault, local tension may result in normal offset on the prior thrust faults.

Ingley Site. The Ingley site is about 300 m northwest of the Cuesta site along trend of the Los Osos fault zone (Fig. 10). Potentially fault-related geomorphic features in the area include a prominent, arcuate topographic scarp near Los Osos Valley Road, a doubly deflected stream channel across the fault zone, and a spring-fed, marshy closed depression in an otherwise integrated drainage system.

At least two fault traces cross the Ingley site. The more southwesterly trace is exposed in a stream cut along Sycamore Canyon Creek (Fig. 16). The trace coincides with a right deflection of Sycamore Canyon Creek and is on trend with the closed depression and spring about 60 m to the southeast. Ingley trench T-1 was excavated across the fault trace between the stream exposure and the closed depression (Fig. 17).

Both the trench and stream cut exposures show a northwest-trending reverse fault that is nearly vertical to steeply northeast-dipping. In the stream cut exposure, warping of beds within older alluvium on the hanging and foot walls is consistent with drag folding on a northeast-dipping reverse fault (Fig. 18). In Ingley trench T-1, the fault separates Pliocene(?) and Quaternary alluvium on the southwest from Franciscan Complex sandstone and shale on the northeast. Older alluvium tentatively correlated with the Pliocene(?) and Pleistocene Paso Robles Formation of Hall and others (1979) is sheared extensively and dips steeply to the southwest. This older alluvium contains well-rounded boulders of dacite up to 0.5 m in diameter and cobbles of Franciscan Complex blueschist, graywacke, chert, and greenstone. This older alluvium is lithologically similar to, although coarser-grained than, the basal gravels in fault contact with the serpentinite in the Ellsworth trench. The stratigraphic relations exposed in the stream cut and trench T-1 indicate northeast-side-up reverse displacement (Figs. 17 and 18).

A buried soil containing charcoal radiocarbon dated at 28,450 ± 550 yr B.P. is developed on the deformed older alluvium (Fig. 17). The soil is faulted, clearly indicating late Pleistocene activity on this fault trace. The faulted soil is overlain by younger alluvium that thickens on the downthrown side of the fault and consists in part of interbedded clayey silt and peat. The silt and peat probably accumulated during a period of quiet-water marsh conditions similar to those presently existing in the nearby closed depression (Fig. 16). Wood fragments in the peat and silt radiocarbon were dated at 2420 ± 90 and 2520 ± 50 yr B.P. These deposits are warped up and pinch out laterally toward the fault. Although they do not extend across the fault where direct evidence of displacement can be observed, their presence adjacent to the fault suggests that local fault-induced warping caused ponding of sediment. Based on the age of the peat, this condition persisted into the late Holocene.

The fault geometry and sense of displacement in Ingley trench T-1 are similar to those observed for the Los Osos fault trace exposed in Ellsworth trench T-1 and those observed along trend at the Cuesta site. Ingley trench T-1, however, presents clear stratigraphic and geomorphic evidence of late Pleistocene and Holocene activity along the Los Osos fault zone.

Ingley trench T-2 was excavated across a prominent northeast-facing, 6-m-high topographic scarp along the Los Osos fault zone (Fig. 10, Plate 1). Franciscan Complex bedrock was not exposed in the trench (Fig. 19). The oldest deposits exposed consist of deeply weathered fluvial deposits containing well-rounded cobbles of decomposed graywacke, dacite, chert, and minor blueschist. This older alluvium is similar in composition to older alluvium exposed in Ingley trench T-1 and is correlated tentatively with the Paso Robles Formation of Hall and others (1979). The older alluvium is overlain by a younger alluvium that lacks dacite clasts. A prominent soil A horizon developed across the younger alluvium, then was buried by colluvium. The buried A horizon, which slopes approximately 6° to the northeast, is a marker horizon that we have used to estimate the amount and timing of latest Quaternary slip on the faults exposed in the trench.

The age of the buried A horizon is poorly constrained. Based on relative soil development in the deposits that overlie it and on comparisons with dated soils in nearby Ingley trench T-1, a tentative age estimate of 10 to 15 ka is assigned to the period of soil development that formed the buried A horizon. The buried soil in Ingley trench T-1, developed on similar parent materials, has a maximum age of 28,450 ± 550 radiocarbon years B.P. The buried A horizon in Ingley trench T-2 is much less developed than this dated soil; we interpret it to be on the order of 10 to 15 thousand years younger. Assuming pedogenesis ceased shortly after burial of the A horizon, displacement of the soil probably occurred during about the past 15,000 years. However, because the buried A horizon soil in Ingley trench T-2 formed primarily under Holocene conditions, whereas the dated Ingley trench T-1 soil formed primarily under late Pleistocene conditions, this age estimate is tentative.

Four low-angle faults displace the buried soil A horizon with up-on-the-southwest displacement (Fig. 19). The fault dips 22° to 29° to the southwest and strikes N54°W to N64°W. Slickensides and mullions on this fault plane trend S42°W to S68°W and plunge 14° to 22°, indicating predominant dip-slip displacement with a minor component of left-lateral displacement. Assuming that the remnants of the buried A soil horizon originally were a single continuous horizon, cumulative vertical separation of the A horizon ranges from about 0.9 to 1.6 m. Cumulative net horizontal shortening of the soil across the four faults is at least 4.0 m, which suggests that this stratum is shortened by about 15 percent within the length of the trench. The ratio of cumulative horizontal to vertical separation, about 3.25 ± 1 to 1, suggests a maximum effective fault dip of about 17 ± 3° within the upper 3 m of exposed strata, although the faults exposed in the trench have dips ranging up to 29° (Fig. 19). Given an estimated age of 10 to 15 ka for the buried A horizon, the late Pleistocene rate of vertical separation across faults exposed in Ingley trench T-2 is 0.06 to 0.16 mm/yr. Assuming a fault dip of 30° to 60°

at depth, we estimate the late Pleistocene net slip rate to range from 0.07 to 0.33 mm/yr.

The stratigraphic record exposed in Ingley trench T-2 provides few data to assess the number of events or displacement per event since development of the buried A horizon. Net displacement of the buried A horizon on each of the four prominent shears ranges from 0.5 to 2.0 m, averaging 1.0 m. No data are available to quantify the number of events represented by each shear or to indicate whether more than one shear was active during a single event. The available data, however, strongly suggest that multiple surface-faulting events have occurred on the shears exposed in Ingley trench T-2 and that the youngest event is late Holocene. Multiple events are indicated by 1) numerous shears (only four of which cut the buried A horizon) within a fault zone approximately 20 m wide; 2) a thick (0.5 to 1 m) clay-gouge zone along one shear that extends through both older and younger alluvium; and 3) a northeasternmost shear that displaces the E horizon of the surface soil and a southwesternmost shear that does not. These relations suggest that the southwesternmost shear predates development of the surface soil and was not involved in coseismic deformation during the most recent event. Thus, at least two and probably more surface-faulting events are recorded in the trench exposures. An MRT radiocarbon date of 1840 $\pm$ 60 yr B.P. from deposits directly beneath the E horizon of the surface soil and the displacement of the E horizon strongly suggest that there has been late Holocene rupture along at least one shear of the Irish Hills segment of the Los Osos fault zone.

Near-surface fault geometry, sense of displacement, and recency of slip indicate that the shears exposed in Ingley trench T-2 represent the primary reverse fault in the Los Osos fault zone. The stratigraphic and structural relationships observed at this site and the Cuesta and Ellsworth sites can be explained by two alternative models for the down-dip geometry of the Los Osos fault zone. These alternative models arise from two alternative interpretations of the high-angle, northeast-dipping dip-slip faults and overlying geomorphic scarps observed at the Ellsworth, Cuesta, and Ingley sites.

If we assume that deformation in the hanging wall of the Los Osos fault zone is controlled primarily by movement of the hanging wall block over non-planar aspects of the primary fault surface and that deformation occurs by simple shear in a homogeneous medium, we can predict the down-dip geometry of that part of the primary fault surface underlying the observed deformation in the hanging wall.

In Alternative 1 (Fig. 20A), the northeast-dipping high-angle faults are shown as southwest verging reverse faults, and represent secondary back thrusts to the primary low-angle, northeast-verging primary thrust fault exposed in Ingley trench T-2. This style of deformation indicates localized contraction of the hanging wall caused by a synclinal fault-bend in the underlying primary thrust surface.

In Alternative 2, the northeast-dipping, high-angle faults are down-on-the-northeast normal faults, consistent with a tectonic origin for the overlying northeast-facing geomorphic scarps. These normal faults detach into the underlying primary thrust fault, and reflect localized tension in one hanging wall that results from an anticlinal fault-bend on the primary fault. Alternatives 1 and 2 are compatible with each other if there is a double-bend in the Los Osos fault

plane in the vicinity of the Irish Hills range front. This local down-dip geometry causes normal-sense shear in the hanging wall to be overprinted on reverse sense shear as the hanging wall moves first over a synclinal fault-bend and then over the anticlinal fault bend as shown in Figure 20b.

The down-dip geometry of the Los Osos fault cannot be determined between the range front and an area approximately 2.5 km to the southwest because of a lack of Tertiary and Quaternary structural data. At this location, however, a local outcrop of Tertiary sandstone, possibly a member of the Pismo formation dips to the northeast indicating that, if the folding is related to faulting, the Los Osos fault steepens at depth beneath this area.

Slip Rate: Irish Hills Segment

Rates of displacement on the Irish Hills segment of the Los Osos fault zone are estimated from the displacement of marine terraces between Montaña de Oro State Park and Morro Bay, the displacement of fluvial terraces along San Luis Obispo Creek, and the displacement history recorded in Ingley trench T-2. Table 2 summarizes the maximum and minimum vertical component of slip for these areas. A range of net slip is also estimated assuming a fault dip of 30° to 60° at depth.

Vertical separation across the western end of the Irish Hills segment is estimated in two ways. The minimum rate of displacement is based on the difference in elevations of marine terraces at Montaña de Oro State Park south of the fault zone and the marine terraces between the towns of Morro Bay and Cayucos north of the fault. The maximum rate of displacement is approximated by combining the rate of uplift of the San Luis/Pismo block and rate of subsidence in the Morro Bay basin and assuming that all deformation is the result of reverse displacement on the Los Osos fault zone.

The substage 5e (120 ka) marine terrace occurs both in the Montaña de Oro State Park area and between the towns of Morro Bay and Cayucos (Hanson and others, this volume). In the area from Cayucos to Morro Bay, the shoreline angle is at an elevation of about 6 ± 1 m (Weber, 1983). Paleosea-level curves indicate that the substage 5e terrace was cut by a highstand of approximately 6 m elevation. This suggests that the coastline between Cayucos and Morro Bay has been relatively stable, with little or no uplift or subsidence. The absence of uplift is supported by the lack of an emergent flight of marine terraces in the Cayucos area (Weber, 1983). Reconnaissance mapping indicates that the 6-m substage 5e terrace drops in elevation to the south into the Los Osos Valley, suggesting that the valley is subsiding at some unknown rate. In the Montaña de Oro State Park area, the shoreline angle for the terrace is at an elevation of about 32 ± 1 m. The minimum rate of vertical separation across the Irish Hills segment of the Los Osos fault zone thus has been 26 m (32 m - 6 m) during the past 120 ka. The minimum vertical component of slip is therefore 0.22 mm/yr (Table 2).

Maximum vertical displacement on the Irish Hills segment outside of the Morro Bay basin is estimated by projecting the southwest-tilted shoreline angle of the substage 5e marine terrace from the Cayucos/Morro Bay area to the Los Osos fault zone. Such a projection suggests that the Los Osos Valley is subsiding at a rate of less than 0.2 mm/yr. Based on the elevation of the substage 5e shoreline angle, uplift of

the San Luis/Pismo block is 0.2 mm/yr. Therefore, the maximum vertical component of slip across the Irish Hills segment is estimated to be 0.4 mm/yr (Table 2).

Fluvial terraces along San Luis Obispo Creek provide another late Pleistocene strain gauge for estimating the vertical component of slip across the southeastern end of the Irish Hills segment of the Los Osos fault zone. As discussed previously, the well-developed flight of fluvial terraces preserved along San Luis Obispo Creek within the San Luis/Pismo structural block is truncated by the Los Osos fault zone. Upstream of the fault trace, the creek meanders within a broad floodplain that lacks a sequence of fluvial terraces. Pliocene(?), Pleistocene, and Holocene valley-fill alluvium suggests that the valley is tectonically quiescent or subsiding at a low rate, and that alluvium is tectonically ponded against the rising Irish Hills subblock along the Los Osos fault zone. The minimum rate of vertical slip on the fault zone is estimated by assuming that the highest fluvial terrace south of the fault correlates with the aggrading valley floor north of the fault. Based on correlation with marine terraces near Avila Beach, the highest recognized fluvial terrace is approximately 430 to 560 ka. This fluvial terrace projects as much as 34 m above the valley floor northeast of the Los Osos fault zone indicating a minimum value for the vertical component of slip on the Irish Hills segment of 34 m/560 ka, or 0.06 mm/yr (Table 2).

The maximum rate of vertical slip is estimated by assuming that gravel deposits recognized in wells north of the fault correlate to the highest fluvial terrace south of the fault and that this terrace is 430 ka. Water-well data suggest that the gravel deposits are at a depth of 76 m below the valley surface. Therefore, the maximum value for the vertical component of slip on the southeastern end of the Irish Hills segment appears to be 110 m/430 ka, or 0.26 mm/yr (Table 2).

LOPEZ RESERVOIR SEGMENT

The Lopez Reservoir segment of the Los Osos fault zone is southeast of the Irish Hills segment (Fig. 2). Faults within this segment are exposed in roadcuts near the Lopez reregulating reservoir, where they strike approximately N73W, dip 50°SW, and place Miocene Monterey diatomite in the hanging wall over weathered older alluvium (the Paso Robles Formation of Hall, 1973a) in the footwall. These relationships indicate that reverse displacement occurred along this segment through at least the early Quaternary.

Geomorphic Expression and Lateral Continuity

The Lopez Reservoir segment extends southeastward along the length of the Edna subblock of Lettis and others (this volume) from directly southeast of San Luis Obispo Creek to south of the Lopez reregulating reservoir, a distance of 16 ± 1 km (Fig. 2). To the northwest, this segment is separated from the Irish Hills segment by a 1- to 2-km en echelon step and the topographic segmentation of the San Luis Range described above. To the southeast, the segment boundary is poorly defined because geomorphic expression of the fault becomes indistinct. We interpret the segment boundary to coincide with the southeastern termination of the Edna subblock as defined by Lettis and others (this volume) and with the change in geomorphic character from a poorly defined range-front fault to an intra-range fault along the Newsom Ridge segment (Fig. 2).

In sharp contrast to the Irish Hills segment to the northwest, the Lopez Reservoir segment has poor topographic and geomorphic expression. The segment is a poorly defined range-front fault. Geomorphic features suggestive of faulting are sparse, laterally discontinuous, and not well defined (Plate 1). These features include linear drainages, anomalous drainage patterns, deflected drainages, topographic saddles, and ponded alluvium. Less prominent features include side-hill benches and tonal lineaments.

The Lopez Reservoir segment generally lies at or near the northeastern margin of the Edna subblock, which generally is characterized by low rolling hills of 180 to 240 m elevation (Fig. 4). Northwest of Pismo Creek, the range front is irregular and deeply dissected, suggesting low rates of late Quaternary uplift. Although the surface trace of the fault segment generally coincides with the base of the range between Pismo and San Luis Obispo creeks, it also lies as much as 2 km from the irregular range front in the adjacent Edna Valley. Between Pismo Creek and Lopez reregulating reservoir, the trace of the fault extends across the eastern foothills of the Edna subblock, an area of moderately dissected rolling hills (Fig. 4). The fault ceases to be a range-front fault in this area, suggesting that there has been little or no late Quaternary uplift of the San Luis/Pismo block along the fault.

The clearest geomorphic expression of Quaternary faulting is the apparent tectonic impoundment of alluvium in the headwaters of the Pismo Creek drainage basin upstream from the Los Osos fault zone (Fig. 3). Quaternary faulting is suggested by the outcrop pattern of both older alluvium (Paso Robles Formation of Hall, 1973a) and younger alluvium in the Edna Valley. In addition, Quaternary fluvial terraces along Pismo Creek appear to be truncated by the Lopez Reservoir segment. These geomorphic and stratigraphic relations suggest late Pleistocene uplift of the Edna subblock of the San Luis/Pismo block accompanied by fluvial incision through the elevated range and by aggradation or impoundment of alluvium upstream of the fault. It is unclear, however, whether this uplift of the Edna subblock is caused by late Quaternary displacement along the Lopez Reservoir segment or whether uplift partially or wholly extends northeast across the Los Osos fault zone into the Edna Valley.

Detailed Site Investigations

Geomorphic features suggestive of recent faulting were investigated by detailed mapping and trenching at four locations along the Lopez Reservoir segment. These locations, shown on Plate 1 and Fig. 3, include the Guidetti Property, Brughelli Property, Glick Property, and the Lopez reregulating reservoir area. Trenches were located across geomorphic features showing the strongest expression of potential late Quaternary faulting. These investigations indicate that older alluvium mapped by Hall (1973a) as the Paso Robles Formation (Pliocene(?) and Pleistocene in age) is displaced against Miocene Monterey Formation along high-angle, southwest-dipping reverse faults (Fig. 21). No evidence for latest Pleistocene (post-40 ka) and Holocene displacement was observed in the trenches. However, the geomorphic relations described above suggest that late Pleistocene uplift may have occurred on the Lopez Reservoir segment.

Slip Rate: Lopez Reservoir Segment

Site-specific data are not available to document the late Pleistocene and Holocene slip rate and behavior of the Lopez

Reservoir segment. Available trenching data do not provide constraints on fault activity during the latest Pleistocene (post-40 ka) and the Holocene. However, the fault has not experienced displacement during the past 750 ± 100 radiocarbon years B.P. (Fig. 21). A late Quaternary slip rate for the segment can be estimated qualitatively from both the topographic relief Edna subblock and from the elevated flight of marine terraces preserved along its southwestern flank (Hanson and others, this volume). Between San Luis Obispo Creek and Arroyo Grande Creek, the shoreline angles for these terraces maintain a relatively uniform elevation. The constant elevation of terraces indicates uniform regional uplift of the subblock along the coastline, with little or no internal deformation. The ages and elevations of these terraces indicate that the subblock is rising as a rigid block at a long-term late Pleistocene rate of 0.11 to 0.13 mm/yr northeast of the Wilmar Avenue fault (Fig. 2).

As described above, geomorphic features suggestive of faulting are sparse, laterally discontinuous, and not well-developed along the Lopez Reservoir segment. Where trenched, these features are not necessarily related to late Pleistocene or Holocene displacement. The long-term uplift rate of the southwestern margin of the Edna subblock provides only a qualitative estimate of the maximum vertical component of slip on the Lopez Reservoir fault segment, which borders the northeastern margin of the subblock. The poor geomorphic expression of the fault suggests that a higher vertical component of slip is unlikely. The fault segment is not a well-defined range-front fault, but becomes an intra-range fault near its southern end (Fig. 4). This suggests that the fault is not separating an area of uplift (the Edna subblock) from an area of subsidence (the Edna Valley), but that some uplift may also be occurring northeast of the fault in the southern Edna Valley. Based on these relations, we conclude that the late Quaternary rate of slip probably is less than 0.1 mm/yr and that the fault may not have experienced any activity during the latest Pleistocene (post-40 ka) or Holocene.

NEWSOM RIDGE SEGMENT

The Newsom Ridge segment of the Los Osos fault zone extends into the Newsom Ridge subblock of the San Luis/Pismo structural block between Arroyo Grande Creek and the West Huasna fault zone, a distance of about 8 ± 1 km (Fig. 2). The trace of the fault is poorly expressed and is based primarily on bedrock relations mapped by Hall (1973b). Hall interpreted the fault to juxtapose rocks of the Franciscan Complex on the northeast against serpentinite and Tertiary Monterey and Lospe formations on the southwest along a generally linear, discontinuous zone of faulting. Aerial photographs along the mapped fault trace show that small, subtle, side-hill benches, tonal lineaments, and linear stream segments are distributed along parts of the fault segment. In part, the fault extends along a northwest-trending linear stream segment of Tar Spring Creek that is deeply incised into the Newsom Ridge range (Plate 1). In contrast to the range-front character of the Irish Hills segment of the Los Osos fault zone, topographic analysis of the San Luis/Pismo block (Figs. 4 and 5) indicates that the Newsom Ridge segment extends into the Newsom Ridge subblock and clearly is an intra-range fault. The northwestern boundary of this fault segment is interpreted to coincide with the northwestern termination of the Newsom Ridge subblock (Fig. 2) and with a change from what clearly is an intra-range fault to a

poorly defined range-front fault along the Lopez Reservoir segment to the northwest. To the southeast, the segment terminates against the West Huasna fault zone near Twitchell Reservoir.

The slip rate and recency of activity of the Newsom Ridge segment are unknown. The poor geomorphic expression and intra-range character of the fault trace suggests that the segment either is not active or has experienced very low rates of activity during the late Quaternary.

ESTERO BAY SEGMENT

The Los Osos fault zone probably continues offshore into Estero Bay northwest of the Irish Hills segment (Fig. 2). Available geophysical and bathymetric data suggest that this segment of the fault zone is a diffuse, structurally complex zone that is 1 to 2 km wide and extends offshore as a northwestern projection of the Irish Hills segment (PG&E, 1988). Bathymetric data and diver geological mapping reveal an east-west trending linear contact between the Miocene Miguelito member of the Pismo formation on the south with unconsolidated, undifferentiated Quaternary sediments on the north. This contact is on line with the offshore projection of the fault reach that trends east-west south of Morro Bay. On seismic reflection data, the fault segment is imaged as a complex zone of diffractions within which reflections are obscured; clear stratigraphic displacement and terminated reflectors are not imaged. Farther offshore, this trace is interpreted to lie along the northeastern margin of a series of northwest-trending, 10- to 25-m-high ridges named "59-meter ridge." We consider the ridge to be the northwestern continuation of the San Luis/Pismo structural block. Several discontinuous northeast-facing scarps border the margin of the ridge. In the current tectonic regime, these relations suggest northeast-verging reverse displacement along a southwest-dipping fault or zone of faults similar in character to the Irish Hills segment onshore. Definitive evidence for recency of displacement along the Estero Bay segment, however, is lacking because of the complex geophysical signature of the fault. Although the northeast-facing scarps serve as a basin-margin for post-late Wisconsinan (post-18 ka) sediments, it is impossible to say whether the sediment-bedrock contacts are faults or buttress unconformities.

The length of the Estero Bay segment is uncertain because of the lack of geophysical resolution of the fault beneath Estero Bay. The fault probably extends to the northwest along the northeastern margin of "59-meter ridge," presumably to an intersection with the Hosgri fault zone. The segment thus is 13 $\pm$ 1 km long from the Hosgri fault zone to the coastline. This length is a maximum because at some distance from the Hosgri, the southwest-dipping Estero Bay segment will be truncated by the vertical to northeast-dipping Hosgri fault zone above seismogenic depths.

SUMMARY

The Los Osos fault zone is a complex reverse or thrust fault along the northeastern margin of the San Luis/Pismo structural block. Quaternary uplift of the block at rates of 0.1 to 0.24 mm/yr has been, in part, accommodated by displacement along this fault zone.

Based on reconnaissance and detailed mapping, trenching, and drilling conducted during this study, we interpret the fault to extend at least from Morro Bay on the

northwest to the Lopez reregulating reservoir on the southeast, a distance of about 36 km. The fault may extend to the northwest an additional 13 km offshore, where it intersects with the Hosgri fault zone in Estero Bay and to the southeast 8 km to an intersection with the West Huasna fault near Twitchell Reservoir. The total possible length of the fault zone therefore is 57 km. Using physical and behavioral characteristics, we have divided the fault into two distinct segments and two poorly defined segments. The central 36 km of the fault is divided into the Irish Hills and Lopez Reservoir segments. Our studies document multiple late Pleistocene and Holocene surface- faulting events along the Irish Hills segment, which we assign a late Quaternary slip rate of 0.2 to 0.8 mm/yr. The segment, which has excellent geomorphic expression, consists of a complex zone of subparallel fault traces up to 2 km wide. The Lopez Reservoir segment has poor geomorphic expression and, with the exception of possibly faulted fluvial terraces along Pismo Creek, exhibits no definitive evidence of late Quaternary activity. Based on uplift of the San Luis/Pismo structural block and the coincidence of most of the segment with the range-front, we interpret the Lopez Reservoir segment to be active in the Quaternary and to have a long-term slip rate of less than 0.1 mm/yr.

The less well-defined northwest and southeast extensions of the Los Osos fault zone are called the Estero Bay and Newsom Ridge segments, respectively. These segments of the fault zone have no clear geomorphic expression, and their existence as active Quaternary structures is uncertain.

The results of this study indicate that the Los Osos fault zone is an important structural element that accommodates regional northeast-southwest Quaternary crustal shortening in the Los Osos/Santa Maria Valley domain (Fig. 1). The fault separates the uplifted San Luis/Pismo structural block from the subsiding or southwest-tilted Cambria block and appears to accommodate relative motion between these blocks. If data from this area are representative of the style of deformation for the domain as a whole, late Quaternary crustal shortening in the domain is occurring primarily by rigid block uplift, subsidence, and tilting that is controlled by reverse displacement on northwest-trending faults.

REFERENCES

California Department of Water Resources (CDWR), 1972, Sea-water intrusion: Morro Bay area, San Luis Obispo County: State of California Bulletin No. 63-6.

Chappell, J., and Shackleton, N.J., 1986, Oxygen isotopes and sea level: Nature, v. 324, p. 137-140.

Dibblee, T.W., Jr., 1974, Geologic map of the San Luis Obispo 15-minute quadrangle, California: U.S. Geological Survey Open File Report 74-223.

Greenhaus, M.R., and Cox, A., 1979, Paleomagnetism of the Morro Rock-Islay Hill complex as evidence for crustal block rotations in central coastal California: Journal of Geophysical Research, v. 84, no. B5, p. 2393-2400.

Hall, C.A., Jr., 1973a, Geologic map of the Morro Bay South and Port San Luis quadrangles, San Luis Obispo County, California: U.S. Geological Survey Miscellaneous Field Studies Map MF-511, scale 1:24,000.

Hall, C.A., Jr., 1973b, Geology of the Arroyo Grande quadrangle, California: California Division of Mines and Geology Map Sheet 24, scale 1:48,000, 8 p.

Hall, C.A., Jr., 1981, Map of geology along the Little Pine Fault, parts of the Sisquoc, Foxen Canyon, Zaca Lake, Bold Mountain, Los Olivos, and Figueroa Mountain quadrangles, Santa Barbara County, California: U.S. Geological Survey Miscellaneous Field Studies Map MF-1285, scale 1:24,000.

Hall, C.A., Jr., Ernst, W.G., Prior, S.W., and Wiese, S. W., 1979, Geologic map of the San Luis Obispo-San Simeon Region, California: U.S. Geological Survey Miscellaneous Investigations Series Map I-1097, scale 1:48,000.

Hanson, K.L., Wesling, J.R., Lettis, W.R., Kelson, K.I., and Mezger, L., 1990, Correlation and ages of Quaternary marine terraces: south-central coastal California: this volume.

Hornafius, S.J., Luyendyk, B.P., Terres, R.R., and Kamerling, M.J., 1986, Timing and extent of Neogene tectonic rotation in the western Transverse Ranges, California: Geological Society of America Bulletin, v. 97, p. 1476-1487.

Killeen, K.M., 1988, Timing of folding and uplift of the Pismo syncline, San Luis Obispo County, California: M.S. Thesis, University of Nevada, Reno, 75 p. (unpublished).

Knuepfer, P.L.K., and Coppersmith, K.J., 1987, Implications of the characteristics of end points of historical surface fault ruptures for the nature of fault segmentation (abs.): EOS Transactions, American Geophysical Union, v. 62, no. 44, p. 1243.

Lettis, W.R., and Hall, N.T., 1988, Methods for evaluating fault segmentation - An example from central coastal California (abs.): Geological Society of America Abstracts with Programs, v. 20, p. 175.

Lettis, W.R., Hamilton, D.H., and Hall, N.T., 1989, Quaternary tectonics of south-central coastal California (abs.): 29th International Geological Congress (in press).

Lettis, W.R., Clark, D.H., Hanson, K.L., Kelson, K.I. and Wesling, J.R., 1990, Quaternary deformation of the San Luis Range, San Luis Obispo County, California: this volume.

Menges, C., 1987, Temporal and spacial segmentation of Plio-Quaternary fault rupture along the base of the western Sangre de Cristo Mountain Front, northern New Mexico: in C. Menges, ed., Quaternary Tectonic Landform Evolution, Soil Chronologies, and Glacial Deposits - Northern Rio Grand Rift of New Mexico, Friends of the Pleistocene, Rocky Mountain Cell, Field Trip Guidebook, p. 71-94.

Mezger, E.L., Hanson, K.L., Hall, N.T., and Hunt, T.D., 1987, Evidence for Quaternary faulting in Los Osos Valley, San Luis Obispo County, California: Geological Society of America Abstracts with Program, v. 19, no. 6, p. 432.

Pacific Gas and Electric Company (PG&E), 1988, Final report of the Diablo Canyon Long-Term Seismic Program: U.S. Nuclear Regulatory Commission Docket Nos. 50-275 and 50-323.

Veeh, H., and Valentine, J.W., 1967, Radiometric ages of Pleistocene fossils from Cayucos, California: Geological Society of America Bulletin, v. 78, p. 547-550.

Weber, G.E., 1983, Geologic investigation of the marine terraces of the San Simeon region and Pleistocene activity of the San Simeon fault zone, San Luis Obispo County, California: U.S. Geological Survey Technical Report 66.

Weber, G.E., Lettis, W.R., and Hanson, K.L., 1987, Late Pleistocene uplift rates along the central California coast, Cape San Martin to Santa Maria Valley (abs.): Geological Society of America Abstracts with Programs, v. 19, no. 6, p. 462.

Yates, E.B., and Wiese, J.H., 1988, Hydrogeology and water resources of the Los Osos Valley ground-water basin, San Luis Obispo County, California: U.S. Geological Survey Water-Resources Investigations Report 88-4081, 112 p.

TABLE 1

CHARACTERISTICS OF FAULT SEGMENTS ALONG THE LOS OSOS FAULT ZONE (FAULT SEGMENTS SHOWN ON FIGURE 2.)

Fault Segment	Topographic Segmentation	Range-front Character	Geomorphic Expression	Recency of Slip	Late Quaternary Slip Rate mm/yr	Length	Characteristics At Segment Boundary
Estero Bay	Poorly defined; deeply eroded bedrock platform with several NW-trending linear ridges.	Borders NE flank of "59-meter ridge." Northern trace unknown.	Onshore trace marked by several NE-facing scarps, tonal lineaments and linear drainages. Offshore extension constrained by linear bedrock/unconsolidated Quaternary sediment contact.	Not well constrained. May displace post-late Wisconsinan sediment.	Not well constrained.	13 ± 2 km	Northwest—inferred to intersect Hosgri fault in Estero Bay. Southeast—segment bends 15° to 25° to more northwesterly trend along southern margin of Morro Bay basin and ends at northwestern margin of Irish Hills subblock.
Irish Hills	Coincident with Irish Hills subblock.	Well-defined range-front fault. Range front linear, steep, moderately dissected.	Well-defined scarps, spring lines, and lineaments. Tectonically impounds Pleistocene and Holocene (?) alluvium.	Multiple late Pleistocene and Holocene events.	Vertical 0.2 to 0.4. Net = 0.25 to 0.5 (60° dip); 0.4 to 0.8 (30° dip)	18 ± 2 km	Northwest— segment ends at Morro Bay basin coincident with en echelon or branching fault relationship or bends to more westerly trend to project into Estero Bay segment (see above). Southeast—1 to 2 km en echelon right step to Lopez Reservoir segment. Coincident with SE termination of Irish Hills subblock, 2 to 4 km right step in range front, and possible intervening basin of subsidence.

Table 1
(continued)

Fault Segment	Topographic Segmentation	Range-front Character	Geomorphic Expression	Recency of Slip	Late Quaternary Slip Rate mm/yr	Length	Characteristics At Segment Boundary
Lopez Reservoir	Coincident with Edna subblock.	Poorly defined range-front fault along NW part. Range front deeply dissected. Fault crosses rolling foothills along SE part.	Poorly defined lineaments. Tectonically impounds Pleistocene and Holocene (?) alluvium.	Displaces early (?) Pleistocene alluvium. Late Pleistocene and Holocene activity suggested by ponded allurium but not documented by displaced strata.	Vertical = < 0.1	17 ± 2 km	Northwest—1 to 2 km en echelon right step to Irish Hills subblock (see above). Coincident with NW termination of Edna subblock. Southeast—poorly defined. Coincident with SE termination of Edna subblock.
Newsom Ridge	Subparallel to and within Newsome Ridge subblock.	Intra-range fault; range deeply dissected.	No topography indicative of Quaternary faulting. Trace may be defined, in part, by linear drainage.	Quaternary displacement not observed.	Vertical = < 0.1 Probably not active.	8 ± 2 km	Northwest—poorly defined (see above). Lies along projection of Lopez Reservoir segment. Southeast—intersects West Huasna fault zone near Twitchell Reservoir.

TABLE 2

LATE QUATERNARY SLIP RATES
IRISH HILLS SEGMENT OF THE LOS OSOS FAULT ZONE

	Vertical Component of Slip (mm/yr)		Net Slip (mm/yr)[1]			
			30° Fault Plane		60° Fault Plane	
	Min.	Max.	Min.	Max.	Min.	Max.
Ingley Trench T-2	0.06	0.16	0.12	0.33	0.07	0.19
Montaña de Oro State Park	0.22	0.4	0.4	0.8	0.25	0.5
San Luis Obispo Creek	0.06	≥0.26	0.12	≥0.5	0.07	≥0.3

Note:

[1]Vertical component of slip is converted into net slip, assuming the fault plane dips 30° or 60° at depth.

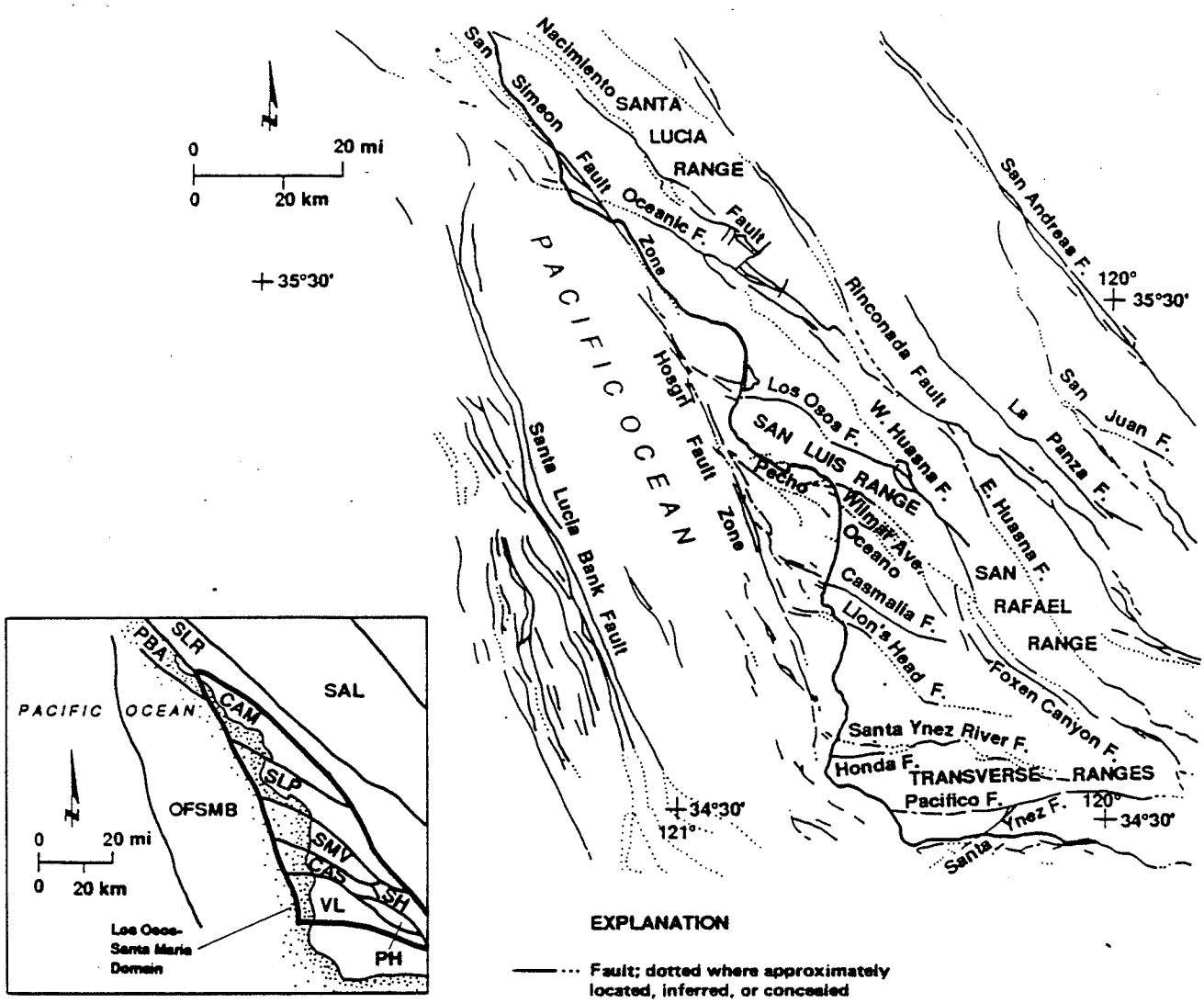

Figure 1. Map of structural blocks and faults in the south-central California coastal region. SAL = Salinian block, SLR = Santa Lucia Range block, PBA = Piedras Blancas anticlinorium, CAM = Cambria block, SLP = San Luis/Pismo block, OFSMB = Offshore Santa Maria basin block, SMV = Santa Maria Valley block, CAS = Casmalia block, VL = Vanderberg/Lompoc block, PH = Purisima Hills block, SH = Solomon Hills block. (After Lettis and others, this volume).

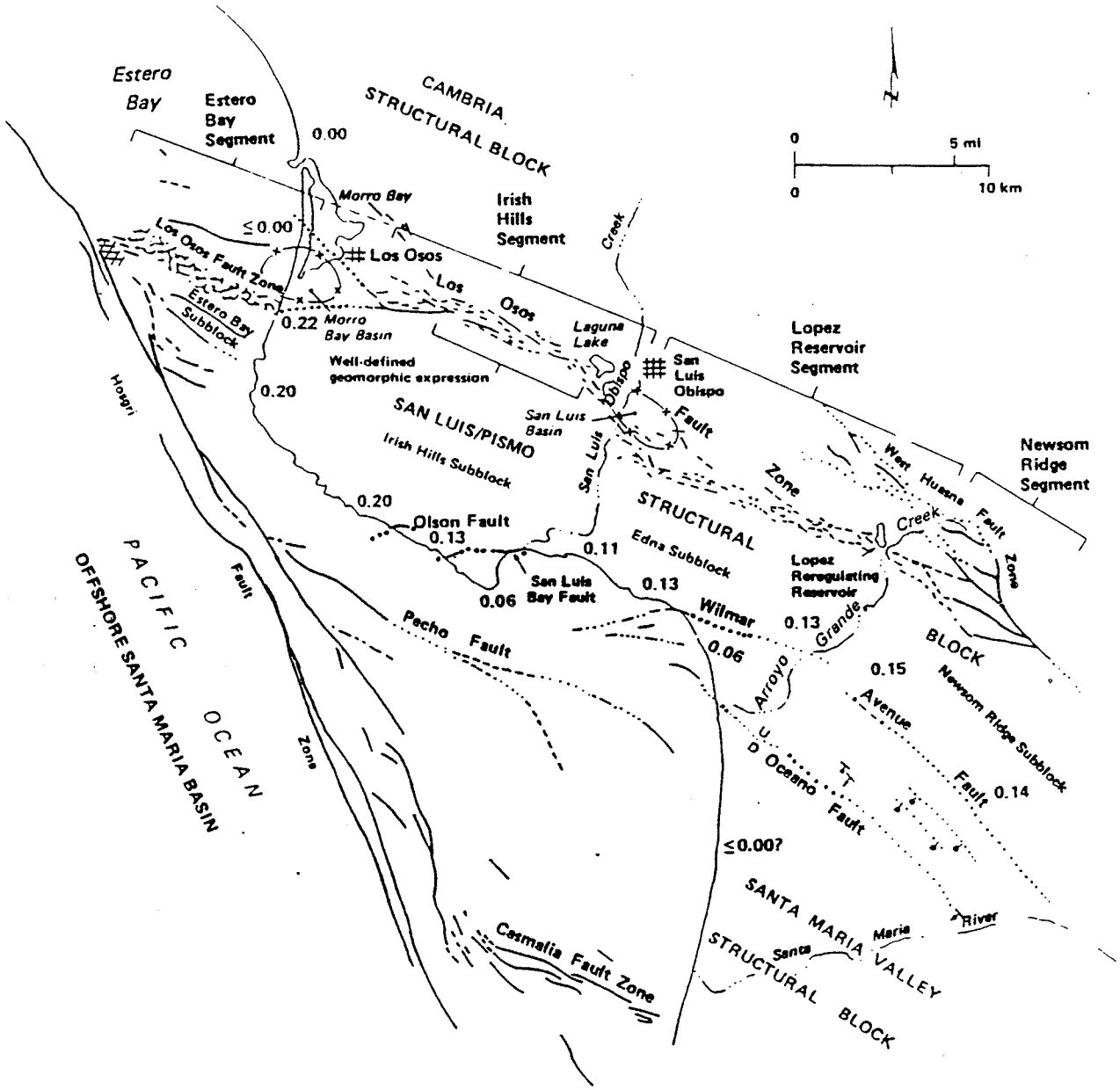

EXPLANATION

Offshore Structures

- Fault; solid where well constrained, dashed where inferred and well located, dotted where inferred and approximately located
- 59-meter ridge
- Structurally complex zone

Onshore Structures

- Fault; dashed where approximately located, heavy dot where concealed but well constrained, light dot where inferred
- Buried monocline; arrow shows direction of downwarp
- Step in bedrock, uncertain origin; ball on lower side
- 0.10 Uplift rate in mm/yr derived from marine terrace investigations
- Inferred structural basin; may or may not be bounded by faults

Figure 2. Regional map showing segments of the Los Osos fault zone and late Quaternary uplift rates of the San Luis/Pismo structural block.

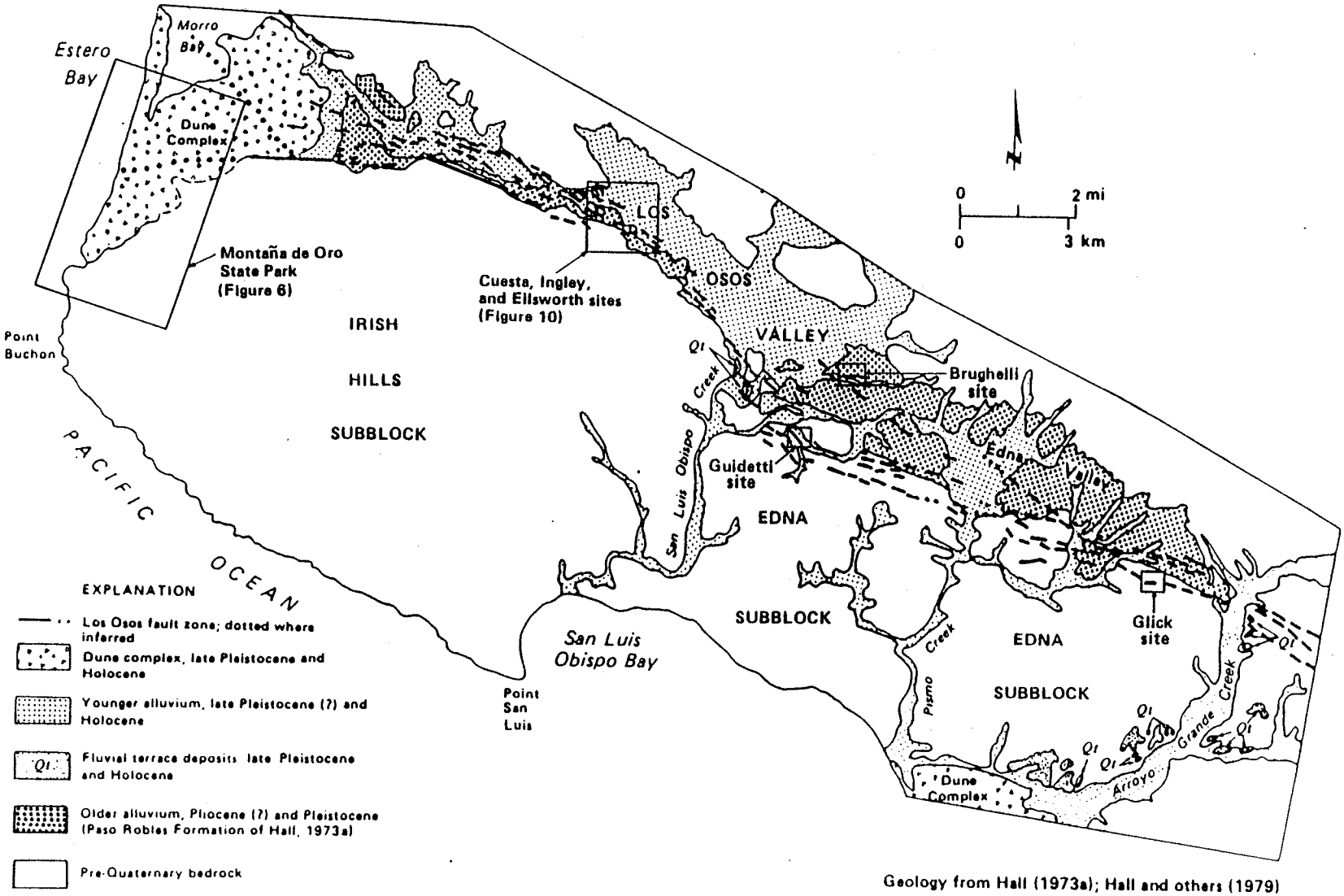

Figure 3. Map showing distribution of Pliocene (?) and Quaternary alluvial deposits along the Los Osos fault zone and the location of areas of detailed geologic investigation.

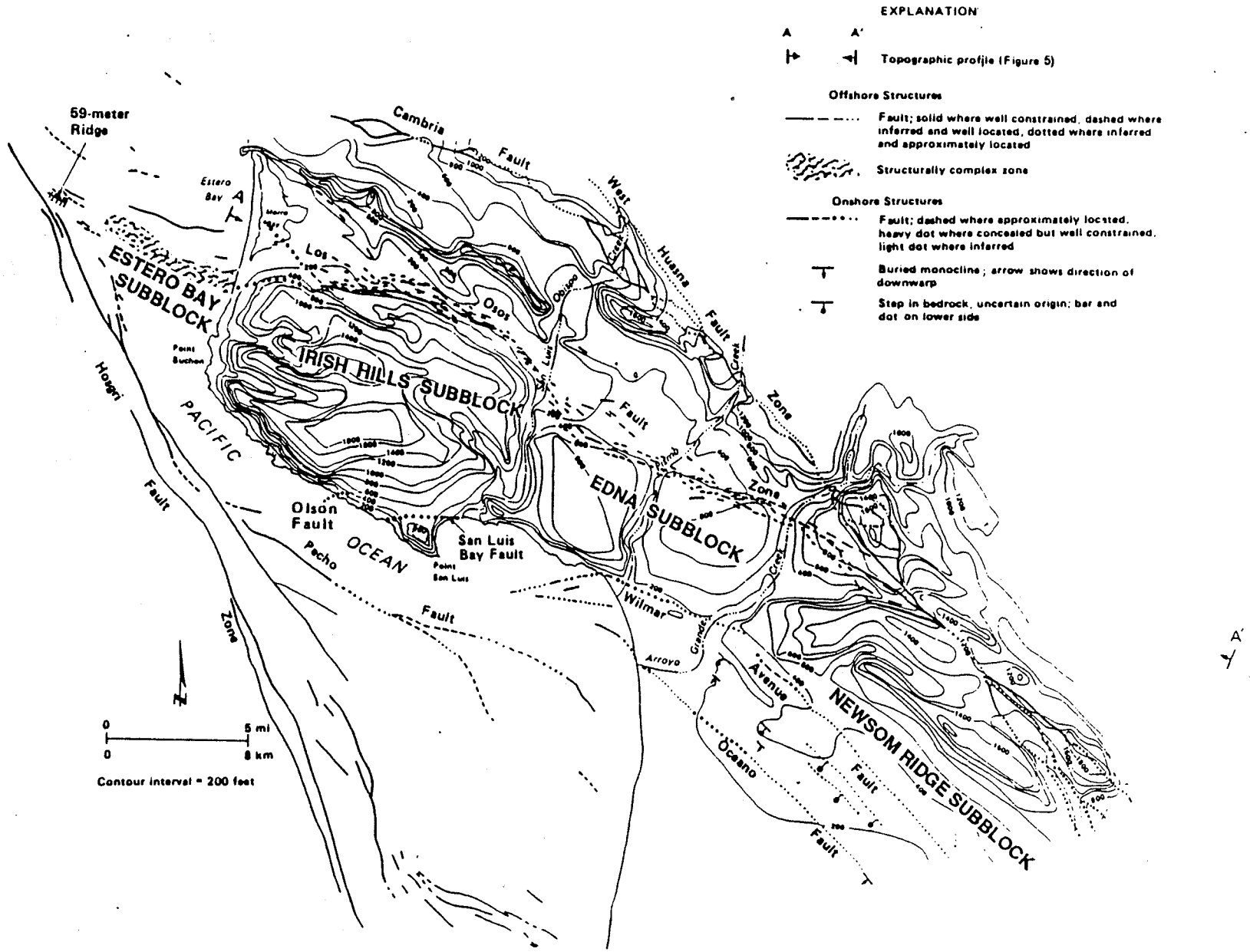

Figure 4 Generalized topographic contour map illustrating subblocks of the San Luis/Pismo structural block. Contours generalized from parts of the Morro Bay South, San Luis Obispo, Port San Luis, Pismo Beach, Arroyo Grande NE, Oceano, Tar Springs, Nipomo, Santa Maria, Huasna, Guadalupe, and Twitchell Dam U.S. Geological Survey 7.5-minute topographic quadrangles (After Lettis and others, this volume).

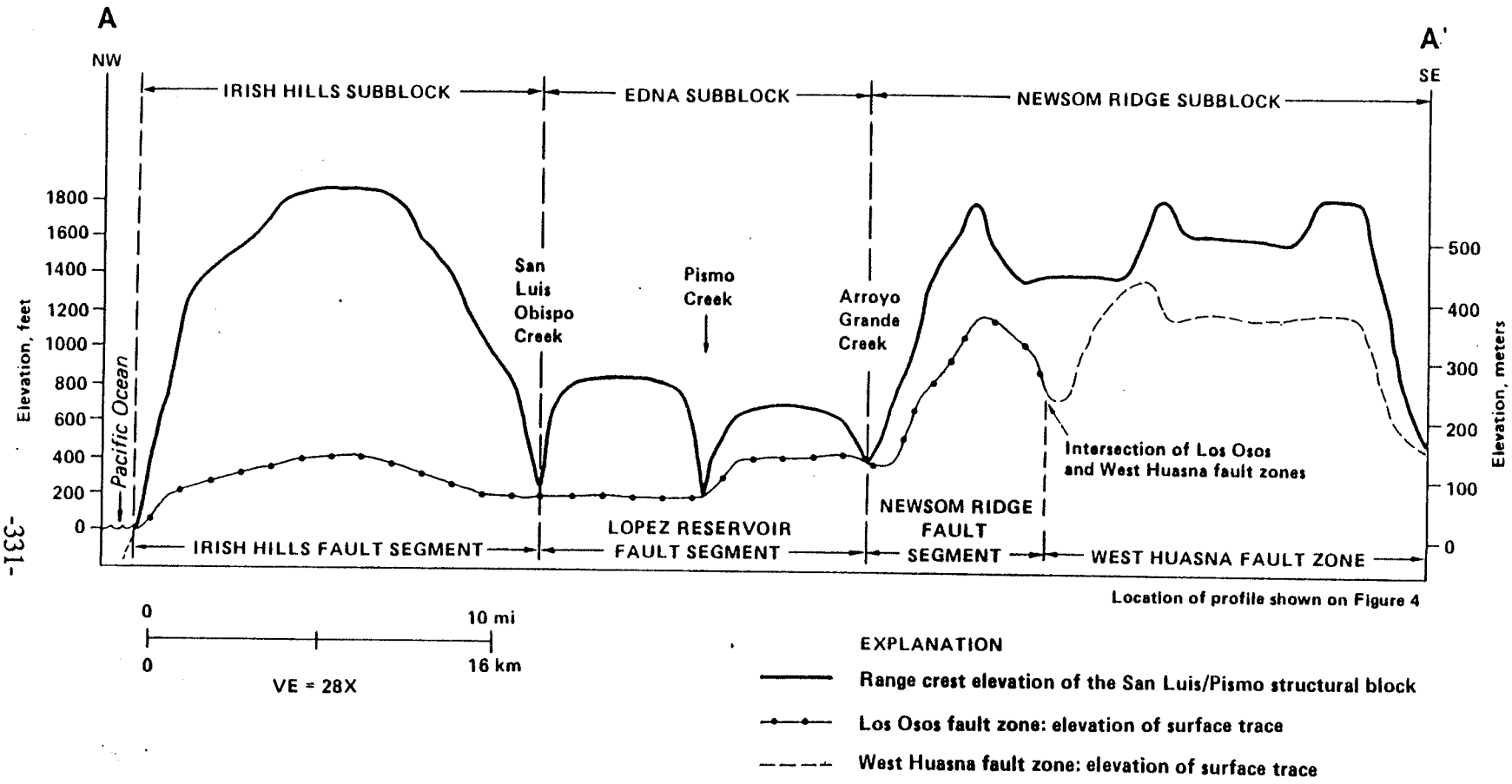

Figure 5 Topographic profiles illustrating: (1) range crest elevation and subblocks of the San Luis/Pismo structural block, and (2) surface-trace elevation and segmentation of the Los Osos fault zone.

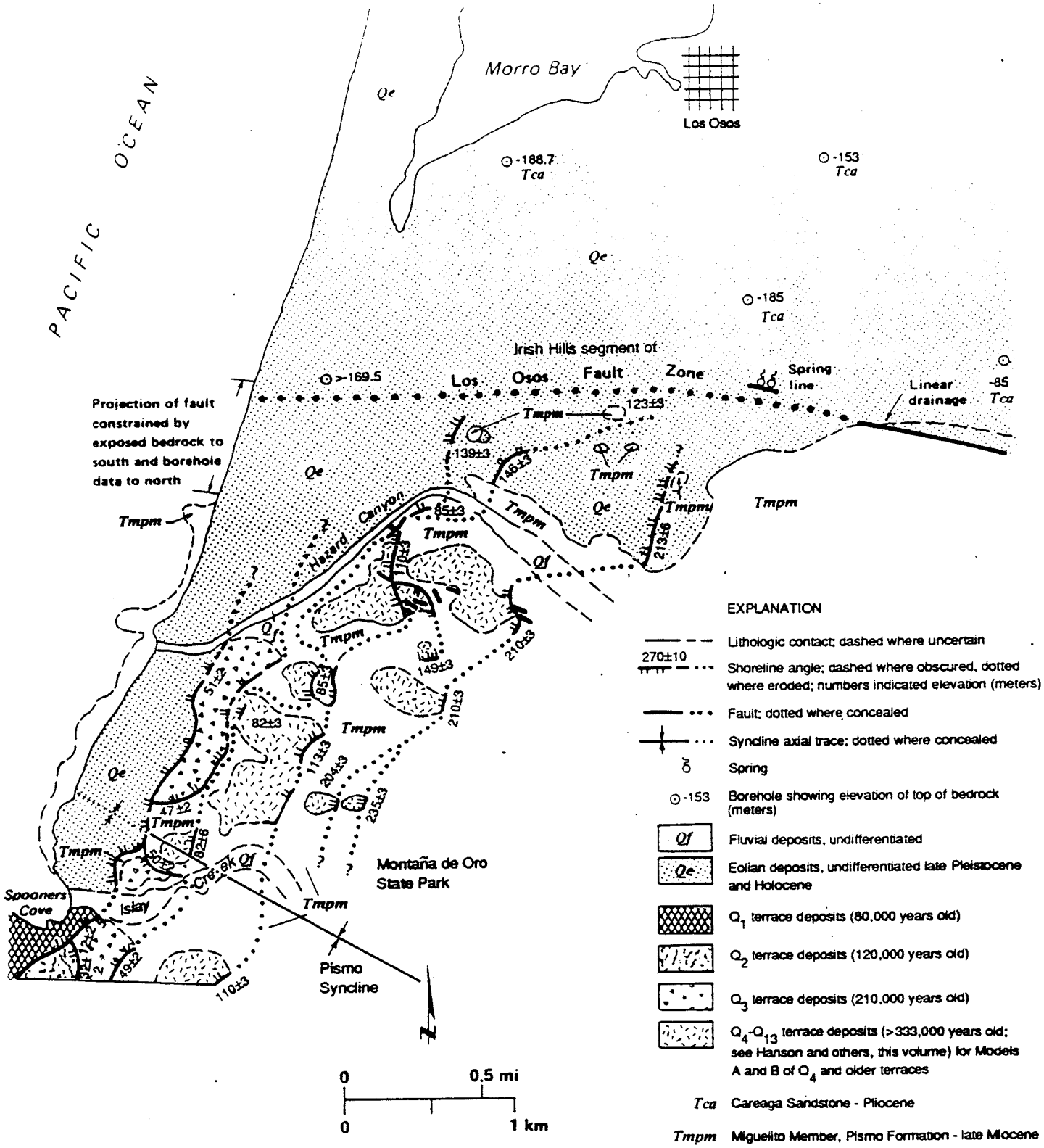

Figure 6. Generalized geologic map of Quaternary deposits in the Montaña de Oro and Morro Bay areas illustrating distribution of marine terraces and interpreted location of the Los Osos fault zone. (After Hanson and others, this volume).

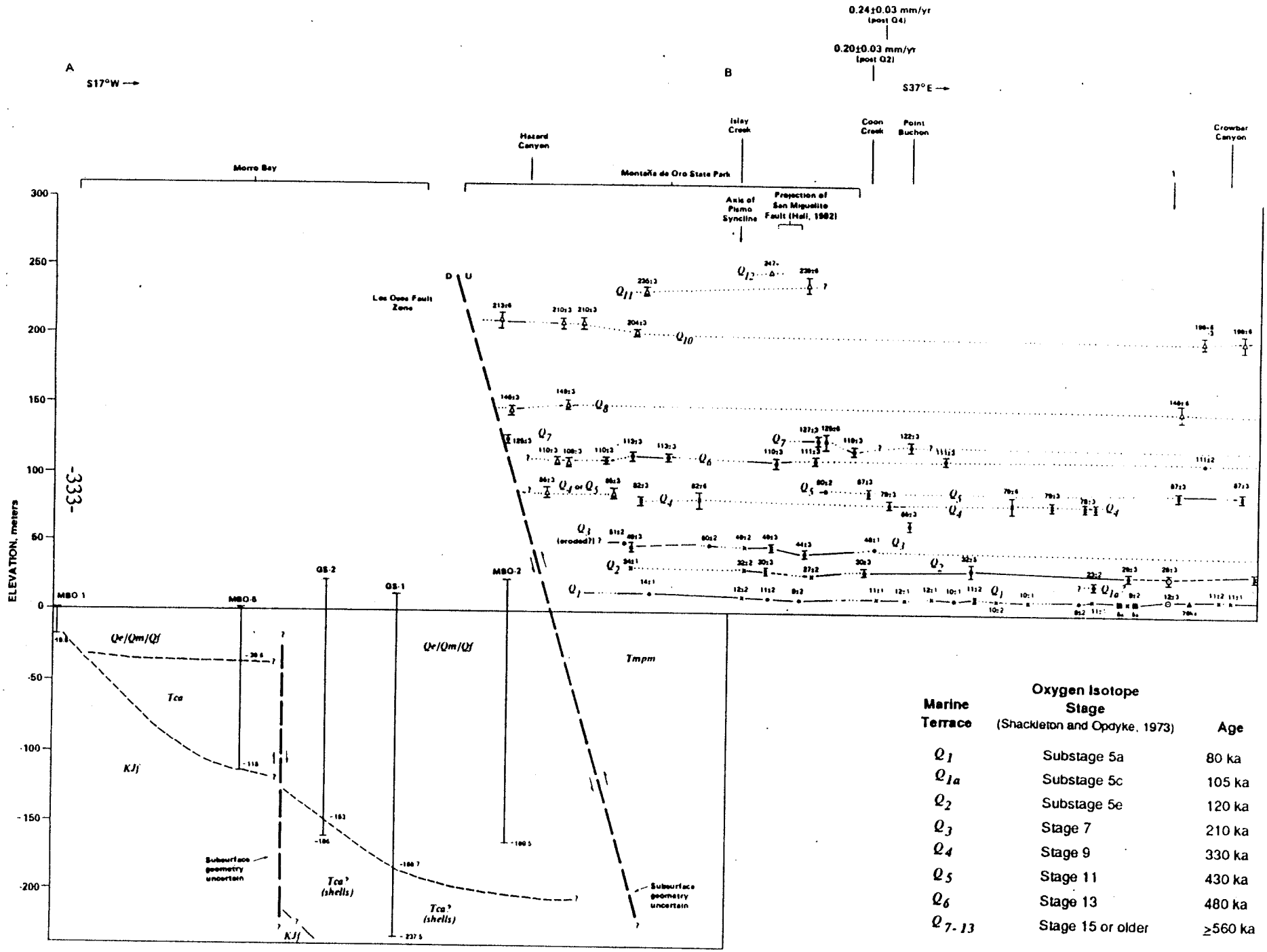

Figure 7. Longitudinal profiles of marine terraces between Morro Bay and Crowbar Canyon, across the Pismo Syncline and projection of the San Miguelit ult. No vertical exaggeration. For location of profile, see Hanson and others (this volume)

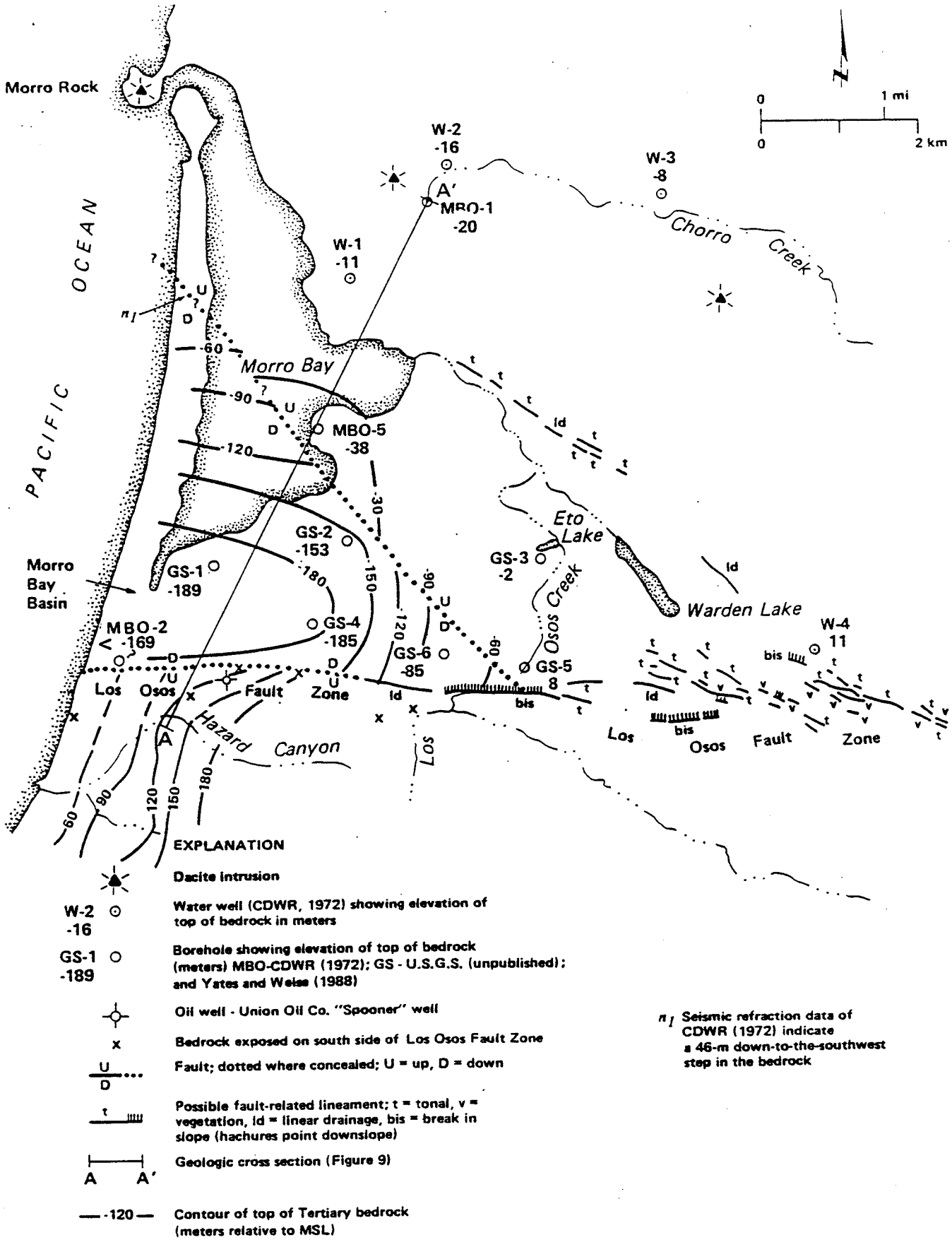

Figure 8. Map of Morro Bay showing locations of wells and interpreted location of the Los Osos fault zone and the Morro Bay basin.

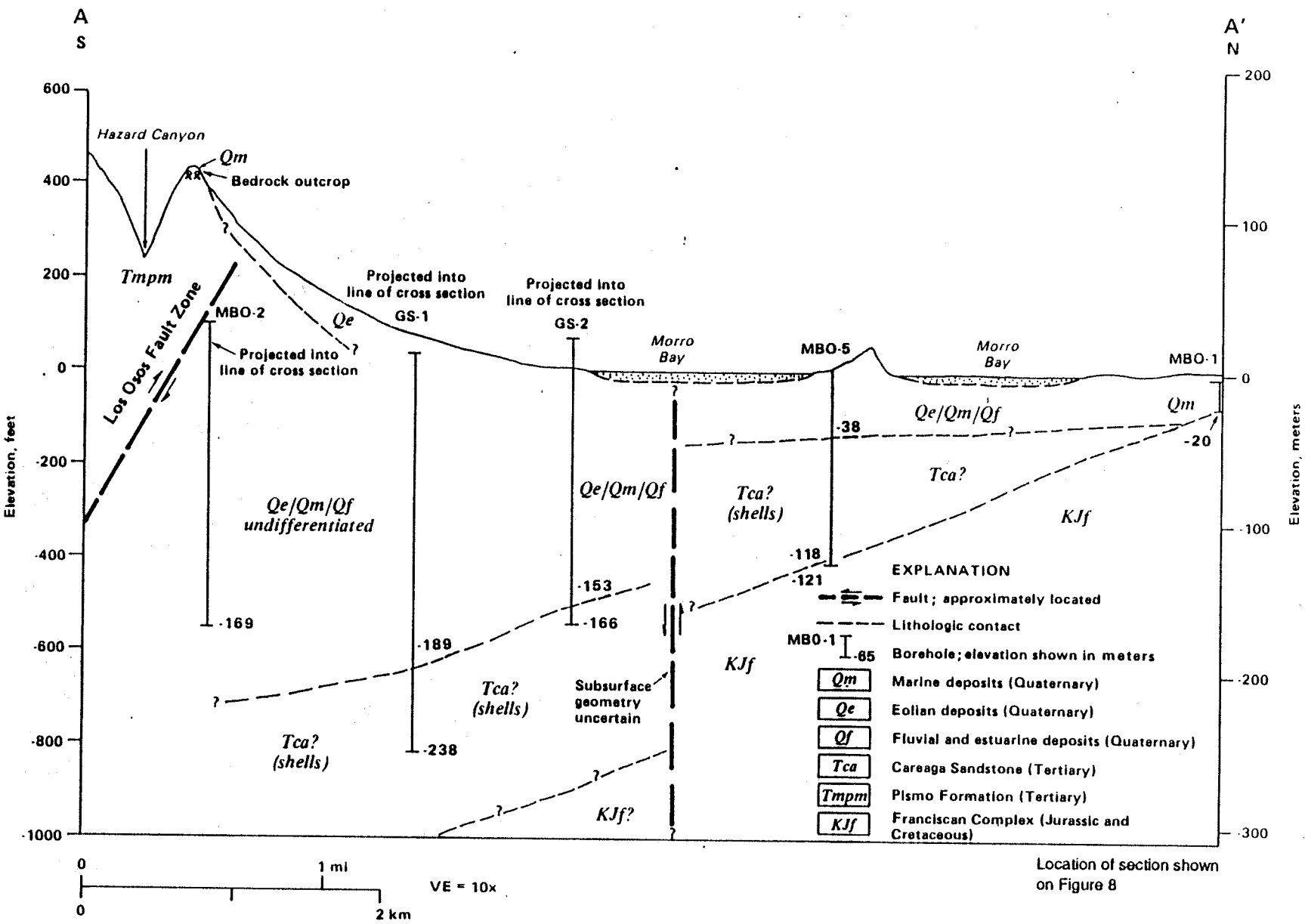

Figure 9. Geologic cross section across Morro Bay area illustrating stratigraphic and structural relationships associated with the Morro Bay basin.

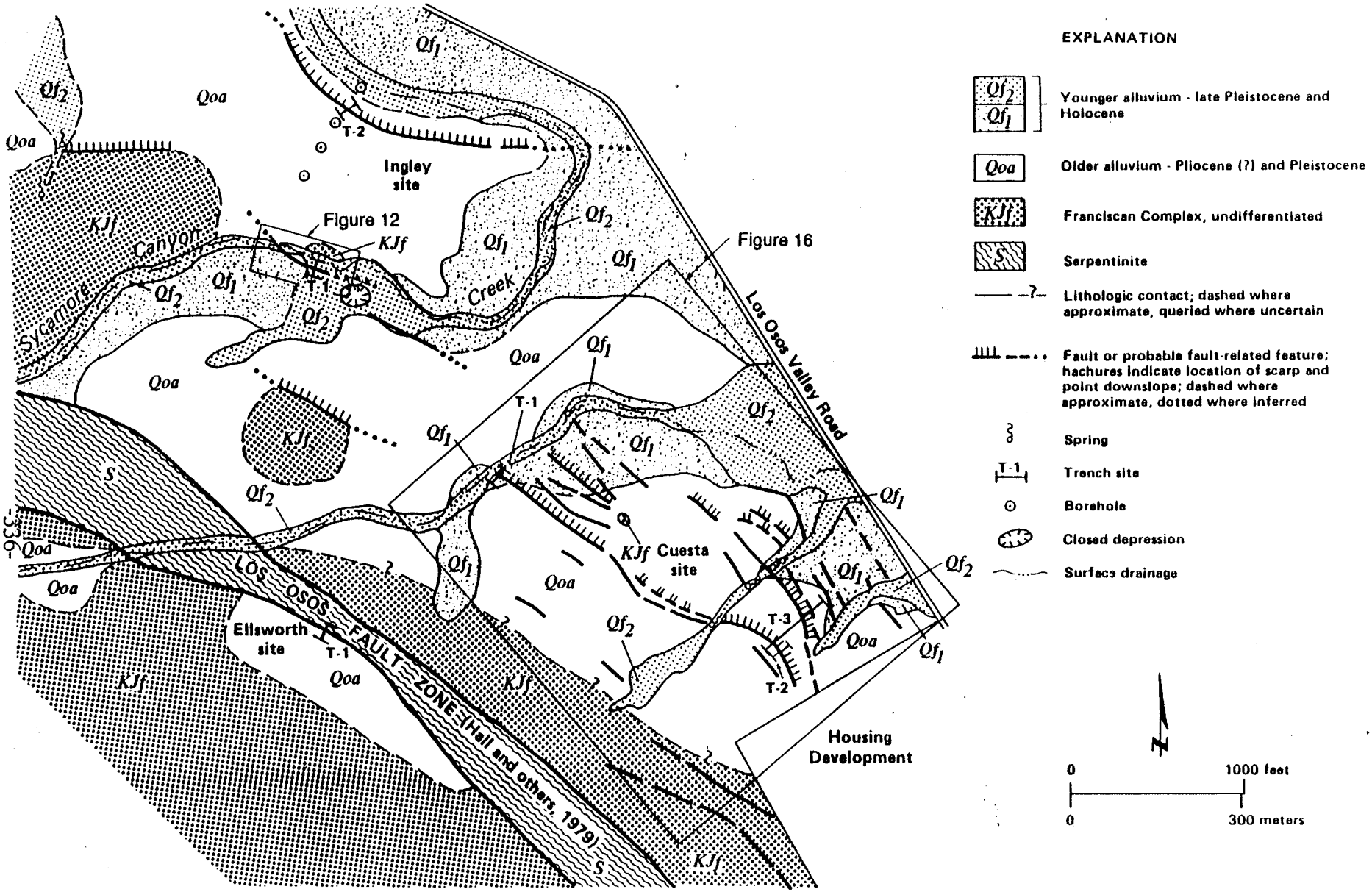

Figure 10. Geologic map of the Cuesta, Ingley, and Ellsworth sites showing location of the Los Osos fault identified by Hall and others (1979) and additional faults and fault-related features identified during this geologic investigation.

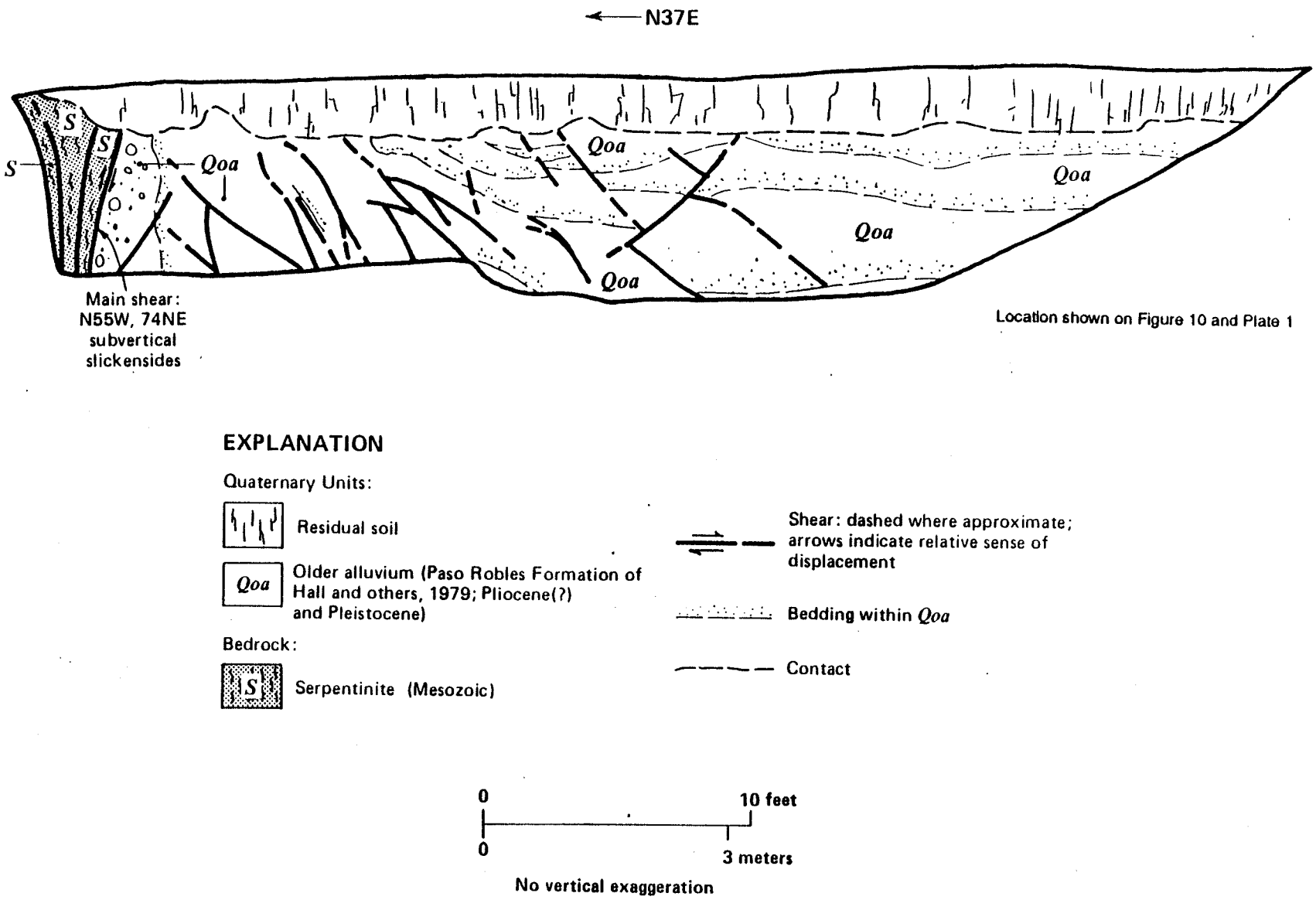

Figure 11. Diagrammatic log of Ellsworth Trench T-1 showing high-angle reverse fault within the Los Osos fault zone.

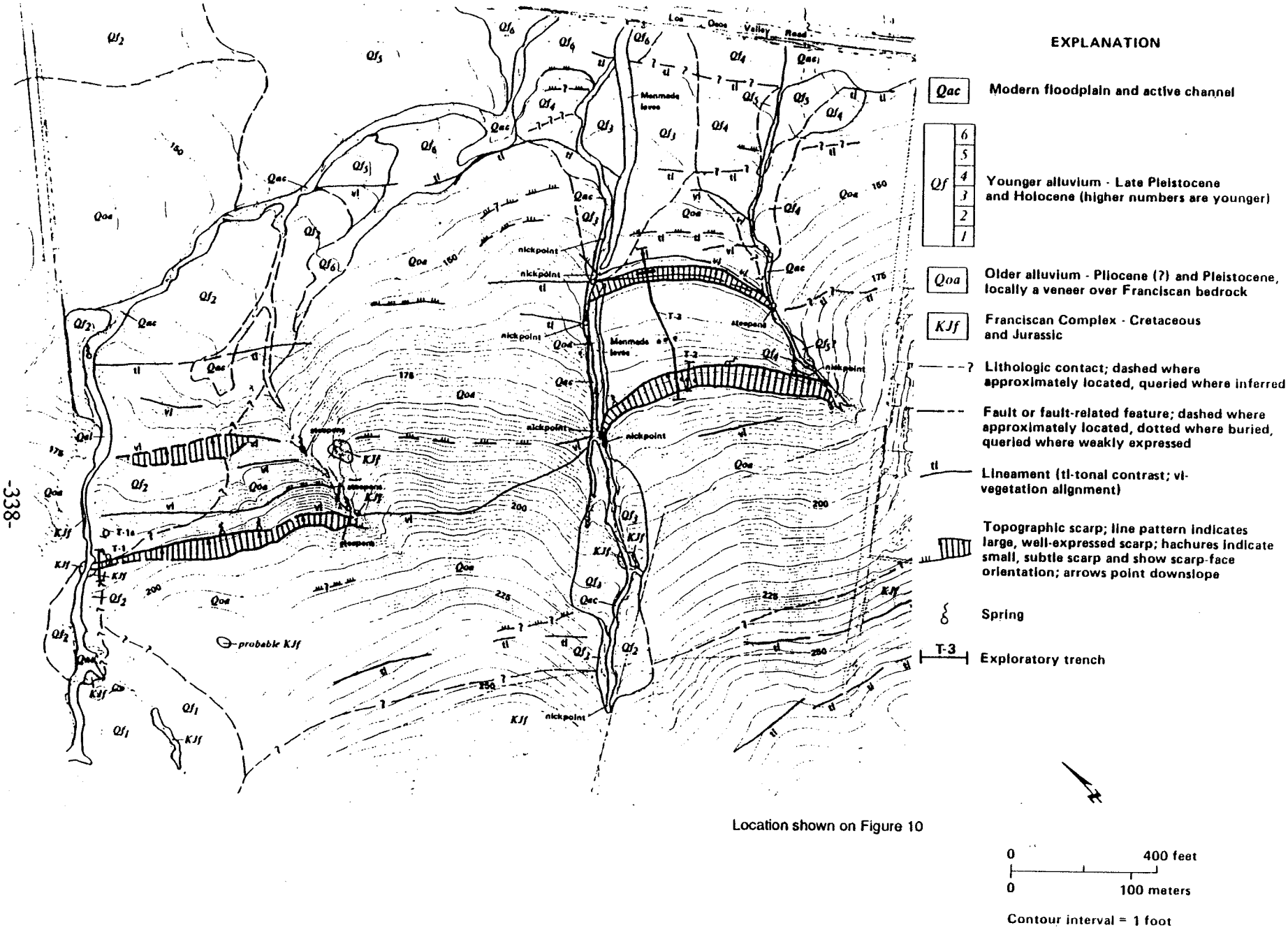

Figure 12. Detailed geologic map of the northeastern part of the Cuesta site, Los Osos fault zone.

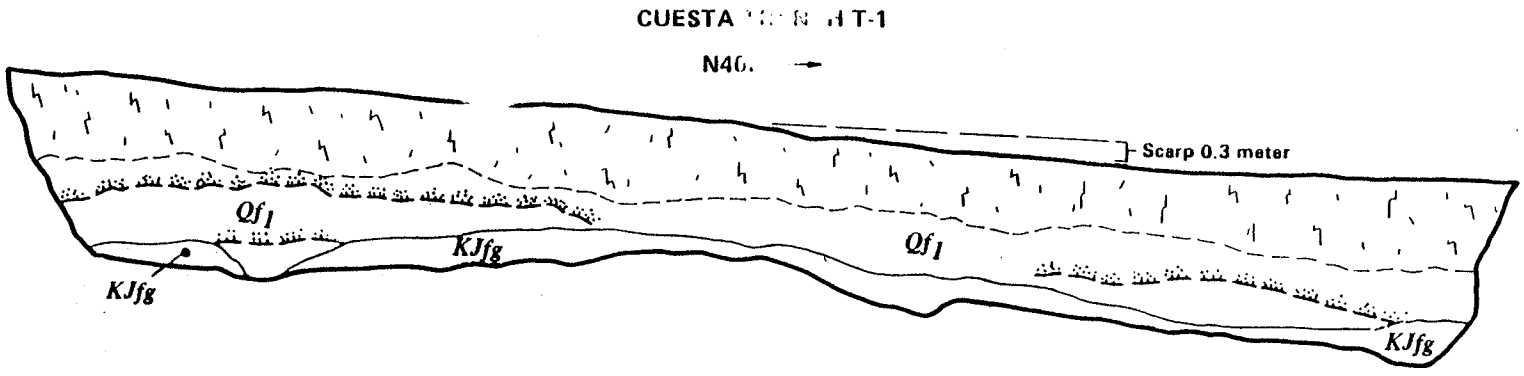

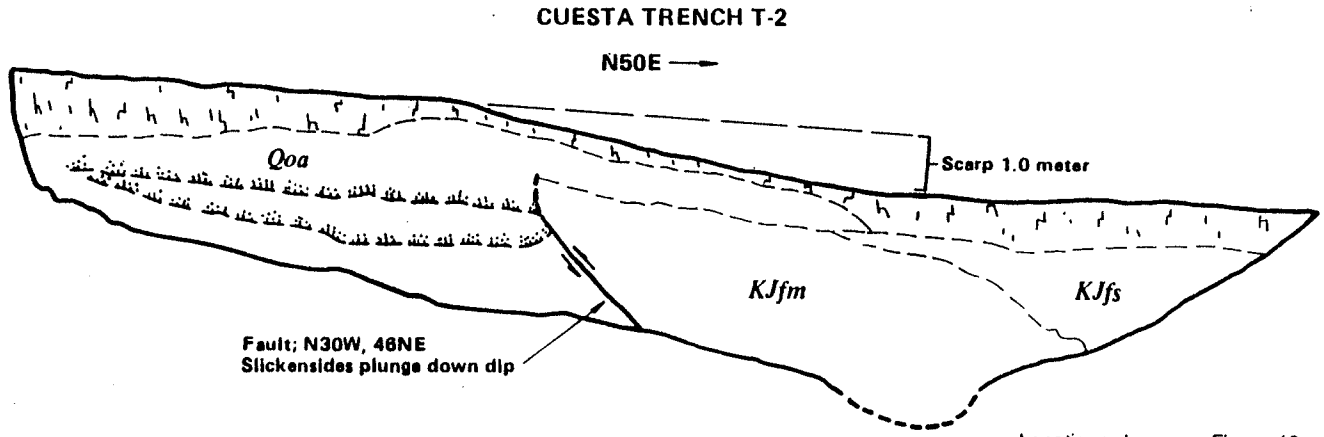

Locations shown on Figure 10 and Plate 1

EXPLANATION

Quaternary Units:

- Cumulic soil (vertisol)
- Qf_1 — Younger alluvium; late Pleistocene and Holocene
- Qoa — Older alluvium (possibly Paso Robles Formation of Hall and others, 1979; Pliocene (?) and Pleistocene)

Bedrock:

- KJf — Franciscan Complex; g = greenstone or ultramafic rock, m = melange, s = siltstone and sandstone (Mesozoic)

- Fault; dashed where approximate; arrows show inferred sense of displacement
- Contact; dashed where approximate
- Bedding

0 — 10 feet
0 — 3 meters

No vertical exaggeration

Figure 13. Diagrammatic logs of Cuesta trenches T-1 and T-2 within the Los Osos fault zone.

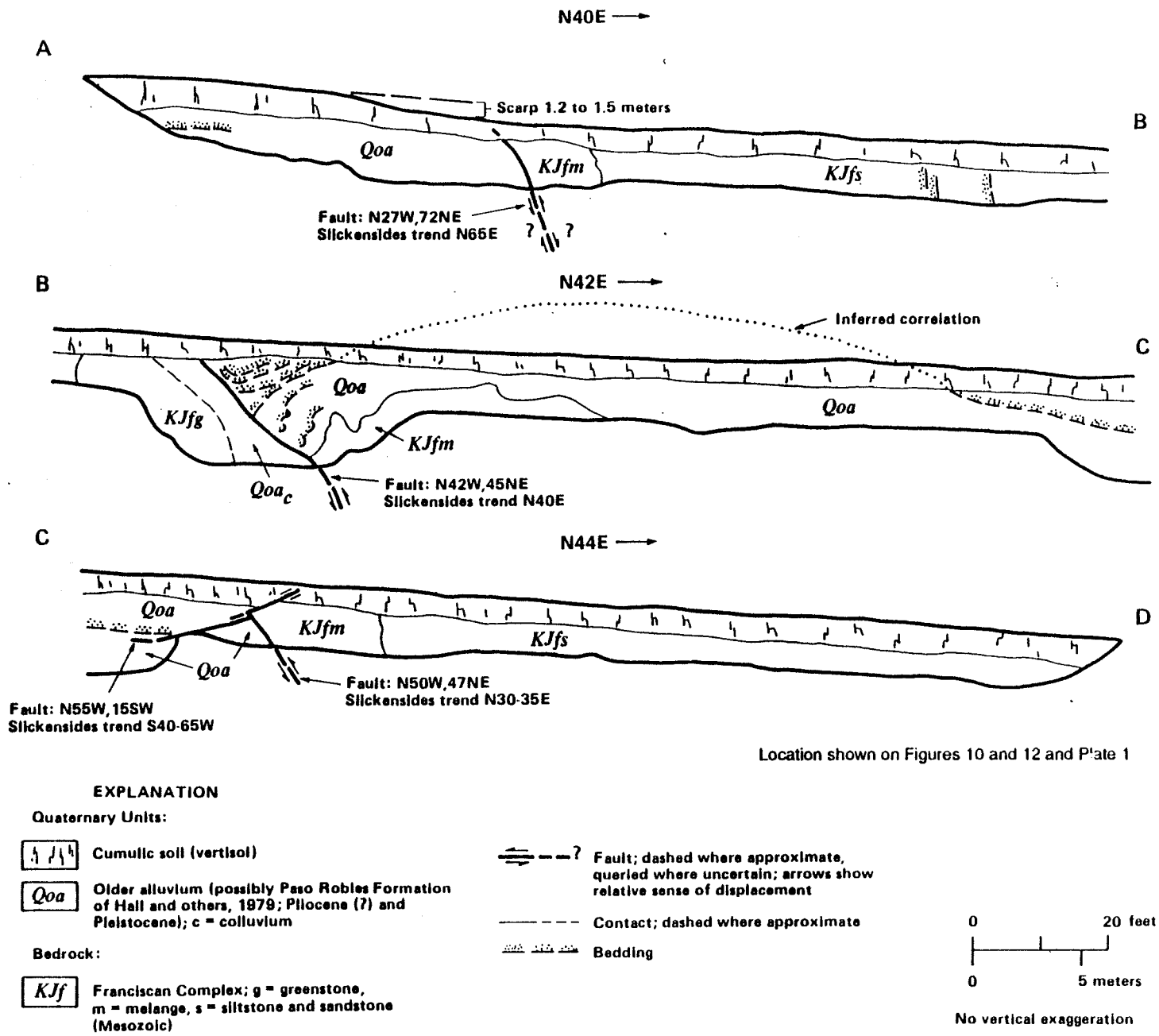

Figure 14. Diagrammatic log of Cuesta Trench T-3 showing dip-slip faults in the inferred hanging wall block of the Los Osos fault.

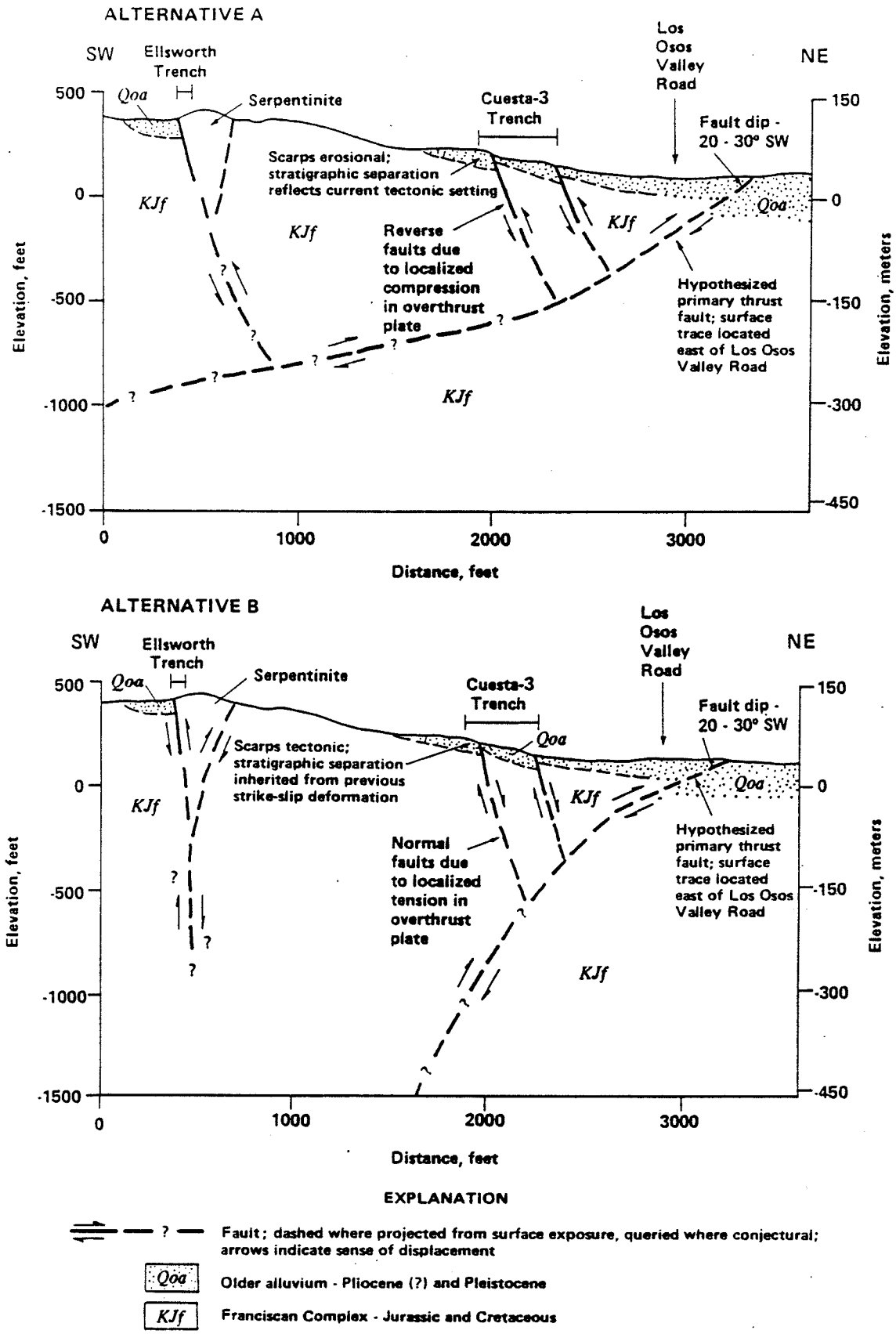

Figure 15. Schematic geologic cross sections between the Ellsworth and Cuesta properties illustrating alternative interpretations of fault geometry based on near-surface stratigraphic, geomorphic and structural relationships. A - primary fault flattens with depth; B - primary fault steepens with depth.

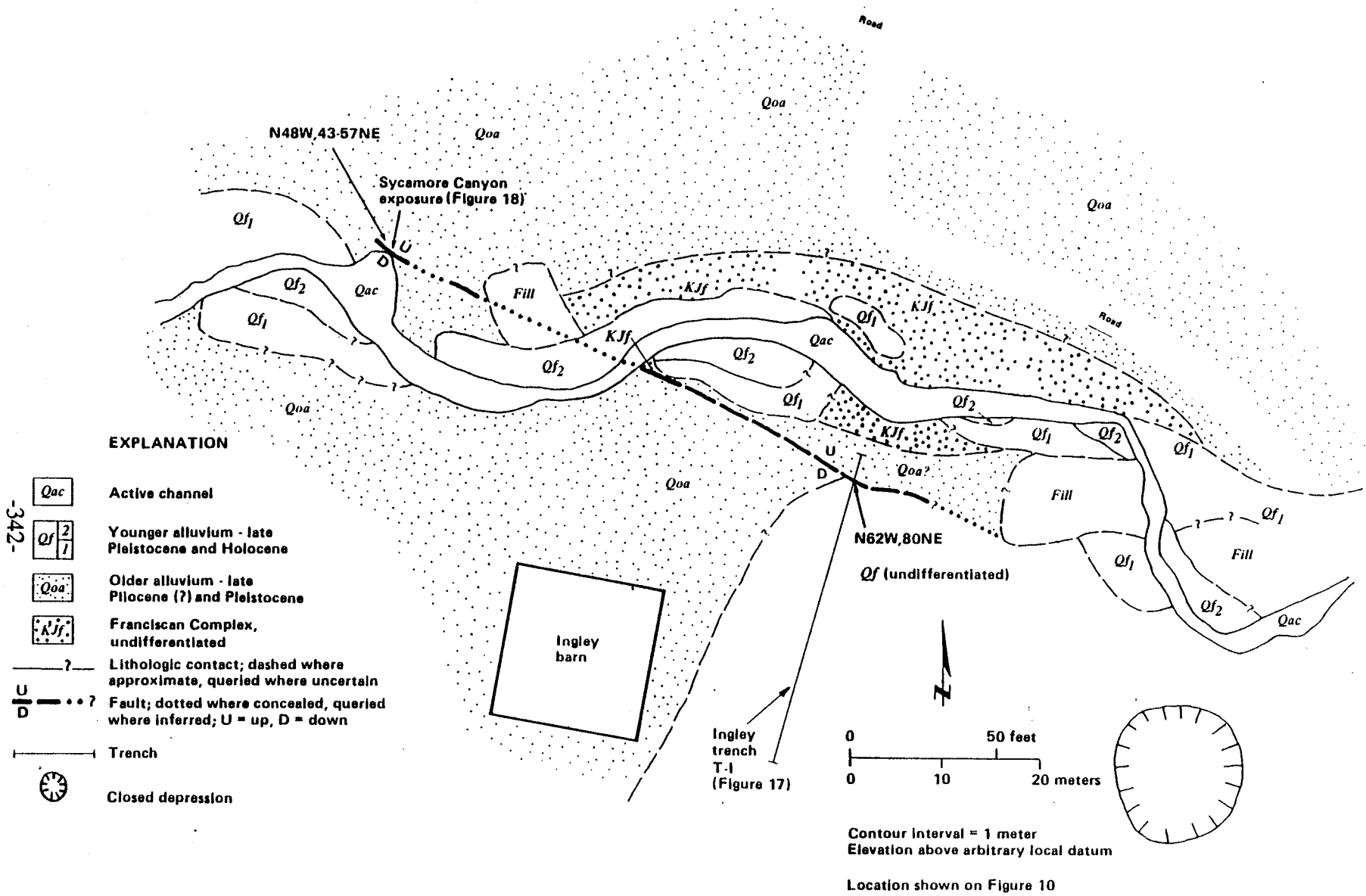

Figure 16. Detailed geologic map of Sycamore Canyon Creek showing location of Sycamore Canyon exposure and Ingley trench T-1.

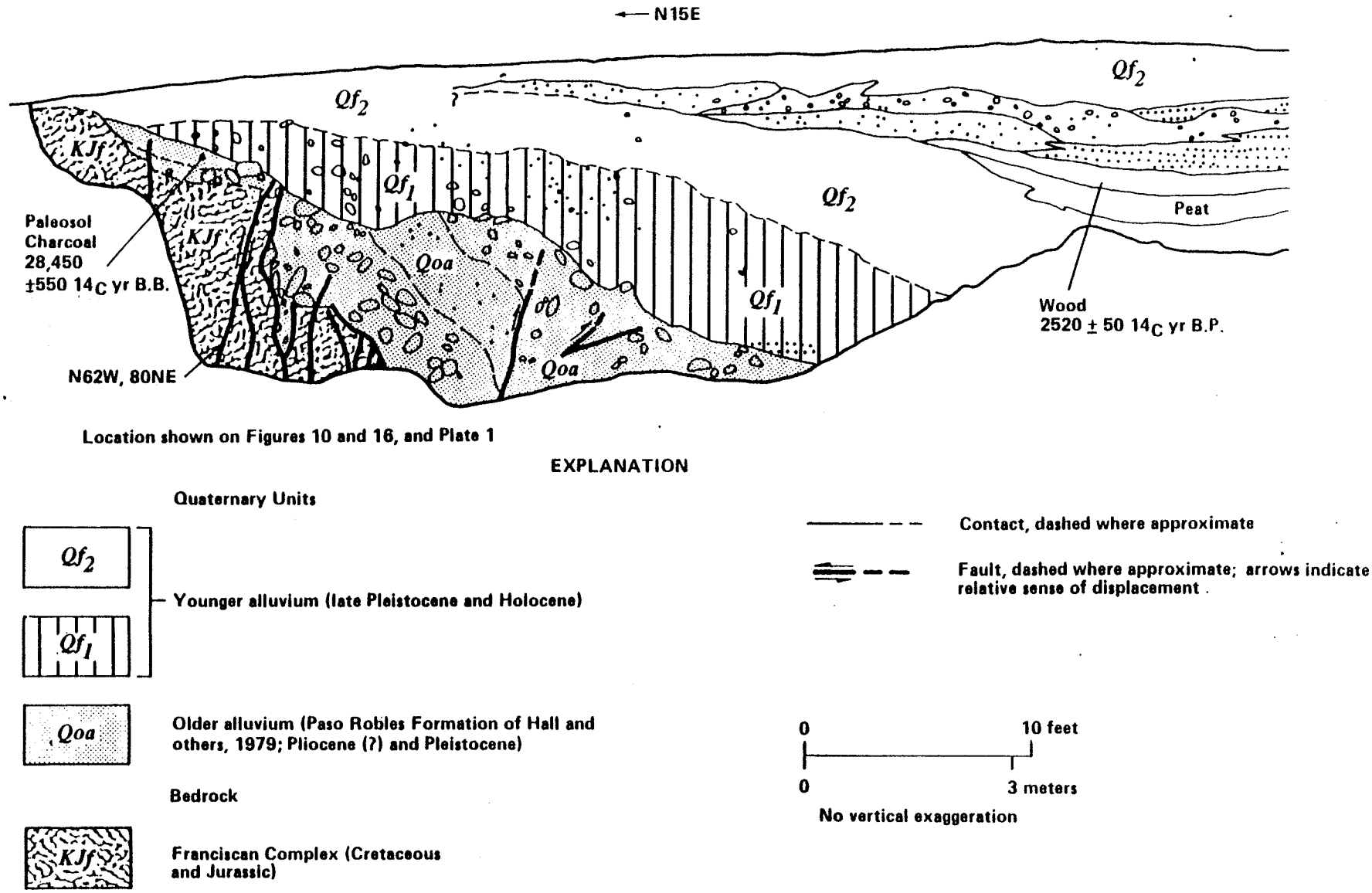

Figure 17. Diagrammatic log of northeastern part of Ingley trench T-1 showing a reverse fault within the Los Osos fault zone.

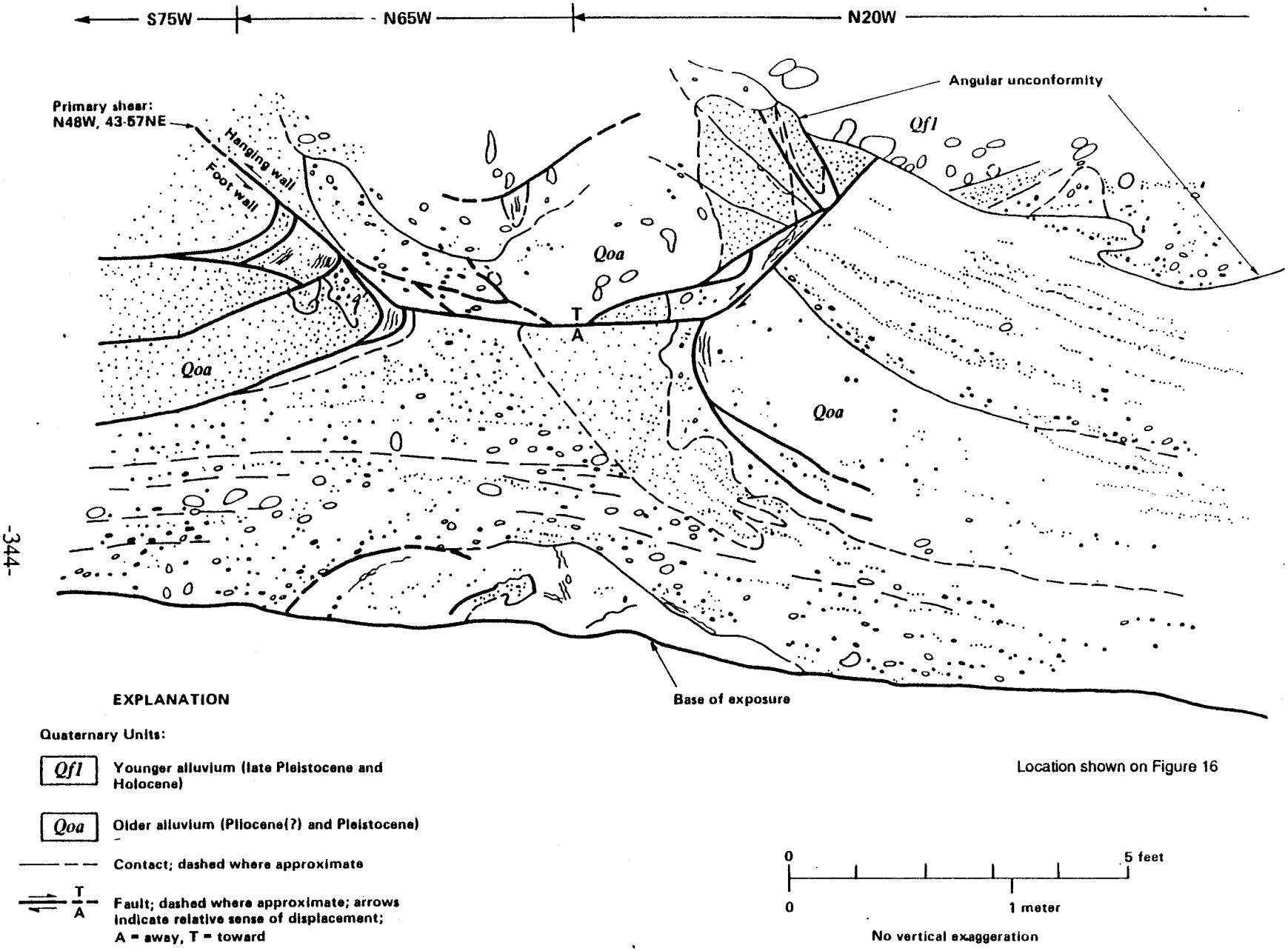

Figure 18. Geologic log of Sycamore Canyon channel wall exposure showing a reverse fault within the Los Osos fault zone.

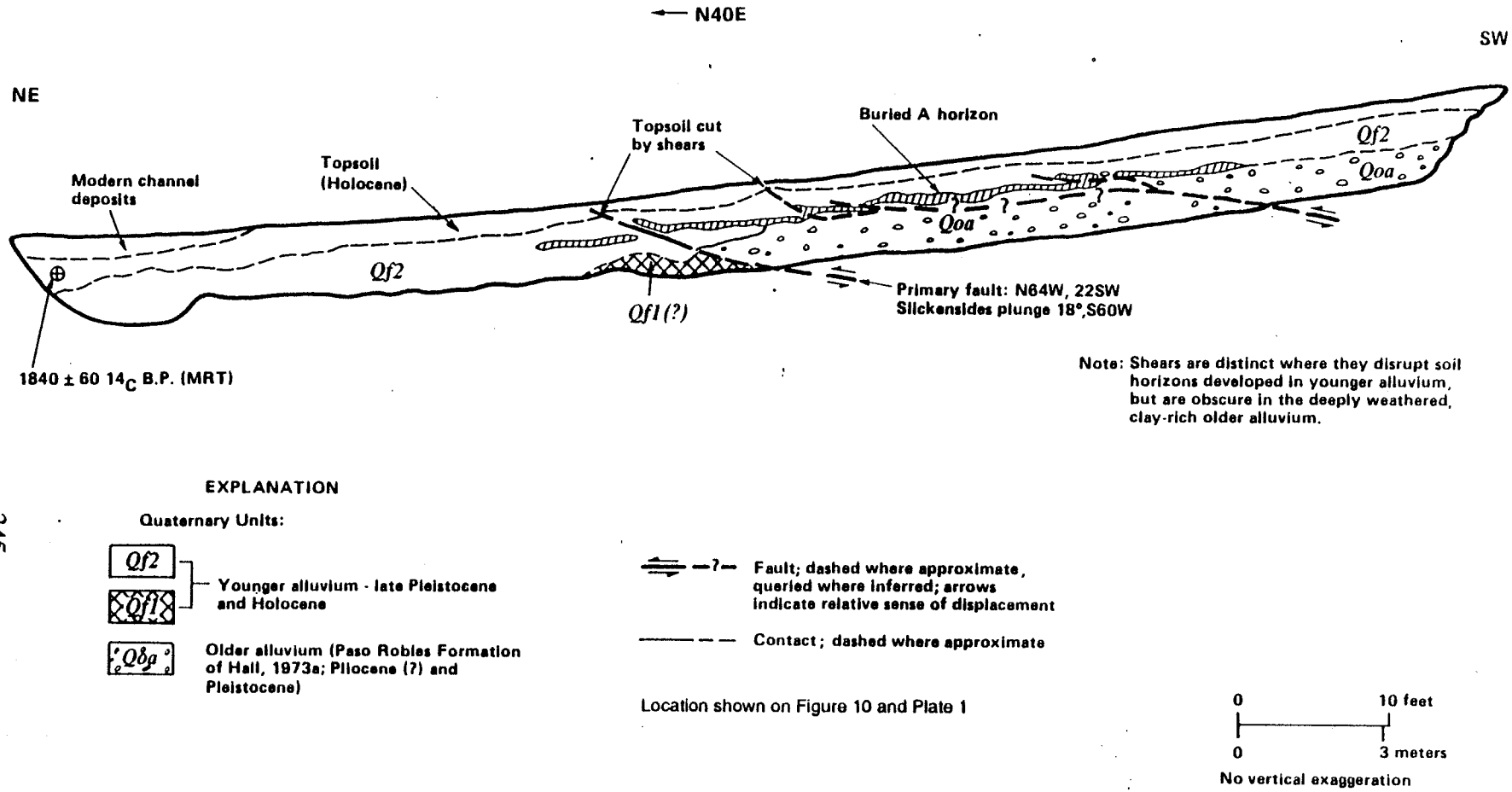

Figure 19. Diagrammatic log of Ingley trench T-2 showing primary zone of thrusting within the Los Osos fault zone.

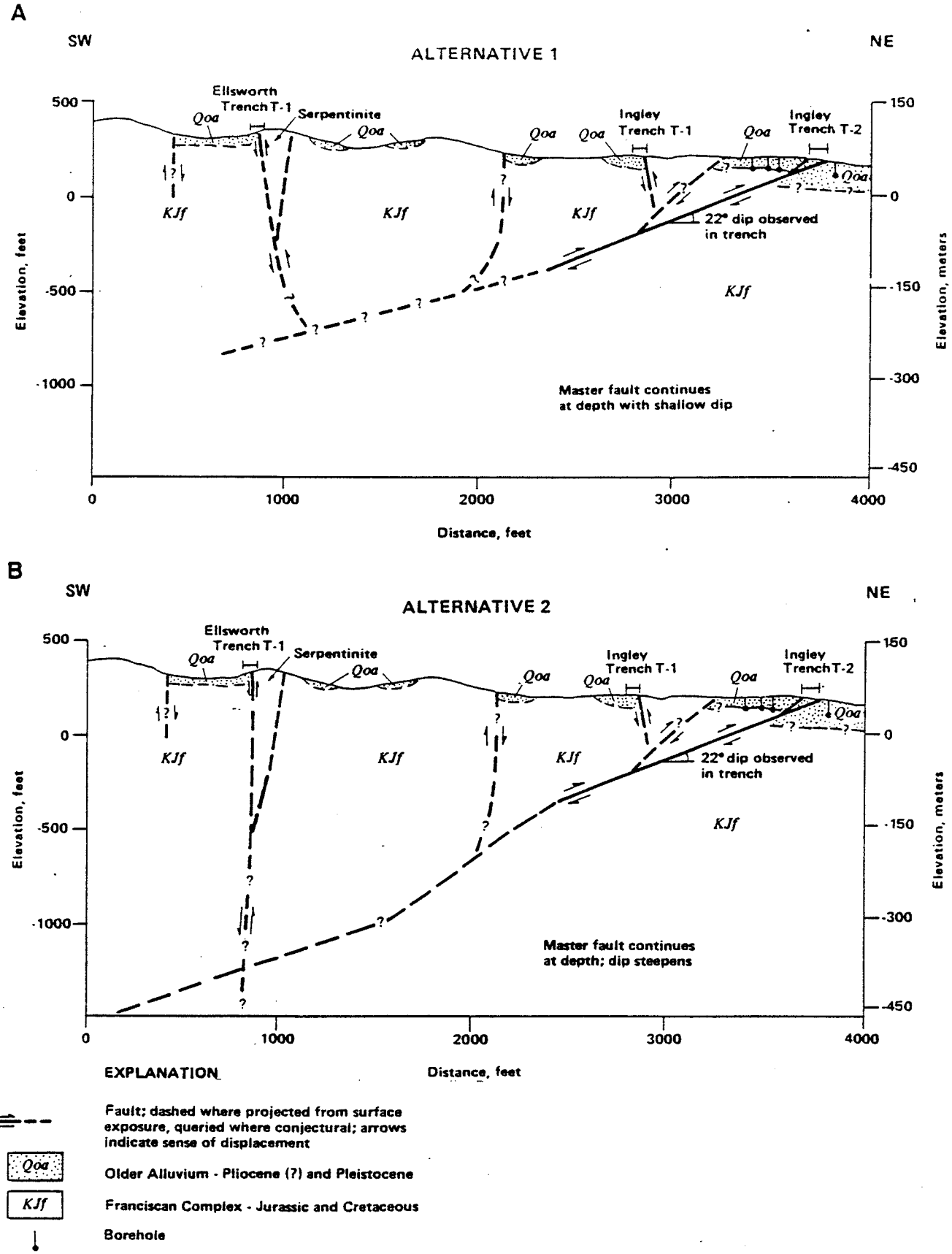

Figure 20. Diagrammatic cross sections illustrating alternative tectonic models to explain stratigraphic and structural relationships observed at the Ingley and Ellsworth sites.

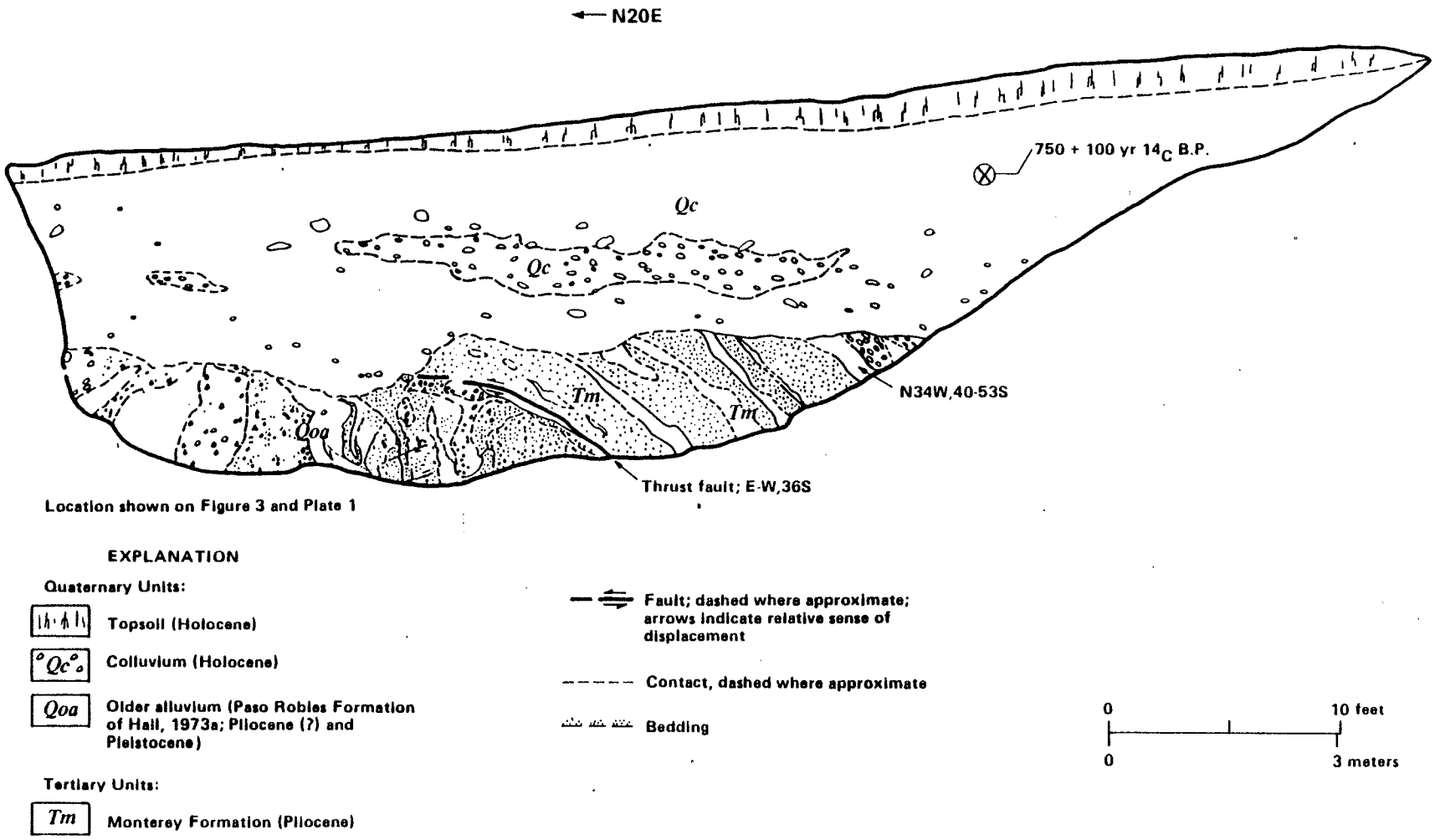

Figure 21. Diagrammatic log of Glick Trench T-1 showing thrust fault along Lopez Reservoir segment of Los Osos fault zone.

LATE QUATERNARY TECTONIC DEFORMATION IN THE CASMALIA RANGE, COASTAL SOUTH-CENTRAL CALIFORNIA

Douglas G. Clark

Center for Neotectonic Studies, University of Nevada, Reno, NV 89557

ABSTRACT

The Casmalia Range is a fault-bounded anticlinal range in the Santa Maria basin geological province. A suite of Quaternary stratigraphic units and geomorphic surfaces on the margins of the range allow assessments of the style and rate of range uplift, the presence or absence of active folding, and the style and recency of activity on the bordering Orcutt Frontal and Lions Head faults. Shoreline angle elevations of dated marine terraces between Point Sal and the Lions Head fault indicate uniform late Quaternary range uplift at a rate of 0.14-0.17 mm/yr, with no significant internal faulting, tilting, or folding. The Orcutt Frontal blind thrust fault uplifts and deforms marine and fluvial terraces and has an estimated late Quaternary dip-slip rate of 0.16 to 0.34 mm/yr. The Lions Head high-angle reverse fault displaces middle and late Quaternary marine terraces at a rate of 0.012-0.018 mm/yr. Surface tectonic deformation in the Casmalia Range can be modeled in various ways, but is most consistent with an interpretation of ongoing fault-propagation-style folding.

INTRODUCTION

The Casmalia Range is a west-northwest-trending coastal mountain range in northern Santa Barbara County, California (Fig. 1). It is one of several fault-bounded fold trends in the Santa Maria basin geological province (Figs. 1 and 2), a late Tertiary sedimentary basin currently undergoing north-northeast-directed crustal shortening (Vittori, 1987; Pacific Gas & Electric, 1988; Feigl and others, 1990). The Casmalia Range is structurally bounded by the Orcutt Frontal fault (or Casmalia fault) on the northeast and the Lions Head fault on the southwest--active, west-northwest-striking thrust or reverse faults (Fig. 2)--and underlain by a series of en-echelon anticlines that continue to the southeast beneath the Solomon Hills and comprise the Casmalia-Orcutt anticlinal trend (Woodring and Bramlette, 1950; Namson and Davis, 1990). The Hosgri fault forms an offshore, western structural boundary.

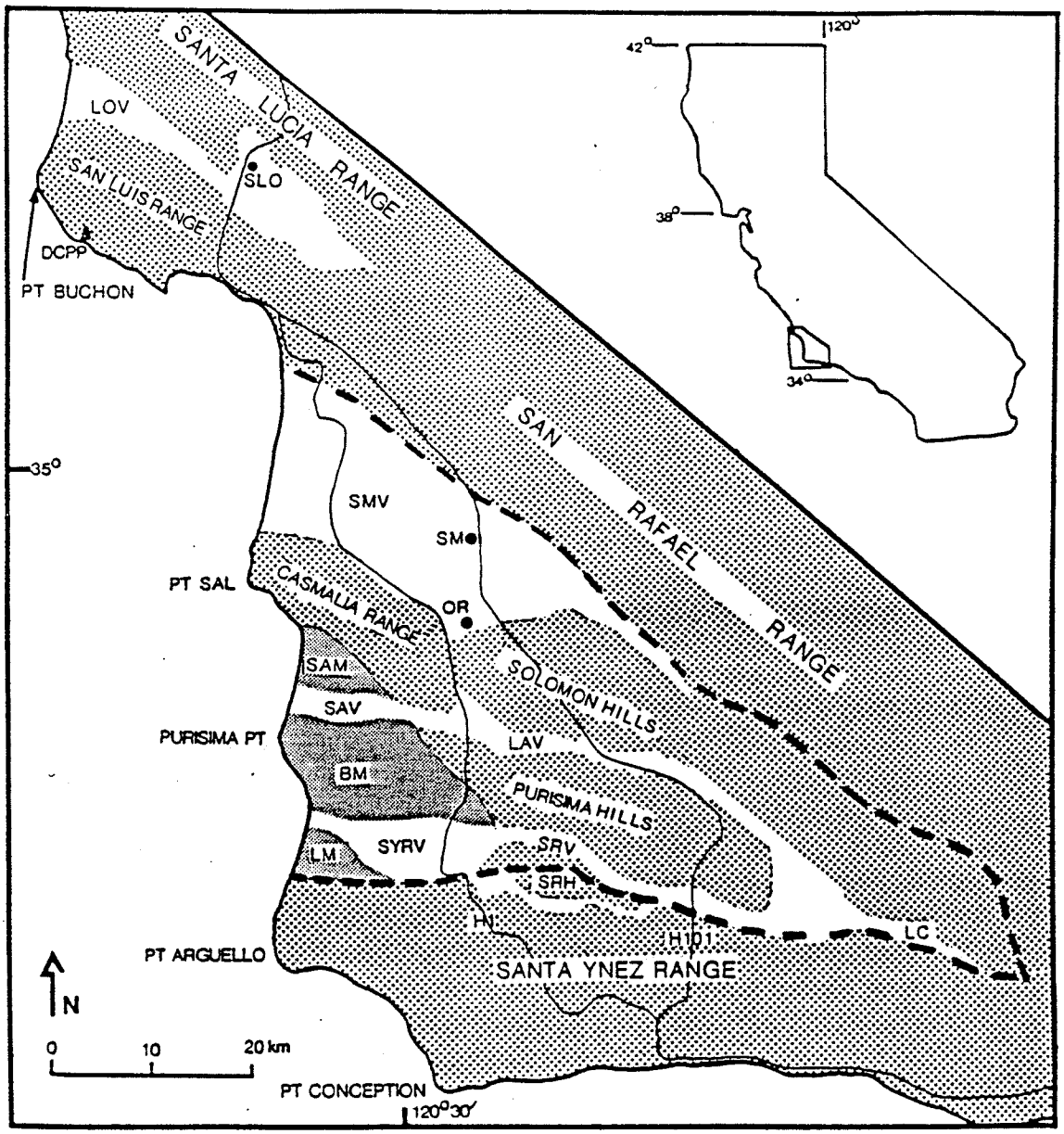

Figure 1--Physiographic map of coastal south-central California. The onshore Santa Maria basin is outlined with a dashed line. Ranges shown with stippled pattern. The San Antonio-Burton-Lompoc Mesa marine terrace complex is shown with fine stippled pattern. BM = Burton Mesa, DCPP = Diablo Canyon nuclear power plant, H1 and H101 = Highways 1 and 101; LAV = Los Alamos Valley, LC = Lake Cachuma, LM = Lompoc Mesa, LOV = Los Osos Valley, OR = Orcutt, SAM = San Antonio Mesa, SAV = San Antonio Valley, SLO = San Luis Obispo, SM = Santa Maria, SMV = Santa Maria Valley, SRH = Santa Rita Hills, SRV = Santa Rita Valley, SYRV = Santa Ynez River Valley.

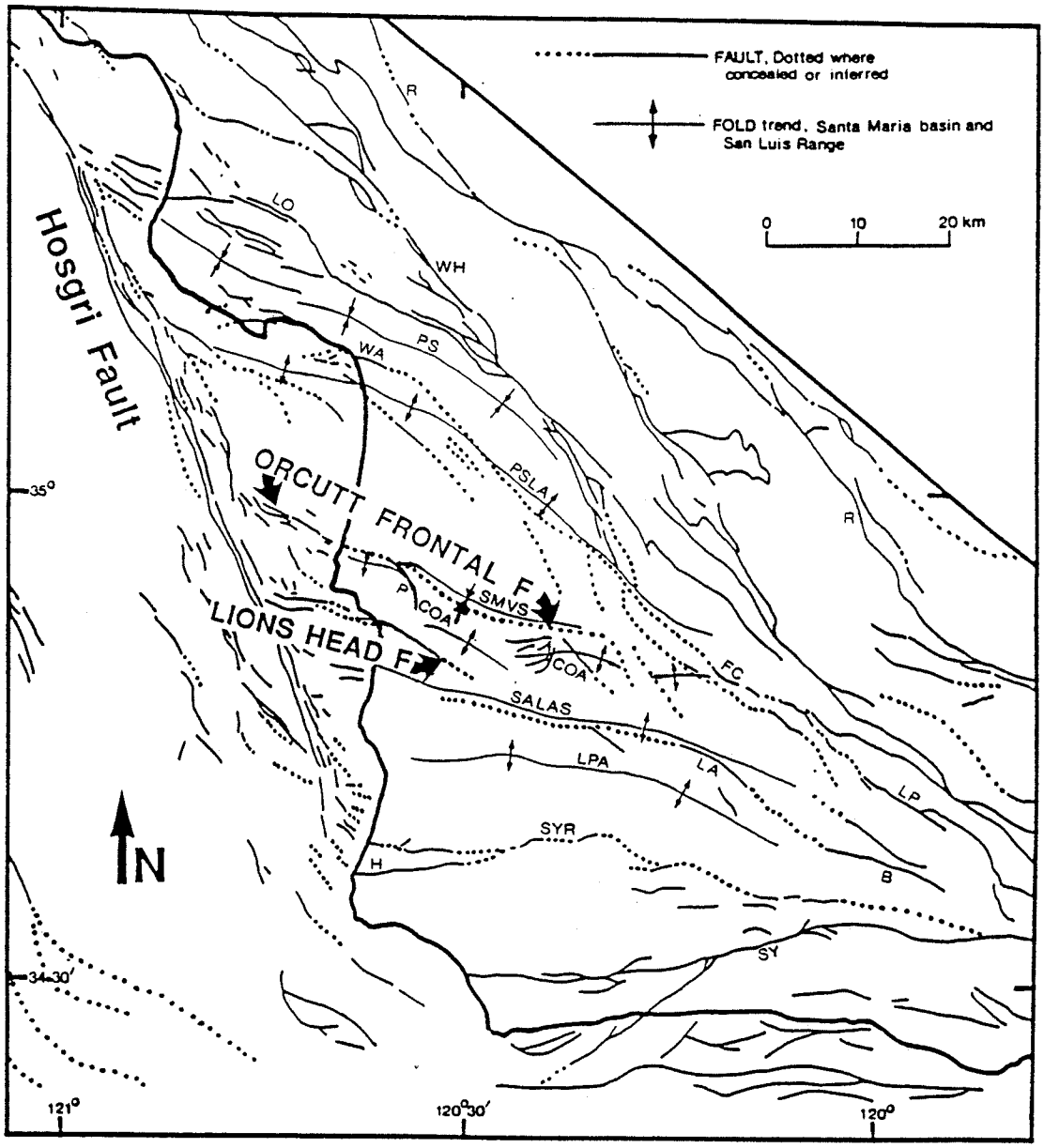

Figure 2--Structural trend map, coastal south-central California. Structural trends in the Santa Maria basin and San Luis Range fan out between the northwest trend of the southern Coast Ranges and the west trend of the western Transverse Ranges, and are abruptly truncated in the offshore by Hosgri fault. Active faulting styles show a progressive change in this region, from reverse and right-lateral reverse-oblique movements in the southern Coast Ranges, to reverse and left-lateral reverse-oblique faulting in the Santa Maria basin and western Transverse Ranges (Eaton, 1984, 1985; Clark and others, 1990). Faults and folds in the offshore Santa Maria basin are oriented subparallel to the Hosgri fault. Faults: B= Baseline, FC= Foxen Canyon, H= Honda, LA= Los Alamos, LO= Los Osos, LP= Little Pine, P= Pezzoni, R=Rinconada, SY= Santa Ynez, SYR= Santa Ynez River, WA= Wilmar Avenue, WH= West Huasna. Fold trends: COA = Casmalia-Orcutt anticlinal trend, LPA = Lompoc-Purisima anticline, PS = Pismo syncline, PSLA = Point San Luis anticline, SALAS = San Antonio-Los Alamos syncline, SMVS = Santa Maria Valley syncline. Modified from Jennings (1975, 1977), Buchanan-Banks and others (1978), PG&E (1988), and Namson and Davis (1990).

A variety of tectonic models have been proposed to explain the recent development of the Santa Maria basin (Sylvester and Darrow, 1979; Luyendyk and others, 1980; Crouch and others, 1984; Hornafius, 1985; Weldon and Humphreys, 1986; Nitchman, 1988; PG&E, 1988; Namson and Davis, 1990). However, testing of tectonic models is handicapped by the lack of detailed documentation of active faulting and folding in this region. The presence of a suite of Quaternary stratigraphic units and geomorphic surfaces within and on the margins of the Casmalia Range, including datable marine terraces, make this an ideal site for quantifying recent tectonic deformation in a portion of the Santa Maria basin. Quaternary deposits and surfaces are used in this study to assess the rate and style of Quaternary range uplift, the presence or absence of active folding, and the style and recency of activity on the bordering Orcutt Frontal and Lions Head faults.

STRATIGRAPHY

The Casmalia Range is part of the Santa Maria sedimentary basin, described by Woodring and Bramlette (1950), Dibblee (1950, 1966), Hall (1978, 1981), and Blake and others (1978). Figure 3 shows the distribution of stratigraphic units in the Casmalia Range and western Solomon Hills.

MESOZOIC AND TERTIARY STRATA

The Casmalia Range is the only locality in the Santa Maria basin where Mesozoic basement rocks are exposed at the surface. Rocks mapped as the Franciscan Complex (Point Sal ophiolite) and Knoxville Formation are exposed in the western part of the range (Fig. 3). Following Upper Jurassic deposition of the Knoxville Formation, a major gap in the geologic record of the Santa Maria basin exists up through late Oligocene time. Tertiary rocks range in age from late Oligocene or early Miocene to Pliocene and consist of a thick sequence of nonmarine, marginal marine, and shallow to moderately deep marine sedimentary rocks (Woodring and Bramlette, 1950). These deposits record a major marine transgression and regression associated with two temporally distinct tectonic regimes. Miocene to early Pliocene rocks were deposited in progressively deepening marine environments during a period of regional transtensional faulting related to the development of the San Andreas fault system (Blake and others, 1978; McCulloch, 1989). Lower Pliocene through Pleistocene rocks record the shallowing and late Pliocene to early Pleistocene emergence of the Santa Maria basin resulting from a change from regional transtension to transpression or compression (Blake and others, 1978; Page and Engebretsen, 1984; Nitchman, 1988; Namson and Davis, 1990).

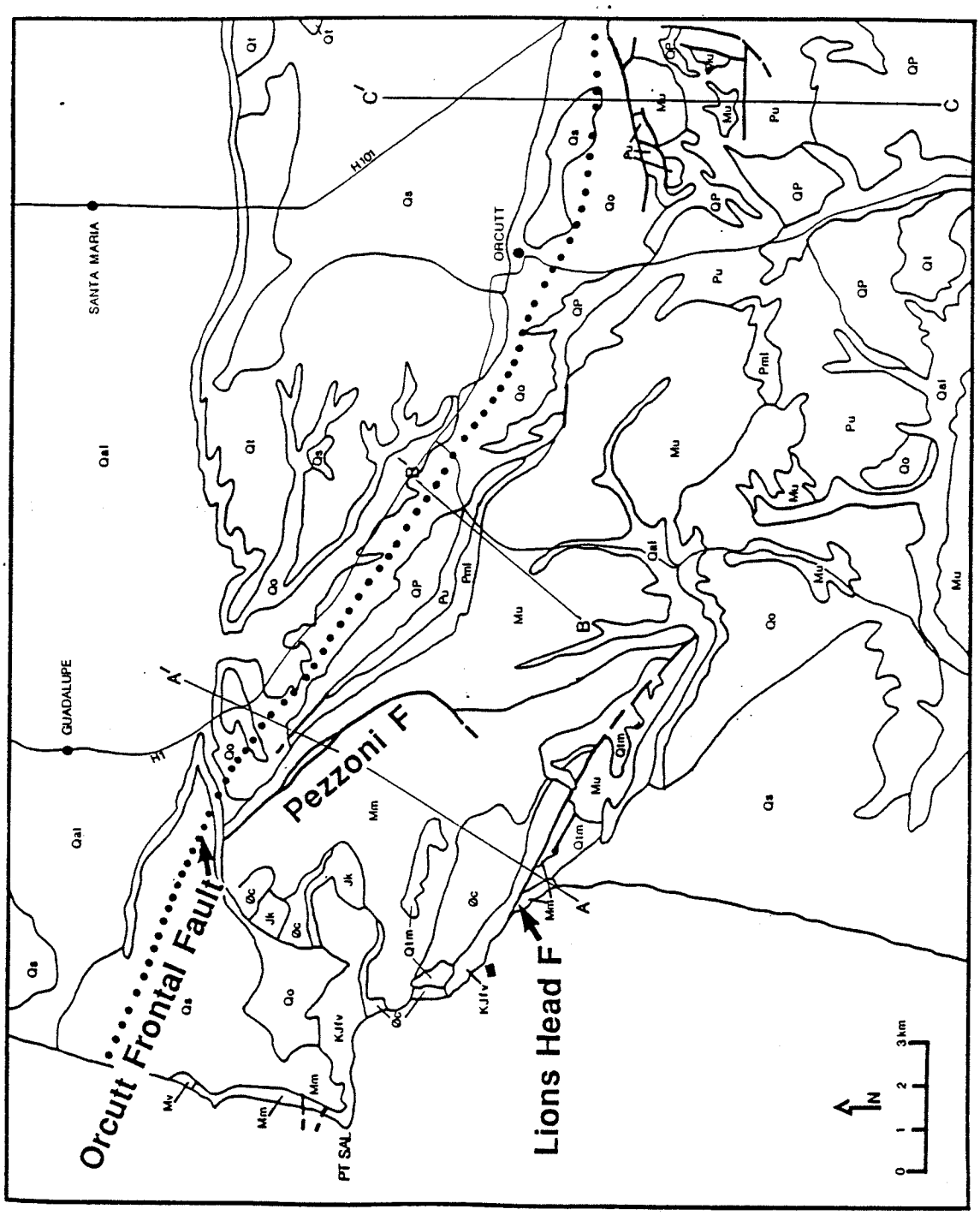

Figure 3--Geologic map of the Casmalia Range and western Solomon Hills. Qal = alluvium, Qs = dune sand, Qt = Quaternary nonmarine terrace deposits, Qtm = Pleistocene marine terrace deposits, Qo = Orcutt sand, QP = Paso Robles Formation, Pu = Careaga Formation, Pml = Foxen Formation, Mu = Sisquoc Formation, Mm = Monterey and Point Sal Formations, Oc = Lospe Formation, Jk = Knoxville Formation, KJfu = Point Sal ophiolite. Cross-section lines: A-A' = Figure 5, B-B' = Figure 16, C-C' = Figure 4. Modified from Jennings, 1959.

QUATERNARY STRATA

Paso Robles Formation

The Paso Robles Formation is a coarse, nonmarine deposit derived from sources in the adjacent San Rafael and Santa Ynez Mountains (Dibblee, 1950). Its age is not well constrained as it rarely contains fossils. It is assigned a late Pliocene to early Pleistocene age based on its position conformably above the Careaga Sand, which contains late Pliocene marine fossils (Woodring and Bramlette, 1950). The Paso Robles Formation consists of moderately to poorly consolidated conglomerate, sandstone, and minor lacustrine limestone. Conglomerate and sandstone units are moderately to poorly sorted, typically with trough cross stratification, pebble imbrication, and scoured channel structures indicating a fluvial floodplain environment. The Paso Robles Formation is at least 500 m thick on the northeast flank of the Casmalia range, where it has been uplifted and folded to a moderately to steeply northeast-dipping orientation and is locally overturned.

Orcutt Sand

The Orcutt sand is described by Woodring and Bramlette (1950) as "sand and gravel unconformably on the Paso Robles and older formations". As implied by this description, the Orcutt sand is a heterogeneous unit consisting of a variety of middle and upper Pleistocene deposits, including fluvial, alluvial fan, eolian, and marine terrace deposits. Its type locality is on the northeast slope of the Casmalia Range near Orcutt, where it is approximately 15 m thick and consists of alluvial fan deposits overlain by and interbedded with eolian sand. The Orcutt sand also has widespread occurrence in the southeastern part of the Casmalia Range, where it consists of flat-lying, mainly eolian and fluvial deposits (Woodring and Bramlette, 1950; Dibblee, 1950).

Marine Terrace Deposits

Marine terraces are present on the southwest, west, and (locally) northeast flanks of the Casmalia Range. Marine terrace deposits typically consist of a thin (0.5-3 m) layer of occasionally fossiliferous marine sand and gravel lying directly above wave-cut bedrock surfaces and capped by variable thicknesses of colluvium and alluvium. Marine deposits are composed of fine- to medium-grained, moderately to well sorted, quartz-rich sands, with variable amounts of gravels, cobbles, and boulders, which commonly occur as basal lag deposits on marine terrace wave-cut platforms. Well rounded cobbles are commonly marked by pholad borings, distinctive

cylindrical holes made by rock-boring clams. Nonmarine deposits consist of moderately to poorly sorted, generally unstratified to poorly stratified sands, silts, and gravels.

Late Quaternary Dune Sand and Alluvium

North of Point Sal, the coastline is mantled by thick eolian sand, which ranges in age from late Pleistocene to Holocene. The northwest margin of the Casmalia Range is covered by active and inactive sand dunes (locally mapped as the Orcutt sand) between sea level and 365 m. These deposits obscure marine terrace relations north of Mussel Rock. Sand dunes are also common south of the Casmalia Range on San Antonio and Burton Mesas. Eolian deposits consist of well sorted, massive to dune cross-stratified, quartz-rich sand with minor amounts of interbedded gravel, which occurs as scattered pebbles and stringers.

Late Pleistocene and Holocene fluvial sediments and alluvial fan deposits overly and are incised into marine terrace deposits, the Orcutt sand, and older deposits.

STRUCTURE

PROPOSED TECTONIC MODELS OF ACTIVE DEFORMATION IN THE SANTA MARIA BASIN

Two types of tectonic models have been proposed for the recent development of the Santa Maria basin. Crouch and others (1984), Nitchman (1988), and Namson and Davis (1990) describe the Santa Maria basin as an active fold-and-thrust belt, with fault-propagation and fault-bend folds developed above blind thrust faults which root into a regional low-angle detachment surface at depth. High-angle faults mapped at the surface are interpreted as secondary tectonic features associated with deformation in the hanging wall of major folds.

In contrast, PG&E (1988) has stated that late Quaternary tectonic deformation is dominated by movements on west- to northwest-striking, high-angle reverse faults and the emergence and subsidence of intervening rigid structural blocks, with only minor, localized folding. This interpretation stems from PG&E's investigation of recent fault activity in the San Luis Obispo region, where Nitchman (1988) and PG&E identified active reverse faults on the northeast and southwest flanks of the San Luis Range (Figs. 1 and 2). The structural block bounded by these faults--the San Luis/Pismo structural block--contains the Pismo syncline, a late Tertiary syncline which Killeen and others (1987) and PG&E showed was no longer actively folding. According to PG&E, the change in structural style in the San Luis Range--from active folding in the late Tertiary to more brittle, fault-dominated upper

crustal deformation throughout much of the Quaternary--applies also to much of the Santa Maria basin.

Both models address neotectonic deformation in the Casmalia Range, but with different implications for earthquake processes and seismic hazard calculations.

STRUCTURAL FEATURES IN THE CASMALIA RANGE

Hosgri Fault

The Hosgri fault forms the western structural boundary of the Casmalia Range, truncating the Orcutt Frontal and Lions Head faults about 10 km west of Point Sal. The Hosgri fault is part of the seismically active San Gregorio-Sur-San Simeon-Hosgri fault zone, a major north-northwest-striking, predominantly right-lateral strike-slip fault system which shows abundant evidence of late Pleistocene and Holocene activity (Coppersmith and Griggs, 1978; PG&E, 1988). The Hosgri fault lies completely offshore. Accordingly, its current style of deformation is not well constrained. PG&E (1988) has documented Holocene right-lateral strike-slip displacements on the onshore San Simeon fault and believe that horizontal slip is transferred to the Hosgri fault across a 5 km wide en-echelon right-stepover. Crouch and others (1984), however, cite reverse faults and fault-parallel folds both onshore and offshore as evidence for mainly thrust or reverse faulting on the Hosgri fault during post-Miocene time. Both types of faulting may be presently active, with oblique strain partitioned in the uppermost crust into strike-slip and reverse and thrust components.

Orcutt Frontal Fault

The Orcutt Frontal fault as originally defined is a high angle, southwest-dipping reverse fault identified in the subsurface from oil field data in the Solomon Hills near Orcutt (Krammes and Curran, 1959; Crawford, 1971), and inferred to extend along the northeast flank of the Casmalia Range and Solomon Hills. PG&E (1988) map the Orcutt Frontal fault (referred to by PG&E as the Casmalia fault) continuing in the offshore to the Hosgri fault. Many aspects of the Orcutt Frontal fault are controversial. PG&E consider the fault to be a continuous, high-angle range-front reverse fault with probable surface expression (PG&E, 1988, Plate 4, Sheet 1). Crouch and others (1984), Nitchman (1988), and Namson and Davis (1990), however, believe that high-angle faults mapped as the Orcutt frontal fault are discontinuous, secondary faults in the hanging wall of a major blind thrust fault system (figs. 4 and 5).

The Orcutt Frontal fault, as referred to in this study, is the master thrust or reverse fault responsible for the Quaternary uplift of the Casmalia

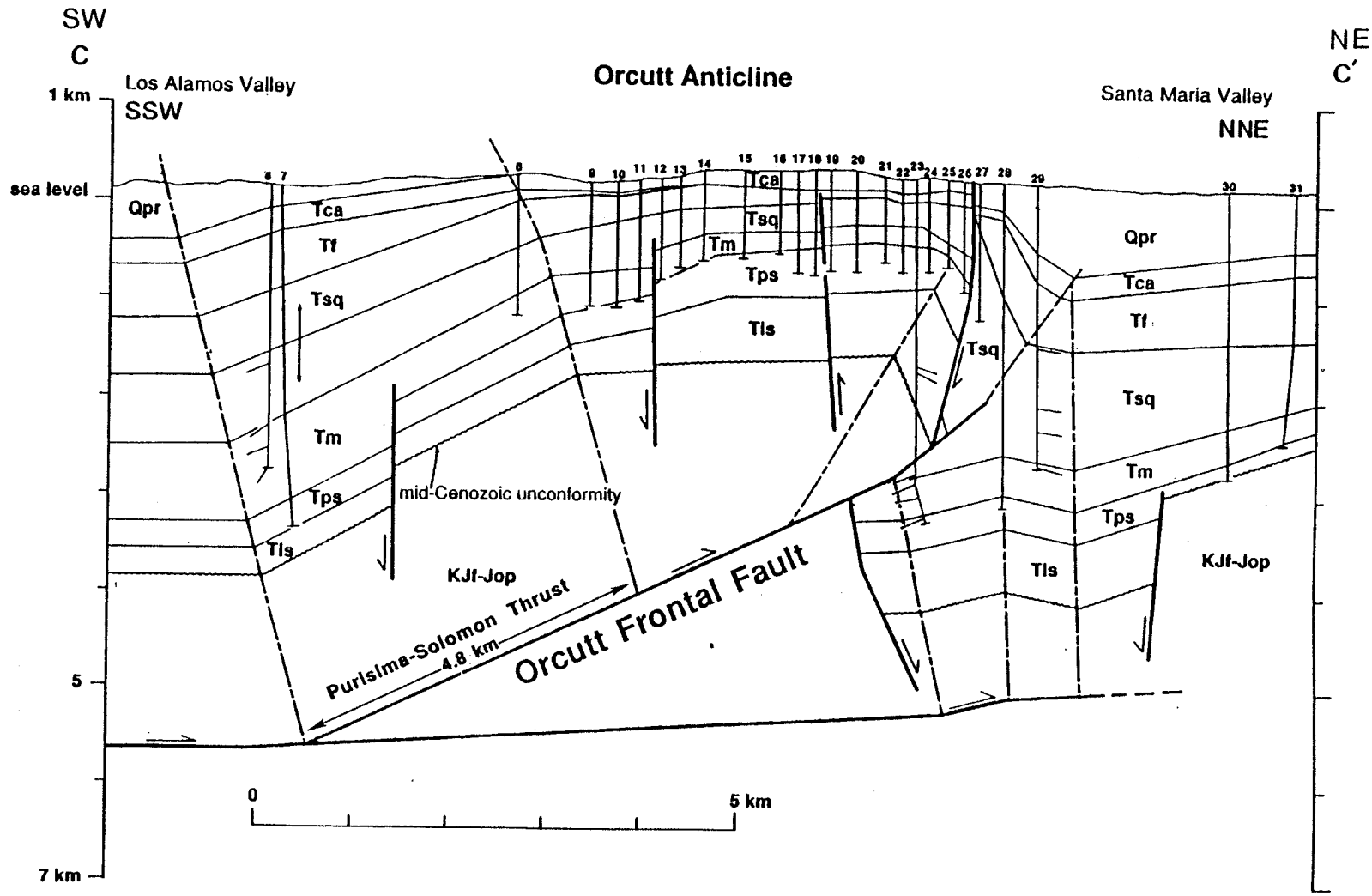

Figure 4--Retrodeformable geologic cross section across the Orcutt anticline, western Solomon Hills (modified from Namson and Davis, 1990). Section line shown in Figure 3. The anticline is interpreted by Namson and Davis as a major fault-propagation fold in the hanging wall of the Lompoc-Purisima thrust (Orcutt Frontal fault).

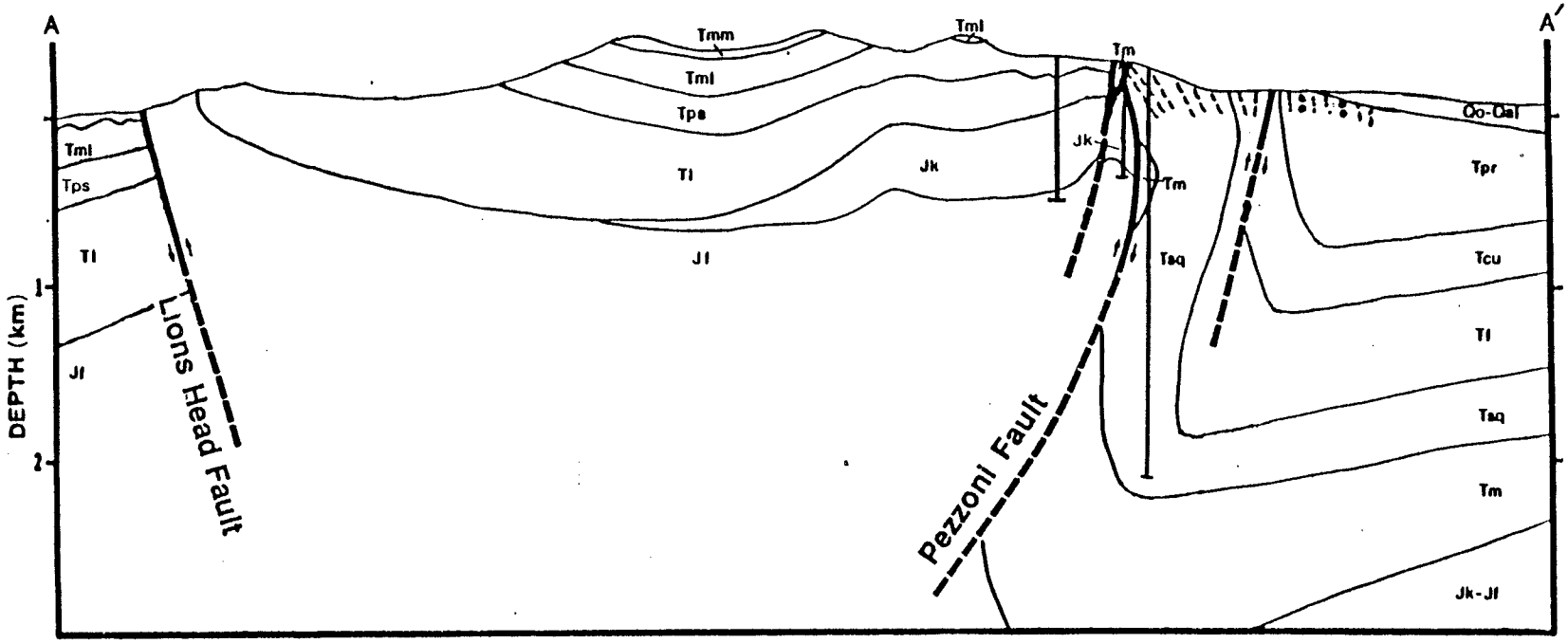

Figure 5--Geologic cross section across the Pezzoni anticline, western Casmalia Range (modified from Woodring and Bramlette, 1950). Section line shown in Figure 3. In their cross section, Woodring and Bramlette interpreted the Lions Head fault as a southwest-dipping normal fault and did not recognize a major thrust or reverse fault north of the Pezzoni fault or the minor reverse fault shown above. The asymmetric geometry of the Pezzoni anticline is consistent with an interpretation of fault-propagation folding above a major blind thrust or reverse fault. If the Orcutt Frontal fault has surface expression, its inferred surface trace probably coincides with the northernmost steeply-dipping Tpr, shown schematically above. Compare with Figure 4.

Range and Solomon Hills. The inferred surface trace of the fault is shown in Figure 3 as a continuous feature immediately north of exposures of steeply-dipping Paso Robles Formation or tilted Orcutt sand. The surface trace may in fact consist of somewhat discontinuous, en-echelon faults and/or fault-related folds.

Figures 4 and 5 are structural cross sections across the Orcutt Frontal fault in the western Solomon Hills and Casmalia Range, respectively. Figure 4 shows approximately 5400 m of post-Monterey structural relief and 2200 m of vertical separation of the base of the upper Pliocene Careaga Formation by a combination of faulting and folding across the fault. The base of the Plio-Pleistocene Paso Robles Formation, which was originally deposited at or near present sea level, is eroded off the crest of the range south of the fault and found at a depth of 1400 m below sea level north of the fault.

The Orcutt Frontal fault is seismically active, as shown by recent seismicity, including the 29 May 1980 Point Sal earthquake (M_L = 5.1). Figure 6 shows PG&E's (1988) relocation of the Point Sal earthquake and several nearby events, and a focal plane solution of the 1980 Point Sal earthquake by Eaton (1984), which suggests predominantly reverse motion on a N72°W-striking, 57°SW-dipping fault plane (Eaton, 1984).

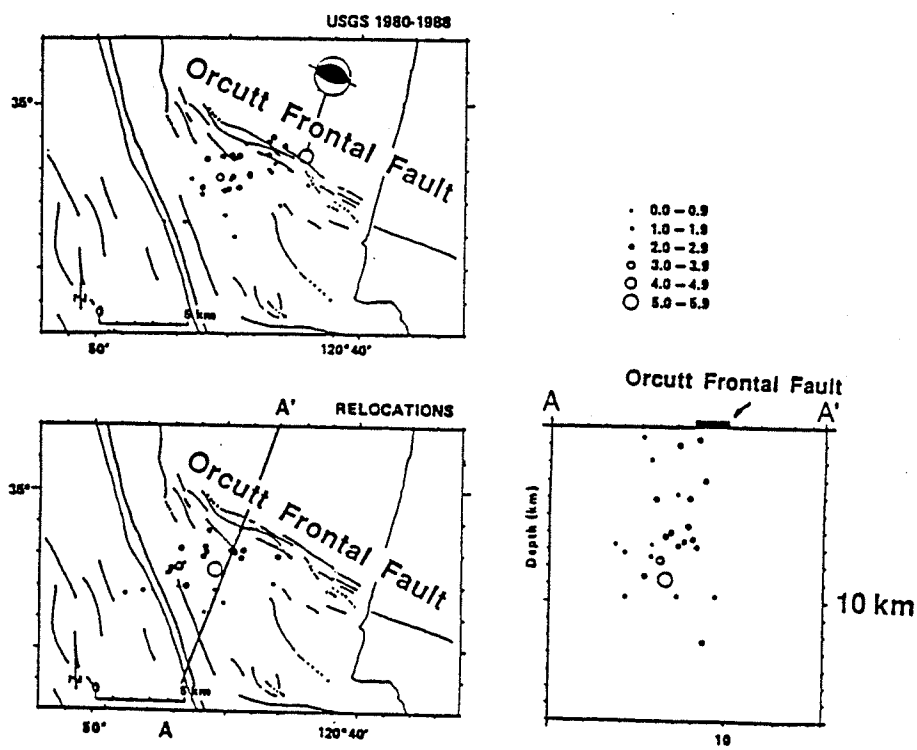

Figure 6--Seismicity map and cross section for recent events near the western end of the Casmalia Range. Epicenter locations from the U.S. Geological Survey seismicity catalog are shown at upper left; event relocations by PG&E (1988) are shown at lower left. Eaton's (1984) fault-plane solution for the 1980 Point Sal earthquake (M_L = 5.1) is also shown. Modified from PG&E (1988).

Pezzoni Fault

Woodring and Bramlette (1950) describe the Pezzoni fault as a northwest-striking, southwest-dipping reverse fault with approximately 3000 m of displacement which juxtaposes Monterey strata on the south against the Sisquoc Formation (Fig. 5). A parallel fault strand separates the Point Sal and Monterey Formations. To the southeast, the Pezzoni fault makes a 100^0 bend and becomes a normal fault. At the surface, the Pezzoni fault is marked by an alignment of topographic saddles and landslides. Woodward-Clyde Consultants (unpublished report, 1988) indicate possible middle or late Pleistocene movements on the southeast portion of the Pezzoni fault, based on apparent offsets of geomorphic surfaces across the fault.

Lions Head Fault

Woodring and Bramlette (1950) describe the Lions Head fault as a high angle, southwest-dipping normal fault which, at the coast, juxtaposes the Point Sal ophiolite on the north against the Monterey Formation. Further inland, the fault separates various stratigraphic units and is shown by Woodring and Bramlette (1950) and by Dibblee (unpublished geologic mapping) as dying out in the Sisquoc Formation (Fig. 3). PG&E (1988) mapped the Lions Head fault and a parallel structure, the "Lions Share fault", continuing offshore and terminating at the Hosgri fault.

Mapping during this study has shown that the Lions Head fault is a steep, northeast-dipping reverse or reverse-oblique fault with an earlier history of strike-slip movement. The fault offsets a series of middle and late Quaternary marine terraces, with north-side-up displacement. Two populations of slickenside orientations occur on steep, northeast-dipping fault planes along the Lions Head fault: (1) pure horizontal, and (2) southeast-plunging, indicating left-lateral reverse-oblique motion. These relations suggest a two-fold history of movement. The first was characterized by strike-slip displacement, as shown by the fault's steep dip and the presence of horizontal striae and mullion on fault surfaces. Plio-Quaternary folding of the Casmalia Range may have subsequently rotated the Lions Head fault to a steep northeast dip, allowing the fault to accommodate minor reverse or reverse-oblique motion in the present compressional regime.

Casmalia-Orcutt Anticlinal Trend

The Casmalia Range and its continuation to the east, the Solomon Hills, are underlain by a series of en-echelon, northwest-trending anticlines (from west to east, the Pezzoni, Casmalia, Graciosa or Orcutt, Mt. Solomon, Las Flores, and Gato Ridge anticlines) which together define the Casmalia-

Orcutt anticlinal trend (Fig. 2). These folds are typically asymmetric in cross section (Woodring and Bramlette, 1950). Southern limbs are long and gently dipping; northern limbs are moderately to steeply dipping, locally overturned, and in some cases override the axes of the adjacent Santa Maria Valley syncline. The highly asymmetric geometries of folds on this trend (Figs. 4 and 5) are consistent with an interpretation of fault-propagation folding in the upper plate of a major blind thrust fault (Nitchman, 1988; Namson and Davis, 1990). Fault-propagation folds form where fault slip at depth is consumed by folding in advance of a propagating fault tip (Suppe, 1985).

MARINE TERRACES IN THE CASMALIA RANGE

Figure 7 shows the terminology commonly used in marine terrace studies. Wave-cut platforms are planar, nearly horizontal erosional surfaces cut into bedrock by the action of waves in the intertidal and nearshore zones. Abandoned wave-cut platforms, or marine terraces, are the geological record of former shorelines. Vertical sequences of marine terraces are commonly found rising stair-step fashion along tectonically emergent coastlines. Each terrace within the sequence is cut during discrete, relatively brief, eustatic sea level highstands which have occurred episodically throughout the Quaternary in conjunction with the advances and retreats of major continental icesheets (Table 1 and Fig. 8).

Oxygen isotope Stage/Substage	Age (Ka)	Elevation (m)	Source
3	60	-24	1
5a	83	-5	1,2,3
5c	105	-2±	1,2,3
5e	120	+6± 2	1,2,3
7	215	-3± 4	1,2
9	320	+4± 4	1,2
11	430	0± 10	1
13	480	0	1
15	560	0	1
17	630	0	1
19	700	0	1
21	755	0	1

Table 1--Paleo-sea level highstand ages and elevations used in this study. Elevations are relative to present sea level. Table 1 is similar to Figure 8, with modifications for the California and Baja, Mexico coast proposed by Muhs and others (1988) and Rockwell and others (1989). Sources: 1 = PG&E (1989) (Modified from Shackleton and Opdyke, 1973; Bender and others, 1979; Bull, 1985; Bloom and others, 1974; Chapell, 1983; Chapell and Shackleton, 1986; Bloom and Yonekura, 1985; Muhs and others, 1987, 1988); 2 = Rockwell and others (1989); 3 = Muhs and others (1990).

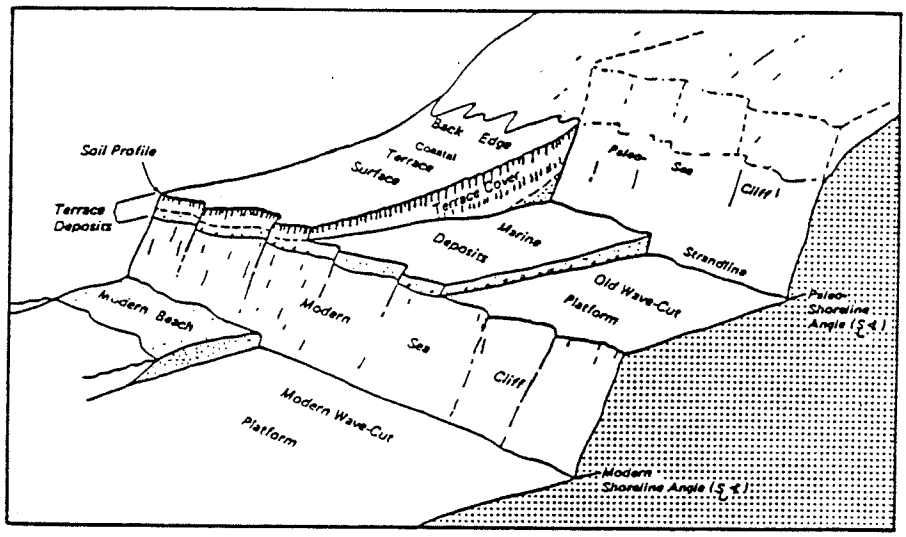

Figure 7--Marine terrace features. Marine terraces consist of planar wave-cut platforms which slope gently seaward at gradients of 0.3 to 1 degree, increasing to 1 to 2 degrees near the platform's back edge (Bradley, 1957; Bradley and Griggs, 1976). The most crucial feature for tectonic studies is the shoreline angle--the line of intersection between the wave-cut platform and the former seacliff. The shoreline angle approximates the location and elevation of the furthest advance of sea level at the time of platform cutting, and was therefore horizontal at the time of formation. Its present elevation is a function of the height of sea level at the time of platform cutting and subsequent tectonic movements. Modified from Weber (1983) and PG&E (1989).

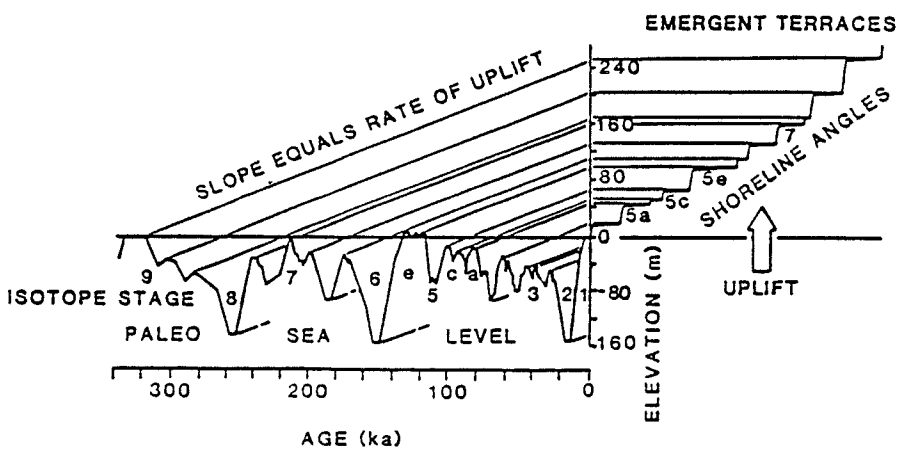

Figure 8--Quaternary sea level fluctuations and origin of emergent marine terraces. Eustatic sea levels are expressed in terminology derived from oxygen-isotope studies. Stage numbers refer to major sea level highstands and lowstands (odd numbers designate highstands; even numbers lowstands). Letters designate substages (a, c and e for highstand substages; b and d for lowstand substages). Modified from Lajoie (1986). Sea-level curve modified from Chapell (1983) and Shackleton and Opdyke (1973).

Because marine terraces are originally horizontal, often datable geomorphic surfaces, they provide ideal tectonic datums for establishing styles and rates of recent coastal uplift, faulting, tilting, and folding. Tectonically active coastlines act as "moving strip charts on which brief sea level highstands were successively recorded as depositional or erosional strandlines (Lajoie, 1986)". The goal of coastal tectonic studies, therefore, is to remove the effects of eustatic sea level fluctuations from the relative sea level history recorded by marine terraces locally, thereby yielding vertical crustal movements.

The presence of well preserved marine terraces on the southwest and west margins of the Casmalia Range (Fig. 3) allow detailed, quantitative assessments of recent tectonic movements in this region. A prominent flight of at least nine marine terraces, with shoreline angle elevations ranging between 9 and 264 m, is present on the southwest margin of the range. This represents a minimum number of marine terraces, as several of the terraces may comprise multiple platforms which cannot be discriminated from surface exposures alone. North of Point Sal Beach, one, and in some cases two, marine terraces are exposed beneath dune sand as far north as Mussel Rock.

Marine terraces in the Casmalia Range are bordered on the south by San Antonio Mesa, remnant of the very extensive, enigmatic San Antonio-Burton-Lompoc Mesa marine terrace complex (Fig. 1). Discrimination of individual marine terraces and dating of surfaces on the Mesas is complicated by a characteristic lack of preserved shoreline angles and datable fossils (Johnson, 1984). Marine terraces are not present on the coast north of the Casmalia Range in the tectonically subsiding Santa Maria Valley.

FIELD METHODS

Marine terraces in the Casmalia Range were mapped at a scale of 1:5000 on five foot contour interval topographic maps provided by Vandenberg Air Force Base (Strategic Air Command, 1978). Wave-cut platform and shoreline-angle elevations were determined by hand leveling using a Lietz survey level and/or brunton compass level, with heights measured from tide-corrected sea level or from well defined elevation points on topographic maps. Critical shoreline angle elevations of the two lowest marine terraces, Q1 and Q2, were surveyed from tide-corrected sea level using a survey level and stadia rod. Marine terrace elevations measured from the shoreline angle of the modern wave-cut platform (which in the Casmalia Range varies from about 0 to 3 m above mean low water) may be a more accurate datum for assessing post-terrace tectonic deformation (Rockwell and others, 1989). Where possible, both heights were measured.

The shoreline angles of higher marine terraces were rarely observed directly; instead, estimates of their elevations were made by projecting known wave-cut platform elevations landward towards likely paleo-seacliffs, assuming average nearshore platform gradients of 1-2^{0}. Table 2 is a summarizes these measurements. Higher, broadly concordant erosional surfaces in the Casmalia Range up to its maximum elevation of 500 m may have wave-cut origins, however, no evidence of pholad-borings, marine fossils, or marine sands have been mapped previously or during this study.

Marine terrace	Shoreline-angle elevation (m)	Fossil sites	Comments
Q1	7-10	12008,9,10	Exposed from S of Lions Head fault to Point Sal
Q2	21-26	12011, 12, 13,14,15	Exposed discontinuously from S of Lions Head to N of Mussel Rock
Q3	58$\pm$ 4		Marine sand on platform. No intermediate terrace recognized between Q1 and Q2. Q3 - Q8 are discontinuously exposed on the range's SW margin.
Q4	69$\pm$ 4	12016	
Q5	75$\pm$ 4		Pholad borings on platform
Q6	96$\pm$ 7		Alignment of erosional notches in bedrock
Q7	161$\pm$ 4		Pholad borings on platform
Q8	188$\pm$ 4	12017	
Q9	264$\pm$ 4	12018	Extensive, well preserved terrace on SW margin of range

Table 2--Marine terrace data, southwest and west margins of the Casmalia Range. Fossil site numbers refer to Los Angeles County Museum of Natural History (LACMNH) collection localities. From Clark (1990).

MARINE TERRACES AGES

Amino Acid Dating

Amino acid racemization causes originally L-form amino acids ("left-handed") to be converted to a mixture of D ("right-handed") and L amino acids. Preliminary amino acid analysis of species of the bivalve Protothaca staminea by Dr. John F. Wehmiller indicates two clusters of D/L ratios in the Casmalia Range fauna (Kennedy and others, 1990). Mean D-alloisoleucene to L-isoleucene values of 0.263 (fossil site 12009) and 0.347 (fossil site

12013) were determined for Q1 and Q2, respectively. D/L ratios, when compared with uranium-series dated marine terraces in the San Luis Range (PG&E, 1988), suggest oxygen isotope substage 5a (80-85 ka) and 5e (120 ka) for the first two marine terraces.

Faunal Assemblage Data

Invertebrate marine faunal assemblages can be used to estimate relative paleo-seawater temperatures (Kennedy, 1978). Extralimital northern species are marine fossils which have a present zoogeographical range that is north of the fossil occurrence, indicating cooler paleo-temperatures than at present. Extralimital southern species indicate paleo-temperatures that are warmer than today. This has proved to be useful in discriminating between the oxygen-isotope substage 5a highstand, characterized by slightly cooler temperatures than present, and the 5e highstand, characterized by slightly warmer paleo-temperatures.

The Casmalia Range fauna contains the extralimital southern species Pteropurpura, Terebra hemphilli, and Nassarius delosi on Q2, consistent with oxygen-isotope substage 5e warmer water conditions (preliminary species identification by Dr. George L. Kennedy; Kennedy and others, 1990). The extralimital northern species Nucella lamellosa is present on both Q1 and Q2.

$^{230}T/^{234}U$ Radiometric Dating of Corals

Several specimens of the solitary coral Balanophyllia elegans were found in the Q2 fauna (fossil site 12013). These are presently being dated using uranium-series techniques by Dr. Daniel R. Muhs.

Terrace Altitudinal Spacing

A graphical age correlation technique outlined by Bull (1985) utilizes comparison of the altitudinal spacing of individual marine terraces within a sequence of terraces and the heights of former sea level highstands. Age correlations were determined as follows. The shoreline angle elevations of marine terraces on the southwest margin of the Casmalia Range were compared with the heights of past sea levels (Table 1). To consider all possible cases, individual marine terraces were assigned a wide range of sea level highstands. The height of the sea level highstand at the assumed time of formation relative to modern sea level was subtracted from the terrace's present shoreline angle elevation to obtain the amount of tectonic uplift. Tectonic uplift was then plotted against terrace age, and the best-fit line for the data was chosen as the most likely correlation. The slope of this line is the inferred uplift rate. A major assumption of this technique is that uplift

rates have remained constant over short periods of geologic time.

A very good fit with the eustatic paleo-sea level curve was achieved by assigning the lowest two marine terraces oxygen isotope interglacial substages 5a and 5e, respectively (Fig. 9). This correlation is consistent with preliminary amino acid and faunal assemblage age data and indicates range uplift at a relatively uniform rate of 0.14 to 0.18 mm/yr over the past approximately 600,000 yrs.

MARINE TERRACE DEFORMATION

Figure 10 is a generalized index map and Figure 11 is a longitudinal profile of Q1 and Q2 shoreline angle elevations and, in cases where shoreline angle positions are buried, wave-cut platform elevations between the Lions Head fault and approximately 1 km north of Mussel Rock. The pattern of shoreline angle elevations indicates relatively uniform late Quaternary range uplift at a rate of 0.14 to 0.17 mm/yr between the Lions Head fault and Point Sal, with no significant internal faulting, tilting, or folding. The arrows on Figure 11 represent the height of the modern shoreline angle, which occurs at about 1 to 3 m above mean low sea level where exposed. Uplift rates determined from the modern shoreline angle elevation reduce the tectonic uplift rates slightly, to 0.13 to 0.16 mm/yr for the 5e terrace. However, the general pattern of uniform range uplift south of Point Sal remains.

Uniform block uplift south of Point Sal is also indicated by the wave-cut platform geometries of higher, older terraces exposed on the southwest margin of the range. Three-point problems using surveyed wave-cut platform elevations of the Q7 and Q9 marine terraces indicate 0.7°-1.9° southwest or seaward gradients, essentially the natural slope of wave-cut platforms.

The one shoreline angle measurement north of Point Sal (Fig. 11), while not as well constrained as other elevations, indicates possible tilting or folding of marine terraces north of Point Sal, and a decreased tectonic uplift rate of about 0.10 mm/yr. This shoreline angle elevation was estimated by projecting the elevation of the exposed Q2 wave-cut platform to a vertical sea cliff in an arroyo immediately south of Mussel Rock, assuming a natural seaward gradient of 1-2°. With the exception of this one point, shoreline angles north of Point Sal are buried by thick eolian sand. Mussel Rock is approximately 1-2 km south of the inferred trace of the Orcutt Frontal fault.

MARINE TERRACE DEFORMATION ALONG THE LIONS HEAD FAULT

Figure 12 shows a schematic diagram of the Lions Head fault in the seacliff. At this location, the fault juxtaposes Franciscan ophiolite on the northeast against Monterey Shale on the southwest. The fault dips about

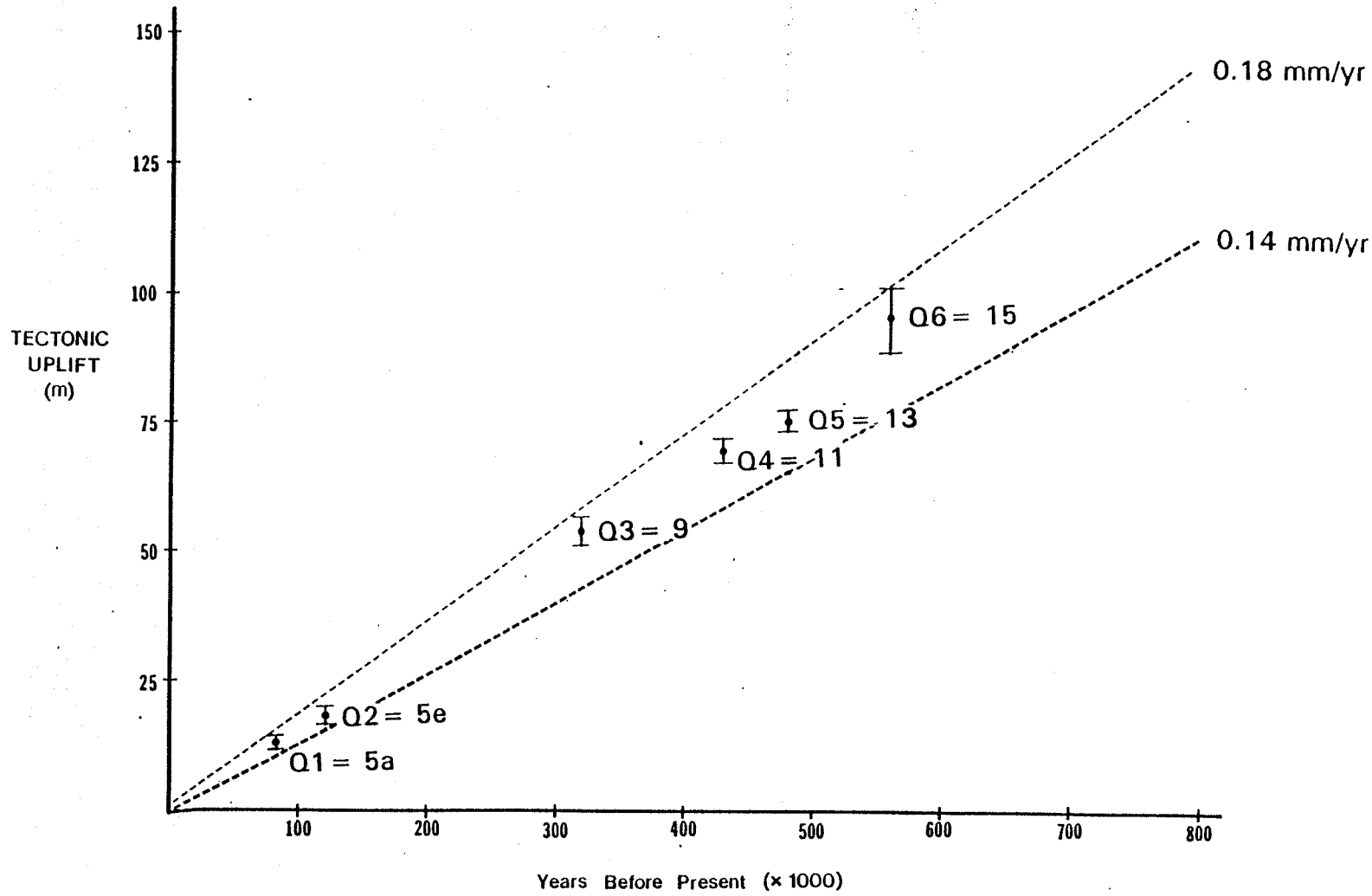

Figure 9--Preferred marine terrace-sea level highstand correlation. Q1 - Q6 are matched with correlative oxygen-isotope sea level highstand stages/substages.

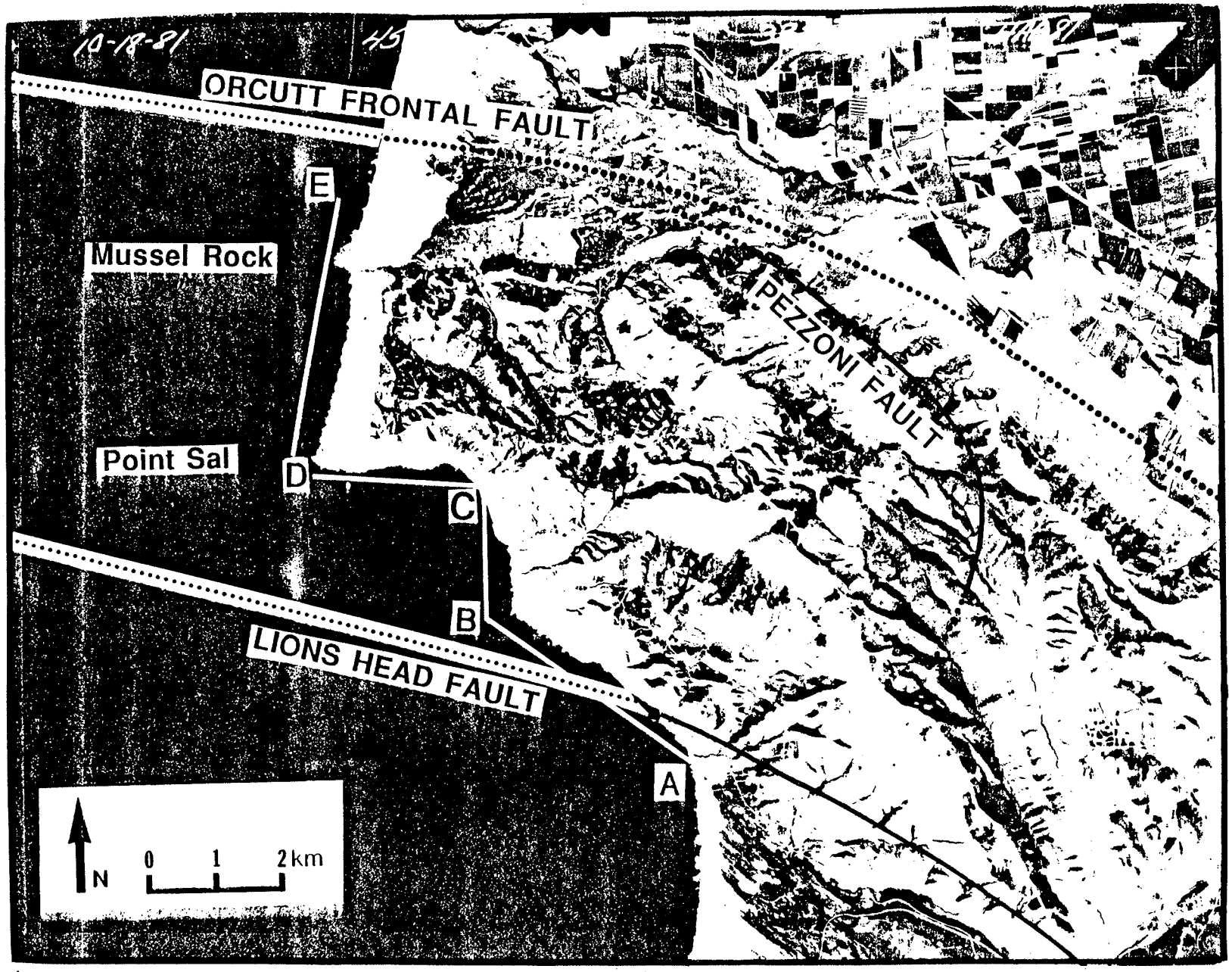

Figure 10--Generalized index map for Q1/Q2 elevation longitudinal profile, Figure 11. Base photograph is National High Altitude Photograph 458-67 (1981).

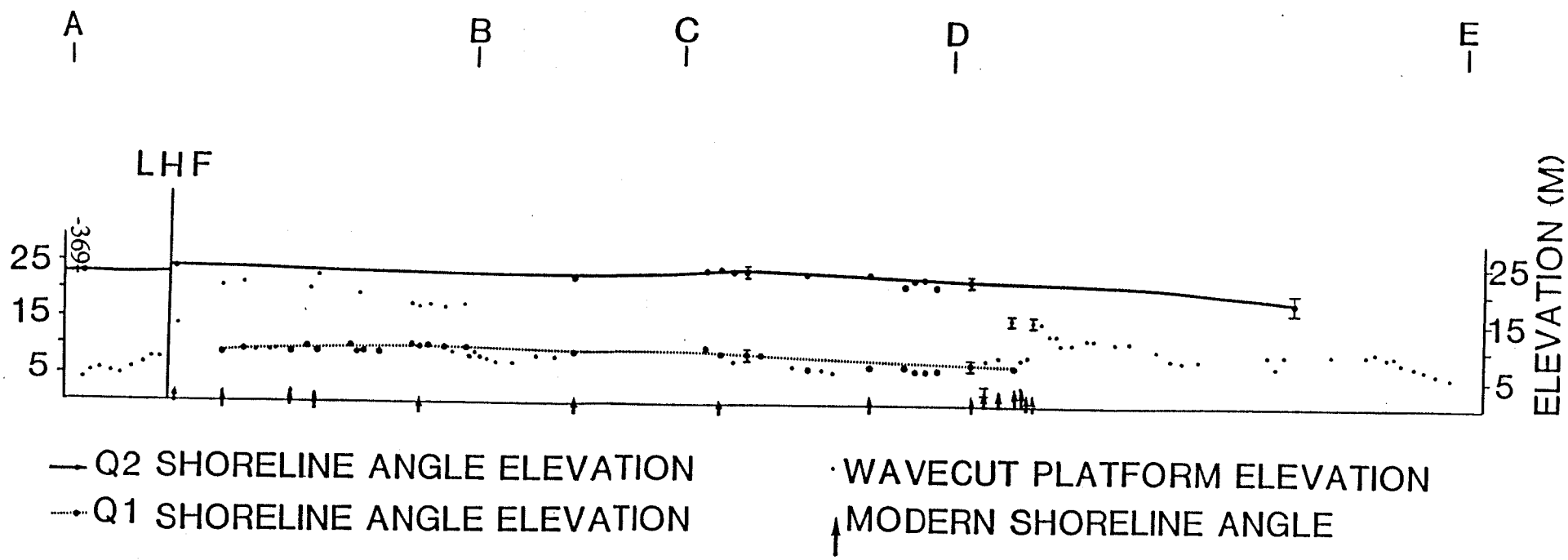

Figure 11--Longitudinal profile of Q1 and Q2 shoreline angle elevations between Mussel Rock and the Lions Head fault. Large circles designate shoreline angle elevations. Smaller circles are wave-cut platform elevations. Elevations are measures from present-day mean low sea level. Arrows show modern shoreline angle elevations, where exposed. LHF= Lions Head fault.

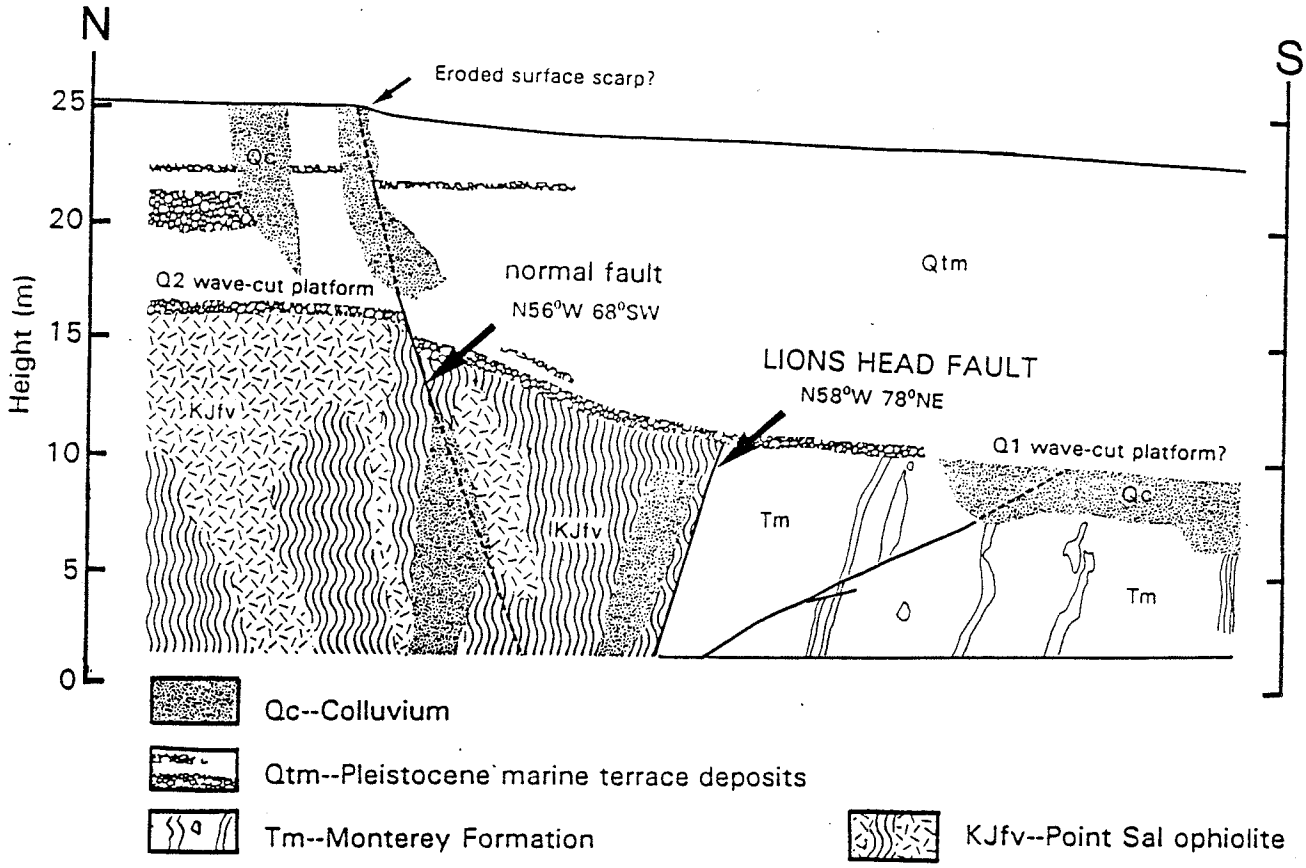

Figure 12--Lions Head fault at its sea cliff exposure.

80° northeast, and does not appear to displace the 5e marine terrace. A low angle thrust fault in the footwall also does not appear to offset the marine terrace, although monoclinal folding associated with this structure cannot be ruled out.

A high angle normal fault in the hanging wall of the fault offsets the 5e marine terrace by 1.4 m vertically and continues up through the overlying marine and alluvial sediments to the surface. Gravel beds and paleosols in the alluvium overlying the marine terrace wave-cut platform are offset 0.6 to 0.7 m along the fault. The fault may be a secondary feature (bending-moment fault) related to hanging wall collapse associated with reverse displacement at depth.

Inland, the Lions Head fault is marked by an eroded scarp, which in many places is probably a fault-line scarp. A zone of anomalous terrace heights, however, occurs within about 0-0.5 km of the trace of the fault and indicates up to 7 to 9 m of north-side-up fault offset and/or monoclinal warping along the Lions Head fault trend. The shoreline angle of the assumed stage 11 marine terrace, for example, appears to be offset approximately 4 to 5 m by the Lions Head fault. Vertical separation rates of middle and late Quaternary marine terraces across the Lions Head fault are no greater than 0.012 to 0.017 mm/yr, yielding a 0.013 to 0.018 mm/yr dip-slip faulting rate for a 70°-80°-dipping fault (this slip rate assumes a uniform 0.14-0.18 mm/yr range uplift rate for terrace age estimates).

NORTHEAST RANGE FRONT OF THE CASMALIA RANGE

The Casmalia Range's northeast range front is underlain by a series of Quaternary stratigraphic units that have undergone differing amounts of tectonic uplift, faulting, and folding. While it is clear that range-front tectonism has occurred throughout the Quaternary and is probably active today, the style and rate of active faulting and folding have not been previously documented. The goal of this part of the study was to identify, characterize, and if possible, quantify recent tectonic deformation along the controversial Orcutt Frontal fault trend.

The upper Pliocene to lower Pleistocene Paso Robles Formation (Fig. 3) is offset by faulting, dips moderately to steeply northeast, and is locally overturned near the inferred trace of the Orcutt Frontal fault. The Paso Robles Formation and older Tertiary strata define the asymmetric north limb of the Casmalia-Orcutt anticlinal trend (Figs. 4 and 5). The Orcutt sand overlies the Paso Robles Formation and older units with marked angular discordance ($\sim 40^0$-90^0) and is itself only gently folded. The Orcutt sand consists primarily of coalescing alluvial fan and eolian deposits and defines what is referred to as the Orcutt uplands or Orcutt terrace (Worts, 1951), a polygenetic middle and late Pleistocene terrace complex that has been uplifted and tilted towards the Santa Maria Valley along the Orcutt Frontal fault. The Orcutt sand is in turn overlain by relatively undeformed debris flow and eolian deposits (shown with the Orcutt sand on Fig. 3).

Tectonic uplift of the Casmalia Range relative to the Santa Maria Valley has resulted in erosional incision of the Orcutt terrace (sea level history undoubtedly plays a major role as well in the geomorphic development of the range front). Streams have responded to lowered base levels by cutting arroyo channels as much as 25 m below the surface of the Orcutt terrace, creating relatively good natural trench exposures of the Orcutt sand and underlying units.

The author examined all of the arroyos between Black Road and the coast, and most of the arroyos between Black Road and Highway 1 for evidence of recent faulting, tilting, or folding along the Orcutt Frontal fault trend (Clark, 1990). The results of this investigation suggest that there is no recent, throughgoing, primary surface faulting along the Orcutt Frontal fault trend. Recent deformation along the fault is instead expressed as folding or tilting of the Orcutt sand and younger deposits, with only minor, secondary surface faulting. This style of deformation differs from the late Quaternary behavior of the Los Osos fault (Fig. 2), characterized by thrust or reverse surface faulting and a lack of significant surface folding (PG&E, 1988).

Figures 13 is a low-sun-angle photograph of the Casmalia Range's northeast range front near Airox Mine. The pronounced west-northwest-trending, north-facing scarp evident in the photograph was identified as a possible fault scarp by Matz and Slemmons (1987) and Matz (1989).

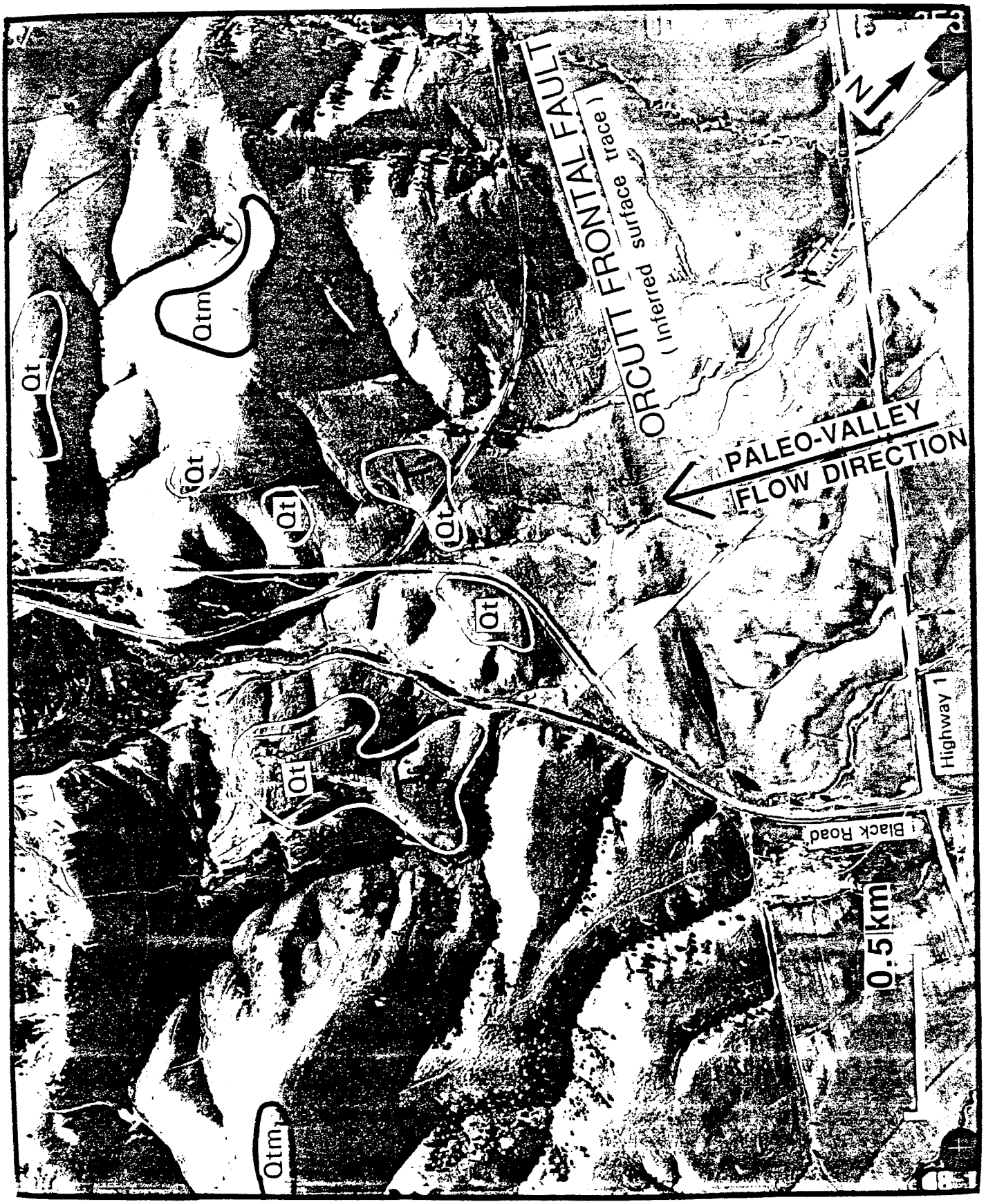

Figure 13--Low-sun-angle photograph of the northeast range front of the Casmalia Range near Airox Mine. Qt = fluvial terrace deposits, Qtm = marine terrace deposits. See text for discussion.

Similar scarps are common along the range front and generally coincide with the northernmost surface exposures of Paso Robles Formation and/or tilted Orcutt sand (mapped as the inferred surface trace of the Orcutt Frontal fault). Field investigation has shown that these very linear features are steeply-dipping to vertical "dip slopes" of resistant beds within the Paso Robles Formation, in many places mantled by thin coverings of Orcutt sand. Prominent scarps are present only where the Paso Robles Formation has dips of about 55^0 or greater. Numerous arroyos cut across these features and do not expose evidence of surface faulting.

The Orcutt sand dips between 5^0-22^0 to the northeast along the range front. The variability in bedding attitudes is due in part to differences in the ages and types of sediments mapped as Orcutt sand. The Orcutt sand is a heterogeneous deposit that includes alluvial fan, fluvial, eolian, and marine terrace deposits. Eolian sand predominates on the northwest and southeast portions of the range front. Eolian deposits have only very slight northeast dips, and may be quite young. Most of the sediments mapped as Orcutt sand along the range front consist of coalescing alluvial fan deposits derived from local sources headed in the Casmalia Range. The deeper arroyo cuts commonly expose moderately to steeply dipping Paso Robles Formation unconformably overlain by moderately to gently dipping Orcutt sand alluvial fan deposits. The Orcutt sand may consist of several successively tilted alluvial fan units. The modern geomorphic surface often cuts across bedding of the underlying Orcutt sand and has very low dips. Successive tilting of alluvial fan deposits may be the result of repeated coseismic folding events along the Orcutt Frontal fault. Similar geomorphic relations were documented at the range front of the $M_s = 7.3$ 1980 El Asnam earthquake area (King and Vita-Finzi, 1981). The El Asnam earthquake produced a complex pattern of folding and surface faulting (Philip and Meghraoui, 1983).

Some of the apparent tilting of alluvial fan deposits is the result of original depositional dip. Young, undissected alluvial fans along the range front dip 3^0-10^0, and occasionally as much as 12^0-15^0, towards Santa Maria Valley. To better constrain the amount of recent tectonic tilting or folding along the Orcutt Frontal fault, I mapped a series of fluvial terrace deposits identified by Woodring and Bramlette (1950) and Woodward-Clyde Consultants (1988). These occur near Black Road (Figs. 13 and 14) and consist of several meters of stratified gravels and sand, with channel structures, trough cross stratification, and pebble imbrication, indicating a floodplain environment. Clast imbrication, trough crossbeds, and the presence of exotic clasts within the paleo-valley deposit (plutonic and volcanic rocks not present as sources in the Casmalia Range or Santa Maria basin) indicate a source to the northeast, in the San Rafael Mountains. These deposits are remnants of a throughgoing, northeast-southwest oriented paleo-drainage inset into the Casmalia Range (Fig. 14). The paleo-valley deposits underlie a large wind gap at the range front and are flanked

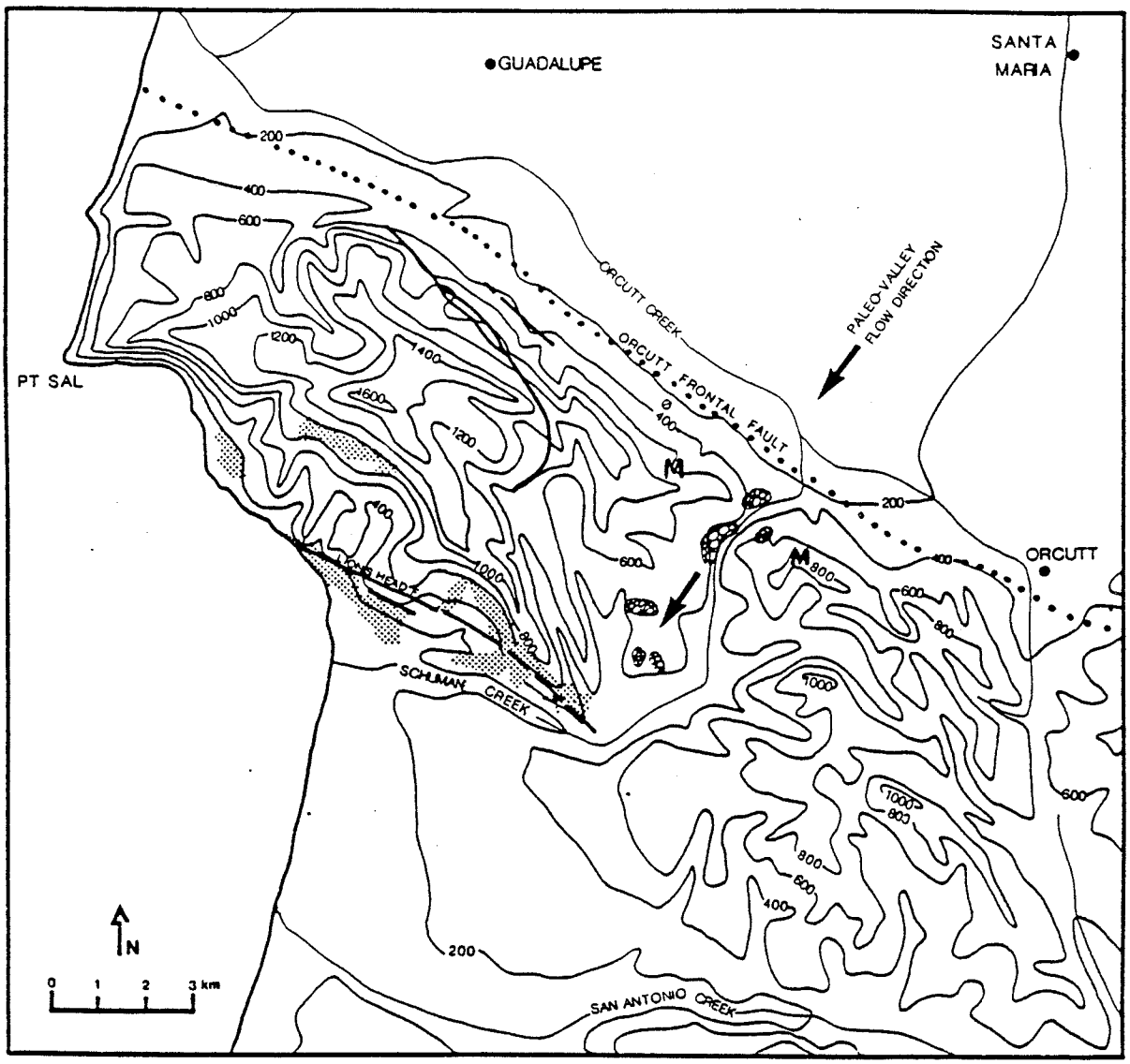

200' Contour Interval

PALEO-VALLEY DEPOSITS

M } MARINE TERRACE DEPOSITS

Figure 14--Generalized topographic map of the Casmalia Range and San Antonio Mesa, and occurrence of marine terrace and paleo-valley deposits in the Casmalia Range.

on the east and west by marine terrace deposits at elevations of approximately 207 m and 244 m, about 36-76 m higher than the paleo-valley deposits. The paleo-valley was apparently cut into the Casmalia Range as it was being uplifted.

Figure 15 shows northeast-southwest oriented topographic profiles of the paleo-valley deposits and of inset modern drainages at the range front and within the range. The latter drainages are non-throughgoing and are separated by a drainage divide. The paleo-drainage originally had a southwest gradient. 0.7 km south of the Orcutt Frontal fault, the deposit dips northeast 7^{0}-10^{0}, indicating at least that much tectonic tilting and/or folding. North-dipping paleo-channel deposits occur only within about 1 km of the Orcutt Frontal fault, suggesting that fold deformation is quite localized. At distances greater than 1.5 km from the Orcutt Frontal fault the paleo-valley deposits are flat-lying or have very slight southeast dips.

The paleo-channel deposits are locally faulted. A northwest-striking, northeast-dipping reverse fault near the intersection of Black Road and the Southern Pacific railroad line has two splays and a total of 0.75 m of dip-slip separation. The fault may be a minor back thrust related to the Orcutt Frontal fault, or may be a flexural slip feature associated with folding of the underlying Paso Robles Formation.

In conclusion, based on investigation of nearly all of the arroyos that cross the inferred trace of the Orcutt Frontal fault, there is no evidence of throughgoing surface faulting. The Orcutt Frontal fault appears to be a blind thrust or reverse fault that has elevated and warped middle and late Quaternary fluvial terraces and alluvial fan deposits along the range front. Discontinuous, secondary faulting is present locally in the hanging wall of the Orcutt Frontal fault. The fault warps and elevates the Casmalia Range structural block, accounting for the step-down in marine terrace shoreline angle elevations and associated uplift rates across the zone, from 0.14-0.17 mm/yr in the Casmalia Range to <0.0 mm/yr in the subsiding Santa Maria Valley block. Using the marine terrace uplift rate, and assuming fault dips of 30 to 60^{0}, the Orcutt Frontal fault has an estimated minimum dip-slip rate of 0.16-0.34 mm/yr. The amount of late Quaternary subsidence of the Santa Maria Valley is not known, but could significantly increase the slip rate of the Orcutt Frontal fault.

LATE QUATERNARY UPLIFT PATTERN: IMPLICATIONS FOR PROPOSED TECTONIC MODELS

The predominant style of late Quaternary, and probably middle Quaternary surface deformation in the Casmalia Range indicated by marine and fluvial terrace data (Figs. 11 and 15) is uniform, block-style uplift, with significant localized folding along the Orcutt Frontal fault and minor reverse movements on the Lions Head fault. This uplift pattern can be interpreted in at least two ways: (1) continued anticlinal folding of the Casmalia Range

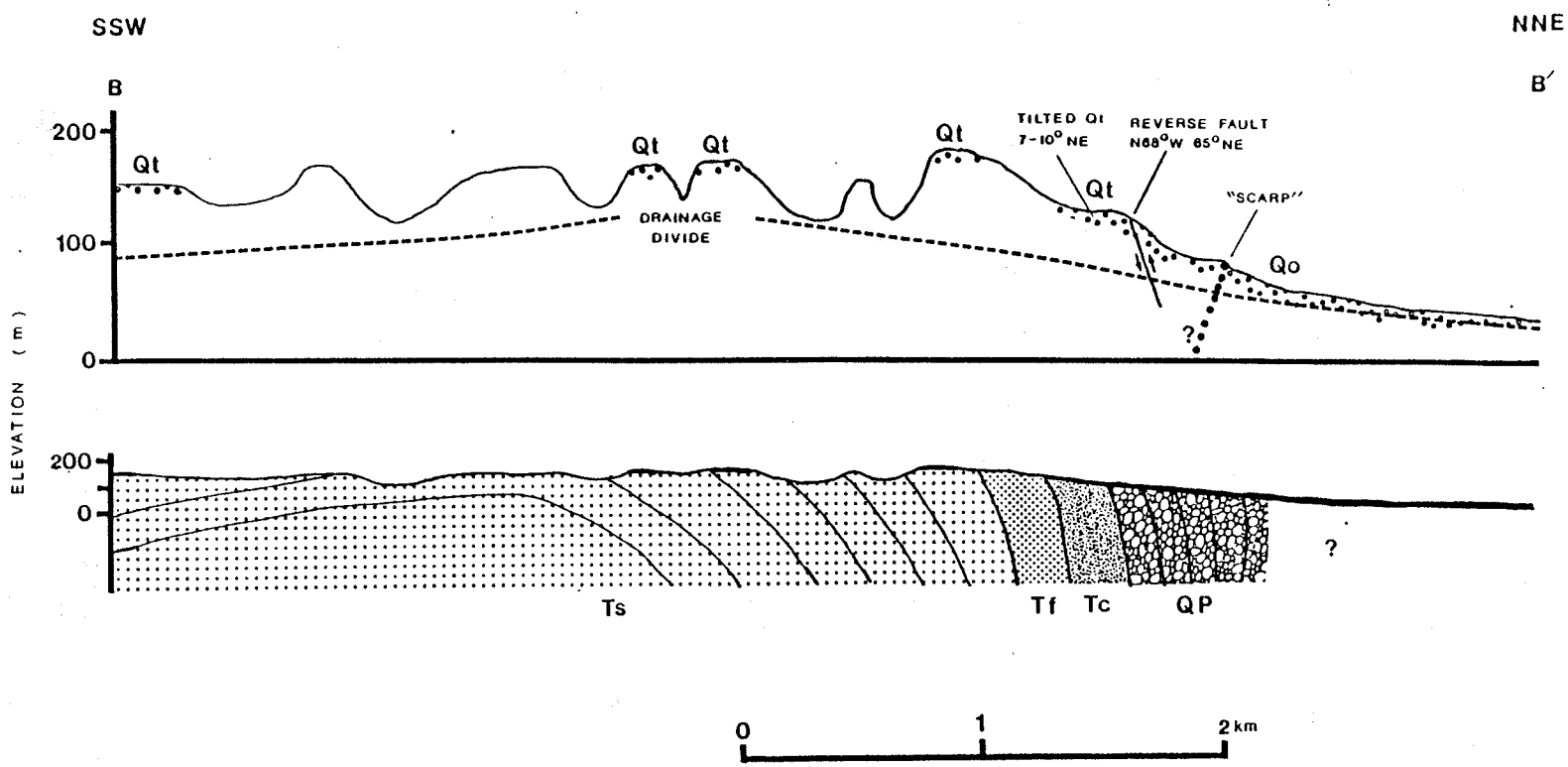

Figure 15--Topographic profile of paleo-valley deposits at the northeast range front of the Casmalia Range near Airox Mine. Section line shown on Figure 3. A stream profile of the modern drainages approximately along Black Road is shown with a dashed line. A generalized geologic cross section along the same section line is shown below (north limb of Casmalia anticline). The upper topographic profile has 5X vertical exaggeration; the geologic cross section has no vertical exaggeration. Qt= fluvial terrace deposits, Qo= Orcutt sand, QP= Paso Robles Formation, Tc= Careaga Formation, Tf= Foxen Formation, Ts= Sisquoc Formation. Geology from Woodring and Bramlette (1950).

above a listric blind thrust or reverse fault; (2) uplift of a rigid structural block along high-angle reverse faults with localized drag folding at the surface along the Orcutt Frontal fault.

The first model is consistent with active fold-and-thrust belt models proposed by Crouch and others (1984), Nitchman (1988), and Namson and Davis (1990). Figures 4 and 5 show the pronounced asymmetry of the Casmalia-Orcutt anticlinal trend. Folds along this trend typically have a broad, flat crest, a gently dipping south limb, and a short, steeply dipping or overturned north limb. The style of middle and late Quaternary range uplift indicated in Figures 11 and 15 generally parallels the underlying fold geometry defined by the Paso Robles Formation and older units. The pattern of tilted marine terraces and alluvial deposits at the north margin of the range is consistent with the asymmetric geometry of the north limb of the Casmalia-Orcutt trend (and similar to the pattern of localized folding at Wheeler Ridge on the north flank of the central Transverse Ranges, a well documented example of active coseismic folding; E.A. Keller, pers. comm., 1989). Marine terrace data north of the Lions Head fault do not show a noticeable south tilt on the south limb of the anticline. However, judging by the relatively shallow dips of the south limb of the anticlinal trend (Fig. 4), late Quaternary data would not be expected to show noticeable southward tilting (also, there may be some south tilting of marine terraces on San Antonio Mesa, south of the Lions Head fault).

The second model is similar to the flower-like structure advanced for the San Luis Range by PG&E (1988) and implies a change from Pliocene and early Pleistocene fault-propagation-style folding to a more brittle, high angle fault-dominated style of deformation in the middle and late Quaternary.

While the data in this study do not preclude either of these models, the first model is favored based on the implied continuity in style between middle and late Quaternary deformation and earlier range folding.

SEISMIC HAZARD

The seismotectonic framework of coastal south-central California is summarized by Gawthrop (1978), Eaton (1985), PG&E (1988), and Clark and others (1990). Ongoing north-northeast-directed compression in the Santa Maria basin and San Luis Range is evidenced by active west- to northwest-striking thrust and reverse faults (Nitchman, 1988; PG&E, 1988; Clark, 1990), uplifted late Pleistocene marine and fluvial terraces, reverse and left-lateral reverse-oblique earthquake focal mechanisms (Eaton, 1984, 1985), in situ stress measurements (Zoback and others, 1987), and geodetic data (Feigl and others, 1990).

Potential earthquake sources in the Casmalia Range vicinity include the Hosgri fault, the Orcutt Frontal fault, and the Lions Head fault, all of which show evidence of late Quaternary surface deformation and are considered "capable" by U.S. Nuclear Regulatory Commission standards.

PG&E (1988) estimated a M_W = 7.2 maximum earthquake for the Hosgri fault. Estimated maximum earthquakes for the Orcutt Frontal fault and Lions Head fault are M_S = 6.5-7.0 and M_S = 6.3-6.7, respectively, based on seismic source characterization, fault segmentation considerations, and regressions by Wyss (1979), Slemmons (1982), Bonilla and others (1984), Slemmons and others (1989) (Clark, 1990). Potential earthquake sources in the Casmalia Range pose significant seismic hazards (i.e., surface rupture and/or strong ground motion) to the growing communities of Santa Maria, Orcutt, and Guadalupe, the Casmalia Resources Hazardous Waste Management Facility (a Class 1 toxic waste dump located near the crest of the Casmalia Range), and structures on North Vandenberg Air Force Base. Low slip rates estimated for the Orcutt Frontal the Lions Head faults suggest very long recurrence intervals for maximum events.

ACKNOWLEDGEMENTS

This study was funded by the U.S. Nuclear Regulatory Commission and is part of the University Nevada, Reno's contribution to the Diablo Canyon Long Term Seismic Program. Support from the U.S. Nuclear Regulatory Commission and from Dr. D. B. Slemmons (Center for Neotectonic Studies) is gratefully acknowledged.

REFERENCES

Bender, M.L., Fairbanks, R.G., Taylor, F.W., Matthews, R.K., Goddard, J.G., and Broecker, W.S., 1979, Uranium-series dating of the Pleistocene reef tracts of Barbados, West Indies: Geological Society of American Bulletin, v. 90, p. 577-594.

Blake, M.C., Jr., Campbell, R.H., Dibblee, T.W., Jr., Howell, D.G., Nilsen, T.H., Normark, W.R., Vedder, J.C., and Silver, E.A., 1978, Neogene basin formation in relation to plate tectonic evolution of the San Andreas fault system, California: American Association of Petroleum Geologists Bulletin, v. 62, p. 344-372.

Bloom, A.L., Broecker, W.S., Chappell, J.M.A., Matthews, R.K., and Mesolella, K.J., 1974, Quaternary sea level fluctuations on a tectonic coast: New Guinea $^{230}Th/^{234}U$ dates from the Huon Peninsula, New Guinea: Quaternary Research, v. 4, p. 185-205.

Bloom, A.L., and Yonekura, N., 1985, Coastal terraces generated by sea-leveel change and tectonic uplift, in Waldenberg, M.J., ed., Models in Geomorphology: Allen and Unwin, p. 139-154.

Bonilla, M.G., Mark, R.K., and Lienkaemper, J.J., 1984, Statistical relations among earthquake magnitude, surface rupture length, and surface fault displacement: Seismological Society of America Bulletin, v. 74, p. 2379-2411.

Bradley, W.C., 1957, Origin of marine-terrace deposits in the Santa Cruz area, California: Geological Society of America, v. 68, p. 421-444.

Bradley, W.C., and Griggs, 1976, Form, genesis, and deformation of central California wave-cut platforms: Geological Society of America, v. 87, p. 433-449.

Buchanan-Banks, J.M., Pampeyan, E.H., Wagner, H.C., and McCulloch, D.S., 1978, Preliminary map showing recency of faulting in coastal south-central California: U.S. Geological Survey Map MF-910, 3 sheets, scale 1:250,000.

Bull, W.B., 1985, Correlation of flights of global marine terraces, in Morisawa, M., and Hack, J., eds., Tectonic Geomorphology, Proceedings of the 15th Annual Binghamton Geomorphology Symposium: Allen and Unwin, p. 129-152.

Chappell, J., 1983, A revised sea-level record for the last 300,000 years from Papua, New Guinea: Search, v. 14, p. 99-101.

Chappell, J., and Shackleton, N.J., 1986, Oxygen isotopes and sea level: Nature, v. 324, p. 137-140.

Clark, D.G., 1990, Quaternary tectonic history and seismic hazard of the Casmalia Range, Santa Barbara County, California [M.S. thesis]: Reno, University of Nevada, ~130 p.

Clark, D.G., Slemmons, D.B., Caskey, J.S., and dePolo, D., 1990, Seismotectonic framework of coastal central California, in Alterman, I.B., ed., Seismotectonics of Central and Coastal California: Geological Society of America Special Paper, (in press).

Coppersmith, K.J., Griggs, G.B., 1978, Morphology, recent activity, and seismicity of the San Gregorio fault zone, in Silver, E.A., and Normark, W.R., eds., San Gregorio-Hosgri Fault Zone, California: California Division of Mines and Geology Special Report 137, p. 33-43.

Crawford, F.D., 1971, Petroleum potential of Santa Maria Valley oil field and adjacent parts of the Santa Maria Valley, in Cram, I.H., ed., Future petroleum provinces of the United States--their geology and potential: American Association of Petroleum Geologists Memoir 15, p. 316-328.

Crouch, J.K., Bachman, S.B, and Shay, J.T., 1984, Post-Miocene compressional tectonics along the central California margin, in Crouch, J.K., and Bachman, S.B., eds., Tectonics and Sedimentation Along the California Margin: Pacific Section ofSociety of Economic Paleontologists and Mineralogists, v. 38, p. 37-54.

Dibblee, T.W., Jr., 1950, Geology of southwestern Santa Barbara County, California: California Division of Mines and Geology Bulletin 150, 95 p.

Dibblee, T.W., Jr., 1966, Geology of the central Santa Ynez mountains, Santa Barbara County, California: California Division of Mines and Geology Bulletin 186, 99 p.

Eaton, J.P., 1984, Focal mechanisms of near-shore earthquakes between Santa Barbara and Monterey, California: U.S. Geological Survey Open-File Report 84-477, 10 p.

Eaton, J.P., 1985, Regional seismic background of the May 2, 1983 Coalinga earthquake, in Rymer, M.J., and Ellsworth, W.L., eds., Mechanics of the May 2, 1983 Coalinga Earthquake: U.S. Geological Survey Open-File Report 85-44, p. 44-60.

Feigl, K.L, King, R.W., and Jordan, T.H., 1990, Geodetic measurement of tectonic deformation in the Santa Maria fold and thrust belt, California: Journal of Geophysical Research, v. 95, p. 2679-2699.

Gawthrop, W.H., 1978, Seismicity and tectonics of the central California coastal region, in Silver, E.A., and Normark, W.R., eds., San Gregorio-Hosgri Fault Zone, California: California Division of Mines and Geology Special Report 137, p. 45-56.

Hall, C.A., Jr., 1978, Origin and development of the Lompoc-Santa Maria pull-apart basin and its relation to the San Simeon-Hosgri strike-slip fault, western California, in Silver, E.A., and Normark, W.R., eds., San Gregorio-Hosgri Fault Zone, California: California Division of Mines and Geology Special Report 137, p. 25-31.

Hall, C.A., Jr., 1981, San Luis Obispo transform fault and middle Miocene rotation of the western Transverse Ranges, California: Journal of Geophysical Research, v. 86, no. B2, p. 1015-1031.

Hornafius, J.S., 1985, Neogene tectonic rotation of the Santa Ynez Range, western Transverse Ranges, California, suggested by paleomagnetic investigation of the Monterey Formation: Journal of Geophysical Research, v. 90, no. B14, p. 12,503-12,522.

Jennings, C.W., Jr., 1959, Geologic map of California, Santa Maria sheet: California Division of Mines and Geology, scale 1: 250,000.

Jennings, C.W., 1975, Fault map of California with locations of volcanoes, thermal springs and thermal wells: California Division of Mines and Geology, 1 map, scale 1: 750,000.

Jennings, C.W., 1977, Geologic map of California: California Division of Mines and Geology, 1 map, scale 1:750,000.

Johnson, D.L., 1984, Quaternary geology and soils in the site area, Chapter 4, Archaeological investigations on the San Antonio Terrace, Vandenberg Air Force Base, California (Consulting report for the Department of the Army, Contract No. DACA09-81-C-0048): Chambers Consultants and Planners, Stanton California, p. 4.1-4.89.

Kennedy, G.L., 1978, Pleistocene paleoecology, zoogeography, and geochronology of marine invertebrate faunas of Pacific Northwest coast (San Francisco to Puget Sound: [Ph.D. dissertation] University of California, Davis, 824 p.

Kennedy, G.L., Clark, D.G., and Wehmiller, J.F., 1990, The southern Oregonian province in the late Pleistocene: changing paleoclimates and sea level history based on integrated faunal and aminostratigraphic studies, Casmalia Hills, coastal California: (abstract) submitted to 1990 Annual Geological Society of America Meeting, Dallas, Texas.

Killeen, K.M., Slemmons, D.B., and Swanson, K.E., 1987, Timing of folding and uplift of the Pismo syncline, San Luis Obispo County, California: Geological Society of America Abstracts with Programs, v. 19, p. 394.

King, G.C.P., and Vita-Finzi, C., 1981, Active folding in the Algerian earthquake of 10 October 1980: Nature, v. 292, p. 22-31.

Krammes, K.F., and Curran, J.F., 1959, Correlation section across Santa Maria basin: American Association of Petroleum Geologists (Pacific Section), Correlation Section 12, 1 sheet.

Lajoie, K.R., 1986, Coastal tectonics, in Wallace, R.E., ed., Active Tectonics: National Academy Press, Washington, D.C., p. 95-124.

Luyendyk, B.P, Kamerling, M.J., and Terres, R., 1980, Geometric model for Neogene crustal rotations in southern California: Geological Society of America Bulletin, v. 91, p. 211-217.

Matz, B., 1989, Remote sensing and geomorphic studies for seismotectonic analysis, Santa Maria basin, California [M.S. thesis]: Reno, University of Nevada, 90 p.

Matz, B., and Slemmons, D.B., 1987, Remote sensing study of Pismo syncline and Santa Maria basin, central coastal California: Geological Society of America Abstracts with Programs, v. 19, p. 429.

McCulloch, D.S., 1989, Evolution of the offshore central California margin, in Winterer, E.L, Hussong, D.M., and Decker, R.W., eds., The Eastern Pacific Ocean and Hawaii: Geological Society of America, The Geology of North America, v. N., p. 439-470.

Muhs, D.R., Kennedy, G.L., and Miller, G.H., 1987, New uranium-series ages of marine terraces and late Quaternary sea level history, San Nicolas Island, California: Geological Society of America Abstracts with Programs, v. 19, p. 780-781.

Muhs, D.R., Kennedy, G.L., and Rockwell, T., 1988, Uranium-series ages of corals from marine terraces, Pacific Coast of North America: Implications for the timing and magnitude of late Pleistocene sea-level changes: American Quaternary Association, Program and Abstracts, p. 140.

Muhs, D.R., Kelsey, H.M., Miller, G.H., Kennedy, G.L., Whelan, J.F., and McInelly, G.W., 1990, Age estimates and uplift rates for Pleistocene marine terraces: Southern Oregon portion of the Cascadia forearc: Journal of Geophysical Research (in press).

Namson, J.S., and Davis, T.L., 1990, Late Cenozoic fold and thrust belt of the southern Coast Ranges and Santa Maria basin, California: American Association of Petroleum Geologists Bulletin, v. 74, p. 467-492.

Nitchman, S.P, 1988, Tectonic geomorphology and neotectonics of the San Luis Range, San Luis Obispo County, California [M.S. thesis]: Reno, University of Nevada, 120 p.

Pacific Gas and Electric Company, 1988, Final Report of the Diablo Canyon Long Term Seismic Program: U.S. Nuclear Regulatory Commission Docket Nos. 50-275 and 50-23.

Pacific Gas and Electric Company, 1989, Diablo Canyon Long Term Seismic Program, response to Q43: U.S. Nuclear Regulatory Commission Docket.

Page, B.M., and Engebretsen, D.C., 1984, Correlation between the geologic record and computed plate motions for central California: Tectonics, v. 3, p. 133-155.

Philip, H., and Meghraoui, M., 1983, Structural analysis and interpretation of the surface deformations of the El Asnam earthquake of October 10, 1980: Tectonics, v. 2, p. 17-49.

Rockwell, T.K., Muhs, D.R., Kennedy, G.L., Hatch, M.E., Wilson, S.H., and Klinger, R.E., 1989, Uranium-series ages, faunal correlations and tectonic deformation of marine terraces within the Agua Blanca fault zone at Punta Banda, northern Baja California, Mexico, in Abbott, P.K., Geologic studies in Baja California: Pacific Section Society of Economic Paleontologists and Mineralogists, Los Angeles, California, p. 1-16.

Shackleton, N.J., and Opdyke, N.D., 1973, Oxygen-isotope and paleo-magnetic stratigraphy of equatorial Pacific core V28-238: oxygen isotopic temperatures and ice volumes on a 10^5-year and 10^6-year scale: Quaternary Research, v. 3, p. 39-55.

Slemmons, D.B., 1982, Determination of design earthquake magnitudes for microzonation: Proceedinngs Third International Earthquake Microzonation Conference, v. 1, p. 119-130.

Slemmons, D.B., Bodin, P., and Zhang, X., 1989, Determination of earthquake size from surface faulting events: Proceedings of the International Seminar on Seismic Zonation, Guangzhou, China, p. 157-169.

Stategic Air Command, 1978, Abbreviated Master Plan, Vandenberg Air Force Base, Lompoc, California. Vol. I (topographic and data maps).

Suppe, J., 1985, Principles of Structural Geology: Prentice-Hall, Englewood Cliffs, New Jersey, 537 p.

Sylvester, A.G., and Darrow, A.C., 1979, Structure and neotectonics of the western Santa Ynez fault system in southern California: Tectonophysics, v. 52, p. 389-405.

Vittori, E., 1987, Structural analysis of Late Cenozoic deformation, southern Coast Ranges, central California: Geological Society of America Abstracts with Programs, v. 19, p. 460.American

Weber, G.E., 1983, Geologic investigation of the marine terraces of the San Simeon region and Pleistocene activity on the San Simeon fault zone, San Luis Obispo County, California: Menlo Park, California, Technical Report to U.S. Geological Survey, Contract No. 14-08-001-18230, 66 p.

Weldon, R., and Humphreys, E., 1986, A kinematic model of southern California: Tectonics, v. 5, p. 33-48.

Woodring, W.P, and Bramlette, M.N., 1950, Geology and paleontology of the Santa Maria district, California: U.S. Geological Survey Professional Paper 222, 185 p.

Woodward-Clyde Consultants, 1988, Geologic Siting Criteria Assessment, Casmalia Resources Hazardous Waste Management Facility, Vol. 1, Oakland, California.

Worts, G.F., Jr., 1951, Geology and ground-water resources of the Santa Maria Valley area, California: U.S. Geological Survey Water-Supply Paper 1000, 169 p.

Wyss, M., 1979, Estimating maximum expectable magnitude of earthquakes from fault dimensions: Geology, v. 7, p. 336-340.

Zoback, M.D., Zoback, M.L., Mount, V.S., Suppe, J., Eaton, J.P., Healy, J.H., Oppenheimer, D., Reasenberg, P., Jones, L., Raleigh, C.B., Wong, I.G., Scotti, O., and Wentworth, C., 1987, New evidence on the state of stress of the San Andreas fault system: Science, v. 238, p. 1105-1111.